

**Faculty of Science and Engineering
School of Civil and Mechanical Engineering**

**Analysis and Design of Stiffened Slab Foundations on
Reactive Soils using 3D Numerical Modelling**

Mohamed A. Shams

**This thesis is presented for the Degree of
Doctor of Philosophy
of
Curtin University**

March 2019

Declaration

This work contains no material which has been accepted for the award of any other degree or diploma at any university or other tertiary institution and, to the best of my knowledge and belief, this thesis contains no materials previously published or written by another person, except where due reference made in the text.

I give consent to this copy of my thesis, when deposited in the University Library, being available for loan and photocopying.

SIGNED

A handwritten signature in blue ink, appearing to read 'M. Shams' with a large, sweeping flourish above the name.

Date

07/03/2019

To my wife and children

Table of Contents

ABSTRACT	v
PUBLICATIONS AND ATTRIBUTING CO-AUTHORSHIPS DECLARATION.....	vii
ACKNOWLEDGEMENTS	xii
LIST OF FIGURES.....	xiii
LIST OF TABLES	xxiv
NOTATIONS	xxvi
ABBREVIATIONS.....	xxx
CHAPTER 1	1
INTRODUCTION	1
1.1 GENERAL	1
1.2 OBJECTIVES AND SCOPE	5
1.3 THESIS ARRANGEMENT	6
CHAPTER 2	7
LITERATURE REVIEW	7
2.1 INTRODUCTION.....	7
2.2 KEY FACTORS AFFECTING DESIGN OF SLAB FOUNDATIONS	8
2.2.1 Active Zone	8
2.2.2 Soil Surface Distortion	12
2.3 TRADITIONAL DESIGN METHODS OF SLAB FOUNDATIONS	15
2.3.1 Building Research Advisory Board (BRAB) Method.....	15
2.3.2 Lytton Method	17
2.3.3 Walsh Method	21
2.3.4 Mitchell Method	23
2.3.5 Swinburne Method	25

2.3.6	Post Tensioning Institute (PTI) Method.....	27
2.3.7	Wire Reinforcement Institute (WRI) Method	29
2.3.8	Australian Standards Method.....	31
2.3.9	Design Comparison among Traditional Design Methods.....	35
2.4	DESIGN OF SLAB FOUNDATIONS USING NUMERICAL MODELLING ..	36
2.5	DISCUSSION	47
2.6	SUMMARY	49
	CHAPTER 3	50
	NUMERICAL MODELLING OF THE BEHAVIOUR OF STIFFENED SLABS ON REACTIVE SOILS USING THE FINITE ELEMENT METHOD.....	50
3.1	INTRODUCTION	50
3.2	MODELLING ASPECTS FOR UNSATURATED SOILS	51
3.2.1.	Coupled versus Uncoupled Analysis	51
3.2.2.	Mechanism of Soil Volume Change	53
3.2.3.	Input Parameters for the Coupled Flow-Deformation Analysis	55
3.3	FINITE ELEMENT MODELLING OF STIFFENED SLAB FOUNDATIONS.	69
3.3.1.	Case Study 1: Formation of a Mound for a Soil with a Flexible Cover Membrane.....	69
3.3.2.	Case Study 2: Suction Simulation.....	79
3.3.3	Case Study 3: Hypothetical Stiffened Slab Foundation	85
3.4	EFFECT OF FLOW-DEFORMATION PARAMETERS ON SOIL MOUND .	101
3.5	SUMMARY.....	113
	CHAPTER 4	115
	NEW DESIGN METHOD FOR STIFFENED SLAB FOUNDATIONS ON REACTIVE SOILS.....	115
4.1	INTRODUCTION	115

4.2	PARAMETRIC STUDY AND DEVELOPMENT OF THE NEW DESIGN METHOD.....	115
4.2.1	Assumptions and conditions of the parametric study and the new design method	118
4.2.2	Discussion of the outputs obtained from the parametric study.....	121
4.2.2.1	Effect of slab dimensions and soil class	124
4.2.2.2	Effect of the type of soil movement: edge lift versus edge drop.....	131
4.2.2.3	Effect of construction type	133
4.3	DEVELOPMENT OF DESIGN EQUATIONS.....	136
4.3.1	Artificial intelligence for modelling design equations	136
4.3.2	Overview of Evolutionary Polynomial Regression (EPR).....	136
4.3.3	Development of EPR models for design of stiffened slab foundations.....	138
4.4	NEW DESIGN METHOD EXPLAINED VIA NUMERICAL EXAMPLE.....	152
4.5	SUMMARY	165
	CHAPTER 5	167
	EFFECT OF USING SAND CUSHION ON THE PERFORMANCE OF STIFFENED SLAB FOUNDATIONS.....	167
5.1	INTRODUCTION.....	167
5.2	HOW DOES SAND CUSHION WORK?	168
5.3	FE MODELLING OF STIFFENED SLAB FOUNDATION WITH SAND CUSHION	170
5.3.1	Modelling of sand cushion	170
5.3.2	Validation of the uniform moisture condition interpretation	173
5.3.3	Parametric study incorporating sand cushion.....	182
5.4	DEVELOPMENT OF EPR MODELS FOR STIFFENED SLAB FOUNDATION WITH SAND CUSHION	185

5.5	NUMERICAL EXAMPLE CONSIDERING SAND CUSHIONS	198
5.6	SUMMARY	202
	CHAPTER 6	204
	SUMMARY, CONCLUSIONS AND RECOMMENDATIONS	204
6.1	GENERAL	204
6.2	SUMMARY AND CONCLUSIONS	206
6.3	ORIGINAL CONTRIBUTION OF THE RESEARCH.....	209
6.4	RECOMMENDATIONS FOR FUTURE WORK	210
	REFERENCES.....	212
	APPENDICES	225
	<i>APPENDIX A: USER-DEFINED SUBROUTINE USDFLD</i>	<i>225</i>
	<i>APPENDIX B: DESIGN CHARTS OF THE NEW DESIGN METHOD</i>	<i>227</i>

ABSTRACT

Reactive soils pose a technical challenge to geotechnical engineers around the world, as they can cause severe distress to the foundations upon moisture variation, leading to unacceptable structural damages. Stiffened slabs are the most common foundation technique used for reactive soils, which are adopted by most international and local standards. However, cracks and damages are still reported worldwide in lightweight structures supported on stiffened slabs, urging the need for a more profound investigation into the reliability and shortcomings of the current design practices of stiffened slab foundations into this type of soils.

In this research, the current design methods of stiffened slab foundations on reactive soils, particularly those adopted by the Australian Standards AS2870, are presented, and their limitations are listed and discussed. New sophisticated three-dimensional (3D) hydro-mechanical finite element (FE) models are developed, using the commercial software package ABAQUS, to address the major shortcomings of the available design methods. The constructed FE models simulate the complex shrink-swell responses of unsaturated soils, by incorporating a coupled flow-deformation analysis that represents realistic soil moisture changes, hence, generating a multi-dimensional transient flow that implements true time-dependent precipitation and evaporation conditions. The interaction between the stiffened slab foundations and the underlying reactive soils is simulated using contact elements, allowing the contact between the slab foundation and the supporting soil to be modelled according to the soil mounds resulted essentially by the moisture changes. A special subroutine is developed to simulate the unsaturated soil conditions realistically and to account for the soil modulus-suction dependency, which is explicitly expressed in ABAQUS as a user-defined model.

The developed FE models are validated through comparisons with field observations reported in the literature. The FE modelling procedure is then used to perform an extensive parametric study involving a wide range of hypothetical stiffened slab foundations of various configurations. The outputs of the parametric study are compiled in the form of

design charts and equations, which now serve as a new, standalone design method for stiffened slab foundations on reactive soils. Finally, the research investigates numerically the design of stiffened slab foundations aided by a sand cushion as a means to reduce the slab thickness. This analysis explores the potential cost saving associated with implementing the sand cushion technique in the routine design of stiffened slab foundations.

PUBLICATIONS AND ATTRIBUTING CO-AUTHORSHIPS DECLARATION

The following publications are produced from the research work conducted in this PhD thesis:

- 1- Shams, M. A., Shahin, M. A., and Ismail, M. A. (2018). “Simulating the behaviour of reactive soils and slab foundations using hydro-mechanical finite element modelling incorporating soil suction and moisture changes.” *Computers and Geotechnics*, 98: 17-34.

Contributing Authors:

Shams, Mohamed



PhD Candidate, Department of Civil Engineering, Curtin University, WA 6845, Australia.

Shahin, Mohamed

Associate Professor, Department of Civil Engineering, Curtin University, WA 6845, Australia.

Ismail, Mostafa

Geotechnical Engineering Consultant, Perth WA, Australia.

	Background /literature	Numerical modelling	Data Presentation interpretation and analysis	Discussion	paper writing/ preparation/ proofread/ final approval
Co-Author #1	20%	10%	20%	20%	20%
I acknowledge that these represent my contribution to the above research output					
Signed:					
Co-Author #2	10%	-----	10%	10%	10%
I acknowledge that these represent my contribution to the above research output					
Signed:					

2- Shams, M. A., Shahin, M. A., and Ismail, M. A. (2018). “Design of stiffened slab foundations on reactive soils using 3D numerical modelling.” *International Journal of Geomechanics*, (submitted).

Contributing Authors:

Shams, Mohamed



PhD Candidate, Department of Civil Engineering, Curtin University, WA 6845, Australia.

Shahin, Mohamed

Associate Professor, Department of Civil Engineering, Curtin University, WA 6845, Australia.

Ismail, Mostafa

Geotechnical Engineering Consultant, Perth WA, Australia.

	Background /literature	Numerical modelling	Data Presentation interpretation and analysis	Discussion	paper writing/ preparation/ proofread/ final approval
Co-Author #1	20%	10%	20%	20%	20%
I acknowledge that these represent my contribution to the above research output					
Signed:					
Co-Author #2	10%	----	10%	10%	10%
I acknowledge that these represent my contribution to the above research output					
Signed:					

3- Shams, M. A., Shahin, M. A., and Ismail, M. A. (2019). “Numerical analysis of slab foundations on reactive soils incorporating sand cushions.” *Computers and Geotechnics*, 112 (2019) 218-229.

Contributing Authors:

Shams, Mohamed



PhD Candidate, Department of Civil Engineering, Curtin University, WA 6845, Australia.

Shahin, Mohamed

Associate Professor, Department of Civil Engineering, Curtin University, WA 6845, Australia.

Ismail, Mostafa

Geotechnical Engineering Consultant, Perth WA, Australia.

	Background /literature	Numerical modelling	Data Presentation interpretation and analysis	Discussion	paper writing/ preparation/ proofread/ final approval
Co-Author #1	20%	10%	20%	20%	20%
I acknowledge that these represent my contribution to the above research output					
Signed:					
Co-Author #2	10%	----	10%	10%	10%
I acknowledge that these represent my contribution to the above research output					
Signed:					

4- Shams, M. A., Shahin, M. A., and Ismail, M. A. (2017). “Analysis and modelling of stiffened slab foundation on expansive soils.” *International Congress and Exhibition, Sustainable Civil Infrastructures: Innovative Infrastructure Geotechnology*, Sharm El Sheikh, Egypt, Springer, 250-261.

Contributing Authors:

Shams, Mohamed



PhD Candidate, Department of Civil Engineering, Curtin University, WA 6845, Australia.

Shahin, Mohamed

Associate Professor, Department of Civil Engineering, Curtin University, WA 6845, Australia.

Ismail, Mostafa

Geotechnical Engineering Consultant, Perth WA, Australia.

	Background /literature	Numerical modelling	Data Presentation interpretation and analysis	Discussion	paper writing/ preparation/ proofread/ final approval
Co-Author #1	20%	10%	20%	20%	20%
I acknowledge that these represent my contribution to the above research output					
Signed:					
Co-Author #2	10%	----	10%	10%	10%
I acknowledge that these represent my contribution to the above research output					
Signed:					

5- Shams, M. A., Shahin, M. A., and Ismail, M. A. (2017). "Comparison between granular pile anchor and stiffened slab foundations for expansive soils using numerical modelling." *Proceedings of the 15th International Conference of the International Association for Computer Methods and Advances in Geomechanics (15th IACMAG)*, Wuhan, China, Proceedings on USB.

Contributing Authors:

Shams, Mohamed



PhD Candidate, Department of Civil Engineering, Curtin University, WA 6845, Australia.

Shahin, Mohamed

Associate Professor, Department of Civil Engineering, Curtin University, WA 6845, Australia.

Ismail, Mostafa

Geotechnical Engineering Consultant, Perth WA, Australia.

	Background /literature	Numerical modelling	Data Presentation interpretation and analysis	Discussion	paper writing/ preparation/ proofread/ final approval
Co-Author #1	20%	10%	20%	20%	20%
I acknowledge that these represent my contribution to the above research output					
Signed:					
Co-Author #2	10%	----	10%	10%	10%
I acknowledge that these represent my contribution to the above research output					
Signed:					

ACKNOWLEDGEMENTS

In the name of Allah, the most gracious, the most merciful. I would like to express my enormous gratitude to my supervisor, Associate Professor Mohamed Shahin, Department of Civil engineering, Curtin University, for his encouragement, thoughtful guidance, continual support in professional and personal matters and invaluable help throughout this research. His patience and availability to answer my queries whenever needed with his heavy workload are deeply appreciated. In addition, his numerous comments, constructive criticisms, suggestions, encouragement and friendship have been of great value to me, and this work would not be possible without his contribution.

My gratitude is also extended to my co-supervisor, Dr. Mostafa Ismail, a geotechnical engineering consultant and former academic, for his kind support, precious suggestions and comments during my candidature, as well as his professional editing of this thesis.

I wish to thank the Department of Civil Engineering, Curtin University, for the provision of excellent research support and facilities. Heartfelt acknowledgements are expressed to all academic and non-academic members of Curtin Civil Engineering and in particular, Associate Professor Andrew Whyte, Deputy Head of the School of Civil and Mechanical Engineering, for his assistance and warm-hearted support during my study. The scholarship awarded to this research project by the Australian Government Research Training Program is greatly acknowledged.

Finally, I am indebted to my family, and in particular my wife Hadil (Software Developer & Computer Engineer), without her encouragement and sacrifices, I may never have come this far in my study. Very special and sincere gratitude is offered to her, for providing the technical support in programming and IT issues. Warm thanks to my son Essam and my daughter Lojain for their patience, love and continuous encouragement throughout my PhD study. Their supports, spoken or unspoken, have helped me to negotiate all the twists and turns of my PhD work.

LIST OF FIGURES

CHAPTER 1. INTRODUCTION

- Figure 1.1 : Distribution of expansive soils (black batches) in Australia 2
(Richards et al. 1983).
- Figure 1.2 : Deformed footing and soil profile: (a) edge heave scenario; and 3
(b) centre heave scenario.

CHAPTER 2. LITERATURE REVIEW

- Figure 2.1 : Moisture variation with depth below ground surface 9
(redrawn from Chen, 1988).
- Figure 2.2 : Typical foundation movement versus time (redrawn from Reins 11
and Volz 2013).
- Figure 2.3 : Histogram of time for stabilisation of 149 sites with no 11
underpinning (redrawn from Reins and Volz 2013).
- Figure 2.4 : Conditions of foundation losing support due to soil heave 12
(Building Research Advisory Borad 1968).
- Figure 2.5 : Support modes assumed by BRAB method (Building Research 16
Advisory Borad 1968).
- Figure 2.6 : Determination of slab support index (C) by BRAB method 16
(Building Research Advisory Borad 1968).
- Figure 2.7 : Soil mound shapes assumed by Lytton method (Li 1996). 19
- Figure 2.8 : Soil mound shapes by Walsh method (Walsh 1974). 21
- Figure 2.9 : Soil mound shapes by Mitchell method (Mitchell 1984). 24
- Figure 2.10 : Soil mound shapes assumed by Swinburne method (Holland et 25
al. 1980).
- Figure 2.11 : Centre heave bending moments by Swinburne method (Pitt 26
1982).
- Figure 2.12 : Soil mound shapes assumed by the Post Tensioning Institute 28
(1980).

Figure 2.13 :	Determination of the cantilever length by WRI method (redrawn from Wire Reinforcement Institute 1981).	30
Figure 2.14 :	Slab length modification factor by WRI method (redrawn from Wire Reinforcement Institute 1981).	30
Figure 2.15 :	Determination of beam spacing by WRI method (redrawn from Wire Reinforcement Institute 1981).	30
Figure 2.16 :	Stiffened raft design for site classes A, S, M, M-D, H1, H2, H1-D, H2-D by Australian Standards AS2870 (2011).	35
Figure 2.17 :	Soil modelling of heave formation by Sinha and Poulos (1996).	38
Figure 2.18 :	Stiffened and unstiffened slab configurations by Sinha & Poulos (1996).	38
Figure 2.19 :	Typical example of output charts in study by Sinha and Poulos (1996).	40
Figure 2.20 :	Illustration of the separation between the soil and concrete slab foundation in the study by Fredlund et al. (2006).	41
Figure 2.21 :	Sketch of slab foundation on curved mounds by Abdelmalak (2007).	43
Figure 2.22 :	Figure 2.22: Typical example of design charts developed by Abdelmalak (2007).	44
Figure 2.23 :	Typical example of design charts developed by Briaud et al. (2016).	45
Figure 2.24 :	Distribution of swelling pressure on corner bays of a foundation grid as developed by Dafalla et al. (2011).	46

CHAPTER 3. NUMERICAL MODELLING USING FINITE ELEMENT

Figure 3.1 :	Typical example of a soil-water characteristic curve for a silty soil (Fredlund and Xing 1994).	55
Figure 3.2 :	Effect of changing fitting parameters (a , m and n) in Equation (3.3) on the shape of the SWCC [modified after Fredlund and Xing (1994)].	57

Figure 3.3	: Idealised soil-water characteristic curve (ISWCC) for empirical parameters: $a = 1000$, $m = 1.25$ and $n = 1$.	58
Figure 3.4	: Typical example of the moisture-swell model by ABAQUS User's Manual (2014).	60
Figure 3.5	: Moisture-swell curves for clay soil obtained from Soko-Ngawi region in Indonesia (Sudjianto et al. 2011).	60
Figure 3.6	: Moisture-swell curves developed by Tripathy et al. (2002).	61
Figure 3.7	: Idealised moisture-swell curve of the current study.	63
Figure 3.8	: Variation of stress-strain curves of black earth clay with suction in triaxial compression test (Li et al. 1992).	67
Figure 3.9	: Plan and cross section of the monitored flexible cover membrane in Maryland, Near Newcastle, Australia (Fityus et al. 1999).	70
Figure 3.10	: Rainfall and evaporation rates of Newcastle, Australia (www.bom.gov.au).	71
Figure 3.11	: Geotechnical profile of the field site in Maryland, Near Newcastle, Australia (Fityus et al. 1999).	71
Figure 3.12	: Profile of the total soil suction and water content of the field site in Maryland, Near Newcastle, Australia (Fityus et al. 1999).	72
Figure 3.13	: Proposed ISWCC used in Case Study (1).	73
Figure 3.14	: Idealised moisture-swell curve used in Case Study (1).	74
Figure 3.15	: Snapshot of the finite element mesh and area of moisture change around the flexible cover membrane of Case Study (1).	74
Figure 3.16	: FE results showing movement with time for some selected points on the flexible cover membrane of Case Study (1).	76
Figure 3.17	: Observed mound formation with time for the flexible cover membrane of Case Study (1) (redrawn from Fityus et al., 1999).	78
Figure 3.18	: Variation of FE predicted mound formation with time for the flexible cover membrane of Case Study (1).	78

Figure 3.19 :	Stratigraphy and soil profile at Amarillo site, Texas (Wray 1990).	79
Figure 3.20 :	SWCC used in the FE modelling for Amarillo site, Texas, of Case Study (2).	80
Figure 3.21 :	IMSC used in the FE modelling for Amarillo site, Texas, of Case Study (2).	81
Figure 3.22 :	FE mesh and boundary of surface suction change used for modelling Amarillo site, Texas, of Case Study (2).	81
Figure 3.23 :	Measured vs FE predicted suction change at Amarillo site, Texas, of Case Study (2), for points located at 0.9 m outside the covered area at depths: (a) 0.9 m; and (b) 2.10 m.	82
Figure 3.24 :	Measured vs FE predicted suction change at Amarillo site, Texas, of Case Study (2), for point located at 3.0 m inside the covered area at depths: (a) 0.9 m; and (b) 2.10 m.	83
Figure 3.25 :	Measured versus FE predicted surface movements at Amarillo site, Texas, of Case Study (2), for points located: (a) 1.8 m outside the covered area along the longitudinal axis; (b) 1.8 m outside the covered area along the short axis; and (c) 0.6 m from the cover centre along the longitudinal axis.	84
Figure 3.26 :	2D FE model of Case Study (3) showing the soil and footing movements in the long span: (a) edge lift scenario; and (b) edge drop scenario (legend values in metres).	88
Figure 3.27 :	2D FE model of Case Study (3) showing the soil and footing movements in the short span: (a) edge lift scenario; and (b) edge drop scenario.	89
Figure 3.28 :	3D FE model used of Case Study (3).	90
Figure 3.29 :	Deformed shapes of 3D FE model of Case Study (3): (a) edge drop scenario; (b) edge heave scenario (legend values in metres).	91

Figure 3.30 :	Comparison between Mitchell’s method, and 2D/3D FE soil movement results of Case Study (3) in the long footing span: (a) edge lift scenario; and (b) edge drop scenario.	93
Figure 3.31 :	Comparison between Mitchell’s method, and 2D/3D FE soil movement results of Case Study (3) in the short footing span: (a) edge lift scenario; and (b) edge drop scenario.	94
Figure 3.32 :	Comparison between Mitchell’s method, and 2D/3D FE footing deformation results of Case Study (3) in the long footing span: (a) edge lift scenario; and (b) edge drop scenario.	95
Figure 3.33 :	Comparison between Mitchell’s method, and 2D/3D FE footing deformation results of Case Study (3) in the short footing span: (a) edge lift scenario; and (b) edge drop scenario.	96
Figure 3.34 :	Comparison between Mitchell’s method, and 2D/3D FE bending moment results of Case Study (3) in long footing span: (a) edge lift scenario; and (b) edge drop scenario.	97
Figure 3.35 :	Comparison between Mitchell’s method, and 2D/3D FE bending moment results of Case Study (3) in the short footing span: (a) edge lift scenario; and (b) edge drop scenario.	98
Figure 3.36 :	Comparison between Mitchell’s method, and 2D/3D FE shear force results of Case Study (3) in the long footing span: (a) edge lift scenario; and (b) edge drop scenario.	99
Figure 3.37 :	Comparison between Mitchell’s method, and 2D/3D FE shear force results of Case Study (3) in the short footing span: (a) edge lift scenario; and (b) edge drop scenario.	100
Figure 3.38 :	SWCC used for analysis of Group 1.	101
Figure 3.39 :	Moisture-swell curve used for analysis of Group 1.	102
Figure 3.40 :	Soil and footing diagonal differential movement progress with time of flow-deformation data for group G1 and G2: (a) edge lift; and (b) edge drop.	104

Figure 3.41 :	Suction change with time for soil at the centre and corner of the footing, for flow-deformation data group G1 and G2: (a) edge lift; and (b) edge drop.	105
Figure 3.42 :	Comparison between soil and footing movement for G1 and G2 for the edge drop scenario: (a) longitudinal direction; and (b) transverse direction.	107
Figure 3.43 :	Comparison between footing bending moments for flow-deformation data of group G1 and G2 for the edge drop scenario: (a) longitudinal direction; and (b) transverse direction.	108
Figure 3.44 :	Comparison between footing shear forces for flow-deformation data of group G1 and G2 for edge drop scenario: (a) longitudinal direction; and (b) transverse direction.	109
Figure 3.45 :	Comparison between soil and footing movement for flow-deformation data group G1 and G2 for edge lift scenario: (a) longitudinal direction; and (b) transverse direction.	110
Figure 3.46 :	Comparison between footing bending moments of flow-deformation data group G1 and G2 for edge lift scenario: (a) longitudinal direction; and (b) transverse direction.	111
Figure 3.47 :	Comparison between footing shear forces for flow-deformation data of group G1 and G2 for edge lift scenario: (a) longitudinal direction; and (b) transverse direction.	112

CHAPTER 4. NEW DESIGN METHOD FOR STIFFENED SLAB FOUNDATIONS ON REACTIVE SOILS

Figure 4.1 :	Typical 3D finite element model used in the parametric study.	118
Figure 4.2 :	Sample design charts for edge lift: $L = 18$ m and $L_d/\Delta_{all} = 800$ (different soil classes).	122
Figure 4.3 :	Sample design charts for edge drop: $L = 18$ m and $L_d/\Delta_{all} = 800$ (different soil classes).	123

Figure 4.4	:	Effect of slab foundation dimensions and soil mound movements on the equivalent slab foundation thickness, T_{eq} , for $\Delta_{all} = L_d/800$: (a) edge drop scenario; and (b) edge lift scenario.	126
Figure 4.5	:	Effect of slab foundation dimensions and soil mound movements on the internal forces of the slab foundation long span for $\Delta_{all} = L_d/800$ and edge drop scenario: (a) bending moments; and (b) shear forces.	127
Figure 4.6	:	Effect of slab foundation dimensions and soil mound movements on the internal forces of the slab foundation short span for $\Delta_{all} = L_d/800$ and edge drop scenario: (a) bending moments; and (b) shear forces.	128
Figure 4.7	:	Effect of slab foundation dimensions and soil mound movements on the internal forces of the slab foundation long span for $\Delta_{all} = L_d/800$ and edge lift scenario: (a) bending moments; and (b) shear forces.	129
Figure 4.8	:	Effect of slab foundation dimensions and soil mound movements on the internal forces of the slab foundation short span for $\Delta_{all} = L_d/800$ and edge lift scenario: (a) bending moments; and (b) shear forces.	130
Figure 4.9	:	Typical mound shape, footing shape and bending moment for flexible slab foundation with large dimensions in the edge drop scenario.	132
Figure 4.10	:	Typical mound shape, footing shape and bending moment for flexible slab foundation with large dimensions in the edge lift scenario.	133
Figure 4.11	:	Effect of allowable slab foundation movement (Δ_{all}) on the equivalent slab foundation thickness (T_{eq}) for soil class (E) and $y_m = 70$ mm; (a) edge drop scenario; and (b) edge lift scenario.	134
Figure 4.12	:	Effect of allowable slab foundation movement (Δ_{all}) on the bending moments of slab foundation for soil class (E) and $y_m = 70$ mm; (a) edge drop scenario; and (b) edge lift scenario.	135

Figure 4.13 :	Graphical performance of the EPR model of Equation 4.3 regarding deflection δ : (a) Training set; and (b) Validation set.	142
Figure 4.14 :	Graphical performance of the EPR model of Equation 4.4 regarding M_s : (a) Training set; and (b) Validation set.	143
Figure 4.15 :	Graphical performance of the EPR model of Equation 4.5 regarding M_t : (a) Training set; and (b) Validation set.	144
Figure 4.16 :	Graphical performance of the EPR model of Equation 4.6 regarding V_s : (a) Training set; and (b) Validation set.	145
Figure 4.17 :	Graphical performance of the EPR model of Equation 4.7 regarding deflection δ : regarding V_t : (a) Training set; and (b) Validation set.	146
Figure 4.18 :	Graphical performance of the EPR model of Equation 4.8 regarding deflection δ : (a) Training set; and (b) Validation set.	147
Figure 4.19 :	Graphical performance of the EPR model of Equation 4.9 regarding M_s : (a) Training set; and (b) Validation set.	148
Figure 4.20 :	Graphical performance of the EPR model of Equation 4.10 regarding M_t : (a) Training set; and (b) Validation set.	149
Figure 4.21 :	Graphical performance of the EPR model of Equation 4.11 regarding V_s : (a) Training set; and (b) Validation set.	150
Figure 4.22 :	Graphical performance of the EPR model of Equation 4.12 regarding V_t : (a) Training set; and (b) Validation set.	151
Figure 4.23 :	Typical <i>L</i> -shape slab foundation used in the numerical example composed of two overlapped rectangular areas.	153
Figure 4.24 :	Sub-beams spacing of the slab foundation of the numerical example.	155
Figure 4.25 :	Flow chart explaining the procedure of the new design method.	157
Figure 4.26 :	Snapshot of SFORS Program developed for the new design method, solving rectangle (6 m \times 18 m) of the numerical example.	158

Figure 4.27 :	Snapshot of SFORS program developed for the new design method, solving rectangle (14 m × 18 m) of the numerical example.	158
Figure 4.28 :	Snapshot of the design report obtained from the SFORS program developed for the new design method, solving rectangle (6 m × 18 m) of the numerical example.	159
Figure 4.29 :	Snapshot of the design report obtained from the SFORS program developed for the new design method, solving rectangle (14 m × 18 m) of the numerical example.	160
Figure 4.30 :	Typical 3D FE mesh of the <i>L</i> -shape slab foundation used in the numerical example.	163
Figure 4.31 :	Service bending moment of the slab foundation used in the numerical example, for the edge drop scenario.	164
Figure 4.32 :	Service shear forces of the slab foundation used in the numerical example, for the edge drop scenario.	165

CHAPTER 5. STUDYING THE EFFECT OF SAND CUSHION ON THE PERFORMANCE OF STIFFENED SLAB FOUNDATION.

Figure 5.1 :	Typical soil-water characteristic curve for sand (Fredlund and Xing 1994).	171
Figure 5.2 :	A typical Finite element model showing the sand cushion (double symmetry).	172
Figure 5.3 :	Saturation contours at soil mound $y_m = 84$ mm, presented on the undeformed shape for the edge lift scenario: (a) no sand cushion; (b) sand cushion depth $S = 0.5$ m; (c) sand cushion depth $S = 1.0$ m; (d) sand cushion depth $S = 1.5$ m.	174
Figure 5.4 :	Saturation contours at soil mound $y_m = 84$ mm, presented on the undeformed shape for the edge drop scenario: (a) no sand cushion; (b) sand cushion depth $S = 0.5$ m; (c) sand cushion depth $S = 1.0$ m; (d) sand cushion depth $S = 1.5$ m.	175

Figure 5.5	: Effect of sand cushion thickness on the soil mound: (a) edge lift scenario; and (b) edge drop scenario.	177
Figure 5.6	: Effect of sand cushion thickness on the footing mound: (a) edge lift scenario; and (b) edge drop scenario.	178
Figure 5.7	: Effect of sand cushion thickness on the footing bending moments: (a) edge lift scenario; and (b) edge drop scenario.	180
Figure 5.8	: Effect of sand cushion thickness on the footing shear forces: (a) edge lift scenario; and (b) edge drop scenario.	181
Figure 5.9	: Effect of the sand cushion thickness on the equivalent slab thickness for different soil mounds: (26 m × 26 m), edge drop scenario, $\Delta_{all} = L_d/300$.	183
Figure 5.10	: Effect of the sand cushion thickness on the equivalent slab thickness for different soil mound: (26 m × 26 m), edge drop scenario, $\Delta_{all} = L_d/400$.	183
Figure 5.11	: Effect of the sand cushion thickness on the equivalent slab thickness for different soil mound: (26 m × 26 m), edge drop scenario, $\Delta_{all} = L_d/600$.	184
Figure 5.12	: Effect of the sand cushion thickness on the equivalent slab thickness for different soil mound: (26 m × 26 m), edge drop scenario, $\Delta_{all} = L_d/800$.	184
Figure 5.13	: Graphical performance of the EPR model of Equation 5.2 regarding deflection δ : (a) Training set; and (b) Validation set.	188
Figure 5.14	: Graphical performance of the EPR model of Equation 5.3 regarding M_s : (a) Training set; and (b) Validation set.	189
Figure 5.15	: Graphical performance of the EPR model of Equation 5.4 regarding M_l : (a) Training set; and (b) Validation set.	190
Figure 5.16	: Graphical performance of the EPR model of Equation 5.5 regarding V_s : (a) Training set; and (b) Validation set.	191
Figure 5.17	: Graphical performance of the EPR model of Equation 5.6 regarding V_l : (a) Training set; and (b) Validation set.	192

Figure 5.18 :	Graphical performance of the EPR model of Equation 5.7 regarding deflection δ : (a) Training set; and (b) Validation set.	193
Figure 5.19 :	Graphical performance of the EPR model of Equation 5.8 regarding M_s : (a) Training set; and (b) Validation set.	194
Figure 5.20 :	Graphical performance of the EPR model of Equation 5.9 regarding M_l : (a) Training set; and (b) Validation set.	195
Figure 5.21 :	Graphical performance of the EPR model of Equation 5.10 regarding V_s : (a) Training set; and (b) Validation set.	196
Figure 5.22 :	Graphical performance of the EPR model of Equation 5.11 regarding V_l : (a) Training set; and (b) Validation set.	197
Figure 5.23	Snapshot of SFORS Program incorporating sand cushion in the new design method, solving rectangle (17 m \times 23 m) of the numerical example.	200
Figure 5.24	Snapshot of the design report obtained from the SFORS program incorporating sand cushion in the new design method, solving (17 m \times 23 m) of the numerical example.	201

LIST OF TABLES

CHAPTER 2. LITERATURE REVIEW

Table 2.1	:	Relative values of e and y_m in the Swinburne method (after Pitt 1982).	27
Table 2.2	:	Profile of soil suction change for certain locations in Australia (Australian Standard AS2870 2011).	32
Table 2.3	:	Site classification by the characteristic surface movement (Australian Standard AS2870 2011).	33
Table 2.4	:	Maximum design differential footing deflection for design of footings and rafts by Australian Standards AS 2870 (2011).	33
Table 2.5	:	Deemed-to-comply design for stiffened slab foundations by Australian Standards AS2870 (2011).	34

CHAPTER 3. NUMERICAL MODELLING USING FINITE ELEMENT

Table 3.1	:	Summary of current methods for predicting in-situ volume change movement of expansive soils (Adem and Vanapalli 2015).	52
Table 3.2	:	Soil modulus-suction dependency (Li 1996).	68
Table 3.3	:	Poisson's ratio suggested by different researchers for unsaturated clay.	68
Table 3.4	:	Soil Properties at various depths at Amarillo site, Texas (Wray 1990).	80
Table 3.5	:	Summary results of Mitchell's method, Case Study (3).	86
Table 3.6	:	Finite element modelling parameters of Case Study (3).	87
Table 3.7	:	Flow-deformation parameters used in the comparison.	102

CHAPTER 4. NEW DESIGN METHOD FOR STIFFENED SLAB FOUNDATIONS ON REACTIVE SOILS

Table 4.1	:	Uniform loads used in the parametric study based on AS1170.1 (2002).	118
-----------	---	--	-----

Table 4.2	:	Range of parameter values used in the parametric study.	120
Table 4.3	:	Comparison between the new design method and Mitchell's method for the numerical example.	162

CHAPTER 5. STUDYING THE EFFECT OF SAND CUSHION ON THE PERFORMANCE OF STIFFENED SLAB FOUNDATION

Table 5.1	:	Comparison between EPR and FE results for the numerical example with sand cushion.	199
Table 5.2	:	EPR results for the numerical example without sand cushion.	202

NOTATIONS

a	depth of soil suction change
a_j	constant
A	non-reactive soil class
A_{sc}	top reinforcement
A_{st}	bottom reinforcement
B	width of slab foundation
B_c	bottom cover
b_f	effective flange width (for T-sections)
B_R	raft width
B_w	breadth of stiffening beam (web width)
C	ratio of the supported area of the slab
C_a	soil compressibility with respect to the change in the soil
C_H	Hazen's empirical coefficient
C_t	soil compressibility with respect to the change in the effective stresses
C_w	climatic rating
D	plate flexure rigidity
D_{10}	the sieve size through which 10 % of the soil pass
e_d	edge distance
e	void ratio
E	modulus of elasticity
$E1$	extremely reactive clay sites, which may experience extreme ground movement (75 mm < y_s ≤ 100 mm)
$E2$	extremely reactive clay sites, which may experience extreme ground movement (100 mm < y_s ≤ 120 mm)
ES	is the matrix of exponents
F	a function constructed by the process
f	a function selected by the user
f'_c	concrete grade
f_y	reinforcement steel yield stress

g	magnitude of gravitational acceleration.
Gh	coupled spring stiffness of foundation soil
G_s	specific gravity
H1	highly reactive clay sites, which may experience high ground movement
H_l	elastic modulus with respect to the change in soil suction
H2	highly reactive clay sites, which may experience very high ground movement
H_s	depth of seasonal moisture fluctuation
H_d	depth of desiccation
I	equivalent moment of inertia of the stiffened slab cross-section
I_{cr}	transformed moment of inertia of the cracked section
I_{eff}	effective moment of inertia
I_g	gross moment of inertia
I_{pt}	instability index
K	Winkler spring stiffness
k_u	permeability of an unsaturated soil
k	permeability of a fully saturated soil
k_s	dependence factor of permeability on the saturation
K_s	soil mound stiffness
L	length of slab foundation
L_d	diagonal length (from corner to corner) of a slab foundation
L_R	raft length
m	mound exponent
m_w	slope of the soil-water characteristic curve
M	moderately reactive clay sites, which may experience moderate ground movement
M	maximum service moment
M_{cr}	cracking moment
M_l	bending moment in the long direction
M_s	bending moment in the short direction
M_{st}	maximum moment of the stiffened raft
M_u	ultimate moment
n	climate frequency (cycle/year)

n^o	initial porosity of the material;
N	500 MPa (f_y steel grade)
N_L	number of beams in the long direction of the slab
N_s	number of beams in the short direction of the slab
q	load per unit length
r	correlation coefficient
r_{ii}	ratios (r_{11}), (r_{22}) and (r_{33}) anisotropic swelling factors
S	slightly reactive clay sites, which may experience slight ground movement
S	thickness of sand cushion
S_L	maximum spacing of beams in the long direction
S_s	maximum spacing of beams in the short direction
t	time variable
T	total load on the rectangle
T_c	top cover
T_s	slab thickness
T_b	depth of the stiffening beam
T_{eq}	equivalent slab thickness
u	soil suction
u_a	air pressure
u_w	water pressure
μ	Poisson's ratio
V_l	shear force in the long direction
V_s	shear force in the short direction
w	beam deflection
X	matrix of input variables
X_i	vector(s)
y	estimated vector of output of the process
y_m	maximum differential movement of the supporting soil
\hat{Y}	vector of target values y
y_m	maximum soil mound differential movement
y_s	characteristic surface heave

α	volumetric swell/shrinkage coefficient
δ	Slab foundation deflection
Δ_{all}	allowable slab foundation differential movement
ε_v	volumetric strain
ε^{ms}	volumetric swelling strain
Δ_{all}	allowable deflection
$\Delta \ell$	typical element dimension
Δu	soil suction change averaged over the thickness of the layer
Δw	reduction in the compaction moisture content
Δ_{st}	differential settlement between the centre and corner of the stiffened raft
Δ_s	differential settlement of the unstiffened raft
σ	total normal stress
θ	volumetric water content
θ_s	saturated volumetric water content
γ_w	unit weight of the wetting liquid
ψ	soil suction
ρ	density of fluid

ABBREVIATIONS

AI	artificial intelligence
AS	Australian Standards
BRAB	building research advisory board
ED	edge drop
EH	edge heave
EL	edge lift
EPR	evolutionary polynomial regression
FE	finite element
ISWCC	idealised soil-water characteristic curve
IMSC	idealised moisture-swell curve
LL	liquid limit
PI	plasticity index
PTI	Post Tensioning Institute
SFORS	stiffened foundations on reactive soils
SWCC	soil-water characteristic curve
WRI	Wire Reinforcement Institute

CHAPTER 1

INTRODUCTION

1.1 GENERAL

Foundations on reactive (or expansive)¹ soils can be exposed to complex modes of deformations. Reactive soils swell and shrink by the increase and decrease of soil moisture, respectively, causing lightweight structures supported by shallow foundations to suffer from different levels of structural damage. The problems associated with reactive soils arise from the fact that the soil moisture can vary between the wet and dry seasons, causing soil volume changes and consequently foundation movements. Man-made soil moisture changes are even more significant than seasonal water precipitation or evaporation (Li et al. 2014); these changes may result from gardening, plantation, vegetation, poor drainage and pipe leakages. The problems associated with reactive soils have been haunting engineers from around the world, since these soils exist all over the globe, including Australia, the United States, Canada, China, India and the Middle East. The financial losses incurred due to the damages caused to structures built on reactive soils are alarming, estimated to be US\$7 billion per year (Krohn and Slosson 1980). Nuhfer (1994) reported that the annual losses in the United States alone due to damages caused to houses and roads by swelling of reactive soils could reach up to US\$11 billion. The American Society of Civil Engineers estimated that nearly 25% of all homes in the United States suffered some damage due to reactive soils, with financial losses exceeding those caused by natural disasters, such as earthquakes, floods, hurricanes and tornadoes combined (Wray 1995). Similarly, expansive soils cover roughly 20% of Australia, as illustrated in Figure 1.1, and these cause structural cracks to nearly 50,000 houses each year, forming about 80% of all housing insurance claims (Robert et al. 1984).

Over the last 50 years or so, stiffened slab foundations have been used as a suitable foundation system for lightweight structures on reactive soils, and they have demonstrated

¹ The terms ‘reactive’ and ‘expansive’ are used interchangeably throughout this thesis.

historical success, despite some inherent shortcomings. This kind of foundation is usually comprised of a concrete slab/raft/mat, typically 100 mm thick, stiffened with ground beams cast monolithically with the slab, and having a spacing of about 4.0 m apart. Both the dimensions of the ground ‘stiffening’ beams and amount of reinforcement depend on the estimated level of the soil movement. The low cost of stiffened slab foundations compared with other foundation types, such as piers and screw piles, made them the first choice for engineers, to reduce the foundation cost relative to the low cost of superstructures.

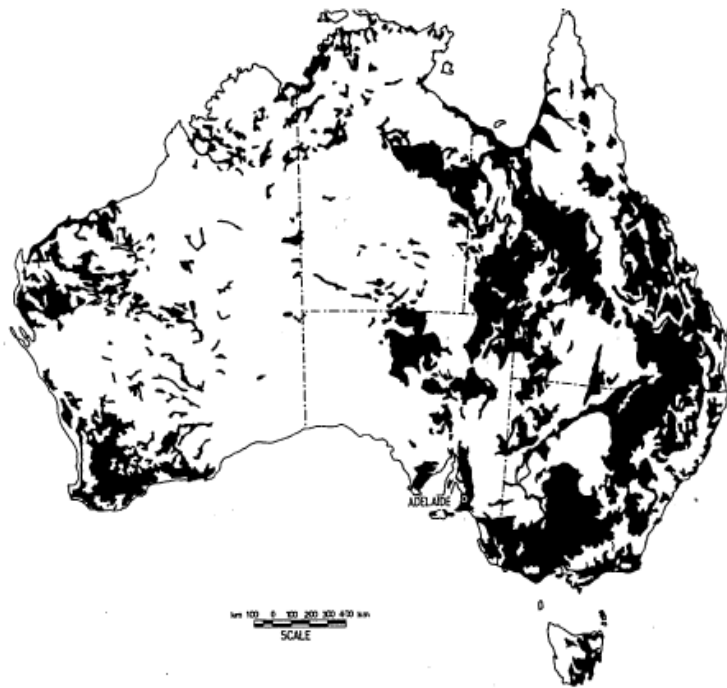


Figure 1.1: Distribution of expansive soils (black batches) in Australia (Richards et al. 1983).

Many traditional methods are available in the literature for the design of stiffened slab foundations on reactive soils, including the Building Research Advisory Board (BRAB) method (1968), Lytton method (Lytton 1970), Walsh method (Walsh 1974), Mitchell method (Mitchell 1980), Swinburne method (Holland et al. 1980), Wire Reinforcement Institute (WRI) method (1981; 1996) and Post Tensioning Institute (PTI) method (1996). Out of these methods, the Walsh (1974) and Mitchell (1980) methods are the most widely adopted by the Australian Standards AS2870 (2011).

The main premise underlying the abovementioned design methods of stiffened slab foundations is to adopt idealised typical patterns of the slab foundation movements caused by the soil heave (namely edge or centre), assuming that these two heave scenarios represent the worst loading cases among an infinite number of possible heave patterns, depending on the site boundary conditions. According to the extreme edge heave scenario, the stiffened slab foundation acts as a simple beam supported by the rising soil at the slab foundation edges, assuming that the centre of the slab foundation loses its contact with the soil [see Figure 1.2 (a)]. Conversely, in the centre heave scenario, the stiffened slab foundation acts as a double cantilever supported by the rising soil at the centre area while the edges of slab lose contact with the soil over a certain edge distance [see Figure 1.2 (b)]. It is postulated that the edge heave beneath the slab footing edges is initiated by the rain water infiltration in the wet seasons, whereas the centre heave is initiated in the hot dry seasons by the moisture propagation from the hot area at the slab edges towards the cooler area beneath the centre (Chen 1988).

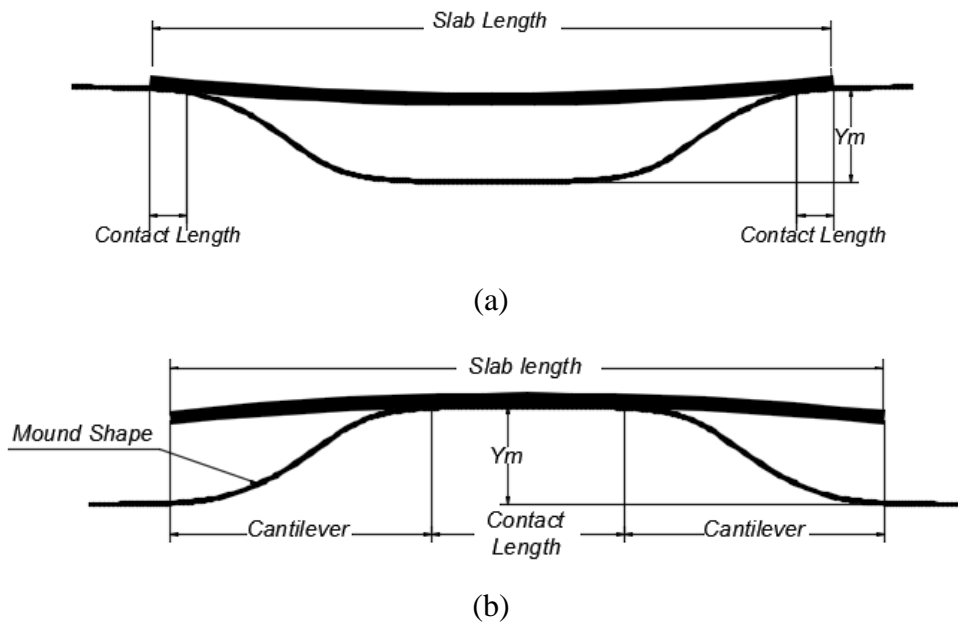


Figure 1.2: Deformed footing and soil profile: (a) edge heave scenario; (b) centre heave scenario.

Iterative analysis of the slab footing over the distorted soil mounds can enable the designers to obtain the required slab stiffness and corresponding internal forces that maintain the foundation differential movements within certain acceptable limits. To

address the complexity of the problem, existing design methods adopt the following simplifications as intrinsic assumptions in the design process:

- Prediction of the distorted soil mound shapes is determined using predefined simple, specific empirical equations, based on the best fit of field observations. In reality, however, there is an infinite number of mound shapes depending on many factors including the soil suction, degree of saturation, permeability, site drainage conditions and irrigation/plantation.
- The actual 3D distorted soil mounds are reduced to simplified 2D plane strain ones; the foundation is then analysed independently in each direction, and the maximum stiffness and internal forces resulting from each direction are adopted in the design.
- The infinite number of foundation plan configurations is simplified by dividing the foundation surface into equivalent overlapped rectangles. Each rectangle is solved separately in both directions under the two heave scenarios, and the maximum stiffness and internal forces are then considered.
- The various loading patterns are simplified into either: (i) a uniformly distributed load over the slab comprising the load of finishing materials, wall load and live load; or (ii) uniformly distributed load comprising the load of finishing materials, live load and partition load, in addition to the central and peripheral line loads representing the internal and edge walls, respectively.
- The change of soil moisture around the footing is assumed to be symmetrical in each of the two modes: precipitation or evaporation; violating this assumption may result in unaccounted differential movements that may not be adequately resisted by the foundation or the superstructure.

During the last few decades, several attempts have been made to enhance the well-established traditional methods by implementing the numerical modelling techniques. However, available numerical modelling studies suffer from the same problem of the traditional methods (in terms of the uncertainty associated with the assumed soil mounds). In addition, none of the available numerical modelling studies were developed into a

general design procedure. In fact, the continual reporting of structural damages of lightweight structures caused by expansive soils reveal that there is an immense need to improve the current design practices, by investigating the intrinsic limitations and assumptions listed above, and this thesis fills out part of this gap. The readily ensuing conclusion is that there is a need to develop a more reliable design method that can closely mimic the real flow mechanism of soil moisture and the subsequent behaviour of stiffened slab foundations on reactive soils.

1.2 OBJECTIVES AND SCOPE

Inspired by the limitations set out earlier for available design methods, this research aims to critically investigate the behaviour of stiffened slab foundations on reactive soils through a sophisticated three dimensional (3D) hydro-mechanical finite element (FE) numerical modelling, using coupled flow-deformation analysis and implementing realistic precipitation and evaporation processes as well as realistic soil water characteristics. The outcomes of this research are synthesised into a set of design charts and equations that can be readily used by practitioners for routine design practices. The specific objectives of this research can thus be summarised as follows:

1. To develop a sophisticated 3D hydro-mechanical FE numerical models capable of simulating realistically the behaviour of stiffened slab foundations on expansive soils under cycles of seasonal wetting and drying. The developed FE models are validated against field observations obtained from existing research results.
2. To carry out a comprehensive parametric study based on the developed FE models, encompassing a wide range of footing slab configurations, construction types and soil parameters.
3. To develop practical procedures for the design of stiffened slab foundations on reactive soils based on the results obtained from the abovementioned parametric study, enabling more realistic and reliable design for adoption by engineers.
4. To investigate the effects of using a sand cushion in a hybrid solution with stiffened slab foundations on reactive soils, potentially enabling a reduction in the slab foundation thickness towards more economical design.

1.3 THESIS ARRANGEMENT

This thesis is divided into six chapters. Chapter 1 provides an introduction on stiffened slab foundations for reactive soils, including the thesis objectives and arrangement.

Chapter 2 covers a literature review on available design methods for stiffened slab foundations on reactive soils, including their assumptions and limitations. This chapter also presents a background on the governing factors affecting the soil mound distorted shapes, which in turn affect the design of stiffened slab foundations.

Chapter 3 describes the development of sophisticated 3D hydro-mechanical FE numerical models that accurately simulate and predict the behaviour and performance of stiffened slab foundations on reactive soils. This chapter also includes verification of the developed FE models through comparisons with field observations and existing research studies.

Chapter 4 comprises an extensive parametric study, using the 3D FE modelling procedure developed and verified in Chapter 3. The parametric study covers a wide range of hypothetical stiffened slab configurations, and the outputs are synthesised into a set of design charts and equations that can be readily used by practitioners for design purposes.

Chapter 5 investigates the efficacy of using sand cushions, as an enhancing technique for slab foundations on expansive soils, and explores the impact of utilising this technique on the required inertia of stiffened slab foundations, aiming at decreasing the depth of stiffening beams and reinforcement, and in turn reducing the overall cost of slab foundations.

Finally, Chapter 6 summarises the research conducted in this thesis and presents the research main contributions and limitations. The chapter also provides the research conclusions and recommendations for possible future work.

CHAPTER 2

LITERATURE REVIEW

2.1 INTRODUCTION

Stiffened slab foundations are the most common type of foundations used to support lightweight structures built on expansive soils. Unfortunately, these foundations are vulnerable to the swelling pressure induced by soil moisture increase, which is likely to exceed the weight of the supported structure. During the last 50 years or so, many design methods have been developed for stiffened slab foundations on expansive soils. Generally speaking, most of these methods are mainly derived from the Building Research Advisory Board (BRAB) method (1968) developed in the United States.

The BRAB method was first generated based on field observations recorded for slab foundations over a decade. The method simplifies the complex distortion of the soil mounds beneath the foundation slab into two extreme scenarios, depending on the location of moisture variation. The first scenario occurs in winter, when the water precipitation causes the soil at the edge of the footing to swell, producing a dish shape soil mound. This scenario is known as the “edge heave scenario” and the foundation in this scenario is usually lifted at the edge over a certain support or contact distance. This distance depends on the footing stiffness and can lose its contact with the soil at the centre, producing a simple beam-like behaviour. Conversely, in summer the soil at the edge of the footing dries by evaporation and shrinks, causing the footing edge to settle or drop, producing a dome shape soil mound. This scenario is known as the “edge drop scenarios” or “centre heave scenario”, in which the footing loses its contact with the soil over a certain edge distance that depends on the footing stiffness. The footing in this scenario becomes supported on the soil over a certain contact distance at the centre, producing a double cantilever-like behaviour. More on this method is presented in Section 2.3.1.

Design of stiffened slab foundations on reactive soils is a soil structure interaction problem that can be solved as a footing resting on idealised mound shapes (formed by in-situ

changes in moisture condition after the footing construction). The key premise of all existing design methods of stiffened slab foundations on expansive soils is similar, which is to design footing slabs that are rigid enough to maintain the footing differential movements (and in turn the super-structure) under all possible movement scenarios within acceptable limits, depending on the super-structure type.

In this chapter, a review of the most commonly used methods for the design of stiffened slab foundations is presented, including their main assumptions and limitations. The chapter starts with a discussion on the key design factors affecting the generation of the distorted soil surface, forming the basis of each available design method. Then, the chapter presents the most common traditional design methods that are widely used in practice, followed by the most recent studies that adopted numerical modelling.

2.2 KEY FACTORS AFFECTING DESIGN OF SLAB FOUNDATIONS

2.2.1 Active Zone

The depth over which a reactive soil can endure a moisture variation (usually denoted as the “active zone”) is a fundamental parameter used to estimate the maximum amount of differential movement of the ensuing soil mound. The active zone can be defined as the depth to which the surface water can penetrate or the thickness of the soil zone considered in estimating the surface heave due to soil expansion at a particular point in time.

An alternative definition of the active zone is proposed by the Australian Standards AS2870 (1996; 2011) as being the depth beyond which no significant change to the soil suction occurs as a result of the seasonal climate conditions. This definition is based on the work done by Mitchell (1984), who related the swelling behaviour to the suction properties, resulting in more accurate estimates of the soil heave. However, McKeen and Johnson (1990) stated that this definition of the active zone excludes the permanent changes in the soil moisture caused by the footing installation that prevents evapotranspiration. Nelson et al. (2001) summarised alternative definitions for the active zone, as follows:

1. *Depth of Seasonal Moisture Fluctuation (or Suction Depth)*: The maximum depth of soil affected by moisture fluctuation due to climate change.
2. *Depth of Wetting*: The maximum depth of soil to which the surface water penetrates. The surface water can be due to some external factors, including the capillary rise after elimination of evapotranspiration from the surface, infiltration due to plantation, irrigation or rainfall, leakage from broken water pipes, perched water tables and flow from water ponds formed due to bad drainage or site topography.
3. *Depth of Potential Heave*: The depth to which the overburden vertical stress equals or exceeds the soil swelling pressure, which represents the maximum active zone depth that may occur.

Chen (1988) indicated that the depth of seasonal moisture fluctuation (H_s) under the slab foundations can increase in the course of several years to reach the depth of desiccation (H_d), which is defined as the depth at which the moisture content below foundations equates that below the uncovered area (see Figure 2.1). The Australian Standards AS2870 (1996) provides fixed values for H_s for different regions across Australia, but emphasised that H_s is not entirely fixed but climate dependent. Chen (1988) mentioned that the exact value of (H_d) cannot be determined, but it has lower and upper bounds between (H_s) and the depth of water table.

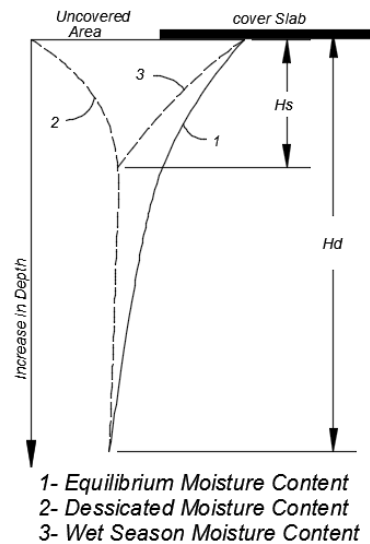


Figure 2.1: Moisture variation with depth below ground surface (redrawn from Chen, 1988).

Since diffusion is time-dependent and because the water below a covered area is not affected by evapotranspiration, the soil below slab foundations uninterruptedly accumulates water due to seasonal precipitation in a successive manner until the soil below the footing reaches a ‘damaging’ saturation degree, resulting in the maximum heave, which typically occurs at the soil’s plastic limit. In fact, in the absence of any tree roots or vegetation excessive transpiration, the foundation movement shows persistent heave behaviour for most field observations until equilibrium is reached after a certain period (Fityus et al. 2004; Reins and Volz 2013). The time required to reach that equilibrium heave is site-specific, and it actually relies on many soil parameters, such as diffusion coefficient, permeability, moisture index and depth of the swelling layer.

Overton et al. (2006) speculated that the depth of wetting should be related to the age of the overlying structure, but Kenneth et al. (2009) argued against this approach. In fact, the speculation made by Overton et al. (2006) agrees well with some field observations. For example, Bligh (1965) reported that the maximum heave was attained after 4 years from construction, while Masia et al. (2004) reported a corresponding three- to five-year period. In addition, the Foundation Performance Association (FPA) (2005) proposed a period of 10 years to achieve the maximum swelling. By observing 149 sites in Colorado, Reins and Volz (2013) found that the a four-year period had the highest frequency (see Figure 2.2), yet they reported that the heave in some buildings continued for more than 20 years, as shown in Figure 2.3.

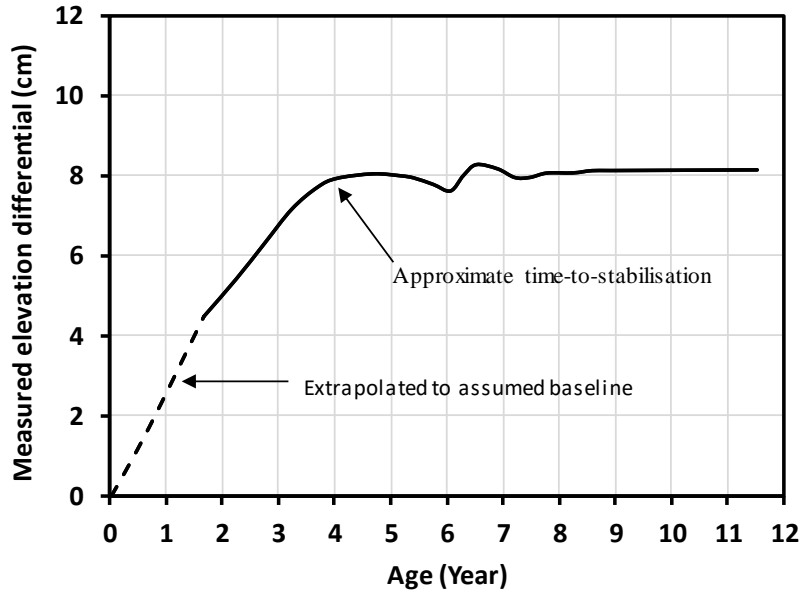


Figure 2.2: Typical foundation movement versus time (redrawn from Reins and Volz 2013).

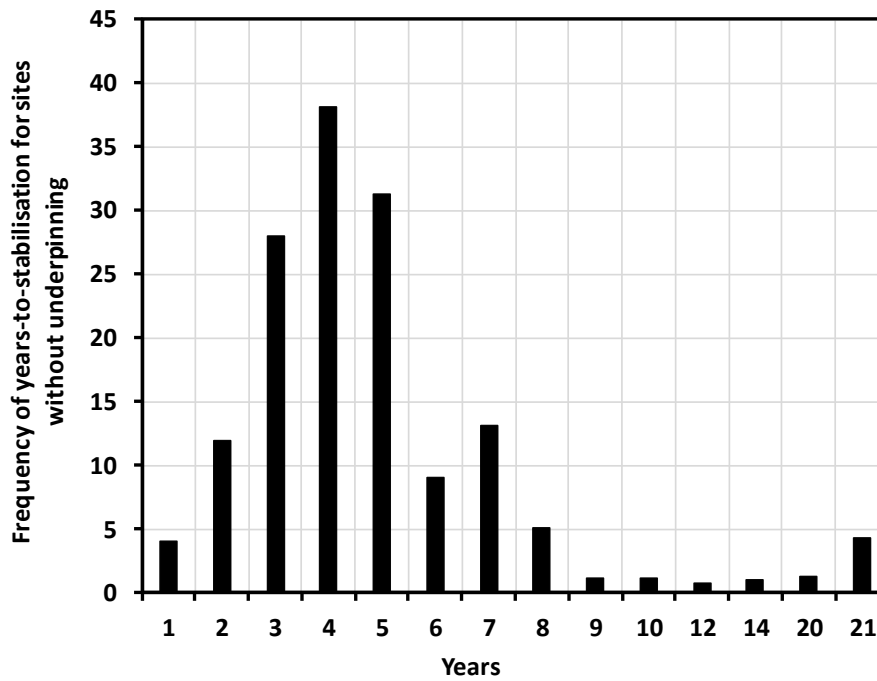


Figure 2.3: Histogram of time for stabilisation of 149 sites with no underpinning (redrawn from Reins and Volz 2013).

It should be noted that the depths of wetting for the two cases of covered and open surfaces are different. Based on the moisture content and movement records below footing slabs in

Maryland, Fityus et al. (2004) found that the design suction changes suggested by the Australian Standards AS2870 (1996) for open ground movement are not entirely appropriate for the wider Newcastle region. The results of that study suggested adopting a deeper active zone and a larger surface suction change for better estimation of the surface heave. Accordingly, in order to cover the worst heave scenario, it can be concluded that in estimating the characteristic surface heave, the fixed value H_s given by the Australian Standards AS2870 (2011) can be used successfully if the depth of the swelling soil layer does not exceed H_s or if the ground water table is encountered at a depth $\leq H_s$. However, this rule should be used with caution for slab foundations resting on expansive soils that extend below the H_s values recommended by the Australian Standards AS2870 (2011), as the actual suction depth may exceed it over time, causing differential mound movement beyond the design values, and leading to cracks and damages in the footings and supported structures.

2.2.2 Soil Surface Distortion

As explained next, the Building Research Advisory Board (BRAB) (1968) assumes the loss of soil support at the foundation edge and centre to approximate the following conditions: edge heave; centre heave; edge settlement; and centre settlement, as shown in Figure 2.4. In fact, in terms of differential settlement, the structural effect of the edge heave is comparable to that of the centre settlement. Correspondingly, the centre heave is similar to the edge settlement. However, the cause of each deformation pattern is different, and it is essential to study the factors conducive to each, as this helps to guide the designer to determine the likelihood of occurrence of each pattern.

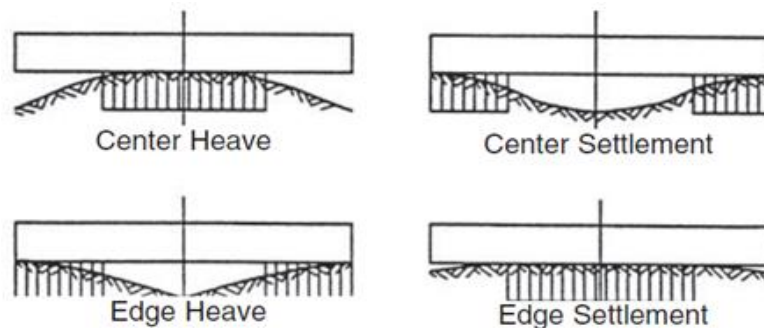


Figure 2.4: Conditions of foundation losing support due to soil heave (Building Research Advisory Borad 1968).

Edge heave is caused by the soil moisture increase around the edges, which can be initiated by many factors; yet, the most common factor is the rainfall in wet seasons. Other man-made factors, such as irrigation or pipe leakage, can have even more detrimental effects (Li 2006). Removal of trees can reduce the water transpiration from the soil, causing the moisture to increase, leading to an edge heave damage (Driscoll 1983). The edge heave due to rainfall is always associated with poor drainage of areas surrounding the footing slabs, causing the water to accumulate into ponds that represent a continuous source of water for the soil. However, as reported by Mitchell (1984), even with good drainage, the edge heave of footing slabs in rainy seasons can always be observed.

Centre heave of footing slabs has two main sources: thermo-osmosis and capillarity action. Thermo-osmosis is the moisture migration from the hot zone at the slab edges to the cooler area at the centre, especially in the hot seasons. A difference in temperature of 1 °C is equivalent to a pressure head of 1 metre (Chen 1988). The capillarity action, on the other hand, causes the moisture to move upwards and accumulates under the footing slab. Other man-made sources of centre heave are also important and can be even more damaging to structures, such as pipe leakage (Li et al. 2014).

The edge settlement of footing slabs can be theoretically caused by water evaporation in the hot dry seasons. However, evaporation from the soil surface slows down as the water available in the soil surface dries out. Hence, the actual drying rates from the soil by evaporation are significantly low (Blight 2004). As a result, the pores are progressively narrowed overtime, as the surface dries out, leading to a significant decrease in the permeability, hence, preventing the water outflow. Chen (1988) pointed out that there is little evidence of appreciable downward movements of foundations under covered areas in buildings due to shrinkage of swelling soils by evaporation; he also noted that shrinkage rarely causes any structural damage, thereby it can be deemed not to be critical. Moreover, Chen (1988) limited the reason for all structural damages to be due to the continuous increase of moisture content below footings. Fityus et al. (1999) compared the seasonal movement of some points at the edge of a flexible membrane and a point at the centre with other points on the uncovered area around the membrane. After 5 years of

observations, it was found that all points of open ground showed a seasonal rise-and-fall in levels, while the points within the covered area, even though on the edge, showed a continuous tendency to heave with no sign of settlement due to seasonal change. In this regard, it should be noted that the edge settlement was accused to be the cause of severe damages to many footings and superstructures based on several observations. However, these observations were always associated with the presence of trees in the vicinity of the footing slabs and the cause was always referred to the transpiration of tree roots (Biddle 1979; Cameron and O'Malley 2002; Goldfinch 1995; Holtz 1983; Jaksa et al. 2002; McInnes 1986; McManus and Brown 1999; Mitchell 1984; Richards et al. 1983). By sucking the water from the soil, especially in the hot dry seasons, tree roots can seriously reduce the moisture in the soil below the footing edges, resulting in settlements that may exceed 300 mm in the case of a row of trees (Crawford 1965). Among 31 case studies of foundation movements on reactive soils in Australia, Mitchell (1984) found that all edge settlement cases were due to the presence of trees. House insurance claims show that trees are repeatedly quoted as the main cause of foundation problems due to root penetration that causes soil drying and shrinking within the tree root zone (Clarke and Smethurst 2008). Some cases of edge settlement were caused by grass transpiration (Mitchell 1984). As mentioned by Blight (2005), the transpiration caused by grass and small bushes is comparable to that of trees.

Centre settlement is more likely to be a theoretical structural design case rather than a realistic one. This is because the soil is completely covered below the centre of the footing slab, thus is not exposed to any source of moisture reduction by evaporation or plant transpiration. On the other hand, no cases of centre settlement have been observed in the literature to be the cause of any footing damage.

It follows from the above discussion that, among the different design patterns of foundation movements on reactive soils, occurrence of both the edge heave and centre heave scenarios is inevitable. Conversely, the edge settlement scenario can be neglected, since its primary reason is the moisture reduction caused by the tree roots or grass transpiration. In such cases, the design standards recommend a definite safe distance

between the slab foundations and trees. As a rule of thumb, a safe distance equal to the expected mature height of the tree (Holland and Richards 1984). Satisfying this recommendation requires some knowledge and instructions for the property owners. Disallowing the edge settlement by the action of trees in the first place eliminates the need to consider the (inevitably) asymmetrical settlement of edges, which violates one of the fundamental assumptions of almost all existing design methods. The edge drop caused by transpiration of grass and small bushes can be avoided, by insulating about 3 metres around the slab foundations using PVC membrane or a concrete slab, then importing 200 mm of grass plantation over the insulated areas for an aesthetic perspective. The idea of surrounding the building with a concrete flatwork is a known treatment to avoid moisture reduction by plantation (Day 1992).

Based on the above review of the causes of moisture changes of reactive soils below slab foundations and the resulting soil mound shapes, the two common movement scenarios of the edge heave and centre heave must be considered in the design by practitioners. However, since numerical simulation of moisture migration due to thermos-osmosis is complicated, the case of the centre heave is simulated in this research as an edge drop due to evaporation. Therefore, the two main soil movement scenarios considered in this work are the edge lift induced by precipitation and the edge drop induced by evaporation. In the following section, most available traditional (empirical) design methods for the design of stiffened slab foundations on reactive soils are presented, followed by the most recent studies using numerical modelling techniques.

2.3 TRADITIONAL DESIGN METHODS OF SLAB FOUNDATIONS

2.3.1 Building Research Advisory Board (BRAB) Method

As indicated earlier, the BRAB (1968) method was developed based on field observations of the performance of residential reinforced concrete slab foundations in the US; the main assumptions of this method are as follows:

1. The total superstructure load is uniformly distributed over the entire slab area; and

2. After the supporting soil swells, the soil pressure is distributed evenly to the centre or at the ends of the slab foundation, as indicated in Figure 2.5. The value of the support index (C) is constant for all slab sizes. The support index (C) is the ratio of the supported area of the slab (i.e. contact area between the slab and underlying soil) to the area of the slab, depending on the climatic rating (C_w) and plasticity index (PI) of the soil. The relationships between C , C_w and PI are shown in Figure 2.6.

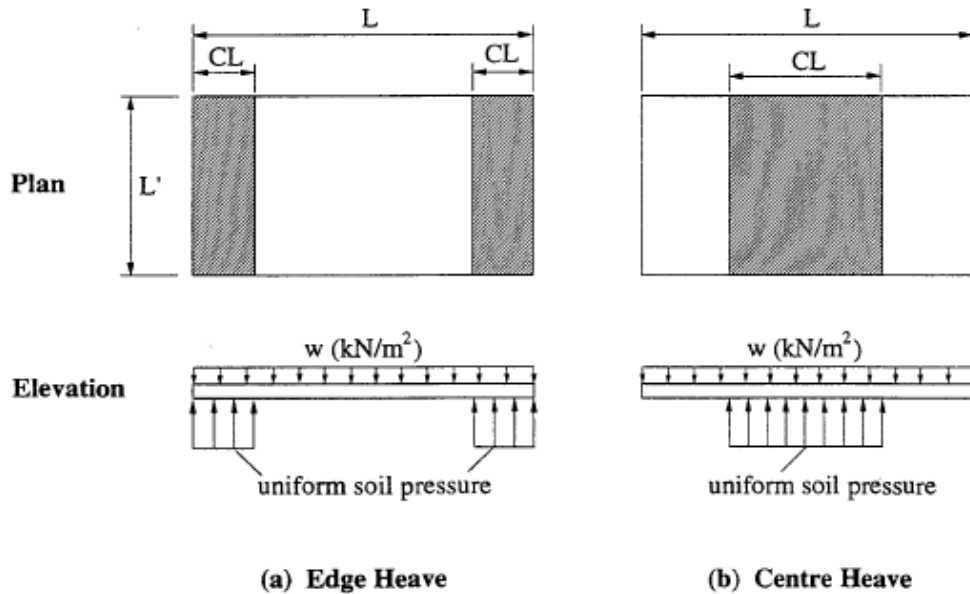


Figure 2.5: Support modes assumed by BRAB method (Building Research Advisory Borad 1968).

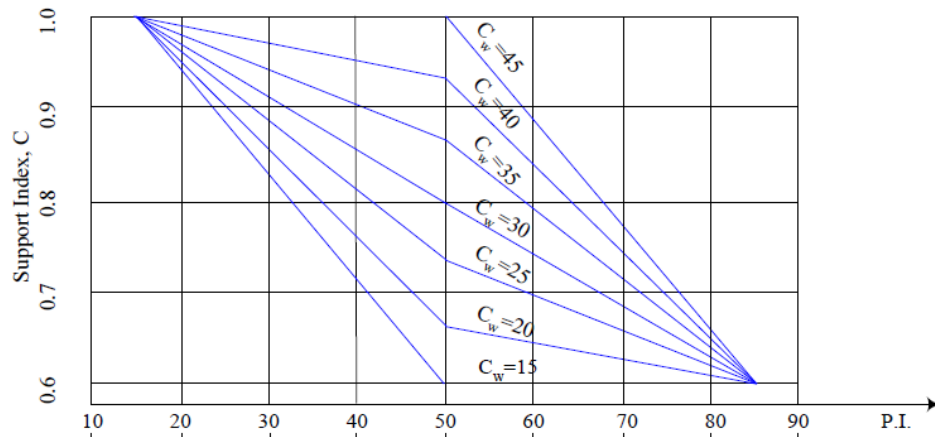


Figure 2.6: Determination of slab support index (C) by BRAB method (Building Research Advisory Borad 1968).

In the BRAB method, a slab foundation of irregular configuration is simplified into rectangular overlapping areas, each having a length (L) and a width (L') (when the design parameters in the short direction are determined, the terms L and L' are transposed). Each rectangle is analysed independently under the edge and centre heave scenarios. In the long direction, the design maximum bending moment (M_{\max}), maximum shear force (V_{\max}) and maximum differential deflection (Δ_{\max}) can be calculated as follows:

$$M_{\max} = \frac{wL^2L'}{8}(1-C) \quad (2.1)$$

$$V_{\max} = \frac{wLL'}{2}(1-C) \quad (2.2)$$

$$\Delta_{\max} = \frac{wL^4L'}{48EI}(1-C) \quad (2.3)$$

where;

C = support index, which varies from 0.6 to 1.0;

w = uniformly distributed load (pressure);

I = equivalent moment of inertia of the stiffened slab cross-section; and

E = modulus of elasticity of the slab concrete.

It should be noted that this method is based on the United States climate rating maps, and is thus not applicable elsewhere. The method of producing the curves in Figure 2.6 is not rational and depends mainly on engineering judgement. Moreover, both the soil and footing are assumed to be rigid with no soil structure interaction being considered. In addition, the assumption of a uniform pressure is not necessarily conservative in hogging distortion in the case of heavy perimeter wall loading (Lytton and Meyer 1971).

2.3.2 Lytton Method

In a major modification to the BRAB method, between 1970 and 1977, Lytton presented the first rational procedure for the design of slab foundations on expansive soils (Lytton

1970; 1970a; 1971; 1972; 1977; Lytton and Meyer 1971; Lytton and Woodburn 1973). Lytton and his co-workers solved the soil-footing interaction problem by simulating the problem as a beam on a curved mound; they implemented a coupled spring foundation model for the edge heave scenario and a Winkler foundation model for the centre heave scenario. The studies were carried out using the finite difference method in which a rigid beam on a Winkler foundation was considered to determine the one-dimensional maximum bending moment, shear forces and required stiffness of the strip footing system. The resulting one-dimensional forces were corrected for the two-dimensional action of the raft using empirical factors based on computer analysis. The differential equation used for the beam on the mound is as follows:

$$\frac{\partial^2}{\partial x^2} \left(EI \frac{\partial^2 w}{\partial x^2} \right) - \frac{\partial}{\partial x} \left[GhB \frac{\partial}{\partial x} (w - y) \right] + kB(w - y) = q \quad (2.4)$$

where;

- w = beam deflection;
- q = load per unit length;
- EI = beam flexural stiffness;
- Gh = coupled spring stiffness of foundation soil;
- k = Winkler spring stiffness;
- B = width of soil that contributes to supporting the beam; and
- x, y = co-ordinates defining the mound shape.

At the location where the beam loses its contact with the soil, the three terms (Gh), (k) and (B) turn into zero. A similar equation for the case of anisotropic elastic plate, which includes the effects of the soil shearing resistance on the same foundation type is given as follows:

$$D\nabla^4 w - \nabla \left[Gh\nabla (w - y) \right] + k(w - y) = p \quad (2.5)$$

where; D and p are the plate flexure rigidity and pressure acting on the plate, respectively. The equation of the soil mound can be obtained as follows:

$$y = Cx^m \quad (2.6)$$

where;

- y = vertical displacement;
- x = horizontal distance from the highest point;
- C = empirical constant; and
- m = mound exponent.

The soil mound exponent (m) is assumed to be the ratio of the footing length (L) to the depth of the soil active zone; it varies between 2 and 8 based on the best fitting curves of field observations of footing slabs that showed a flatter soil mound for a larger footing length. The soil mound equations thus produce convex and double convex shapes for the centre and edge heave scenarios, respectively, as shown in Figure 2.7.

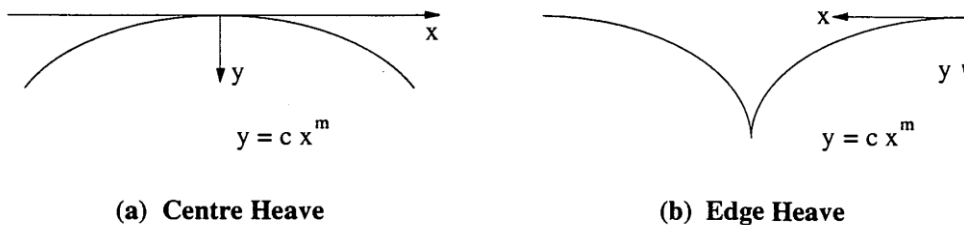


Figure 2.7: Soil mound shapes assumed by Lytton method (Li 1996).

Similar to the BRAB method, the Lytton method uses the concept of overlapped rectangles, to simplify the complex foundation configurations. The loads on the footing slab is assumed to be as follows: (i) an edge load (q_e) that accounts for the perimeter walls; (ii) a central line load (q_c) that accounts for the partitions and roof support; and (iii) a uniform distributed load (w_l) over the slab, consisting of the slab self-weight, finishes and live loads. The maximum bending moment is obtained in each direction using the following equations.

For the maximum positive moment in the case of edge heave:

$$M_{\max} = \frac{q_c LL'}{4} + \frac{L^2}{8} (2q_e + w_1 L') \quad (2.7)$$

For the maximum negative moment in the case of centre heave:

$$M_{\max} = \frac{q_c LL'}{2} + \frac{L^2}{8} (2q_e + q_c + w_1 L') \quad (2.8)$$

where; L and L' are the length and width of each rectangle, respectively. The obtained moments are then reduced to account for the soil compressibility, as follows:

$$M_1 = M_{\max} - C \frac{TL}{8} \quad (2.9)$$

where; T is the total load on the rectangle, L is the length in the direction under consideration and C is the support index obtained from:

$$C = \frac{m+1}{m+2} \left[\frac{m+1}{m} \cdot \frac{T}{A} \cdot \frac{1}{kym} \right]^{\frac{1}{(m+1)}} \quad (2.10)$$

where;

m = mound exponent;

A = total rectangle area;

k = Winkler spring stiffness; and

y_m = maximum differential movement of the supporting soil.

The Lytton method was used successfully in Australia for the design of many slab footings on highly expansive soils. However, the equation defining the mound shape exponent (m) is entirely empirical. In addition, the assumption of a rigid, uncracked foundation is unrealistic and usually leads to a very conservative design, since it produces higher

bending moments compared to the values produced in reality. Furthermore, as mentioned by Li (1996) the method can become conservative when the permissible footing deflection approaches the soil differential movement.

2.3.3 Walsh Method

Over a decade, Walsh (1974; 1978; 1978a; 1984) improved the rigid beam model of Lytton by analysing a flexible beam on a coupled Winkler foundation using the finite element analysis; he eventually developed a design method suitable for strip and raft footings. Walsh method uses the two extreme mound shapes of the edge heave and centre heave; both heave scenarios consist of a central flat section with parabolic edges (Figure 2.8). The method adopts the assumption of dividing the footing into overlapped rectangles and solving each rectangle separately.

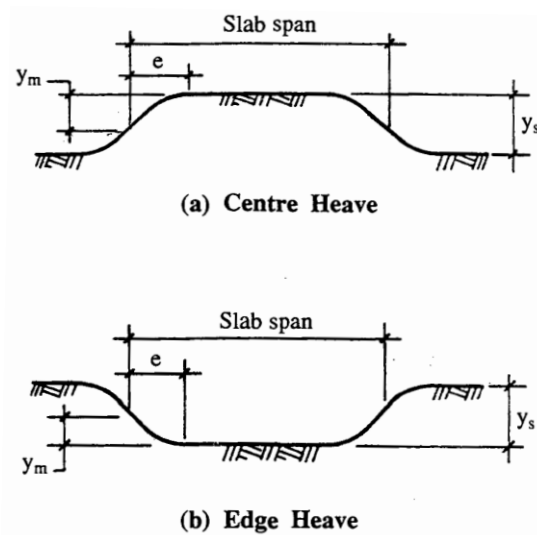


Figure 2.8: Soil mound shapes by Walsh method (Walsh 1974).

According to Walsh method, the mound shapes are defined using two parameters: the footing differential movement (y_m); and the edge distance (e_d). The footing differential movement is expressed empirically in terms of the characteristic surface heave (y_s), based on the work of Holland (1981), as follows:

$$y_m = 0.7 y_s \quad (\text{for the centre heave}) \quad (2.11)$$

$$y_m = 0.5y_s \quad (\text{for the edge heave}) \quad (2.12)$$

The edge distance (e_d) is estimated as follows:

$$e_d = \left(0.5 + \frac{y_m}{36} \right) \quad (\text{for the centre heave}) \quad (2.13)$$

$$e_d = 0.2L \leq \left(0.6 + \frac{y_m}{25} \right) \quad (\text{for the edge heave}) \quad (2.14)$$

where; L is the span in meters and y_m is in millimetres. For design purposes, the slab is divided into overlapping rectangles, then the rectangles are further idealised as single beams. These beams are solved in each direction separately as beams on coupled Winkler foundations using the following equation:

$$EI \frac{\partial^4 y}{\partial x^4} + Kw_b^2 \frac{\partial^2 (y - y_o)}{\partial x^2} + K(y - y_o) = q \quad (2.15)$$

where;

EI = beam stiffness per unit width;

q = loading per unit area;

K = footing stiffness; and

w_b = co-operating width.

When the beam loses its contact with the supporting soil, the above equation becomes:

$$EI \frac{\partial^4 y}{\partial x^4} = q \quad (2.16)$$

The method proposes that the analysis is carried out in two phases: first by using a soft mound until one-eighth of the soil free swell remains; subsequently, the rest of the swell can be simulated as a hard mound. However, Walsh et al. (1986) developed a computer design package called CORD (Code Oriented Raft Design) in which a single value for the soil spring stiffness (k) was adopted. The value of (k) was proposed to be 100 times the average loading, but should not be less than 1000 kPa/m. In order to account for the effect of cracking on the required stiffness, the beam stiffness was calculated based on Branson's formula (1963), as follows:

$$I_e = I_{cr} + \left(\frac{M_{cr}}{M} \right)^3 (I_g - I_{cr}) \quad (2.17)$$

where;

M = maximum moment in the beam

M_{cr} = cracking moment of the beam section;

I_{cr} = transformed moment of inertia of the cracked section

I_e = effective moment of inertia; and

I_g = gross moment of inertia.

The Walsh method was adopted by the Australian Standards AS2870 since 1990. However, similar to all previous methods, this method simplifies the 3D distorted slab foundation problem into a simplified 2D one. In addition, the coupled spring model adopted in this method does not reflect the nature of the soil structure interaction process (Li 1996).

2.3.4 Mitchell Method

Mitchell (1980) developed a design method for stiffened slab foundations on expansive soils based on the finite difference analysis of a beam on an uncoupled Winkler spring foundation using constant spring stiffness. The method was incorporated into a computer program called Slab-on-Grade (SLOG) (Mitchell 1980). The beam in this method is

analysed on a pre-formed mound, having a concave shape for the edge heave and a convex shape for the centre heave, as shown in Figure 2.9. In this method, the maximum surface heave and the associated soil mound are estimated more accurately based on the analytical solution of the steady- state soil suction diffusion. The assumed mound shape equation is similar to that proposed by Lytton, as follows:

$$y = \left(\frac{2X}{L} \right)^{1.5L/a} Y \quad (2.18)$$

where;

- Y = maximum differential heave;
- L = Length of beam under consideration; and
- a = depth of soil suction change.

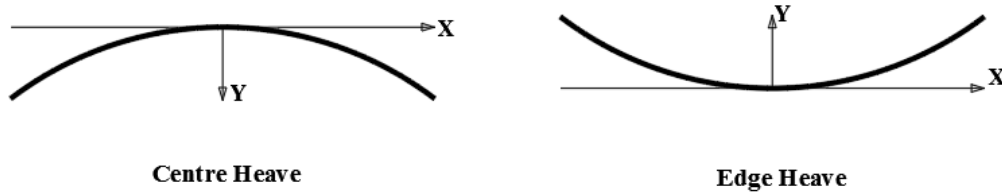


Figure 2.9: Soil mound shapes by Mitchell method (Mitchell 1984).

In the computer program SLOG, a non-linear swell-pressure relationship is proposed, by defining the slope (k) of the pressure versus the soil swell curve, as follows:

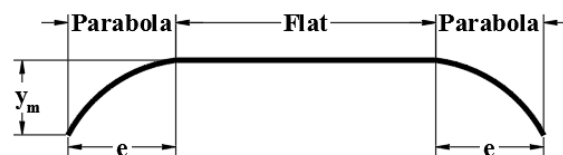
$$k = A y^x \delta^t \quad (2.19)$$

where; A , x and t are soil constants. Mitchell (1990) suggested that a constant value of (k) = 1000 kPa/m could be used for routine design practice. Branson's formula (1963) was first used in order to relate the inertia of the beam to the bending moment. In a latter development, the beam curvature was related to the moment through a multilinear curve.

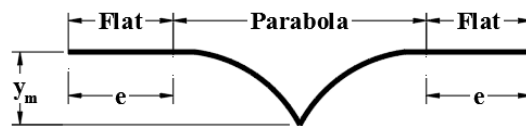
Mitchell method is recommended in the Australian Standards AS2870 (2011) for residential slabs and footings. However, the method has similar limitations to those of previous methods in terms of simplifying the actual 3D problem into a simple 2D one. In addition, the use of the simple Winkler spring model is less rigorous than the coupled (connected) spring model. The method also uses a pre-formed soil mound neglecting the load path and the effects of loading and suction changes on the soil stiffness.

2.3.5 Swinburne Method

In the Swinburne Institute of Technology method, Holland et al. (1980) and Pitt (1982) modified the FOCALS program, originally developed by Fraser and Wardle (1975), in order to generate design charts for routine design of house footings on expansive clays. The method calculates the moments, deflections and slab thickness for assumed values of maximum differential heave (y_m), edge distance (e_d), concrete strength and number and width of the underlying cross-beams. The method also uses the concept of overlapped rectangles. The design soil mound shape adopted in this method has a flat top with parabolic convex edges over an edge distance (e_d) for the centre heave (see Figure 2.10a), while it has flat edges over the edge distance (e_d) which turn into a convex parabola at the centre for the edge heave (see Figure 2.10b).



(a) Centre Heave



(b) Edge Heave

Figure 2.10: Soil mound shapes assumed by Swinburne method (Holland et al. 1980).

The proposed mound shapes in the Swinburne method provide much better support to the footing slab under the edge heave condition than for the centre heave. Therefore, the centre

heave is predominant in this method. However, this shape is not consistent with field observations made for covered shapes (Jackson 1980). Figure 2.11 shows a typical example of the developed design charts depicting the centre heave bending moment in the Swinburne method.

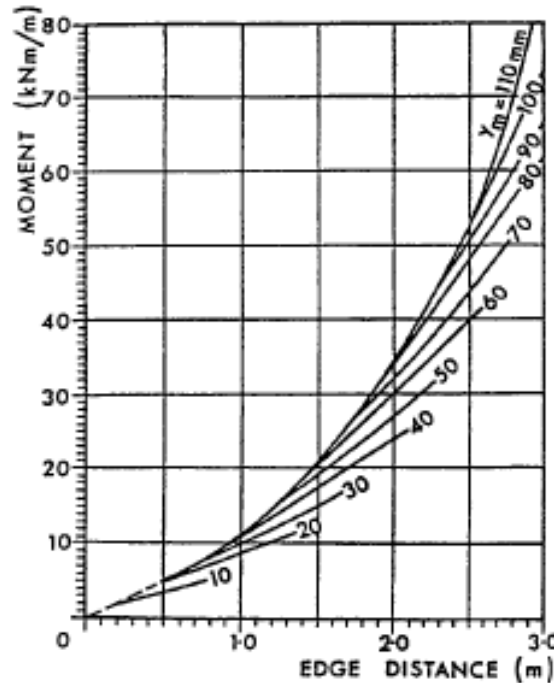


Figure 2.11: Centre heave bending moments by Swinburne method (Pitt 1982).

Holland et al. (1980) proposed a relationship between the edge distance (e_d) and magnitude of the mound heave (y_m) based on experiments performed on covered cases, as summarised in Table 2.1. However, as mentioned by Mitchell (1984), the proposed relationship is very approximate. Another important limitation of the Swinburne method is that the design charts were developed for a single storey brick veneer loading, despite the authors' claims that the method can also be used for two-storey brick veneer loading. This assumption was criticised by Wray (1980) and Mitchell (1984), and even rejected by Pidgeon (1983) who stated that this assumption is unsound and could lead to under-designing of stiffened slabs. Moreover, the method uses a unique value for the soil modulus while it is actually suction dependant. The Swinburne method presumes that the centre heave controls the design, based on a proposed edge heave mound shape that is not consistent with field observations (Jackson 1980). In fact, the proposed edge heave

mound shape provides a large soil support to the footing slab, resulting in reduced internal forces.

Table 2.1: Relative values of e and y_m in the Swinburne method (after Pitt 1982)

Edge distance, e_d (m)	Differential movement, y_m (mm)
0.0 to 0.5	0 to 20
0.5 to 1.0	10 to 40
1.0 to 1.5	20 to 60
1.5 to 2.0	30 to 80
2.0 to 2.5	40 to 100
2.5 to 3.0	60 to 120

2.3.6 Post Tensioning Institute (PTI) Method

Through a three dimensional finite element analysis of a slab resting on a heaving elastic soil, Wray (1978) developed design equations for raft footings, which were later manipulated to develop the Post Tensioning Institute (PTI) method (1996) in which the moment, shear and required stiffness of the raft can be calculated for the edge and centre heave scenarios. The soil mound shapes, as shown in Figure 2.12, were determined by a computer simulation for the moisture propagation beneath the slab edges. The mound shape is defined in terms of the edge distance (e_d) over which the moisture is propagated and the movement occurs; a prior knowledge for the value of (e) is required.

The edge distance (e_d) is empirically related to the climate pattern only as measured by the Thornthwaite Moisture Index (TMI). Therefore, the modified PTI (2004) method was introduced in which the edge distance (e_d) was adjusted by introducing the soil fabric factor which depends on the soil profile content of the roots, soil layers and fractures or joints. This method has the same disadvantage of other previous methods in terms of uncoupling the problem using a pre-defined soil mound and simplified 2D analysis.

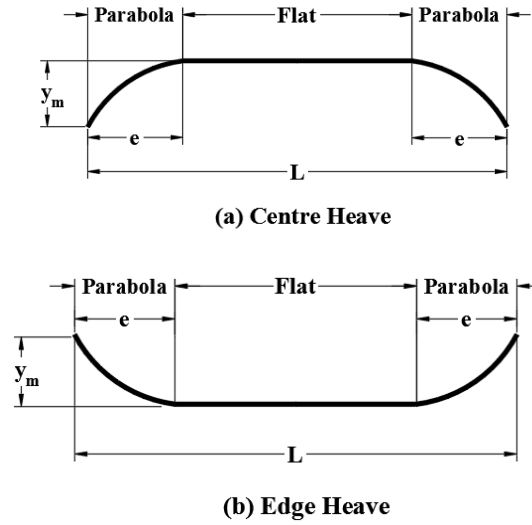


Figure 2.12: Soil mound shapes assumed by the Post Tensioning Institute (1980).

Similar to the previously presented methods, this method uses the concept of overlapping rectangles for irregular slab shapes. In the case of centre heave, the moment in the long direction (M_{lc}) and short direction (M_{sc}) for $e > 1.5$ m, mound movement (Y) and differential deflection (Δ), with an edge load (P), sub-beam spacing (S), and depth (d), can be calculated as follows:

$$M_{lc} = A \left[B(e)^{1.238} + C \right] \quad (2.20)$$

where;

$$A = \frac{1}{727} \left[(L)^{0.013} (S)^{0.306} (d)^{0.688} (P)^{0.534} (Y)^{0.193} \right] \quad (2.21)$$

$$B = (Y - 1)/3 \quad (2.22)$$

$$C = \left(8 - \frac{P - 613}{255} \right) \left(\frac{4 - Y}{3} \right) \quad (2.23)$$

$$M_{sc} = \left(\frac{58 + e}{60} \right) M_{lc} \quad (2.24)$$

$$\Delta = \frac{(YL)^{0.205} (S)^{1.059} (P)^{0.523} (e)^{1.296}}{380(d)^{1.214}} \quad (2.25)$$

For the edge heave, the bending moment in the long direction (M_{le}), short direction (M_{se}) and deflection (Δ) can be calculated as follows:

$$M_{le} = \frac{(s)^{0.10} (ed)^{0.78} (Y)^{0.66}}{7.2(L)^{0.0065} (P)^{0.04}} \quad (2.26)$$

$$M_{se} = (d)^{0.35} \left(\frac{19 + e}{57.75} \right) M_{le} \quad (2.27)$$

$$\Delta = \frac{(L)^{0.35} (S)^{0.88} (e)^{0.74} (Y)^{0.76}}{15.9(d)^{0.85} (P)^{0.01}} \quad (2.28)$$

2.3.7 Wire Reinforcement Institute (WRI) Method

The Wire Reinforcement Institute (WRI) method (1996) can be considered as a modified version of the BRAB method. It is empirically derived by developing and modifying the design equations to best match field observations. The method uses the same climate rating index (C_w) and support index (C) of the BRAB method. The cantilever length (l_c) is obtained from Figure 2.13, which is then modified for the long- and short-directions (L and L') using the modification factor (k) shown in Figure 2.14. The beam spacing (S) is obtained from Figure 2.15. By determining the cantilever length (l_c) in each direction and knowing the applied loads, the bending moments and shear forces are calculated analytically and the associated required beam depth and reinforcement determined. The WRI method has the same main limitations of the BRAB method, being applicable only in the US, for which the climate rating index map was generated.

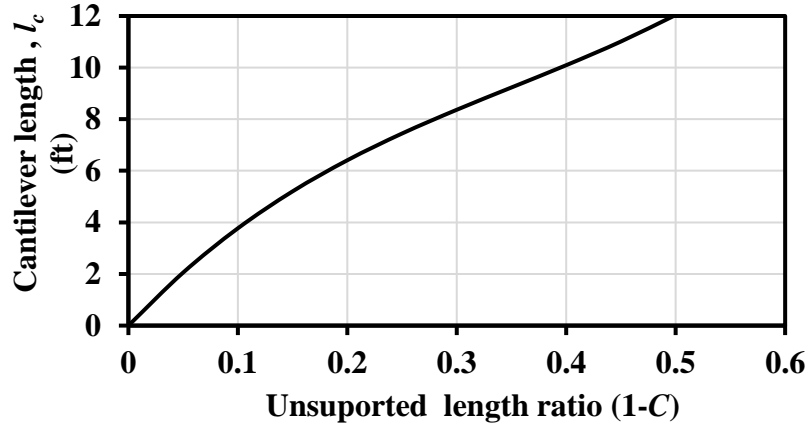


Figure 2.13: Determination of the cantilever length by WRI method (redrawn from Wire Reinforcement Institute 1981).

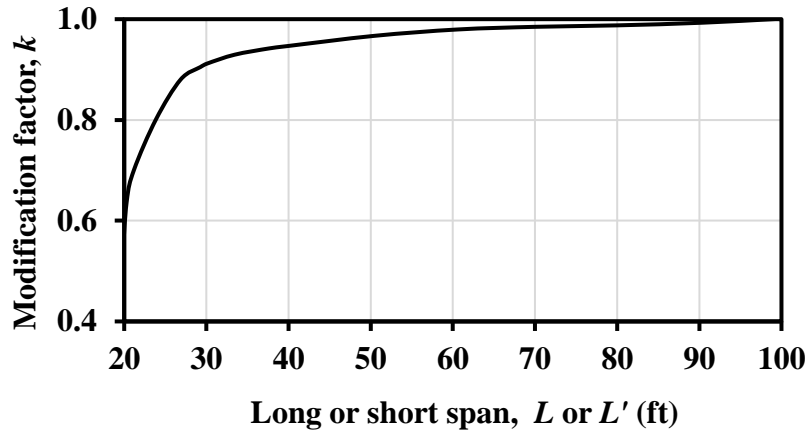


Figure 2.14: Slab length modification factor by WRI method (redrawn from Wire Reinforcement Institute 1981).

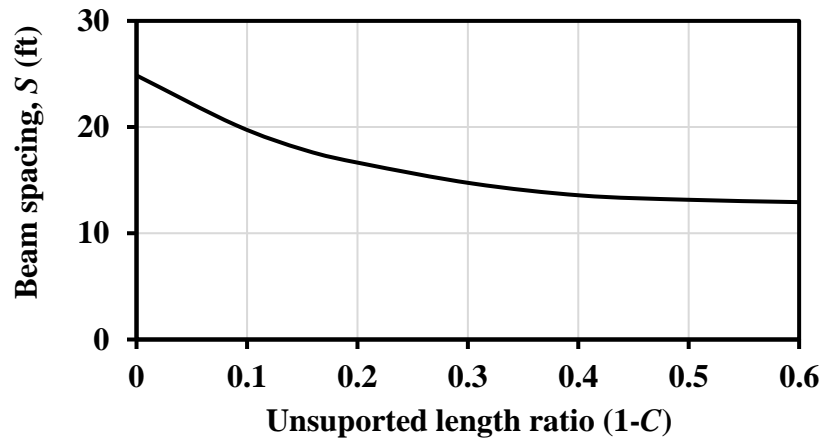


Figure 2.15: Determination of beam spacing by WRI method (redrawn from Wire Reinforcement Institute 1981).

2.3.8 Australian Standards Method

Australian Standards AS2870 (2011) recommend the use of one of the two following design pathways: (i) deemed-to-comply design method; and (ii) design by engineering principles using either Walsh method or Mitchell method.

In the deemed-to-comply design method, the Australian Standards provide typical design tables to be readily used by practitioners without the need to carry out any calculations, as follows. First, the soil characteristic surface (free) heave (y_s) is calculated by integrating the soil movement of all soil layers from layer 1 to layer N within the depth at which a significant change of soil suction occurs. Thus, the characteristic surface heave can be calculated, as follows:

$$y_s = \frac{1}{100} \sum_{n=1}^N (I_{pt} \cdot \overline{\Delta u} h)_n \quad (2.29)$$

where:

y_s = characteristic surface movement (in millimetres);

I_{pt} = instability index (in % pF);

$\overline{\Delta u}$ = soil suction change averaged over the thickness of the layer (pF);

h = thickness of layer under consideration (in millimetres); and

N = number of soil layers within the design depth of the suction change (H_s).

The depth of suction change in this context is the depth of the soil at which no significant change in suction occurs by seasonal conditions. The Australian Standards provide values for the depth of suction change and expected surface suction change for different locations across Australia, as shown in Table 2.2. By estimating the characteristic surface heave (y_s), the soil class can be specified according to Table 2.3. Knowing the site class and slab dimensions, the beam depth, reinforcements, beam spacing and slab mesh can be obtained from typical design tables provided by the Australia Standards, depending on the type of construction of the superstructure and associated allowable differential movement, as

shown in Table 2.4. The deemed-to-comply design tables are provided for rafts, strip footings, waffle slabs and stiffened slabs. Typical example of the deemed-to-comply design cases are shown in Table 2.5 and Figure 2.16. Although the deemed-to-comply method is easy to use, the Australian Standards restrict its applicability to the following cases:

- (i) class *E* sites;
- (ii) buildings longer than 30 m;
- (iii) slabs containing permanent joints (e.g. contraction or control joints);
- (iv) buildings incorporating wing walls or masonry arches unless specially detailed;
- (v) construction of three or more storeys;
- (vi) single leaf-earth or stone masonry walls greater than 3 m in height; and
- (vii) construction using concrete strength ≥ 32 MPa.

**Table 2.2: Profile of soil suction change for certain locations in Australia
(Australian Standard AS2870 2011).**

Location	Ratio of change in soil suction, Δu (pF)	Depth of design soil suction change, H_s (m)
Adelaide	1.2	4.0
Albury/Wodonga	1.2	3.0
Brisbane/ Ipswich	1.2	1.5-2.3 *
Gosford	1.2	1.5-1.8 *
Hobart	1.2	2.3-3.0 *
Hunter Valley	1.2	1.8-3.0 *
Launceston	1.2	2.3-3.0 *
Melbourne	1.2	1.8-2.3 *
Newcastle	1.2	1.5-1.8 *
Perth	1.2	1.8
Sydney	1.2	1.5-1.8 *
Toowoomba	1.2	1.8-2.3 *

*Note: The variation in H_s depends largely on the climate changes.

**Table 2.3: Site classification by the characteristic surface movement
(Australian Standard AS2870 2011).**

Characteristic surface movement, y_s (mm)	Site class	Site classification
$0 < y_s < 20$	S	Slightly reactive clay sites, which may experience only slight ground movement from moisture changes
$20 < y_s < 40$	M	Moderately reactive clay or silt site, which may experience moderate ground movement from moisture changes
$40 < y_s < 60$	H1	Highly reactive clay sites, which may experience high ground movement from moisture changes
$60 < y_s < 75$	H2	Highly reactive clay sites, which may experience very high ground movement from moisture changes
$y_s > 75$	E	Extremely reactive sites, which may experience extremely ground movement from moisture changes

Table 2.4: Maximum design differential footing deflection for design of footings and rafts by Australian Standards AS 2870 (2011).

Type of construction	Maximum differential deflection, as a function of the span (mm)	Maximum differential deflection (mm)
Clad frame	$L/300$	40
Articulated masonry veneer	$L/400$	30
Masonry veneer	$L/600$	20
Articulated full masonry	$L/800$	15
Full masonry	$L/1000$	10

Table 2.5: Deemed-to-comply design for stiffened slab foundations by Australian Standards AS2870 (2011).

Site class	Type of construction	Edge and internal beams				
		Depth (D) mm	Bottom reinforcement		Top bar reinforcement	Max beam spacing cc m
			Mesh	Bar alternative		
Class A	Clad frame	300	3-L8TM	2N12	—	—
	Articulated masonry veneer	300	3-L8TM	2N12	—	—
	Masonry veneer	300	3-L8TM	2N12	—	—
	Articulated full masonry	400	3-L8TM	2N12	—	—
	Full masonry	500	3-L8TM	2N12	—	—
Class S	Clad frame	300	3-L8TM	2N12	—	—
	Articulated masonry veneer	300	3-L8TM	2N12	—	—
	Masonry veneer	300	3-L11TM	3N12	—	—
	Articulated full masonry	500	3-L11TM	3N12	2N12	—
	Full masonry	700	2x3-L11TM	3N16	2N16	5
Class M	Clad frame	300	3-L11TM	3N12	—	6
	Articulated masonry veneer	400	3-L11TM	3N12	—	6
	Masonry veneer	400	3-L11TM	3N12	—	5
	Articulated full masonry	625	3-L11TM	3N12	2N12	4
	Full masonry	950	2x3-L11TM	3N16	2N16	4
Class M-D	Clad frame	400	3-L11TM	3N12	—	5
	Articulated masonry veneer	400	3-L11TM	3N12	1N12	4
	Masonry veneer	500	3-L12TM	3N12	2N12	4
	Articulated full masonry	650	3-L12TM	2N16	2N16	4
	Full masonry	1050	2x3-L11TM	3N16	3N16	4
Class H1	Clad frame	400	3-L11TM	3N12	—	5
	Articulated masonry veneer	400	3-L11TM	3N12	1N12	4
	Masonry veneer	500	3-L11TM	3N12	3N12	4
	Articulated full masonry	750	2x3-L11TM	3N16	2N16	4
	Full masonry	1050	2x3-L12TM	3N16	3N16	4
Class H1-D	Clad frame	400	3-L11TM	3N12	1N12	4
	Articulated masonry veneer	500	3-L11TM	3N12	2N12	4
	Masonry veneer	650	2x3-L11TM	3N16	1N16	4
	Articulated full masonry	800	2x3-L11TM	3N16	2N16	4
	Full masonry	1100	2x3-L12TM	3N16	3N16	4
Class H2	Clad frame	550	3-L11TM	3N12	2N12	4
	Articulated masonry veneer	600	3-L12TM	3N12	2N12	4
	Masonry veneer	750	2x3-L11TM	3N16	2N16	4
	Articulated full masonry	1000	2x3-L11TM	3N16	2N16	4
	Full masonry	—	—	—	—	—
Class H2-D	Clad frame	550	2x3-L11TM	3N16	2N16	4
	Articulated masonry veneer	700	2x3-L11TM	3N16	2N16	4
	Masonry veneer	750	2x3-L11TM	3N16	2N16	4
	Articulated full masonry	1000	2x3-L11TM	3N16	2N16	4
	Full masonry	—	—	—	—	—

NOTE: Slab reinforcement for all site classes shall be as follows:

(a) SL72, where slab length <18 m

(b) SL82, where slab length 18 to 25 m

(c) SL92, where slab length >25 and <30 m

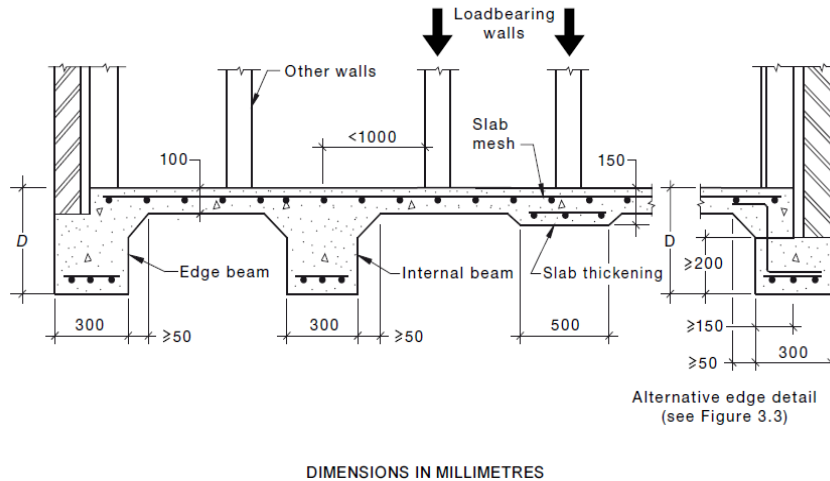


Figure 2.16: Stiffened raft design for site classes A, S, M, M-D, H1, H2, H1-D, H2-D by Australian Standards AS2870 (2011).

The Australian Standards AS2870 (2011) did not clarify the reason behind all of the abovementioned restrictions imposed on the deemed-to-comply method; however, it may be attributed to the boundaries assumed in producing the design tables. In fact, when using the deemed-to-comply method, the designers are confronted with an issue of professional responsibility and legal liability, since no design calculations are carried out and the designer is required to just lookup the provided design tables. Moreover, the method does not adequately consider the effect of the superstructure size and dead load values. For instance, the method gives identical design configurations for a “4 m × 3 m” garden shed or a “24 m × 15 m” double storey house (Frank 2000), when designed for the same soil class and construction type, which is quite alarming. In fact, practitioners should be aware that this method might lead to a non-conservative design in some cases, particularly for heavily loaded stiffened slabs used for double storey structures.

2.3.9 Design Comparison among Traditional Design Methods

Mitchell (1984) compared the design outputs obtained from Walsh, Mitchell, Lytton, Swinburne and PTI methods for a single storey brick veneer house (10 m²), having a slab foundation stiffened with a grillage of sub beams 3.3 m apart. The design parameters were the same for all methods. Comparison of the design output showed that, for the centre

heave case, the Swinburne, PTI and Mitchel methods gave very close bending mode at the lower level of the heave, while for the higher heave values the results showed considerable scatter. The variation was much greater for the edge heave case. Mitchell (1984) indicated that the difference in the results is attributed to the difference in the initial mound shape and assumed load distribution.

Abdelmalak (2007) compared the beam depth calculated by the three methods: WRI, PTI (as the most common methods used in the US) and AS 2870 method (as the most common method used in Australia). A number of 27 cases were designed, comprising three simple rectangular stiffened slabs built on three different shrink-swell soils and loaded with uniform pressure and perimeter line load and subjected to three different weather patterns. Among the 27 cases, only one case gave identical beam depth using the three selected design methods. The WRI and PTI methods produced the closest results while the PTI and AS2870 showed the poorest correlation. Abdelmalak (2007) highlighted that the large scatter in the design outputs raises the need for more observations and comparisons with field data.

In light of the above comparisons, it is obvious that there is a need for more reliable design methods that can overcome the limitations of existing methods. One way of achieving this is by tackling the intrinsic assumptions of the existing methods, using complex numerical analysis. Some of the major efforts spent for solving the problem of slab foundations on expansive soils using numerical modelling are presented and discussed below.

2.4 DESIGN OF SLAB FOUNDATIONS USING NUMERICAL MODELLING

As indicated in the previous section, although existing traditional design methods of stiffened slab foundations on expansive soils showed some degree of success, the magnitude of damage is still alarming. Therefore, during the last few decades, many attempts have been made to enhance existing methods by implementing the numerical modelling techniques. For example, Fraser and Wardle (1975) carried out a three dimensional (3D) finite element (FE) analysis for stiffened rafts on a semi-infinite elastic soil, using a program called FOCALS. The worst and only loading condition was assumed

to be the centre heave. The footing was analysed iteratively on a pre-formed soil mound based on Walsh method, in order to define the areas where the soil loses contact with the footing. The approach produced smaller sections than any of the previously described methods. However, the method of analysis had the same problem of the traditional methods in terms of the uncertainty associated with the proposed soil mounds; moreover, the method was not developed into a general raft design procedure.

Poulos (1983) used the mound shapes proposed by the Lytton method in the analysis and design of strip footings and beams using the finite element method. Through his investigation, it was found that the use of a lower value of the mound exponent (m) results in large bending moments and a more conservative design. The mound exponent was considered to be 2, producing a parabolic mound shape. The soil was modelled as an isotropic homogeneous elastic half-space with a soil modulus (E) that was considered to vary along the length of the strip footing. Both concentrated and distributed loads were considered in the analysis. The method was developed to be used only for analysis of strip footings and was not deemed suitable as a general design procedure for rafts.

Sinha and Poulos (1996) carried out a study using a 3D FE technique addressing the importance of the stiffening beams on slab foundations. Again, the soil mound equations proposed by Lytton method were adopted in the analysis with a mound shape exponent (m) equal 2, resulting in a conservative parabolic soil mound in all directions, as shown in Figure 2.17. The analysis was carried out for different values of surface movement under edge drop and edge lift scenarios considering the twisting effect from the 3D analysis for a stiffened and unstiffened 10 m \times 10 m slab, as shown in Figure 2.18. The effect of separation between the soil and raft, and the local yielding of the soil underneath the raft were included in the analysis. The relative raft stiffness was calculated as follows:

$$K_R = \frac{4E_R t_R^3 B_R (1 - \nu_s^2)}{3\pi E_s L_R^4} \quad (2.30)$$

where;

E_R and E_s = concrete and soil moduli, respectively;

t_R = raft thickness;

L_R and B_R = raft length and width, respectively; and

ν_s = Poisson's ratio of the soil.

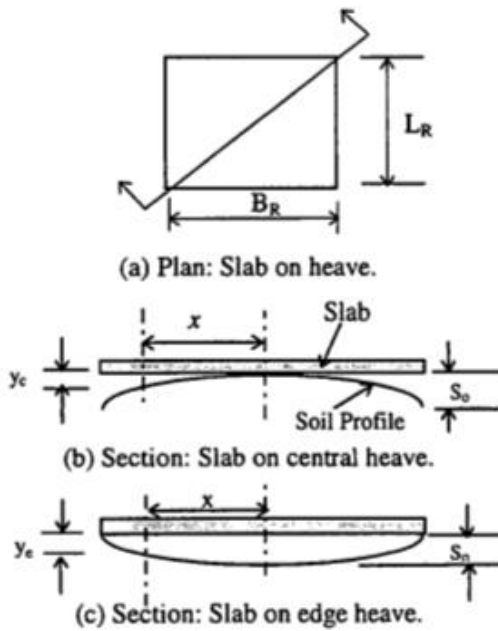


Figure 2.17: Soil modelling of heave formation by Sinha and Poulos (1996).

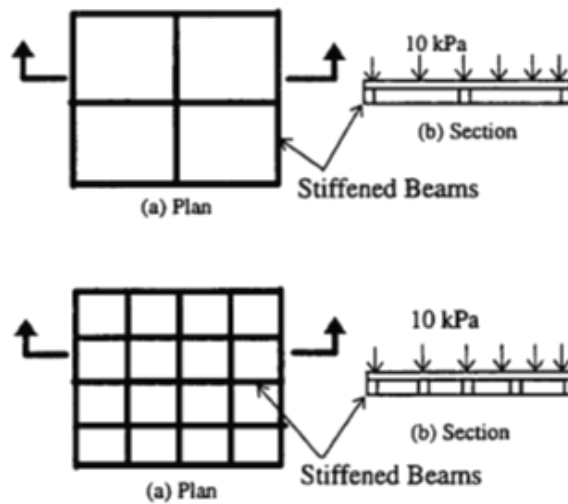


Figure 2.18: Stiffened and unstiffened slab configurations by Sinha & Poulos (1996).

Figure 2.19 presents a typical example of the output charts derived from the study. It is obvious that the increase in the beam depth causes a reduction in the differential settlement and an increase in the maximum moment. The notations used in the curves shown in Figure 2.19 are as follows:

Δ_{st} = differential settlement between the centre and corner of the stiffened raft;

Δ_s = differential settlement of the unstiffened raft;

M_s = maximum moment of the unstiffened raft;

M_{st} = maximum moment of the stiffened raft;

T_b = stiffened beam thickness; and

T_s = raft slab thickness.

In general, the study did not develop a generalised design method but rather focused on the benefits of stiffening the raft and emphasised its settlement restrictive features.

Li (1996) adopted a thermo-mechanical analogy for the moisture diffusion and soil shrink-swell movement. This was based on the fact that the diffusion equation is identical to the general governing equation in the heat transfer analysis, and the transient diffusion of the soil suction was numerically solved in both 2D and 3D set-up analyses. The behaviour of the expansive soil was modelled as a function of both the soil suction and structural loads. The non-linear behaviour of the reinforced concrete was also taken into account. The change in suction over time and depth considered in the analysis were calculated through the thermal diffusion model and were found to compare well with Mitchell's (1980) analytical diffusion equation. The results showed that the instability index, lateral swell pressure, skin friction and edge beam depth had noticeable effects on the slab performance, while the influence of the elastic modulus of concrete and elastic modulus and Poisson's ratio of the soil were relatively small and could be ignored. Li (1996) also found that the perimeter load had a larger influence on the footing behaviour than the uniformly distributed load and highlighted that the current two-dimensional design methods are inadequate for the U shape slab geometry. The study did not provide general design charts or tables, yet it introduced the coupled thermo-mechanical analogy as an

acceptable and relatively accurate methodology that can be utilised to simulate coupled 2D and 3D seepage and stress analyses, with consideration of many factors affecting the performance of the slab foundations on expansive soils, such as the skin friction along the beam sides as induced by the lateral swelling.

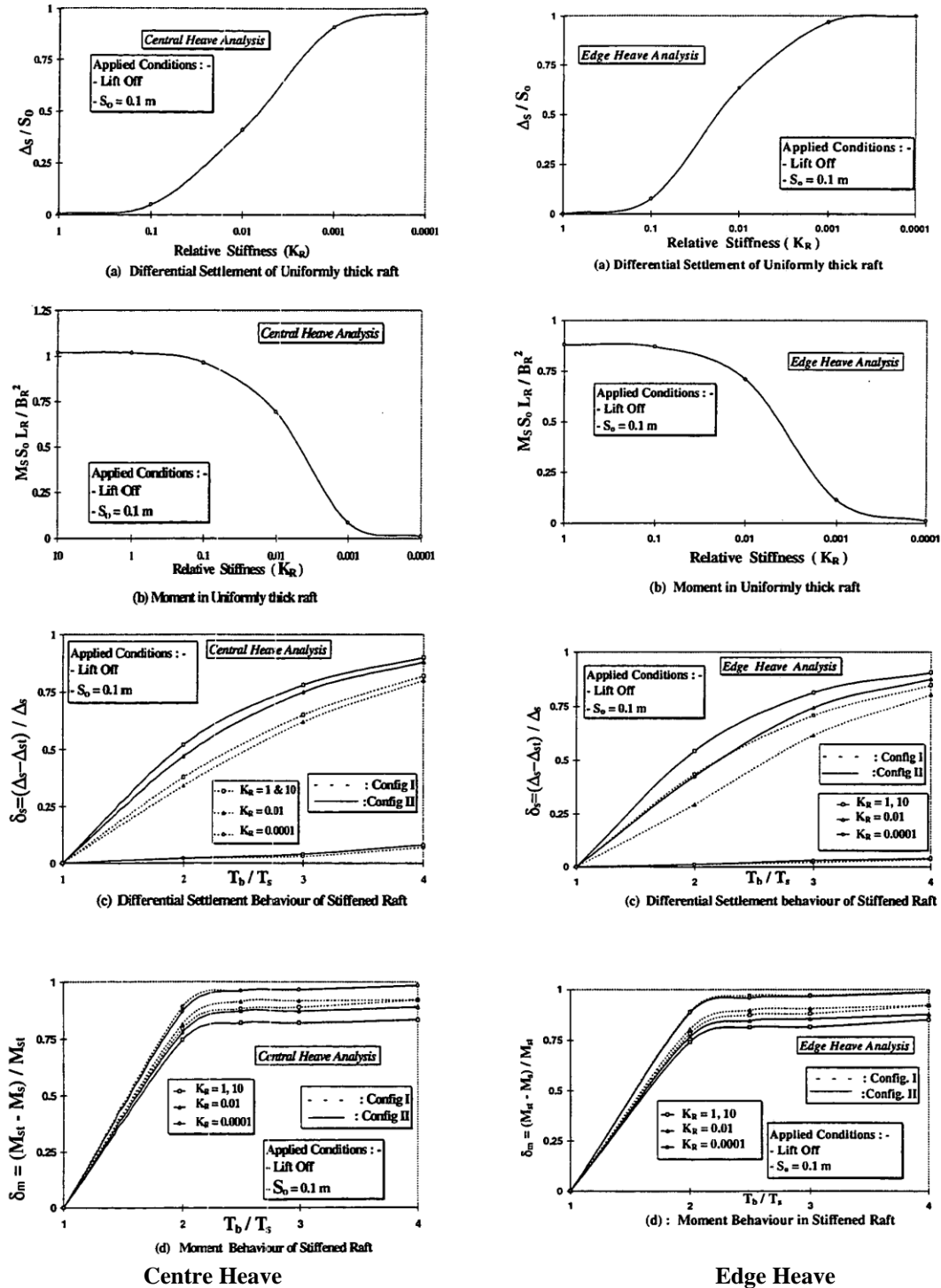


Figure 2.19: Typical example of output charts in study by Sinha and Poulos (1996).

El-Garhy and Wray (2004) and Wray et al. (2005) used an uncoupled modelling approach to calculate the suction distribution over time and the corresponding volume change and surface movement of expansive soils. This work estimated, to a certain accuracy, the edge moisture change distance but no stress analysis or soil structure interaction was involved. The analysis was based on two steps: (i) calculating the suction distribution based on the 3D diffusion equation of Mitchell (1980); and (ii) using the suction data over the soil mass at a certain time, the soil vertical surface heave was calculated from Wray method (1997), which is based on the soil suction. No precipitation or evaporation was modelled; instead, a sinusoidal suction change over time was applied. A FORTRAN computer program named SUCH was written, utilising the finite difference technique to solve the transient suction diffusion equation in 3D. The program was able to predict the suction distribution and the corresponding volumetric change of expansive soils.

Fredlund et al. (2006) carried out a 2D FE uncoupled analysis to evaluate the separation distance under the footing edge in the case of the edge drop scenario. The seepage analysis was carried out using the program SVFLUX (2001), utilising an estimated soil water characteristic curve that relates the soil saturation with the suction profile and hydraulic conductivity. The output of the final pore pressure distribution over a certain time increment was then utilised in a stress analysis using a program called SVSOLID (2002). The footing was assumed initially to have no separation from the soil; an iterative procedure was then suggested to evaluate the tensile zone under the footing slab. The tensile zone was then simulated as a gap between the footing and soil in a stress analysis step (see Figure 2.20).

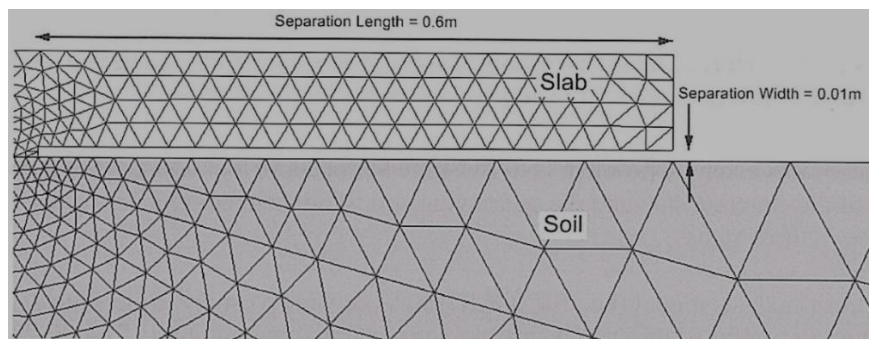


Figure 2.20: Illustration of the separation between the soil and concrete slab foundation in the study by Fredlund et al. (2006).

This study provided a methodology to estimate the edge moisture variation distance (e), which is the distance from the footing slab edge beyond which the change in both suction and deformation are negligible. It was concluded that the edge moisture variation distance can be estimated from the seepage analysis, and that it depends on the rate of precipitation, duration of precipitation and unsaturated soil properties. The proposed methodology to design the footing focused on the edge drop only. The method requires the use of FE modelling in an iterative, uncoupled procedure, which made it difficult to be used as a routine design method.

By considering an exponential decay suction distribution under the cover edge, Abdelmalak (2007) modified Mitchell's diffusion equation (1980) to derive a new solution for the suction distribution under cover. The new equation was proposed to estimate a more realistic mound shape under cover for soils subjected to cyclic weather patterns. The distribution of the suction change was integrated with the depth to derive the distorted mound shape. This mound shape was adopted in a parametric study as a predefined soil mound under a flat foundation in an iterative 2D FE simulation in order to obtain the footing deflection and the associated internal forces. The following slab foundation parameters were examined in the parametric study: slab lengths (L) = 4 m, 6 m, 8 m, 10 m and 12 m; slab beam depth = 0.3 m, 0.6 m, 0.9 m, 1.2 m and 1.5 m; with beam width = 0.3 m; beam spacing = 4 m (these beam depth values provide stiffness values equivalent to that of a flat slab with thicknesses = 0.127 m, 0.253 m, 0.3795 m, 0.506 m and 0.633 m, respectively); slab total imposed area loads = 2 kPa, 2.75 kPa, 3.5 kPa, 4.25 kPa and 5 kPa; slab concrete modulus of elasticity = 20, GPa. Based on the equivalent cantilever length (L_{eqv}) shown in Figure 2.21, the output of the parametric study was used to develop the design charts in Figure 2.22.

The design charts proposed by Abdelmalak (2007) in Figure 2.22 were limited to uniform loadings over the footing slab length; therefore, Magbo (2014) extended the above design method to account for the line loads at the slab edge for simulating the wall loads, and he developed the design charts presented in Figure 2.23 plus a spreadsheet called TAMU-SLAB (Briaud et al. 2016) to automate the design calculations. This design procedure

accounted only for the edge drop and edge lift cantilever moments, shear and deflections, (without considering the general case of the edge lift that may result in loss of support beneath the footing centre, producing a simply supported beam pattern). Moreover, the mound shape adopted was a pre-defined soil distorted surface without considering the normal loading history that involves the footing construction and its loading before the development of the soil mounds, a common disadvantage in most of the existing design methods.

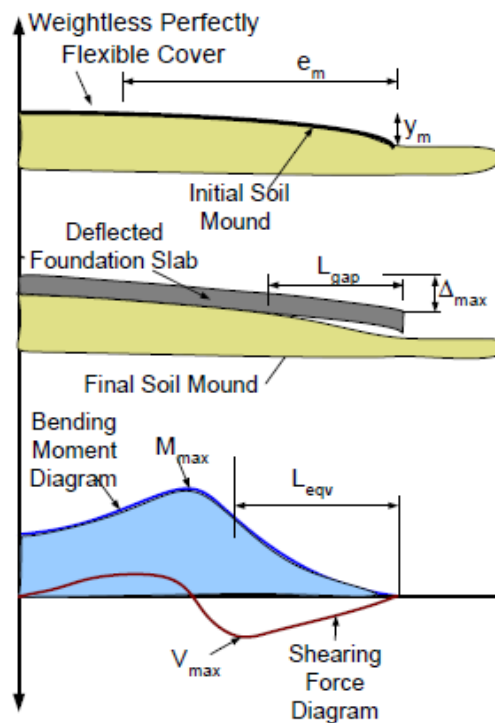


Figure 2.21: Sketch of slab foundation on curved mounds by Abdelmalak (2007).

[e_m = edge moisture distance; y_m = vertical movement; L_{eqv} = equivalent cantilever length (i.e. length of slab that gives the slab maximum bending moment when used with the formula $M_{max} = qL_{eqv}^2/2$); L_{gap} = unsupported length (i.e. length of slab without the soil support underneath); Δ_{max} = difference in elevation between the slab centre and slab edge; M_{max} = maximum bending moment of the slab foundation; and V_{max} = maximum shear force in the slab]

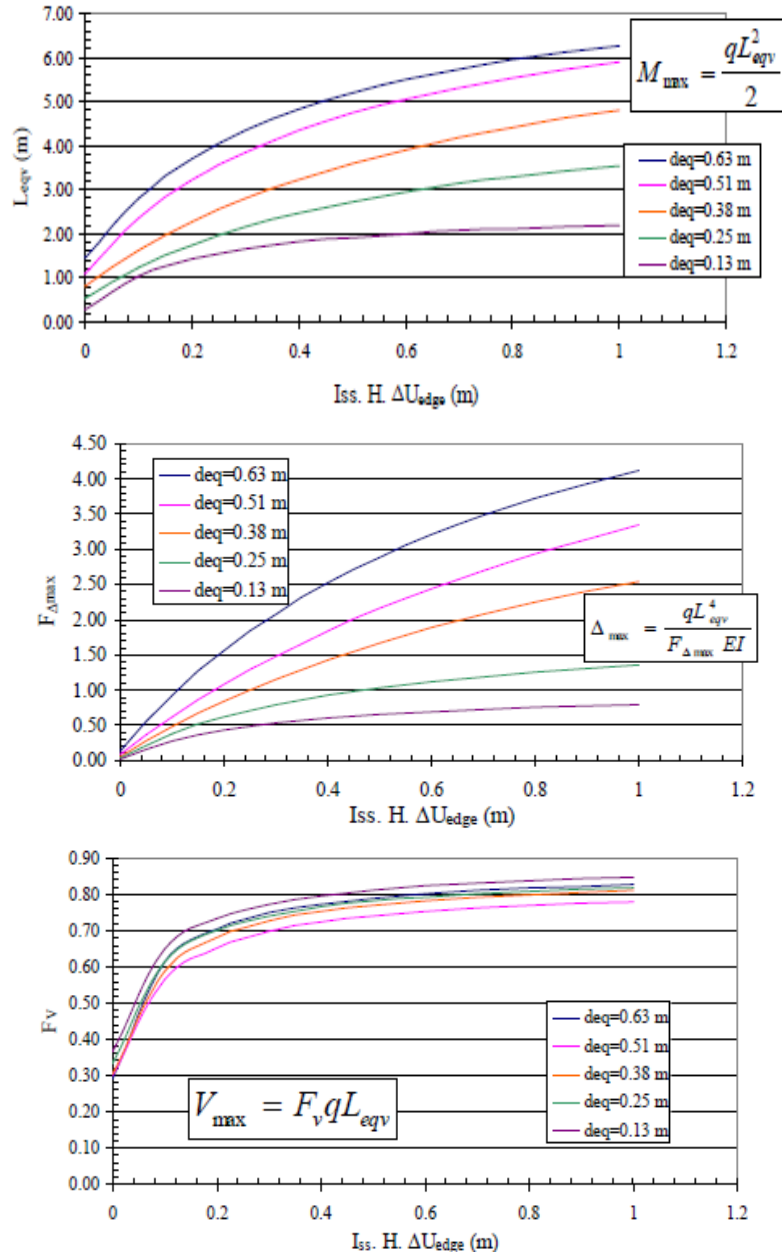


Figure 2.22: Typical example of design charts developed by Abdelmalak (2007).

[H = depth of active zone; ΔU_0 = change in suction; I_{ss} = shrink-swell index; q = total slab foundation loads (including self-weight and imposed loads); L_{eqv} = equivalent cantilever length; Δ_{max} = difference in elevation between the slab centre and slab edge; $F_{\Delta_{max}}$ = maximum deflection factor = $qL_{eqv}^4/\Delta_{max} EI$; and F_v = maximum shear factor = $V_{max}/q L_{eqv}$].

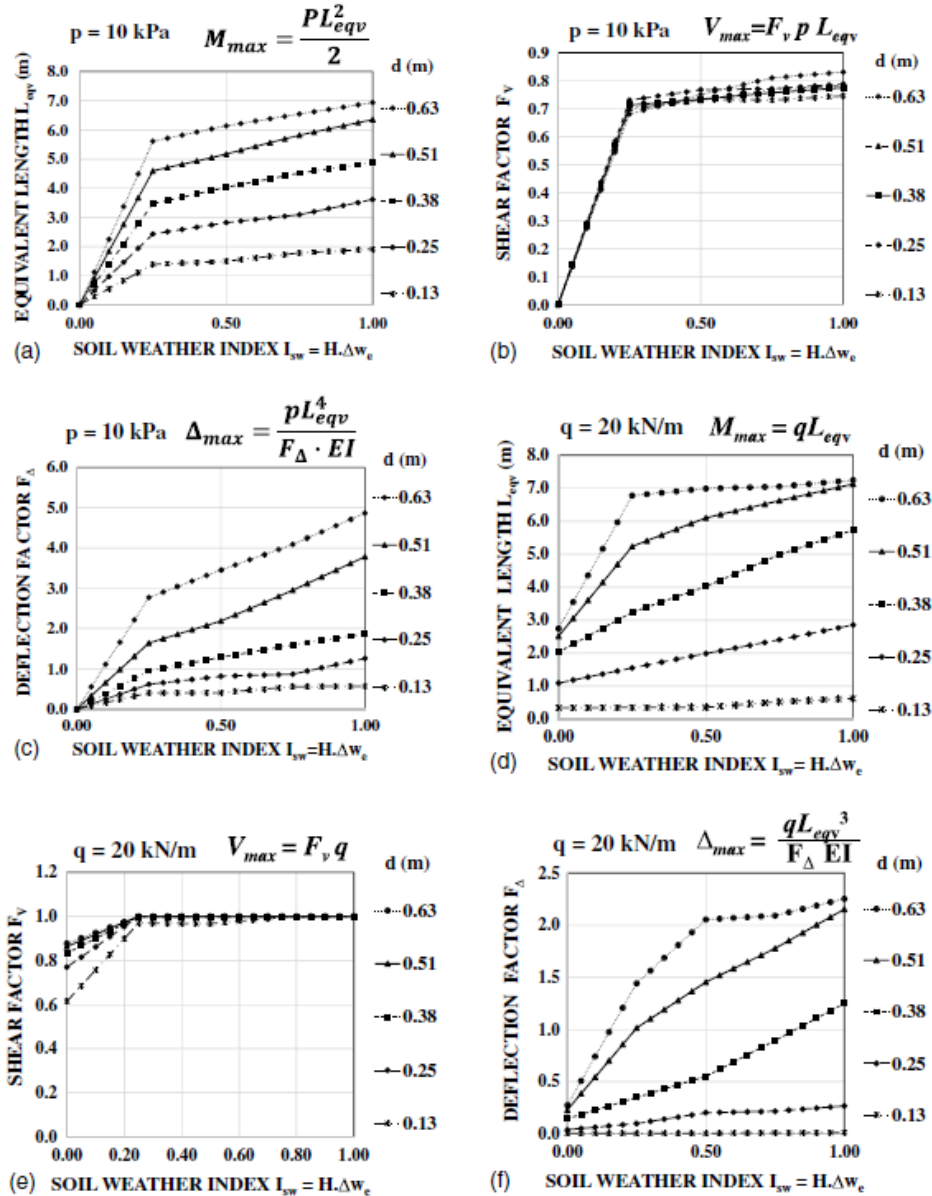


Figure 2.23: Typical example of design charts developed by Briaud et al. (2016).

Dafalla et al. (2011) proposed a simplified design concept for a rigid substructure foundation in the form of an inverted-T of a two-storey concrete frame structure on expansive soils. The upheaval forces of the swelling soils was determined through a one-dimensional odometer test and was then reduced by a factor of 3, as suggested by Al Shamrani et al. (2002), to account for the effect of lateral restraint. These forces were applied on the corner bays of the foundation grids in order to induce the edge heave scenario, as shown in Figure 2.24. The centre heave scenario was omitted from the

analysis, since the concept was developed for a two-storey building and the authors believed that the dead load of the central columns can overcome the swelling forces. The structural analysis of the inverted-T beams grid could be carried out using an ordinary commercial finite element software in order to get the corresponding internal forces. This rigid design methodology has certain limitations. It was recommended only for sites indicating a swelling pressure of less than 300 kPa. In addition, the edge and corner bays on which the swelling pressure is applied, should have limited spans in order to get reasonable bending moments and shear forces, thus, restricting the geometry of the foundations. Moreover, the centre heave scenario was not considered in this approach despite its high potential of occurrence, since the internal columns loads are unlikely to cause stresses on the soil exceeding the proposed design limit of 300 kPa.

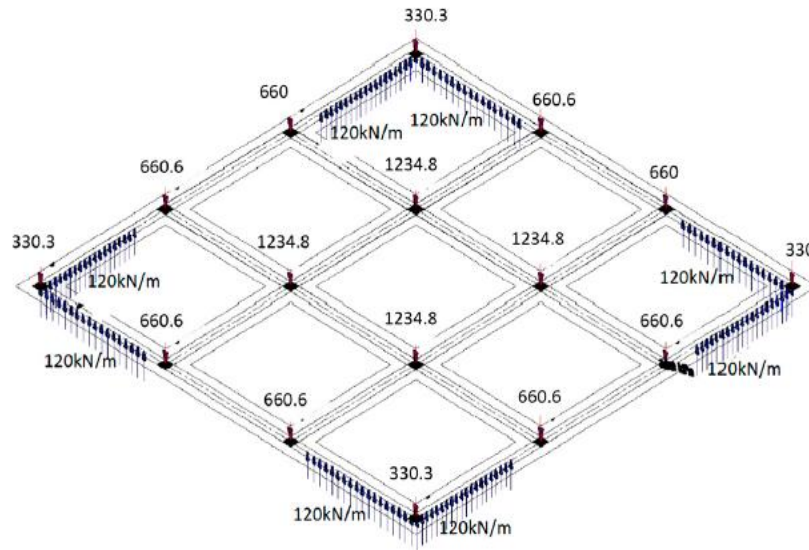


Figure 2.24: Distribution of swelling pressure on corner bays of a foundation grid as developed by Dafalla et al. (2011)

Zhang et al. (2015) carried out a coupled 3D FE transient analysis for isolated footings on expansive soils by adopting the thermal analogy. In this study, the climate and vegetation factors were included to determine the boundary conditions of the problem. The work did not provide a design methodology but rather focused on the prediction of soil movement due to the evapotranspiration of grass roots and crops, assuming all infiltration is intercepted by plantation and utilising the FAO 56 PM method (Allen et al. 1998). The predicted movement of the isolated footing studied agreed well with field observations

made over two years. However, it should be mentioned that the use of the FAO 56 PM equation requires specific vegetation data, which in most cases would not be available to geotechnical engineers. This work is somehow robust, but the proposed analysis mainly tackles the effect of evapotranspiration caused by the grass, trees or crops, hence, it requires thorough vegetation and agriculture knowledge in order to accurately predict the input parameters controlling the evapotranspiration. In addition, the account for evapotranspiration for the tree or grass roots in the calculation of the reactive soil deformations increases the likelihood of violating the symmetrical application of loads, which is a fundamental assumption in the design of slab footings on reactive soils. In fact, a safe distance between the tree roots and foundation is the most feasible solution to avoid their detrimental effects on the slab footing deformations. Unfortunately, the method was not generalised into an engineering design methodology.

2.5 DISCUSSION

The review presented above concerning the traditional method used for designing stiffened slab foundations on expansive soils reveals the following common limitations:

- The slab foundation is usually analysed using pre-formed mound shapes, which neglects the influence of the actual stress path, since the soil mound is formed after the footing is constructed and loaded (Li 1996). In fact, the mound configuration should reflect the influence of the coupled deformation flow that captures the realistic soil moisture changes.
- The complex, irregular and unsymmetrical soil mounds as well as the loading and boundary conditions that are usually experienced in practice, are all overly simplified.
- The use of simple 2D mound shapes to simulate the behaviour of a rather complicated 3D problem is conservative (Kay and Mitchell 1990).
- Adoption of the overlapping rectangles approach by most design methods may cause underestimation of the slab foundation movement and the associated internal forces, especially for the U-shape foundation configurations (Li 1996).

- Determination of the mound shapes in all methods is based primarily on empiricism without scientific guidance, leaving the designer to his/her own experience or available field observations.
- The soil structure interaction problem is normally simulated using a constant soil modulus of subgrade reaction, while in reality this interaction is more complicated and the soil modulus actually varies with the evolving soil suction.

Studying the performance of stiffened slab foundations on reactive soils using numerical modelling or thermal analogy produced promising results. However, most published studies did not provide generic design methodologies and were mainly based on uncoupled approaches implementing pre-defined soil mound shapes, which misrepresents reality.

The above discussion indicates clearly that there is still a need for more reliable and advanced methods for the design of stiffened slab foundations on reactive soils that can overcome the limitations of the existing methods. In this regard, sophisticated 3D FE models can be used to develop an advanced design methodology that is capable of implementing 3D transient coupled hydro-mechanical modelling involving both the seepage and stress calculations, so that the moisture and suction distribution beneath the slab foundation can be accurately simulated. The following features should be considered along the proposed 3D analysis:

- The method should be generalisable by adopting realistic and representative unsaturated soil properties, including the soil moisture-swell dependency, hydraulic conductivity and soil-water characteristic curves (SWCC);
- The seepage analysis should be based on realistic climate precipitation and evaporation conditions, so that the distorted soil mound beneath the slab footings can be calculated rather than estimated (a shortcoming in all previous design methods);
- The external loads should be applied before carrying out the flow analysis to produce a more realistic distorted profile;

- The method should be integrated into the standards requirements with respect to the allowable footing deformations and soil expansiveness classes; and
- Finally, the method should be easy to use by engineers and practitioners for routine design practices.

2.6 SUMMARY

This chapter presented and discussed the existing traditional methods of the design of stiffened slab foundations on expansive soils. In addition, the recent research and design development using the numerical modelling were also highlighted. The assumptions used in the existing design methods were summarised and their limitations were critically discussed. Careful review of the broad range of relevant literature showed that the existing methods along with the recent design development lack the following two major aspects: (i) using realistic 3D simulation of the problem (rather than using a simplified 2D approach); and (ii) implementing a coupled flow-deformation and stress analysis approach that allows the soil mound to be determined through a seepage process that involves the soil suction and moisture-swell characteristics. The current practice of using uncoupled approach in which the slab foundation is analysed using a pre-defined soil mound is prone to misjudgement and inaccuracy. In order to resolve these two main shortcomings, sophisticated 3D finite element hydro-mechanical models are developed and presented in Chapter 3, along with relevant seepage and deformation parameters. The FE numerical modelling set-up is calibrated and validated against field observations. The general features of the proposed modelling methods were discussed in Section 2.5.

CHAPTER 3

NUMERICAL MODELLING OF THE BEHAVIOUR OF STIFFENED SLABS ON REACTIVE SOILS USING THE FINITE ELEMENT METHOD

3.1 INTRODUCTION

As described in Chapter 1, the main objective of this research is to enhance the current design practice of stiffened slab foundations on reactive soils using advanced numerical modelling. Chapter 2 revealed that a major assumption adopted by almost all existing design methods of stiffened slab foundations on reactive soils is that the real case of three-dimensional (3D) moisture flow can be reduced to a simple two-dimensional (2D) problem, resulting in deformation incompatibility between the soil mound and supported footing. In addition, most existing methods implement uncoupled approaches in which the footing is designed for stress analysis using a pre-defined soil mound obtained from a separate seepage analysis, with no consideration to the effect of the slab loading on the formation of the soil mound. In this chapter, an advanced 3D finite element (FE) numerical modelling is pursued to simulate the complex behaviour of stiffened slab foundations, which otherwise are not captured by the currently available design methods. Through a hydro-mechanical approach, the resulting FE modelling is capable of simulating the true performance of stiffened slab foundations on reactive soils, by involving a coupled flow-deformation analysis based on realistic moisture flow and suction evolution, which lead to formation of a realistic soil mound beneath the footing. As a precursor to the 3D modelling process, the following section presents some modelling aspects relating to unsaturated soils and the corresponding associated parameters are presented and discussed. This will be followed by development of the FE numerical model and its verification through three case studies.

3.2 MODELLING ASPECTS FOR UNSATURATED SOILS

3.2.1. Coupled versus Uncoupled Analysis

Design of stiffened slab foundations on reactive soils is typically a moisture transient, unsaturated soil problem (Fredlund et al. 2006). Most of the studies carried out on this topic usually adopt uncoupled approaches in which the problem is solved via two phases, as follows. The first phase comprises an independent transient seepage analysis to obtain the distribution of the degree of saturation and/or soil suction within the soil mass, for a certain time increment; the soil movement is then estimated using one of the available theories listed in Table 3.1, so that the soil distorted mound can be determined. In the second phase, a separate stress-deformation analysis is carried out for the soil structure interaction problem, by analysing the footing slab using the pre-calculated distorted soil mound obtained from the first phase. Although this approach is generally acceptable, the accuracy of the results depends on the duration of the selected time increment. In addition, the actual soil distorted mound and the corresponding maximum differential movement are greatly affected by the stresses induced by the loaded footing, an aspect ignored in the seepage phase. Moreover, the soil in the stress phase is most often assumed to be homogeneous; however, unsaturated soil properties are highly nonlinear and depend on the moisture variation and the ensuing suction changes. Additionally, unlike in the fully coupled flow-deformation analysis, the excess pore water pressure developed due to application of the external load cannot be simulated in the uncoupled analysis (Zhang and Briaud 2015). Formation of the soil distorted mound underneath the slab foundation in the coupled approach directly accounts for the combined effect of the suction evolution and the stresses induced by the footing loading. The abovementioned limitations of the uncoupled analysis indicate clearly that it oversimplifies the real situation compared with the coupled approach, and this compromise can inevitably lead to inaccurate design. To circumvent these limitations, this thesis adopts a robust, fully coupled flow-deformation transient analysis for simulating the problem of stiffened slab foundations on reactive soils.

Table 3.1: Summary of current methods for predicting in-situ volume change movement of expansive soils (Adem and Vanapalli 2015).

Description	Consolidation theory-based methods		Water content-based methods		Suction-based methods	
	Based on elastic constitutive models (Vu and Fredlund, 2004; Zhang, 2004)	Based on elastoplastic constitutive models (Abed, 2008)	Briaud et al. (2003)	Overton et al. (2006)	Wray et al. (2005)	Adem and Vanapalli (2013)
Governing equations	Water continuity, and stress equilibrium	Water continuity, and stress equilibrium	The equation of the soil movement formulated by extending the parallel between the shrink test–water content method and settlement methods	Free field heave equation	Mitchell's transient suction diffusion equation, and suction-based empirical model	Simplified volume change constitutive equation for soil structure, and semi-empirical model for estimating F_{unsat}
State variables	Matric suction, $u_s - u_w$ and net normal stress, $\sigma_m - u_s$	Matric suction, $u_s - u_w$ and net normal stress, $\sigma_m - u_s$	Water content, w	Volumetric water content, θ	Total soil suction	$u_s - u_w$
Required tests	Vu and Fredlund (2004): Conventional oedometer test, oedometer or triaxial shear tests with suction control; Zhang (2004): Consolidation-swell test, free shrink test, suction test, and specific gravity test	Conventional oedometer test, oedometer or triaxial shear tests with suction control	Shrink test	Filter paper tests, consolidation-swell test, constant-volume test	Tests to measure the diffusion coefficient and the suction compression index	Filter paper tests, Conventional tests to measure saturated modulus of elasticity, E_{sw} , such as triaxial or oedometer test
Computer programs	Vu and Fredlund (2004): FlexPDE for uncoupled analysis, COUPSO for coupled analysis; Zhang (2004): Abaqus/standard program	PLAXFLOW for simulating the unsaturated ground water flow, and PLAXIS for predicting the movements of expansive soils over time ($u_s - u_w$), ($\sigma_m - u_s$), ($\sigma_m - u_s$)	None	VADOSE/W for simulating water migration in response to atmospheric conditions	SUCH with two models: (i) moisture flow model, and (ii) a volume change model	VADOSE/W for simulating saturated and unsaturated flow in response to environment changes
Initial conditions	Initial matric suction, ($u_s - u_w$), and initial net normal stress, ($\sigma_m - u_s$)	None	None	Initial water content profile	Initial total suction	Initial matric suction profile or initial water content profile
Boundary conditions	Matric suction, water flux, applied load, and soil displacements	Matric suction, water flux, applied load, soil displacements	None	Water flux, pore water pressure, climate data	Total suction, u	Matric suction, water flux, climate data, thermal data, and vegetation data
Results	Vu and Fredlund (2004): 1D, 2D, and 3D heave over time; Zhang (2004): Vertical movement of the ground surface (heave/shrink) over time	Vertical movement of the ground surface (heave/shrink) over time	Vertical movement of the ground surface (heave/shrink) over time	Free field heave over time	Soil surface movements (heave/shrink) under covered surfaces	Vertical movement (heave/shrink) at any depth over time
Applications	Vu and Fredlund (2004): A light industrial building in Regina, Saskatchewan, Canada; Zhang (2004): To simulate footings' movements for a site in Arlington, Texas, USA	To predict the movements of expansive soils underneath a trial wall built in Barakat site, Sudan	To simulate footings' movements for a site in Arlington, Texas, USA	Soil profiles in the Denver area of Colorado, USA	Amarillo test site and College Station test site located in Texas, USA, and Al-Ghatt, Saudi Arabia, test site	Four case studies from two countries: Canada and China (see Table 1)

3.2.2. Mechanism of Soil Volume Change

Fredlund et al. (1976) described the volume change constitutive relations of an unsaturated, linear, elastic, isotropic s, as follows:

$$\varepsilon_x = \frac{(\sigma_x - u_w)}{E_1} - \frac{\mu_1}{E_1}(\sigma_y + \sigma_z - 2u_w) + \frac{(u_a - u_w)}{H_1} \quad (3.1)$$

where:

ε_x = normal strain in the x -direction;

E_1 = elastic modulus with respect to the change in effective stress $(\sigma - u_w)$;

μ_1 = Poisson's ratio with respect to the relative strains in x , y and z directions;

H_1 = elastic modulus with respect to the change in soil suction $(u_a - u_w)$;

σ = total normal stress;

u_a = air pressure; and

u_w = water pressure.

Similar equations can be written in the y - and z -directions. The soil volumetric strain is equal to the sum of the normal strain components, calculated as follows:

$$\varepsilon_v = C_t \cdot \partial(\sigma - u_w) + C_a \partial(u_a - u_w) \quad (3.2)$$

where:

C_t = soil compressibility with respect to the change in effective stresses; and

C_a = soil compressibility with respect to the change in soil suction.

Equation 3.2 shows that the volume change in unsaturated soils is induced by the soil compressibility due to the change in the net stress caused by both loading and suction. Because suction within a soil mass results in a volumetric change, it can be simulated mechanically in the FE modelling as an equivalent mean effective stress (compressive).

Many researchers assume a constant value for the air pressure during flow-deformation analysis (e.g. Gay 1993; Wray 1978; Zhang and Briaud 2015), and the same approach is adopted in the current study.

It should be noted that most available FE studies on the topic of simulating the volume change of expansive soils are based only on the suction and stress variations, with no consideration to the soil mineralogy (e.g. Briaud et al. 2010; Li 1996; Wray et al. 2005; Zhang and Briaud 2015). However, the influence of the mineralogy of a particular clay should be included in any robust analysis, as the swelling potential is a direct function of the soil's mineralogy. For example, clayey soils without highly swelling minerals in the form of montmorillonite are of no danger when exposed to a high suction variation. This is evident from the volumetric shrinkage strain tests performed by Puppala et al. (2013) on clay samples from Texas; these tests showed that a clay with a high content of montmorillonite experienced a volumetric shrinkage strains that is twice that experienced by a clay of a lower montmorillonite content. In fact, only a few studies accounted for the effect of minerals on the volume change of reactive soils, as the main focus of these studies was directed to the suction variation and not on the compressibility per se. However, a recent study carried out by Pulat et al. (2014) suggests that suction is independent of the soil mineralogy and cannot be used alone to accurately predict the volume change of reactive soils.

To account for the effect of suction and mineralogy on the volume change of expansive soils, sorption and moisture-swell models are introduced in the FE analyses performed in this thesis to relate the volumetric strain with r , the degree of saturation (Williams 1982). The sorption model is represented by the soil-water characteristic curve (SWCC), which simulates the suction changes within the soil matrix with respect to the change in the degree of saturation. The moisture-swell model, on the other hand, defines the volumetric swelling-saturation dependency of the soil matrix during the partially saturated flow condition, and it requires volumetric strain data with respect to the changes in the degree of saturation. The SWCC and moisture-swell models are discussed in detail below.

3.2.3. Input Parameters for the Coupled Flow-Deformation Analysis

3.2.3.1 Soil-water characteristic curve (SWCC)

The soil water characteristic curve (SWCC) is one of the primary soil properties required for the transient seepage analysis in unsaturated soils. As mentioned earlier, the SWCC defines the suction-saturation dependency within the soil matrix. The soil suction may be matric or total. The matric suction is the capillary pressure exerted by the soil on its surroundings (i.e. $u_a - u_w$; where u_a is the pore-air pressure and u_w is the pore-water pressure). The total suction is the sum of the matric suction and osmotic suction (arising from the salt content of the soil pore fluid). At high suction values > 1500 kPa, the total suction equates the matric suction (Fredlund and Xing 1994). Figure 3.1 shows a typical example of a soil-water characteristic curve for a silty soil. In this figure, the air-entry value is the soil matric suction in which the air starts to enter the largest pores of the soil. The residual water content is the water content below which the extraction of water from the soil requires a very high suction change.

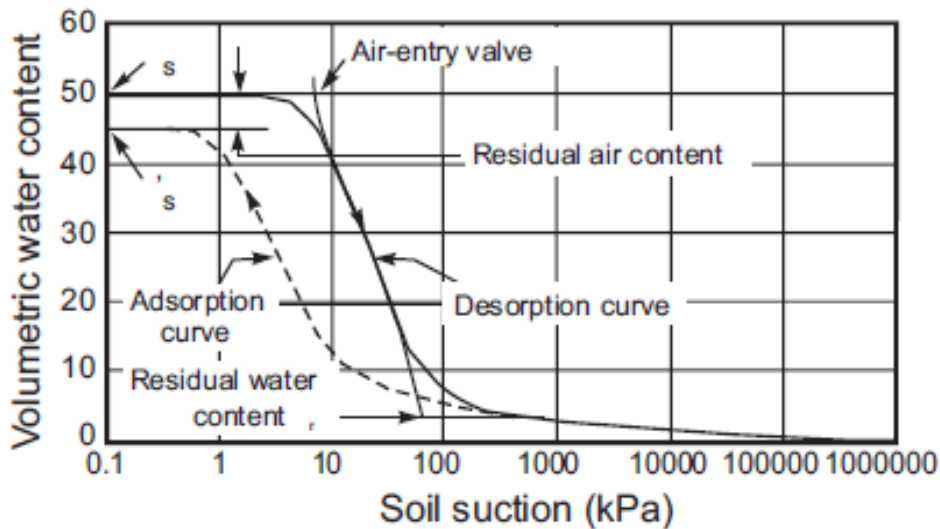


Figure 3.1: Typical example of a soil-water characteristic curve for a silty soil (Fredlund and Xing 1994).

Numerous empirical equations were proposed in the literature to generate different forms of SWCC based on laboratory test results. The following equation suggested by Fredlund et al. (1994) is an example:

$$\theta = \theta_s \left[\frac{1}{\ln \left[e + (\psi / a)^n \right]} \right]^m \quad (3.3)$$

where:

- θ = volumetric water content;
- θ_s = saturated volumetric water content;
- ψ = soil suction; and
- a, m and n = empirical fitting parameters.

Figures 3.2a to 3.2c show the effect of changing the empirical parameters (a, m and n) on the shape of the SWCC for a soil with a volumetric water content = 0.5 and a saturated volumetric water content = 0.5. Fredlund et al. (1994) reported that the parameter (a) determines the air entry value, whereas the parameters (m) and (n) control the slope of the curve (i.e. the degree of soil diffusion). As mentioned earlier, the SWCC is deemed essential for the hydro-mechanical FE numerical modelling as an indirect means to account for the clay mineralogy. A representative, idealised SWCC is thus proposed (called herein ISWCC) to describe the saturation-suction relationship of unsaturated swelling clays; the following section describes the way the ISWCC is constructed.

Based on field suction data taken from the north-east of Adelaide, South Australia, Li (1996) found that the surface suction could be assumed to vary in a sinusoidal manner in response to the climate cycles, as follows:

$$u(0,t) = 4.0 + \cos(2\pi n t) \quad (3.4)$$

where:

- u = surface suction in pico-Farad (pF) [logarithm to the base 10 of the pressure in centimetres of water];
- n = climate frequency (cycle/year); and
- t = time variable (in months).

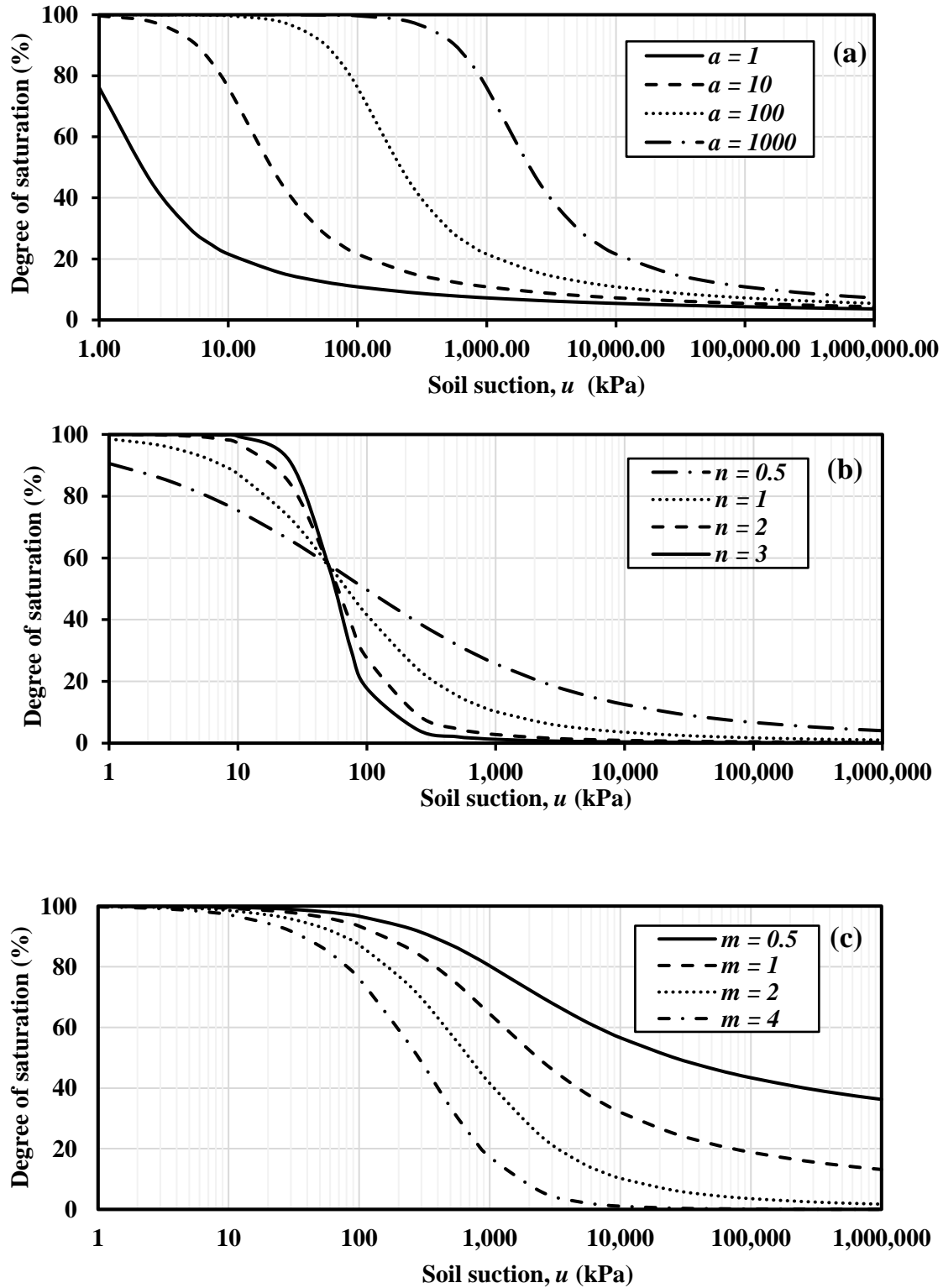


Figure 3.2: Effect of changing fitting parameters (a , m and n) in Equation (3.3) on the shape of the SWCC [modified after Fredlund and Xing (1994)].

Equation 3.4 indicates that the SWCC should cover the range of the expected suction values between 3.0 and 5.0 pF, which are equivalent to 100 and 100,000 kPa for the dry and wet conditions, respectively. Therefore, based on these limits, the fitting parameters (a) and (m) are fixed to 1000 and 1.25, respectively, to produce an ISWCC covering the required seasonal suction fluctuation range. In fact, the soil aggregation (structure) and initial moisture have no influence on the SWCC in the high ranges of suction greater than 20,000 kPa (Vanapafli et al. 1999). Moreover, suction values less than < 100 kPa are considered negligible. For soil surfaces exposed directly to water, Mitchell (1984) suggested that the suction value should be 2.75 pF.

The fitting parameter (n) is assumed to be 1.0 in this study. Therefore, ISWCC fitting parameters (a), (m) and (n) are chosen to be 1000, 1.25 and 1.0, respectively. These values are chosen so that the ISWCC produces the least expected suction of 100 kPa at a reasonably high degree of saturation of about 95% and also the maximum expected suction of 10,000 kPa at a respectively low degree of saturation of about 30%. The proposed ISWCC is compared with field data obtained from five different sites, and the comparison is shown Figure 3.3.

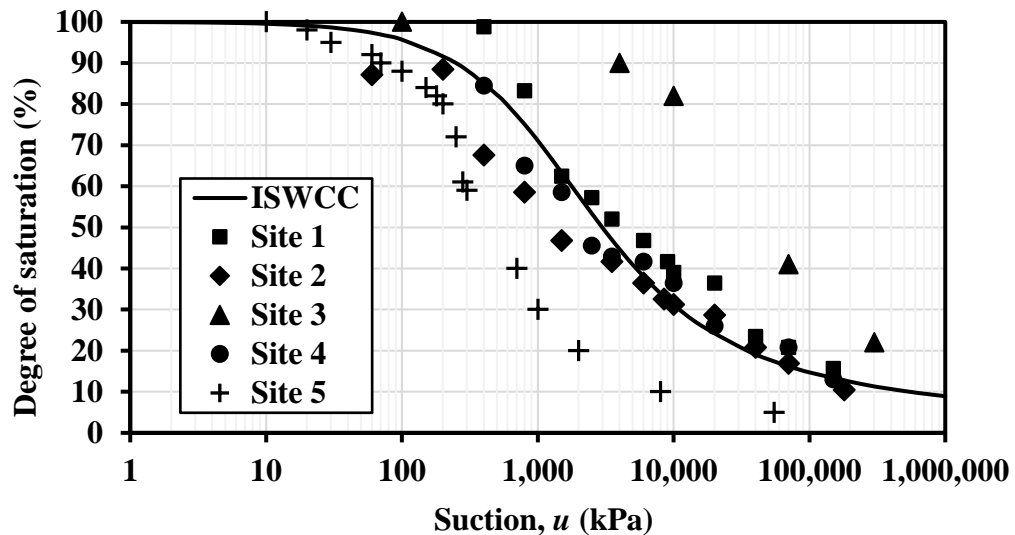


Figure 3.3: Idealised soil-water characteristic curve (ISWCC) for empirical parameters: $a = 1000$, $m = 1.25$ and $n = 1$.

[Site 1: Paris Soil (Puppala et al., 2013); Site 2: Houston Soil (Puppala et al., 2013); Site 3: Regina Clay (Fredlund et al., 1994); Site 4: Fort Worth Soil (Pupalla et al., 2013); Site 5: Kidd Greek Tailings (Fredlund et al., 1994)]

It can be seen from Figure 3.3 that the proposed ISWCC reasonably predicts the relationship between the degree of saturation and suction for many swelling soils obtained from different sites. Consequently the ISWCC shown in Figure 3.3 will be used with reasonable accuracy in the cases where site data is not available. It should be noted that, in the course of estimating the characteristic surface heave (y_s), the Australian Standards AS2870 (1996; 2011) do not recommend using a definitive SWCC, but rather proposes design values of suction changes (maximum of 1.2 pF). However, Mitchell (2008) recommends higher values up to 1.8 pF for the suction change in arid regions.

3.2.3.2 Moisture-swell model

The moisture-swell model relates the volumetric swelling of porous soil materials to the degree of saturation of the wetting liquid in the partially saturated flow condition. A partially saturated condition is postulated when the pore liquid pressure is negative. A typical example of a moisture-swell model is represented by the curve shown in Figure 3.4 in which the moisture-swell strain (ϵ_{ii}^{ms}) in any single direction can be calculated with reference to the initial saturation, as follows (ABAQUS User's Manual 2014):

$$\epsilon_{ii}^{ms} = r_{ii} \frac{1}{3} (\epsilon^{ms}(s) - \epsilon^{ms}(s^I)) \quad (\text{no sum on } i) \quad (3.5)$$

where:

$\epsilon^{ms}(s)$ = volumetric swelling strain at the current saturation;

$\epsilon^{ms}(s^I)$ = volumetric swelling strain at the initial saturation; and

r_{ii} = represents the ratios (r_{11}), (r_{22}) and (r_{33}), which allow for anisotropic swelling.

A few moisture-swell curves are found in the literature and an example is shown in Figure 3.5, for a very high expansive clay from Soko-Ngawi region in Indonesia. The soil used to develop such curves had a liquid limit (LL) = 101%, a plasticity index (PI) = 71.3%

and a montmorillonite mineral content = 49.7%. A modified oedometer apparatus was used to develop the curves where the ring supporting the soil samples was replaced by a calibrated rubber to allow for the soil lateral swell. The soil samples were allowed to swell with no applied seating loads. More details about the tests conducted and the reading procedures can be found in Sudjianto et al. (2011).

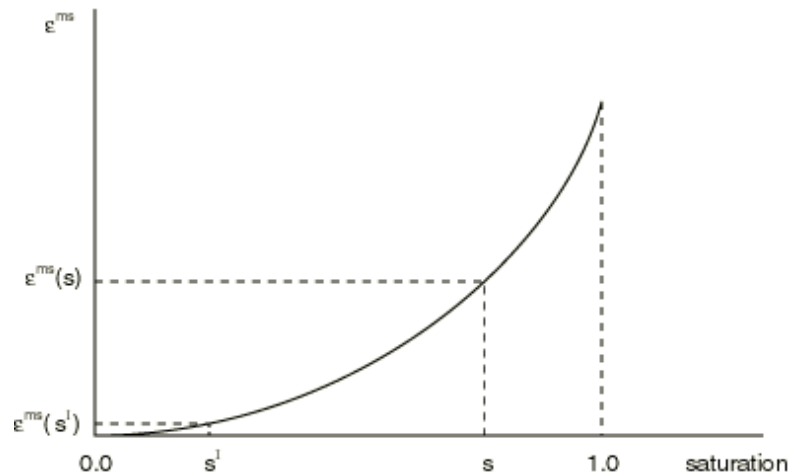


Figure 3.4: A typical example of the moisture-swell model implemented in ABAQUS User's Manual (2014) .

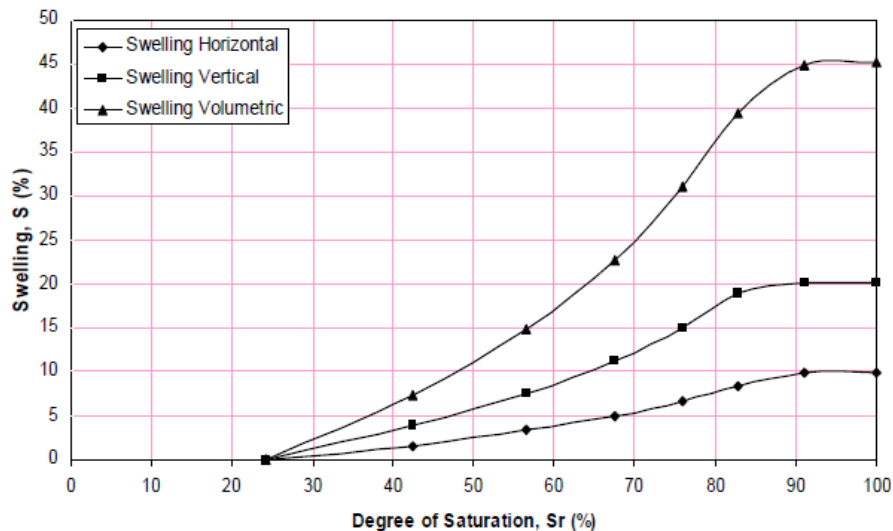


Figure 3.5: Moisture-swell curves for a clay soil obtained from Soko-Ngawi region in Indonesia (Sudjianto et al. 2011).

Tripathy et al. (2002) carried out a study on cyclic swelling and shrinkage paths for compacted expansive soil specimens, and Figure 3.6 shows the moisture-swell curves obtained from the study. The results show the following features:

- (i) The swell-shrink path is reversible once the specimen reaches an equilibrium condition where the vertical deformation during swelling and shrinkage are equal. This generally occurred after about four swell–shrink cycles;
- (ii) The swell–shrink path represents a curve of an S-shape (i.e. three phases) for soil specimens subjected to cycles of swelling and full shrinkage. For specimens subjected to cycles of full swelling and partial shrinkage, the path comprises only two phases (i.e. a curvilinear phase and a linear normal phase); and
- (iii) Almost 80% of the total volumetric strain occurred in the linear portion of the S-shape curve. The linear portion is found within a degree of saturation that ranges between 50–80%. It should be noted that the soil vertical deformation shown in Figure 3.6 is relatively high, since the readings were obtained from a normal oedometer apparatus.

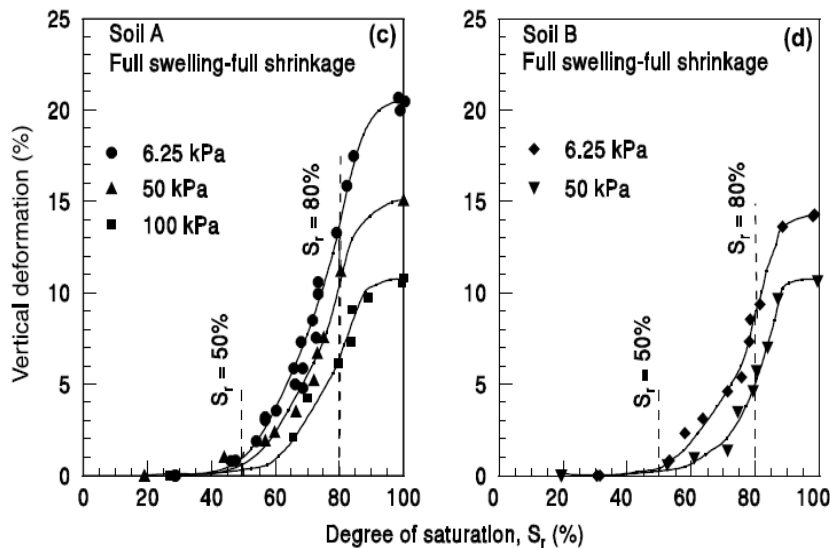


Figure 3.6: Moisture-swell curves developed by Tripathy et al. (2002).

Kodikara and Choi (2006) showed that the relationship between the volumetric shrinkage or swell strain ($\varepsilon_{vol,swell/shrink}$) and the reduction in the compaction moisture content (Δw)

observed during shrinkage tests follow a linear correlation that is valid for slurry and compacted clayey specimens. This relationship can be expressed as follows (Kodikara and Choi 2006):

$$\varepsilon_{vol,swell/shrink} = \alpha \Delta w \quad (3.6)$$

where: (α) is the volumetric swell/shrinkage coefficient. The value of (α) is reported as 0.7 and 0.6 for the case of swelling and shrinkage, respectively. In terms of the degree of saturation for highly plastic clays, these values are 0.26 and 0.24, respectively. The results obtained by Tripathy et al. (2002) show a value of (α) of about 0.4 for both the swell and shrinkage volumetric strains, in terms of the degree of saturation. On the other hand, Al-Shamrani and Dhowian (2002) show that (α) = 0.18 from the triaxial compression test, which corresponds to a value of 0.5 for the oedometer test. In the current research, (α) = 0.15 is used, which is close to the value reported by Al-Shamrani and Dhowian (2002), for the linear section of the moisture-swell curve.

Chen (1988) reported that very dry clays having a moisture content less than 15% can absorb moisture of as high as 35%, resulting in swelling that can cause damages to structures. On the other hand, a moisture content of more than 30% in a clay indicates that most of the swelling already took place. Thakur et al. (2005) carried out volumetric strain oedometer tests on montmorillonite and bentonite mineral samples at different compaction water contents; the maximum potential volumetric strain of reported was about 25%. Al-Shamrani and Dhowian (2002) showed that field measurements of surface heave are best predicted by data obtained from the triaxial compression test; they reported that the actual surface heave is about one-third of that obtained from the traditional oedometer test. From the facts above, a maximum volumetric strain of 8 % is considered in the present research, which is approximately equivalent to one-third of the maximum free swell value obtained by Thakur et al. (2005) for the maximum range he measured for swelling clays.

By integrating the range of parameters discussed above, an idealised moisture-swell curve (IMSC) can be constructed, in which the full swelling takes place at a water content of say 30%, following an S-shape curve as obtained by Tripathy et al. (2002). For a highly plastic clay of a porosity ranging from 0.4 to 0.6, the degree of saturation corresponding to a 30% moisture content is about 90%. Therefore, the moisture-swell function can be constructed to satisfy 100% swelling at a degree of saturation of about 90%. The slope of the linear portion of the S-shape curve can be considered to be 0.15, as described earlier, and the maximum volumetric swell strain can be limited to 8%. The constructed IMSC is shown in Figure 3.7, which also presents the curve prepared on Soko-Ngawi region clay for comparison, and a good agreement is evinced.

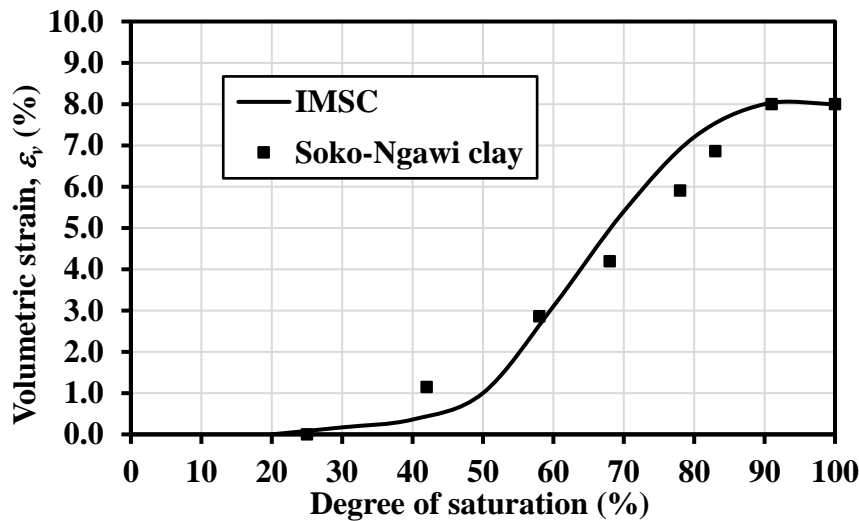


Figure 3.7: Idealised moisture-swell curve (IMSC) of the current study.

It should be noted that the original data of the volumetric strain in Figure 7 for the Soko-Ngawi clay (measured using odometer tests) are divided by 3.0 to account for the equivalent triaxial test data, as recommended by Al-Shamrani and Dhowian (2002). It should also be noted that the IMSC shown in Figure 3.7 is representative of unsaturated clays with high contents of montmorillonite. Other moisture-swell curves can be constructed for clays having less montmorillonite minerals in the same manner, but with different values of the maximum expected volumetric strains to be used for better surface heave simulation. This means that, in order to predict the surface heave for any site, an individual moisture-swell curve for this specific site should be constructed.

3.2.3.3 Soil permeability and flow duration

Soil permeability is an important parameter in the calculation of seepage and, in turn, formation of the soil distorted surface (i.e. the soil mound). In the coupled flow-deformation analysis, the partial differential equation governing the seepage flow of unsaturated soils is calculated as follows (Fredlund and Rahardjo 1993):

$$\frac{\partial}{\partial x} \left(k_x \frac{\partial h}{\partial x} \right) + \frac{\partial}{\partial y} \left(k_y \frac{\partial h}{\partial y} \right) = m_w^2 \gamma_w \frac{\partial h}{\partial t} \quad (3.7)$$

where:

h = total pressure head;

k_x = soil permeability in the x -direction;

k_y = soil permeability in the y -direction;

γ_w = unit weight of water; and

m_w^2 = slope of the soil-water characteristic curve (SWCC).

Unlike the constant permeability premise used in saturated soils, the permeability of unsaturated soils shown in Equation 3.7 is not constant but dependant on the degree of saturation or soil suction (Fredlund and Rahardjo 1993; Richards 1967). According to Forchheimer (1901), the permeability of unsaturated soils is dependent on the fluid flow velocity, and can be calculated as follows:

$$k_u = k_s k = \left(\frac{q \gamma_w}{[(\partial u / \partial x) - \rho g]} \right) \quad (3.8)$$

where:

k_u = permeability of unsaturated soils;

k = permeability of fully saturated soils;

k_s = dependence factor of permeability on the saturation;

- q = volumetric flow rate of the wetting liquid per unit area of the soil;
 γ_w = unit weight of the wetting liquid;
 $\partial u / \partial x$ = change in pore water pressure with the unit length in x -direction;
 ρ = density of fluid; and
 g = magnitude of gravitational acceleration.

At low flow velocity, as in the case of unsaturated soils, the term (ρg) in Equation 3.8 (known as the Forchheimer's term) approaches zero, and the permeability function is thus reduced to:

$$k_u = k_s k = \left(\frac{q \gamma_w}{(\partial u / \partial x)} \right) \quad (3.9)$$

Mitchell et al. (1965) proposed that dependence factor of permeability (k_s) on the degree of saturation (S) can be calculated as follows:

$$k_s = S^3 \quad (3.10)$$

3.2.3.4 Stiffness of soil mound

The stiffness of the soil mound influences the soil-structure interaction between the soil and the slab footing at the contact surface. The lower the soil mound stiffness (i.e. higher compressibility) the more ability of the footing to punch through the soil, and vice versa. The most frequently used soil-structure interaction model that represents the soil mound stiffness is the Winkler foundation model. However, this model has a major shortcoming in that it accounts only for the normal stiffness of the soil (i.e. the form of vertical springs), with no consideration to the lateral friction (which is inevitably mobilised) between the soil and the footing. Another problem associated with this model is that the springs support both compressive and tensile stresses, and this does not allow for the expected separation that should occur under tension between the soil and the footing (as in the case of the slab foundations on expansive soils under different edge movement scenarios). One way to

circumvent this limitation is to adopt an iterative procedure for the simulation of the separation distance that may develop between the footing and the supporting soil mound. This can be achieved (for example) by using the elastic half-space foundation model, which is more advanced than Winkler's model for the soil-structure interaction problems. However, this model is limited to soil mounds with a constant stiffness profile over depth. But in reality, the soil modulus is greatly affected by both the applied stresses (from the footing) and the evolving matric suction (Zhang and Briaud 2015). Contact elements is another advanced approach that can be used successfully to simulate the complex soil-structure interaction problems. This approach is used in this research to simulate the soil-structure interaction between the soil mound and stiffened slab foundation. The approach allows for the soil-structure separation under tensile stresses and can simulate both the vertical support and lateral friction. Penetration of the footing slab into swelling soil can also be simulated with this approach.

According to the Australian Standards AS2870 (2011), the maximum design value of the mound stiffness (K_s) is $100q$, where (q) is the total building load force divided by the area of slab foundation, with a minimum value equal to 1,000 kPa. For shrinking soils, being dry and hard, the Australian Standards proposes a minimum value of 5,000 kPa for K_s . In light of this recommendation, the K_s values assumed in the current study are 5,000 kPa for the edge drop and 1,000 kPa for the edge lift. The footing-soil separation is allowed under tensile stresses and the friction between the soil and footing is simulated using a coefficient of friction equal to 0.35.

3.2.3.5 Soil modulus and Poisson's ratio

The stress-strain relationship of an expansive soil is nonlinear and highly dependent on the soil suction (Richards and Gordon 1972). As expected, triaxial compression tests carried out on Black Earth expansive clay from Australia indicated that the both the soil strength and modulus (E) are proportional to the soil suction, as shown in Figure 3.8. In fact, the soil modulus (E) has a significant impact on the amount of surface heave in FE numerical modelling, since the suction change is simulated as a change in the mean effective stresses within the soil mass, producing vertical strains as described in

Section 3.2.2. the suction has a dual effect, as it can both increase/decrease the soil modulus and also causes compressive/extensional volumetric strain in a complex constitutive manner. The effect of the in-situ confining pressure on (E) is also important in foundation problems involving soil-structure interaction. However, the effect of the in-situ confining pressure on (E) is usually marginal compared with the effect of soil suction resulting from a reduced degree of saturation, as experimentally confirmed by Hangge et al. (2015). The concept of considering the reliance of (E) on the soil suction for reactive soils and neglecting the effect of the overburden confining pressure was previously adopted by many researches (e.g. Briaud et al. 2016; Li 1996; Li et al. 2014; Wray et al. 2005; Zhang and Briaud 2015). As an additional confirmation on this matter, a case study discussed later in Section 3.3.1 is modelled, with and without the effect of the confining pressure on (E), and the difference is found to be relatively small (refer to Case study No 3). Consequently, in this thesis, it is decided to consider only the effect of the soil suction on (E) and omit the effect of the confining pressure. The user-defined subroutine (USDFLD) is specifically developed to express the soil modulus – suction dependency implemented in the ABAQUS models constructed in this thesis. In this subroutine, the soil modulus, as a material property, is related to the soil suction (negative pore water pressure) through the dependency relationship shown in Table 3.2, based on the study reported by Li (1996). The negative pore water pressure represents the output of the equilibrium phase of the combined stages of the initial moisture condition and water precipitation event. The subroutine is generated using Intel Visual Fortran, and a copy is provided in Appendix-A.

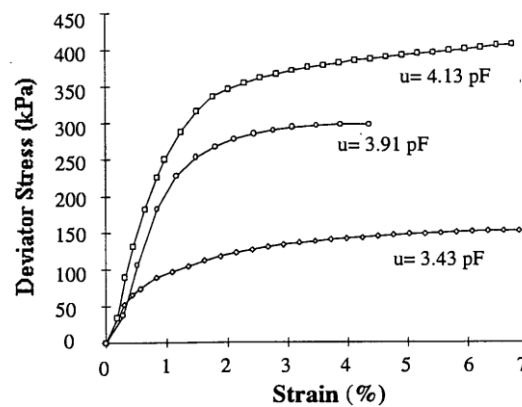


Figure 3.8: Variation of stress-strain curves of black earth clay with suction in triaxial compression test (Li et al. 1992).

Table 3.2: Soil modulus-suction dependency (Li 1996).

Soil modulus, E (MPa)	Soil suction, u	
	(pF)	(kPa)
11	3.0	100
20	3.4	250
30	3.8	650
40	4.2	1,600
50	4.6	3,900

By definition, Poisson's ratio (μ) contributes to the volumetric strain in unsaturated soils as shown earlier in Equation 3.1. The effect of μ on the deflection of footings was reported to be negligible by some researchers (e.g. Pidgeon 1980). However, Li (1995) opposed this assumption and proved through FE analyses that the vertical displacement of slab foundations increases with higher values of μ . He attributed this to the fact that, as the value of μ increases, a larger proportion of the otherwise lateral swelling strain (which is suppressed by the adjacent soil mass) is transferred into vertical swelling strain, increasing the slab foundation movement in the vertical direction (i.e. in a 1-D manner). It is the view of the author that, although the value of μ has a direct impact on the absolute deformation of footings, its effect on the differential mound or footing movement is negligible. Some values of μ found in the literature for unsaturated clays are given in Table 3.3; a constant value of $\mu = 0.3$ is reasonably assumed for the swelling soil modelled in this research.

Table 3.3: Poisson's ratio suggested by different researchers for unsaturated clays.

Study	Poisson's ratio (μ)
Wallace and Lytton (1992)	0.20-0.35
Linveh et al. (1973)	0.25
Richards (1979)	0.40
Poulous (1984)	0.30
Wray (1978) and Pitt (1982)	0.40
Zhang et al.(2015)	0.40

3.3 FINITE ELEMENT MODELLING OF STIFFENED SLAB FOUNDATIONS

It is critically prudent to ensure that the process of finite element (FE) numerical modelling adopted in this thesis is capable of providing reliable outcomes. To this end, the proposed advanced FE modelling performed in this thesis is verified against three different stages of case studies. Firstly, the 3D FE modelling is applied to a case study involving field observations of a soil mound formation for a flexible cover membrane. This stage of modelling verification is meant to confirm the capability of the adopted hydro-mechanical approach used in the FE modelling to generate realistic soil distorted mound shapes. Secondly, the efficiency of the FE modelling in simulating the water diffusion and suction changes through the soil medium is verified against another case study of corresponding field observations. Thirdly, the FE modelling is applied to a hypothetical case study of a stiffened slab foundation on reactive soil, and the results are compared with those obtained from Mitchell's method.

As mentioned earlier, FE models developed in this thesis are carried out using the commercial software package ABAQUS. This particular software is used due to its ability to conduct a coupled flow-deformation analysis using a hydro-mechanical moisture-swell model capable of relating the soil reactivity to its degree of saturation and the ensuing suction. In this way, the soil distorted mound (a fundamental factor in the design of stiffened slab foundations on reactive soils) is intuitively calculated rather than pre-assumed, a weakness intrinsic to most current available design methods. The calculation of the soil distorted mound in the current FE modelling is based on accurate moisture contours initiated from a transient seepage analysis. The moisture contours generate the corresponding water pore pressure (following the soil-water characteristic curve utilised in the analysis), thereby the volumetric strain simulating the soil heave or shrinkage is readily generated.

3.3.1. Case Study 1: Formation of a Mound for a Soil with a Flexible Cover Membrane

In this case study, a 3D FE model is developed and verified against field measurements of soil mound formation for a flexible cover membrane resting on an expansive soil in Maryland, Near Newcastle, Australia. This case study involves a field monitoring program

carried out by Fityus et al. (1999) for the soil movement over a period of 5 years. Figure 3.9 shows the field test configuration and distribution of the monitored points located at the edge and centre of the flexible cover membrane. Similar to the site set-up, a peripheral beam of 300 mm × 500 mm is generated in the model and a load equivalent to 100 mm of sand is applied on top of the surface of the membrane. The study did not reveal any data for the average seasonal rainfall and evaporation at the site; therefore, these missing data are obtained from the Bureau of Meteorology of Australia (www.bom.gov.au) and shown in Figure 3.10. The geotechnical profile of the site is shown in Figure 3.11. The soil profile is comprised of 250-350 mm of silty topsoil underlain by high plasticity clay to a depth of approximately 1.0 m, followed by medium plasticity silty clay to a depth of approximately 2.3 m where highly to extremely weathered siltstone is encountered. There is no water table up to 5 m depth. The site is classified as highly expansive (H-class), following the Australian Standards AS 2870 (1996), with a characteristic surface heave (y_s) that ranges from 40 mm to 70 mm. In the 3D FE model, the active zone is taken to be 2.5 m, based on the soil stratification. As mentioned previously, the numerical analysis involves invoking the developed user defined subroutine USDFLD to achieve the soil modulus and suction dependency. Figure 3.12 shows variation of the suction profile and moisture content over the monitoring period.

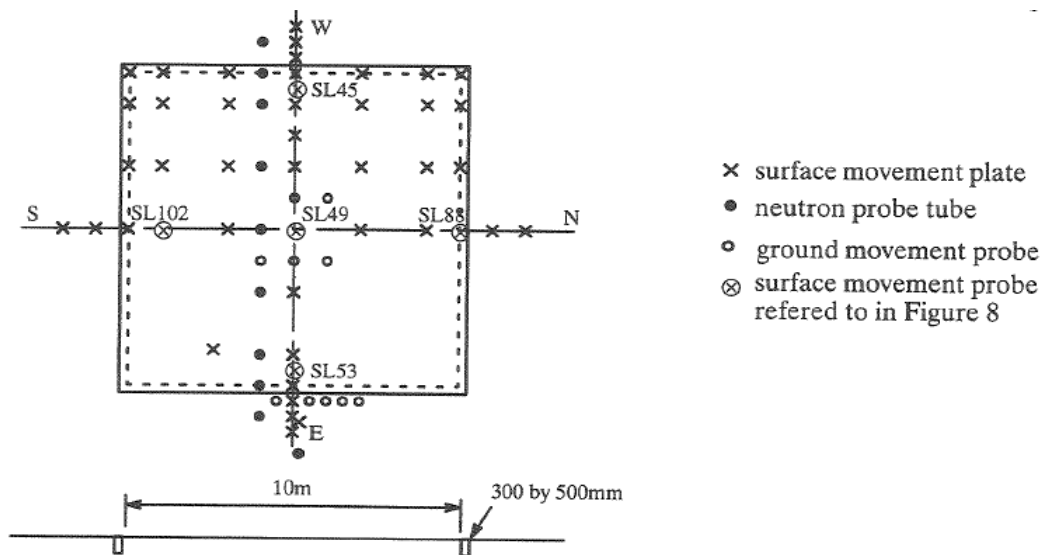


Figure 3.9: Plan and cross section of the monitored flexible cover membrane in Maryland, Near Newcastle, Australia (Fityus et al. 1999).

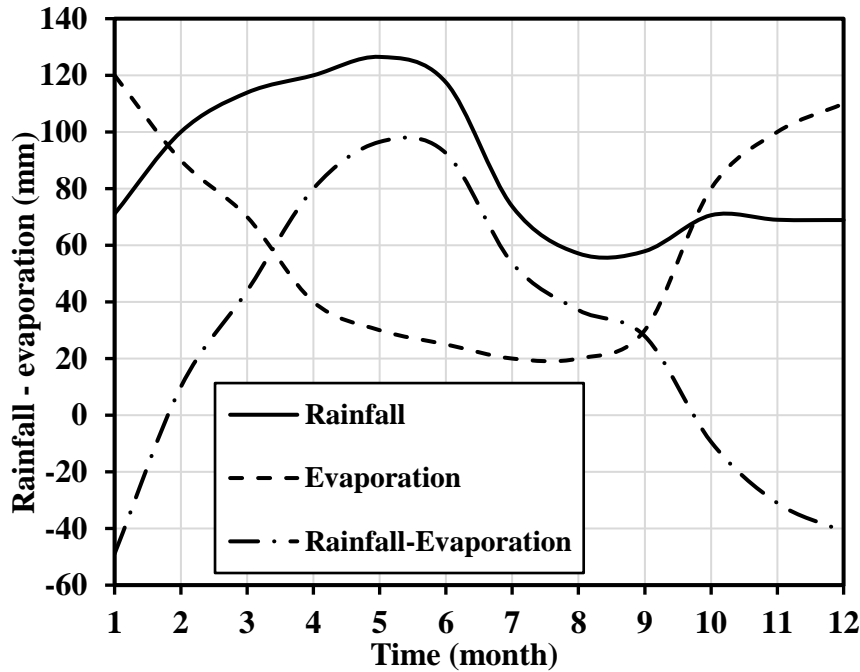


Figure 3.10: Rainfall and evaporation rates of Newcastle, Australia (www.bom.gov.au).

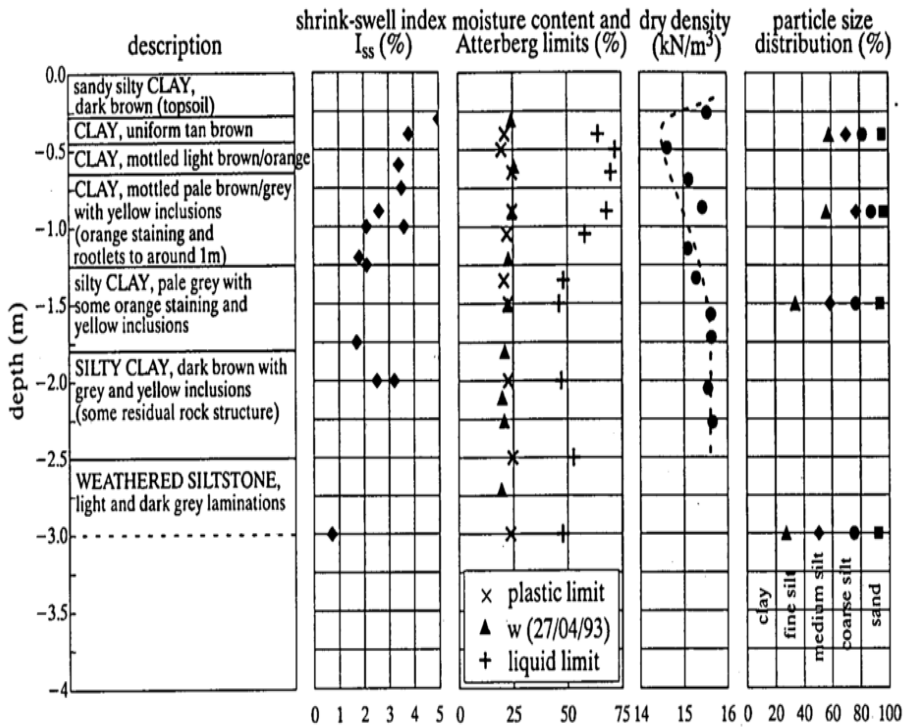


Figure 3.11: Geotechnical profile of the field site in Maryland, Near Newcastle, Australia (Fityus et al. 1999).

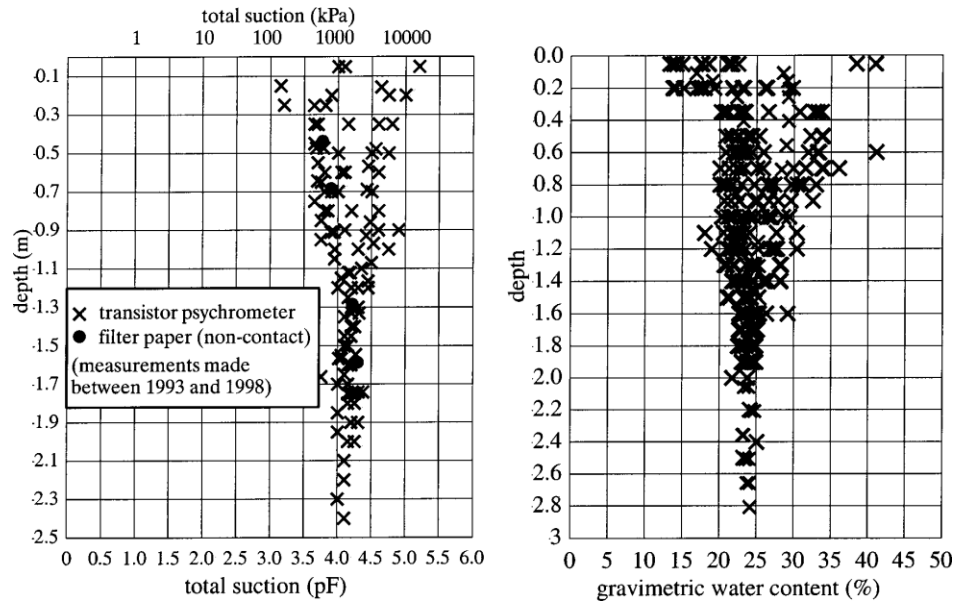


Figure 3.12: Profile of the total soil suction and water content of the field site in Maryland, Near Newcastle, Australia (Fityus et al. 1999).

There is no SWCC available in the geotechnical data, but based on the measured suction and gravitational water content data shown in Figure 3.12, some points in the SWCC could be predicted by considering a soil specific gravity (G_s) of 2.7 and a soil void ratio (e) of 1.2. The ISWCC proposed in Section 3.2.3.1 is then found to match the measured data fairly well, as shown in Figure 3.13, and is thus used in the FE analysis.

The moisture-swell information are also not available in the geotechnical data and the IMSC proposed in Section 3.2.3.2 with a maximum volumetric strain equal to 3% is thus used, as shown in Figure 3.14. For better prediction of the surface movement, the IMSC is adjusted to obtain a maximum volumetric strain at saturation values between 40-70 %.

The initial condition of the saturation is set according to the data obtained from the field tests, with a uniform suction over the whole depth of the soil mass equal to 4.70 pF and a degree of saturation of 40% following the ISWCC. The simulation is carried out in two steps as follows. Firstly, a geostatic analysis is performed in order to generate the in-situ stresses and nullify the soil deformation caused by the initial suction condition. Secondly, a transient flow-deformation analysis is conducted by applying a time dependent surface

load of precipitation and evaporation following the amplitude curve presented in Figure 3.10, repeated for a period of 5 years. It should be noted that the precipitation value is reduced to 30% owing to the presence of grass and trees in the site, which usually absorb 70% of the rainfall. A similar approach was adopted by Zhang et al. (2015) who estimated that the precipitation is usually absorbed by plants. A linear elastic model is used, since there is no need to consider plasticity in such analysis when the focus is on the mound formation. The soil mass is simulated using an 8-node brick, trilinear displacement, trilinear pore pressure element. Figure 3.15 shows a snapshot of the FE mesh used in this case study, including the soil mass and the ground perimeter beam; a double symmetry condition is used in the model (i.e. one-quarter of the model is used).

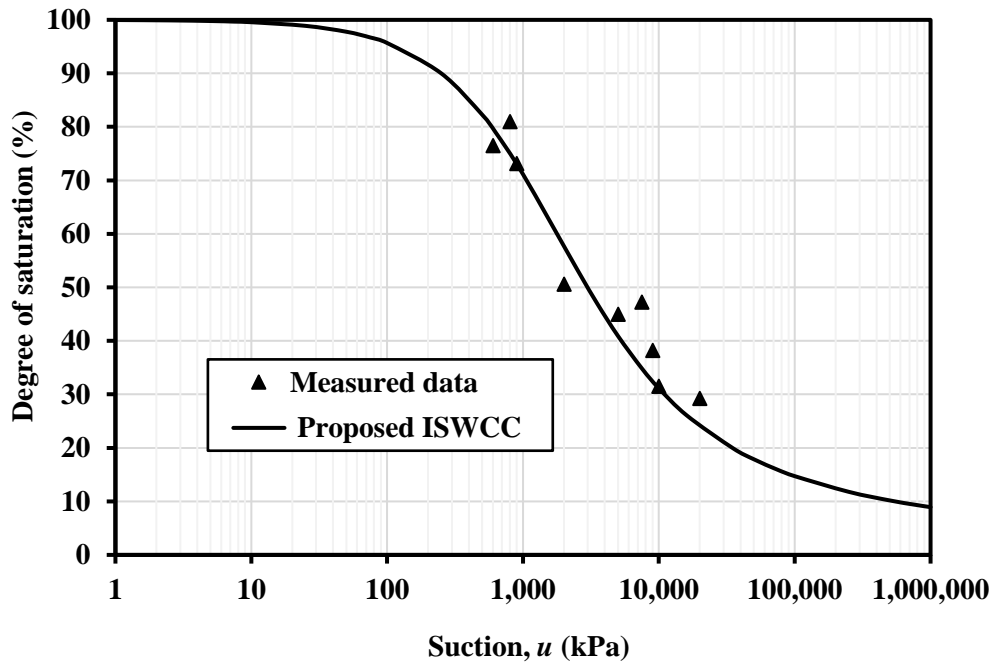


Figure 3.13: Proposed ISWCC used in Case Study (1).

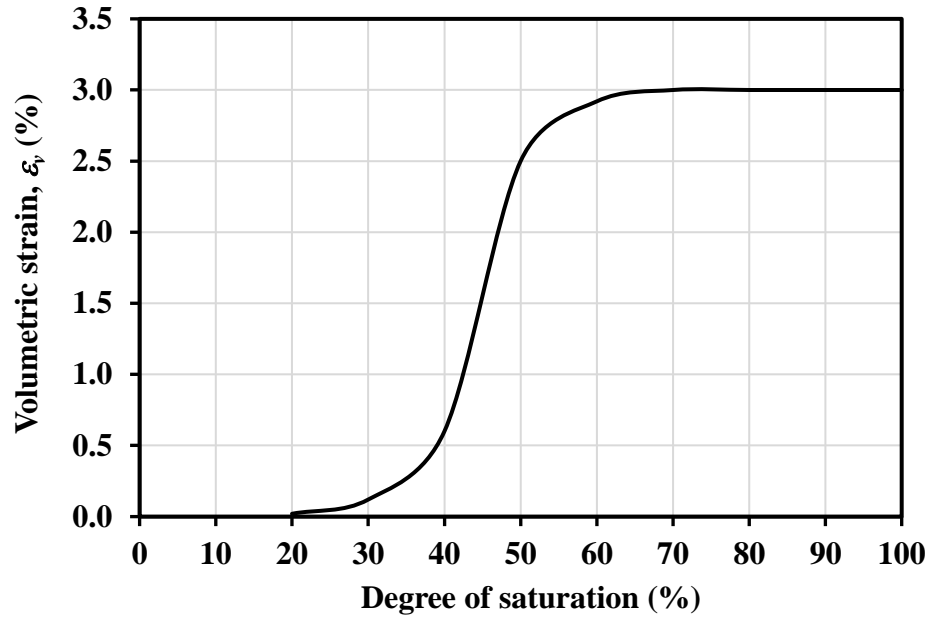


Figure 3.14: Idealised moisture-swell curve used in Case Study (1).

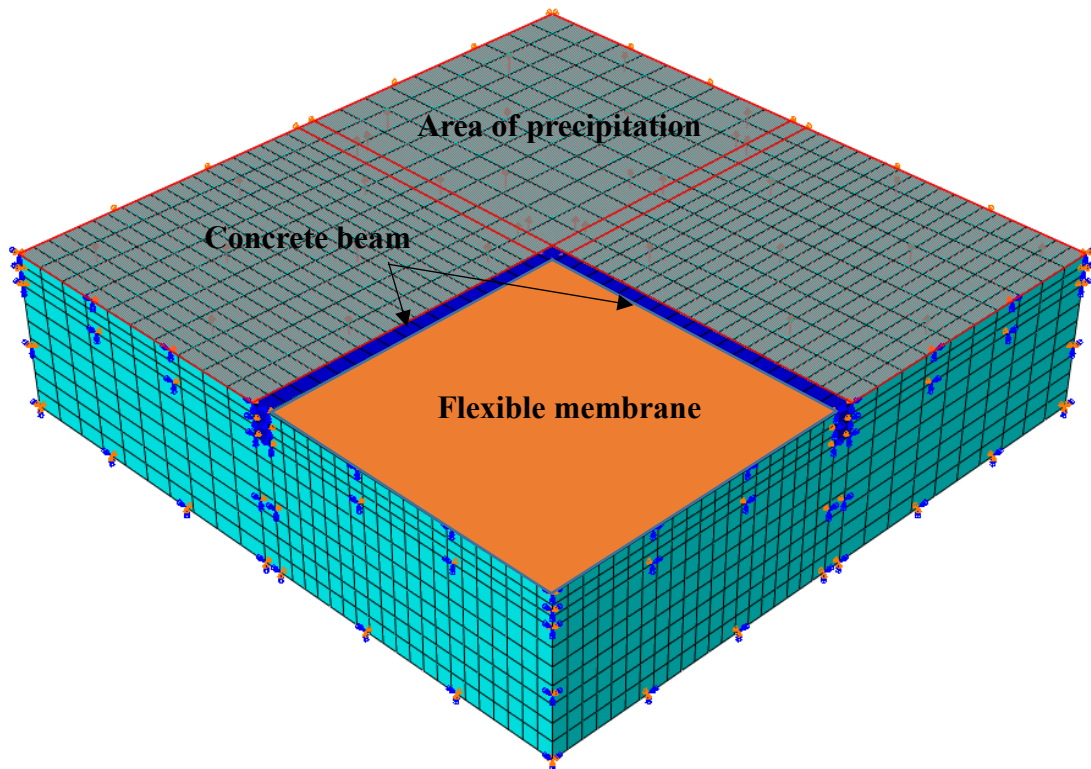


Figure 3.15: Snapshot of the finite element mesh and area of moisture change around the flexible cover membrane of Case Study (1).

In simulating the seepage numerically, the FE size, model boundaries and time increment have to be selected carefully to ensure accuracy of the results. Particularly critical is the choice of the initial time increment in the transient partially saturated flow problem to avoid spurious solution oscillations. The criterion used for a minimum usable time increment in the partial-saturation conditions is expressed as follows:

$$\Delta t > \frac{\gamma n^o}{6k_s k} \frac{ds}{du} (\Delta \ell)^2 \quad (3.11)$$

where:

- γ = specific weight of the wetting liquid;
- n^o = initial porosity of the soil;
- k = permeability of the fully saturated soil;
- k_s = permeability-saturation influence factor;
- ds/du = rate of change of saturation with respect to pore pressure as defined in the suction profile of the soil; and
- $\Delta \ell$ = typical element dimension.

In general, the size of the model (total soil mass) should be selected so that the boundary conditions have minimal effects on the output results. In this case study, the soil mass plan dimensions is selected with a clear length of 5.0 m away from each edge of the footing. The boundary conditions are set so that the bottom of the soil mass is restrained against the vertical movement, while the sides are restrained horizontally, allowing only for vertical strains. Since swelling can cause significant deformation with respect to the element size, geometric nonlinearity is adopted to account for the effect of large strains on the stiffness matrix formulation; this way the stiffness matrix is adjusted at every time increment when large deformation occurs with respect to the tolerance limits. Interaction properties are defined between the perimeter ground beams and surrounding soil, allowing for a friction contact with a penalty friction coefficient equal to 0.3.

Figure 3.16 shows a comparison between the field observations and FE results, for the movement of two points: one at the centre and another at the edge. It can be seen that the FE results are in relatively good agreement with the field observations. The two selected points experience continuous heave over time, with low tendency to settle even during the dry season, but the points show less tendency to heave towards the end of the observation period. It can also be seen that the point at the centre, being the least affected by the moisture change, suffered the least heave compared to that at the edge, which one would expect. This is attributed to the fact that the water propagates with time towards the centre of the membrane, and the heave at the centre approaches that of the edge at the end of the 5-year period. The difference in the heave values between the field observations and FE results may be due to the actual precipitation rates which may differ from the average rate used in the FE analysis.

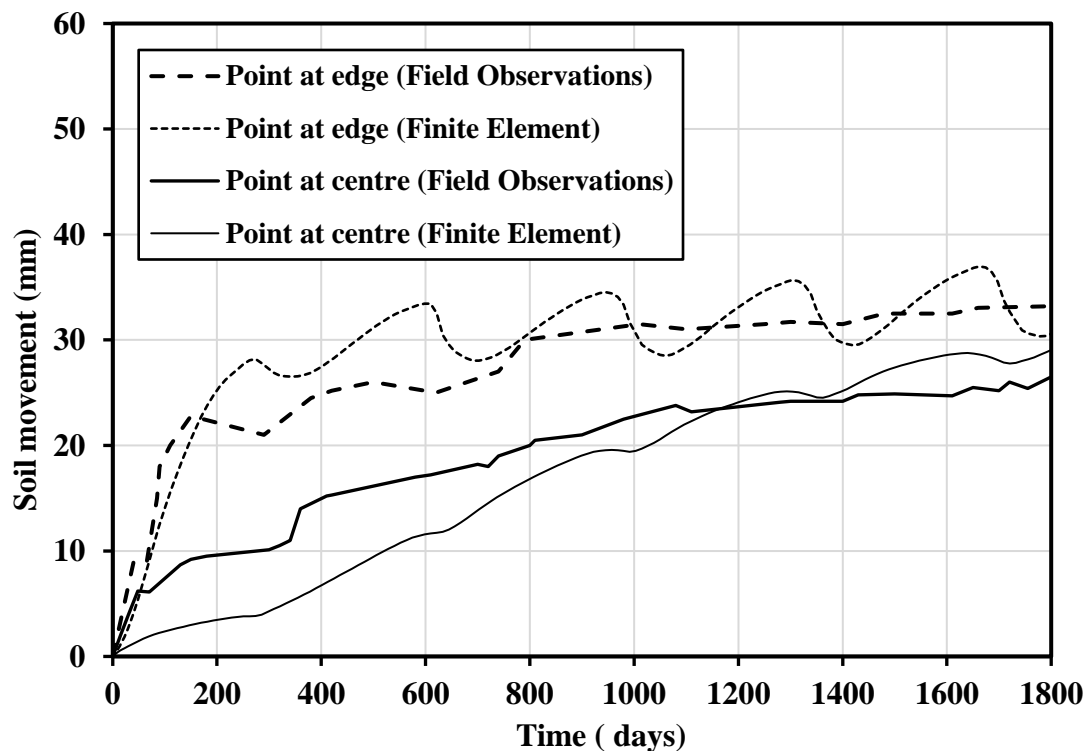


Figure 3.16: FE results showing movement with time for some selected points on the flexible cover membrane of Case Study (1).

Figures 3.17 shows the progress of the measured mound formation over the 5-year observation period, whereas Figure 3.18 shows the predicted mound formation obtained

from the FE analysis. It can be seen from Figure 3.17 that the ground outside the membrane undergoes repeated shrinkage and heave cycles due to seasonal variations. On the other hand, the area beneath the cover incurred consistent heave until the initial dry soil becomes wet and approaches its equilibrium water content. Figure 3.18 shows that the FE results are in general agreement with the field observations; the mound shapes have a prominent dish shape under all climate conditions. In the FE model, the water accumulated beneath the cover membrane cause progressive heave during the course of the 5-year observation period. Numerically, the mound profile shows a drop at the location of the perimeter beams (Figure 3.18). According to Fityus et al. (1999), the reduction in the swelling at the beam location is due to the reduction of the thickness of the welling soil mass by the depth of the perimeter beams, resulting in a reduction of the final surface heave at these locations.

The FE model reveals that the differential mound movement between the centre and edges continuously decreases due to the progressive soil wetting beneath the cover. The points located outside the cover membrane are exposed and therefore experience cycles of heave and shrinkage; however, their overall dominant movement is heave (Figures 3.17 and 3.18). The discrepancies between the FE results and field observations for the points located away from the cover in terms of the higher tendency to shrinkage in the dry season for the field data is most probably due to the presence of trees in the site. This greatly increases the suction and causes much higher shrinkage in the uncovered area than what is achieved using the evaporation only in the FE analysis; this phenomenon was discussed in detail in Chapter 2 (Section 2.2.2). In fact, the large settlements in the open areas cannot be achieved without the transpiration of the tree roots, which is not considered in the FE model.

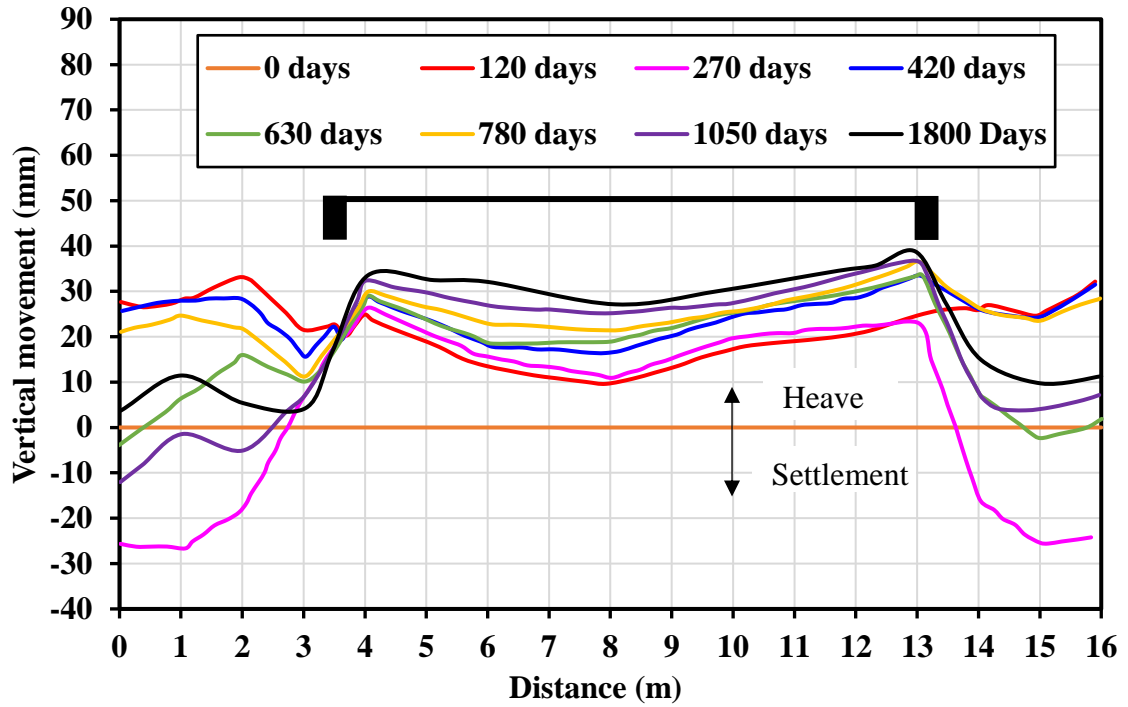


Figure 3.17: Observed mound formation with time for the flexible cover membrane of Case Study (1) (redrawn from Fityus et al., 1999).

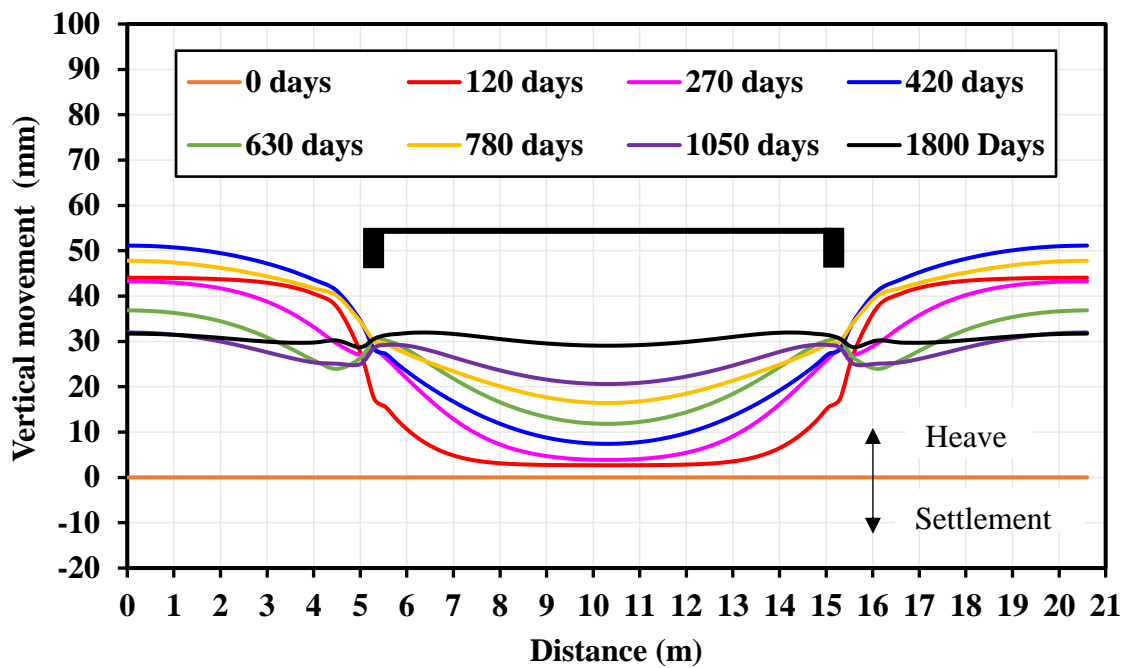


Figure 3.18: Variation of FE predicted mound formation with time for the flexible cover membrane of Case Study (1).

3.3.2. Case Study 2: Suction Simulation

In this section, the 3D model developed in this chapter is used to investigate the evolution of soil diffusion and suction variation with depth in response to the surface suction change, and the results are verified against field observations for a case study in Amarillo site, Texas. Description of the site conditions is provided by Wray (1990). The different soil strata identified in the site are shown in Figure 3.19. The third light grey silty clay stratum is underlain by another very similar light grey clay that extends to at least 27.5 ft (9.1 m) depth; this stratum is slightly sandy and less plastic. The active zone, below which no suction change is observed, is reported to be 13 ft (4.3 m). The mean values determined from multiple Atterberg limits tests, percent passing sieve No. 200, and the clay content for the site (determined by the hydrometer test) are reported for each foot in Table 3.4. The SWCC shown in Figure 3.20 is used in the FE modelling for this site. The SWCC is developed based on best fit for the measured data. Based on the site specific data listed in Table 3.4, the soil in this site is not highly reactive. Therefore, the IMSC curve is used for a maximum volumetric strain of 1.5%, as shown in Figure 3.21. The site has a covered area of 11.0 m × 15.8 m, and the model dimensions are extended to a distance of 5.0 m outside the cover membrane. The suction change over the 5-year period using Equation 3.4 is applied around the covered area, with an initial uniform suction of 4.5 pF. The double symmetry is again used in the FE model. Figure 3.22 shows the 3D FE model after highlighting the area of the surface suction change.

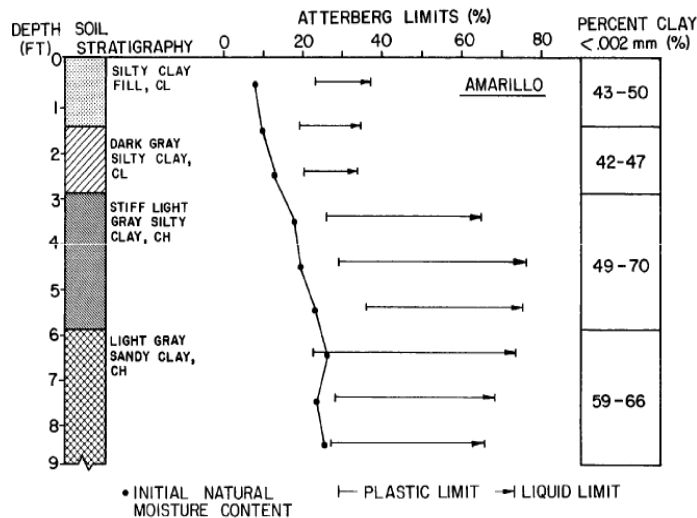


Figure 3.19: Stratigraphy and soil profile at Amarillo site, Texas (Wray 1990).

Table 3.4: Soil Properties at various depths at Amarillo site, Texas (Wray 1990).

DEPTH (ft)	MOISTURE CONTENT (%)		PLASTIC LIMIT (%)		LIQUID LIMIT (%)		PLASTICITY INDEX (%)		PERCENT PASSING No. 200 SIEVE (%)		PERCENT CLAY (<0.002 mm) (%)	
	Mean	(Range)	Mean	(Range)	Mean	(Range)	Mean	(Range)	Mean	(Range)	Mean	(Range)
0 - 1	8.3	(4.9-9.8)	23.2	(19.8-25.7)	37.3	(35.6-39.8)	14.1	(11.5-16.7)	62	(49-66)	47	(43-50)
1 - 2	10.5	(7.1-13.1)	19.8	(18.4-21.9)	35.0	(32.2-37.1)	15.3	(13.7-18.4)	57	(55-61)	46	(43-47)
2 - 3	13.8	(8.2-18.0)	20.5	(17.7-24.8)	33.9	(32.4-36.8)	14.1	(11.9-15.5)	59	(50-65)	42	(38-47)
3 - 4	17.8	(15.8-19.8)	26.0	(21.8-33.8)	64.3	(57.9-73.3)	38.4	(35.6-40.0)	82	(64-96)	62	(49-70)
4 - 5	19.7	(17.3-22.2)	29.3	(27.1-31.6)	77.2	(67.4-83.1)	54.2	(52.5-56.2)	75	(66-87)	59	(50-68)
5 - 6	21.7	(17.5-24.5)	36.5	(26.9-44.2)	75.8	(69.5-81.3)	39.3	(31.1-54.3)	83	(83-89)	63	(57-67)
6 - 7	24.2	(20.9-27.0)	31.0	(26.3-38.4)	74.3	(72.0-77.3)	43.4	(33.6-49.1)	83	(79-87)	64	(61-66)
7 - 8	22.7	(20.8-25.7)	28.6	(25.4-34.6)	68.7	(64.3-72.9)	40.1	(29.7-47.0)	78	(77-80)	64	(62-66)
8 - 9	23.5	(16.8-26.8)	27.4	(25.8-30.3)	66.3	(54.2-76.9)	34.8	(15.8-51.1)	81	(80-84)	61	(59-64)

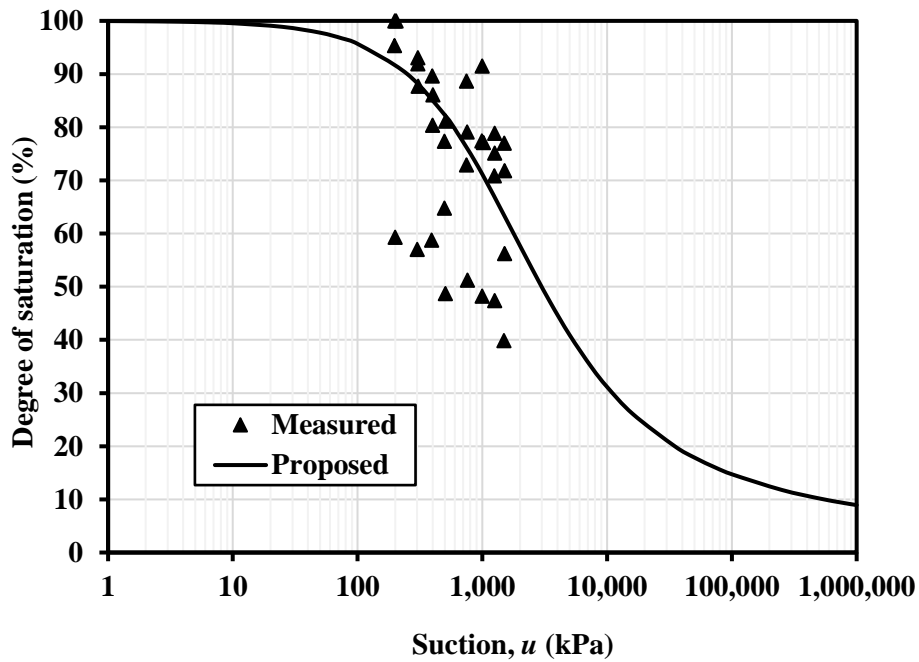


Figure 3.20: SWCC used in the FE modelling for Amarillo site, Texas, of Case Study (2).

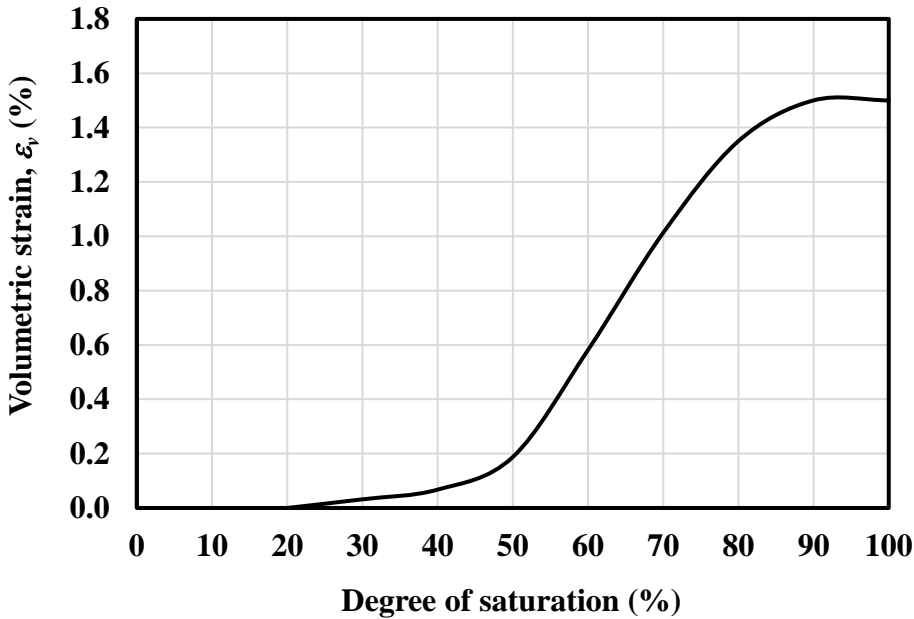


Figure 3.21: IMSC used in the FE modelling for Amarillo site, Texas, of Case Study (2).

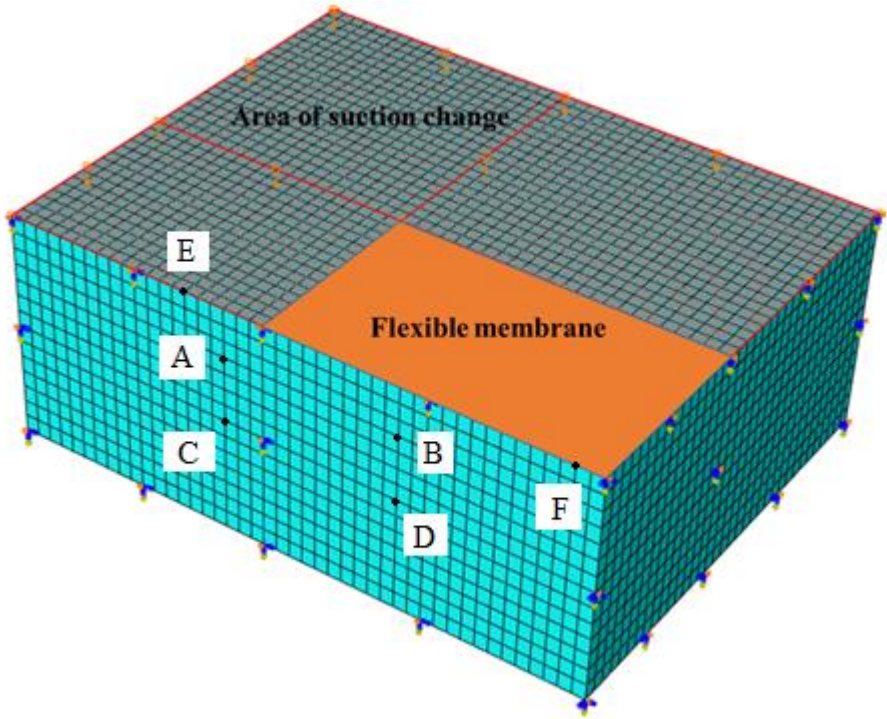


Figure 3.22: FE mesh and boundary of surface suction change used for modelling Amarillo site, Texas, of Case Study (2).

Figures 3.23 and 3.24 present results of the predicted and measured suction variation with time for points located at 0.9 m outside the covered area and 3.0 m inside the covered area, along the long dimension of the cover membrane, at depths of 0.9 m (points A and C) and 2.1 m (points B and D), respectively (shown in the model of Figure 3.22). In general, the predicted values of the suction change with time agree reasonably well with the measured data (the suction change diminishes over time and with depth), despite the fact that the measured values are slightly higher, presumably due to the presence of grass and cracks in the site. It should be noted that grass evapotranspiration increases the suction while cracks provide easy access for the surface water into the soil, hence, affecting the amount of diffusion. These factors contribute to the difference in the results between measured and predicted suction values at the points investigated.

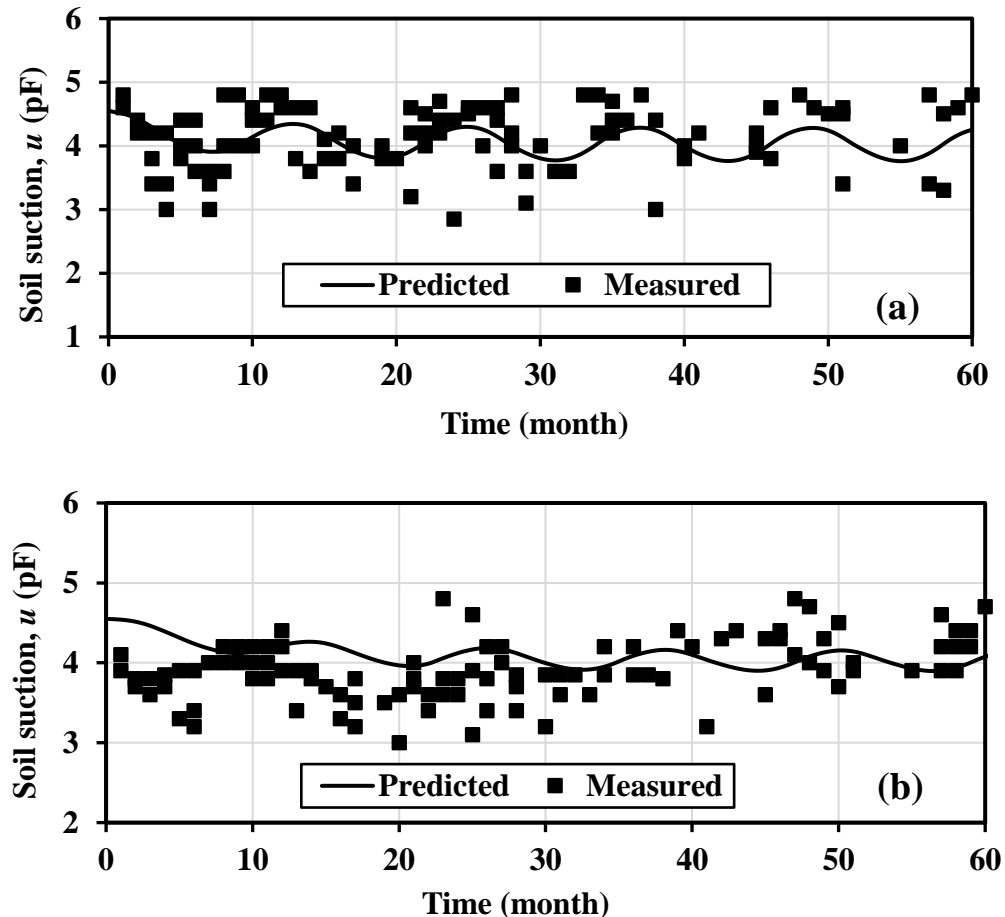


Figure 3.23: Measured versus FE predicted suction change at Amarillo site, Texas, for Case Study (2), for points located at 0.9 m outside the covered area at depths: (a) 0.9 m; and (b) 2.10 m.

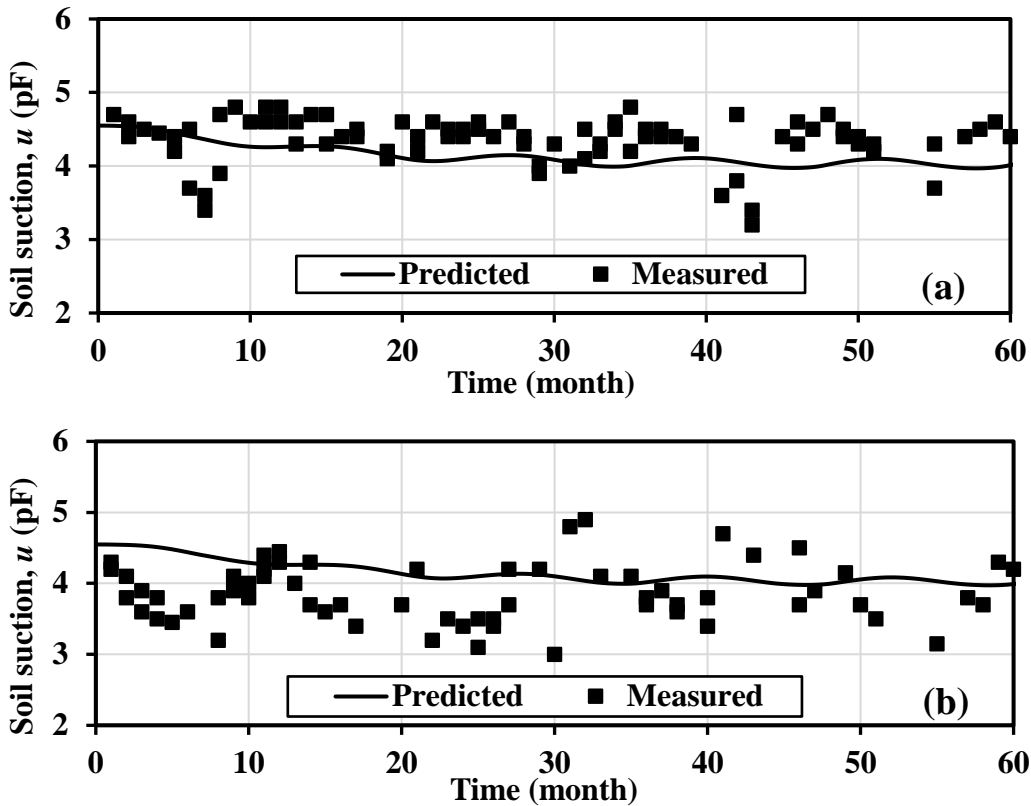


Figure 3.24: Measured versus FE predicted suction change at Amarillo site, Texas, of Case Study (2), for point located at 3.0 m inside the covered area at depths: (a) 0.9 m; and (b) 2.10 m.

Figure 3.25 presents a comparison between the measured and FE predicted soil movement with time for points located at the surface, 1.8 m outside the covered area along the longitudinal directions (point E), and a point located at 0.6 m from the centre of the covered area along the long axis (point F). Some disagreement may be noticed in Figure 3.25(a) between the measured and predicted data for the point located outside the cover area along the longitudinal direction. As explained earlier, this may be attributed to the presence of grass and cracks affecting the diffusion and violating the symmetry assumed in the FE modelling. On the other hand, Figure 3.25(b) demonstrates that the predicted movement with time for the point located outside the cover area along the short direction of the cover agrees fairly well with the measured data. For the point located at 0.6 m from the cover centre along its longitudinal direction, Figure 3.25(c) shows slight disagreement in the movement values with time for the FE prediction compared to the

measured data. Again, this difference may be due to the presence of grass around the cover, which absorbs the excess water from the seasonal rainfall, thereby, preventing the moisture to accumulate below the cover and keeping the soil dry with higher suction values and less movement. However, despite this discrepancy, the general trend of movement outside and inside the cover is almost similar, showing a continuous tendency of heave and suction reduction over time.

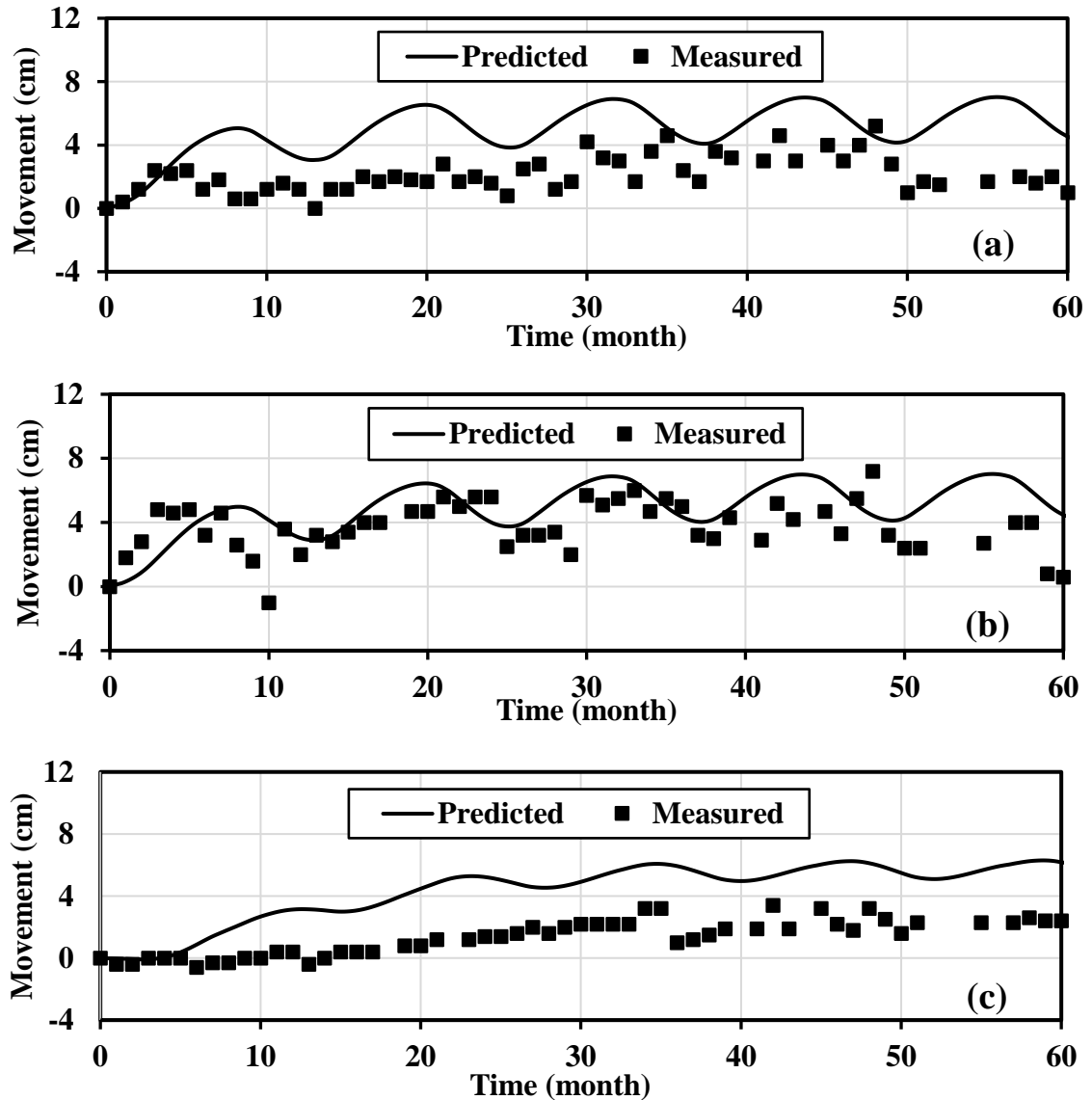


Figure 3.25: Measured versus FE predicted surface movements at Amarillo site, Texas, of Case Study (2), for points located: (a) 1.8 m outside the covered area along the longitudinal axis; (b) 1.8 m outside the covered area along the short axis; and (c) 0.6 m from the cover centre along the longitudinal axis.

3.3.3 Case Study 3: Hypothetical Stiffened Slab Foundation

In this section, the efficacy of the FE coupled flow-deformation analysis in simulating the behaviour of stiffened slab foundations for light-weight structures on expansive soils is investigated. To this end, the results of the FE modelling are compared with those obtained using Mitchell's method, which is one of the most commonly used design methods currently adopted by the Australian Standards AS2870 (2011). Since Mitchell's method adopts 2D analysis, a 2D FE model is firstly generated for verification with Mitchell's method, then a more realistic 3D FE model is developed for the purpose of comparison with the 2D analysis.

A hypothetical slab stiffened foundation of dimensions (16 m × 8 m) is assumed to support an articulated masonry veneer of a single storey building. The footing slab is 100 mm thick and stiffened with ground beams spaced at 4 m in each direction (i.e. a total of 5 beams having 8 m span and 3 beams having 16 m span). Each beam has a width of 300 mm; the question is to determine the depth that can sustain the internal forces induced by the volumetric change resulting from the moisture variation. The footing slab is resting on 4.0 m highly reactive soil of class H-D, following the classification of the Australian Standards AS 2870 (2011), with an expected surface characteristic heave (y_s) of 70 mm. The footing slab is subjected to a uniform load comprising the finishing and long term live loads of 1.5 kPa. An edge load of 6.0 kN/m is applied on the perimeter, simulating the combined loads from the edge walls and roof. For the articulated masonry veneer, the Australian Standards AS 2870 (2011) allow for a maximum footing differential movement equal to $L/400 \leq 30$ mm (where: L is the footing dimension in the direction under consideration). The differential mound movement (y_m) is considered in accordance with the Australian Standards AS2870 (2011) to be 70% of the characteristic surface heave (i.e. $y_m = 0.7 y_s = 49$ mm). A normal stiffness values of 1,000 kPa and 5,000 kPa are assumed to simulate the soil mound under the edge lift and edge drop, respectively, following the recommendation of the Australian Standards AS2870 (2011).

The footing stiffness (EI) required to limit the differential movement according to the standards is first calculated using Mitchell's method. By considering a concrete elastic

modulus = 15 GPa, the required beam depth of the stiffened footing is calculated. In the design of the stiffening beam for the case of edge heave (i.e. slab in compression), a *T*-section is considered with an equivalent flange width = $0.1 L$, whereas for the case of edge settlement (i.e. slab in tension) a rectangular section for the stiffened beam is considered. The calculation is carried out for the edge lift and edge drop for the footing two spans (i.e. 16.0 m and 8.0 m) separately. Table 3.5 summarises the required equivalent footing slab thickness (having same inertia as the stiffened slab) calculated from Mitchell's method.

Table 3.5: Summary results of Mitchell's method, Case Study (3).

Heave scenario	Footing equivalent rectangular thickness (m)	
	Long span	Short span
Edge lift	0.350	0.175
Edge drop	0.270	0.220

The same footing slab stiffness obtained from Mitchell's method are then used in the 2D FE model. In real design, the maximum inertia would be used; however, in this study the same slab inertia calculated by Mitchell's method for each heaving scenario is utilised for the purpose of comparison with the FE modelling. A linear elastic material is used for both the footing slab and the swelling clay layer, since the focus is on the volumetric response due to swelling (refer to Table 3.6). This assumption is reasonable, because light-weight structures are expected to produce stresses that are relatively low anyway. The permeability of the clay layer and rate of precipitation are assumed to be 1.0×10^{-9} m/s and 3.8×10^{-8} m/s (about 100 mm/month), respectively.

Table 3.6: Finite element modelling parameters of Case Study (3).

Material	Element type of FE mesh	Elastic modulus, E (GPa)	Poisson's ratio, μ
Swelling Clay	C3D8P: An 8-node brick, trilinear displacement, trilinear pore pressure element	Following user subroutine USDFLD (refer to Appendix A)	0.30
Footing Slab	S4R: a 4-node doubly curved shell element	15	0.16

The initial void ratio of the swelling clay is taken as 1.2. The idealised moisture-swell curve (IMSC) shown earlier in Figure 3.7 is used in the FE modelling. The flow period for the edge lift and the evaporation period for the edge drop are imposed to achieve the target differential mound movement (i.e. $y_m = 49$ mm), based on the pre-calculated slab thickness using Mitchell's method. The boundary conditions of the FE model are set to restrict the vertical displacement at the bottom of the model, while no lateral movement is allowed at the vertical sides. The initial saturation and suction conditions are set following the idealised soil-water characteristic curve (ISWCC) shown earlier in Figure 3.3, so that the initial conditions of the edge lift are set to be dry (i.e. saturation = 40 % and uniform suction = 4.69 pF) over the depth of the soil mass, whereas these conditions for the edge drop are set to be wet (i.e. saturation = 95% and uniform suction = 3.0 pF).

The time increment is chosen to allow for monitoring the mound formation and capturing the time required to achieve the target differential mound movement (i.e. $y_m = 49$ mm). The geometric nonlinearity is considered as explained in the previous sections. The modelling is performed in 3 steps. In the first step, a geostatic analysis is carried out as in the previous validation examples (Case Study 2) to eliminate the deformation of the initial suction and generate in-situ stresses. In the second step, the loading of the slab foundation is applied, including all uniform loads, edge line loads and self-weight. In the third step, the flow or evaporation inducing the edge lift or edge drop is activated. It should be noted that the self-weight of the slab foundation, which is simulated as a plate of uniform thickness, is adjusted to consider the actual self-weight of an equivalent stiffened slab

having the same inertia. Figures 3.26 and 3.27 show the deformed shape of the 2D FE model in the long and short footing slab dimensions under the edge lift and edge drop scenarios, respectively.

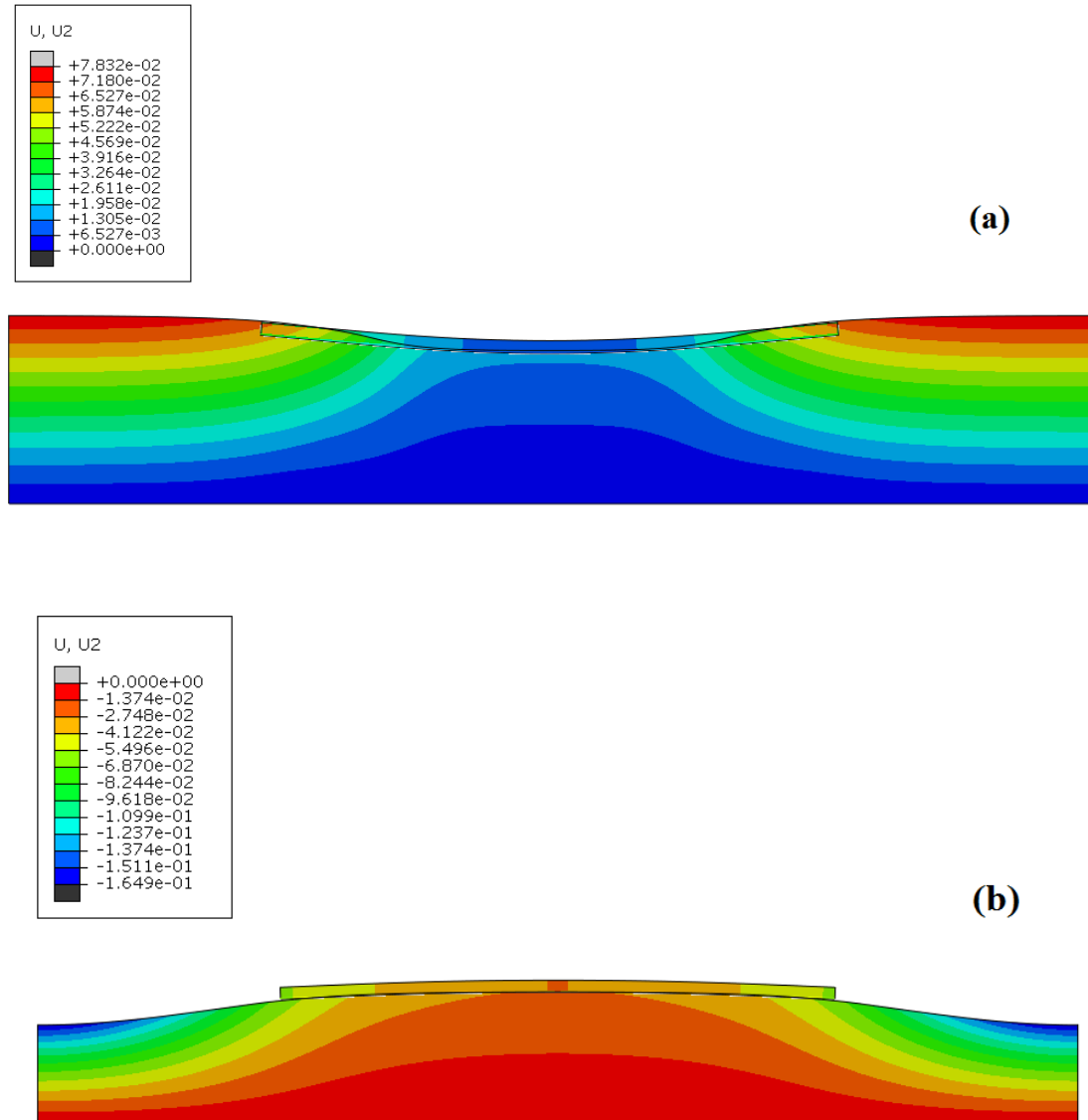


Figure 3.26: 2D FE model of Case Study (3) showing the soil and footing movements in the long span: (a) edge lift scenario; and (b) edge drop scenario (legend values in metres).

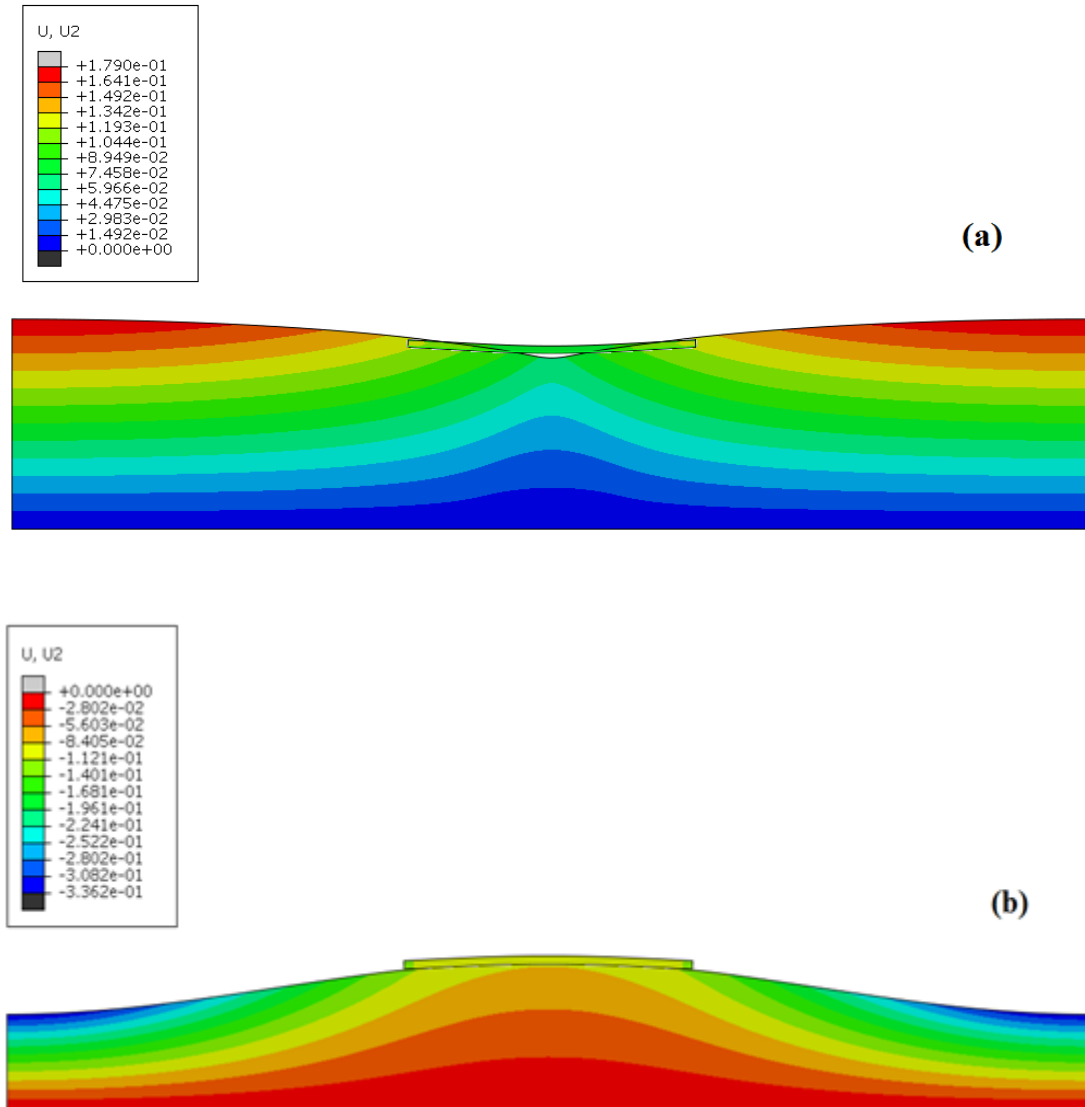


Figure 3.27: 2D FE model of Case Study (3) showing the soil and footing movements in the short span: (a) edge lift scenario; and (b) edge drop scenario (legend values in metres).

In reality, the mound shape forms a complicated three-dimensional surface (Pile 1984; Walsh and Walsh 1986). This particular feature highlights the power of the FE modelling in reproducing and carrying out a more realistic coupled 3D flow-deformation and stress analysis. This feature can overcome the 2D major assumption adopted by most existing methods, eliminating the need to undertake the analysis of the footing slab in each direction separately, which invariably violates the deformation compatibility of the soil

and footing. For instance, if a rectangular slab is analysed using 2D simulation, the analysis would consider different values for the maximum differential mound movement (y_m) in each direction, being the difference between the soil beneath the centre of the footing and the soil beneath the edge of the footing. However, under the more realistic 3D analysis, the footing would be analysed as a plate resting on a 3D mound having a maximum differential mound movement (y_m) as being the difference between the soil beneath the centre of the footing and the soil beneath the corner of the footing. Consequently, for the deformation compatibility, the maximum differential mound movement between the centre and edges (either in the long or short span) would be much less than the target (y_m) used in the 2D analysis and accordingly the required inertia that limits the deformation would thus be reduced.

In the 3D FE analysis, the same case study used in the 2D FE analysis, with the same maximum differential mound movement, is considered. However, the maximum differential mound movement is defined to be the difference in movement between the soil beneath the centre of the footing and the soil beneath the corner of the footing, as mentioned above. Figure 3.28 shows a snapshot of the 3D FE model.

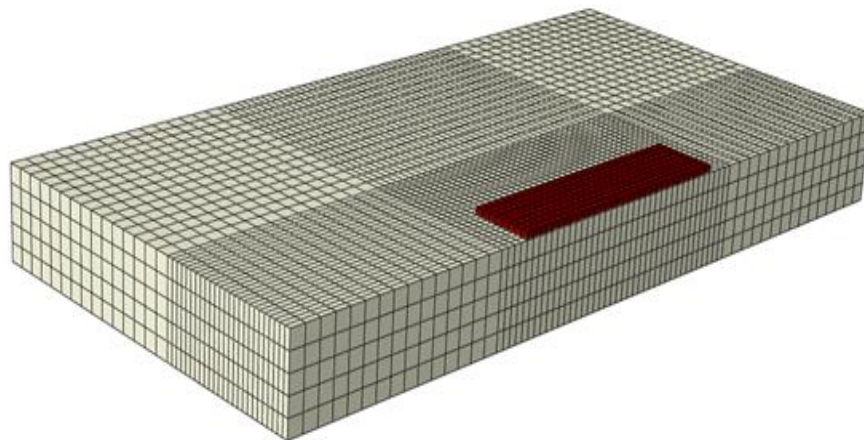
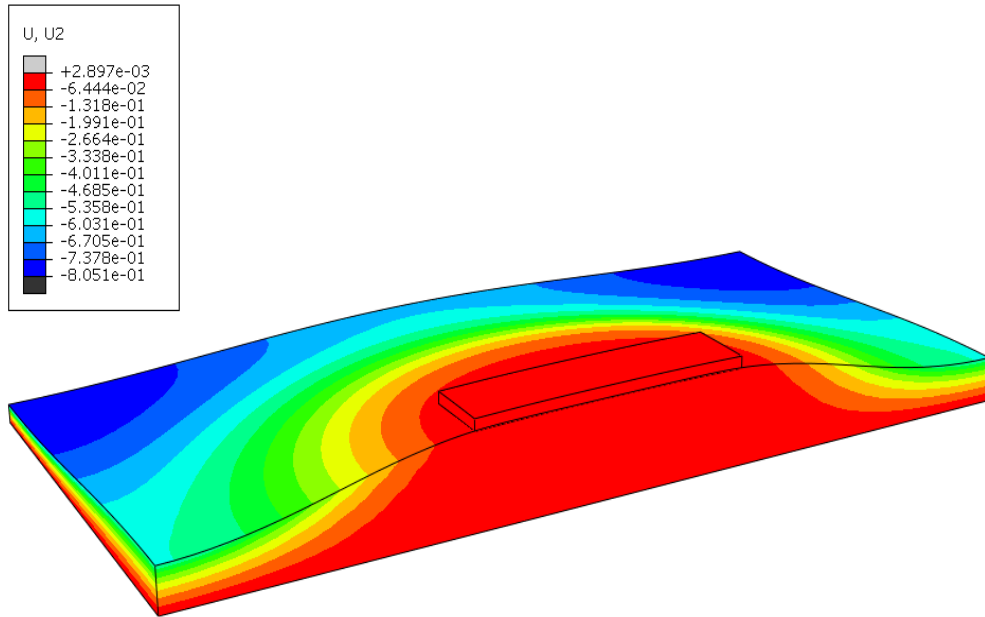


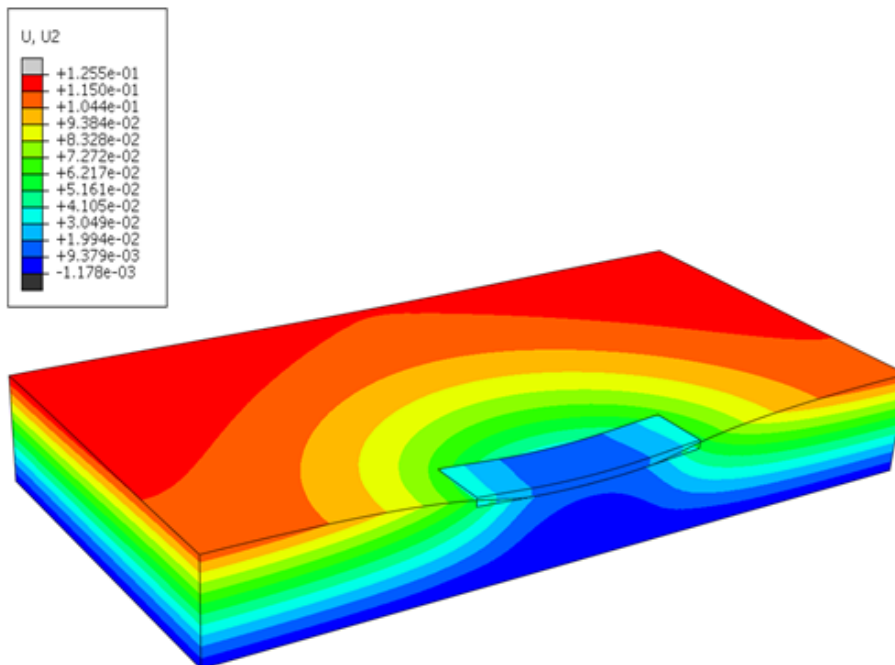
Figure 3.28: 3D FE model used of Case Study (3).

Under both the edge lift and edge drop scenarios, the maximum allowable footing movement (i.e. $L/400 \leq 30$ mm) is achieved by using a slab foundation of uniform thickness = 200 mm. Compared with the maximum thickness obtained from the 2D FE analysis (i.e. 350 mm), the 200 mm slab thickness obtained from the 3D represents a

considerable reduction in the slab foundation thickness for the loading conditions used. Figure 3.29 demonstrates the deformed shapes of the soil and footing in the 3D FE analysis.



(a)



(b)

Figure 3.29: Deformed shapes of 3D FE model of Case Study (3): (a) edge drop scenario; (b) edge heave scenario (legend values in metres).

A comparison is made in Figures 3.30-3.37 between the output obtained from Mitchell's method and the 2D and 3D FE analyses for a 1.0 m strip parallel to the flow direction, for both the edge lift and edge drop scenarios. It can be seen from all the figures that the overall results of the 2D FE analysis and Mitchell's method agree fairly well. Under the edge lift scenario, in the long footing span, the soil mound is flatter in the 2D FE analysis than in Mitchell's method, while in the short footing span both methods produced similar soil movements. The footing slab thicknesses calculated by Mitchell's method showed similar footing deformation to that of the 2D FE analysis. The bending moment obtained from Mitchell's method in the long direction slightly exceeds that obtained from the 2D FE due to the difference in the soil mound, which provided less support to the footing in Mitchell's method. Similar to the bending moment, the shear forces of the 2D FE analysis are very close to those obtained from Mitchell's method, for both the edge lift and edge drop scenarios.

The soil mound differential movements obtained from the 3D FE analysis are significantly less than those obtained from both the 2D FE analysis and Mitchell's method. This is attributed to the way the 3D FE analysis handles the differential movement between the centre and edges in each case, as mentioned above. In other words, the reason is due to the lack of compatibility in Mitchell's method and 2D FE analysis, compared with the 3D FE analysis. The compatibility effect is expressed in the slab spatial bending that distributes the acting loads rather than in one direction as in the 2D FE analysis and Mitchell's method. The end result is less internal forces for the 3D analysis under the edge lift and edge drop scenarios, as shown in the bending moment and shear force diagrams.

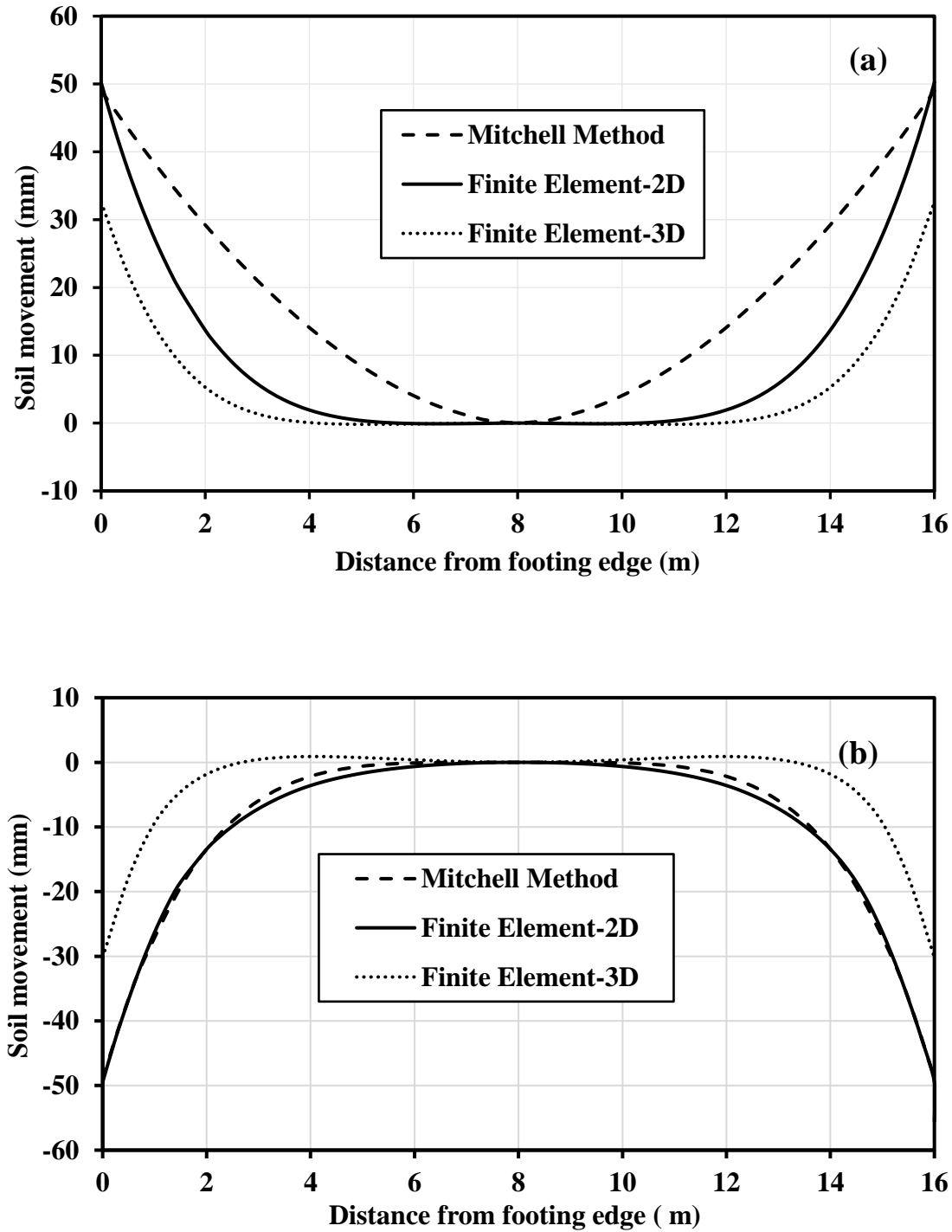


Figure 3.30: Comparison between Mitchell’s method, and 2D/3D FE soil movement results of Case Study (3) in the long footing span: (a) edge lift scenario; and (b) edge drop scenario.

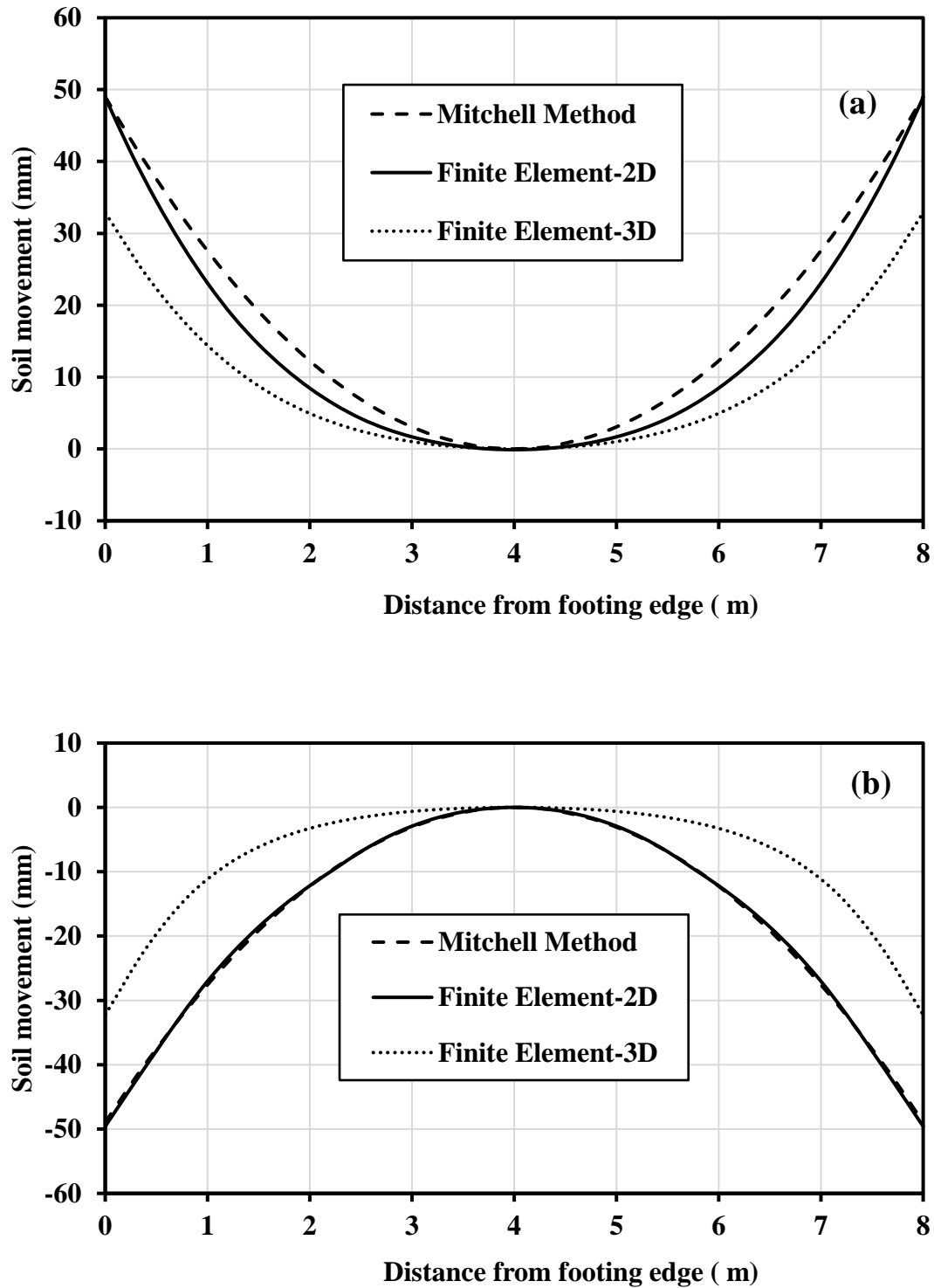


Figure 3.31: Comparison between Mitchell's method, and 2D/3D FE soil movement results of Case Study (3) in the short footing span: (a) edge lift scenario; and (b) edge drop scenario.

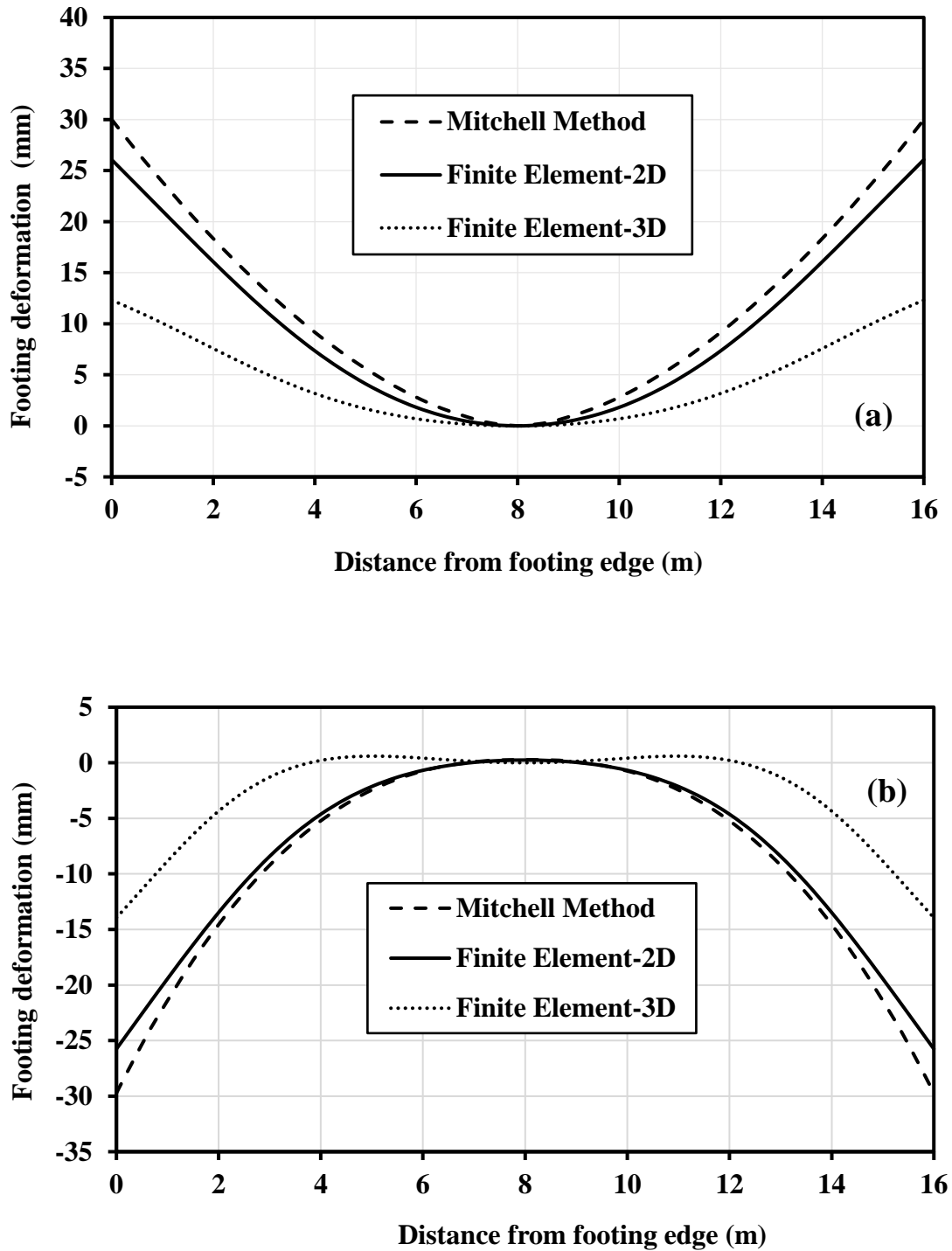


Figure 3.32: Comparison between Mitchell's method, and 2D/3D FE footing deformation results of Case Study (3) in the long footing span: (a) edge lift scenario; and (b) edge drop scenario.

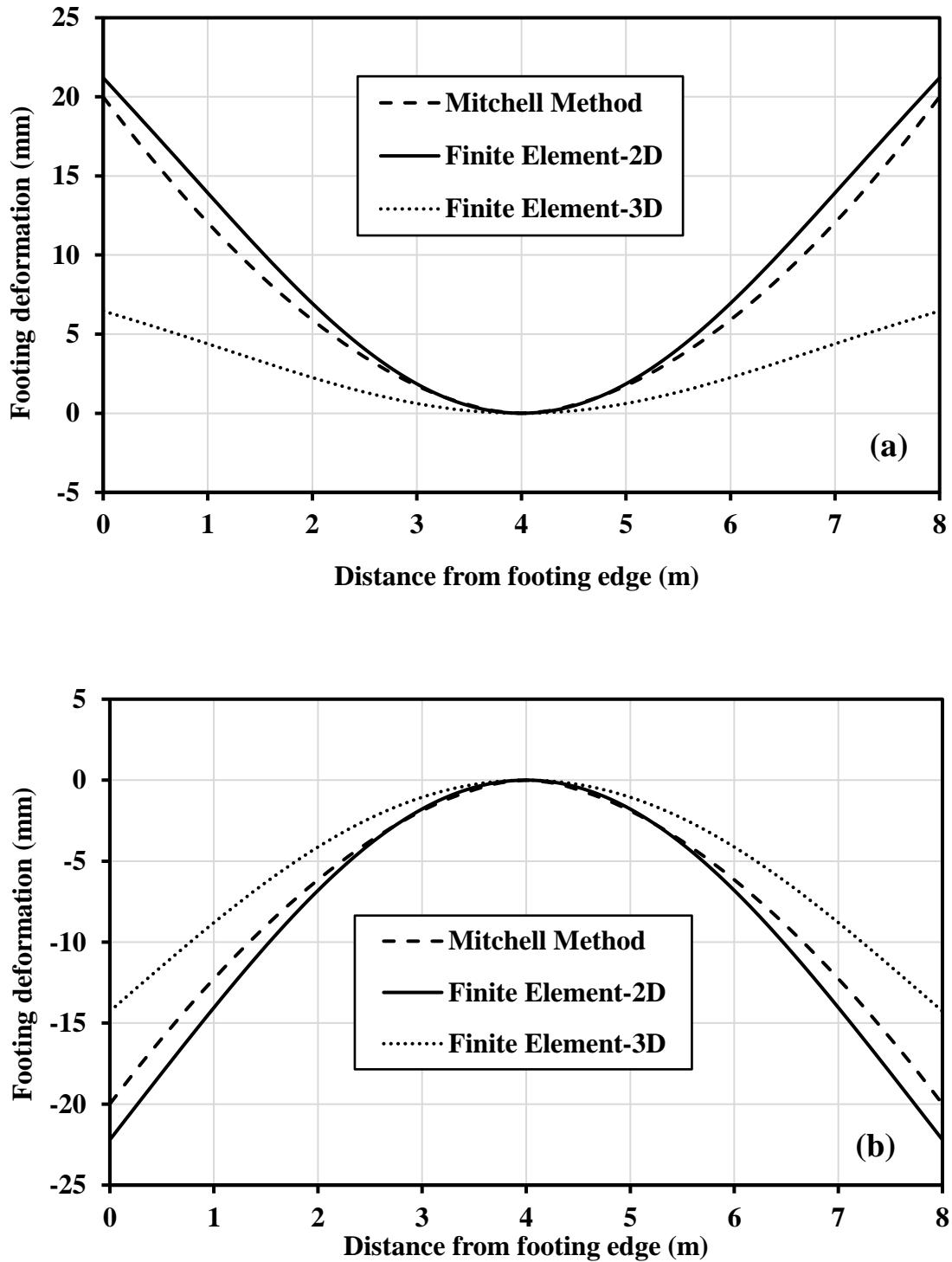


Figure 3.33: Comparison between Mitchell's method, and 2D/3D FE footing deformation results of Case Study (3) in the short footing span: (a) edge lift scenario; and (b) edge drop scenario.

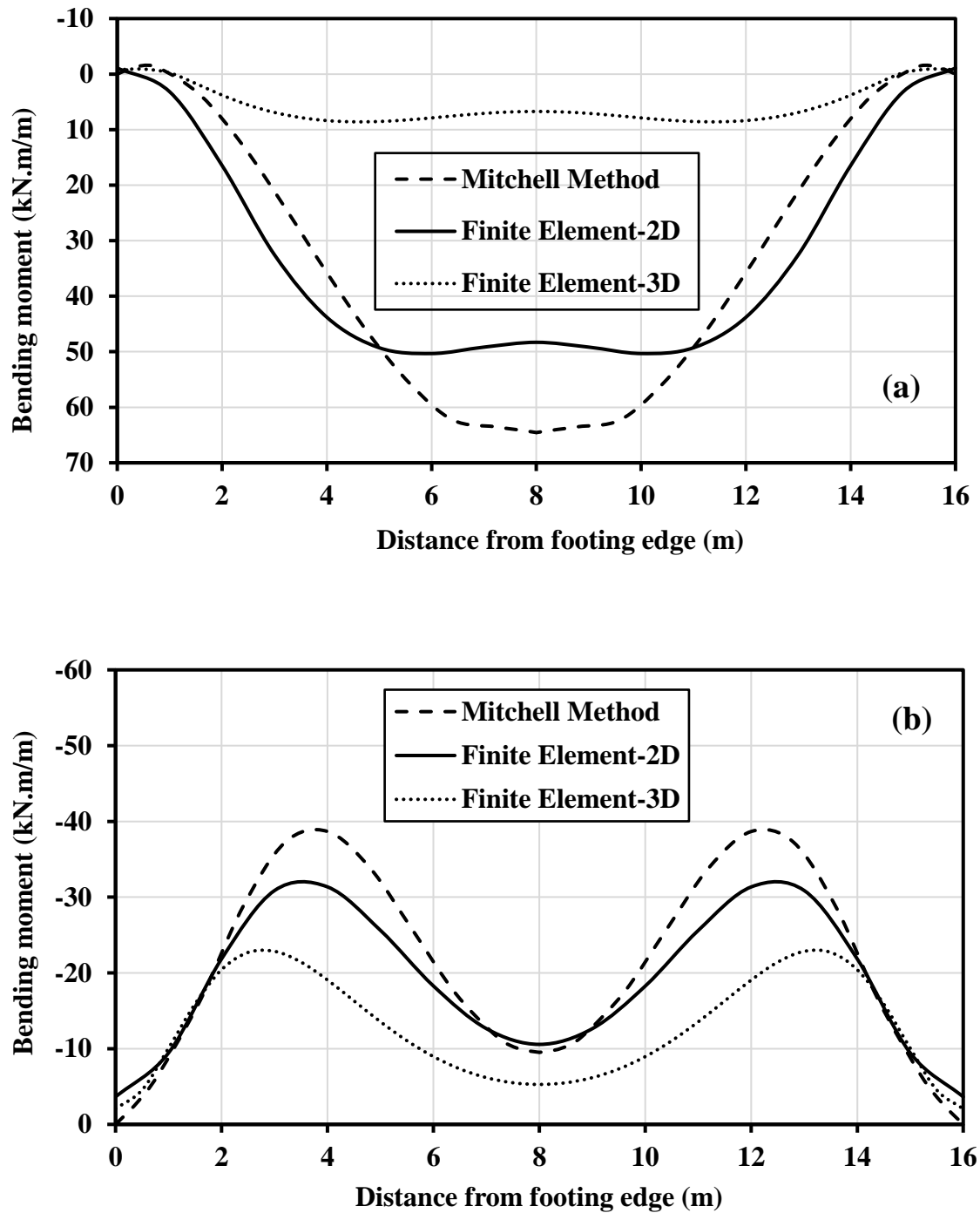


Figure 3.34: Comparison between Mitchell’s method, and 2D/3D FE bending moment results of Case Study (3) in long footing span: (a) edge lift scenario; and (b) edge drop scenario.

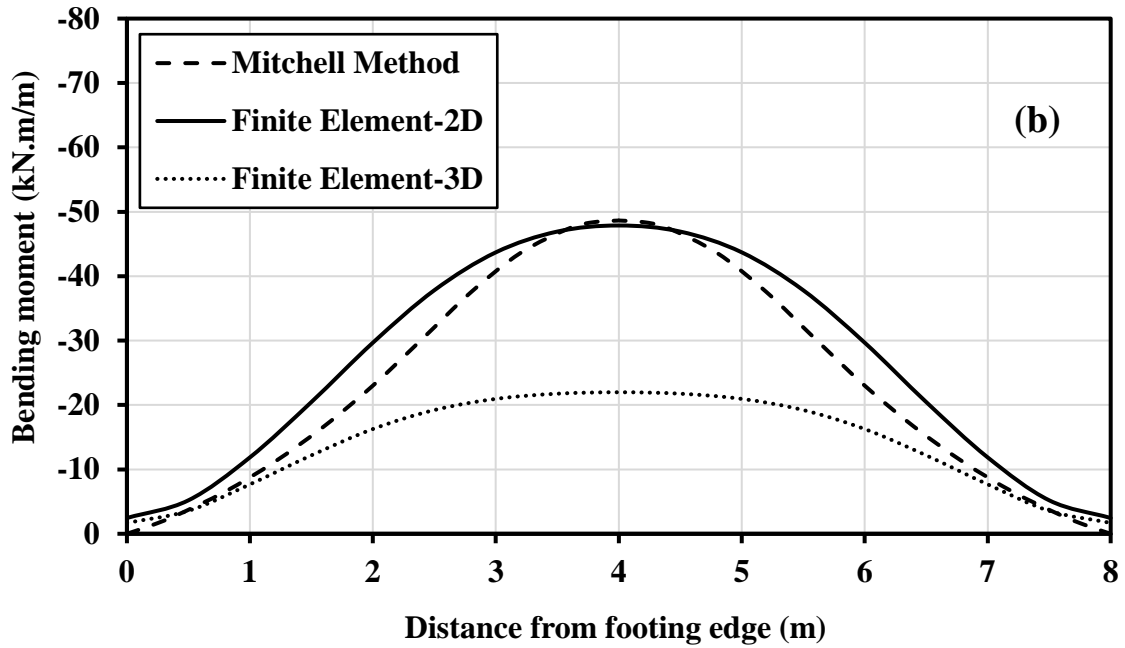
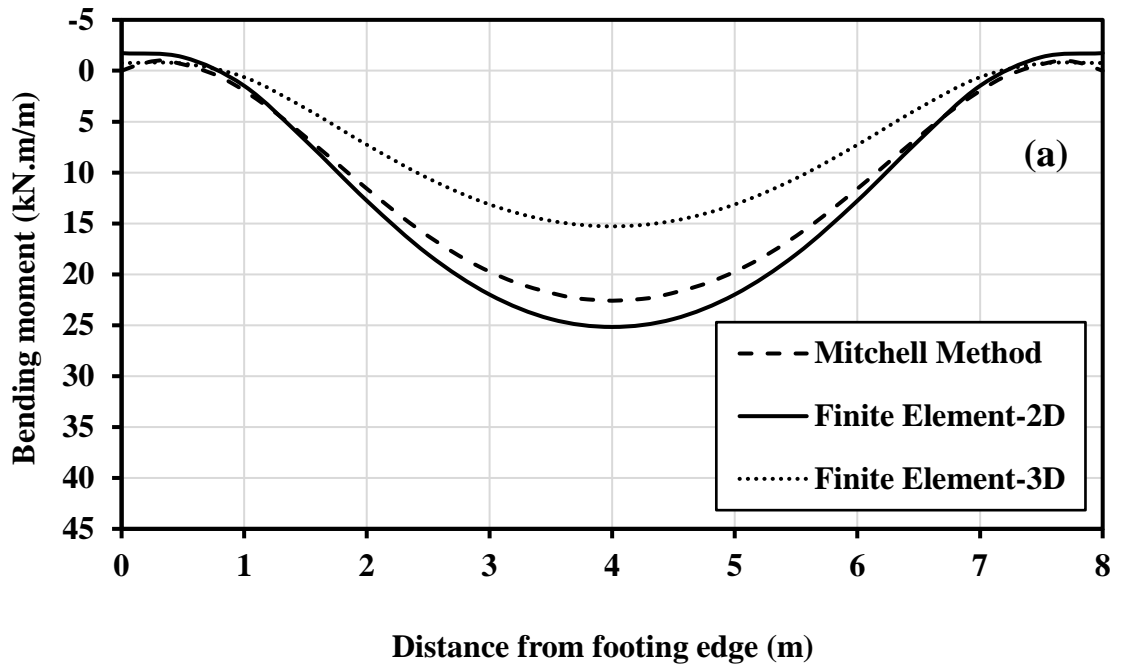


Figure 3.35: Comparison between Mitchell's method, and 2D/3D FE bending moment results of Case Study (3) in the short footing span: (a) edge lift scenario; and (b) edge drop scenario.

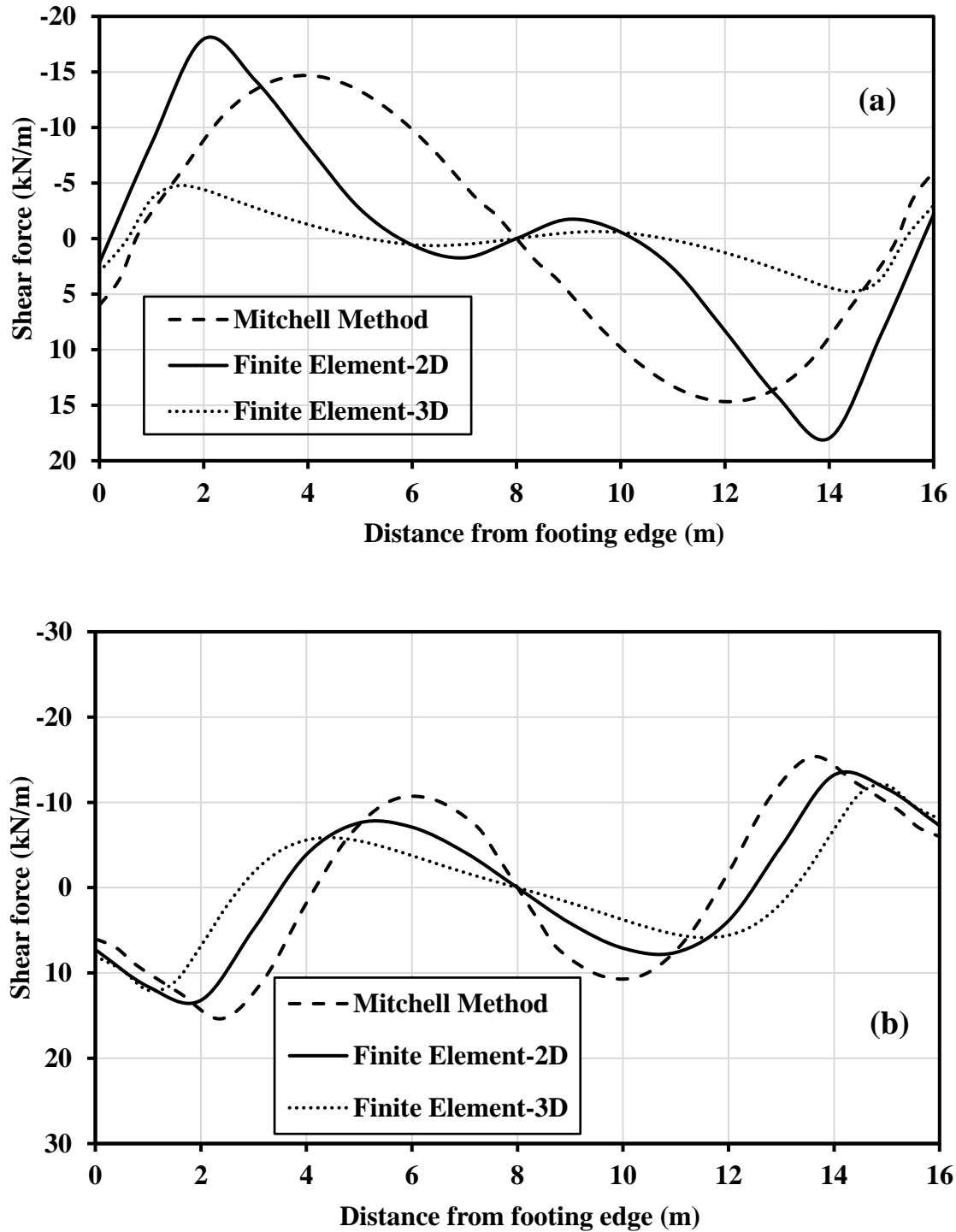


Figure 3.36: Comparison between Mitchell’s method, and 2D/3D FE shear force results of Case Study (3) in the long footing span: (a) edge lift scenario; and (b) edge drop scenario.

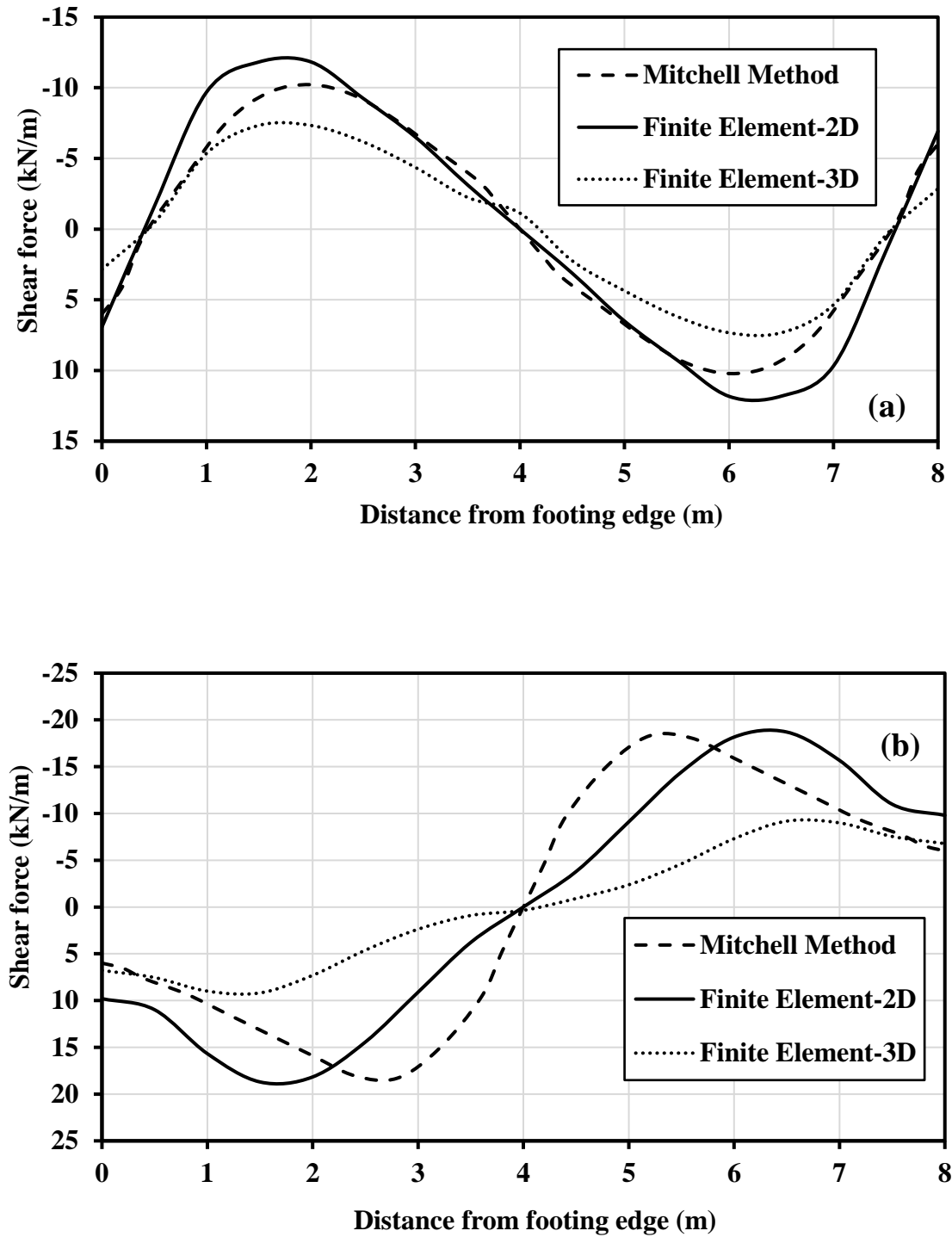


Figure 3.37: Comparison between Mitchell’s method, and 2D/3D FE shear force results of Case Study (3) in the short footing span: (a) edge lift scenario; and (b) edge drop scenario.

3.4 EFFECT OF FLOW-DEFORMATION PARAMETERS ON SOIL MOUND

The idealised soil-water characteristic curve (ISWCC) and moisture-swell curve (IMSC) were used in some of the previous case studies assuming that they can logically describe the behaviour of unsaturated clays. However, it is believed that the use of different SWCC and MSC than the idealised ones may have an impact on the formation of the soil mound with time and the corresponding final soil movement and footing internal forces. Consequently, in this section, the effect of using different SWCC and MSC on the mound shape and behaviour of slab foundation is investigated for the slab foundation presented in Case Study 3 (Section 3.3.3). For this purpose, this case study is re-analysed using different curves of SWCC (refer to Figure 3.38) and MSC (refer to Figure 3.39) than the idealised ones previously used in Section 3.3.3, and the difference is presented and discussed. The analysis using the new curves (i.e. Figures 3.38 and 3.39) is denoted herein as Group 1 (G1), whereas the analysis using the idealised curves (Figures 3.3 and 3.7) is denoted as Group 2 (G2). Table 3.7 shows the different flow-deformation group parameters used for the comparison.

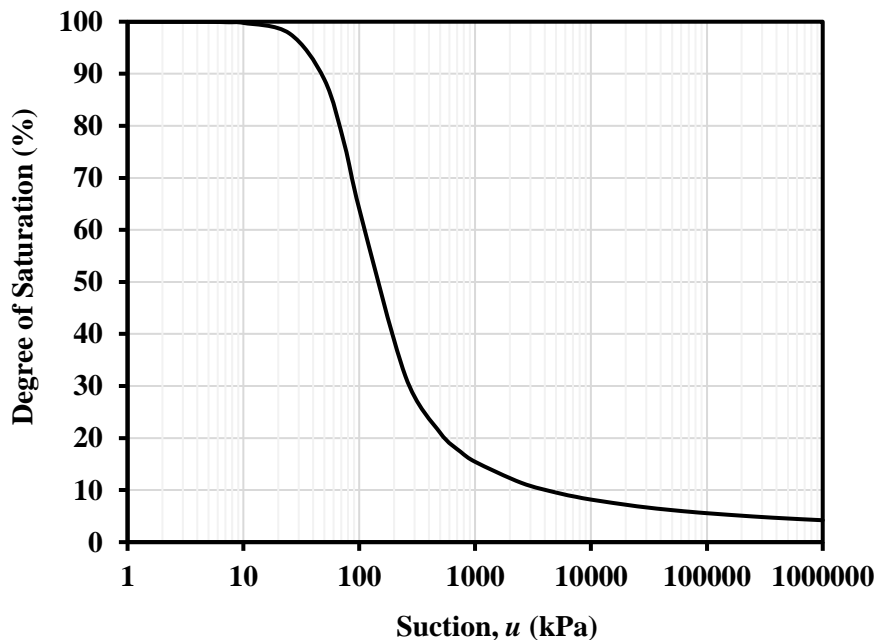


Figure 3.38: SWCC used for analysis of Group 1.

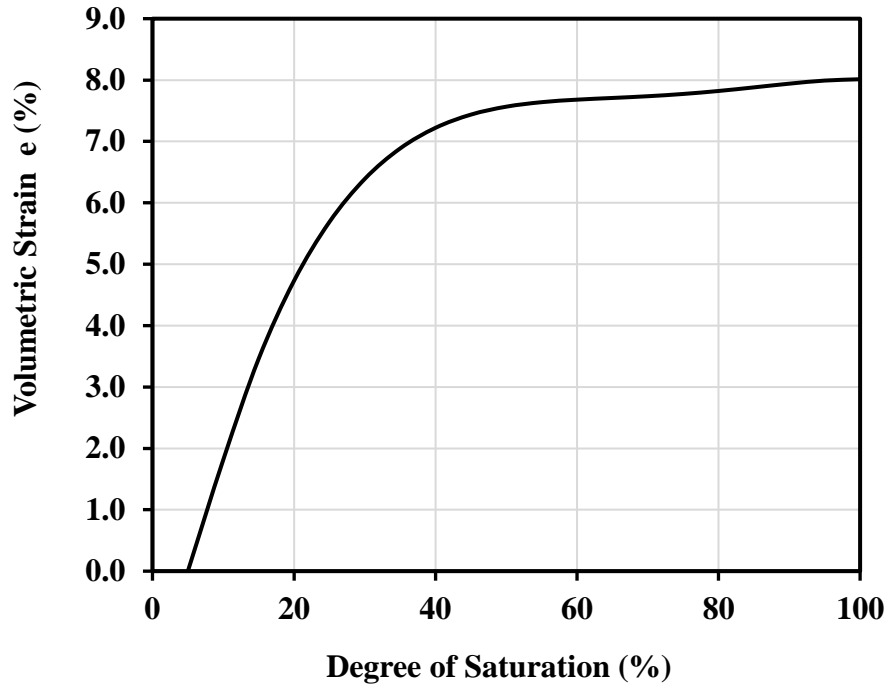


Figure 3.39: Moisture-swell curve used for analysis of Group 1.

Table 3.7: Flow-deformation parameters used in the comparison.

Group	SWCC	MSC	k_{sat} (m/s)	Initial suction, u (Pf)	Initial saturation, S (%)
G1 (edge drop)	Figure 3.38	Figure 3.39	5×10^{-8}	2.7	89
G1 (edge lift)	Figure 3.38	Figure 3.39	1×10^{-8}	4	15
G2 (edge drop)	Figure 3.3	Figure 3.7	5×10^{-10}	3.4	90
G2 (edge lift)	Figure 3.3	Figure 3.7	1×10^{-9}	4.7	41

The initial conditions of the soil degree of saturation and suction are modified in the new analysis following the new SWCC. As can be seen in Table 4.1, the soil permeability (k_{sat}) has to be changed since the new SWCC has a different slope from that of the ISWCC, which has a direct effect on the equation of flow (refer to Section 3.2.3.3). Therefore, in order to achieve the same target (y_m) of 49 mm used in Case Study 3, the saturated permeability is changed. It has to be noted that the ideal value of (k_{sat}) is the one that maintains the initial conditions of the degree of saturation and soil suction beneath the centre of the slab foundation nearly unchanged, for a complete cycle of the edge lift or edge drop. If the soil beneath the centre of the footing suffers a significant change in the initial conditions of moisture and suction, it means that the permeability used is too high, which can be reflected in the soil movement at the centre of slab foundation. For example, a differential mound movement of ± 50 mm can be achieved if the soil movement at the corner of the slab foundation is ± 100 mm, while the soil movement at the centre of the slab foundation is only ± 50 mm. Similarly, a differential mound movement of ± 50 mm can also be achieved if the movement at the corner of slab foundation is 52 mm, while the movement at the centre is ± 2 mm. Although both cases achieve the target differential mound movement of ± 50 mm, the first approach would have large deformation at the centre, indicating that the used permeability is too high and the mound shape produced is thus not representative. On the contrary, for the second case, the soil beneath the centre of the footing would move by a small amount, indicating a successful choice of the value of soil permeability.

By re-analysing the 3D FE model of the slab foundation of Section 3.6 using the parameters in Group 1 (G1), the 200 mm footing thickness is found to be satisfactory in limiting the footing differential movement to 30 mm, similar to the findings obtained from the parameters in Group 2 (G2), with an accuracy of $\pm 6\%$. Figure 3.40 shows the progress of the soil and footing diagonal differential movement with time, measured between the centre and corner of the slab footing for the edge lift scenario (Figure 3.40a) and edge drop scenario (Figure 3.40b), for G1 and G2. It should be noted that the time required to achieve the target differential mound movement ($y_m = 49$ mm) is highly dependent on the flow-deformation input parameters, mainly the saturated permeability and the slope of the

SWCC (refer to Equation 3.3). However, when the target ($y_m = 49 \text{ mm}$) is achieved, the soil movement beneath the centre of the footing is found to be minimum for both groups, indicating successful simulation of the problem despite the difference in the transient flow-deformation data. This can be seen in the change in suction with time for points at the corner and at the centre of the slab foundation, as shown in Figure 3.41, for both G1 and G2. The change in suction beneath the footing centre is minor with respect to the amount of suction change beneath the footing corner, starting from the beginning of the analysis until a time at which the target mound movement is achieved. This trend is applicable for both the edge lift and edge drop scenarios.

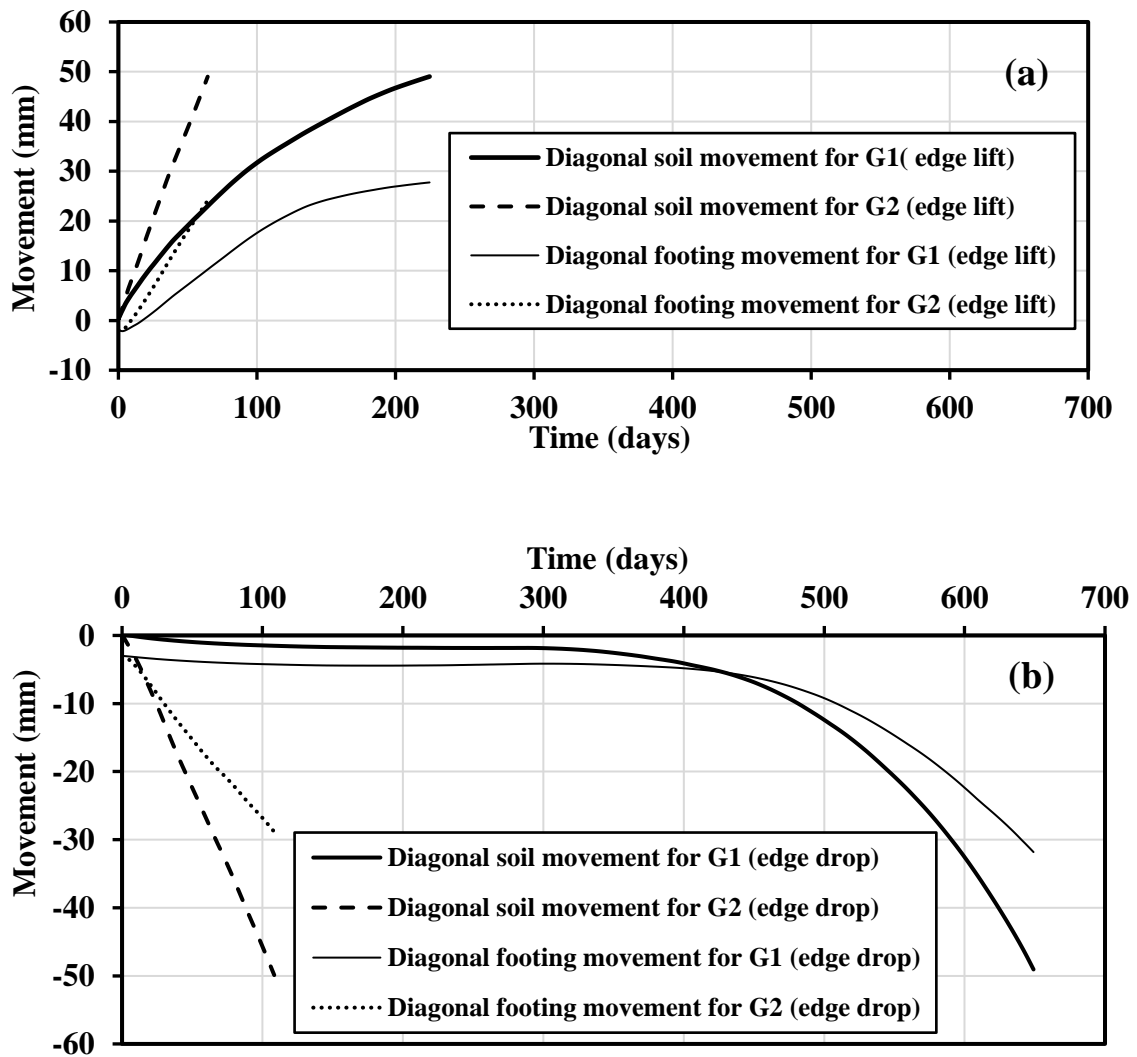


Figure 3.40: Soil and footing diagonal differential movement progress with time of flow-deformation data for group G1 and G2: (a) edge lift; and (b) edge drop.

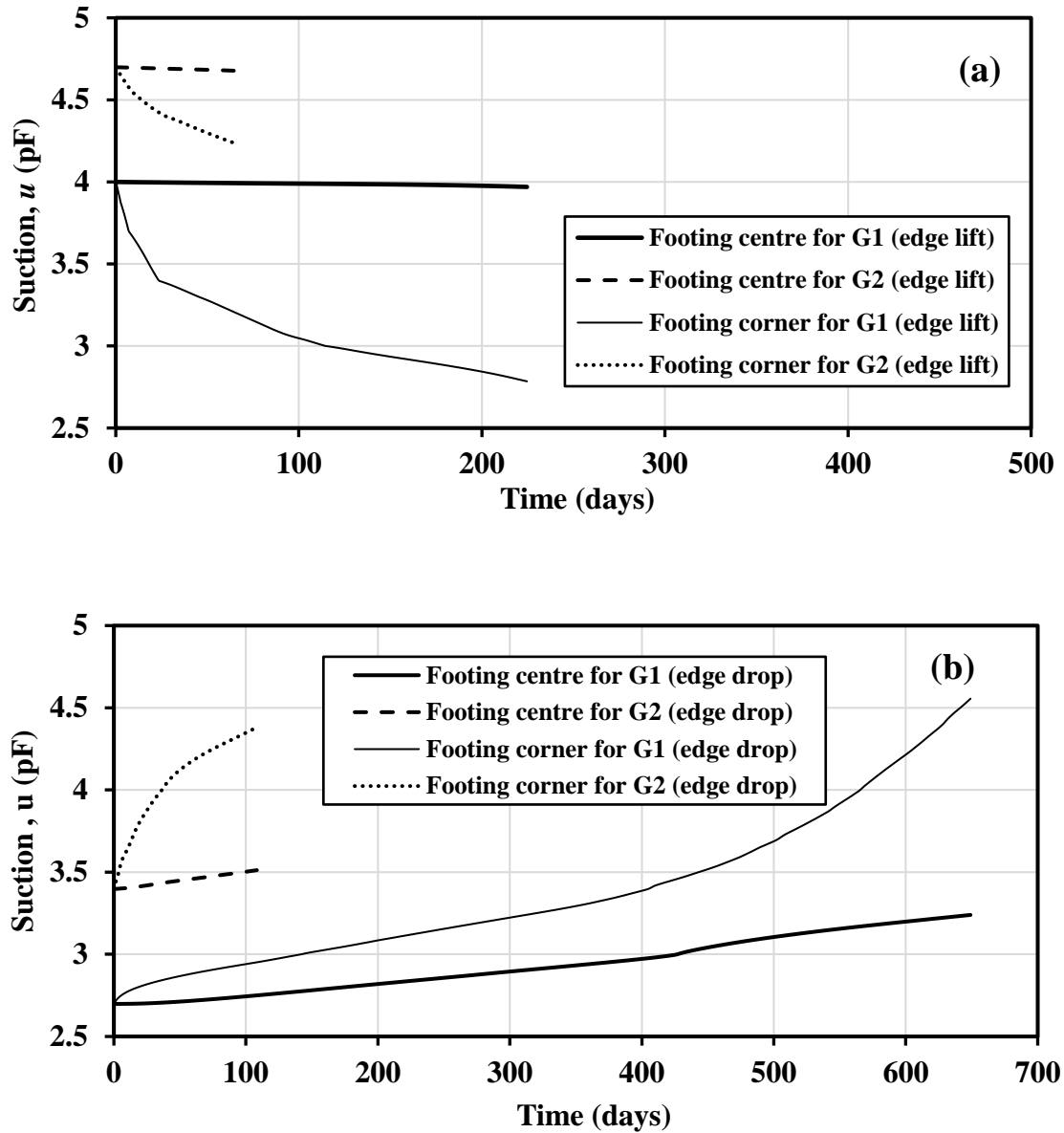


Figure 3.41: Suction change with time for soil at the centre and corner of the footing, for flow-deformation data group G1 and G2: (a) edge lift; and (b) edge drop.

Figures 3.42 to 3.47 show the comparison between the analyses using the two seepage data groups G1 and G2 for a strip at the slab footing centre, in the longitudinal and transverse directions. The target mound movement (y_m) of 49 mm is achieved between the corner and the centre of the slab footing for both seepage data groups, and the mound

movement in the longitudinal and transverse footing direction (between the centre and the edges of the slab foundation in both directions) are much less for both seepage data groups, as shown in Figure 3.42. For the edge drop scenario, the soil and footing movements in the longitudinal direction are almost identical, while in the transverse direction the seepage data group G2 produced more parabolic mound shape, which is more conservative with respect to the flatter mound shape produced by G1. The similarity of the soil and footing movements in the longitudinal direction resulted in similar footing internal forces, while the parabolic mound shape of G2 resulted in slightly higher bending moments and shear forces than those obtained from G1, as shown in Figures 3.43 and 3.44. However, despite these differences, the design forces of the footing are very similar for both seepage data groups. For the edge lift scenario, clear similarity in the soil and footing movements is observed, for both seepage data groups, as shown in Figure 3.45, and this resulted in similar footing internal forces, as shown in Figures 3.46 and 3.47.

The results of the above comparison reflect the robustness of the hydro-mechanical simulations. The seepage input parameters are interconnected; if they are changed within a logical range, there will be no major differences in the resulting footing design forces for a certain target differential soil movement in the edge lift or edge drop scenario. The logical range of the seepage input data is the one that can achieve the target differential soil movement without causing major disturbance to the saturation and suction initial conditions of the soil beneath the centre of the footing in the edge lift or edge drop scenario. Selecting the seepage input data based on this guideline guarantees successful simulations of the problem at hand and yields realistic outputs in terms design forces of slab foundation. From the above study, it can be concluded that changing the SWCC and the MSC data can have a considerable impact on the amount of slab movement with time; however, it has little impact on the differential mound movement and the corresponding internal forces. Therefore, in the parametric study presented in Chapter 4 the ISWCC and IMSC presented earlier in Chapter 3, are used to represent the seepage and deformation parameters in the numerical modelling.

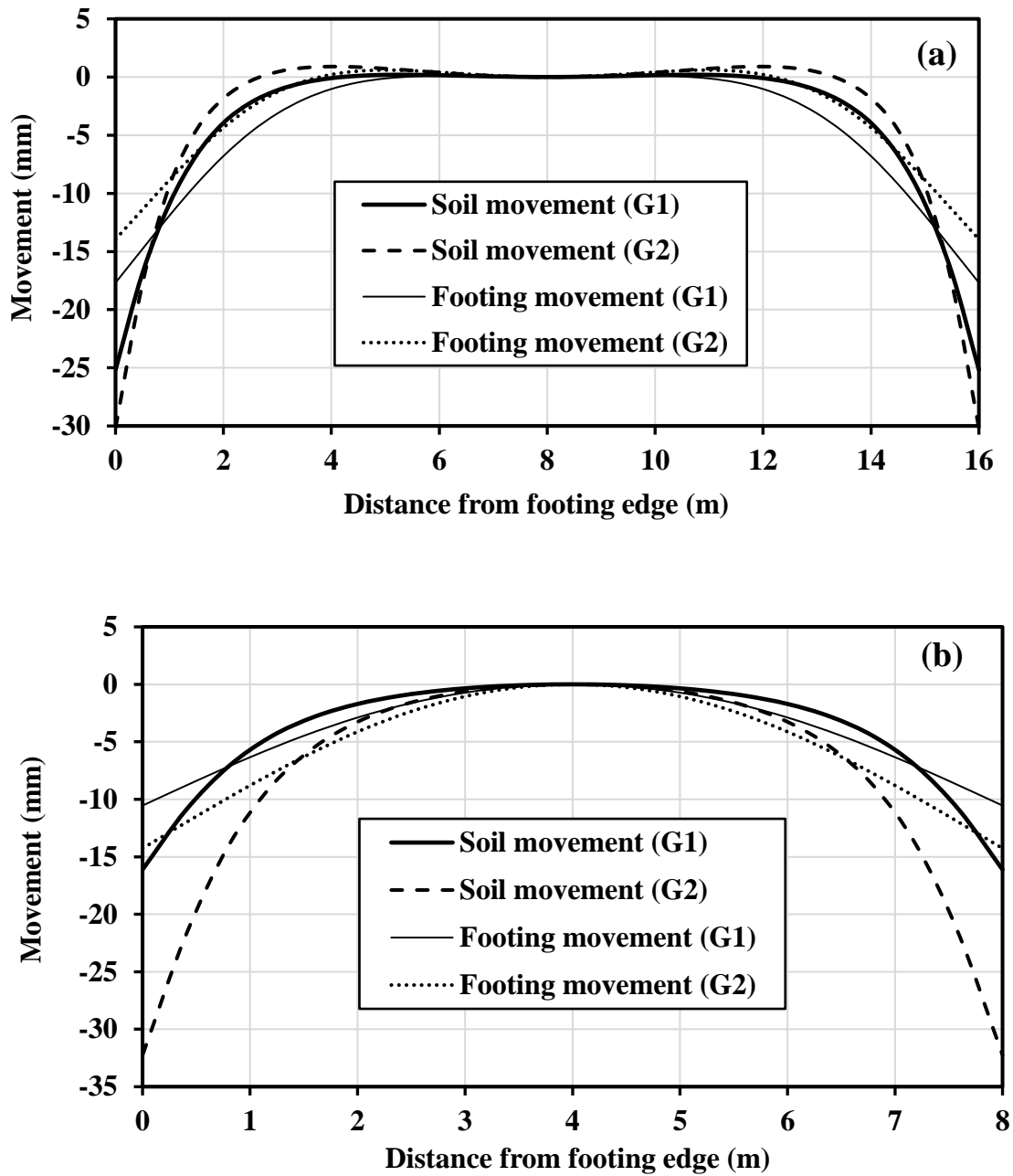


Figure 3.42: Comparison between soil and footing movement for G1 and G2 for the edge drop scenario: (a) longitudinal direction; and (b) transverse direction.

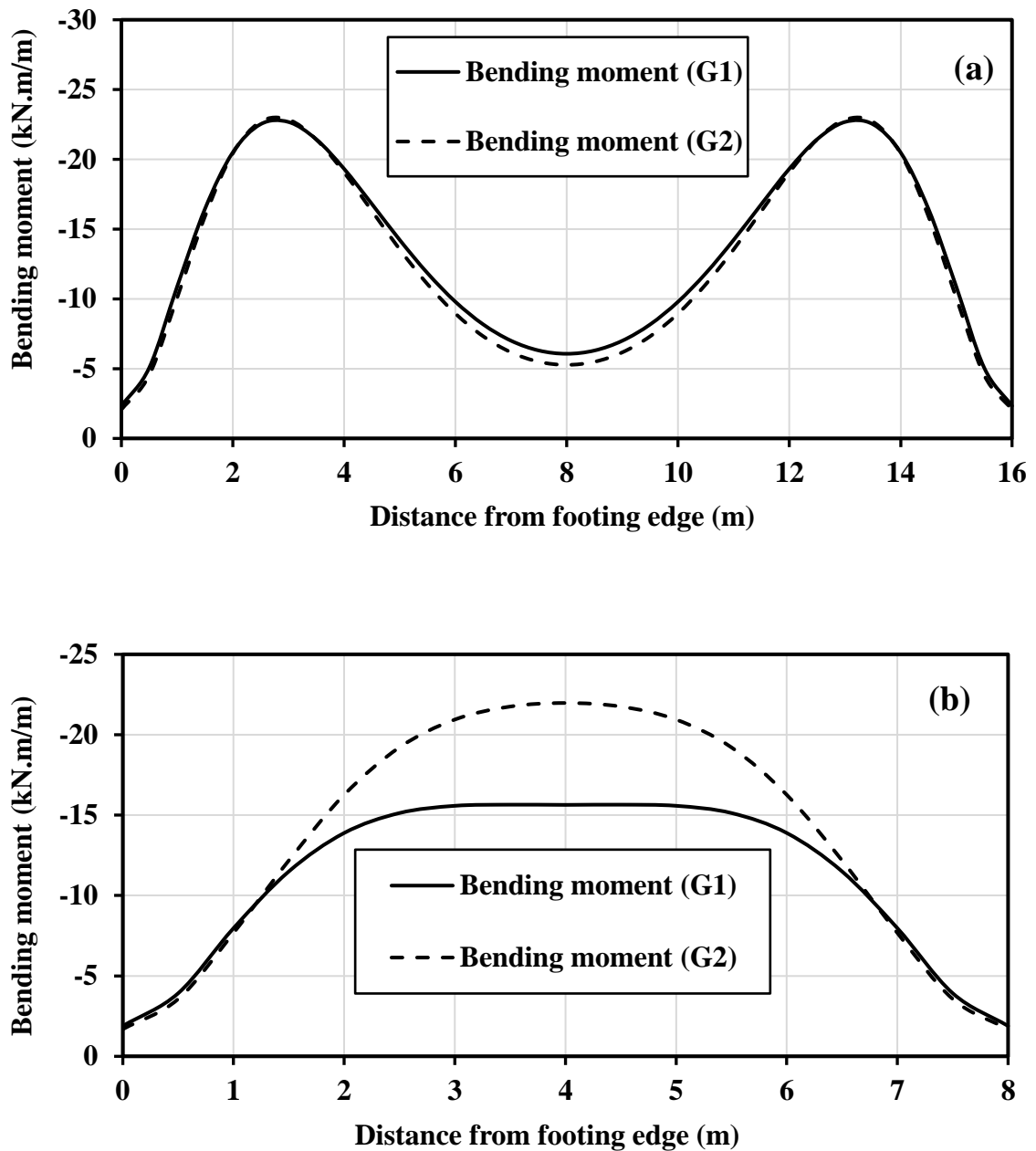


Figure 3.43: Comparison between footing bending moments for flow-deformation data of group G1 and G2 for the edge drop scenario: (a) longitudinal direction; and (b) transverse direction.

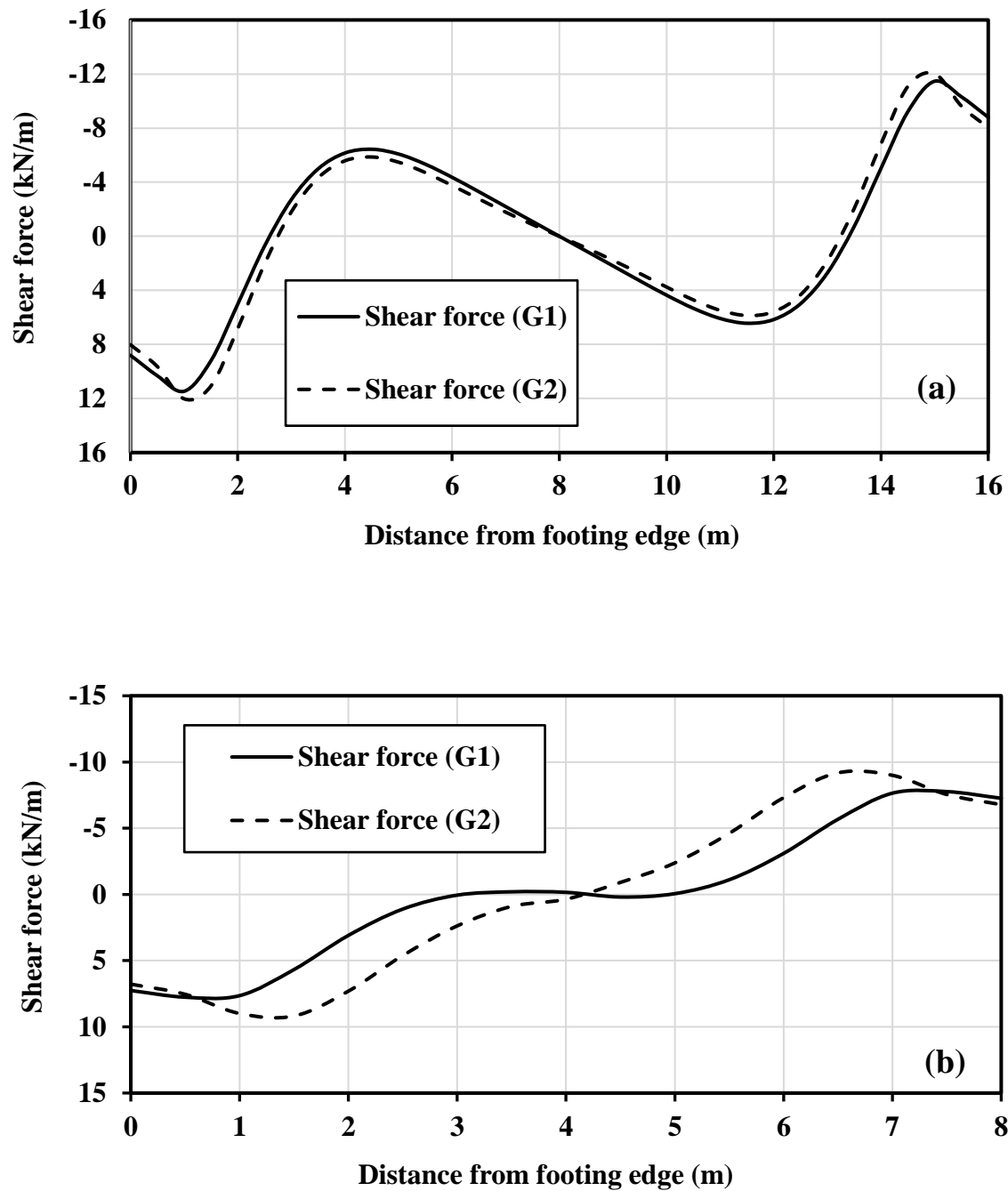


Figure 3.44: Comparison between footing shear forces for flow-deformation data of group G1 and G2 for edge drop scenario: (a) longitudinal direction; and (b) transverse direction.

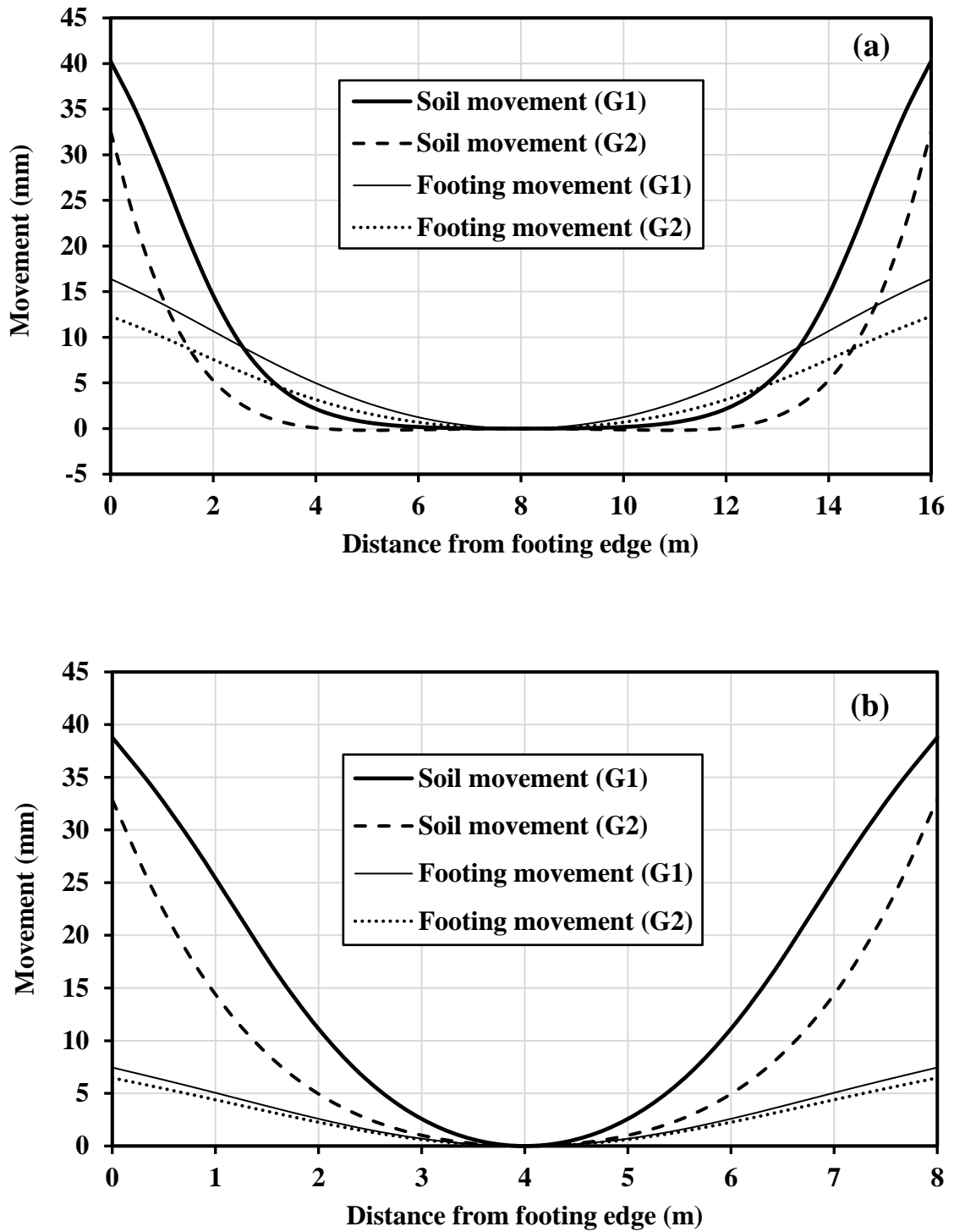


Figure 3.45: Comparison between soil and footing movement for flow-deformation data group G1 and G2 for edge lift scenario: (a) longitudinal direction; and (b) transverse direction.

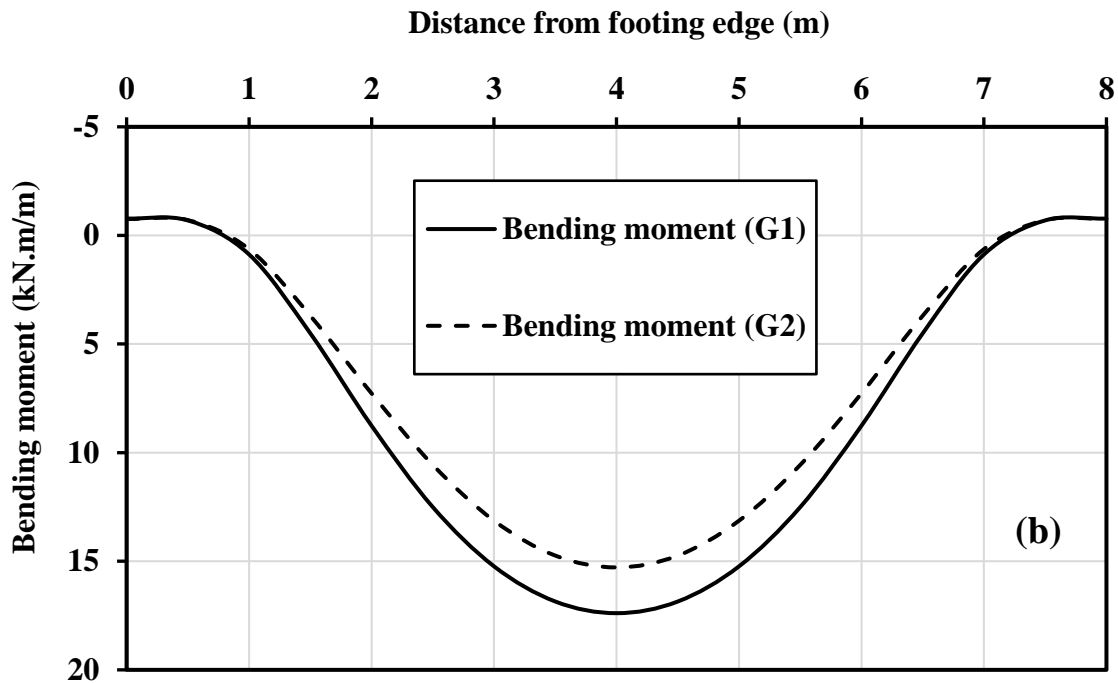
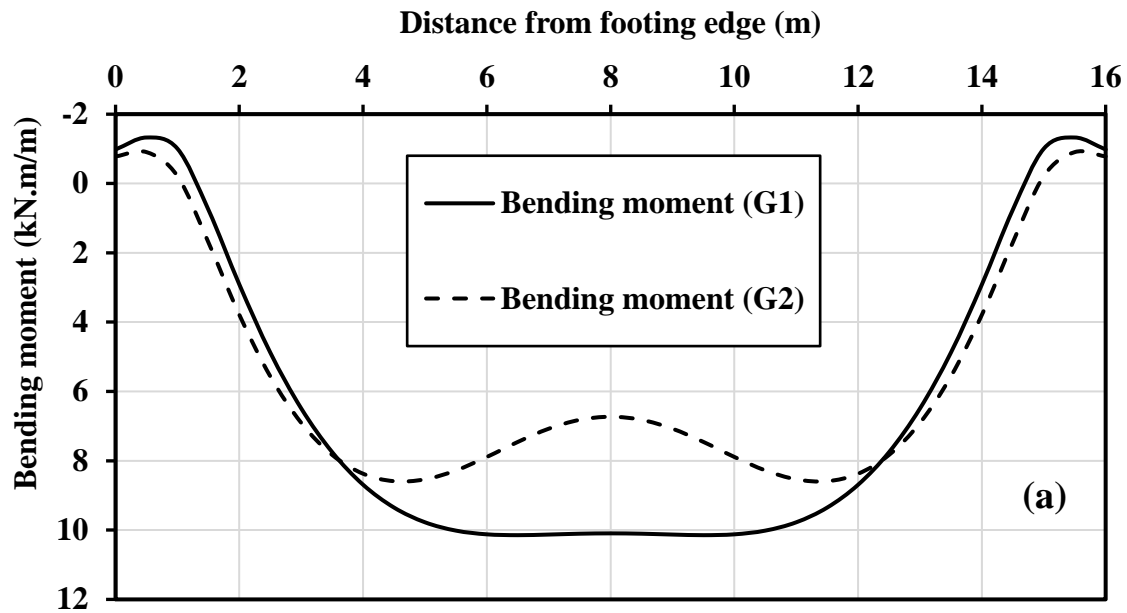


Figure 3.46: Comparison between footing bending moments of flow-deformation data group G1 and G2 for edge lift scenario: (a) longitudinal direction; and (b) transverse direction.

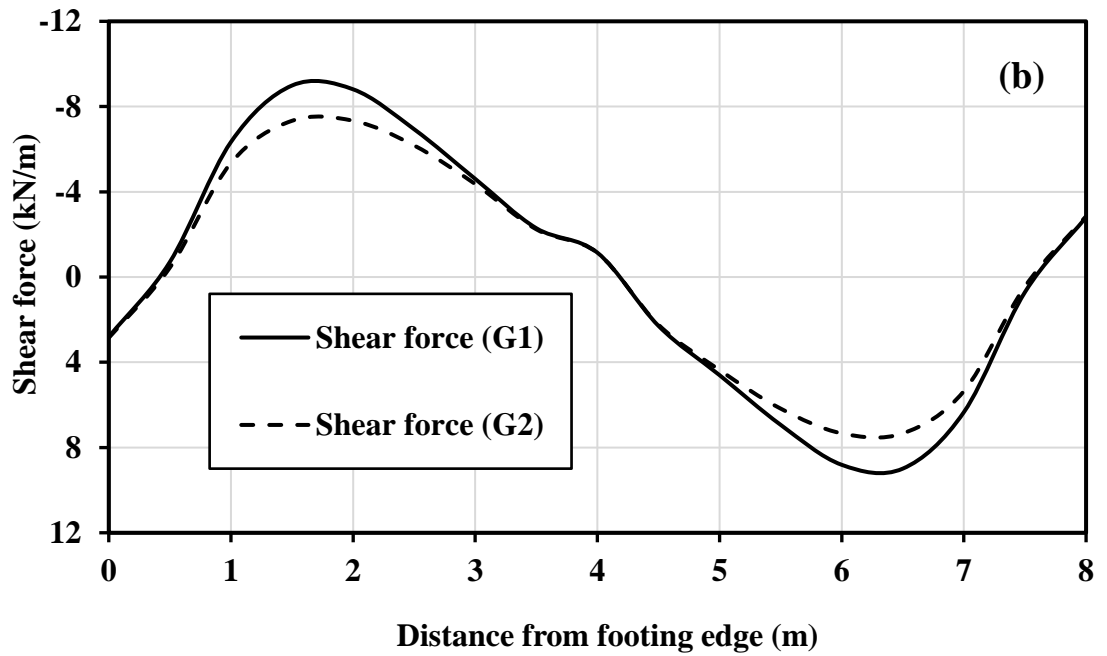
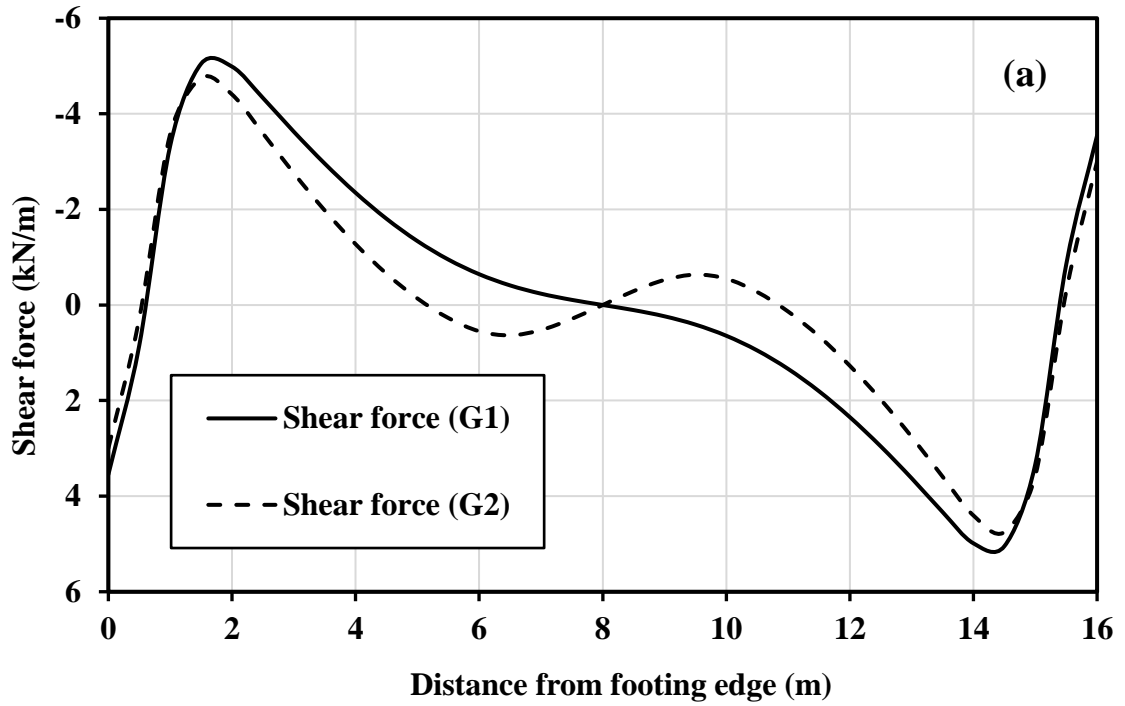


Figure 3.47: Comparison between footing shear forces for flow-deformation data of group G1 and G2 for edge lift scenario: (a) longitudinal direction and (b) transverse direction.

3.5 SUMMARY

The behaviour of stiffened slab foundations on expansive soils (including formation of a mound from the distorted soil surface beneath the footing) due to moisture precipitation or evaporation depends on many parameters, such as the soil-water suction characteristics (called here the SWCC), moisture-swell characteristics, soil permeability/duration of flow, initial saturation/suction conditions, soil modulus and footing loads. In this chapter, an advanced FE modelling using a hydro-mechanical approach and a coupled flow-deformation analysis was performed, with due consideration of the abovementioned parameters, which is the thrust of the current research. The proposed FE modelling was verified through three cases studies. The first case study involved field observations of a soil mound formation of a flexible cover membrane resting on a highly expansive soil over a period of 5 years in Newcastle, Australia. The mound formation over the course of observations was found to be reasonable predicted by the FE analysis. This stage of modelling confirmed the reliability of the developed FE modelling procedure in generating realistic soil distorted mound shapes. The second case concerned testing the ability of the FE model to reproduce the results obtained from field observations of the suction change and soil movement for a site in Amarillo, Texas. The results of the FE modelling agreed fairly well with the field observations, which verified the efficiency of the FE modelling in simulating the water diffusion and suction change through a soil medium. The third case study involved a hypothetical stiffened slab foundation on reactive soil, which was designed by the 3D FE modelling approach developed in this chapter and compared with both Mitchell's method and a dependent 2D analysis. The 2D FE analysis showed good agreement with Mitchell's method. However, the 3D FE analysis produced more realistic mound shapes and achieved deformation compatibility; a matter usually disregarded in the 2D analysis adopted by most existing design methods.

The effect of using different SWCCs and MSCs from the idealised ones adopted by default in this Chapter is investigated, and the results showed that changing the flow parameters associated with the construction of these curves affect the amount of transient movement; with only little effect on the differential movement and the corresponding internal slab

forces. Since the excess differential movement is responsible for most of structural damage of stiffened slab foundations on reactive soils, it is decided to use the idealised models (i.e. ISWCC and IMSC) in the parametric study presented next in Chapter 4.

The results presented in this chapter provided insights into the capability of the proposed 3D coupled flow-deformation and stress analysis in realistically simulating the behaviour of stiffened slab foundations on expansive soils, overcoming some major limitations inherent in most existing design methods. These include: (i) realistic formation of the spatial (3D) soil mounds, based on coupled seepage and deformation analyses, rather than the pre-defined 2D soil mounds adopted in the existing; and (ii) simultaneous stress analysis and transient seepage, by involving the effect of suction change on the soil stiffness and implementing representative contact elements for the soil-footing interaction. In the next chapter, a comprehensive parametric study involving different slab foundation dimensions (using the same 3D FE set-up developed in this chapter) will be carried out with the intention to develop design charts and procedures that can be readily used for design purposes by engineers and practitioners.

CHAPTER 4

NEW DESIGN METHOD FOR STIFFENED SLAB FOUNDATIONS ON REACTIVE SOILS

4.1 INTRODUCTION

In Chapter 3, an advanced 3D finite element (FE), hydro-mechanical numerical model was developed for the analysis of stiffened slab foundations on reactive soils. The proposed modelling method was presented and verified against three case studies, involving surface moisture change, surface suction change and design comparison of a hypothetical stiffened slab foundation. The results proved very promising, demonstrating the ability of the proposed modelling method to accurately simulate the behaviour of stiffened slab foundations on reactive soils.

In this chapter, an extensive parametric study is carried out utilising the 3D FE modelling approach developed in Chapter 3, aiming to produce data that can be incorporated into a new design method for routine use by practitioners. The new design method is believed to be more reliable than the methods available in the literature, since it is based on advanced 3D FE coupled flow-deformation and stress analyses, addressing the three salient weaknesses reported previously for the existing methods, namely: (1) using an ad-hoc soil mound that is independent of the processes and parameters affecting its characteristics; (2) using an uncoupled approach for the slab/soil interaction; and (3) oversimplifying the inherently spatial problem by adopting a 2D model.

4.2 PARAMETRIC STUDY AND DEVELOPMENT OF THE NEW DESIGN METHOD

In this section, the sophisticated 3D FE hydro-mechanical model that was developed earlier in Chapter 3 is used to perform a parametric study to develop a set of design charts and equations that form the core of a new ‘standalone’ design method for stiffened slab foundations on reactive soils. This section presents the process leading to the development

of the new design method; the input is a limiting differential movement and a certain soil class, and the output is the required slab foundation stiffness that can satisfy these input requirements and the internal forces associated. The limits adopted in the parametric study are those used by the Australian Standards AS2870 (2011), with respect to the soil classes and allowable deformations (refer to Tables 2.3 and 2.4 in Chapter 2). The site class (S), which is classified as a slightly reactive site, is not considered in the current analysis, since it is unlikely to cause damage to footings or structures. Moreover, the construction type involving a full masonry is also omitted from the current analysis, postulating that it involves an old fashion construction technique that is hardly used nowadays.

The process of developing the design charts is carried out by generating 3D FE hydro-mechanical models for several plan dimensions of slab foundations. Each model is analysed with a set of different foundation thicknesses, under both the edge drop and edge lift scenarios, for a period of time that is long enough to generate the soil mound differential movement (y_m) that defines a specific soil class. For each y_m , an equivalent rectangular thickness (T_{eq}) is calculated to produce an adequate stiffened slab inertia that can successfully limit the footing deformation; the corresponding internal forces of the designed slab foundation are then obtained and recorded. The internal forces are then used in a design procedure involving the cracked inertia of the slab foundation, in order to obtain the final stiffened slab configurations including the slab thickness, the depth of the stiffening beams, the stiffening beams grid spacing in each direction, and the required reinforcement for both flexure and shear. The above-mentioned steps are integrated into a simple design computer program called Slab Foundations on Reactive Soils (SFORS), which will be described later. This program can perform the required design calculations, without the need for the design charts, by defining simple input data including the slab dimensions, the configurations of the stiffening beams, the construction type (allowable slab foundation deformation limit, Δ_{all}) and the soil movement (y_m).

Figure 4.1 shows a typical example of the 3D FE model used in the parametric study, generated for one of the slab foundation plan dimensions. Details about the size of the mesh used in the FE model and the corresponding boundary conditions were explained

earlier in Chapter 3 (Section 3.3.1). Conveniently, the depth of the swelling clay is selected to be 4.0 m, corresponding to the maximum suction depth recommended by the Australian Standards AS2870 (2011). This depth is found to be sufficient for the formation of the different mound movements (y_m) up to ± 84 mm without significant distortion of the elements of the FE model. In order to omit the effect of the lower boundary on the swelling soil movement, the swelling clay layer is followed by a non-swelling clay soil of 1.0 m thickness. The idealised soil water characteristic curve (ISWCC) and the idealised moisture-swell curve (IMSC) presented in Chapter 3 are assigned for the swelling soil in the present parametric study. An elastic soil model is used for the swelling soil with a suction-dependent soil modulus through the user defined subroutine explained earlier in Chapter 3. The soil element used is an 8-node brick, trilinear displacement, trilinear pore pressure element (C3D8P). The double symmetry is used in the generated FE models to save the computation time.

For the concrete slab foundation, an elastic model is also used, with a concrete modulus of 15 GPa and a unit weight of 25 kN/m³. The slab foundation is simulated using a 4-node double curved shell element (S4R). The mound stiffness is considered to be 1,000 and 5,000 kPa for the case of the edge lift and edge drop, respectively, as recommended by the Australian Standards AS2870 (2011). Contact elements are used to allow for a footing-soil separation according to the generated soil mound. The initial conditions are set to be dry with high suction and low saturation for the case of the edge lift scenario, while they are set to be saturated with low suction and high degree of saturation for the case of the edge drop scenario.

The analysis of each model starts with a geostatic step, in which the soil deformation caused by the initial suction is nullified and the gravity loads are then activated by considering the slab self-weight. Finally the stage of infiltration or evaporation (according to the edge movement scenario) is activated with a rate of ± 100 mm/month. This final analysis stage is extended until all the design mound movements of the different assigned soil classes are achieved.

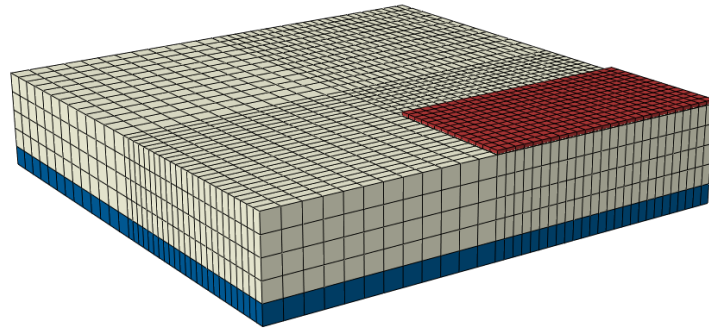


Figure 4.1: Typical 3D finite element model used in the parametric study.

4.2.1 Assumptions and conditions of the parametric study and the new design method

The FE analysis concerning the parametric study, and in turn the ensuing new design method, are based on certain assumptions and a range of parameters, as follows:

1. The analysis is mainly developed for the design of slab foundations of single storey houses subjected to a uniform service area load comprising the finishes, internal partitions (single leaf walls), utilities, live loads and roof loading, not exceeding 4.5 kPa, as shown in Table 4.1. In addition, a perimeter line load of 6.0 kN/m representing the external walls corresponding to 2.50 m high double leaf wall, and no central line loads are considered. The loads shown in Table 4.1 do not include the self-weight of the slab, which is taken into consideration in the FE modelling.

Table 4.1: Uniform loads used in the parametric study based on AS1170.1 (2002).

Load type	Load (kPa)
Internal wall loads	2.6
Roof: 0.8 mm steel sheet	0.1
10 mm plasterboard	0.083
12 mm hardwood T and G lining	0.126
Insulation wiring fittings and battens	0.058
Flooring: 13 mm clay tiling	0.27
live load (permanent)	1.25
Total service load on slab foundation	4.50

2. The differential soil mound movement (y_m) beneath the slab foundation is taken as 70% of the characteristic surface heave (y_s), as per the Australian Standards AS2870 (2011). The maximum characteristic surface heave considered in this method is 120 mm.
3. The top slab thickness is fixed to 100 mm and the spacing of the stiffened beams should not be less than 3.0 m and not more than 4.0 m, so that they do not exceed the self-weight of the stiffened slab foundations considered in the study.
4. The method is developed for slab foundations with rectangular plan dimensions; however, the concept of overlapped rectangles can be adopted for the L and U -shape foundation plans. Note that, even with this limitation the design method would still produce results that are more reliable than the existing methods that use the same assumption, because the spatial nature of the problem is still taken into consideration in the 3D modelling from which the charts and the design software were derived.
5. The analysis is based on a symmetrical precipitation or evaporation around the slab foundation, without consideration to the suction change induced by any nearby trees or plant roots; a safe separation between the slab foundation and the trees equal to the mature height of the tree is recommended in this regard.
6. The soil mound stiffness is considered to be equal to 1,000 kPa for the edge lift scenario and 5,000 kPa for the edge drop scenario, and the soil modulus is considered to be a suction-dependent parameter (refer to Chapter 3).
7. For ductility, the ratio of the flexural capacity (M_u) of the stiffening beam section and cracking moment (M_{cr}) should be at least 1.2, as per the Australian Standards AS2870 (2011).
8. Branson's equation (1963) is used to calculate the effective inertia (I_{eff}) of the stiffening beams (refer to Chapter 2).
9. In the edge lift scenario and under the uncracked conditions, the stiffening beams act as T -sections, with part of the 100 mm top slab acting as a flange, according to the recommendations in Section 4.4 (Clause e) of the Australian Standards AS 2870 (2011), which states that "the flange width to be the minimum of half the distance

between the sub-beams centrelines and $B_w + 0.2 L$ (where: B_w is the stiffening beam web width and L is the sub-beams span for the direction under consideration).

10. In order to calculate the cracking moments used in the effective inertia of the stiffening beams, the tensile stress of concrete taken as $0.4\sqrt{f'_c}$ for the edge drop and $0.6\sqrt{f'_c}$ for the edge lift, in accordance with the Australian Standards AS2870 (2011). The concrete grade (f'_c) is fixed to 20 MPa and the concrete modulus for the slab foundation is fixed to 15 GPa.
11. The minimum inertia of the slab foundation considered in this method is equivalent to the inertia of a 200 mm thick slab. Table 4.2 lists the different parameters used in the parametric study.

Table 4.2: Range of parameter values used in the parametric study.

Parameter	Values used
Rectangular slab foundation dimension, L (m)	6, 10, 14, 18, 22 and 26
Rectangular slab foundation dimension, B (m)	6, 10, 14, 18, 22 and 26
Thickness of equivalent rectangular section of stiffened slab foundation (m)	0.200, 0.225, 0.250, 0.275, 0.300, 325, 0.350, 0.375, 0.400, 0.425, 0.450, 0.500, 0.550, 0.600, 0.650, 0.700, 0.750, 0.800, 0.850, 0.900, 0.950, 1.000, 1.100 and 1.200
Differential soil mound movement, y_m (mm), corresponding to soil class	28.0 – Class (M) 42.0 – Class (H1) 52.5 – Class (H2) 70.0 – Class (E1)* 84.0 – Class (E2)*
Maximum allowable differential movement of slab foundation, Δ_{all} , corresponding to the construction type	$L_d/300 \leq 40$ mm (Clad frame)** $L_d/400 \leq 30$ mm (Articulated masonry veneer)** $L_d/600 \leq 20$ mm (Masonry veneer)** $L_d/800 \leq 15$ mm (Articulated full masonry)**

*The extremely expansive soil as per Australia Standards AS2870 is divided in this study into two categories, E1 and E2, for the sake of interpolation refinement.

**Dimension L_d is measured between the corners of the foundation slab.

4.2.2 Discussion of the outputs obtained from the parametric study

The outputs obtained from the parametric study are compiled in the form of design charts, as shown in Appendix (B). Figures 4.2 and 4.3 are typical samples of these design charts, for a slab having a length (L) of 18.0 m and different width dimensions (B) varying from 6.0 m to 26.0 m. The slab is also subjected to different mound movements (y_m) corresponding to different soil classes (i.e. M, H1, H2, E1 and E2). The limits of the slab foundation differential movement (Δ_{all}) based on the required inertia are calculated as $L_d/300$, $L_d/400$, $L_d/600$ and $L_d/800$, corresponding to the different codified construction types referred to in Table 4.2. The samples of the design charts in Figures 4.2 and 4.3 are for an allowable movement of $L_d/800$. The data provided on the top left side of each design chart represent the parameters considered in the design, including loading, dimension of the slab foundation in one direction (L), type of edge movement (i.e. edge lift or edge drop) and the allowable slab foundation differential movement, L_d/Δ_{all} .

Slab foundation main span, L (m)	18.00
Edge movement scenario	EL
Span to deflection ratio (L_d/Δ_{all})	800
Service Loads:	
Internal wall loads, W_{int} (kPa)	2.6
Roof: 0.80 mm steel sheet, R (kPa)	0.1
10 mm Plasterboard (kPa)	0.083
12 mm hardwood lining	0.126
Insulation, wiring, fittings (kPa)	0.058
Flooring (13 mm clay tiling)	0.27
Permanent live load, q (kPa)	1.25
Total uniform load* (kPa)	4.50
Edge wall line load (kN/m)	6.00
*Exclude slab/beams self-weight	

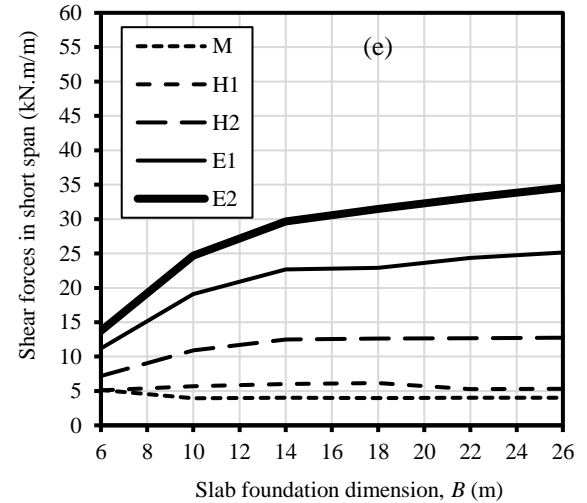
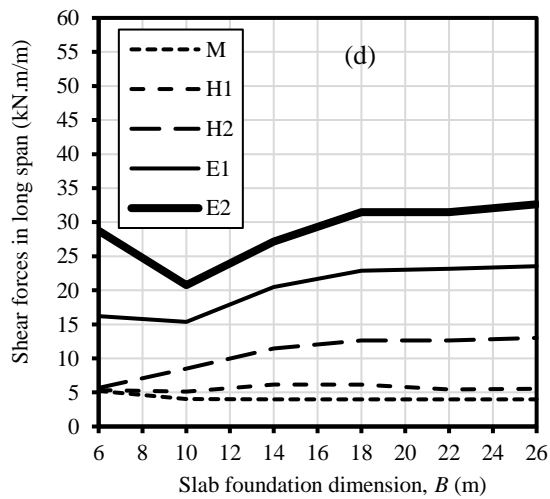
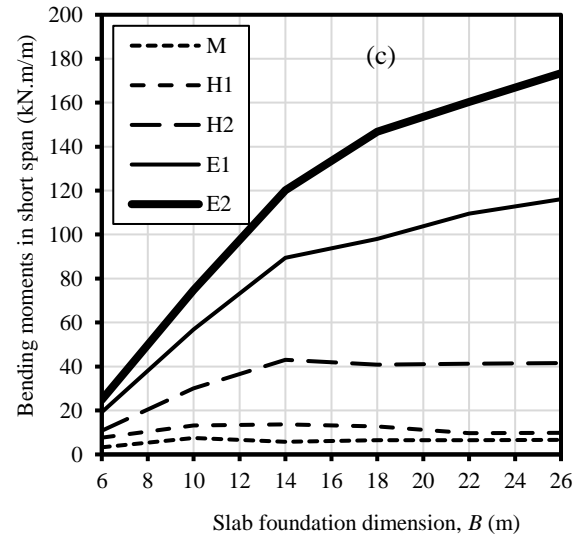
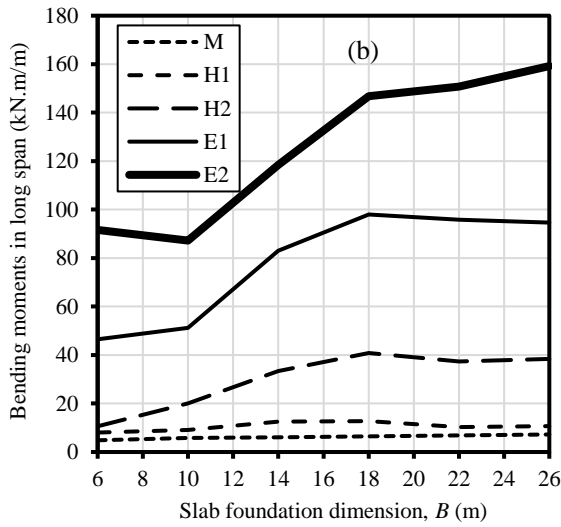
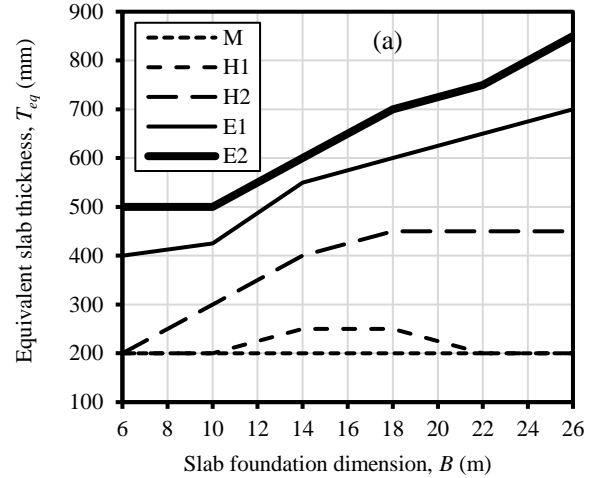


Figure 4.2: Sample design charts for and edge lift scenario:

$L = 18$ m and $L_d/\Delta_{all} = 800$ (different soil classes: M, H1, H2, E1, E2).

Slab foundation main span, L (m)	18.00
Edge movement scenario	ED
Span to deflection ratio (L_d/Δ_{all})	800
Service Loads:	
Internal wall loads, W_{int} (kPa)	2.6
Roof: 0.80 mm steel sheet, R (kPa)	0.1
10 mm Plasterboard (kPa)	0.083
12 mm hardwood lining	0.126
Insulation, wiring, fittings (kPa)	0.058
Flooring (13 mm clay tiling)	0.27
Permanent live load, q (kPa)	1.25
Total uniform load* (kPa)	4.50
Edge wall line load (kN/m)	6.00
*Exclude slab/beams self-weight	

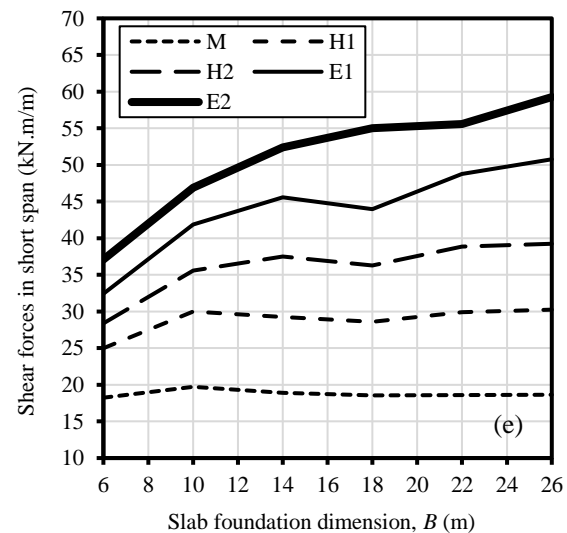
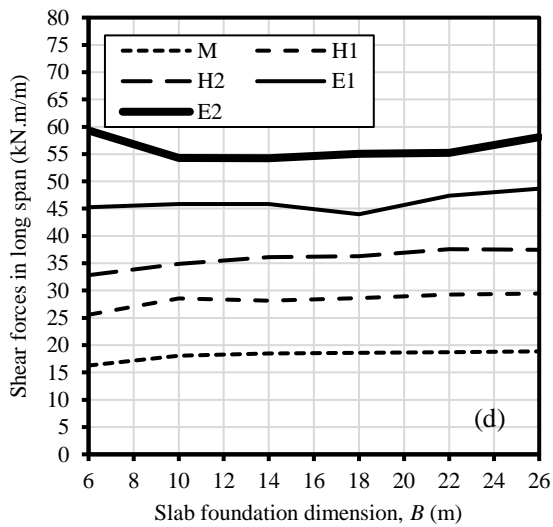
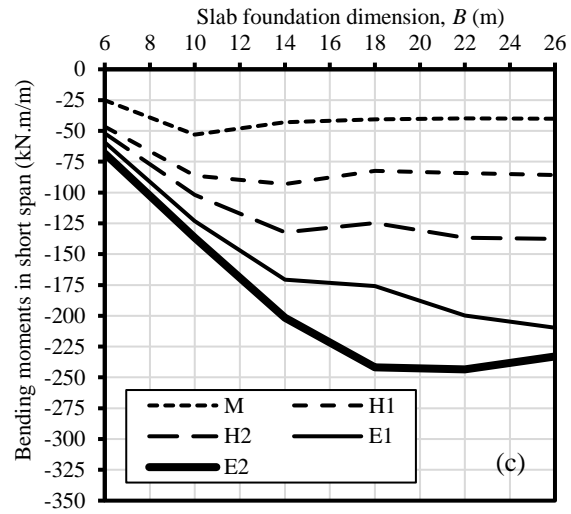
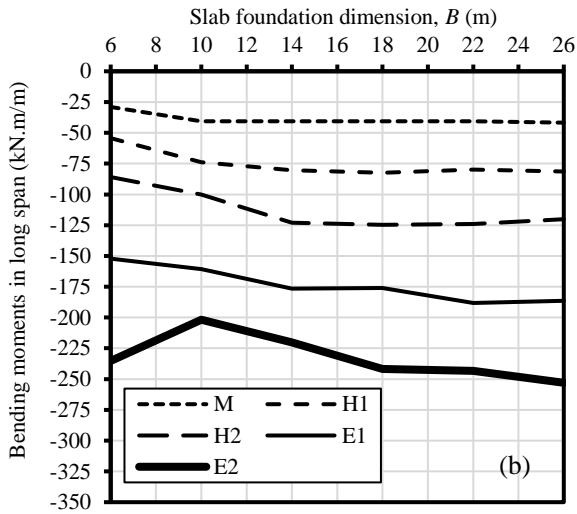
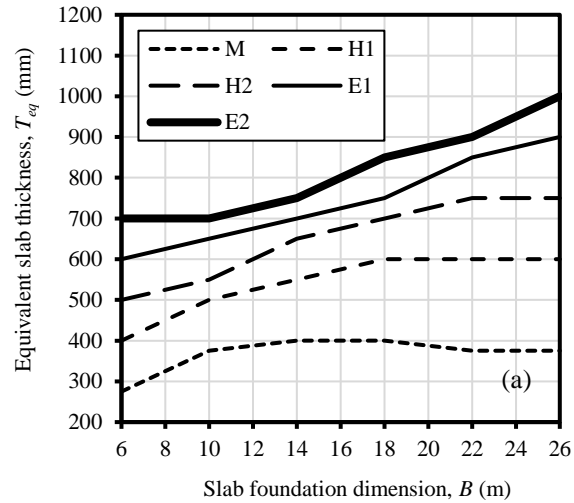


Figure 4.3: Sample design charts for and edge drop scenario:

$L = 18$ m and $L_d/\Delta_{all} = 800$ (different soil classes: M, H1, H2, E1, E2).

Note that the bending moment presented in the chart represents the design values needed to calculate the reinforcement in the slab/beam system. In the following section, many affecting factors are extracted from the parametric study through the design charts; these factors are discussed below.

4.2.2.1 Effect of slab dimensions and soil class

In the parametric study performed here, each soil class is represented by an upper bound soil mound differential movement (y_m), as referred to in Table 4.2. The slab inertia is represented by an equivalent slab thickness (T_{eq}), which is the thickness of a rectangular cross section slab having an inertia per unit metre equal to that of a stiffened slab with a *T*-shape cross section consisting of a 100 mm thick slab and one stiffening beam. Figure 4.4 shows the effect of varying the slab dimension and soil movement on the equivalent slab thickness. Figure 4.4 is generated considering an allowable slab foundation movement (Δ_{all}) of $L_d/800$; similar figures with similar trends can be generated for the other allowable slab foundation deformations included in the parametric study (refer to Table 4.2). It can be seen from Figure 4.4 that the equivalent slab thickness has a continuous tendency to increase by increasing both the slab area and soil mound movement (y_m), for both the edge lift and edge drop scenarios. It can also be seen that the slab inertia (or equivalent thickness) is more sensitive to the increase of the mound movement than the slab area. It is moreover evident that the extremely expansive site classes (E₁ and E₂) corresponding to mound movements (y_m) of 70 mm and 84 mm, respectively, require much stiffer slab foundations than the other (less reactive) site classes. Another interesting aspect derived from Figure 4.4 is that the increase in the required equivalent slab foundation thickness (T_{eq}) with the increase of the soil mound (y_m) becomes almost linear starting from a soil mound value of 52.5 mm corresponding to the H2 soil class, for both the edge lift and edge drop scenarios.

Figures 4.5 to 4.8 show the effect of slab dimension and soil movement on the internal forces (i.e. bending moments and shear forces) of the slab foundation, considering an allowable foundation differential movement Δ_{all} of $L_d/800$, for the case of the edge drop and edge lift scenarios. It can be seen that the bending moments and shear forces in the

short and long spans of the slab foundation increase with the increase in the slab dimensions and soil mound movement. It can also be seen that, in general, the internal forces are more sensitive to the increase of the mound movement than to the increase of slab dimension. It should be noted that, unlike the structure of the two-way slab supported at its edges where the dimensions are more significant than the loading on the slab bending moments, the slab foundation resting on swell-shrink soils is a soil-structure interaction problem in which the bending moment is generated according to the way the soil supports or loses its contact with the slab as well as the final soil support pattern at the time when the design mound movement is achieved.

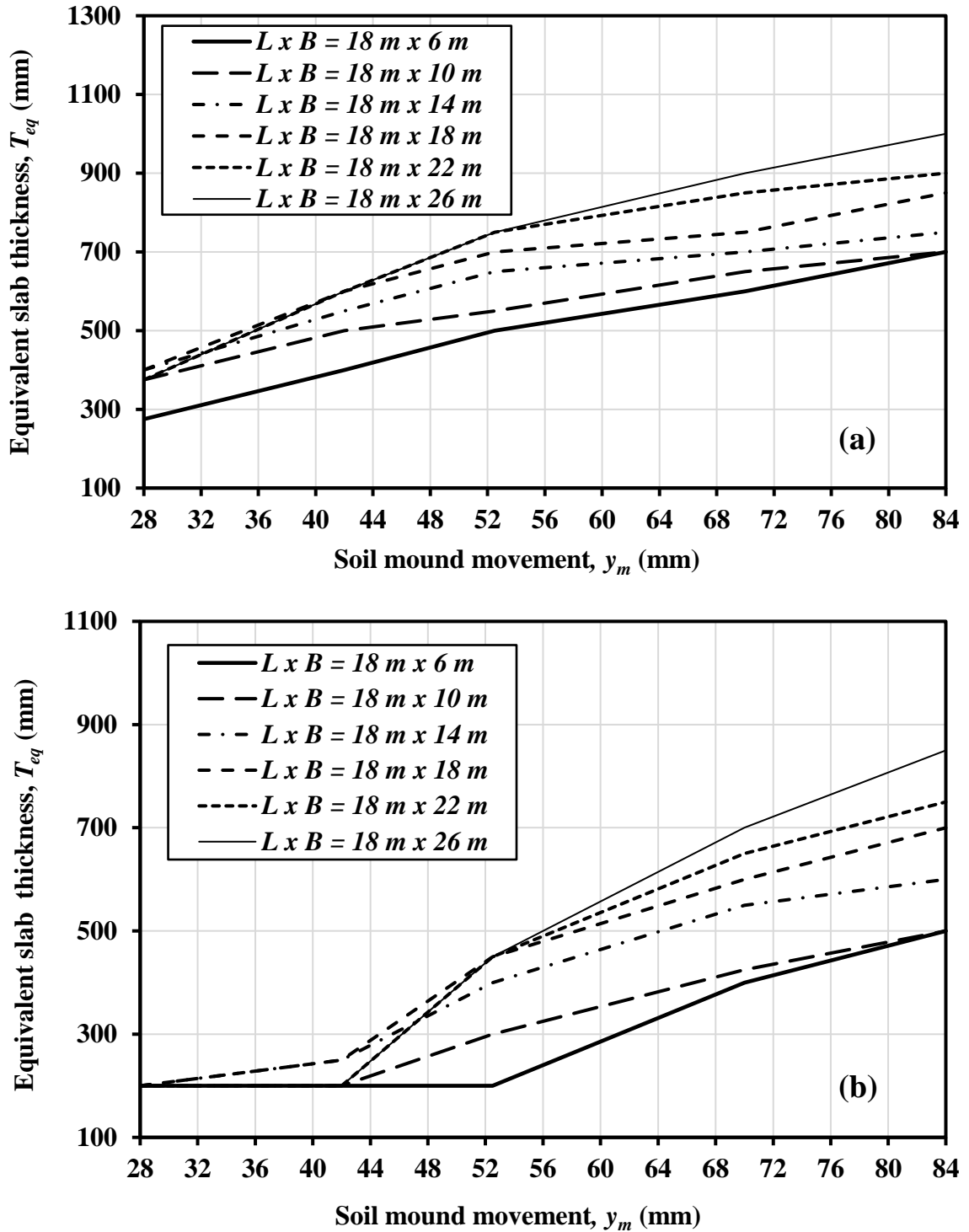


Figure 4.4: Effect of slab foundation dimensions and soil mound movements on the equivalent slab foundation thickness, T_{eq} , for $\Delta_{all} = L_d/800$

(a) edge drop scenario; and (b) edge lift scenario.

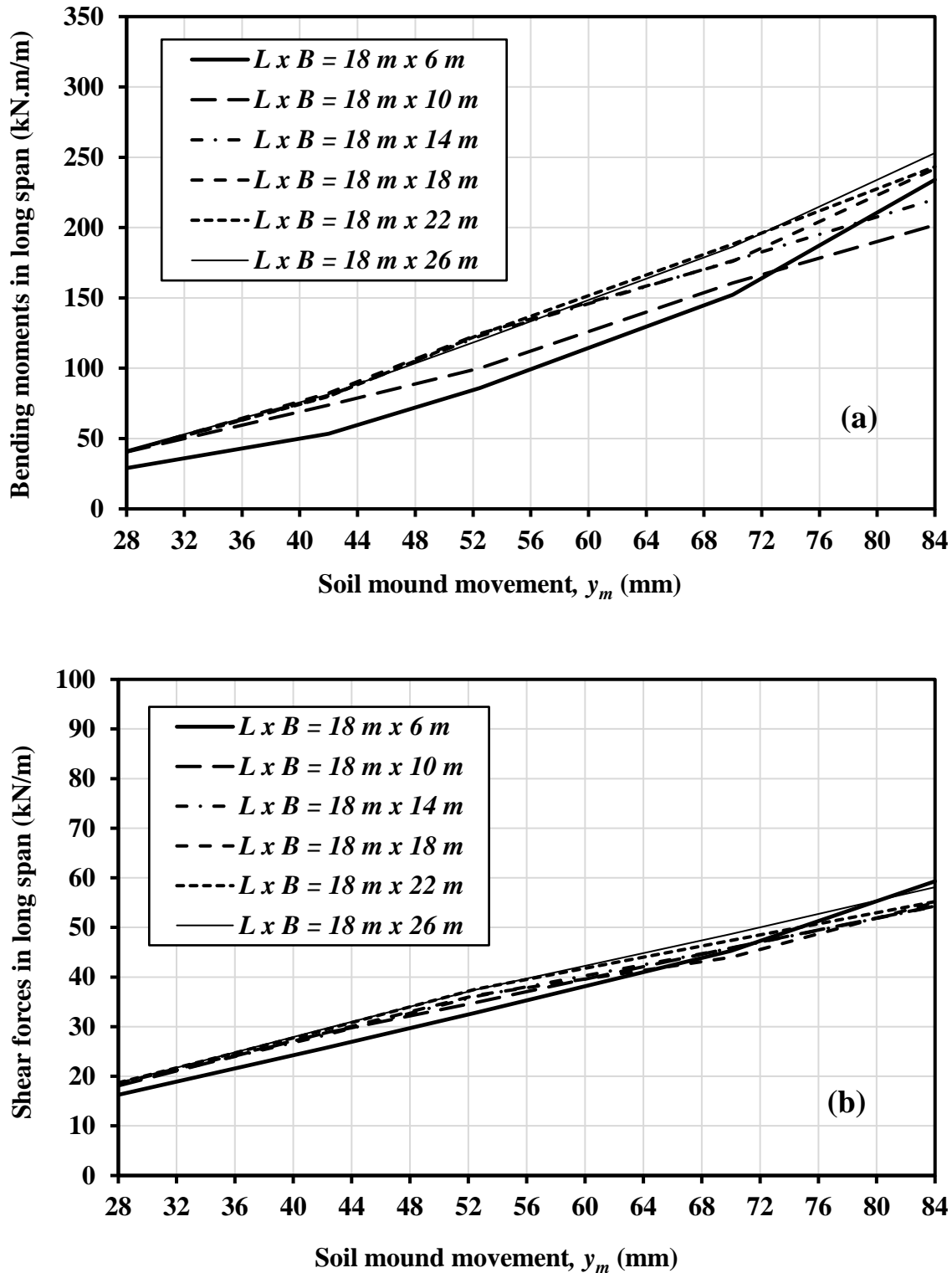


Figure 4.5: Effect of slab foundation dimensions and soil mound movements on the internal forces of the slab foundation long span for $\Delta_{all} = L_d/800$ and edge drop scenario: (a) bending moments; and (b) shear forces.

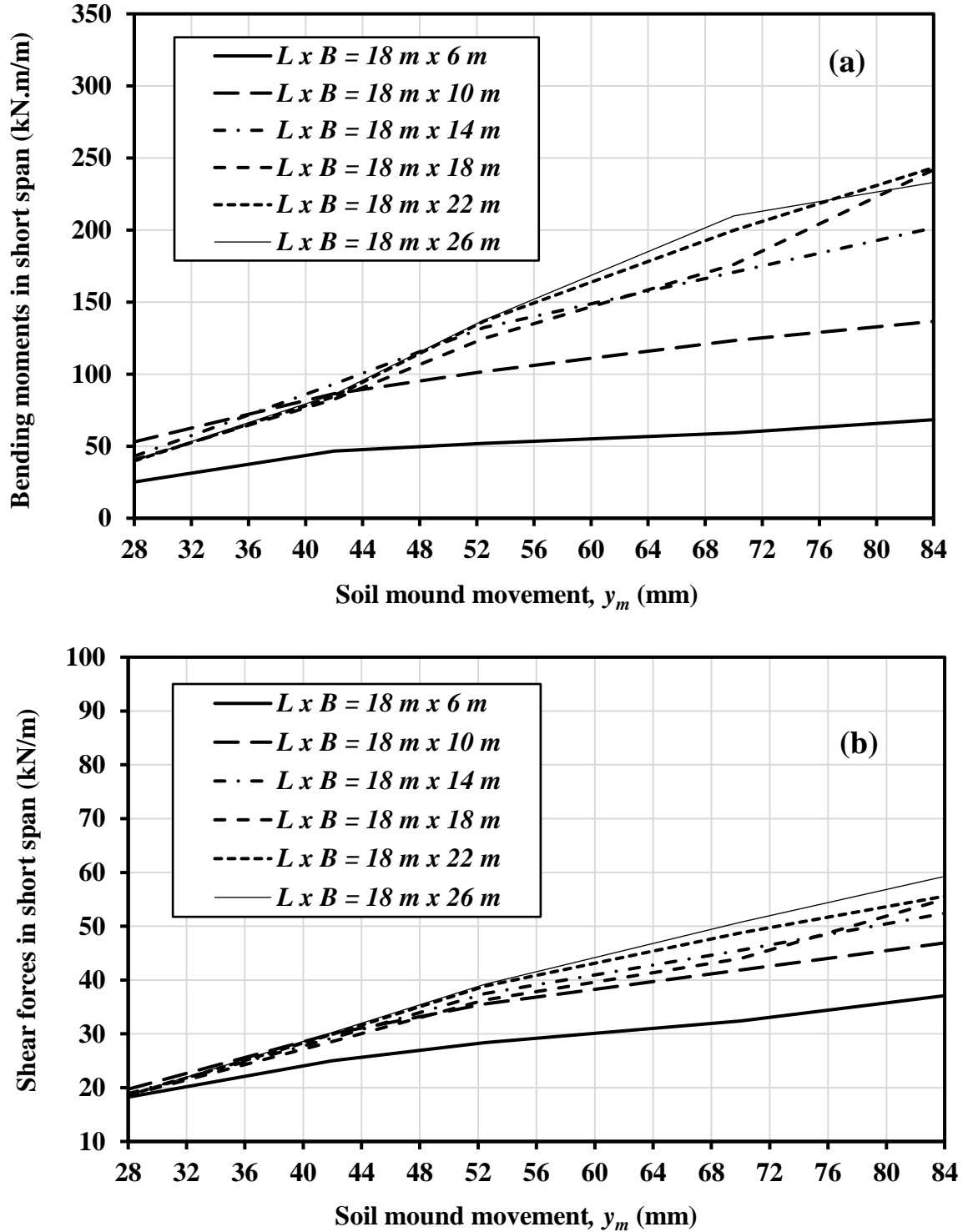


Figure 4.6: Effect of slab foundation dimensions and soil mound movements on the internal forces of the slab foundation short span for $\Delta_{all} = L_d/800$ and edge drop scenario: (a) bending moments; and (b) shear forces.

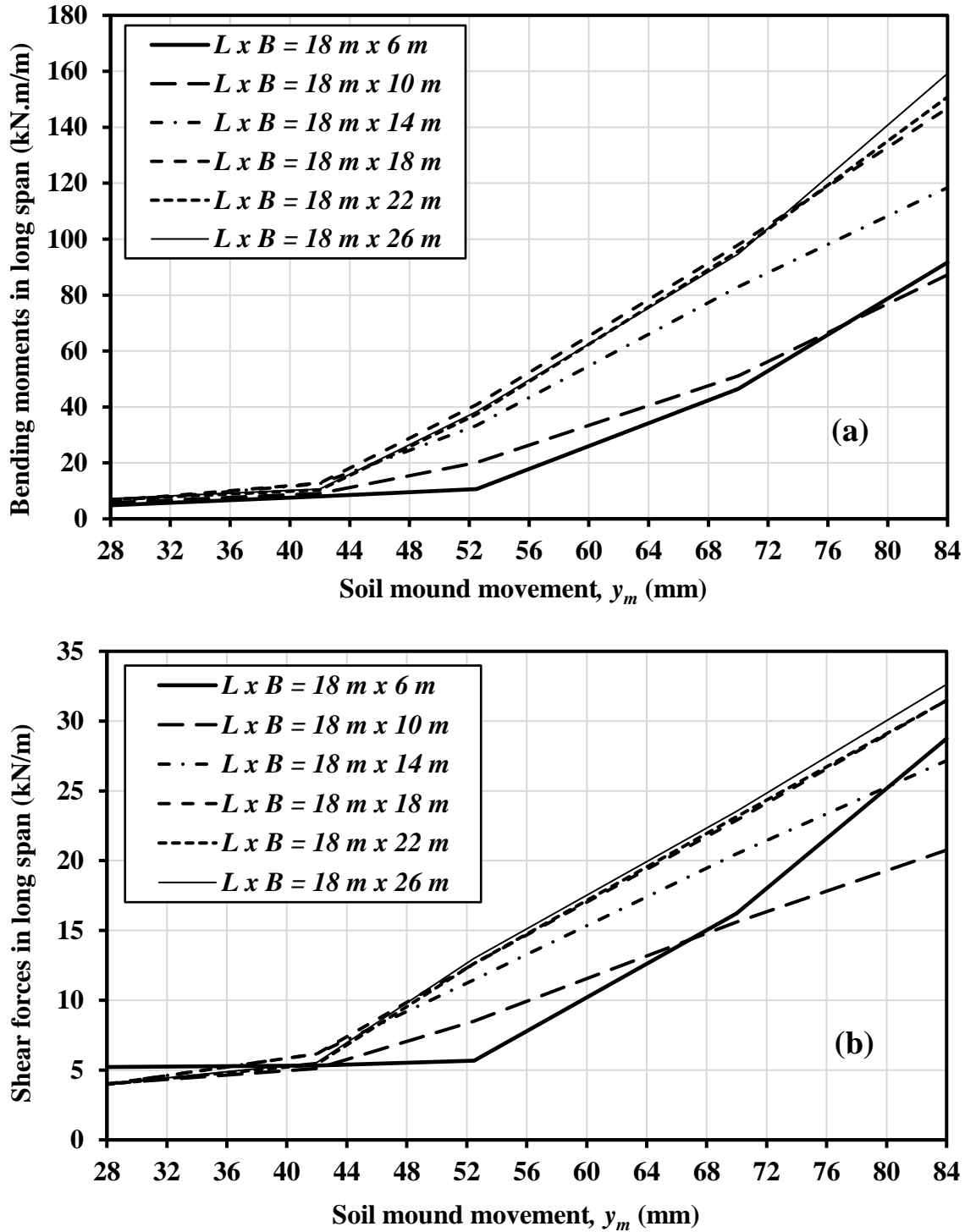


Figure 4.7: Effect of slab foundation dimensions and soil mound movements on the internal forces of the slab foundation long span for $A_{alt} = L_d/800$ and edge lift scenario: (a) bending moments; and (b) shear forces.

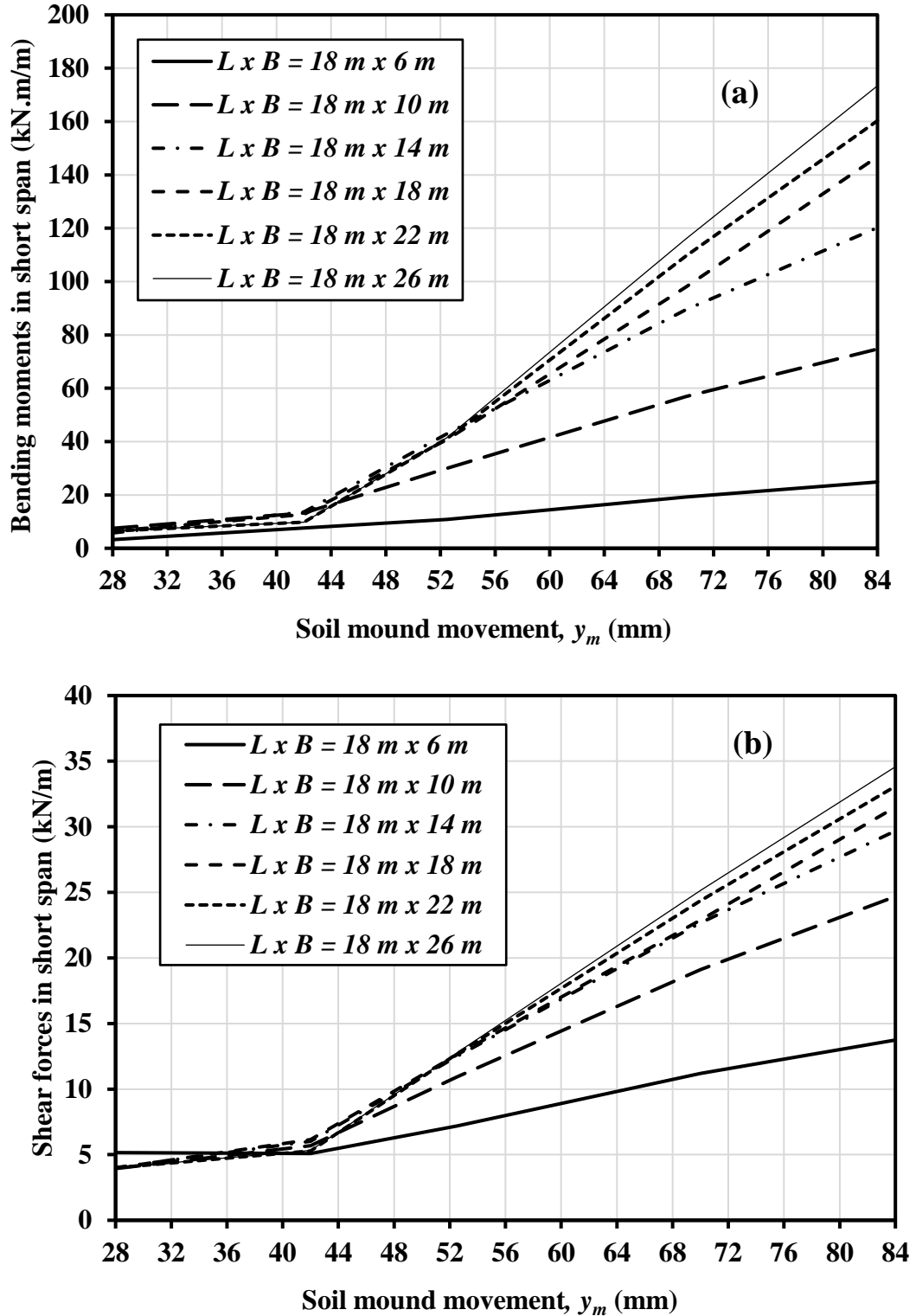


Figure 4.8: Effect of slab foundation dimensions and soil mound movements on the internal forces in the slab foundation short span for $\Delta_{all} = L_d/800$ and edge lift scenario: (a) bending moments; and (b) shear forces.

4.2.2.2 Effect of the type of soil movement: edge lift versus edge drop

The overall results of the parametric study revealed that the edge drop scenario is in general more critical in the design than the edge lift scenario. For example, for the same slab foundation dimensions, loading conditions and soil mound (y_m), the edge drop scenario requires an equivalent slab foundation thickness (T_{eq}) that is higher than that required for the edge lift scenario. Moreover, the internal forces in the slab foundation that govern the design result from the edge drop scenario. The above results are in agreement with the recommendations by the Swinburne's method (Holland 1981), although other researchers argued that the mound shape used in the Swinburne's method is not adequate (refer to Chapter 2). In the current study, however, the mound shapes used in both the edge drop and edge lift scenarios are obtained from a thorough 3D FE hydro-mechanical modelling that lends itself to more robust analysis, as explained earlier. In effect, the reason behind the edge lift scenario being less critical is due to the lower value of the mound stiffness used in the edge lift scenario with respect to that used in the edge drop scenario. [As mentioned earlier, the mound stiffness in the case of the edge lift scenario is logically assumed to be only 1,000 kPa, since under the heave condition (i.e. edge lift scenario) the soil is softened due to loss of suction, while under the shrinkage condition (i.e. edge drop scenario) the soil becomes drier and stiffer, warranting a higher stiffness value of say 5,000 kPa]. The low mound stiffness value in the case of the edge lift allows the slab foundation to penetrate inside the swelling soil at the beginning of the mound formation, thus, delaying the slab uplift and allowing water to infiltrate beneath the slab by a larger edge moisture distance. This provides a larger supportive area beneath the slab foundation and a smaller free span of the slab, which consequently reduces both the required thickness and resulting internal forces.

Another important reason why the edge drop scenario is more critical than the edge lift scenario in the design is the consideration of the perimeter wall loads (in the former: ED) and neglecting the central line loads (in the latter: EL). In the current study, it is assumed that the edge loads simulating the external walls are relatively heavy and serve as an indispensable requirement in construction of houses; on the other hand, the internal

partition loads can be light and may be included in the distribution of the wall loads over the slab foundations.

For both the edge lift and edge drop scenarios, the bending moments do not necessarily increase with the increase in the slab foundation dimensions, unlike the equivalent slab thickness. This is because the slab foundation becomes more flexible for large dimensions, allowing for edge deformation while maintaining large contact with soil at the slab centre. Therefore, the bending moment patterns for the edge drop and edge lift scenarios tend to be different from those of the double cantilever-like or simple beam-like in ordinary slabs with small cantilevers, which are relatively more rigid. Consequently, for the edge drop scenario, instead of having a central support area, as in the small rigid slab, a larger slab will have two symmetrical support areas, resulting in two cantilevers at the edges and a continuous beam at the central span, as shown in Figure 4.9. Similarly, in the case of the edge lift, instead of having a simple beam-like structure with full soil supports at the edges and loss of soil support at the centre as in small rigid footings, larger slabs tend to have a two-span beam structure with support area at the edges and centre of the slab, as shown in Figure 4.10.

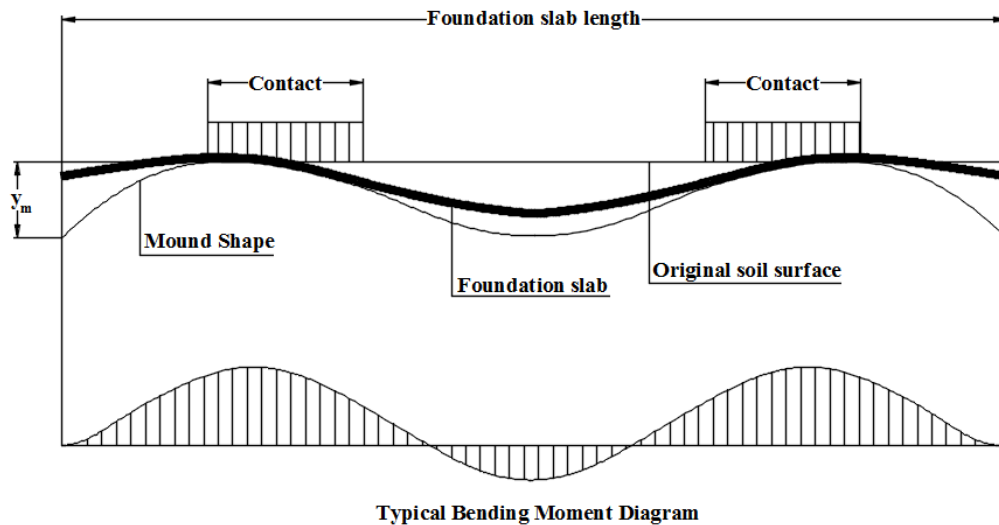


Figure 4.9: Typical mound shape, footing shape and bending moment for flexible slab foundation with large dimensions in the edge drop scenario.

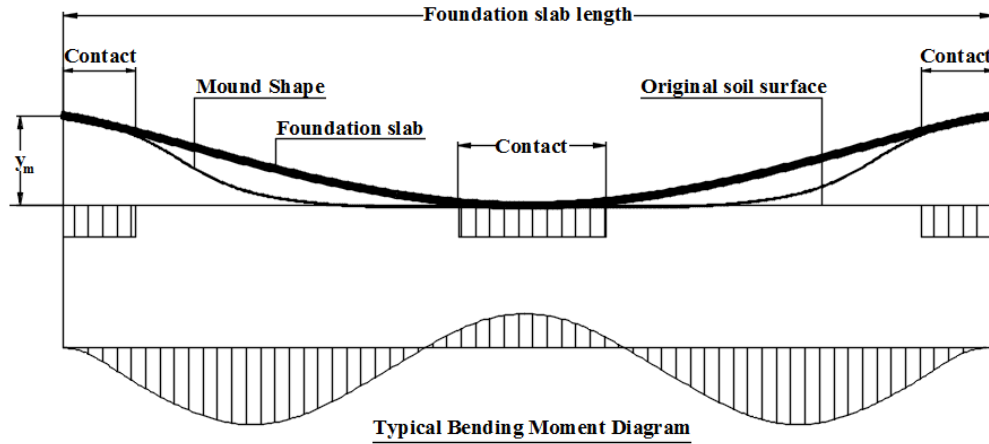


Figure 4.10: Typical mound shape, footing shape and bending moment for flexible slab foundation with large dimensions in the edge lift scenario.

4.2.2.3 Effect of construction type

In the parametric study, the effect of the construction type is expressed through the ratio of the diagonal length of the slab foundation to the allowable differential movement (L_d/Δ_{all}), where (Δ_{all}) has limits corresponding to specific construction types. Figure 4.11 shows the effect of the allowable slab foundation differential movement (Δ_{all}) (construction type) on the equivalent slab thickness (T_{eq}), for different slab dimensions. It can be seen that the equivalent slab thickness (T_{eq}) is inversely proportional to the deformation limits of the slab foundation, for both the edge lift and edge drop scenarios. Logically speaking, more slab inertia (i.e. thickness) is required to reduce the slab foundation differential movement in response to the soil deformation. It can also be seen that the equivalent slab thickness is more sensitive to the construction type than to the slab dimensions, as illustrated in Figure 4.11.

Figure 4.12 shows that the bending moment of the slab foundation increases by decreasing the allowable movement or increasing the ratio (L_d/Δ_{all}). This is attributed to the fact that a rigid construction with a small margin of allowable movement requires rigid slab configurations, thus, increasing the self-weight of the slab and in turn increasing the generated bending moments induced by the ground movement. In addition, the internal forces induced by the mound movement are generally high for rigid slab foundations.

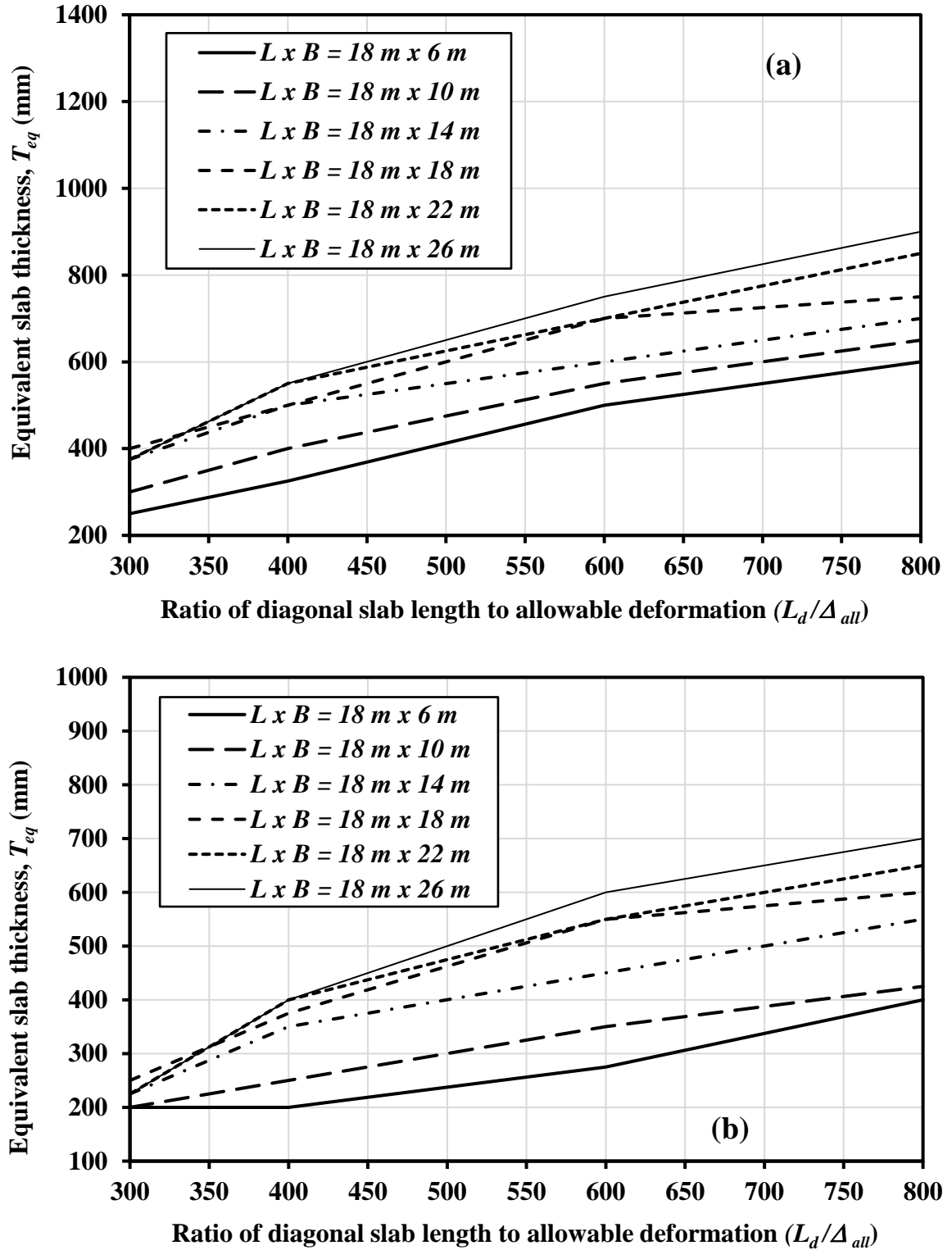


Figure 4.11: Effect of allowable slab foundation movement (Δ_{all}) on the equivalent slab foundation thickness (T_{eq}) for soil class (E) and $y_m = 70 \text{ mm}$; (a) edge drop scenario; and (b) edge lift scenario.

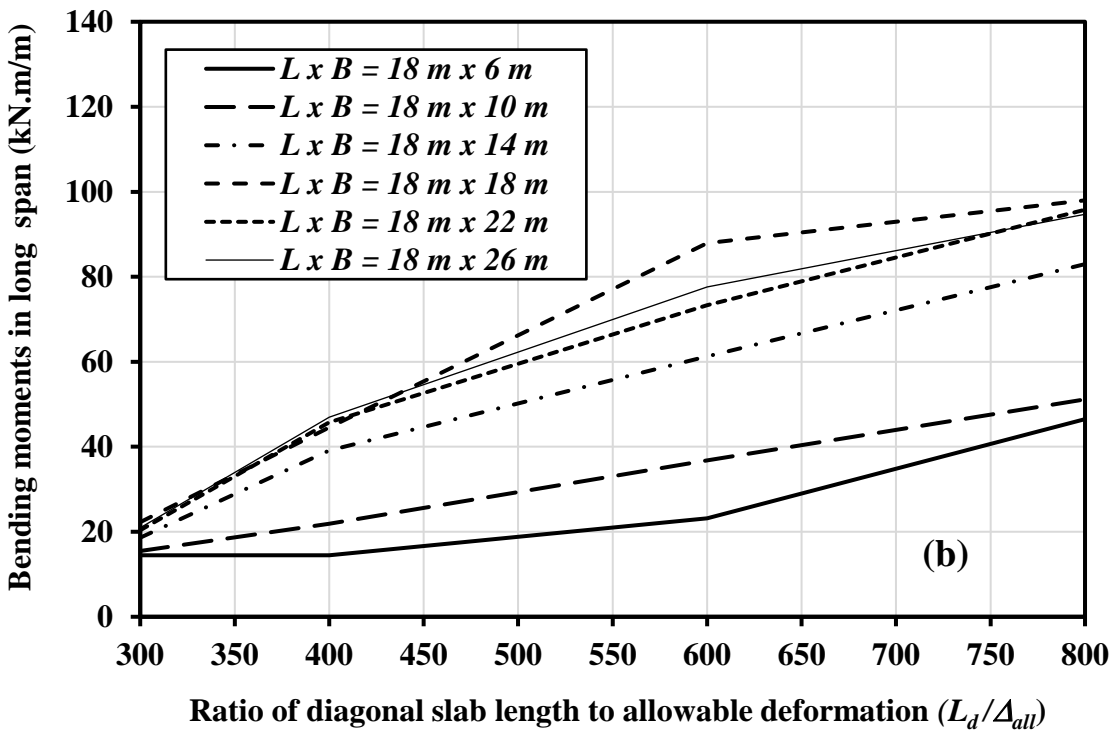
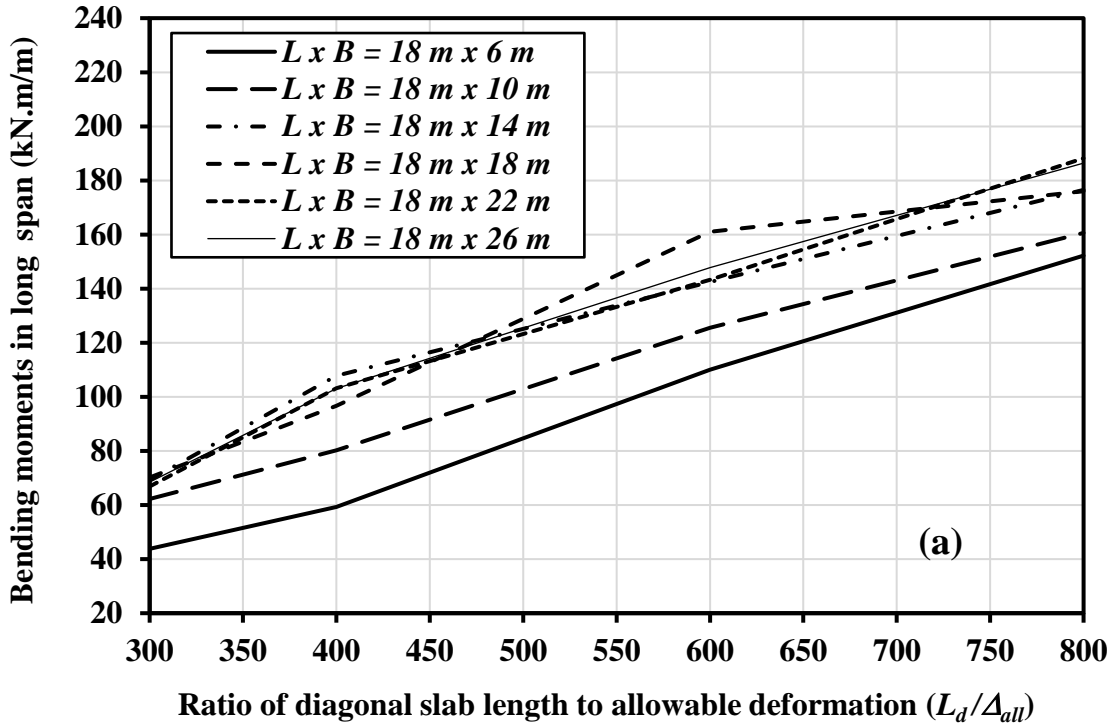


Figure 4.12: Effect of allowable slab foundation movement (Δ_{all}) on the bending moments of slab foundation for soil class (E) and $y_m = 70$ mm; (a) edge drop scenario; and (b) edge lift scenario.

4.3 DEVELOPMENT OF DESIGN EQUATIONS

As explained in Section 4.2, a computer program called SFORS is developed to perform all required design calculations. In order to reduce the inaccuracy associated with the linear interpolation of data obtained from the design charts and to reduce the complexity of integrating the design charts into this computer program, an alternative set of design equations using artificial intelligence (AI) are developed and used instead of the design charts. Details of the AI models are described below, followed by a description of how these design equations are integrated into a new design method. An illustrative numerical example is then presented to show how the new design method can be used in practice, and the results obtained are compared with 3D FE analysis and Mitchell's method.

4.3.1 Artificial intelligence for modelling design equations

In this section, the outputs obtained from the parametric study are compiled to form a database for deriving design equations using artificial intelligence (AI) techniques. These techniques are practically amenable to modelling many complex geotechnical engineering problems and have been applied successfully other authors for the design of foundations (e.g. Shahin 2010; 2014; 2015; Shahin and Jaksa 2006; Shahin et al. 2002). The most commonly used AI techniques in geotechnical engineering include (Shahin 2013): artificial neural networks (ANNs), genetic programming (GP), evolutionary polynomial regression (EPR), and support vector machines (SVM). Of these, EPR is becoming more popular and frequently used in geotechnical engineering; it will be the focus of the current work. Particularly, the EPR technique is used herein as it can provide simple symbolic forms, as usually defined in the mathematical literature, from presented trained information (data). Details of the EPR models developed for the new design method of stiffened slab foundations are described below.

4.3.2 Overview of Evolutionary Polynomial Regression (EPR)

Evolutionary polynomial regression (EPR) is a hybrid regression technique that is based on evolutionary programming, developed by Giustolisi and Savic (2006). The EPR technique was applied since then to some civil engineering problem and already has a

record of success (e.g. Ahangar-Asr et al. 2011; Berardi et al. 2008; Savic et al. 2006; Shahin and Elchalakani 2014). A detailed description of the EPR technique is beyond the scope of this research and can be found elsewhere (e.g. Giustolisi and Savic 2006).

Briefly, the EPR technique constructs symbolic models by integrating the soundest features of numerical regression, with genetic programming and symbolic regression (Koza 1992). It involves two main steps that roughly describe its underlying features. In the first step, the selection of exponents for polynomial terms is carried out, using an evolutionary searching strategy by means of genetic algorithms (Goldberg 1989). In the second step, a numerical regression step using the least square method is conducted to obtain the parameters of the previously selected polynomial terms. The general form of expression in EPR can be presented by the following equation (Savic et al. 2006):

$$y = \sum_{j=1}^m F(X, f(X), a_j) + a_o \quad (4.1)$$

where, (y) is the estimated vector of output of the process; (m) is the number of terms of the target expression; (F) is a function constructed by the process; (X) is the matrix of input variables; (f) is a function defined by the user; and (a_j) is a constant. A typical example of EPR pseudo-polynomial expression that belongs to the class of Eq. (1) is as follows (Giustolisi and Savic 2006):

$$\hat{Y} = a_0 + \sum_{j=1}^m \left(a_j \cdot (X_i)^{ES(j,1)} \dots (X_k)^{ES(j,k)} \cdot f \left[(X_i)^{ES(j,k+1)} \dots (X_k)^{ES(j,2k)} \right] \right) \quad (4.2)$$

where, (\hat{Y}) is the vector of target values; (m) is the length of the expression; (a_j) is the value of the constants; (X_i) is the vector(s) of the (k) candidate inputs; (ES) is the matrix of exponents; and (f) is a function selected by the user.

The EPR method uses two features for modelling physical phenomena (Savic et al. 2006):

(i) introduction of prior knowledge about the physical system/process – to be modelled at

three different times (i.e. before, during and after EPR modelling calibration); and (ii) production of symbolic formulas, enabling data mining to discover patterns that can describe the desired parameters. In EPR feature (i) above, the modeller (before the construction of the EPR model) selects the relevant inputs and arranges them in a suitable format according to their physical meaning. During construction of the EPR model, the model structures are determined following some user-defined settings, such as the general polynomial structure, user-defined functions (e.g. natural logarithms, exponentials, and tangential hyperbolics) and searching strategy parameters. EPR starts from true polynomials and at the same time allows for the development of non-polynomial expressions containing user-defined functions (e.g. natural logarithms). The user's physical insight and engineering judgement can also be incorporated into the EPR model by making hypotheses on the elements and structure of the selected objective functions, enabling refinement of the final models (Giustolisi and Savic 2006). After calibrating the EPR model, an optimum model can be selected from among the series of returned models; the optimum model is then selected based on the modeller's judgement, as well as the statistical performance indicators (e.g. coefficient of correlation). The strategy used herein for assessing the best models out of several generated models is that: (i) the model performs well in the validation set; (ii) the model's performance in the validation set is consistent with that of the training set; and (iii) the model has a simple structure with a minimum number of model parameters.

4.3.3 Development of EPR models for design of stiffened slab foundations

In this study, the EPR models are developed using the computer-based software package EPR TOOLBOX Version 2.0 (Laucelli et al. 2009). The modelling steps are as follows. The data used to calibrate and validate the EPR models are obtained from the outcomes of the parametric study. The available data are divided into two sets: a training set (the extreme values of the data are included in this set) for model calibration and an independent validation set for model verification. In total, a number of 389 data cases are compiled from the parametric study for the edge drop scenario, whereas 248 data cases are collected for the edge heave scenario. In both scenarios, 90% of the available data are used for model training and 10% for model validation. The data division is carried out in

such a way that the training and validation sets are statistically consistent and thus represent the same statistical population. Therefore, the training and the validation sets had close averages and standard deviations. The inputs include the slab foundation breadth (B), the slab foundation length (L), the maximum soil mound differential movement (y_m), the allowable slab deformation (Δ_{all}), and the equivalent rectangular slab foundation thickness (T_{eq}). The outputs include the slab foundation differential movement (δ), which involves the construction type, the service bending moment in the short direction of slab foundation (M_s), the service bending moment in the long direction of slab foundation (M_l), the service shear force in short direction of slab foundation (V_s), and the service shear force in the long direction of the slab foundation (V_l). It should be noted that the EPR modelling is carried out separately for each of the abovementioned inputs using the same inputs, for both the edge lift and edge drop scenarios, leading to ten derived equations to be used in the new design method, as explained later.

Following the data division, the input and output variables are presented to the EPR for model training and a set of internal model parameters are tried in an attempt to arrive at an optimal model, by selecting the related internal parameters for evolving the model. The optimization phase is undertaken as follows. Before presenting the data to the EPR for training, the input and output variables were pre-processed by scaling them between 0.0 and 1.0 for normalisation and to ensure that all variables receive equal weight during training. The polynomial structure of the EPR is assumed in such a way that each regression term consists of elements from X that are raised to pre-specified power values; the assumed range of possible exponents of terms from X was (-2; -1; -0.5; 0; 0.5; 1; 2). As explained by Giustolisi et al. (2007), the exponent 0 is useful for deselecting the non-necessary inputs, the exponents (-0.5 and 0.5) smooth the effect of the inputs, the exponents (-1 and 1) produce a linear effect of the inputs and the exponents (-2 and 2) amplify the inputs. The maximum length of the polynomial structure is assumed to be 5 terms and the bias term is assumed to be zero. Finally, the least square search is performed for positive coefficients only (i.e. $a_j > 0$), and is obtained using the singular value decomposition based solver (Giustolisi and Savic 2006).

Once the training phase is accomplished successfully, the performance of the trained models is verified using the validation set. Performance of the proposed EPR models in the training and validation sets is evaluated using the coefficient of correlation, r , which is a measure used to determine the relative correlation between the predicted and observed outputs. It is the most commonly used measure to examine the performance of AI models. The developed EPR equations are shown below, along with their graphical representation performance (i.e. Figures 4.13 to 4.22):

For the edge lift scenario (EL):

$$\delta = 0.33689 \frac{T_{eq}^2}{B^2 L \sqrt{y_m}} - 0.00067293 \frac{y_m T_{eq}^2}{L^2 \sqrt{B}} + 3.7501 y_m \sqrt{\frac{B}{T_{eq}}} - 6099.0209 \frac{B y_m}{L T_{eq}^2} - 0.037446 \frac{B^2 L \sqrt{y_m}}{T_{eq}} - 16.502 \quad (4.3)$$

$$M_s = -1.1912 \times 10^{-6} \frac{y_m^2 T_{eq}^2}{B \sqrt{L}} + 1.2662 \times 10^{-7} \frac{y_m^2 T_{eq}^2 \sqrt{B}}{L} + 0.00086523 y_m T_{eq} \sqrt{B} - 2.427 \times 10^{-5} \frac{B^2 y_m T_{eq}}{\sqrt{L}} - 6.0017 \quad (4.4)$$

$$M_l = -1.8296 \frac{y_m}{\sqrt{BL}} + 5.4937 \times 10^{-7} \frac{y_m^2 T_{eq}^2}{L} + 0.27403 \sqrt{y_m T_{eq}} - 12.2302 \quad (4.5)$$

$$V_s = -0.01545 \frac{y_m T_{eq}}{B^2} + 7131.6238 \frac{1}{y_m \sqrt{B T_{eq}}} + 0.022426 y_m \sqrt{T_{eq}} - 6.452 \times 10^{-5} B y_m^2 - 8.5607 \quad (4.6)$$

$$V_l = 9.4532 \times 10^{-7} \frac{y_m^2 T_{eq}^2}{B^2 \sqrt{L}} + 0.014984 \frac{y_m \sqrt{B T_{eq}}}{\sqrt{L}} - 1.9426 \frac{B Y_m}{L \sqrt{T_{eq}}} + 1.7681 \quad (4.7)$$

Likewise for the edge drop scenario (ED):

$$\delta = -0.097655 \frac{y_m T_{eq}}{L^2} - 7.0882 \sqrt{\frac{T_{eq}}{y_m}} + 8.6118 y_m \sqrt{\frac{B}{L T_{eq}}} - 64.182 \frac{B^2}{L T_{eq}} + 33.8095 \quad (4.8)$$

$$M_s = 0.000190377 T_{eq}^2 - 3.9791 \times 10^{-5} y_m^2 T_{eq} + 1.9208 \times 10^{-8} L^2 \sqrt{y_m^2} e^{0.5B} + 0.0026711 y_m T_{eq} \sqrt{B} - 0.00027428 B^2 y_m \sqrt{T_{eq}} + 3.296 \quad (4.9)$$

$$M_l = 0.0038785 y_m T_{eq} - 3.4044 \times 10^{-6} y_m^2 L \sqrt{B T_{eq}} \quad (4.10)$$

$$V_s = 126.1764 \frac{1}{B^2} \sqrt{\frac{y_m}{L}} - 0.017714 \frac{y_m T_{eq}}{B^2} + 0.31019 \sqrt{y_m T_{eq}} - 0.0018124 B y_m \sqrt{\frac{T_{eq}}{L}} - 10.5604 \quad (4.11)$$

$$V_l = 0.35345 \sqrt{y_m T_{eq}} - 0.0088593 \sqrt{B L y_m T_{eq}} + 5.1508 \times 10^{-5} B L^2 \sqrt{T_{eq}} - 9.9742 \quad (4.12)$$

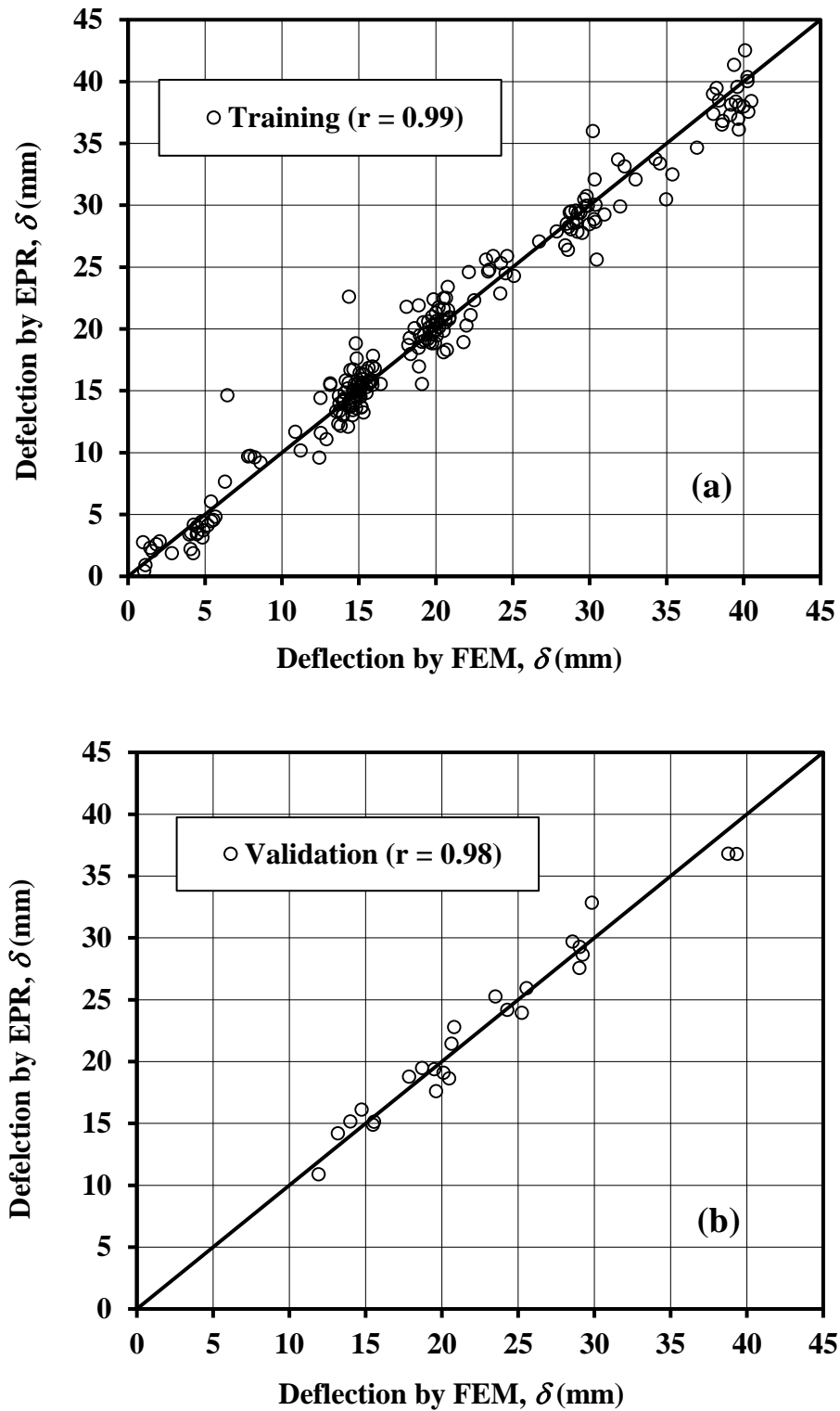


Figure 4.13: Graphical performance of the EPR model of Equation 4.3 regarding deflection δ : (a) Training set; and (b) Validation set.

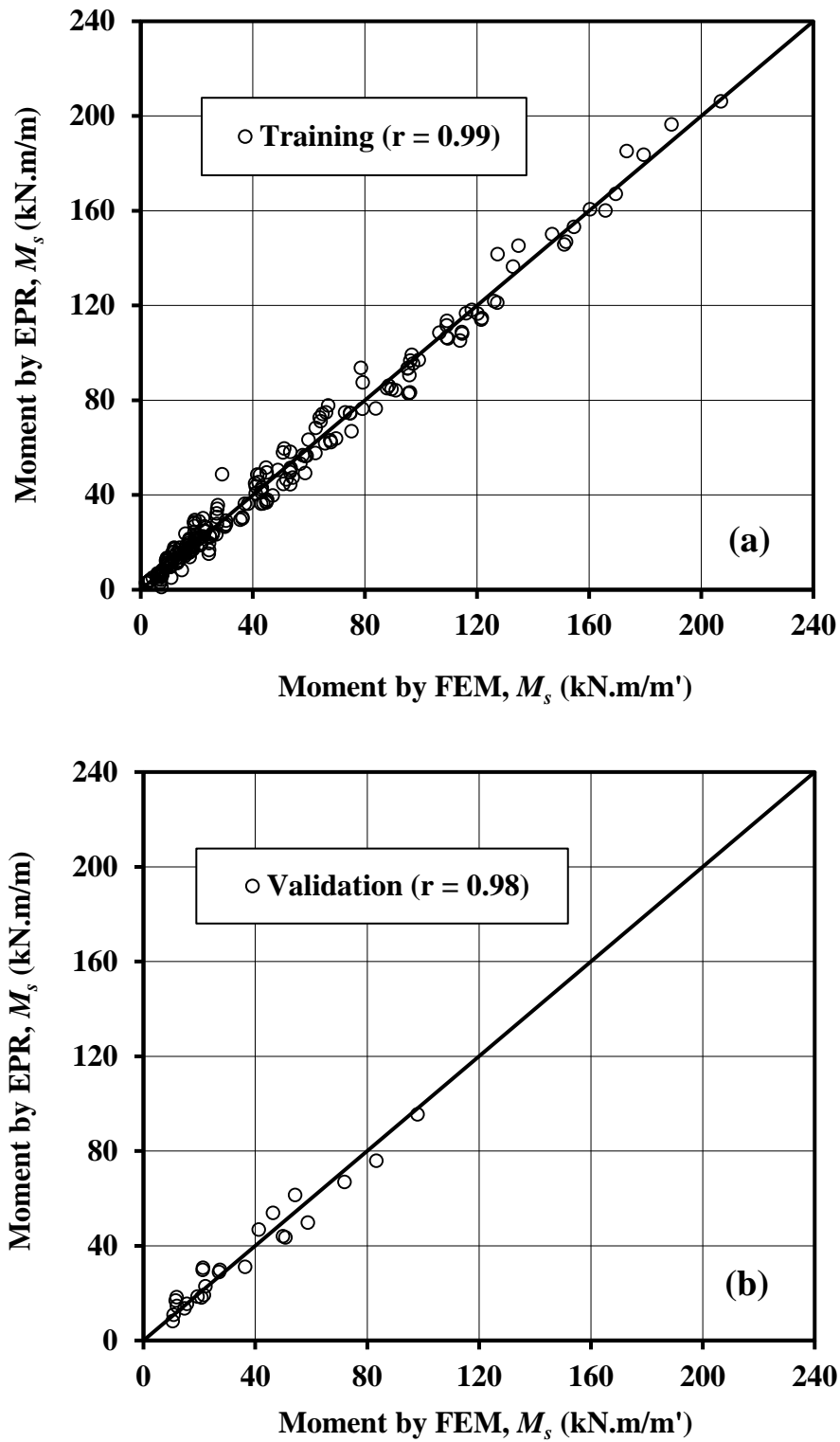


Figure 4.14: Graphical performance of the EPR model of Equation 4.4 regarding M_s : (a) Training set; and (b) Validation set.

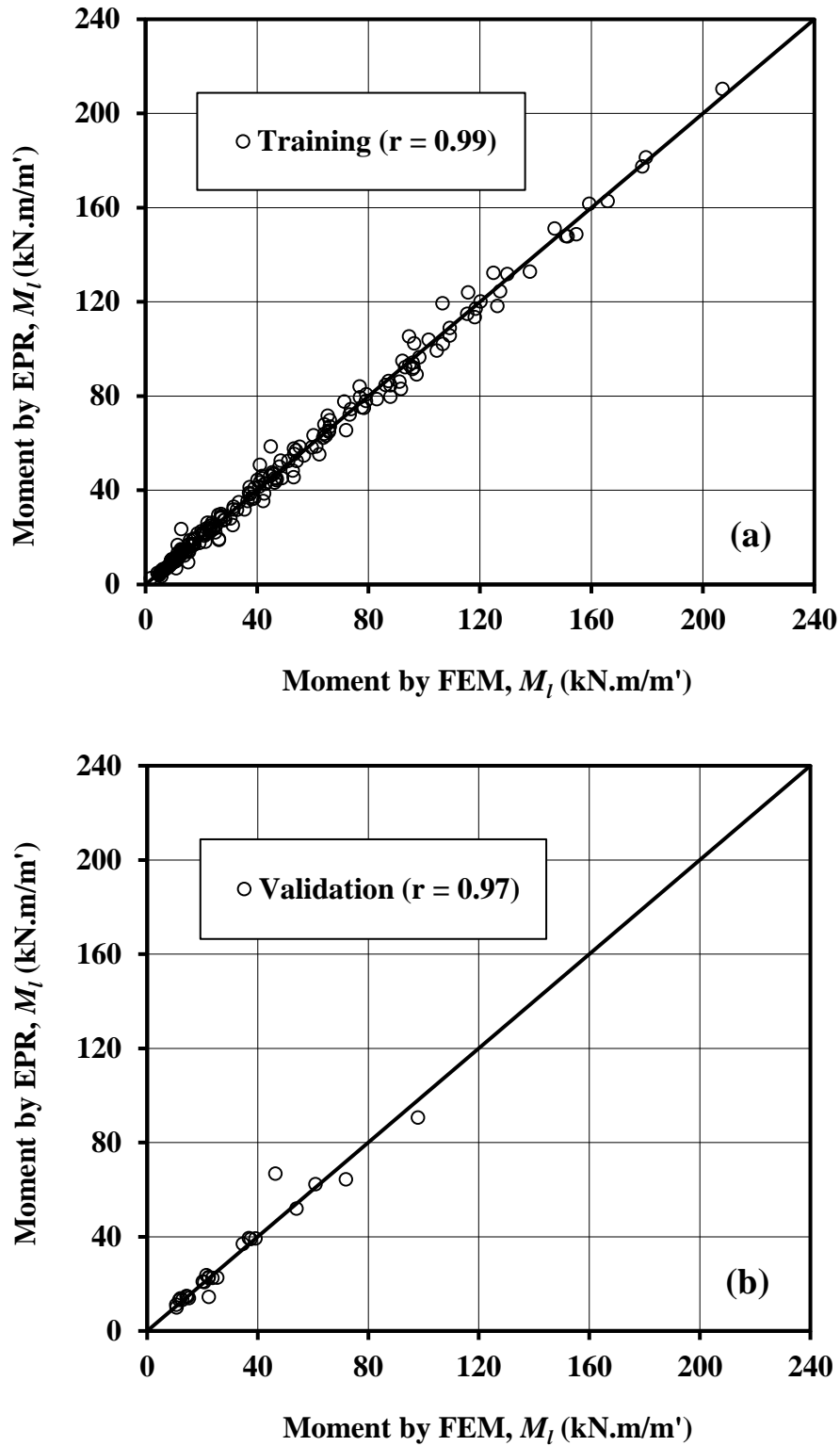


Figure 4.15: Graphical performance of the EPR model of Equation 4.5 regarding M_I : (a) Training set; and (b) Validation set.

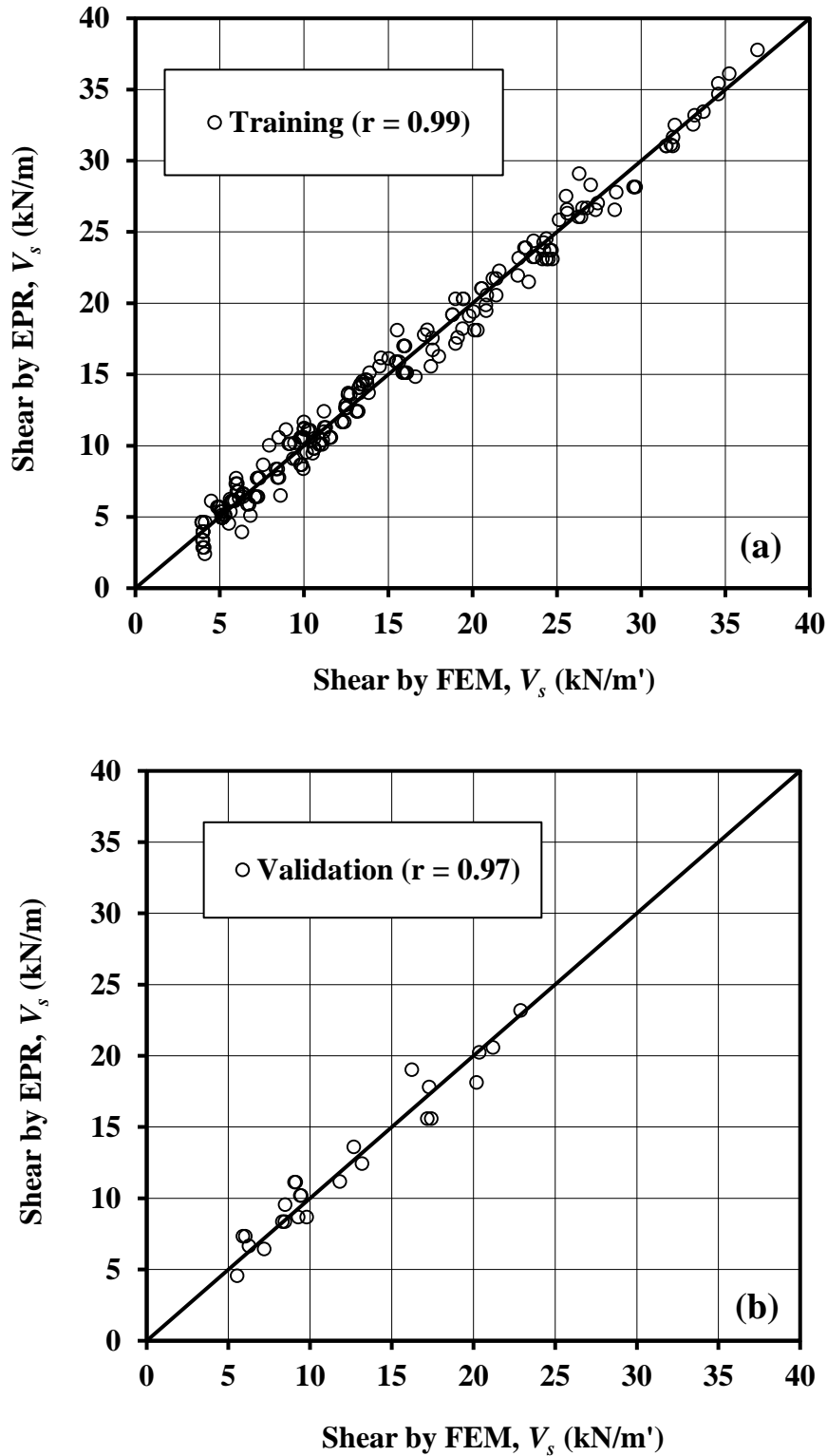


Figure 4.16: Graphical performance of the EPR model of Equation 4.6 regarding V_s : (a) Training set; and (b) Validation set.

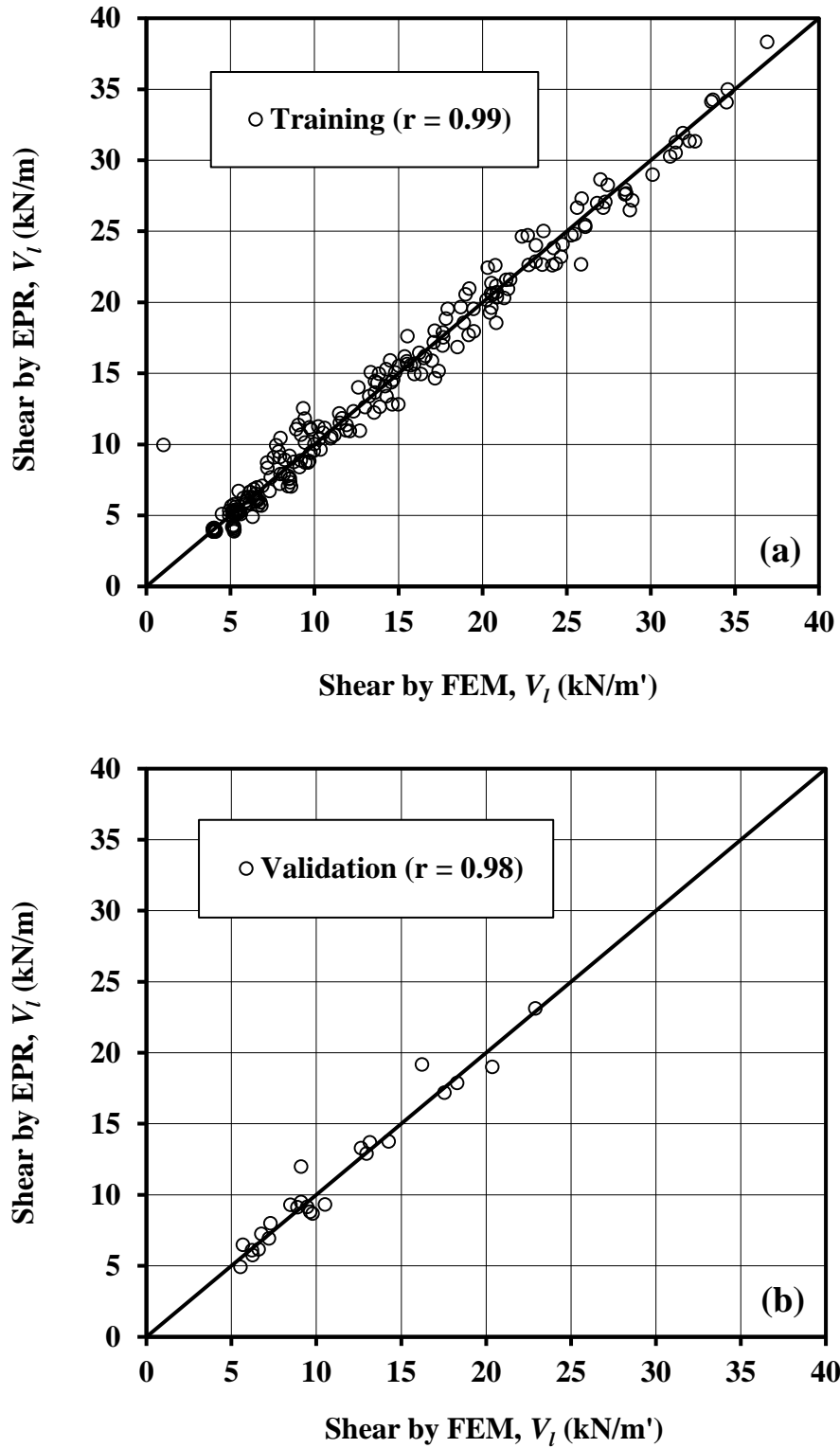


Figure 4.17: Graphical performance of the EPR model of Equation 4.7 regarding V_l : (a) Training set; and (b) Validation set.

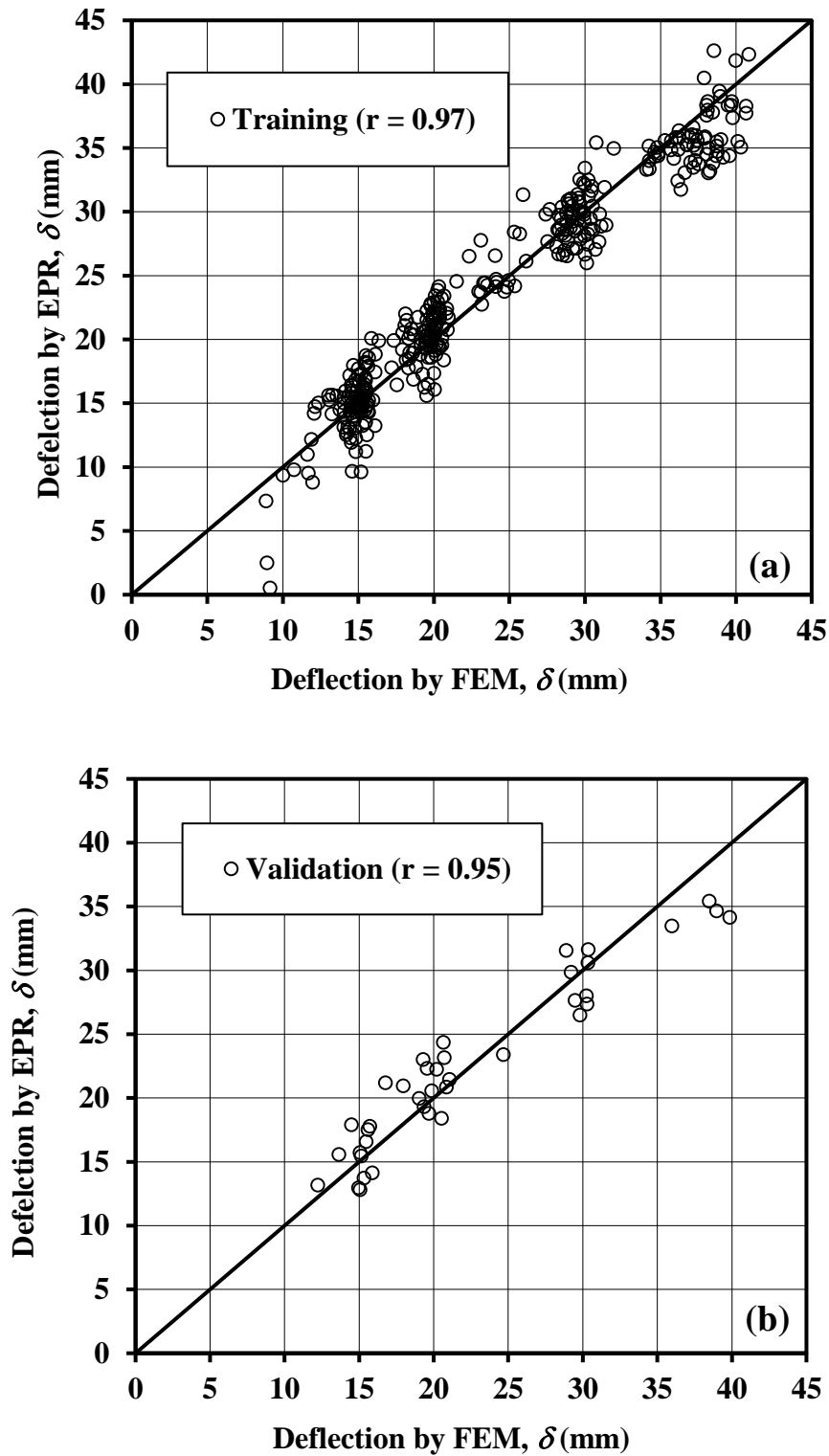


Figure 4.18: Graphical performance of the EPR model of Equation 4.8 regarding deflection δ : (a) Training set; and (b) Validation set.

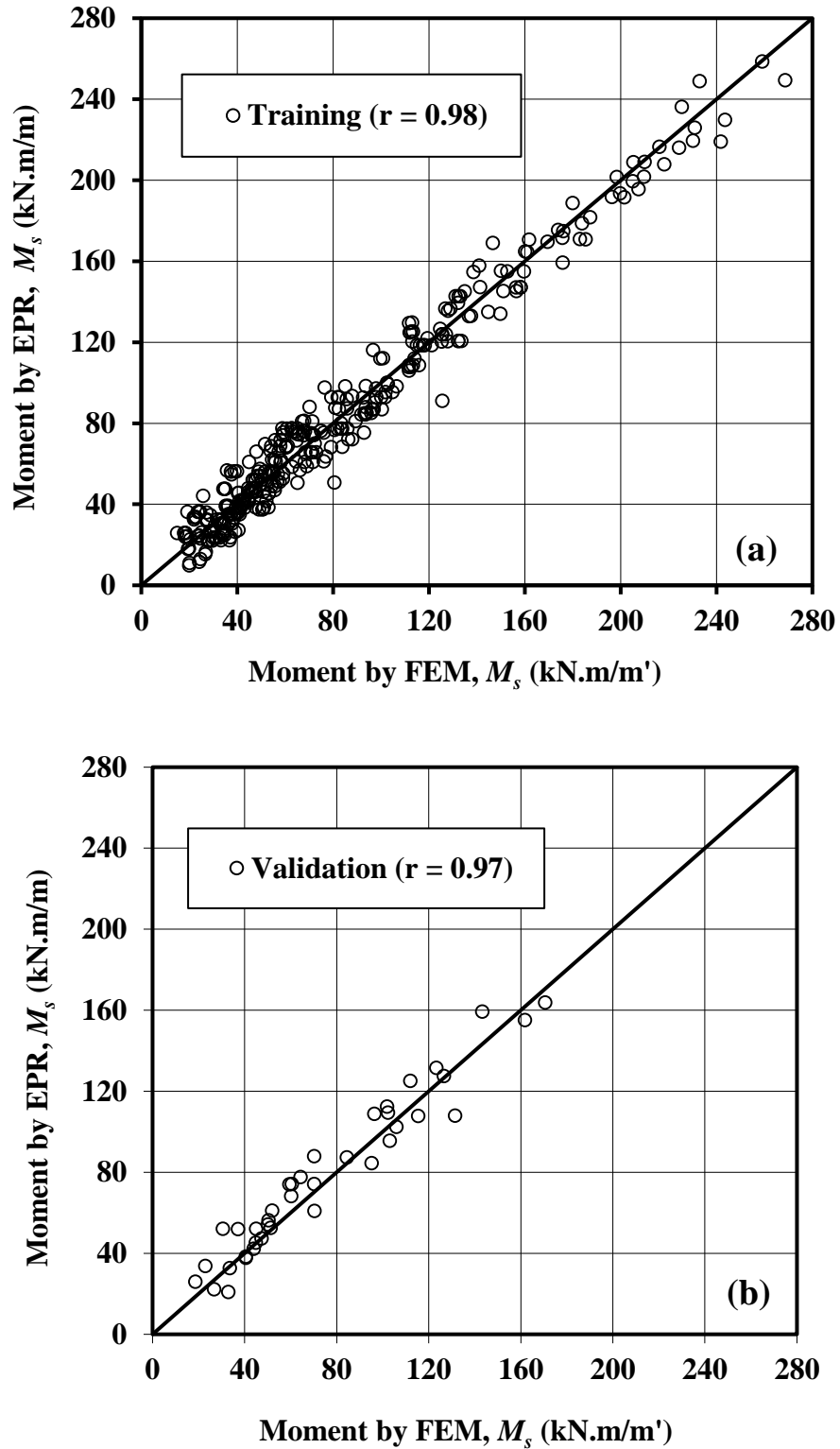


Figure 4.19: Graphical performance of the EPR model of Equation 4.9 regarding M_s : (a) Training set; and (b) Validation set.

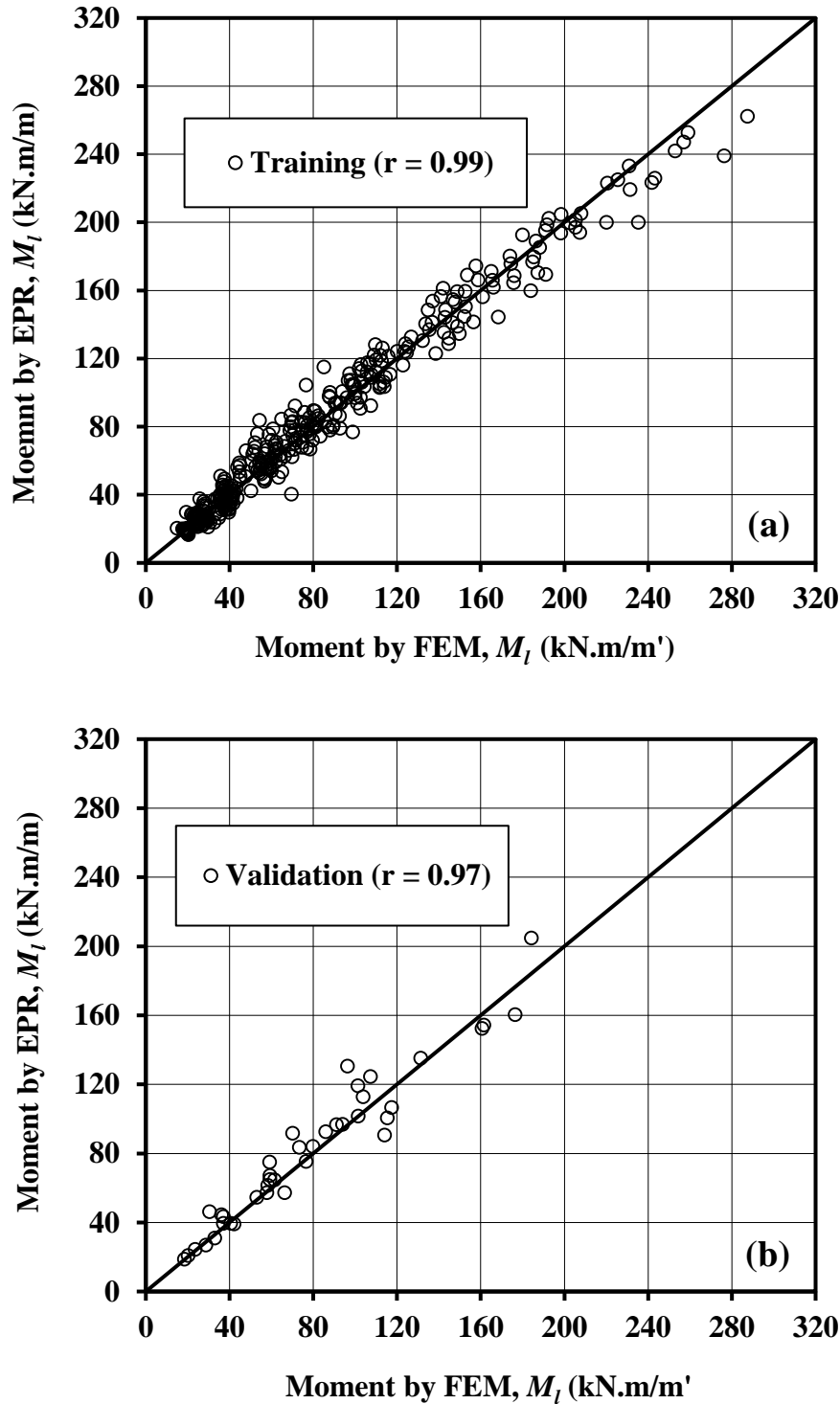


Figure 4.20: Graphical performance of the EPR model of Equation 4.10 regarding M_l : (a) Training set; and (b) Validation set.

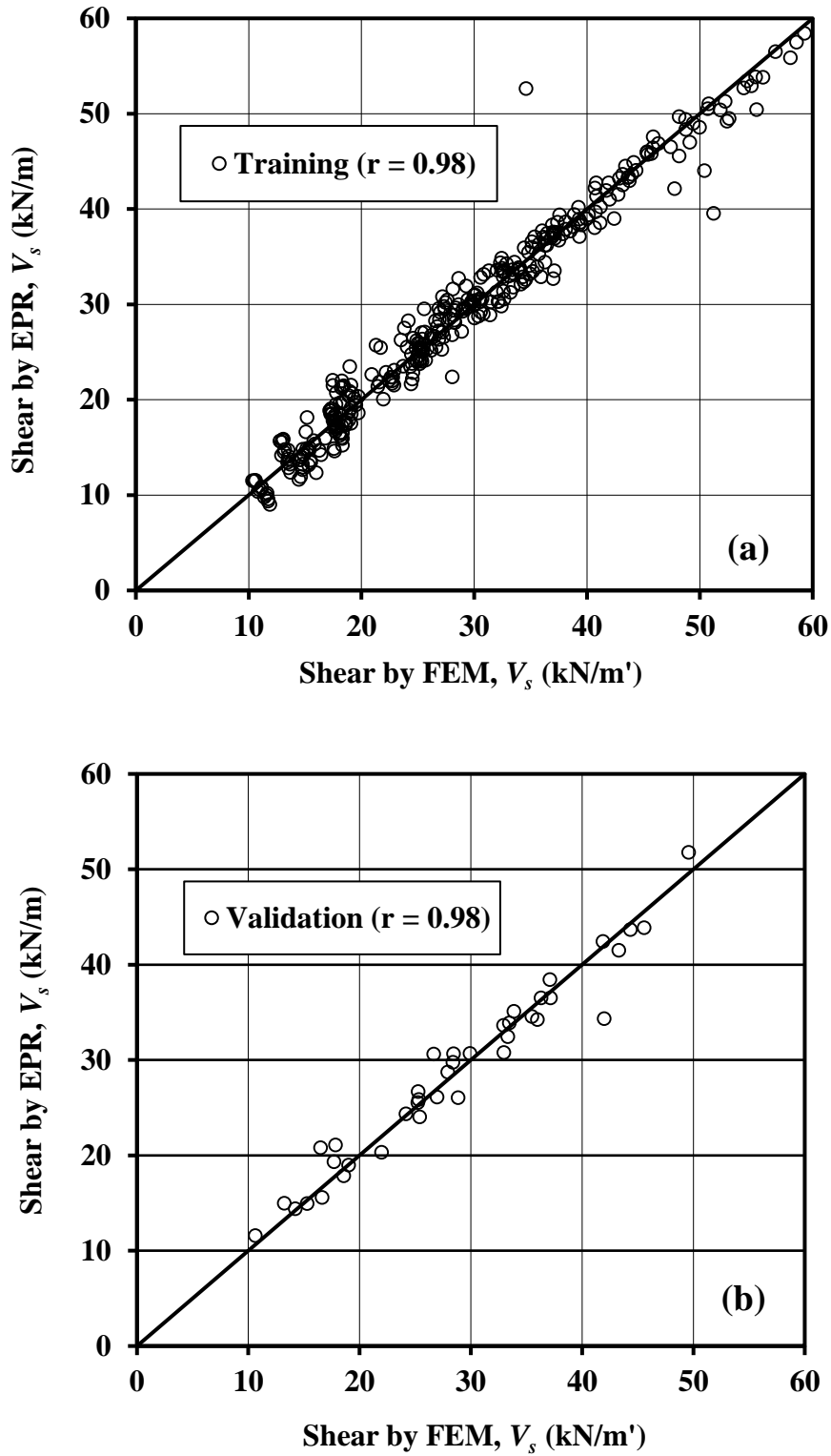


Figure 4.21: Graphical performance of the EPR model of Equation 4.11 regarding V_s : (a) Training set; and (b) Validation set.

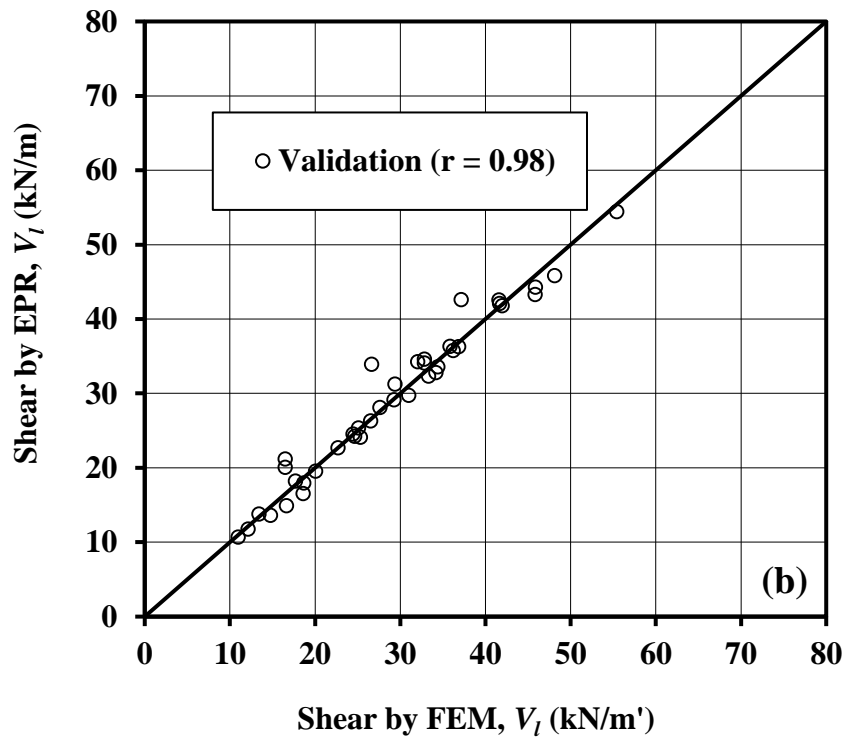
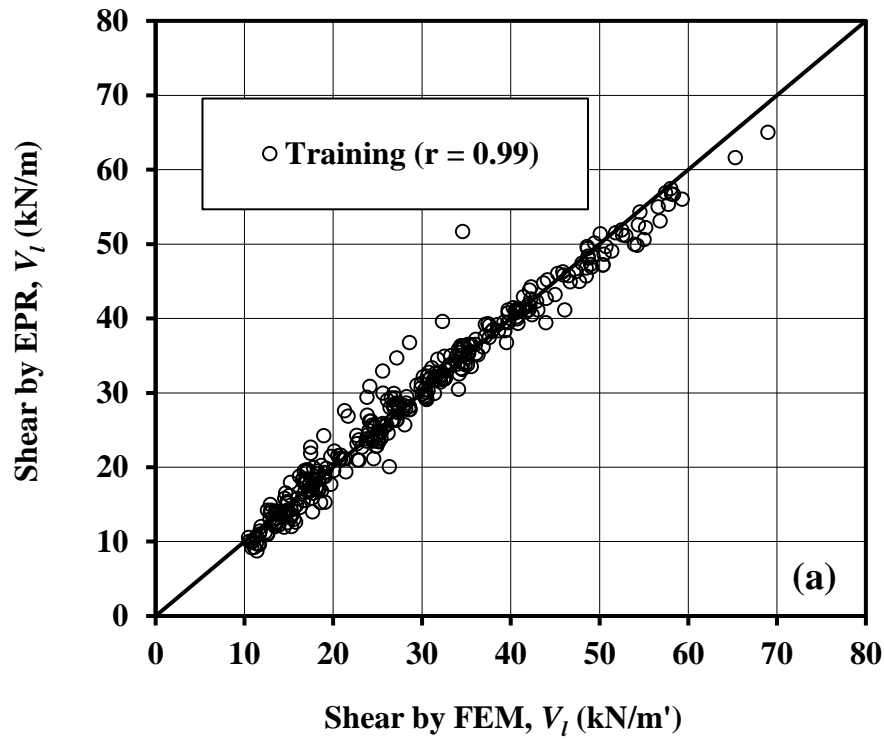


Figure 4.22: Graphical performance of the EPR model of Equation 4.12 regarding V_l : (a) Training set; and (b) Validation set.

4.4 NEW DESIGN METHOD EXPLAINED VIA NUMERICAL EXAMPLE

The steps of the new design method and how it can be used in practice are best explained through an illustrative numerical example. The example postulates that an arbitrary slab having *L*-shape plan layout, as shown in Figure 4.23, is to be designed to support a single storey articulated masonry veneer house on a highly reactive class (H1) with a characteristic surface heave, $y_s = 60$ mm. The design implies the following steps:

1. Verify the design service loads acting on the slab foundation and make sure they do not exceed those shown in Table 4.1. Note that, as mentioned in Section 4.2, these loads do not include the self-weight of the foundation elements (slab and beams).
2. Apply the concept of overlapped rectangles to *L*-shape slabs by dividing it into two overlapped rectangle slab areas (14 m × 18 m) and (6 m × 18 m), as highlighted in Figure 4.23.
3. Calculate the soil mound movement (y_m) in accordance with the Australian Standards AS2870 (2011), as $y_m = 0.7 y_s = 0.7 \times 60$ mm = 42 mm.
4. The construction type is defined as ‘articulated masonry veneer’, which has an allowable slab foundation differential movement ($\Delta_{all} = L_d/400$) not exceeding 30 mm; where (L_d) is the slab diagonal dimension. For the 14 m × 18 m slab, $\Delta_{all} = 22800/400 = 57$ mm > 30 mm, hence, the 30 mm is the limit, and for the 6 m × 18 m slab, $\Delta_{all} = 18970/400 = 47$ mm > 30 mm, hence, 30 mm is the limit.

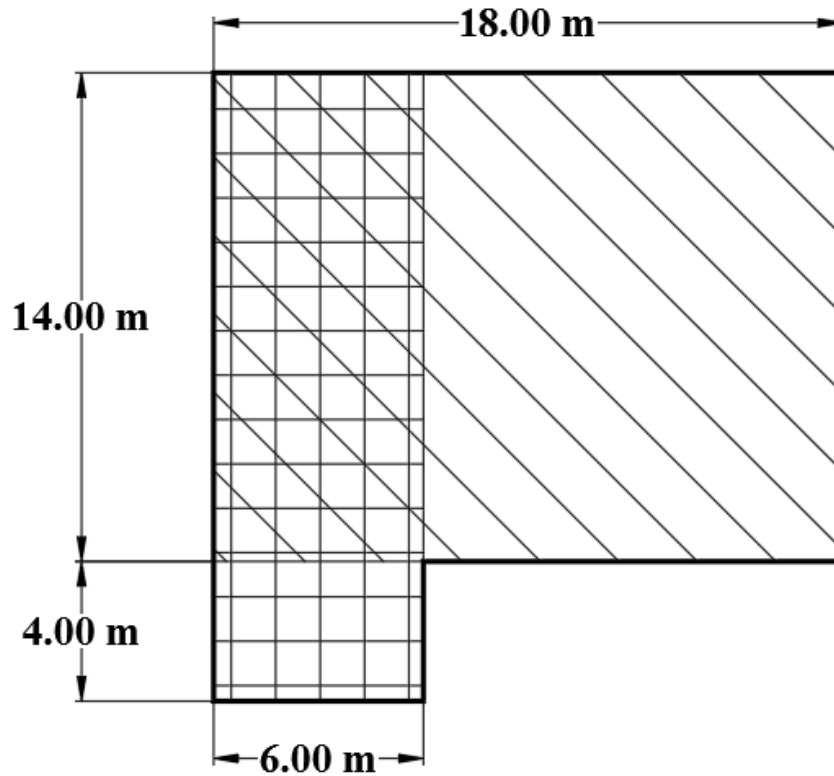


Figure 4.23: Typical L-shape slab foundation used in the numerical example composed of two overlapped rectangular areas.

5. The following outputs, which are derived from the EPR models, are determined for the footing dimensions (6 m × 18 m) and the edge drop scenario:
 - The required equivalent thickness, $T_{eq} = 200$ mm
 - The bending moment in the short direction, $M_s = 30.74$ kN.m/m
 - The bending moment in the long direction, $M_l = 28.84$ kN.m/m
 - The shear force in the short direction, $V_s = 17.57$ kN/m
 - The shear force in the long direction, $V_l = 15.40$ kN/m

6. Likewise, the following outputs, are determined for the footing dimensions (14 m × 18 m) and the edge drop scenario:
 - The required equivalent thickness, $T_{eq} = 260$ mm
 - The bending moment in the short direction, $M_s = 44.90$ kN.m/m

- The bending moment in the long direction, $M_l = 35.79$ kN.m/m
- The shear force in the short direction, $V_s = 17.78$ kN/m
- The shear force in the long direction, $V_l = 16.02$ kN/m

7. Similarly, the following outputs (derived from the EPR models), are determined for the footing dimensions (6 m × 18 m) and the edge lift scenario:

- The required equivalent thickness, $T_{eq} = 200$ mm
- The bending moment in the short direction, $M_s = 7.99$ kN.m/m
- The bending moment in the long direction, $M_l = 7.65$ kN.m/m
- The shear force in the short direction, $V_s = 5.37$ kN/m
- The shear force in the long direction, $V_l = 5.42$ kN/m

8. Finally, the following outputs are determined for the footing dimensions (14 m × 18 m) and the edge lift scenario:

- The required equivalent thickness, $T_{eq} = 200$ mm
- The bending moment in the short direction, $M_s = 12.22$ kN.m/m'
- The bending moment in the long direction, $M_l = 10.20$ kN.m/m
- The shear force in the short direction, $V_s = 5.71$ kN/m
- The shear force in the long direction, $V_l = 5.21$ kN/m

9. Estimate the configuration of the sub-beams based on the following limits: minimum spacing = 3.0 m and maximum spacing = 4.0 m. Based on these limits, the configuration shown in Figure 4.24 is deemed acceptable. Note that the width of all sub-beams is chosen to be 300 mm.

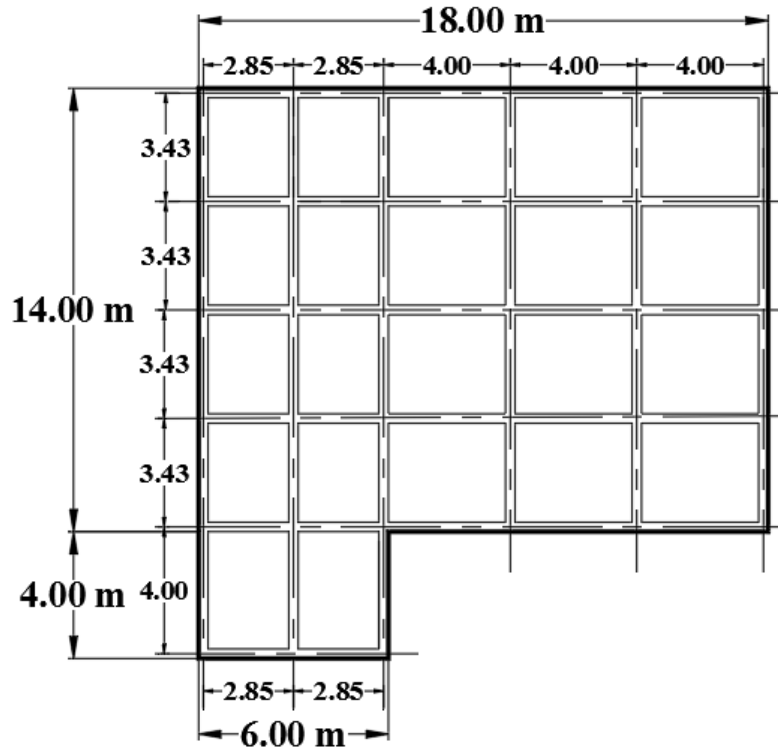


Figure 4.24: Sub-beams spacing for the slab foundation of the numerical example.

10. From the plan layout of Figure 4.24, the maximum width served by the sub-beams is determined in the long span and short span for each rectangular part of the slab, which in this numerical example are found to be 3.43 m and 4.0 m, for the 14 m \times 18 m rectangular part of the slab, and 2.85 m and 3.71 m for the 6 m \times 18 m rectangular part of the slab. Consequently, the flange width (b_f) in the short and long directions can be verified against the recommendations of Section 4.4 of the Australian Standards AS 2870 (2011). In this example, the effective flange width (b_f) is conservatively calculated as 1500 mm and 1850 mm for the 6 m \times 18 m rectangle, in the long and the short direction respectively, whereas it is computed as 1750 mm and 2000 mm for the 18 m \times 14 m rectangle, in the long and short directions, respectively.
11. The design in the long and short directions is carried out under both the edge lift and edge drop scenarios, in order to find the required sub-beams depth for certain top and bottom reinforcement considering the effective section inertia based on Section 4.2.1 (items 9 to 11). An iterative procedure is required, as follows:

- The top and bottom reinforcements are first estimated along with the top and bottom concrete covers. In this numerical example, the top cover is considered to be 30 mm, while the bottom cover is taken to be 50 mm.
 - The width of the sub-beam (B_w) is considered to be 300 mm, the width of the flange is already known (refer to Step 4) and the depth of the sub-beam (T_b) is estimated.
 - The effective inertia of the sub-beam section (I_{eff}) is calculated using Branson's equation, by knowing the following: the dimensions of the T-section of the stiffening beam (i.e. B_w , b_f and T_b), as well as the steel reinforcements, and the applied moments obtained from the EPR equations.
 - The effective inertia of the sub-beam per unit width ($I_{eff}/\text{served width}$) is then compared with the inertia calculated from the required equivalent thickness (T_{eq}) obtained from the EPR models.
 - The iteration is carried out by changing (T_b) and the reinforcement until ($I_{eff}/\text{served width}$) equals the inertia calculated from the required equivalent thickness (T_{eq}).
12. After obtaining the maximum required sub-beams depth, the flexural reinforcement and the shear capacity are verified based on the Australian Standards AS3600 (2009). Note that the values of the internal forces of the slab foundations are service (working forces) and factorised by 1.35 to obtain the factored design moments and shearing forces.

A flow diagram that explains the above design procedure is shown in Figure 4.25. As explained earlier, for the ease of use by design engineers and practitioners, the abovementioned steps as well as EPR models are integrated into the SFORS computer program that can perform all of the above design calculations and iterations. This computer program is user-friendly and will be available for interested readers upon request. Figures 4.26-4.29 show screenshots of the program's input and output modules.

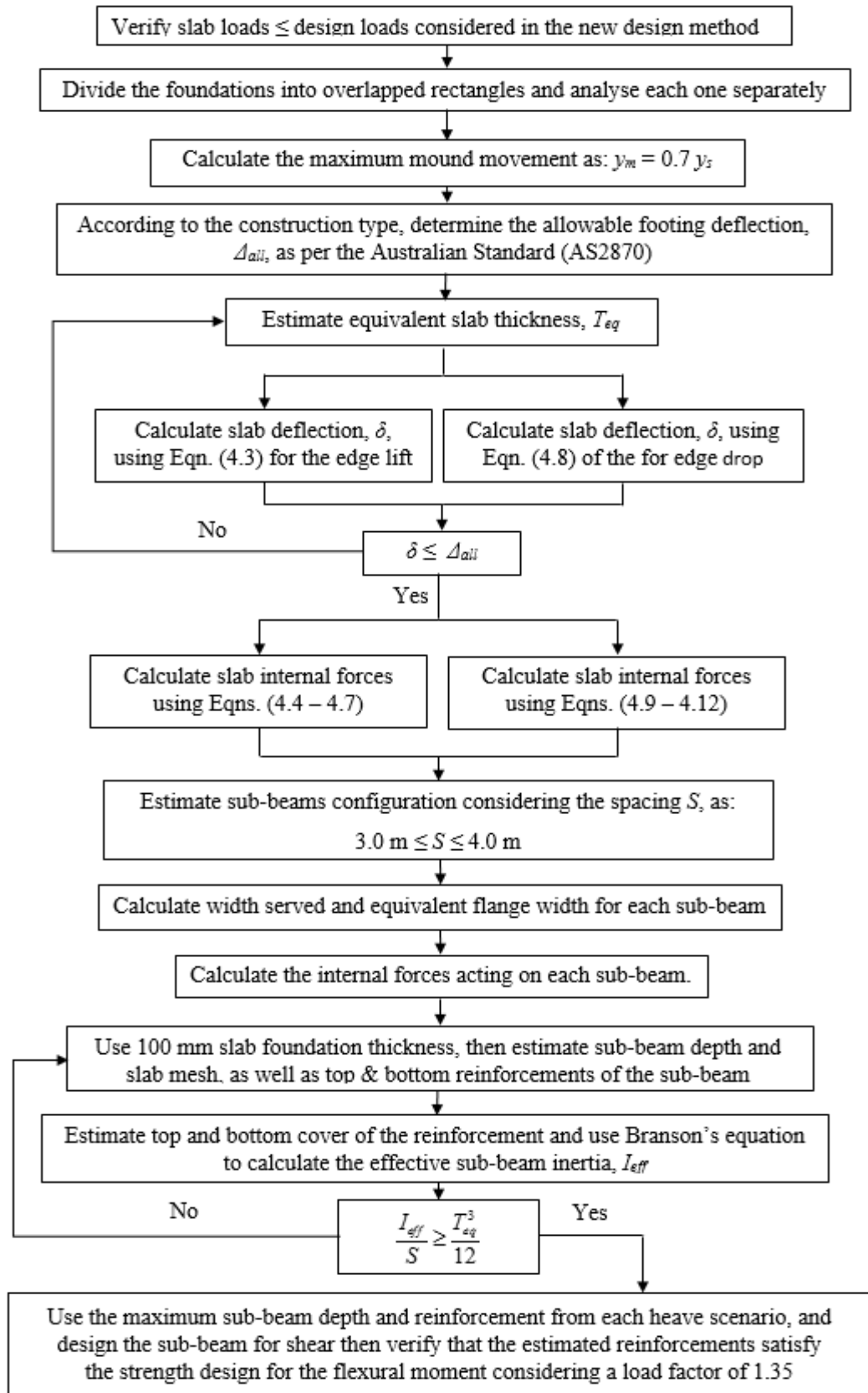


Figure 4.25: Flow chart explaining the procedure of the new design method.

SFORS

Slab long span	L	18.00	m
Slab short span	B	6.00	m
No. of beams in long span	N_L	3	Max. spacing CL to CL in long direction 3.000 m
No. of beams in short span	N_S	6	Max. spacing of beams in short direction 3.700 m
Beam web width	b_w	300.00	mm
Top rebars	A_{sc}	3	16.00 ▾
Bottom rebars	A_{st}	3	16.00 ▾
Slab reinforcement	S_r	175.00	mm ² /m'
Top cover	T_c	30.00	mm
Bottom cover	B_c	50.00	mm
Soil movement	γ_m	42.00	mm
Allowable deflection	L/Δ	400.00	▾

Solve Clear

Figure 4.26: Screenshot of the SFORS Program developed for the new design method, solving rectangle (6 m × 18 m) of the numerical example.

SFORS

Slab long span	L	18.00	m
Slab short span	B	14.00	m
No. of beams in long span	N_L	5	Max. spacing CL to CL in long direction 3.500 m
No. of beams in short span	N_S	6	Max. spacing of beams in short direction 4.000 m
Beam web width	b_w	300.00	mm
Top rebars	A_{sc}	3	16.00 ▾
Bottom rebars	A_{st}	3	16.00 ▾
Slab reinforcement	S_r	175.00	mm ² /m'
Top cover	T_c	30.00	mm
Bottom cover	B_c	50.00	mm
Soil movement	γ_m	42	mm
Allowable deflection	L/Δ	400.00	▾

Solve Clear

Figure 4.27: Screenshot of the SFORS Program developed for the new design method, solving rectangle (14 m × 18 m) of the numerical example.

<div style="text-align: center;"> <h1 style="margin: 0;">SFORS</h1> <p style="margin: 0;">Slab Foundation On Reactive Soil</p> </div>		Project			
		Client			
		Date	Rev.		
Input Data:					
Slab foundation length	L	18	m		
Slab foundation breadth	B	6	m		
No. of beams in long direction	N_L	3			
Max. CL to CL distance in long direction	S_L	3	m		
No. of beams in short direction	N_s	6			
Max. CL to CL distance in short direction	S_s	3.7	mm		
Beam web width	b_w	300	mm		
Top cover to reinforcement	T_c	30	mm		
Bottom cover to reinforcement	B_c	50	mm		
Slab reinforcement	S_r	175	mm ² /m'		
Concrete grade	f'_c	20	MPa		
Reinforcement yield strength	f_y	500	MPa		
Soil mond movement	y_m	42	mm		
Allowable slab deflection	L/Δ	400			
Top reinforcement	A_{sc}	3	N	16	
Bottom reinforcement	A_{st}	3	N	16	
Slab thickness	T_s	100	mm		
Output Data :					
		Edge drop		Edge lift	
		Long span	Short span	Long span	Short span
Equivalent slab thickness	mm	200	200	200	200
Equivalent slab inertia	m ⁴ /m'	6.67E-04	6.67E-04	6.67E-04	6.67E-04
Service BM per metre width	kN.m/m'	28.835	30.739	7.648	7.985
Service BM per beam	kN.m/m'	86.505	113.734	22.944	29.545
Effective flange width	m	1.500	1.850	1.500	1.850
Cracking moment/beam	kN.m'	55.987	72.801	22.763	27.863
Required beam depth	m	0.458	0.486	0.349	0.380
Eff. inertia of stiffened slab	m ⁴ /m'	6.67E-04	6.67E-04	6.67E-04	6.66E-04
Max. required beam depth	m	0.486			
Max. flexural rebars	mm ²	5137	5477	3590	3964
Min. flexural rebars	mm ²	495	611	288	335
Max. service shear force	kN/m'	15.398	17.567	5.420	5.374
Required shear rebars	mm ²	63.000			
Required shear rebars spacing	mm	300.000			
Summary:					
Total height of sub-beam	mm	486			
Top rebars		3	N	16	
Bottom rebars		3	N	16	
Shear rebars		2	N	8	@ 300.000
Slab rebars (both directions)	mm ² /m'	175			

Figure 4.28: Screenshot of the design report obtained from the SFORS program developed for the new design method, solving (6 m × 18 m) of the numerical example.

<div style="text-align: center;"> <h1 style="margin: 0;">SFORS</h1> <p style="margin: 0;">Slab Foundation On Reactive Soil</p> </div>		Project			
		Client			
		Date		Rev.	
Input Data:					
Slab foundation length	L	18	m		
Slab foundation breadth	B	14	m		
No. of beams in long direction	N_L	5			
Max. CL to CL distance in long direction	S_L	3.5	m		
No. of beams in short direction	N_s	6			
Max. CL to CL distance in short direction	S_s	4	mm		
Beam web width	b_w	300	mm		
Top cover to reinforcement	T_c	30	mm		
Bottom cover to reinforcement	B_c	50	mm		
Slab reinforcement	S_r	175	mm ² /m'		
Concrete grade	f'_c	20	MPa		
Reinforcement yield strength	f_y	500	MPa		
Soil mond movement	y_m	42	mm		
Allowable slab deflection	L/Δ	400			
Top reinforcement	A_{sc}	3	N	16	
Bottom reinforcement	A_{st}	3	N	16	
Slab thickness	T_s	100	mm		
Output Data :					
		Edge drop		Edge lift	
		Long span	Short span	Long span	Short span
Equivalent salb thickness	mm	259.689	259.689	200	200
Equivalent slab inertia	m ⁴ /m'	1.46E-03	1.46E-03	6.67E-04	6.67E-04
Service BM per metre width	kN.m/m'	35.785	44.896	10.201	12.216
Service BM per beam	kN.m/m'	125.248	179.584	35.704	48.864
Effective flange width	m	1.750	2.000	1.750	2.000
Cracking moment/beam	kN.m'	94.090	122.712	30.666	38.135
Required beam depth	m	0.579	0.637	0.400	0.442
Eff. inertia of stiffened slab	m ⁴ /m'	1.46E-03	1.46E-03	6.67E-04	6.67E-04
Max. required beam depth	m	0.637			
Max. flexural rebars	mm ²	6583	7286	4204	4704
Min. flexural rebars	mm ²	550	759	382	467
Max. service shear force	kN/m'	16.016	17.784	5.210	5.713
Required shear rebars	mm ²	63.000			
Required shear rebars spacing	mm	300.000			
OK OK					
Summary:					
Total height of sub-beam	mm	637			
Top rebars		3	N	16	
Bottom rebars		3	N	16	
Shear rebars		2	N	8	@ 300.000
Slab rebars (both directions)	mm ² /m'	175			

Figure 4.29: Screenshot of the design report obtained from the SFORS program developed for the new design method, solving (14 m × 18 m) of the numerical example.

A summarised comparison between the results obtained from the new design method and those obtained from Mitchell's method (1980) is given in Table 4.3. It can be seen that the new design method produces stiffening beam dimensions of 300 mm × 637 mm, with top reinforcement of 953 mm² (3-N16 bars in addition to the slab mesh) and bottom reinforcement of 603 mm² (3-N16 bars). On the other hand, Mitchell's method requires stiffening beam dimensions of 300 mm × 540 mm, with top reinforcement of 519 mm² (2-N16 in addition to the slab mesh) and bottom reinforcement of 591 mm² (3-N16). Both solutions are based on the same material properties (i.e. $f'_c = 20$ MPa and $f_y = 500$ MPa), having a top slab of 100 mm thickness and 175 mm²/m reinforcement mesh. In general the amount of reinforcement obtained from the new design method is higher than that of Mitchell's method, since the minimum code requirement for the tensile steel according to the Australian Standards AS 3600 (2009) is considered, which contributes directly to the effective inertia of the section of the stiffened slab foundation (I_{eff}). Note that Mitchell's method is based on an assumption that the mound movement is within a certain edge distance (e_d), as explained in Chapter 2, over which the slab foundation moves and generates the corresponding internal forces, while the rest of the slab foundation is assumed to be in direct contact with the soil, thus, generating no or minor internal forces. On the contrary, in the new design method there is no predefined boundaries on the slab foundation movement, therefore, the whole slab is subjected to movements following the generated mound, yet the differential movement between the slab corner and slab centre is satisfied according to the Australian standards limits. Mitchell's assumption is that the slab deformation takes place within the edge distance (e_d), with the maximum deformation at the edge, while in the 3D FE analysis of the new design method the deformation is within the whole slab, with its maximum value at the corner and least value at the centre. Allowing all the deformation to be within the edge distance only requires a more flexible footing slab and this explains why the depth of the stiffened beam obtained from Mitchell's method is less than that obtained from the new design method. The flexible footing obtained from Mitchell's method results in less bending moment and therefore less reinforcement. It is presumed that the conservatism provided by the new method in this regard may help in reducing the case histories of damage that is still reported in the literature due to the use of the existing design methods including Mitchell's method.

Table 4.3: Comparison between the new design method and Mitchell’s method for the numerical example.

Area (m ²)	Required stiffening beam dimensions (mm)		Reinforcement (mm ²)			
	New method	Mitchell’s method	Top		Bottom	
			New method	Mitchell’s method	New method	Mitchell’s method
6 m × 18 m	300 × 486	300 × 540	926	519	603	591
14 m × 18 m	300 × 637	300 × 450	953	349	603	413

To confirm the validity of the new design method, the illustrative numerical example solved earlier using the new design method, is analysed using an iterative 3D FE analysis, trying to obtain the equivalent slab foundation thickness and the corresponding internal forces, for the same input conditions. The results obtained from the 3D FE analysis are then compared with those obtained from the new design method. Figure 4.30 shows a typical 3D mesh of the FE model. All of the material properties, flow parameters, initial conditions, boundaries and loading data utilized in the parametric study are used in the 3D FE model. The equivalent slab thickness (T_{eq}) required to limit the maximum differential slab foundation movement (δ) to the standard requirement (Δ_{all}) is obtained through an iterative analysis and is found to be 275 mm for the edge drop scenario and 200 mm for the edge lift scenario. Consequently, the edge drop scenario governs, as it resulted in higher T_{eq} ; the edge drop scenario also governed when the new design method is used. Figures 4.31 and 4.32 show the bending moment and shear force in both directions of slab foundation for the 275 mm slab foundation thickness. The maximum service bending moment from the 3D FE is 40.0 kN.m /m and the maximum service shear force is 19.2 kN/m. These values are found to be equal to 44.9 kN.m/m for the maximum service bending moment and 17.8 kN/m for the maximum service shear force when the new design method is used, implying a good agreement with the results of the 3D FE analysis. By adopting the same beam configuration in Figure 4.24, the required dimensions of the stiffening beams are 300 mm × 613 mm with 4-N16 bars top and bottom reinforcements, in addition to the slab mesh reinforcement of 175 mm²/m. Again, these results are also in

good agreement with the output of the new design method, which gave a section of 300 mm × 637 mm with the same slab mesh, 3-N16 bars top reinforcement, and 3-N16 bottom reinforcement.

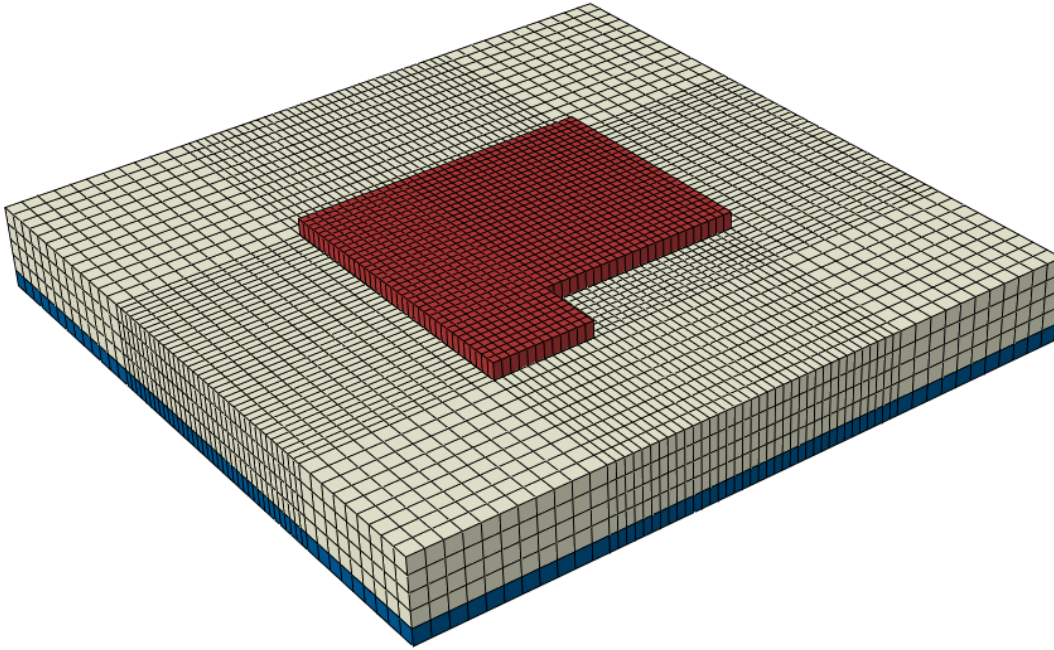


Figure 4.30: Typical 3D FE mesh of the L-shape slab foundation used in the numerical example.

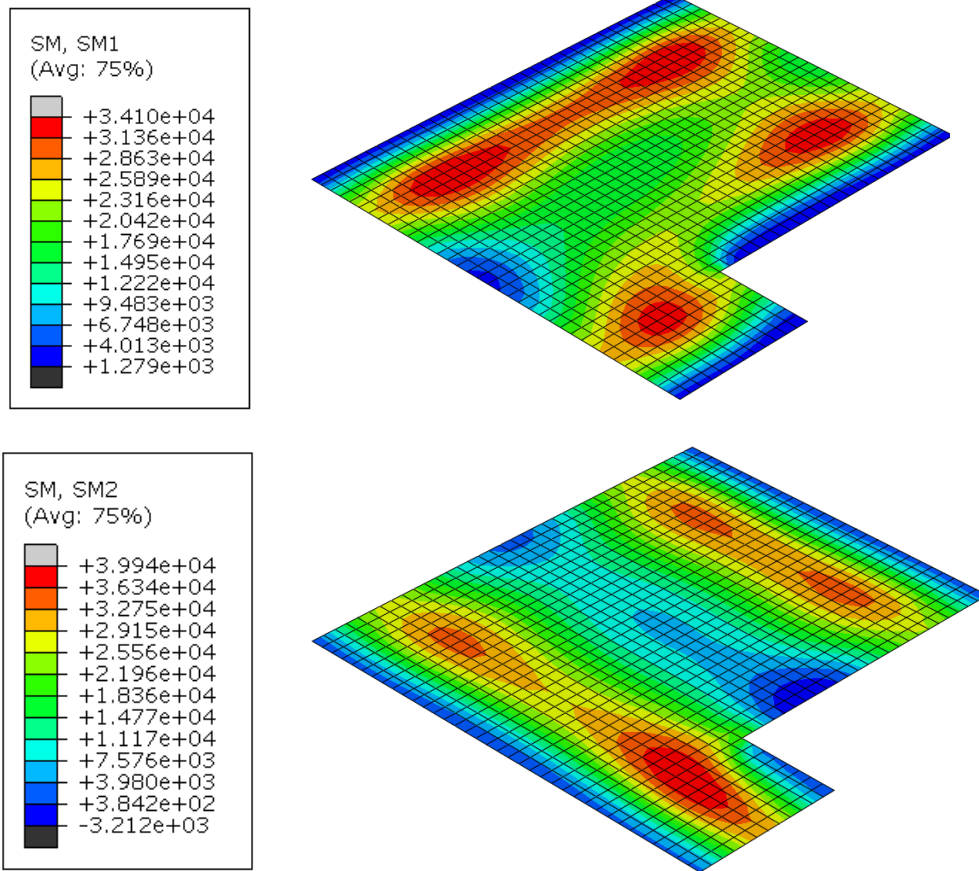


Figure 4.31: Service bending moment of the slab foundation used in the numerical example, for the edge drop scenario.

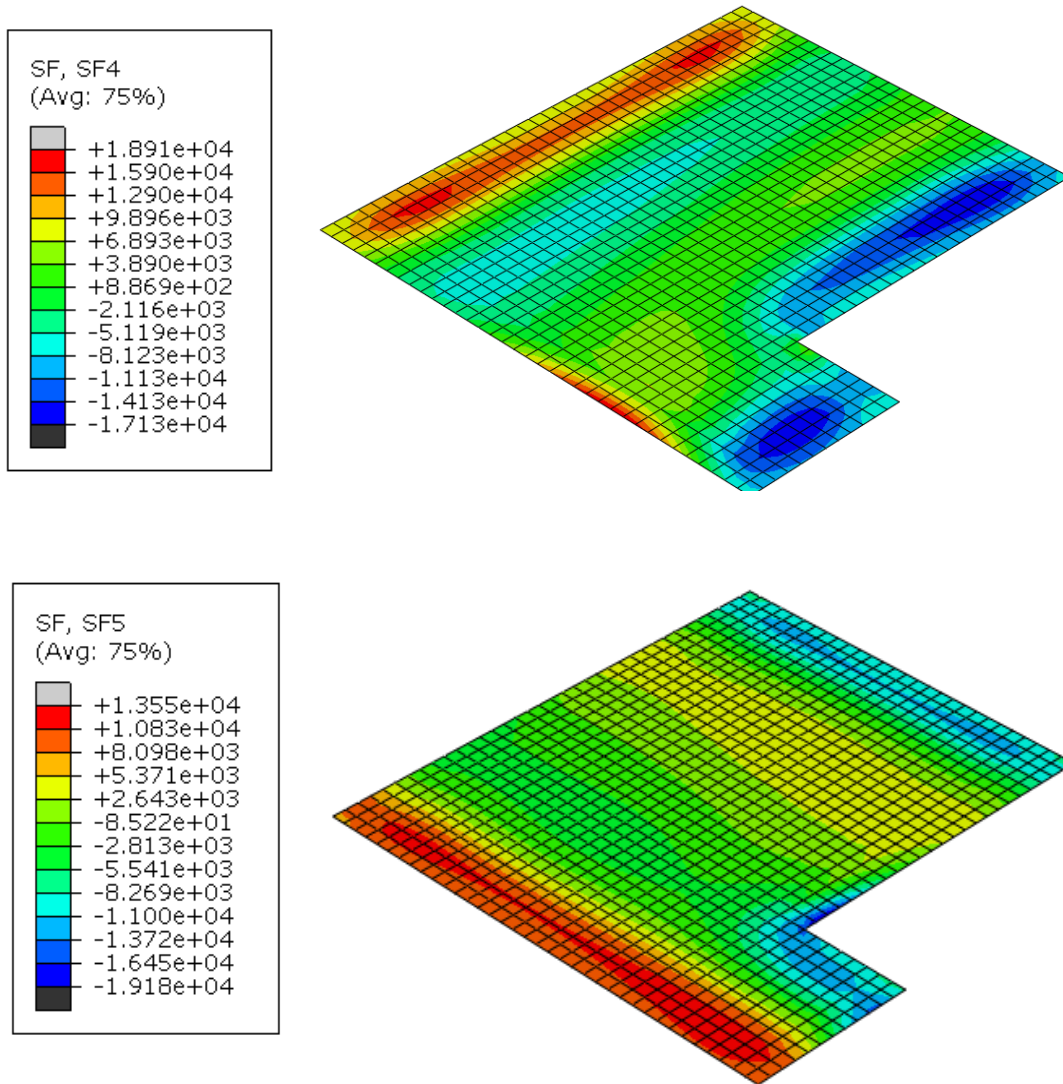


Figure 4.32: Service shear forces for the slab foundation used in the numerical example, for the edge drop scenario.

4.5 SUMMARY

In this chapter, an intensive parametric study was carried out based on the advanced 3D FE hydro-mechanical model proposed and explained in detail in Chapter 3. The different parameters used in the parametric study were defined and the results were presented and analysed. The outcomes of the parametric study were then congregated into a series of

design charts. In order to avoid the inaccurate linear interpolation when using the design charts, the charts were substituted by design equations. Subsequently, the data obtained from the parametric study were compiled and trained using artificial intelligent (AI) to generate a set of design equations, which formed a standalone new design method for stiffened slab foundations on reactive soils. These design equations along with all design and iteration procedures were integrated into a user-friendly computer program called SFORS. The assumptions and limitations of the new design method were discussed. The new method was then applied to an illustrative numerical example involving *L*-shape slab foundations, and the results were compared with those obtained from the well-known Mitchell's method as well as the 3D FE analysis. The results of the new design method were found to agree well with the common engineering practice and the outputs of the 3D FE analysis, and were thus deemed to be more realistic than those obtained from Mitchell's method. The particular example tried here shows that the new method is slightly more conservative than Mitchell's method.

CHAPTER 5

EFFECT OF USING SAND CUSHION ON THE PERFORMANCE OF STIFFENED SLAB FOUNDATIONS

5.1 INTRODUCTION

The use of a sand cushion underneath slab foundations is known worldwide as an effective solution to the problems associated with expansive soils. By partial replacement of the reactive soil layer below the foundation with a stable, clean sand layer extended laterally to a certain limit beyond the foundation footprint, the expected foundation deformation resulting from moisture variation is reported to be reduced or entirely omitted (Moussa et al. 1985). In this chapter, an investigation is carried out (based on the 3D hydro-mechanical model presented in the previous chapters) to better understand how the sand cushion works and how far it can mitigate the damage caused by reactive soils. The chapter begins with a study on the mechanism associated with the sand cushion which leads to enhancement of the performance of stiffened slab foundations. Following that, the chapter presents a comprehensive parametric study to quantify the efficacy of the sand cushion using the EPR modelling process presented in Chapter 4. The parametric study covers 3 practical depths for the sand cushion layer (i.e. 0.5, 1.0 and 1.50 m), aiming to investigate the effect of the sand cushion depth on the reduction of the slab foundation thickness. The results of the parametric study is used as input data in a regression analysis using the EPR method in order to obtain a set of design equations which can be easily used by practitioners to estimate the reduced slab foundation equivalent thickness (T_{eq}) and its reduced internal forces in the presence of a specific thickness of sand cushion. Eventually, designing stiffened slab foundations with a sand cushion is illustrated by example, using an extended version of the computer program SFORS presented in Chapter 4.

5.2 HOW DOES SAND CUSHION WORK?

There are a number of different interpretations regarding the mechanism associated with the role of sand cushions in mitigating the soil movement upon moisture variation. The most common of these interpretations are:

- 1- *The replacing sand cushion adapts to the deformability of the underlying swelling soil:* A very common understanding of the mechanism of the sand cushion refers to its adaptability to the soil movement of the underlying swelling clay (Rao et al. 2008). In order to achieve this adaptability, the sand cushion should be loose enough to absorb most of the deformation of the soil to suppress any excessive uplift pressure on the slab foundation. However, a loose sand cushion may violate the settlement design limits under gravity loading; moreover, a sand cushion would normally provide easy access for the surface water into the deeper expansive soil. It is experimentally proven that the swelling pressure exerted by an expansive soil is proportional to the density of the sand cushion and is inversely proportional to its fineness (Moussa et al. 1985). Accordingly, a highly compacted sand cushion will be inefficient in reducing the swelling pressure due to its lower adaptability. Moreover, a coarse sand with a higher hydraulic conductivity would increase the potential of moisture migration towards the deep expansive soil, which may exacerbate the problem.
- 2- *The weight of the sand cushion suppresses heave:* As previously discussed in Chapter 2, the swelling pressure of an expansive soil can be counteracted when the soil is loaded. Replacing a thickness of the swelling soil with a stable sand layer reduces the volume of the swelling clay and poses a surcharge on the remaining reactive deposit, hence reducing the overall swelling. This can be effective for the case of relatively shallow swelling layers of up to 2 m to 3 m thickness; however, this role of the sand cushion will diminish as the swelling clays becomes thicker (Nelson and Miller 1992). However, as iterated above, the high permeable sand with respect to the original low permeable swelling clay eases access of the surface water to the reactive soil, hence, increasing the potential surface heave.

- 3- *A cohesive, non-swelling clay cushion serves as a moisture barrier to the lower swelling clay:* Many researchers favour the use of a ‘Cohesive Non-swelling Soil’ cushion (CNS) over the sand cushion for its lower hydraulic conductivity, which can be controlled to be even lower than that of the original swelling soil. Such cushion can serve as a water barrier that efficiently diminishes or prevents increase in the moisture of the underlying swelling clay and reduces heave (Bharadwaj 2013). However, efficiency of the CNS critically requires that the cushion must extend beyond the slab boundaries, which in most practical cases does not exceed beyond a margin of 1 to 2 metres. However, it appears that the CNS actually delays the moisture propagation to the lower swelling layers rather than preventing it; this may explain the findings of Subba Rao (2000) that the CNS cushion becomes ineffective after the first shrink-swell cycle, presumably after the moisture finds alternative flow paths into the reactive soil.

- 4- *Loaded sand cushion reduces swelling by confinement:* Field observations confirm that, when the soil under a sand cushion heaves, only the lightly loaded parts of the sand cushion will experience heave (like in the case of the areas between footings), while the footings will not experience substantial movement (Varghese 2012). Experiments also showed that partially confining the top surface of the sand cushion has a great effect in reducing the swelling beneath the loaded areas (Moussa et al. 1985). In fact, this feature of the sand cushion is directly attributed to the effect of gravity loading on the reduction of heave as described in detail in Chapter 2; this effect is more pronounced in the case of isolated footings, which exerts relatively high stresses on the top of the sand cushion. Obviously, this effect is not applicable to the particular case of stiffened slab foundations, since there is no unloaded parts within the slab area.

- 5- *Sand cushion creates a condition of uniform degree of saturation:* As previously presented in earlier chapters, differential rather than total movements of the slab foundations is mostly responsible for major structural damages associated with expansive soils. As explained in the following section, using a sand cushion below

the slab foundation allows for a more uniform change in the moisture content, and, consequently, more uniform shrink swell deformation. According to this argument, even if a deep reactive soil swells by the ingress of moisture through the highly permeable sand cushion, the differential movements will probably be uniform, and hence more tolerable (Chen 1988).

5.3 FE MODELLING OF STIFFENED SLAB FOUNDATION WITH SAND CUSHION

This section investigates the actual mechanism responsible for the efficacy of the sand cushion in improving the performance of stiffened slab foundations on reactive soils, through 3D FE modelling, emphasising the concept that a sand cushion creates a condition of uniform degree of saturation. A parametric study is then carried out on the 3D FE model to produce data from which design equations for slab foundations on reactive soils incorporating sand cushions are derived, for use by practitioners.

5.3.1 Modelling of sand cushion

The 3D FE hydro-mechanical model presented and validated in Chapter 3 is used in this chapter with the inclusion of the sand cushion, considering 3 practical thicknesses of 0.5 m, 1.0 m and 1.5 m. A reactive soil of a constant thickness of 4.0 m underlying the sand cushion is maintained in all cases. As explained in Chapter 4, this thickness was found to be sufficient to generate the soil mound without significantly distorting the soil elements in the FE mesh; furthermore, this thickness represents the maximum suction depth adopted by the Australian Standards AS2870 (2011). Except for the sand cushion, the soil model, soil properties (including the soil-water characteristic curve, SWCC, Moisture-Swell model) and the finite element type are similar to those used in Chapter 4. The slab foundation parameters are also similar to those used in Chapter 4 (model, modulus, loading and element type). For the sand cushion, an elastic model is used which is justified by the fact that the study focusses on the deformation caused by the shrink-swell process rather than the relatively lower expected settlement from the slab light loading. A representative soil-water characteristic curve from the literature is used (Figure

5.1) is also used, with an initial void ratio of 0.6 and a Poisson's ratio of 0.3. The soil element type used is 8-node brick trilinear displacement, trilinear pore pressure element (C3D8P).

Since the aim of using a sand cushion is to increase its efficiency in producing a nearly uniform saturation field, as explained earlier, a relatively highly permeable sand cushion layer is used with a saturated permeability of 5×10^{-4} m/sec (Ishibashi and Hazarika 2011), corresponding to slightly silty sand. Sand cushion layers comprising more fine particles with lower permeability are not recommended.

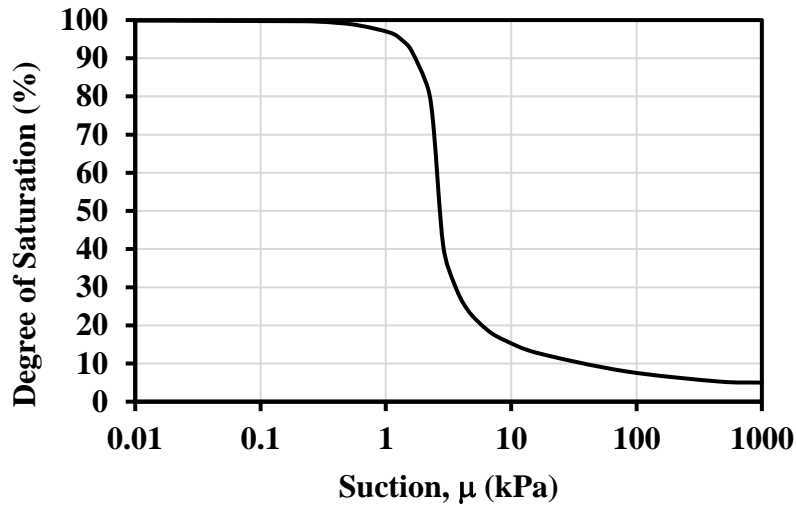


Figure 5.1: Typical soil-water characteristic curve for the cushion sand (Fredlund and Xing 1994).

To achieve such permeability for the sand cushion, Hazen's (1892; 1911) formula can be used as follows:

$$k = C_H D_{10}^2 \quad (5.1)$$

where (k) is the sand permeability in cm/s; (C_H) is Hazen's empirical coefficient (usually = 100); and (D_{10}) is the effective particle size in (cm). This formula is developed for sands with coefficient of uniformity (D_{60}/D_{10}) of less than about 2. By using Hazen's formula, the (D_{10}) of the recommended sand is about 0.22 mm.

The soil mound stiffness is fixed to be 5000 kPa for both the edge lift and edge drop scenarios. This value is the same for the stiff clay in the case of the edge drop scenario, but it is much higher than the 1000 kPa used in Chapters 3 and 4 for the swelling soil in the case of the edge lift scenario; the reason is that, in the case of the edge lift scenario, even when the swelling soil is softened, the sand cushion mound stiffness (K), which is in direct contact with the footing will not be affected. The analysis steps are also similar to those presented in Chapter 4, starting with (1) application of a geostatic step in which the in-situ stresses are calculated, (2) application of a second geostatic gravity analysis to account for the slab foundation loading, and (3) simulation of the precipitation or evaporation event to initiate the edge lift or the edge drop scenario, respectively. The analysis is carried out using the ABAQUS (2014) package, and a typical 3D FE model is shown in Figure 5.2. Normally, the sand cushion extends outside the slab foundation footprint; however, in certain cases, when the slab foundations is located on the allotment limit, the extension is not possible. Accordingly, the sand cushion is assumed to have the same dimensions of the slab foundation, as a worst case scenario.

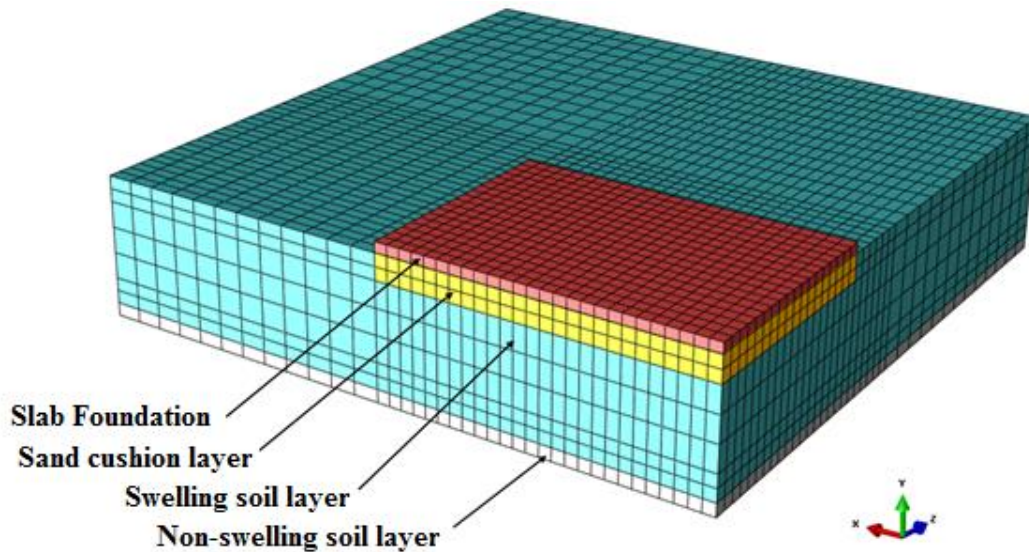


Figure 5.2: A typical Finite element model showing the sand cushion (double symmetry).

As explained in Chapters 3 and 4, for the case of no sand cushion, the target mound movement defining the soil class, is measured as the difference between the movement of

the reactive soil beneath the corner of the footing and beneath its centre. However, in the case of using a sand cushion layer beneath the slab foundation, and since the sand cushion provides a uniform condition of moisture change which results in almost uniform deformation beneath the slab, it is found that the target mound differential movement (y_m) is achieved after a very long period of flow which generates a huge surface heave (y_s) that violates the rule of thumb adopted by the Australian Standards ($y_m = 0.5$ to $0.7 y_s$) and may reach a value of 5 times y_m . Therefore, in case of sand cushion the target y_m is deemed to be achieved when the surface heave of the uncovered area y_s reaches conservatively twice the target y_m . For instance, if the target $y_m = 70$ mm, the soil mound, the slab movement and its internal forces are recorded when the surface heave reaches 140 mm. This criterion is adopted for both the edge drop and edge heave scenarios.

5.3.2 Validation of the uniform moisture condition interpretation

In order to validate the uniform moisture conditions initiated by the sand cushion, resulting in improving the performance of stiffened slabs on reactive soils, a hypothetical case is modelled considering a slab foundation of $26 \text{ m} \times 26 \text{ m}$ dimensions for a soil mound differential movement of 84 mm corresponding to an E2 soil class. An allowable differential movement $\Delta_{all} = L_d/600$ is considered for the two scenarios of edge lift and edge drop. The results of this exercise are displayed in terms of both the saturation contours within the soil layers under the slab (i.e. the sand cushion and the reactive soil) and the shape of the soil and footing mound. As described earlier, three thicknesses are considered for the sand cushion: 0.5 m, 1.0 m and 1.5 m.

The degree of saturation contours shown in Figures 5.3 and 5.4, demonstrate the role of the sand cushion in providing more uniform saturation to the soil with respect to the case with no sand cushion, for both cases of edge lift and edge drop scenarios. Without a sand cushion the variation of the degree of saturation at the soil beneath the edges is huge for both scenarios, besides the degree of saturation beneath the centre of the footing is almost unchanged. On the other hand, in case of using a sand cushion, the degree of saturation has almost same values at the edges and the centre. In addition, the uniformity of the moisture change and the depth of wetting increases with the depth of sand cushion.

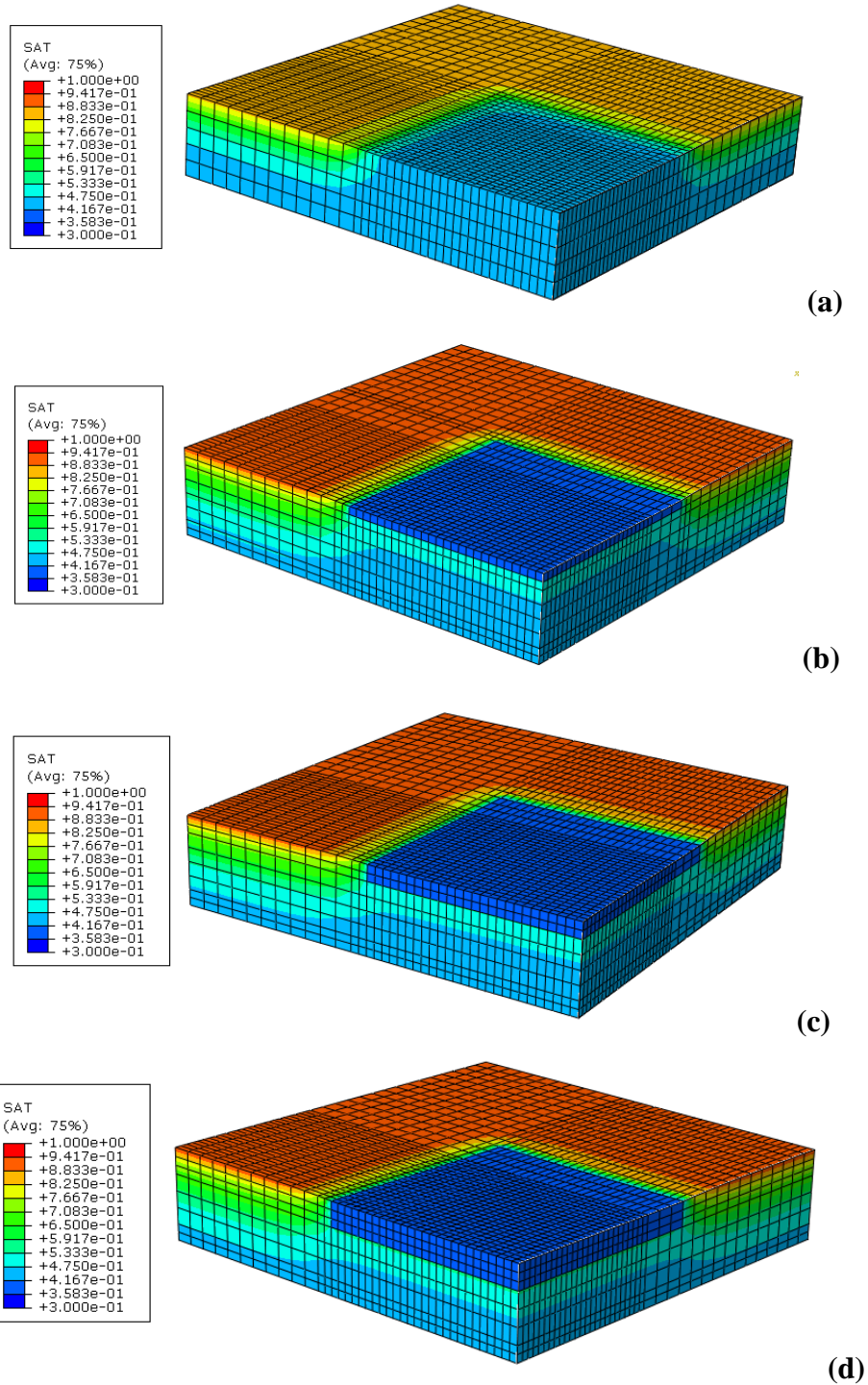


Figure 5.3: Saturation contours at soil mound $y_m = 84$ mm, presented on the undeformed shape for the edge lift scenario: (a) no sand cushion; (b) sand cushion depth $S = 0.5$ m; (c) sand cushion depth $S = 1.0$ m; (d) sand cushion depth $S = 1.5$ m.

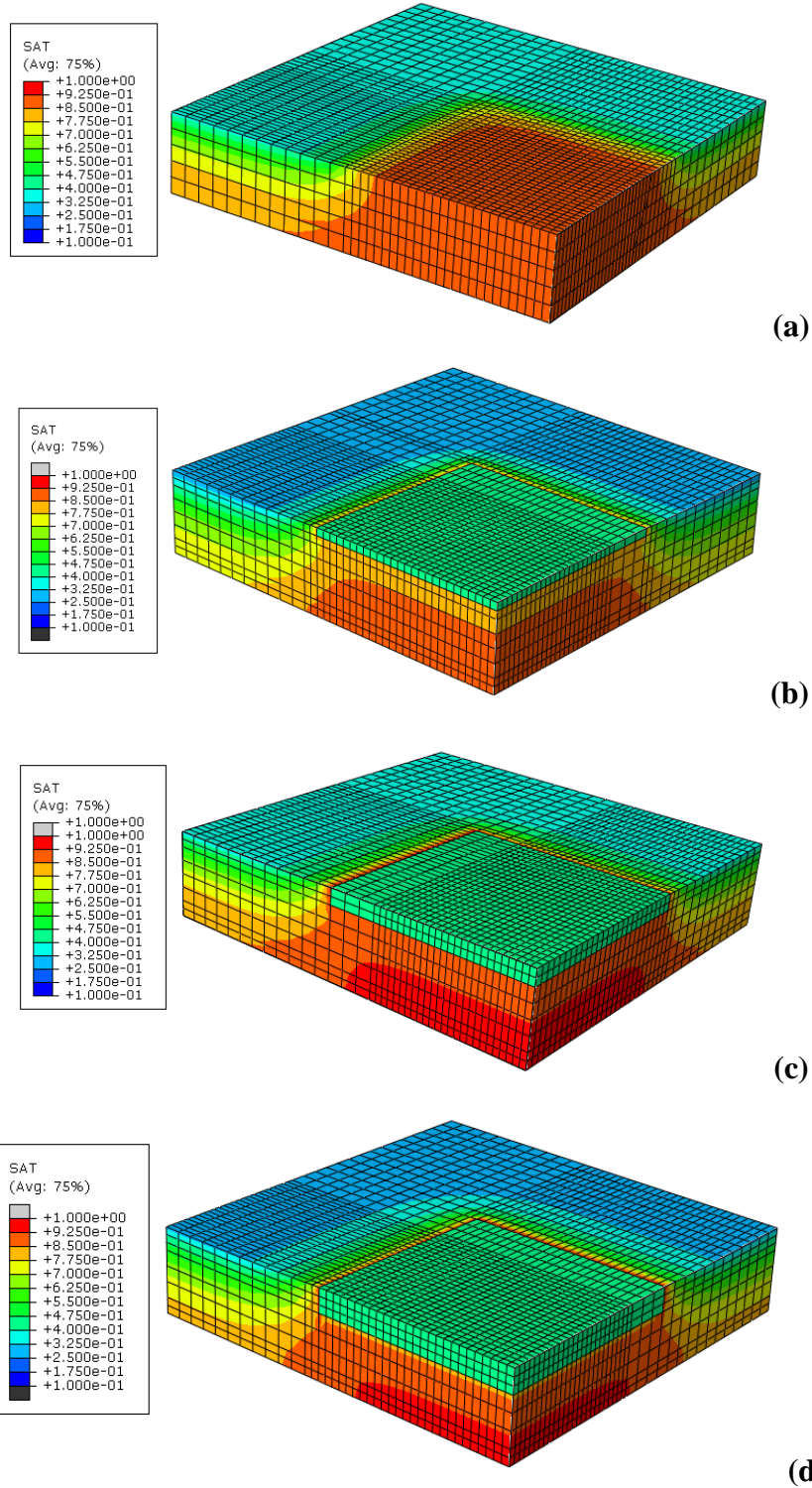


Figure 5.4: Saturation contours at soil mound $y_m = 84$ mm, presented on the undeformed shape for the edge drop scenario: (a) no sand cushion; (b) sand cushion depth $S = 0.5$ m; (c) sand cushion depth $S = 1.0$ m; (d) sand cushion depth $S = 1.5$ m.

The role of the sand cushion explained above is manifested in Figures 5.5. Scrutiny of Figure 5.5 reveals that the vertical movement profile is more uniform than in the case of no sand cushion. This applies to both the edge lift and edge drop scenarios. Uniformity of the soil movement increases by increasing the sand cushion thickness. Since the differential movement rather than the total movement is responsible for generating the slab foundation deflection and its internal forces, one should expect a reduction in the required slab thickness and the internal forces. This aspect is discussed later.

Based on the FE results and discussion presented above in Figures 5.3 to 5.5 that primary contribution of the sand cushion is to serve as a permeable blanket that attracts the moisture and redistributes it uniformly into the underlying reactive soil (in the absence of this blanket, the moisture will eventually reach the reactive soil but in a non-uniform manner). In other words, the high permeability of the sand cushion with respect to the surrounding reactive soil allows water to migrate horizontally beneath the footing much faster than vertically towards the underlying soil. This in turn produces a uniform moisture field within the reactive soil as the accumulated moisture within the sand cushion tends to migrate downward under gravity. Eventually, this results in a much uniform deformation for both the soil (Figure 5.5) and the slab foundation as shown in Figure 5.6. Similarly, for the case of edge drop, evaporation of the soil moisture is much faster horizontally (within the sand cushion) than vertically, which guarantees a much uniform settlement of both the soil and the slab.

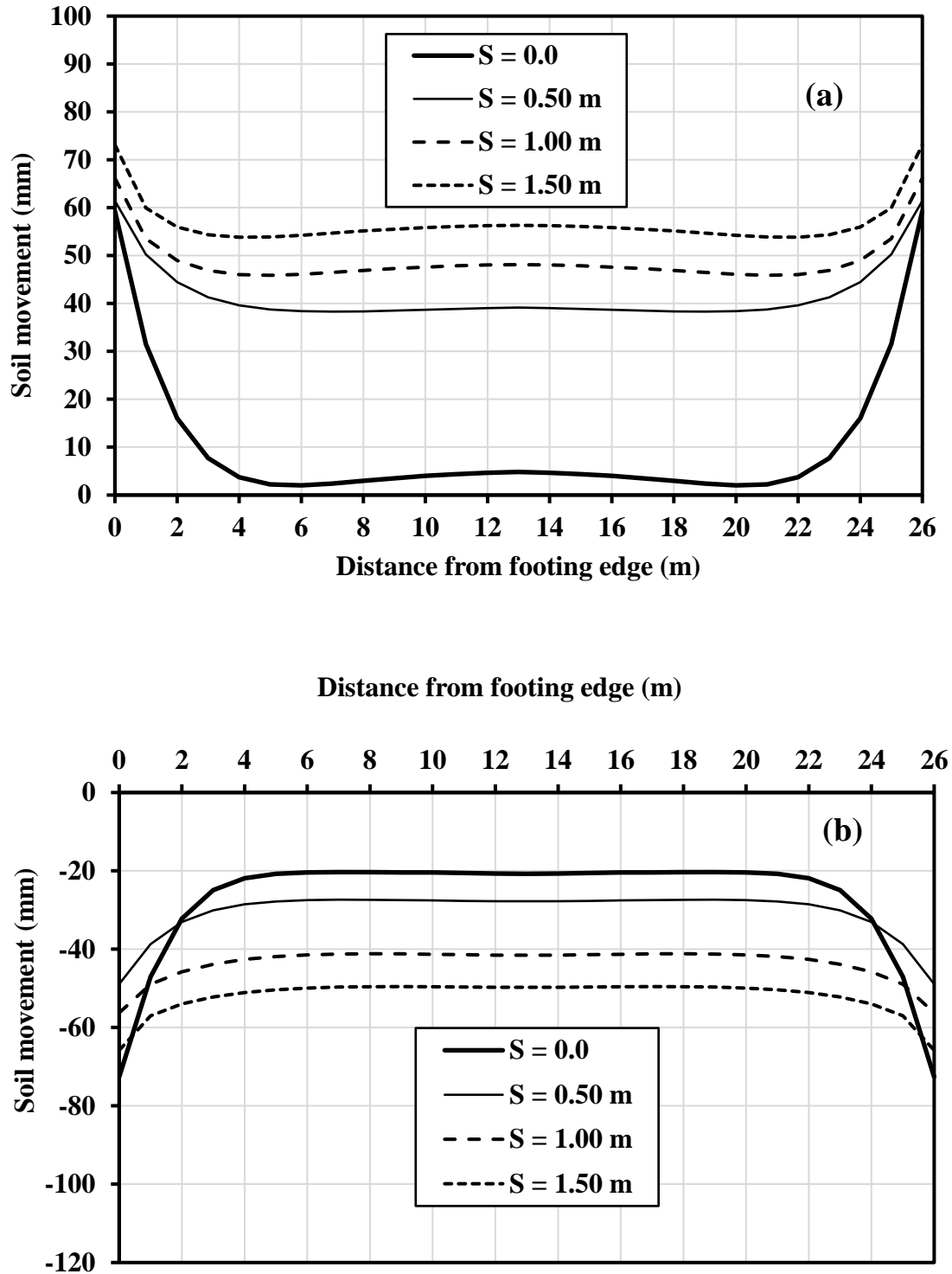


Figure 5.5: Effect of sand cushion thickness on the soil mound: (a) edge lift scenario; and (b) edge drop scenario.

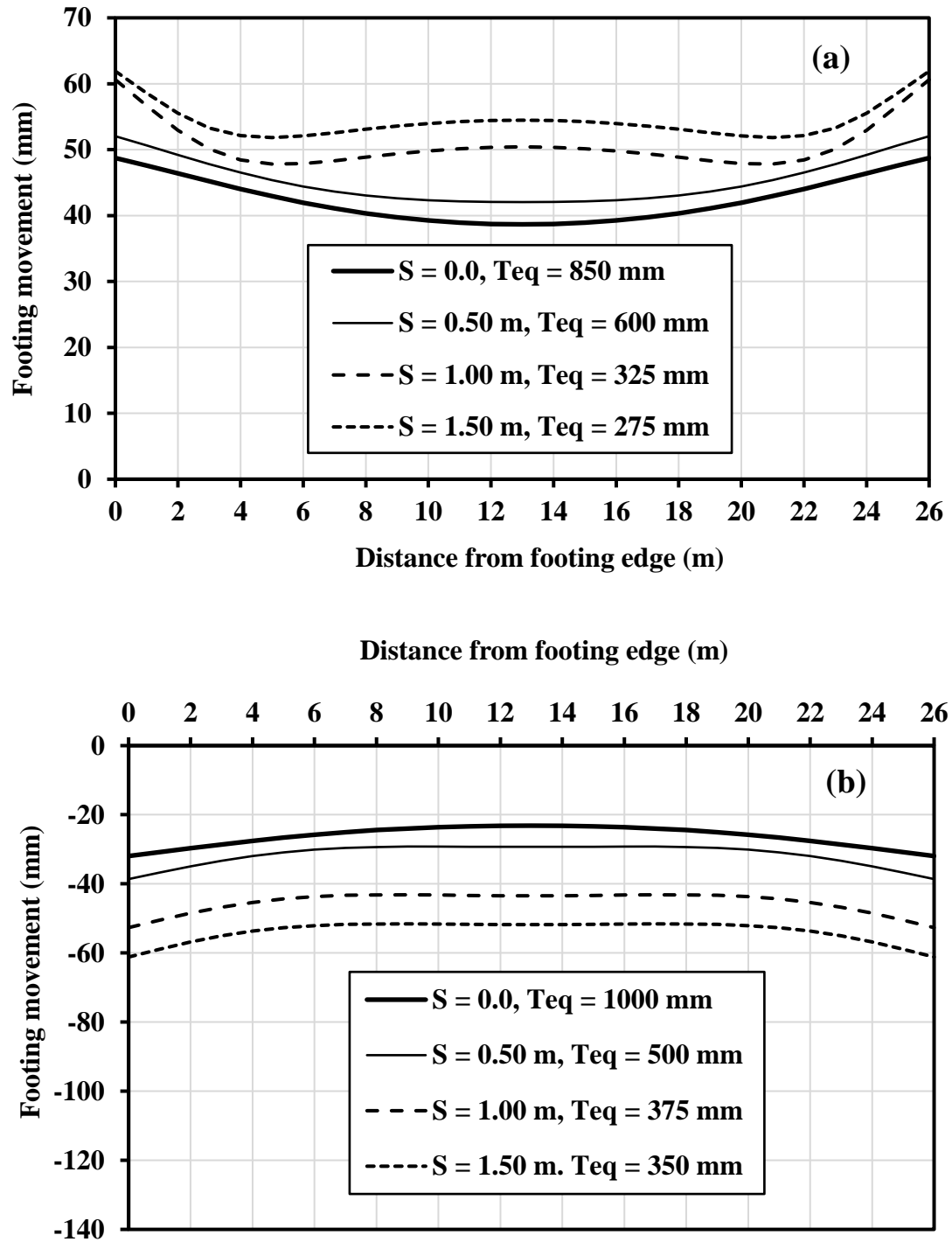


Figure 5.6: Effect of sand cushion thickness on the footing mound: (a) edge lift scenario; and (b) edge drop scenario.

It is now interesting to examine how the implementation of the sand cushion can affect the internal forces of the slab foundation. To this end, Figures 5.7 and 5.8 are prepared for the cases presented above. The equivalent slab thickness T_{eq} required to limit the slab deformation to the codified limit ($\Delta_{all} = L_d/600$) under the mound value $y_m = 84$ mm is first determined for each thickness of sand cushion and then the internal forces are generated. It is clear from Figures 5.7 and 5.8 that the internal forces generated in the slab foundations are reduced by the presence of the sand cushion. For the specific cases presented in Figure 5.7, a massive reduction in the bending moment of up to 50% and 70% is achieved for the edge lift and edge drop, respectively, when a sand cushion thickness of 0.5 m is used. Further reduction is achieved by increasing the thickness of sand cushion. Similarly, the shear forces are reduced by increasing the depth of sand cushion for both cases of edge lift and edge drop, as shown in Figure 5.8.

It should be noted that using the sand cushion is criticised on the grounds that it increases the depth of the active zone and, hence, the soil total heave. However, this is not completely true, since, as explained in Chapter 2, a permanent change occurs in the soil moisture conditions beneath the slab, due to the fact that the slab itself does not allow the water to evaporate in dry seasons at a rate that matches its infiltration during wet seasons. Therefore, for an extended swelling soil layer, in the course of several years the water accumulates below the slab and the active zone increases until reaching the depth of desiccation (H_d), as reported by Chen (1988) (refer to Chapter 2). A similar behaviour was reported by Fityus et al. (2004) (refer to Chapter 3). Accordingly, it can be argued that the deep seated heave of reactive soils beneath slab foundations is inevitable, whether a sand cushion is used or not. The sand cushion actually speeds up the process of deep seated heave, but does not initiate it. Furthermore, one should recall that, there is no limitations in the foundation design standards as to the total foundation movement; the limits are available only for the differential movement. However, the foundation's total movement is always governed by the building usage and the movement tolerance of the utility fittings and connections.

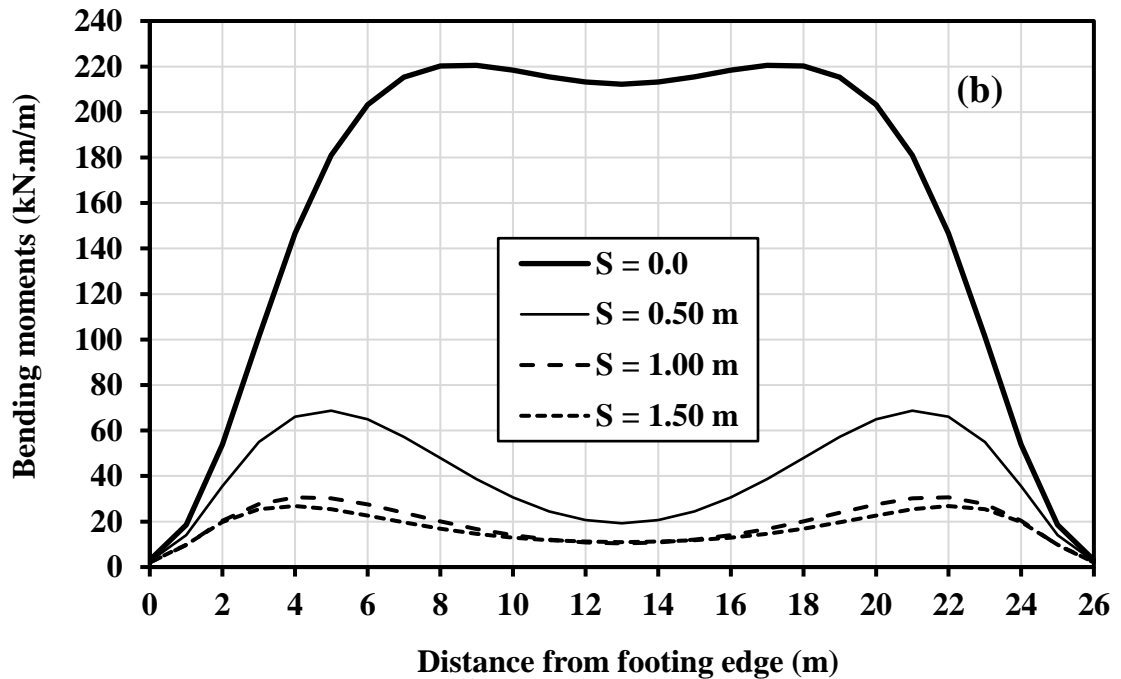
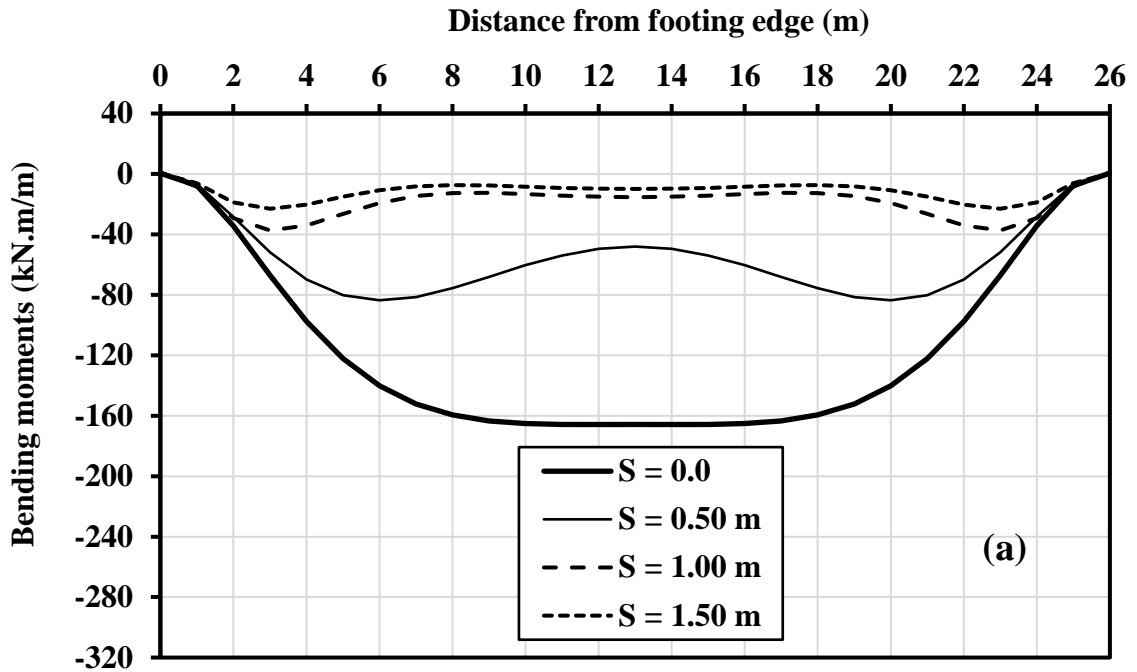


Figure 5.7: Effect of sand cushion thickness on the footing bending moments: (a) edge lift scenario; and (b) edge drop scenario.

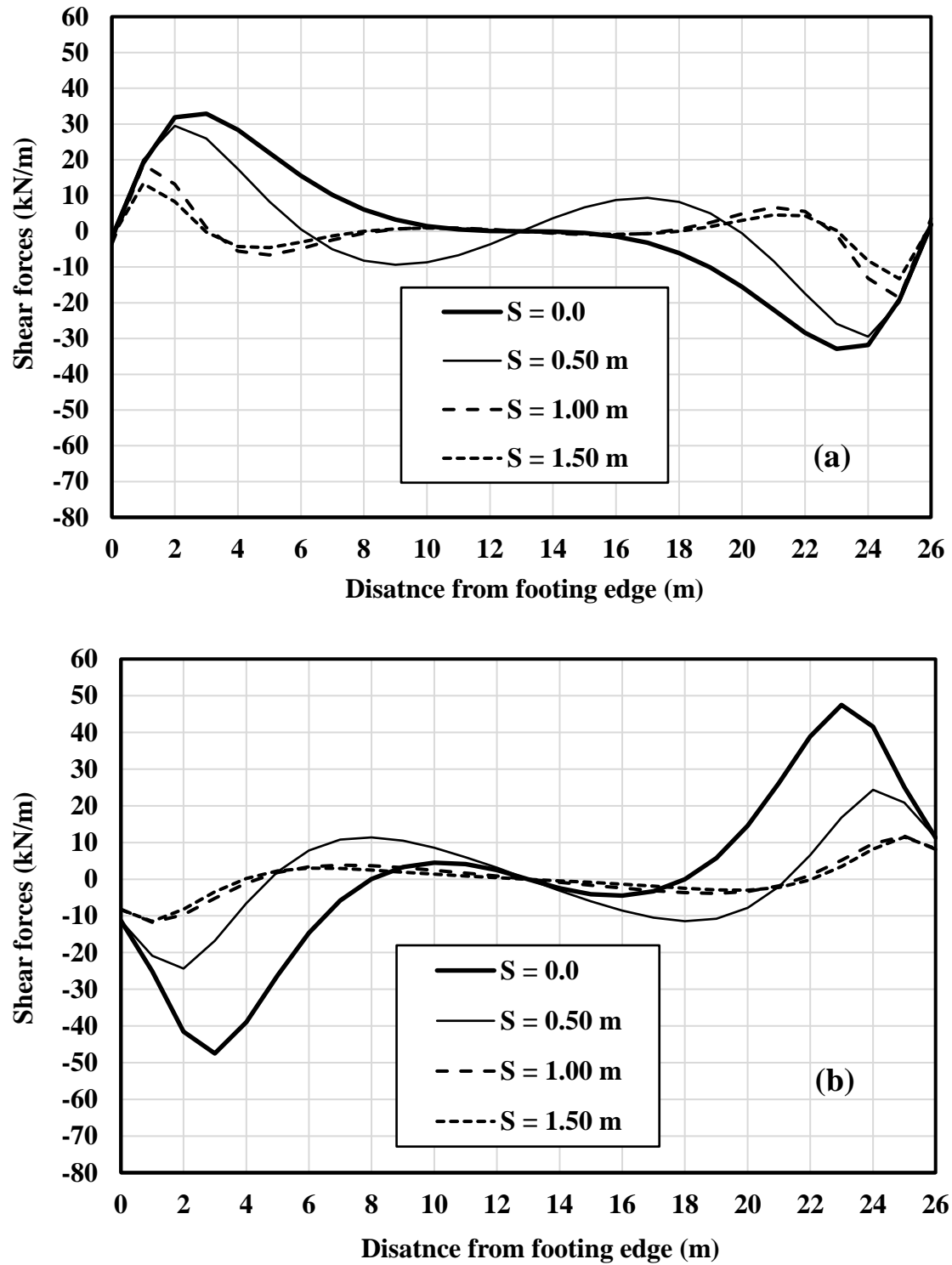


Figure 5.8: Effect of sand cushion thickness on the footing shear forces: (a) edge lift scenario; and (b) edge drop scenario.

5.3.3 Parametric study incorporating sand cushion

As explained earlier, one of the objectives of this study is to generate design equations for stiffened slab foundations on reactive soils considering a specific thickness of sand cushion. Consequently, a parametric study is carried out, similar to that of Chapter 4 with the inclusion of the new parameter, S , representing the sand cushion thickness. The range and limits of the parametric study are similar to those of Chapter 4 (refer to Table 4.2) and as described earlier, three practical sand cushion thicknesses are used 0.5 m, 1.0 m and 1.5 m. Similar to the parametric study in Chapter 4, for each slab foundation combination, a set of iterative analyses is carried out with different slab foundation thicknesses. The slab thickness selected is the value that maintains the differential movement of the slab within the standard limits, for a certain mound movement $\pm y_m$ corresponding to a certain edge movement scenario. The outcome recorded from the analysis is the corresponding internal forces (bending moments and shear forces). The effect of the sand cushion is manifested in reducing the slab thickness and the corresponding internal forces in comparison with the similar case where no sand cushion is used.

Figures 5.9 to 5.12 show the reduced slab foundation thickness as a function of the sand cushion thickness, for different construction types (different allowable deformation limits) and for different site classes (soil mound movement y_m). These figures are generated for a rectangular slab foundation of 26 m \times 26 m dimensions and for the case of an edge drop scenario. Similar behaviour is also found for the case of edge lift scenario and other dimensions.

In general, the sand cushion can significantly reduce the required slab thickness. As expected, the efficacy of the sand cushion in reducing the required slab thickness increases with increasing mound movement; the benefit also increases with a reduced deflection limit. Interestingly, it can be seen from the figures that the efficacy of the sand cushion drops beyond a certain thickness, which may call for optimisation of the sand cushion quantity.

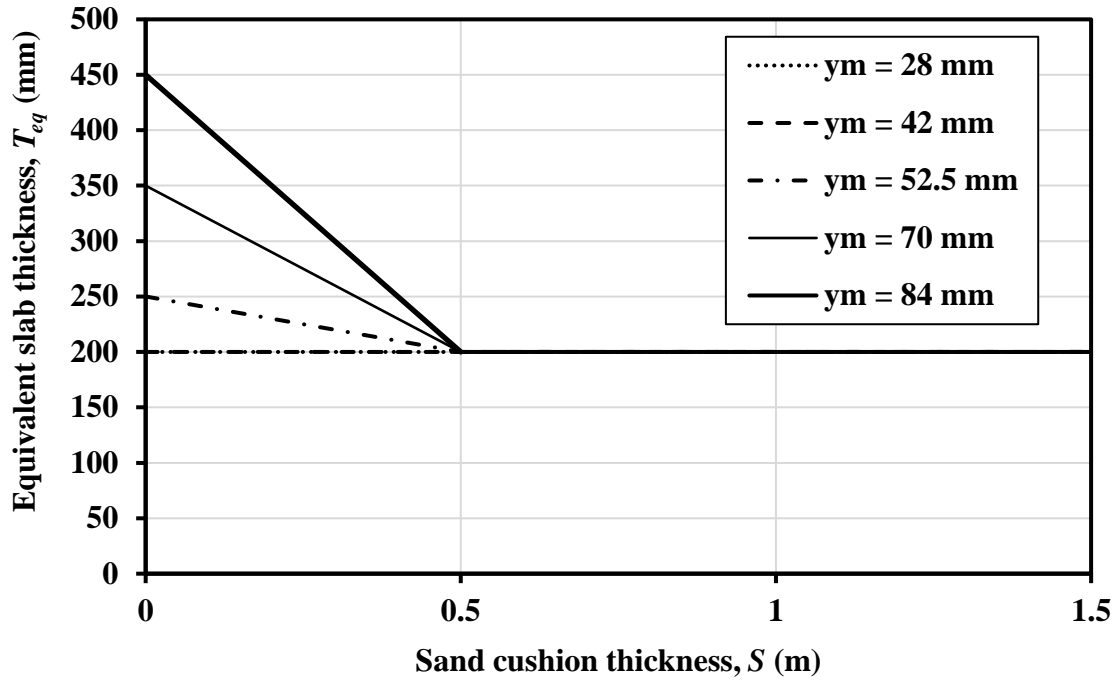


Figure 5.9: Effect of the sand cushion thickness on the equivalent slab thickness for different soil mounds- 26 m \times 26 m- edge drop scenario, $\Delta_{all} = L_d/300$.

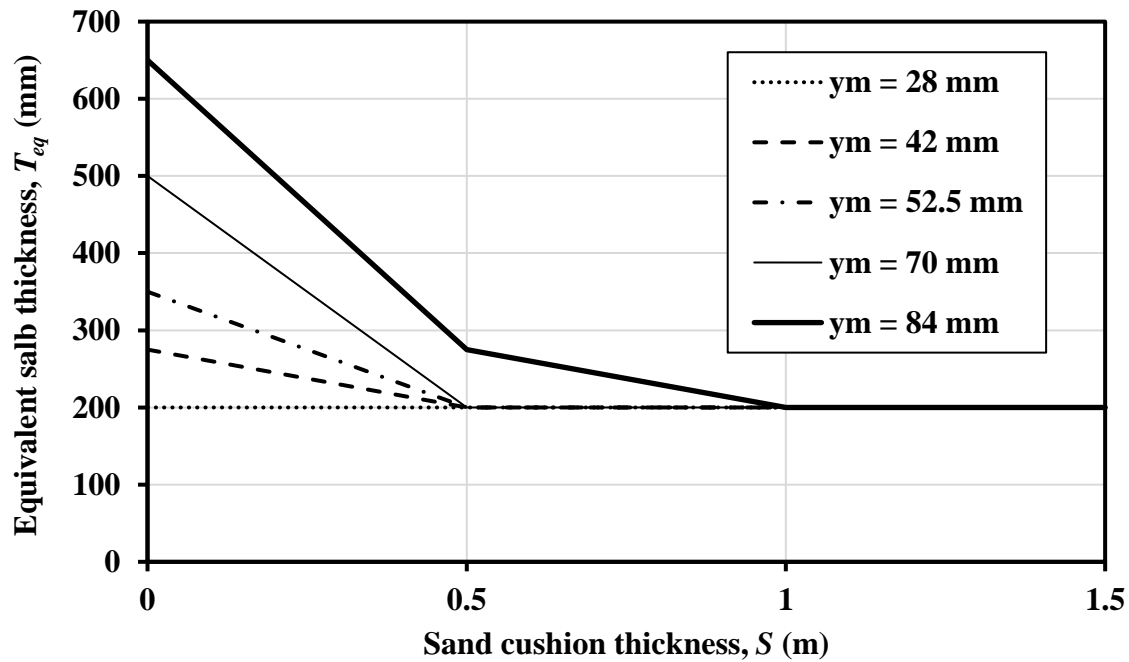


Figure 5.10: Effect of the sand cushion thickness on the equivalent slab thickness for different soil mound- 26 m \times 26 m- edge drop scenario, $\Delta_{all} = L_d/400$.

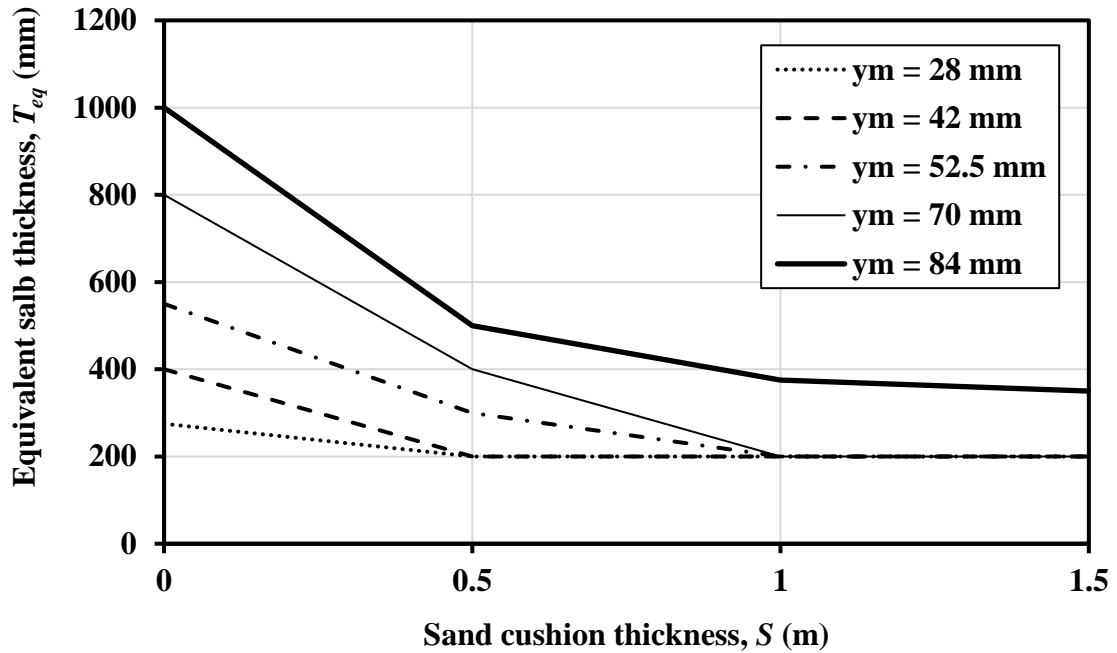


Figure 5.11: Effect of the sand cushion thickness on the equivalent slab thickness for different soil mound- 26 m × 26 m- edge drop scenario, $\Delta_{all} = L_d/600$.

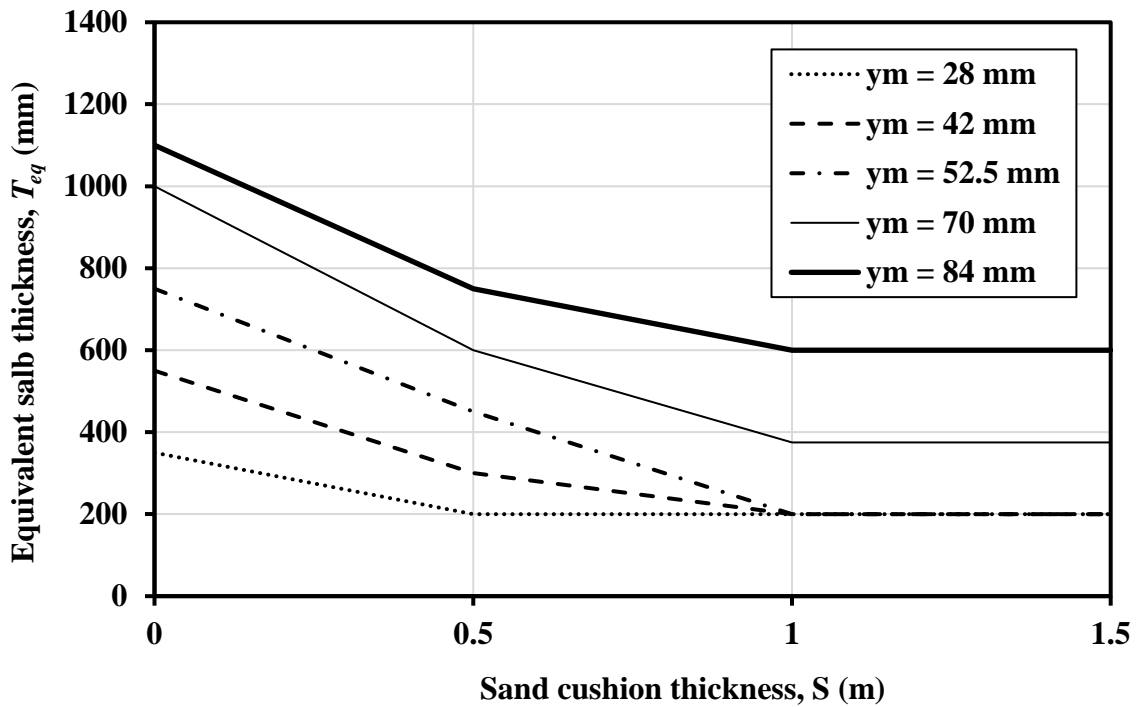


Figure 5.12: Effect of the sand cushion thickness on the equivalent slab thickness for different soil mound- 26 m × 26 m- edge drop scenario, $\Delta_{all} = L_d/800$.

The results presented above in Figures 5.9 to 5.12 agree with the results of Bharadwaj (2013), who found numerically that the reduction in the total heave of an extremely expansive, deep reactive layer reached 22% after replacing 750 mm of the reactive soil with a non-reactive cushion of higher saturated permeability. By increasing the thickness of the cushion to 2.0 m, a further reduction in the total heave of only 15% was achieved, whereas a further increase in the cushion thickness to 4.0 m added only a further 7.3% reduction in the total heave. The fact that the efficacy of the sand cushion reduces with its thickness indicates that the recommendations made by Chen (1988), regarding the use of a minimum thickness of 3.0 feet (1.0 m) for the sand cushion, are questionable.

5.4 DEVELOPMENT OF EPR MODELS FOR STIFFENED SLAB FOUNDATION WITH SAND CUSHION

Currently, there is no definite codified method or guideline to evaluate or design the thickness of the sand cushion. Chen (1988) recommended a minimum depth of 3 feet (1.0 m) and preferred 5 feet (1.5 m). Nelson and Miller (1992) suggested that the depth of the cushion should be governed by the weight required to counter the expected uplift. Obviously, this recommendation may lead to impractical thicknesses, considering that the expected total heave and the corresponding swelling pressure is proportional to the active zone which is even quite challenging to estimate in the presence of a sand cushion. To fill this gap in design practice, this section aims at providing a tool that can help engineers quantify the role of the sand cushion into specific design output. This is accomplished using the EPR method presented in Chapter 4.

The input data concerning the EPR method presented here are similar to those of Chapter 4 with the inclusion of the new parameter (S), representing the thickness of the sand cushion. The outputs are the same as in Chapter 4, including the internal forces in the slab foundation (bending moments and shear forces in both directions) and the slab foundation deflection. In total, a number of 569 data cases were compiled from the parametric study for the edge drop scenario, whereas 524 data cases were collected for the edge heave scenario. Similar to the EPR model developed in Chapter 4, 90% of the parametric study outputs data, considering the sand cushion is used for training the model, while 10% of

the data is used for validation. The training and validation data are divided in a way to be statistically consistent to properly represent the same statistical population. Consequently, the training and validation data are selected to have very close averages (means) and standard deviations. The minimum and maximum values of the parameters are used in the training data to avoid extrapolation. The EPR analysis returned 4 models for each output parameter and the optimal models along with their performance graphical representation (see Figures 5.13 to 5.22) are as follows:

For the edge lift scenario:

$$\begin{aligned} \delta = & -5.1918 \frac{y_m^2}{B^2 \sqrt{LT_{eq} S}} - 3.6456 \frac{1}{B} \sqrt{\frac{Ly_m}{S}} + 22.6104 \frac{y_m}{\sqrt{BT_{eq} S}} \\ & + 0.00034027 y_m^2 \sqrt{L} - 169.8056 \frac{B^2}{T_{eq} L^2} \sqrt{\frac{y_m}{S}} - 1.8647 \end{aligned} \quad (5.2)$$

$$\begin{aligned} M_s = & -0.00029804 \frac{y_m T_{eq}^2}{B^2} + 6.682 \times 10^{-5} \frac{y_m T_{eq}^2}{B} - 2735.1374 \frac{1}{T_{eq} \sqrt{y_m}} \\ & - 0.12701 \frac{B^2 y_m \sqrt{S}}{L^2} + 29.6343 \end{aligned} \quad (5.3)$$

$$\begin{aligned} M_l = & -0.19758 \frac{LT_{eq}}{B^2} + 1.8388 \sqrt{\frac{LT_{eq}}{B}} + 0.00037881 \frac{T_{eq}^2 \sqrt{y_m}}{L} \\ & + 0.0019695 y_m \sqrt{\frac{LT_{eq}}{S}} - 27.987 \end{aligned} \quad (5.4)$$

$$V_s = 5.4069 \times 10^{-5} \frac{y_m^2 T_{eq} S}{B \sqrt{L}} + 0.2136 \sqrt{y_m T_{eq}} - 0.12401 y_m \sqrt{\frac{BS}{L}} - 9.6441 \quad (5.5)$$

$$V_l = 1.3563\sqrt{T_{eq}} + 0.005287y_m\sqrt{T_{eq}} + 0.016455y_m\sqrt{\frac{B}{S}} - 0.036346\frac{B^2y_m}{L\sqrt{T_{eq}}} - 18.3312 \quad (5.6)$$

For the edge drop scenario:

$$\delta = \frac{-1.0492y_mT_{eq}}{B^2L^2\sqrt{S}} - \frac{0.067123y_m\sqrt{LT_{eq}S}}{B^2} + \frac{541.2089}{\sqrt{LT_{eq}}} + 6.7279\frac{y_m}{\sqrt{T_{eq}}} - 261.1665\frac{B^2\sqrt{y_mS}}{L^2T_{eq}} - 7.8074 \quad (5.7)$$

$$M_s = -2.2822 \times 10^{-7} \frac{y_m^2 T_{eq}^2 \sqrt{L}}{B^2} + \frac{951.5144}{\sqrt{BT_{eq}}} + 0.030299T_{eq}\sqrt{y_m} - 0.00055127\frac{B^2T_{eq}\sqrt{y_mS}}{L} + 0.21723B^2\sqrt{\frac{S}{y_m}} - 44.4641 \quad (5.8)$$

$$M_l = 0.00072314\frac{T_{eq}^2}{L}\sqrt{\frac{y_m}{B}} + 0.0011386y_mT_{eq} + 6.4991 \times 10^{-5}L^2T_{eq}\sqrt{\frac{B}{y_m}} - 0.0033012\frac{B^2T_{eq}S\sqrt{y_m}}{L^2} - 0.63052 \quad (5.9)$$

$$V_s = -8.1225 \times 10^{-8} \frac{y_m^2 T_{eq}^2}{B^2 S^2} + 4.8926 \times 10^{-6} \frac{y_m T_{eq}^2}{S^2 L \sqrt{B}} + 0.01597T_{eq}\sqrt{\frac{y_m}{B}} + 0.1518\sqrt{Ly_m} - 1.9909 \quad (5.10)$$

$$V_l = -0.002312\frac{Ly_m\sqrt{T_{eq}}}{B^2S} + 0.0016866\frac{y_mT_{eq}}{\sqrt{B}} + 0.00077552\frac{T_{eq}}{S^2}\sqrt{\frac{y_m}{L}} + 0.0002231L^2\sqrt{T_{eq}} + 2.8124 \quad (5.11)$$

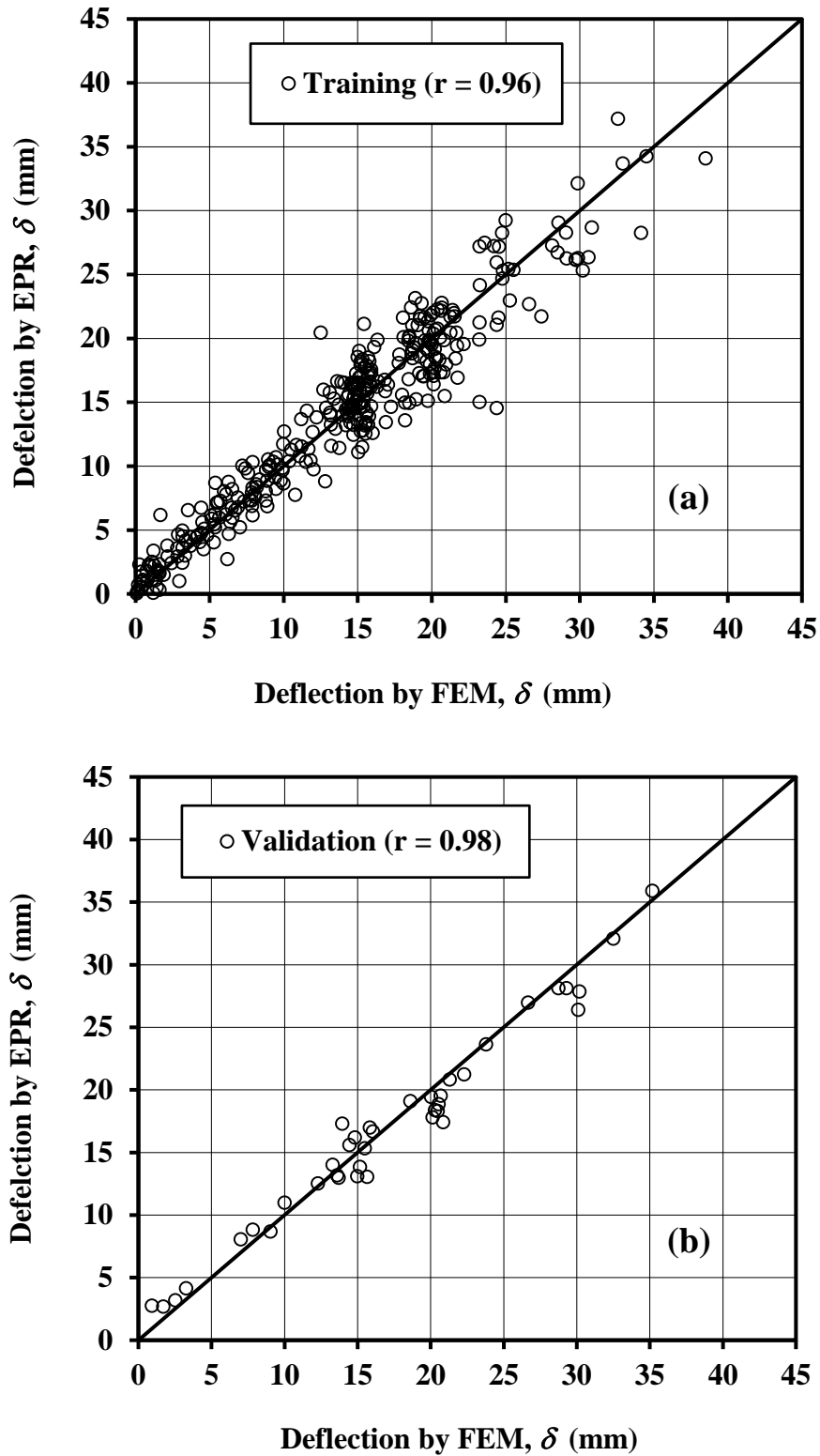


Figure 5.13: Graphical performance of the EPR model of Equation 5.2 regarding deflection δ : (a) Training set; and (b) Validation set.

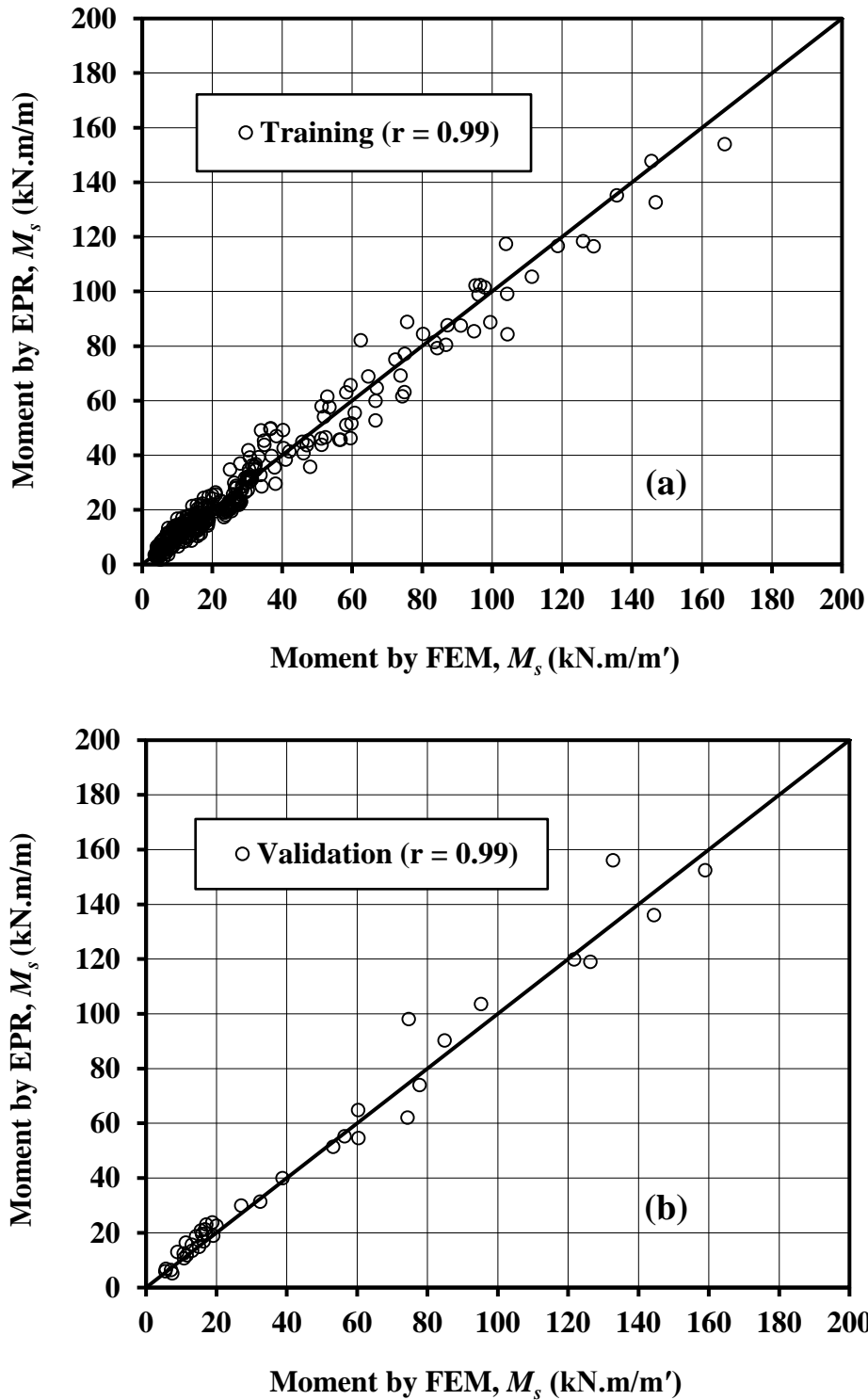


Figure 5.14: Graphical performance of the EPR model of Equation 5.3 regarding M_s : (a) Training set; and (b) Validation set.

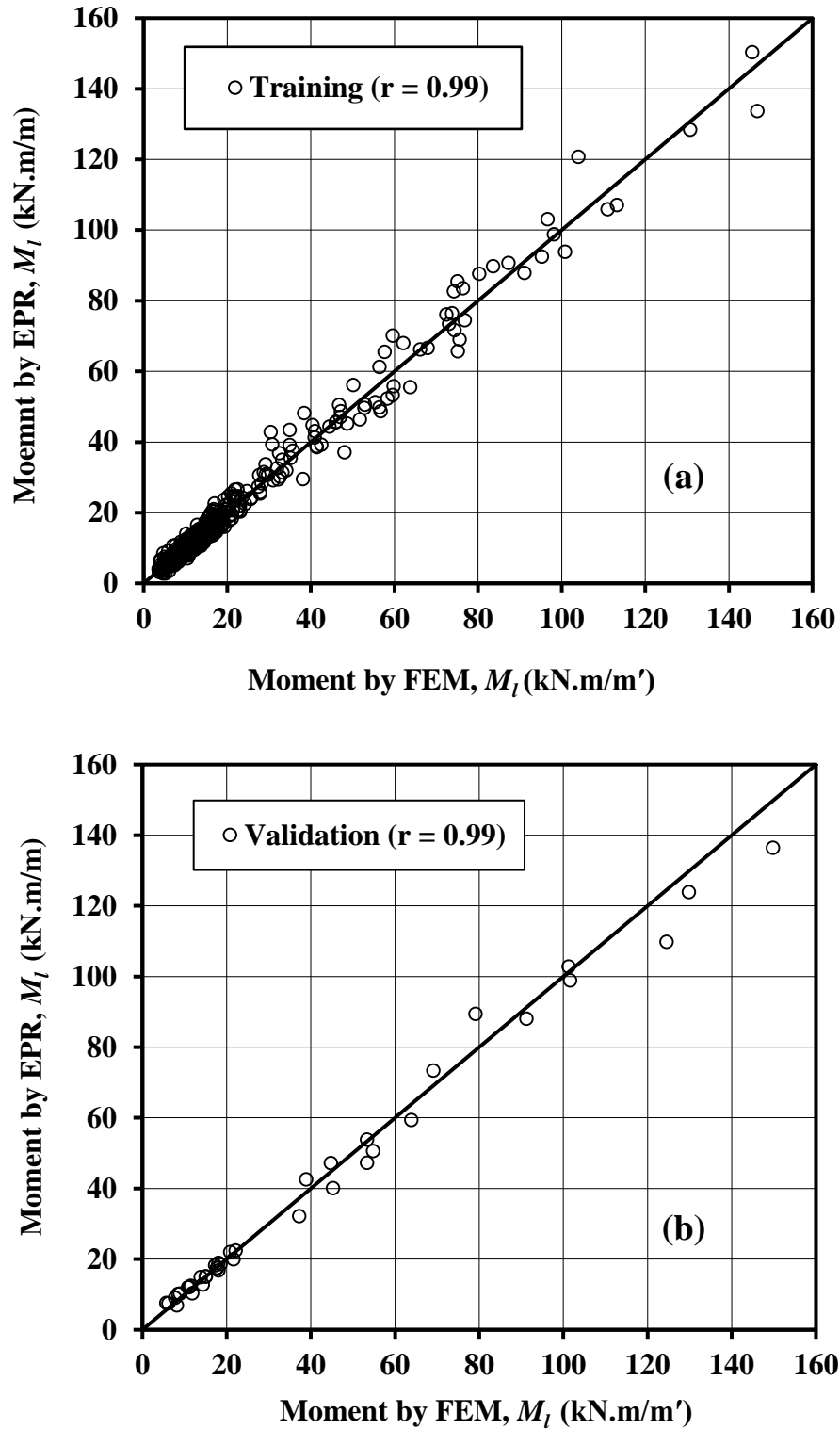


Figure 5.15: Graphical performance of the EPR model of Equation 5.4 regarding M_l : (a) Training set; and (b) Validation set.

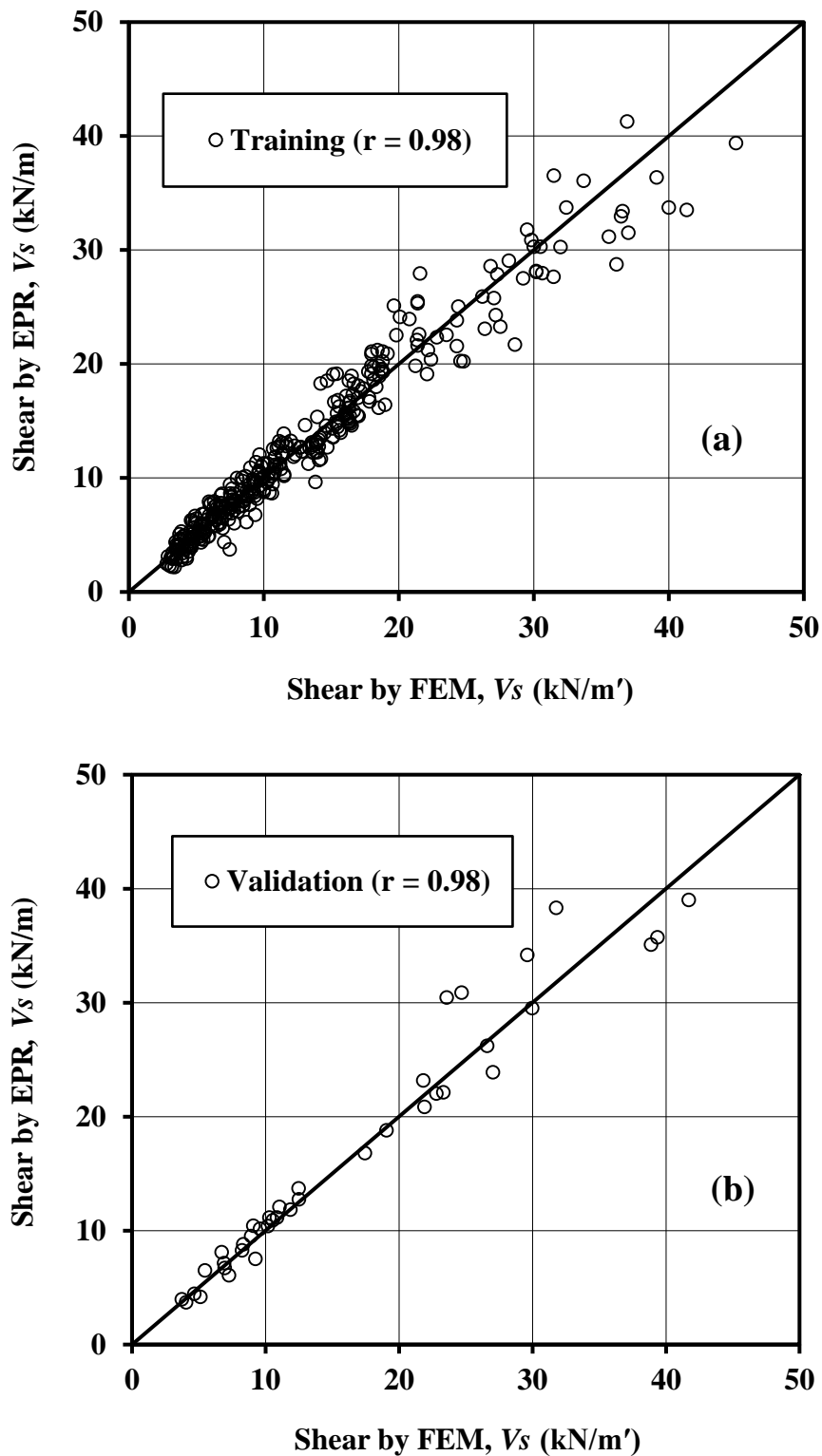


Figure 5.16: Graphical performance of the EPR model of Equation 5.5 regarding V_s : (a) Training set; and (b) Validation set.

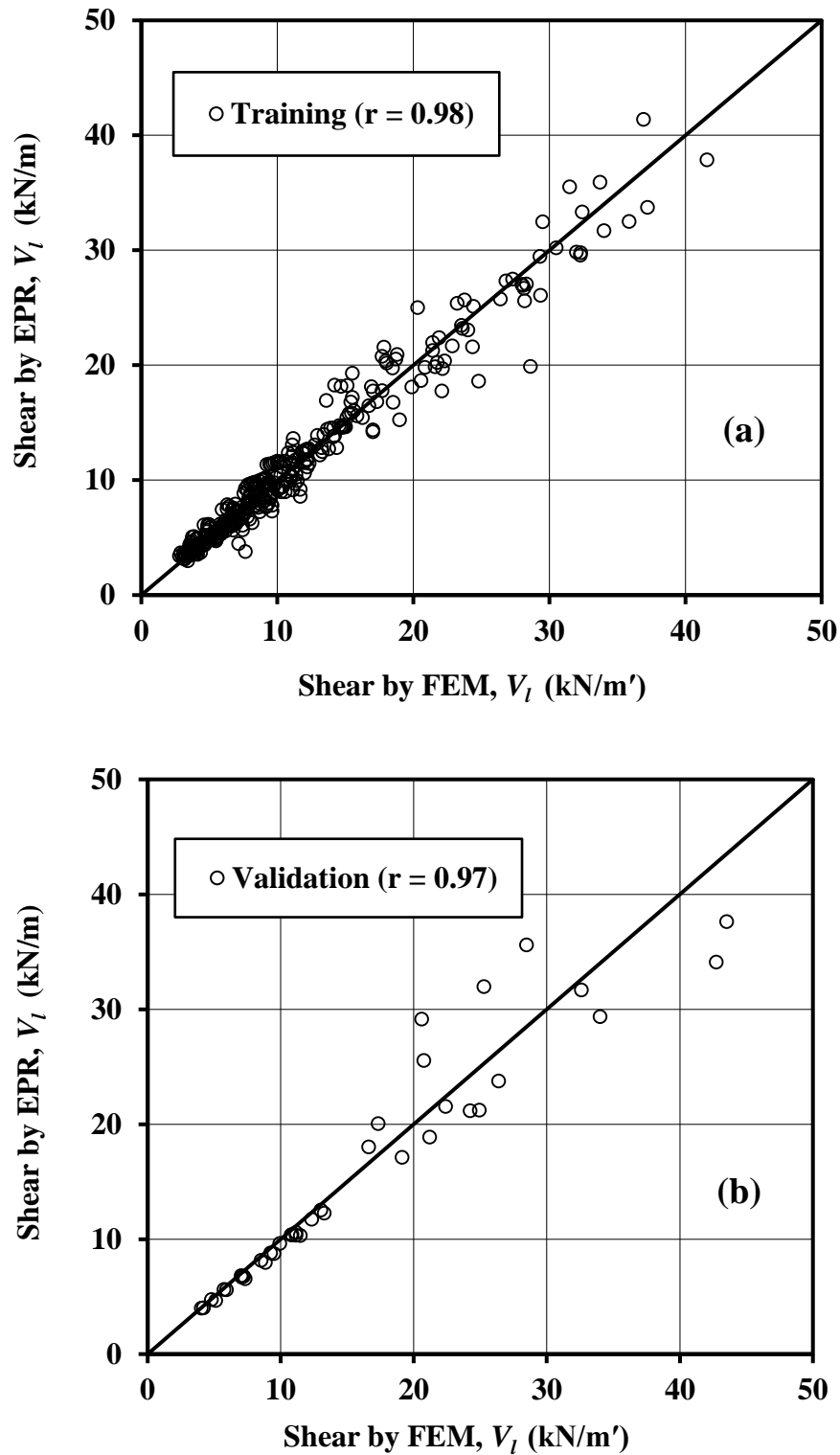


Figure 5.17: Graphical performance of the EPR model of Equation 5.6 regarding V_l : (a) Training set; and (b) Validation set.

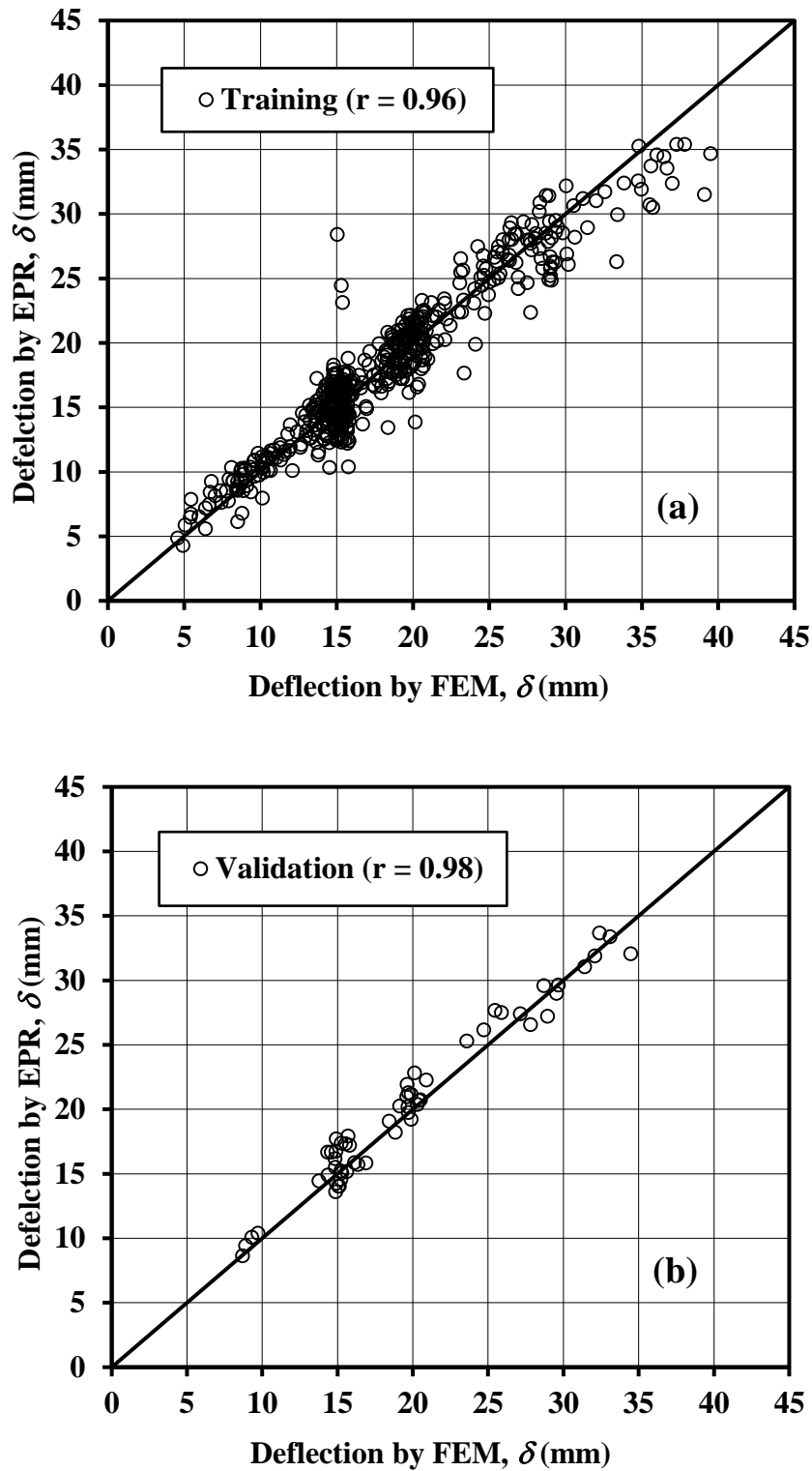


Figure 5.18: Graphical performance of the EPR model of Equation 5.7 regarding deflection δ : (a) Training set; and (b) Validation set.

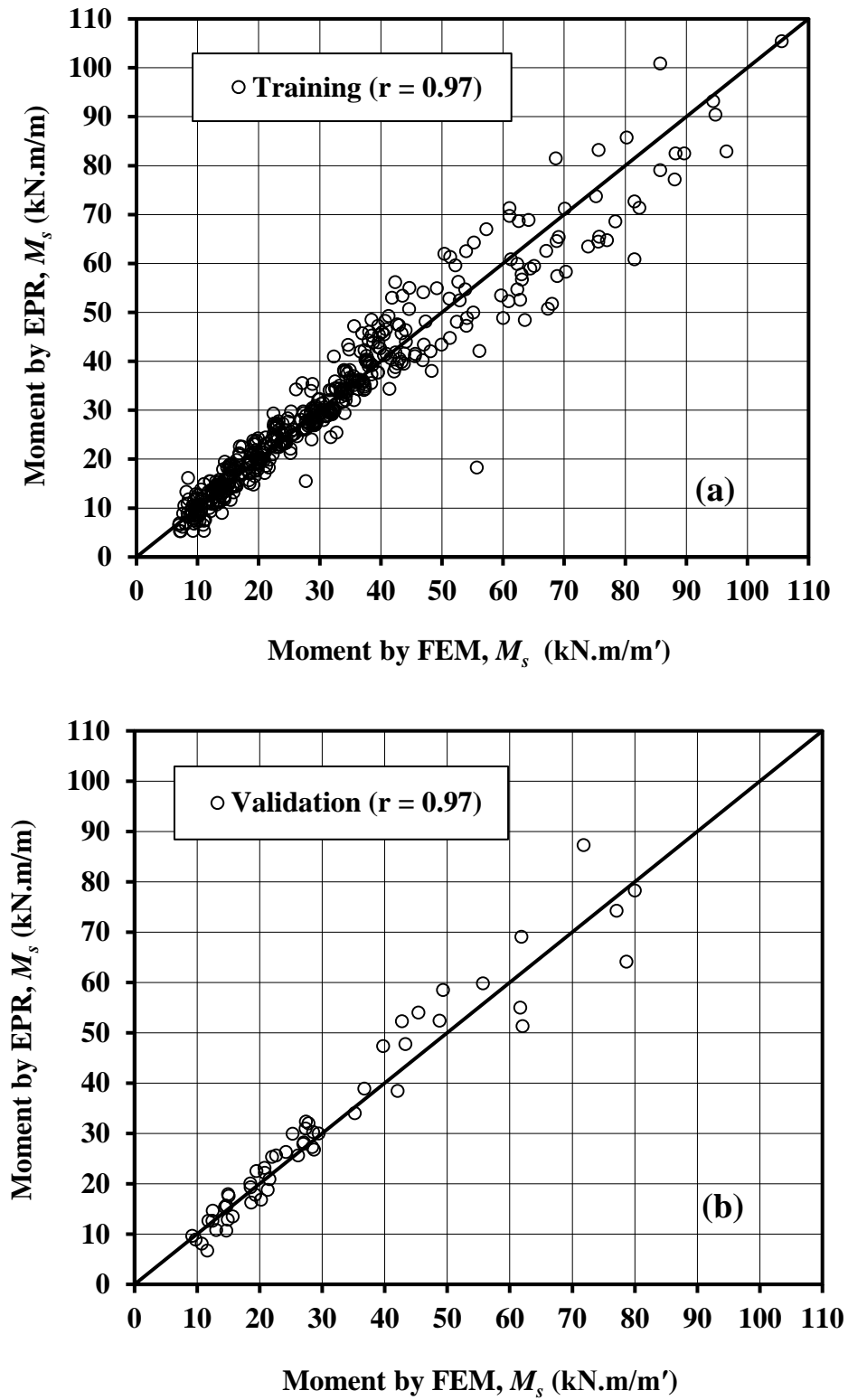


Figure 5.19: Graphical performance of the EPR model of Equation 5.8 regarding M_s : (a) Training set; and (b) Validation set.

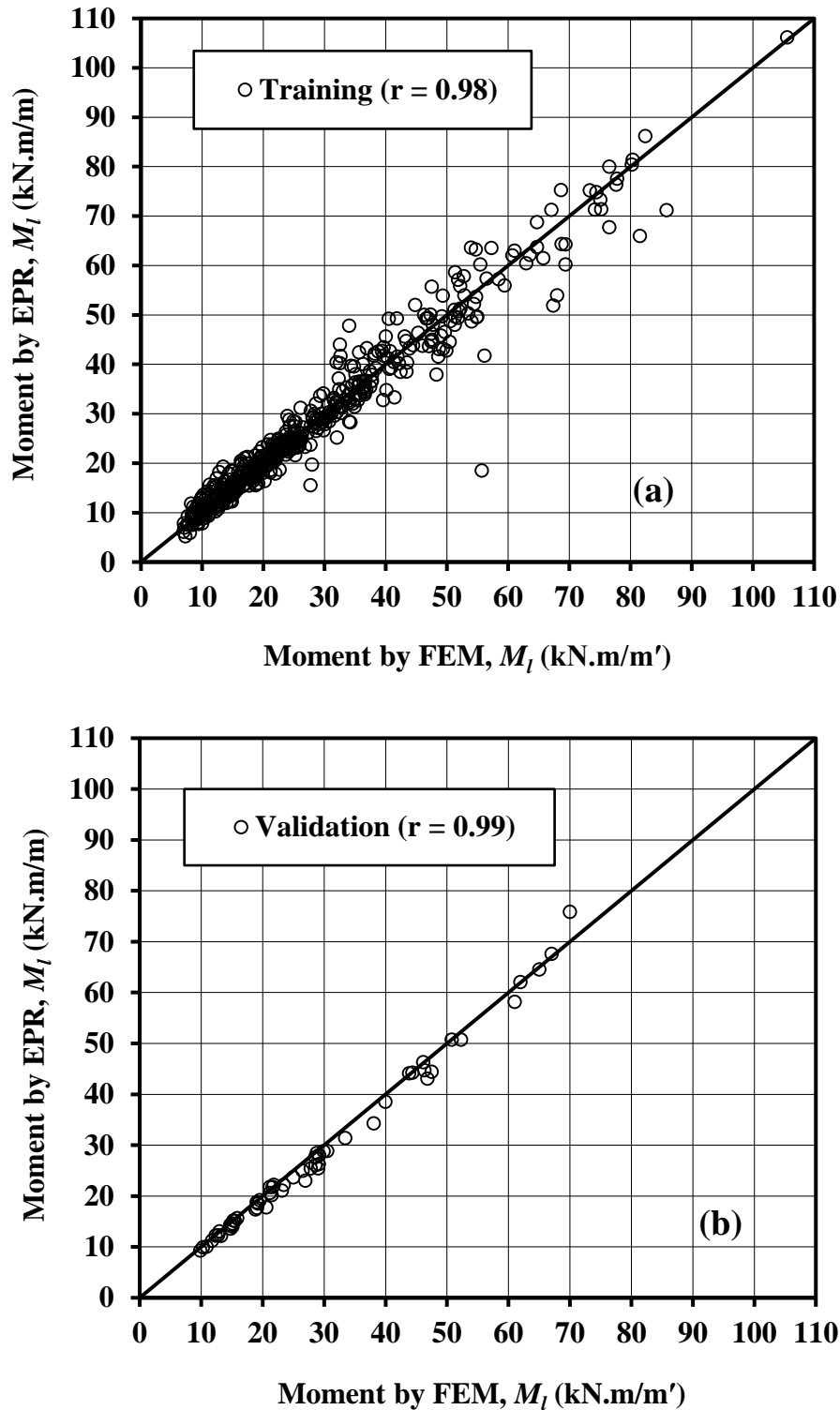


Figure 5.20: Graphical performance of the EPR model of Equation 5.9 regarding M_l : (a) Training set; and (b) Validation set.

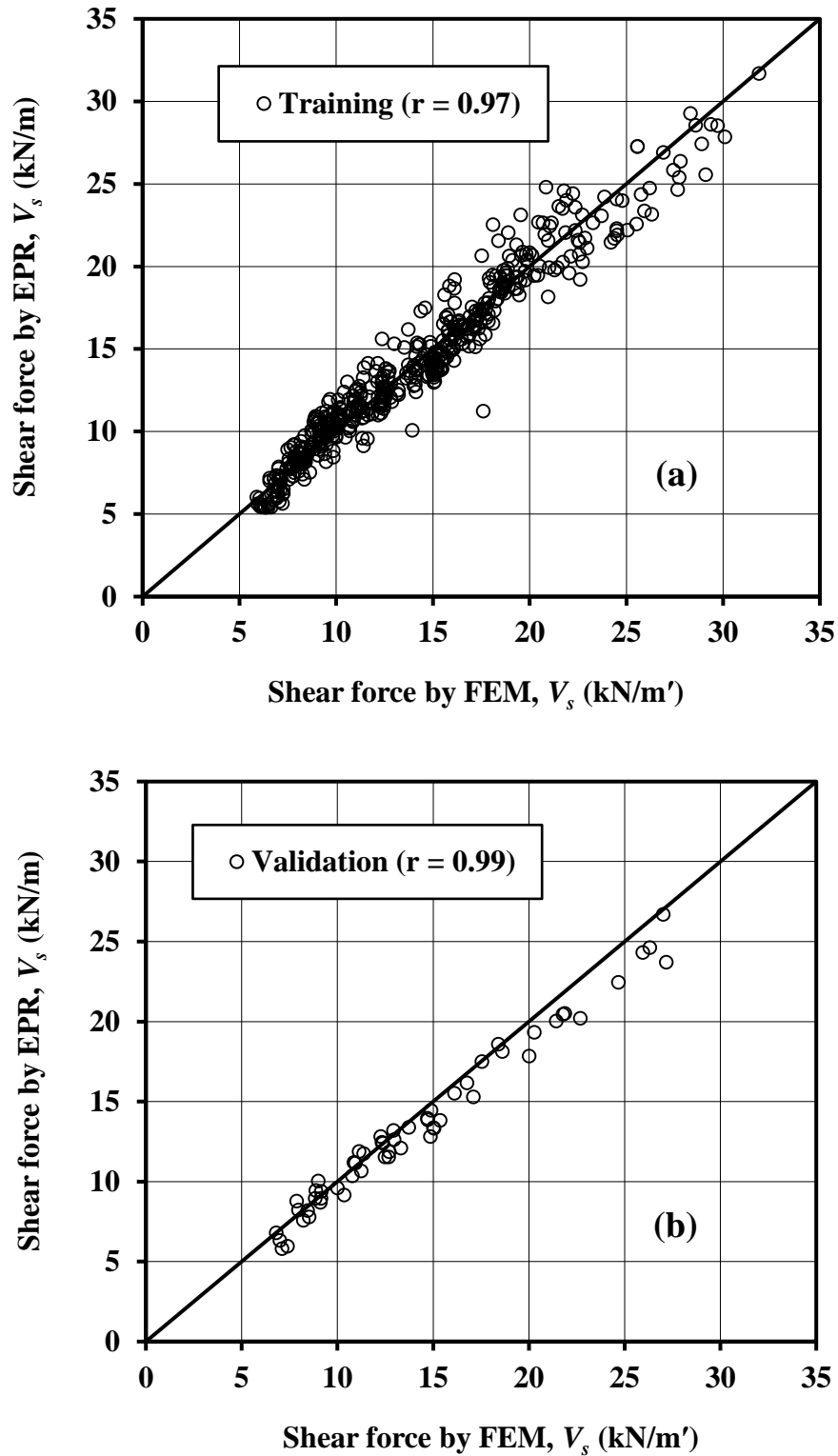


Figure 5.21: Graphical performance of the EPR model of Equation 5.10 regarding V_s : (a) Training set; and (b) Validation set.

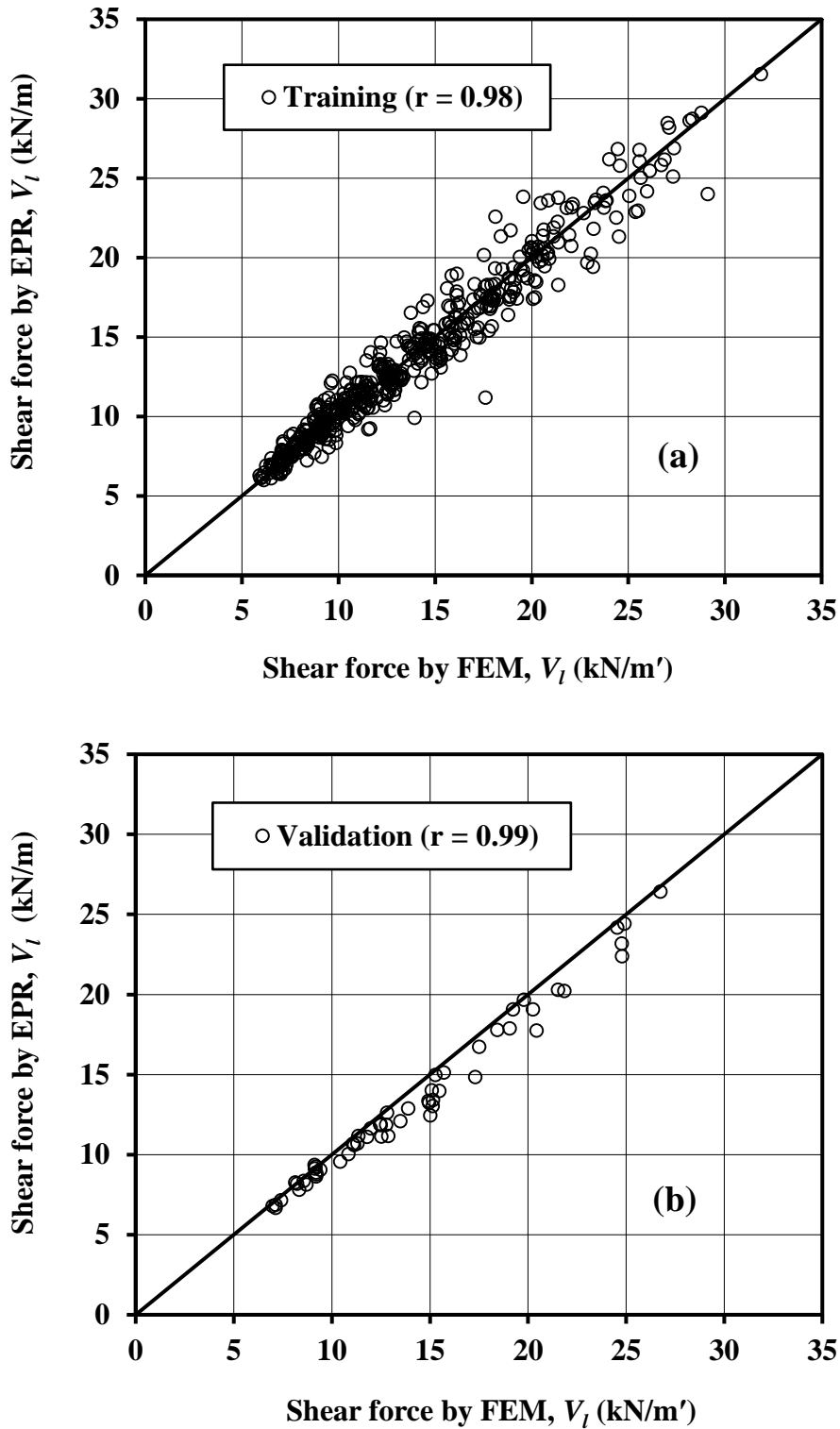


Figure 5.22: Graphical performance of the EPR model of Equation 5.11 regarding V_l : (a) Training set; and (b) Validation set.

The results of the EPR analysis are implemented in the new design method and the SFORS computer program, so that the designer can select the option to consider the use of a predefined thickness of a sand cushion beneath the slab foundation. The computer program carries out the required calculations using the EPR models shown above in order to get the required equivalent slab thickness and the corresponding slab internal forces. The rest of the procedure is similar to that explained in Chapter 4, in terms of accounting for the effective inertia of the stiffened slab foundation and delivery of the final design, including the dimensions and reinforcement of the stiffening beams. In the following section the new design method using the SFORS program with the feature of a sand cushion is illustrated and tested through an illustrative numerical example.

It should be noted that, instead of investigating the optimal sand cushion depth required to reduce or eliminate the surface heave or reduce the swelling pressure, this section focuses on how the sand cushion can be used to reduce the required foundation stiffness needed to maintain the foundation differential movement within the standard limits.

5.5 NUMERICAL EXAMPLE CONSIDERING SAND CUSHION

In order to validate the EPR models, the following example of slab foundation with sand cushion is examined; first using the EPR models and second using a separate finite element analysis. The results of the two methods are then compared. The example is for a hypothetical 17.0 m × 23.0 m slab foundation, supporting a single storey masonry veneer house, and subjected to a characteristic surface heave (y_s) of 109 mm. The loading is similar to that used in the parametric study with a uniform load of 4.5 kPa and perimeter edge line load of 6.0 kN/m'. A 750 mm sand cushion layer is assigned beneath the footing, with properties and permeability comparable to those used in the parametric study. The two scenarios of edge lift and edge drop are evaluated.

Using Equations 5.2 and 5.7, and by iteration, the equivalent slab thickness (T_{eq}) required to limit the deflection of the slab foundations δ to the allowable deformation, Δ_{all} , to 20 mm (according to the type of construction—refer to Table 4.2), is determined, along with corresponding internal forces. A separate, 3D FE model is constructed for the same

slab foundation and the same equivalent thickness T_{eq} obtained from the EPR models is used for each soil mound scenario. Overall, the results of the finite element modelling are found to be in very good agreement with the EPR models, as shown in the comparison outcomes in Table 5.1.

Table 5.1: Comparison between EPR and FE results for the numerical example with sand cushion.

Movement Scenario	T_{eq} (mm)	δ (mm)	M_s (kN.m/m)	M_l (kN.m/m)	V_s (kN/m)	V_l (kN/m)
ED EPR	376	20	50.5	43.3	17.5	17.7
ED FE	375	18.5	41.4	43.3	18.3	18.7
EL EPR	321	20	38.2	35.1	17.3	17.7
EL FE	325	22.2	35.6	38.3	18.0	18.9

Using the internal forces obtained from the EPR model and applying the same procedures for the calculation of the effective slab inertia in Chapter 4 (considering 6 beams in the long slab direction and 7 beams in the short direction) the stiffening beam design depth is found to be 790 mm (including the 100 mm top slab), with top and bottom reinforcements of 3N16 and 4N16, respectively, and a slab steel mesh of $178 \text{ mm}^2/\text{m}'$. Note that if the design is carried out considering the relatively lower moment obtained from the FE results (a maximum of 18% lower, M_s), the depth will be 750 mm; however, this difference has little effect on the design, and the EPR models can be developed to have acceptable conservatism. Figures 5.23 and 5.24 show screenshots of the SFORS program's input and output modules incorporating a sand cushion. Solving the same example without the sand cushion gives much higher results, as shown in Table 5.2, emphasising the benefit of using a sand cushion.

SFORS

With Sand Cushion

Slab long span	L	23.00	m
Slab short span	B	17.00	m
No. of beams in long span	N_L	6	Max. spacing CL to CL in long direction
No. of beams in short span	N_S	7	Max. spacing of beams in short direction
Beam web width	b_w	300.00	mm
Top rebars	A_{sc}	3	16.00
Bottom rebars	A_{st}	4	16.00
Slab reinforcement	S_r	178.00	mm ² /m'
Top cover	T_c	30.00	mm
Bottom cover	B_c	50.00	mm
Soil movement	y_m	76.50	mm
Allowable deflection	L/Δ	600.00	
Sand cushion thickness	S	0.75	m

Solve Clear

Figure 5.23: Screenshot of the SFORS Program incorporating sand cushion in the new design method, solving rectangle (17 m × 23 m) of the numerical example.

The stiffening beam design depth considering the results shown in Table 5.2, is 1800 mm (including the 100 mm top slab), with top and bottom reinforcements of 4N20 and 4N20, respectively, and a slab steel mesh of 178 mm²/m'. It is obvious that the 750 mm sand cushion reduced the depth of the stiffening beam of the slab foundation significantly by 56%. This reduction results in a remarkable saving in the volume of concrete of about 65.0 m³ for the size of the footing under consideration (17.0 m × 23.0 m). A detailed cost comparison would eventually add the contribution of excavation and standard backfilling for the construction of the 750 mm sand cushion (compared to the over-excavation for the construction of the 1800 mm deep stiffening beam without the sand cushion), and other items including the cost of insulation, top and bottom beams' reinforcement and shear reinforcement, which is most likely to provide an overall cost reduction in favour of the sand cushion option.

<div style="text-align: center;"> <h1 style="margin: 0;">SFORS</h1> <p style="margin: 0;">Slab Foundation On Reactive Soil</p> </div>		Project			
		Client			
		Date	Rev.		
Input Data:					
Slab foundation length	L	23	m		
Slab foundation breadth	B	17	m		
No. of beams in long direction	N_L	6			
Max. CL to CL distance in long direction	S_L	3.4	m		
No. of beams in short direction	N_s	7			
Max. CL to CL distance in short direction	S_s	3.833	mm		
Beam web width	b_w	300	mm		
Top cover to reinforcement	T_c	30	mm		
Bottom cover to reinforcement	B_c	50	mm		
Slab reinforcement	S_r	178	mm ² /m'		
Concrete grade	f'_c	20	MPa		
Reinforcement yield strength	f_y	500	MPa		
Soil mond movement	y_m	76.5	mm		
Allowable slab deflection	L/Δ	600			
Top reinforcement	A_{sc}	3	N	16	
Bottom reinforcement	A_{st}	4	N	16	
Slab thickness	T_s	100	mm		
Sand cushion depth	S	0.75	m		
Output Data :		Edge drop		Edge lift	
		Long span	Short span	Long span	Short span
Equivalent salb thickness	mm	376.576	376.576	321.139	321.139
Equivalent slab inertia	m ⁴ /m'	4.45E-03	4.45E-03	2.76E-03	2.76E-03
Service BM per metre width	kN.m/m'	43.276	50.539	35.100	38.172
Service BM per beam	kN.m/m'	147.138	193.716	119.340	146.313
Effective flange width	m	1.700	1.917	1.700	1.917
Cracking moment/beam	kN.m'	135.682	168.487	92.811	108.092
Required beam depth	m	0.731	0.790	0.698	0.747
Eff. inertia of stiffened slab	m ⁴ /m'	4.45E-03	4.45E-03	2.76E-03	2.76E-03
Max. required beam depth	m	0.790			
Max. flexural rebars	mm ²	8415	9115	7775	8363
Min. flexural rebars	mm ²	589	638	691	787
Max. service shear force	kN/m'	17.714	17.470	17.707	17.266
Required shear rebars	mm ²	63.000			
Required shear rebars spacing	mm	300.000			
Summary:					
Total height of sub-beam	mm	790			
Top rebars		3	N	16	
Bottom rebars		4	N	16	
Shear rebars		2	N	8	@ 300.000
Slab rebars (both directions)	mm ² /m'	178			

Figure 5.24: Screenshot of the design report obtained from the SFORS program incorporating sand cushion in the new design method, solving (17 m × 23 m) of the numerical example.

The above illustrative example shows how efficient the sand cushion can be in reducing the beam depth of the stiffened slab foundation, especially with high differential mound movements and strict allowable deformation limits. By incorporating the option of the sand cushion in the design tool presented in Chapter 4 in terms of the EPR models, this research now enables engineers to quantify the exact contribution of the sand cushion in terms of the exact equivalent design depth of the stiffened slab foundation; this corresponds to a particular thickness of the sand cushion. Adoption of this tool will remove the element of empiricism that engulfs application of the sand cushions in the design of stiffened slab foundation on reactive soils (such that engineers are no longer forced to follow the rule-of-thumb of using either 1.0 m or 1.5 m of sand cushion, without knowing its actual impact on the design).

Table 5.2: EPR results for the numerical example without sand cushion.

Movement Scenario	T_{eq} (mm)	δ (mm)	M_s (kN.m/m')	M_l (kN.m/m')	V_s (kN/m')	V_l (kN/m')
ED EPR	765.4	20	191.1	174.8	48.1	46.0
EL EPR	615.2	20	111.0	93.0	26.0	23.3

5.6 SUMMARY

This chapter investigated the role of the sand cushion in the performance of stiffened slab foundations on reactive soils. The mechanism behind the ability of the sand cushion to improve the performance of this type of foundations was determined numerically. The chapter revealed that the sand cushion actually works as a filter that provides a path for moisture to accumulate in a uniform manner before it, inevitably, reaches the underlying reactive soil under the work of gravity. This eventually creates a field of much more uniform degree of saturation within the reactive stratum, leading to reduced differential movement of the slab foundation.

The effect of using sand cushions on the design of stiffened slab foundation was investigated in this chapter. This study succeeded in mathematically relating the equivalent slab foundation thickness T_{eq} (and consequently the depth of the stiffening sub-beams) to the thickness of the sand cushion (S). In order to achieve this goal, an intensive parametric study was carried out similar to that presented in Chapter 4 after including a parameter representing the thickness of the sand cushion (S). The results of the parametric study were compiled using the artificial intelligence, evolutionary polynomial regression (EPR) technique, in the form of design equations for the case of edge drop and edge heave scenario. The EPR models (design equations) were validated through an illustrative numerical example and the results of the EPR models showed good agreement compared to the results of the finite element analysis. The same numerical example was solved without a sand cushion using the EPR models developed in Chapter 4 in order to compare the results with and without the sand cushion. Efficacy of the sand cushion was clearly demonstrated in this example. The design equations of the EPR models can be easily used by designers to estimate the equivalent slab thickness (T_{eq}) and the corresponding slab internal forces for a slab foundation supporting a single storey house having a specific construction type and subjected to a specific mound movement, for a specific thickness of the sand cushion.

CHAPTER 6

SUMMARY, CONCLUSIONS AND RECOMMENDATIONS

6.1 GENERAL

Stiffened slab foundations are the most common foundation technique used worldwide to support light-weight structures on reactive soils. Careful review of the existing design methods and other studies on stiffened slab foundations revealed that a major assumption adopted by almost all methods involves simplifying the real, complex 3D moisture flow aspect into a 2D problem, resulting in deformation incompatibility between the soil mound and the supported footing. This is manifested by analysing the slab in each direction separately, by adopting uncoupled approaches in which the footing is designed for stress analysis using pre-defined soil mound shapes obtained empirically or from a separate seepage analysis in each direction, with no consideration to the effect of slab loading on the formation of the soil mounds. In fact, determination of the soil mound shapes in the existing methods is based on simple empirical equations, based on best fit of minimal field observations. However, in reality, formation of the soil mound depends on several factors, including evolving soil suction, degree of saturation, hydraulic conductivity, site drainage conditions and irrigation/plantation events.

This research tackled the above mentioned shortcomings in current design practices by developing a robust, hydro-mechanical finite element (FE) model able to simulate the intricate behaviour of unsaturated reactive clays and their response to soil moisture and suction variations. The range of parameters needed for the developed hydro-mechanical FE model were identified, investigated and verified against previous studies. The model was then used in a 3D coupled flow-deformation and stress analysis involving multidimensional transient flow simulating realistic events of moisture precipitation and evaporation. The resulting model simulated the corresponding soil moisture and suction changes to produce a realistic soil mound beneath the slab foundation. Contact elements were used to allow for the separation between the slab foundation and the soil based on the generated soil mound and the stiffness of the slab foundation. The developed hydro-

mechanical FE model was verified through two case studies involving field observations in order to investigate its ability to simulate the soil response in situations involving surface moisture and suction changes. The results of the verification work proved the success and strength of the model in simulating the soil deformations and suction changes in a 3D fashion that reflected the true behaviour of stiffened slab foundations. A third case study involving a design of a hypothetical stiffened slab foundation using the developed model and the well-known Mitchell's method was also presented.

Following the verification phase, the developed 3D FE hydro-mechanical model was used in an extensive parametric study involving slab foundations of variable dimensions, subjected to different soil mounds and supporting different construction types. The results of the parametric study were compiled into a set of design charts. However, to avoid the inaccuracy in the linear interpolation from the design charts, the data of the parametric study were used to generate design equations through a robust artificial intelligence techniques. These design equations along with the design procedures formed a new standalone design method for stiffened slab foundations on reactive soils supporting light-weight structures. The procedures of the new design method (including iterations and verifications) were congregated into a user-friendly computer program that can be readily used by engineers and practitioners.

In addition to the contribution above, this thesis investigated the effect of sand cushion as a well-known remedial technique for foundations in reactive soils. The actual role of sand cushions was investigated and identified via 3D analysis using the hydro-mechanical FE model mentioned above. The actual contribution of sand cushions to the design of stiffened slab foundations was carefully quantified in terms of the reduction in the overall slab foundation thickness. To this end, an extensive parametric study was carried out similar to that used to develop the new design method, with the inclusion of 3 commonly used depths of sand cushion. The results of the parametric study were used to generate design equations using the AI technique, and the computer program developed for the new design method was then extended to include the sand cushion thickness in the design of stiffened slab foundations.

6.2 SUMMARY AND CONCLUSIONS

This thesis developed a new design method for stiffened slab foundations on reactive soils, based on a robust 3D, coupled flow-deformation and stress analysis, considering an advanced hydro-mechanical model, and implementing realistic moisture precipitation and evaporation algorithms. The thesis comprises six main chapters:

Chapter 1 presented the premises underlying the design of stiffened slab foundations, highlighting the main shortcomings. The chapter also presented the research objectives and scope.

Chapter 2 presented a critical review of the existing and most commonly used design methods for stiffened slab foundations on reactive soils, exploring their assumptions and limitations. The chapter investigated the recent researches into design and analysis of stiffened slab foundations on reactive soils that involved the finite element techniques. The chapter summarised the specific shortcomings of existing design methods (which were tackled and resolved later in this research). These shortcomings included: oversimplifying the real 3D real problem into a 2D one, which violates the soil and footing mound deformation compatibility; the empirical estimation of the soil mound; and the use of uncoupled approach in the flow- deformation problem.

In Chapter 3, an advanced 3D finite element (FE) numerical modelling was pursued to simulate the complex behaviour of stiffened slab foundations, which otherwise cannot be realistically captured by the currently available design methods. Through a hydro-mechanical approach, the resulting 3D FE model was proven capable of simulating the true performance of stiffened slab foundations on reactive soils, by: (1) involving a coupled flow-deformation analysis based on realistic moisture flow and suction evolution; and (2) inducing a realistic formation of the soil mound beneath the footing. The chapter presented and discusses some modelling aspects relating to unsaturated soils and the corresponding associated parameters. Development of the adopted FE numerical models is then explained and verified through three case studies. The first case study involved field observations of a soil mound formation of a flexible cover membrane resting on a

highly expansive soil over a period of 5 years in Newcastle, Australia. The mound formation over the course of observations was found to be similar to that produced by FE analysis. This modelling step confirmed reliability of the adopted FE modelling process and capability of the model in generating realistic soil distorted mound shapes. The second case study presented field observations of the suction change and soil movement for a site in Amarillo, Texas. The results of the FE modelling agreed fairly well with the field observations, and this proved the efficacy of the FE model in simulating the water diffusion and suction changes through a soil medium. The third case study involved a hypothetical stiffened slab foundation on reactive soil, solved via 2D/3D FE modelling and compared with Mitchell's method. The 2D FE analysis showed a good agreement with Mitchell's method. However, the 3D FE analysis produced more realistic mound shapes and achieved deformation compatibility; a matter that is usually unaccounted for in the 2D analysis adopted by most existing design methods.

Chapter 4 detailed the comprehensive parametric study carried out using the hydro-mechanical model presented in Chapter 3. The assumptions and conditions associated with the parametric study were presented and the results of the parametric study were compiled into a set of design charts. Analysis of the design charts was presented through by example to demonstrate the design process and associated elements. To avoid any inaccuracy during interpolation from the design charts, the output data of the parametric study were classified into a training set (90 % of the data) and validation set (10% of the data) and then used to generate design equations using the evolutionary polynomial regression (EPR) method, as a robust artificial intelligence (AI) technique. The design equations along with all design procedures presented a new design methods for stiffened slab foundations on reactive soils supporting light weight structures. The new design method was validated through an illustrative numerical example involving a slab of L-shape. The results of the new design method were compared with those of the well-known Mitchell's method (adopted by the Australian Standards) and also the results obtained from the 3D finite element analysis of the same foundation problem. The outcomes of the new design method were found to agree well with the common engineering practice and the outputs of the 3D FE analysis, and were thus deemed to be more realistic than those obtained from

Mitchell's method, given the shortcomings reported previously for the latter. The new design method procedures were integrated into a user-friendly computer program called (SFORS).

Chapter 5 explored the effect of sand cushion on the design of slab foundations. The actual role of the sand cushion was investigated numerically and shown to be manifested in producing a relatively uniform moisture field beneath the slab, which eventually reduce the differential movement of the slab foundation. A study was then carried out on the effect of sand cushion thickness on reducing the thickness demand of the stiffened slab foundation for different soil mound differential movements, different construction types, different foundation dimensions and different movement scenarios. An extensive parametric study similar to that used to develop the new design method presented in Chapter 4 was carried out considering 3 commonly used sand cushion depths. The ability of the sand cushion to reduce the differential slab foundation movement and internal forces, led to reduction in the required design thickness of the slab. The results of the parametric study were synthesized into design equations, using the EPR method considering a specific thickness of sand cushion. The design equations were validated through an illustrative numerical example solved by the design equations and by the 3D finite element method. The results of both methods were found to agree fairly well, confirming the ability of the EPR model to calculate the reduced thickness of stiffened slab foundations using a specific sand cushion thickness. Considerable cost saving can be achieved through the use of sand cushions. This is believed to be contribution critical tool, since designers can now discard the empirical rule-of-thumb of using 1.0 to 1.5 m of sand cushion, since this method does not lend itself to engineering conviction. Instead, the new design tool can be used to specify the thickness of the sand cushion required to achieve a specific reduction in the slab foundation thickness.

6.3 ORIGINAL CONTRIBUTION OF THE RESEARCH

To the author's best knowledge, this thesis made the following original contributions:

- 1- Development of a robust hydro-mechanical model capable of simulating the complex behaviour of reactive soils and their response to surface moisture and suction variations.
- 2- Successfully implementing the developed hydro-mechanical in a 3D coupled flow-deformation and stress FE analysis, involving realistic surface moisture and suction changes by generating 3D transient flow process, simulating true time-dependent precipitation and evaporation conditions.
- 3- Using the developed model in a comprehensive parametric study that was carefully designed to produce an efficient database to develop design equations through the Artificial Intelligence method called EPR (Evolutionary Polynomial Regression).
- 4- Using the design equations from EPR along with traditional design procedure to develop a new design method for stiffened slab foundations on reactive soils, supporting light weight structures. This new design method is more realistic than available methods, since it mitigates many of the limitations and shortcomings of these methods.
- 5- Providing clear understanding of the role of sand cushion when used under stiffened slab foundations, and integrating the role of sand cushion in the design process of stiffened slab foundation using the EPR method.
- 6- Development of a computer program integrating the new design method for stiffened slab foundation on reactive soils with and without the inclusion of a sand cushion layer of a specific thickness.

6.4 RECOMMENDATIONS FOR FUTURE WORK

Despite the good performance of the new design method, there are still more enhancements that can be made as explained below:

- 1- The new design method was developed based on a parametric study that had certain conditions/limitations, and overcoming these limitations will broaden applicability of the method. For example, partition loads were converted to a uniform pressure load in the analysis, and this can be enhanced by considering a centre line load in each direction to produce more accurate results.
- 2- Using separate parameters for the edge, centre and uniform loads by adding 3 new parameters to cover a wider range of load configuration.
- 3- The new design method was developed for a highly expansive soil, by considering a moisture-swell model with 8% strain upon saturation. Future studies may use lesser strain potential, specifically with relatively low soil mound differential movement (y_m). Consequently, it may also be recommended to study the effect of varying the soil-water characteristic curve (SWCC) for different soil classes.
- 4- The new design method is developed for slab dimensions from 6.0 m to 26.0 m. It is recommended in future researches to use a wider range of the dimensions parameter.
- 5- The study on the sand cushion was carried out using a relatively high permeability corresponding to slightly silty sand. Lower values of sand permeability are recommended in future work.
- 6- The concrete strength and modulus were fixed in the study to 20 MPa and 15 GPa, respectively. Increasing these two parameters will lead to a reduction in the design equivalent thickness (T_{eq}) of the stiffened slab foundation. Therefore, higher ranges of concrete strengths and corresponding concrete modulus can be used in future studies.

7- The proposed new design method for stiffened slab foundations on reactive soils with and without sand cushion is based on pure numerical modelling. Experimental models, full scale field models, and field observations to slabs designed using the new design method is highly recommended for more validation and future development. The experimental work may also extend to produce data for the variation of the mound stiffness with the degree of saturation, as this parameter was fixed in this study to 1,000 MPa and 5,000 MPa for the edge lift and the edge drop, respectively.

REFERENCES

- ABAQUS User's Manual. (2014). Version 6.14: Moisture Swelling, Hibbit, Karlsson and Sorenson Inc., 1080 Main Street, Pawtucket, RI02860-4847, U.S.A.
- Abdelmalak, R. I. (2007). "Soil structure interaction for shrink-swell soils. new design procedure for foundation slabs on shrink-swell soils." PhD Thesis, Texas A&M University, Texas, USA.
- Adem, H. H., and Vanapalli, S. K. (2015). "Review of methods for predicting in situ volume change movement of expansive soil over time." *Journal of Rock Mechanics and Geotechnical Engineering*, 7 (1): 73-86.
- Ahangar-Asr, A., Faramarzi, A., Mottaghifard, N., and Javadi, A. A. (2011). "Modeling of permeability and compaction characteristics of soils using evolutionary polynomial regression." *Computers & Geosciences*, 37 (11): 1860-1869.
- Al-Shamrani, M. A., and Dhowian, A. W. (2002). "Experimental study of lateral restraint effects on the potential heave of expansive soils." *Engineering Geology*, 69 (1): 63-81.
- Allen, R. G., Pereira, L. S., Raes, D., and Smith, M. (1998). "Crop evapotranspiration-guidelines for computing crop water requirements." *Irrigation and Drainage*, 56 (9): D05109.
- Australian Standard AS1170.1 (2002). "Structural design actions: permanent, imposed and other actions." Standards Australia, Sydney NSW.
- Australian Standard AS2870 (1996). "Residential slabs and footings." Standard House, Sydney NSW.
- Australian Standard AS2870 (2011). "Residential slabs and footings." Standard House, Sydney NSW.
- Australian Standard AS3600 (2009). "Concrete structures." Standards Australia, Sydney, NSW.
- Berardi, L., Giustolisi, O., Kapelan, Z., and Savic, D. A. (2008). "Development of pipe deterioration models for water distribution systems using EPR." *Journal of Hydroinformatics*, 10 (2): 113-126.

- Bharadwaj, A. (2013). "Effect of soil replacement option on surface deflections for expansive clay profiles." PhD Thesis, Arizona State University, Arizona, USA.
- Biddle, P. G. (1979). "Tree root damage to buildings-an arboriculturist's experience." *Arboricultural Journal*, 3 (6): 397-412.
- Blight, G. (1965). *The time-rate of heave of structures on expansive clays*, Butterworth & Company (Australia) Limited.
- Blight, G. E. (2004). "Measuring evaporation from soil surfaces for environmental and geotechnical purposes." *Water SA*, 28 (4): 381-394.
- Blight, G. E. (2005). "Desiccation of a clay by grass, bushes and trees." *Geotechnical and Geological Engineering*, 23 (6): 697-720.
- Branson, D. E. (1963). "Instantaneous and time-dependent deflections of simple and continuous reinforced concrete beams." Alabama Highway Research Department, Bureau of Public Roads, Alabama, USA, 1-78.
- Briaud, J. L., Abdelmalak, R., Xiong, Z., and Magbo, C. (2016). "Stiffened slab-on-grade on shrink-swell soil: New design method." *Journal of Geotechnical and Geoenvironmental Engineering*, 142 (7): 04016017, doi: 10.1061/(ASCE)GT.1943-5606.0001460.
- Briaud, J. L., Abdelmalak, R., and Zhang, X. (2010). "Design of stiffened slabs-on-grade on shrink-swell soils." *Proceedings of the 5th International Conference on Unsaturated Soil*, International Center for Numerical Methods in Engineering, Barcelona, Spain.
- Building Research Advisory Board (1968). "Criteria for selection and design of residential slabs on ground." Report No. 33, Federal Housing Administration, USA.
- Cameron, D. A., and O'Malley, A. P. K. (2002). "Established street trees, soil suction and leaf water potential." *Australian Geomechanics*, 37 (1): 35-46.
- Chen, F. H. (1988). *Foundations on expansive soils*, Elsevier Science Publishing Company INC, New York.
- Clarke, D., and Smethurst, J. (2008). "Buildings on clay- the effects of geology, climate and vegetation on heave and settlement." <http://www.buildingconservation.com/articles/buildclay/buildclay.htm>.

- Crawford, C. B. (1965). "Engineering studies of Leda clay: In soils in Canada (rf legget ed.)." University of Toronto Press for the Royal Society of Canada, Special Publications, 200-217.
- Dafalla, M. A., Al-Shamrani, M. A., Puppala, A. J., and Ali, H. E. (2011). "Design guide for rigid foundation systems on expansive soils." *International Journal of Geomechanics*, 12 (5): 528-536.
- Day, R. W. (1992). "Irrigation, drainage, and landscaping for expansive soil." *Journal of Irrigation and Drainage Engineering*, 118 (2): 285-290.
- Driscoll, R. (1983). "The influence of vegetation on the swelling and shrinking of clay soils in Britain." *Geotechnique*, 33 (2): 93-105.
- El-Garhy, B. M., and Wray, W. K. (2004). "Method for calculating the edge moisture variation distance." *Journal of Geotechnical and Geoenvironmental Engineering*, 130 (9): 945-955.
- Fityus, S. G., Allman, M. A., and Smith, D. W. (1999). "Mound shapes beneath covered areas." *Proceedings of the 8th Australia New Zealand Conference on Geomechanics: Consolidating Knowledge*, Australian Geomechanics Society, Barton, ACT, 163-170.
- Fityus, S. G., Smith, D. W., and Allman, M. A. (2004). "Expansive soil test site near Newcastle." *Journal of Geotechnical and Geoenvironmental Engineering*, 130 (7): 686-695.
- Forchheimer, P. (1901). *Wasserbewegung durch boden (water movement through soil)*, Z. Ver. Deutsch. Ing. 45, Germany, 1782–1788.
- Foundation Performance Association (2005). "Homebuyers' guide for foundation evaluation." *FPA-SC-06-0*, , 2005Houston,Texas 16, <http://www.foundationperformance.org/Projects/FPA-SC-06-0.pdf>.
- Frank, V. W. (2000). Raft software - design of stiffened slabs on reactive soils- user manual
- Fraser, R. A., and Wardle, L. J. (1975). "The analysis of stiffened raft foundations on expansive soil." *Symposium on Recent Developments in the Analysis of Soil Behaviour and their Application to Geotechnical Structures*, University of New South Wales, Australia, 89-98.

- Fredlund, D. G., and Morgenstern, N. R. (1976). "Constitutive relations for volume change in unsaturated soils." *Canadian Geotechnical Journal*, 13 (3): 261-276.
- Fredlund, D. G., and Rahardjo, H. (1993). "An overview of unsaturated soil behaviour." *Proceedings of the American Society of Civil Engineers , Geotechnical Special Publication on Unsaturated Soil Properties*, Dallas, Texas, USA, 1-31.
- Fredlund, D. G., and Rahardjo, H. (1993). *Soil mechanics for unsaturated soils*, John Wiley & Sons, New York, USA.
- Fredlund, D. G., and Xing, A. (1994). "Equations for the soil-water characteristic curve." *Canadian Geotechnical Journal*, 31 (4): 521-532.
- Fredlund, M. D., Stianson, J. R., Fredlund, D. G., Vu, H., and Thode, R. C. (2006). "Numerical modeling of slab-on-grade foundations." *Proceedings of the 4th International Conference on Unsaturated Soils*, Arizona, USA, 2121-2132.
- Gay, D. A. (1993). "Development of a predictive model for pavement roughness on shrink-swell clay." PhD Thesis, Department of Civil Engineering, A&M University, Texas, USA.
- Giustolisi, O., Doglioni, A., Savic, D. A., and Webb, B. W. (2007). "A multi-model approach to analysis of environmental phenomena." *Environmental Modelling and Software*, 22 (5): 674-682.
- Giustolisi, O., and Savic, D. A. (2006). "A symbolic data-driven technique based on evolutionary polynomial regression." *Journal of Hydroinformatics*, 8 (3): 207-222.
- Goldberg, D. E. (1989). *Genetic algorithms in search optimization and machine learning*, Addison-Wesley, Reading, MA.
- Goldfinch, J. C. (1995). "Relationship between Soil Movement, Buildings and Trees." *Trees in the Urban Environment Seminar, Royal Australian*, Institute of Parks and Recreation, Adelaide, Australia, 1-18.
- Hangge, E. E., Hardiyatmo, H. C., Adi, A. D., and Rifa'i, A. (2015). "Influence of swell on stress-strain behaviour of expansive soils under confining pressure." *International Organization of Scientific research, Journal of Engineering*, 05 (06): 48-54.

- Hazen, A. (1892). "Some physical properties of sands and gravels: with special reference to their use in filtration." Publication document No. 34, 539–556, Massachusetts State Board of Health.
- Hazen, A. (1911). "Discussion of dams on sand foundations by AC Koenig." *Transactions of the American Society of Civil Engineers*, 73: 199–203.
- Holland, J. E. (1981). "The design, performance and repair of housing foundations." Swinburne College Press, Melbourne, Australia.
- Holland, J. E., Cimino, D. J., Lawrance, C. E., and Pitt, W. G. (1980). "The behaviour and design of housing slabs on expansive clays." *Proceedings of the 4th International Conference on Expansive Soils*, Denver, Colorado, USA 448-468.
- Holland, J. E., and Richards, J. (1984). "The practical design of foundations for light structures on expansive clays." *Fifth International Conference on Expansive Soils 1984: Preprints of Papers*, Institution of Engineers, Australia, 154.
- Holtz, W. G. (1983). "The influence of vegetation on the swelling and shrinking of clays in the United States of America." *Géotechnique*, 33 (2): 159-163.
- Ishibashi, I., and Hazarika, H. (2011). *Soil mechanics fundamentals*, CRC Press Taylor & Francis Group, USA.
- Jackson, J. D. (1980). "Field study of the performance of slab-on-ground under Australian conditions." Master of Engineering Thesis, Swinburne Institute of Technology, Melbourne, Australia.
- Jaksa, M. B., Kaggwa, W. S., Woodburn, J. A., and Sinclair, R. (2002). "Influence of large Gum trees on the soil suction profile in expansive soils." *Australian Geomechanics*, 1 (37): 23-33.
- Kay, J. N., and Mitchell, P. W. (1990). "Stiffened raft design for houses using a probabilistic format." *Australian Civil Engineering Transactions, Institution of Engineers Australia*, CE32 (3): 144-150.
- Kenneth, D. W., Colby, C. A., Houston, W. N., and Houston, S. L. (2009). "Method for evaluation of depth of wetting in residential areas." *Journal of Geotechnical and Geoenvironmental Engineering*, 135 (2): 169-176.
- Kodikara, J. K., and Choi, X. (2006). "A simplified analytical model for desiccation cracking of clay layers in laboratory tests." *Proceedings of the 4th International*

- Conference on Unsaturated Soils*, American Society of Civil Engineers (ASCE), Carefree, Arizona, 2558-2569.
- Koza, J. R. (1992). "On the programming of computers by natural selection." The MIT Press, Cambridge MA.
- Krohn, J. P., and Slosson, J. E. (1980). "Assessment of expansive soils in the United States." *Proceedings of the 4th International Conference on Expansive Soils*, ASCE, Denver, Colorado, USA, 596-608.
- Laucelli, D., Berardi, L., and Doglioni, A. (2009). Evolutionary polynomial regression EPR Version 2. SA.
- Li, J. (1995). "Finite element analysis of deep beams in expansive clays." *1st International Conference on Unsaturated Soils*, Paris, France 1109-1115.
- Li, J. (1996). "Analysis and modelling of performance of footings on expansive soils." PhD Thesis, Civil Engineering, University of South Australia, Australia.
- Li, J. (2006). "Two dimensional simulation of a stiffened slab on expansive soil subject to a leaking underground water pipe." *4th International Conference on Unsaturated Soils. Geotechnical Special Publication No. 147*, Carefree, Arizona, USA, 2098-2109.
- Li, J., Cameron, D. A., and Ren, G. (2014). "Case study and back analysis of a residential building damaged by expansive soils." *Computers and Geotechnics*, 56: 89-99, <http://dx.doi.org/10.1016/j.compgeo.2013.11.005>.
- Li, J., Cameron, D. A., and Symons, M. G. (1992). "Three-dimensional analysis of stiffened slabs on expansive soils ", *Proceeding of International Conference on Computational Methods in Engineering*, Singapore, 119-204.
- Livneh, M., Shklarsky, E., and Uzan, J. (1973). "Cracking of flexible pavements based on swelling clay: Preliminary theoretical analysis." *Proceedings of the 3rd International Conference on Expansive Soils*, Haifa, Israel, 257-266.
- Lytton, R. L. (1970). "Analysis for design of foundations on expansive clay." *Proceedings of the Symposium of Soils & Earth Structures in Arid Climates*, Australian Geotechnical Society & Institute of Engineers Australia, Adelaide, Australia, 29-37.

- Lytton, R. L. (1970). "Design criteria for residential slabs and grillage rafts on reactive clay." *CSIRO Report, Division of Applied Geomechanics*, Melbourne, Australia.
- Lytton, R. L. (1970a). "Analysis for design of foundations on expansive clay." *Proceedings of the Symposium of Soils & Earth Structures in Arid Climates*, Australian Geomechanics & Institution of Engineers Australia, Adelaide, Australia, 29-37.
- Lytton, R. L. (1971). "Risk design of stiffened mats on clay." *Proceedings of the 1st International Conference on Applications of Statistic and Probability to Soil and Structural Engineering*, Hong Kong, 154-171.
- Lytton, R. L. (1972). "Design methods for concrete mats on unstable soils." *Proceedings of the 3rd International -American Conference on Materials Technology*, Rio de Janeiro, Brazil, 171-177.
- Lytton, R. L. (1977). *Foundations in expansive soils, in numerical methods in geotechnical engineering*, McGraw-Hill Book Company, New York, 783.
- Lytton, R. L., and Meyer, K. T. (1971). "Stiffened mats on expansive clay." *Journal of the Soil Mechanics and Foundations Division*, 97 (7): 999-1019.
- Lytton, R. L., and Woodburn, J. A. (1973). "Design and performance of mat foundations on expansive clay." *Proceedings of the 3rd International Conference on Expansive Soils*, Haifa, Israel, 301-307.
- Magbo, C. (2014). "Design method for stiffened slab on grade placed on shrink-swell soils and subjected to uniform pressure and line loads." Master's Thesis, Zachry Dept. of Civil Engineering, A&M University, Texas, USA.
- Masia, M. J., Totoev, Y. Z., and Kleeman, P. W. (2004). "Modeling expansive soil movements beneath structures." *Journal of Geotechnical and Geoenvironmental Engineering*, 130 (6): 572-579.
- McInnes, D. B. (1986). "Drying effect of different verge planted tree species on urban roads." *13th Australian Road Research Board (ARBB) and 5th Road Engineering Association of Asia and Australasia (REAAA) Comb. Conference Proceedings*, 54-66.
- McKeen, R. G., and Johnson, L. D. (1990). "Climate-controlled soil design parameters for mat foundations." *Journal of Geotechnical Engineering*, 116 (7): 1073-1094.

- McManus, K., and Brown, R. I. (1999). "The performance of light structures founded in expansive clays following active moisture recharge." *Proceedings of the 8th Australia New Zealand Conference on Geomechanics: Consolidating Knowledge*, Australian Geomechanics Society, Hobart, Tasmania, Australia, 201-205.
- Mitchell, J. K., Hooper, D. R., and Campanella, R. G. (1965). "Permeability of compacted clay." *Journal of Soil Mechanics & Foundations Division*, SM4 (91): 41-65.
- Mitchell, P. W. (1980). Slab-on-grade (SLOG) user manual-Residential slab and footing design program, Adelaide, Australia.
- Mitchell, P. W. (1980). "The structural analysis of footings on expansive soil." *Proceedings of the 4th International Conference on Expansive Soils*, Denver, Colorado, USA, 438-447.
- Mitchell, P. W. (1984). "The design of shallow footings on expansive soil." PhD Thesis, Civil Engineering Department, University of Adelaide, Australia.
- Mitchell, P. W. (1990). "Design of footings on expansive soil considering two-way action." *Seminar on Computing in Geomechanics: Seminar Papers*, Australian Geomechanics Society, 48.
- Mitchell, P. W. (2008). "Footing design for residential type structures in arid climates." *Australian Geomechanics.*, 43 (4): 51-68.
- Moussa, A. A., Abd-El-Meguid, M. A., Okdah, S. M., and Heikal, A. H. (1985). "Effect of sand cushion on swelling and swelling pressure of expansive silty clay." *Proceedings of the 11th International Conference on Soil Mechanics and Foundation Engineering* Balkema (AA), San Fransisco, USA, 1023-1026.
- Nelson, J. D., and Miller, D. J. (1992). *Expansive soils: problems and practice in foundation and pavement engineering*, John Wiley & Sons, New York.
- Nelson, J. D., Overton, D. D., and Durkee, D. B. (2001). "Depth of wetting and the active zone." *Expansive Clay Soils and Vegetative Influence on Shallow Foundations*, Geo-Institute Shallow Foundation and Soil Properties Committee Sessions, Reston, Virginia, 95-109.
- Nuhfer, E. B. (1994). "What's a geologic hazard?" *Geotimes*, 39 (7): 4.
- Overton, D. D., Chao, K.-C., and Nelson, J. D. (2006). "Time rate of heave prediction for expansive soils." *Proceedings of the ASCE Conference GeoCongress*, 162-168.

- Pidgeon, J. T. (1980). "The interaction of expansive soil and a stiffened raft foundation." *Proceedings of the 7th Regional Conference for Africa on Soil Mechanics and Foundation Engineering*, Ghana, 811-822.
- Pidgeon, J. T. (1983). *The design of stiffened raft foundation on expansive soils, ground profiles, no. 33*, Council of Scientific & Industrial Research (CSIR), 4-23.
- Pile, K. C. (1984). "The deformation of structures on reactive clay soils." *5th International Conference on Expansive Soils*, Institution of Engineers Australia, Barton, ACT, 292-299.
- Pitt, W. G. (1982). "Correlation between the real behaviour and the theoretical design of residential raft slabs." Master of Engineering Thesis, Swinburne Institute of Technology, Melbourne, Australia.
- Post-Tensioning Institute (PTI). (1980). "Design and Construction of Post-Tensioned Slab-on-Ground, 1st Edition." Phoenix, AZ, USA.
- Post Tensioning Institute (1996). "Design and construction of post-tensioned slabs-on-ground." 2nd Edition Phoenix, AZ, USA.
- Post Tensioning Institute (2004). "Design and construction of post-tensioned slab-on-ground." 3rd Edition Phoenix, AZ, USA.
- Poulos, H. G. (1983). "Analysis of strip footings on expansive soils." Report No. R459, School of Civil and Mining Engineering, University of Sydney, Australia.
- Poulos, H. G. (1984). "Parametric solutions for strip footings on swelling and shrinking soils." *5th International Conference on Expansive Soils 1984: Preprints of Papers*, Institution of Engineers, Australia, Adelaide, Australia, 149-153.
- Pulat, H. F., Yukselen-Aksoy, Y., and Egeli, I. (2014). "The effect of soil mineralogy and pore fluid chemistry on the suction and swelling behavior of soils." *Bulletin of Engineering Geology and the Environment*, 73 (1): 37-42.
- Puppala, A. J., Manosuthikij, T., and Chittoori, B. C. (2013). "Swell and shrinkage characterizations of unsaturated expansive clays from Texas." *Engineering Geology*, 164: 187-194.
- Rao, M. R., Rao, A. S., and Babu, R. D. (2008). "Efficacy of cement-stabilized fly ash cushion in arresting heave of expansive soils." *Geotechnical and Geological Engineering*, 26 (2): 189-197.

- Reins, J. D., and Volz, J. J. (2013). "Monitoring and mitigation of movements affecting foundations on expansive soils in Colorado." *Journal of Performance of Constructed Facilities*, 27 (6): 731-736.
- Richards, B. G. (1967). "Moisture flow and equilibria in unsaturated soils for shallow foundations-Special technical publication no. 417." *Symposium on Permeability and Capillarity of Soils*, ASTM International, Philadelphia, USA, 4-34.
- Richards, B. G. (1979). "A method of analysis of the effects of volume change in unsaturated expansive clays on engineering structures." *Australian Geomechanics Journal*, G9: 27-41.
- Richards, B. G., and Gordon, R. (1972). "Prediction and observation of the performance of a flexible pavement on expansive clay subgrade." *3rd International Conference on the Structural Design of Asphalt Pavements*, Grosvenor House, Park Lane, , London, England, 11-15.
- Richards, B. G., Peter, P., and Emerson, W. W. (1983). "The effects of vegetation on the swelling and shrinking of soils in Australia." *Geotechnique*, 33 (2): 127-139.
- Robert, L., Andrew, B., and Mary, L. C. (1984). "Soils shrink, trees drink, and houses crack." *ECOS Magazine*, The Science Communication Unit of CSIRO's Bureau of Scientific Services, 13-15.
- Savic, D. A., Giustolisi, O., Berardi, L., Shepherd, W., Djordjevic, S., and Saul, A. (2006). "Modelling sewer failure by evolutionary computing." *Proceedings of the Institution of Civil Engineers-Water Management*, Thomas Telford Ltd, 111-118.
- Shahin, M. A. (2010). "Intelligent computing for modelling axial capacity of pile foundations." *Canadian Geotechnical Journal*, 47 (2): 230-243.
- Shahin, M. A. (2013). "Artificial intelligence in geotechnical engineering: applications, modeling aspects, and future directions." *Metaheuristics in water, geotechnical and transport engineering*, Elsevier, 169-204.
- Shahin, M. A. (2014). "Load-settlement modelling of axially loaded drilled shafts using CPT-based recurrent neural networks." *International Journal of Geomechanics*, 14 (6): Article Number 06014012.

- Shahin, M. A. (2015). "Use of evolutionary computing for modelling some complex problems in geotechnical engineering." *Geomechanics & Geoengineering: An International Journal*, 10 (2): 109-125.
- Shahin, M. A., and Elchalakani, M. F. (2014). "A new model based on evolutionary computing for predicting ultimate pure bending of steel circular tubes." *Journal of Constructional Steel Research*, 94: 84-90.
- Shahin, M. A., and Jaksa, M. B. (2006). "Pullout capacity of small ground anchors by direct cone penetration test methods and neural networks." *Canadian Geotechnical Journal*, 43 (6): 626-637.
- Shahin, M. A., Maier, H. R., and Jaksa, M. B. (2002). "Predicting settlement of shallow foundations using neural networks." *Journal of Geotechnical and Geoenvironmental Engineering*, 128 (9): 785-793.
- Sinha, J., and Poulos, H. G. (1996). "Behaviour of stiffened raft foundations.", 7th *Australia New Zealand Conference on Geomechanics: Geomechanics in a Changing World*, Institution of Engineers, Australia, Barton, ACT, 704-709.
- Soil Vision Systems Ltd. (2001). SVFLUX Users Manual, Saskatoon, Sask, Canada.
- Soil Vision Systems Ltd. (2002). SVSOLID Users Manual, Saskatoon, Sask, Canada.
- Subba Rao, K. (2000). "Swell–shrink behaviour of expansive soils—geotechnical challenges." *Indian Geotechnical Journal*, 30 (1): 1-68.
- Sudjianto, A. T., Suryolelono, K. B., and Mochtar, I. B. (2011). "The effect of water content change and variation suction in behavior swelling of expansive soil." *International Journal of Civil & Environmental Engineering*, 11 (3): 11-17.
- Thakur, V. K., and Singh, D. N. (2005). "Rapid determination of swelling pressure of clay minerals." *Journal of Testing and Evaluation*, 33 (4): 239-245.
- Tripathy, S., Rao, K. S., and Fredlund, D. G. (2002). "Water content-void ratio swell-shrink paths of compacted expansive soils." *Canadian Geotechnical Journal*, 39 (4): 938-959.
- Vanapafli, S. K., Fredlund, D. G., and Pufahl, D. E. (1999). "The influence of soil structure and stress history on the soil-water characteristics of a compacted till." *Geotechnique*, 49 (2): 143-159.

- Varghese, P. C. (2012). *Foundation engineering*, PHI Learning Pvt. Ltd., New Delhi, India.
- W.K, W. (1978). "Development of a design procedure for residential and light commercial slab-on-ground constructed over expansive Soils." PhD Thesis, A&M University, Texas, USA.
- Wallace, K. B., and Lytton, R. L. (1992). "Lateral pressure and swelling in a cracked expansive clay profiles." *Proceedings of the 7th International Conference on Expansive Soils*, Dallas, Texas, 245-250.
- Walsh, P. F. (1974). "The design of residential slab on ground." Technical Report No. 5, Commonwealth Scientific and Industrial Research Organization (CSIRO) Division of Building Research, Melbourne, Australia.
- Walsh, P. F. (1978). "The analysis of stiffened rafts on expansive clays." Technical report No. 23, Commonwealth Scientific and Industrial Research Organization, CSIRO, Division of Building Research, Melbourne, Australia.
- Walsh, P. F. (1978a). *Concrete slabs for houses. Technical Report No. 25*, Commonwealth Scientific and Industrial Research Organization, CSIRO, Division of Building Research, Melbourne, Australia.
- Walsh, P. F. (1984). "Concrete slabs for houses." Technical Report No. 48, Commonwealth Scientific and Industrial Research Organization, (CSIRO), Division of Building Research, Melbourne, Australia.
- Walsh, P. F., and Walsh, S. F. (1986). "Structure/reactive clay model for a microcomputer." Report No. 86/9, CSIRO, Australia.
- Williams, P. J. (1982). *The surface of the Earth: An introduction to geotechnical science*, Longman Inc., New-York.
- Wire Reinforcement Institute (1981). "Design of slab-on-ground foundations." Wire Reinforcement Institution, Findlay, Ohio, USA.
- Wire Reinforcement Institute (1996). "Design of slab-on-ground foundations." Wire Reinforcement Institution, Findlay, Ohio, USA.
- Wray, W. K. (1978). "Development of a design procedure for residential and light commercial slabs-on-ground constructed over expansive soils " PhD Thesis, Texas A&M University, Texas, USA.

- Wray, W. K. (1980). "Analysis of stiffened slabs-on-ground over expansive soil." *Proceedings of the 4th International Conference on Expansive soils*, Denver, Colorado, USA, 558-581.
- Wray, W. K. (1990). "Mitigation of damage to structures supported on expansive soils." Report No. Eke-8320493, US Department of Commerce, National Technical Information Service, Washington, D. C.
- Wray, W. K. (1995). *So your home is built on expansive soils: a discussion of how expansive soils affect buildings*, American Society of Civil Engineers, Virginia, USA.
- Wray, W. K. (1997). "Using soil suction to estimate differential soil shrink or heave." *Proceedings of Unsaturated Soil Engineering Practice, Geotechnical Special Publication No. 68*, Reston, VA, 66-87.
- Wray, W. K., El-Garhy, B. M., and Youssef, A. A. (2005). "Three-dimensional model for moisture and volume changes prediction in expansive soils." *Journal of Geotechnical and Geoenvironmental Engineering*, 131 (3): 311-324.
- Zhang, X., and Briaud, J. L. (2015). "Three dimensional numerical simulation of residential building on shrink–swell soils in response to climatic conditions." *International Journal for Numerical and Analytical Methods in Geomechanics*, 39 (13): 1369-1409.

Every reasonable effort has been made to acknowledge the owners of copyright material. I would be pleased to hear from any copyright owner who has been omitted or incorrectly acknowledged.

APPENDICES

APPENDIX A: USER-DEFINED SUBROUTINE USDFLD

```
SUBROUTINE USDFLD(FIELD,STATEV,PNEWDT,DIRECT,T,CELENT,  
1 TIME,DTIME,CMNAME,ORNAME,NFIELD,NSTATV,NOEL,NPT,LAYER,  
2 KSPT,KSTEP,KINC,NDI,NSHR,COORD,JMAC,JMATYP,MATLAYO,  
3 LACCFLA)
```

C

```
INCLUDE 'ABA_PARAM.INC'
```

C

```
CHARACTER*80 CMNAME,ORNAME
```

```
CHARACTER*3 FLGRAY(15)
```

```
DIMENSION FIELD(NFIELD),STATEV(NSTATV),DIRECT(3,3),
```

```
1 T(3,3),TIME(2)
```

```
DIMENSION ARRAY(15),JARRAY(15),JMAC(*),JMATYP(*),
```

```
1 COORD(*)
```

C

```
CALL GETVRM('Por',ARRAY,JARRAY,FLGRAY,JRCD,JMAC,JMATYP,
```

```
1 MATLAYO,LACCFLA)
```

```
Por = ARRAY(1)
```

C Use the pore pressure as a field variable

```
FIELD(1) = ARRAY(1)
```

C Store the Pore Pressure as a solution dependent state

C variable

```
STATEV(1) = FIELD(1)
```

```
RETURN
```

```
END
```

Keyword File for Soil Modulus-Suction Dependency

** MATERIALS

*Material, name=Swelling-soil

*Elastic, dependencies=1

5e+07., 0.3, ,-3900000

4e+07.,0.3, ,-1600000

3e+07., 0.3, ,-650000

2e+07., 0.3, ,-250000

*USER DEFINED FIELD

*DEPVAR

1

APPENDIX B: DESIGN CHARTS OF THE NEW DESIGN METHOD

Slab foundation main span, L (m)	6.00
Edge drop scenario	ED
Span to deflection ratio (L_d/Δ_{all})	300
Service Loads:	
Internal wall loads (kPa)	2.6
Roof: 0.80 mm steel sheet (kPa)	0.1
10 mm Plasterboard (kPa)	0.083
12 mm hardwood lining	0.126
Insulation, wiring, fittings (kPa)	0.058
Flooring (13 mm clay tiling)	0.27
Permanent live load (kPa)	1.25
Total uniform load* (kPa)	4.50
Edge wall line load (kN/m)	6.00
*Without the self-weight of slab foundation	

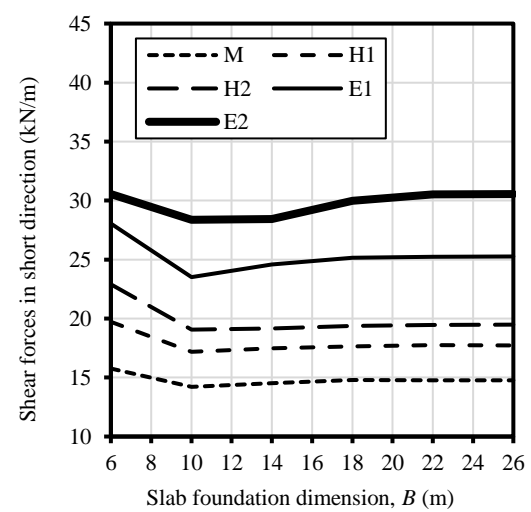
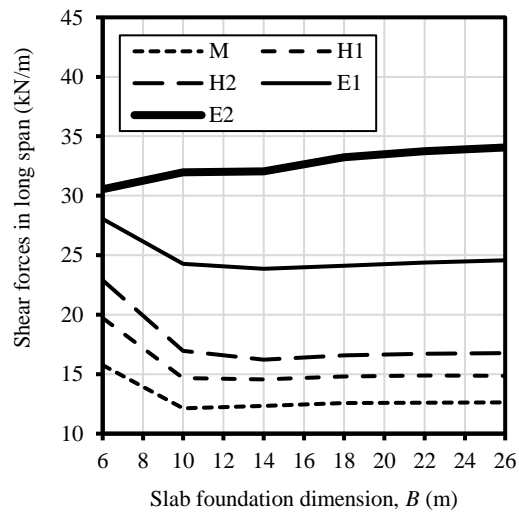
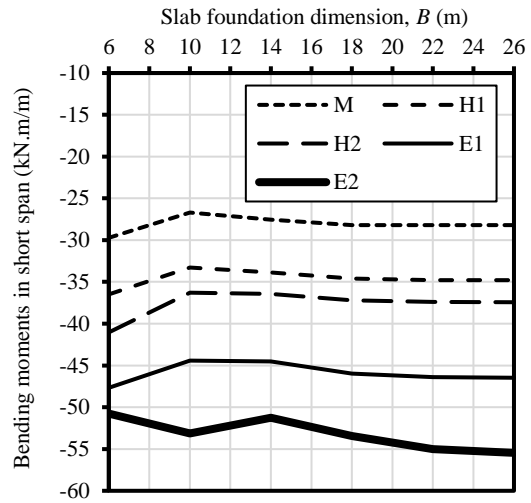
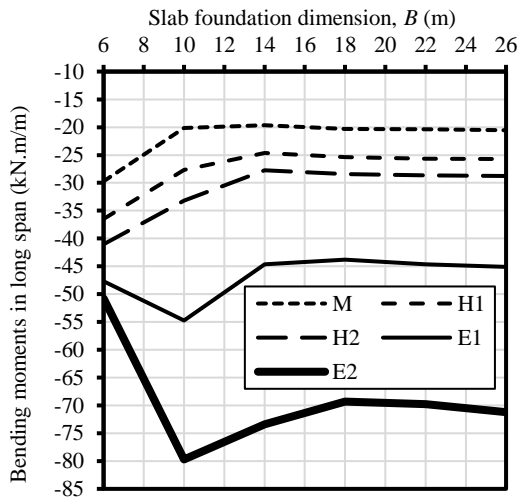
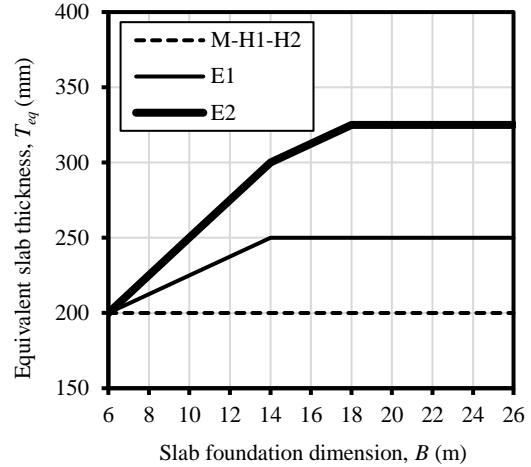


Figure B-1: $L = 6$ m, edge drop and $L_d/\Delta_{all} = 300$.

Slab foundation main span, L (m)	6.00
Edge drop scenario	ED
Span to deflection ratio (L_d/Δ_{all})	400
Service Loads:	
Internal wall loads (kPa)	2.6
Roof: 0.80 mm steel sheet (kPa)	0.1
10 mm Plasterboard (kPa)	0.083
12 mm hardwood lining	0.126
Insulation, wiring, fittings (kPa)	0.058
Flooring (13 mm clay tiling)	0.27
Permanent live load (kPa)	1.25
Total uniform load* (kPa)	4.50
Edge wall line load (kN/m)	6.00
*Without the self-weight of slab foundation	

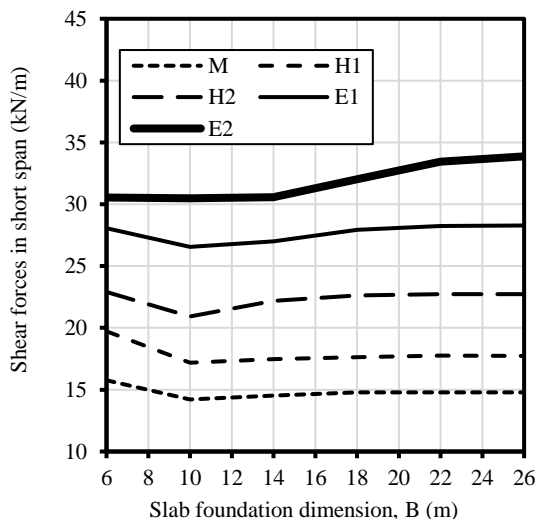
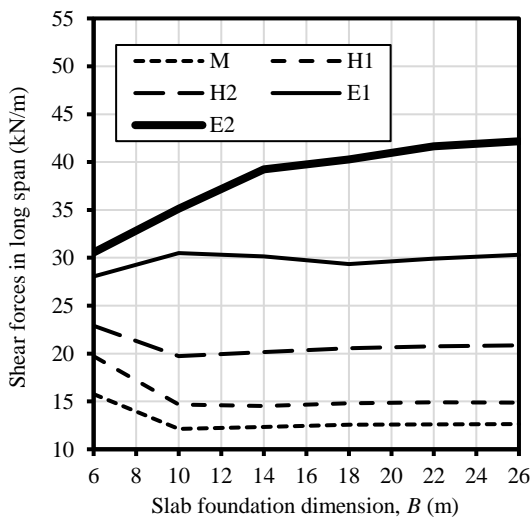
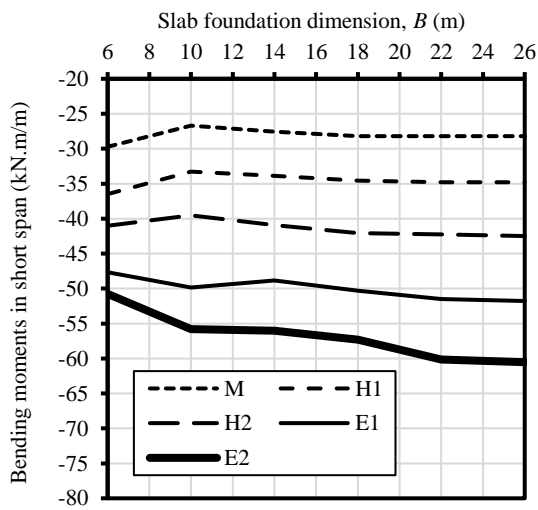
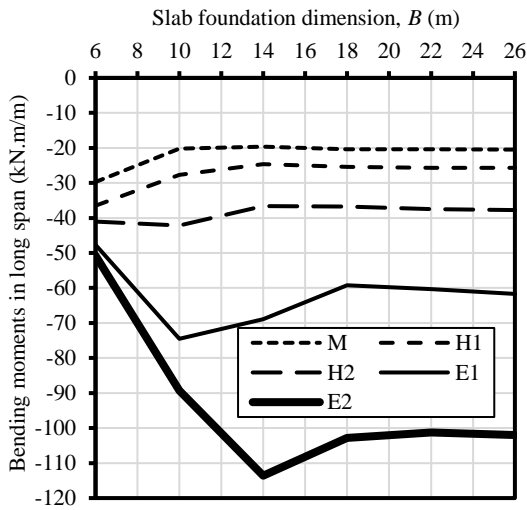
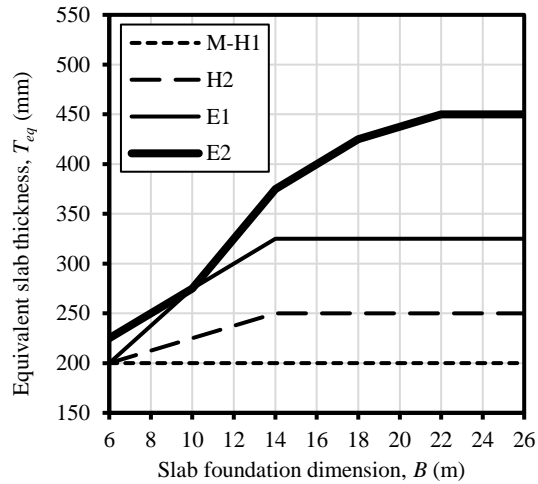


Figure B-2: $L = 6$ m, edge drop and $L_d/\Delta_{all} = 400$.

Slab foundation main span, L (m)	6.00
Edge drop scenario	ED
Span to deflection ratio (L_d/Δ_{all})	600
Service Loads:	
Internal wall loads (kPa)	2.6
Roof: 0.80 mm steel sheet (kPa)	0.1
10 mm Plasterboard (kPa)	0.083
12 mm hardwood lining	0.126
Insulation, wiring, fittings (kPa)	0.058
Flooring (13 mm clay tiling)	0.27
Permanent live load (kPa)	1.25
Total uniform load* (kPa)	4.50
Edge wall line load (kN/m)	6.00
*Without the self-weight of slab foundation	

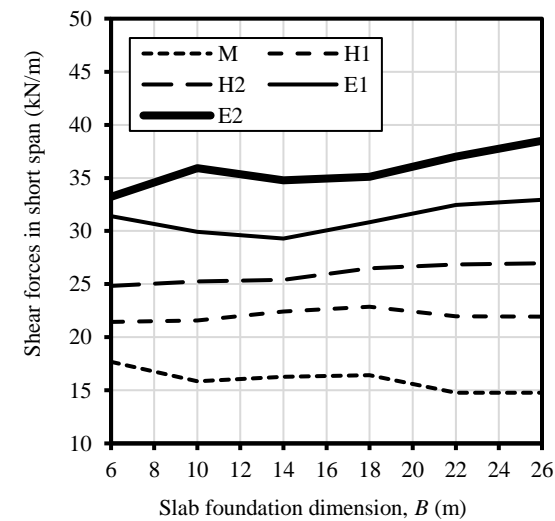
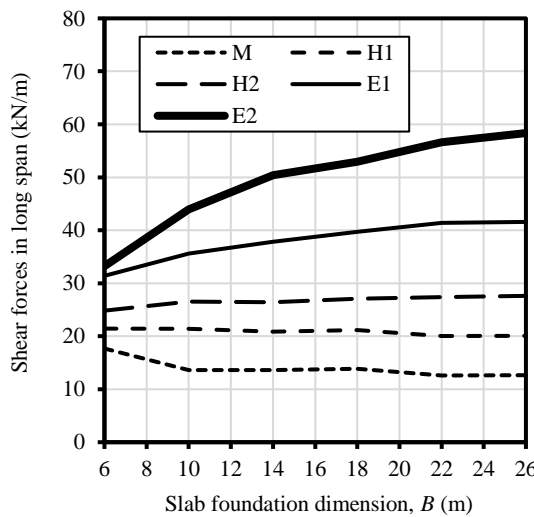
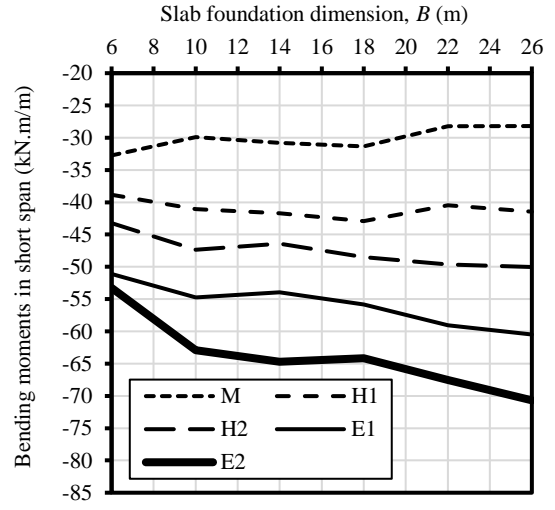
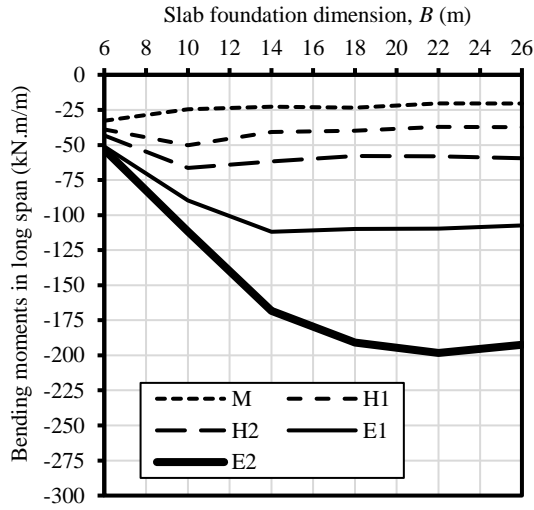
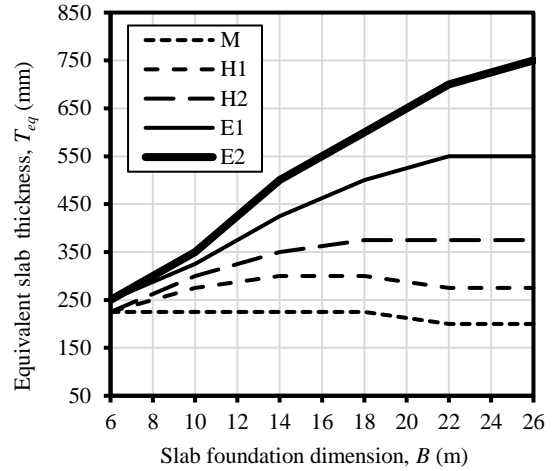


Figure B-3: $L = 6$ m, edge drop and $L_d/\Delta_{all} = 600$.

Slab foundation main span, L (m)	6.00
Edge drop scenario	ED
Span to deflection ratio (L_d/Δ_{all})	800
Service Loads:	
Internal wall loads (kPa)	2.6
Roof: 0.80 mm steel sheet (kPa)	0.1
10 mm Plasterboard (kPa)	0.083
12 mm hardwood lining	0.126
Insulation, wiring, fittings (kPa)	0.058
Flooring (13 mm clay tiling)	0.27
Permanent live load (kPa)	1.25
Total uniform load* (kPa)	4.50
Edge wall line load (kN/m)	6.00
*Without the self-weight of slab foundation	

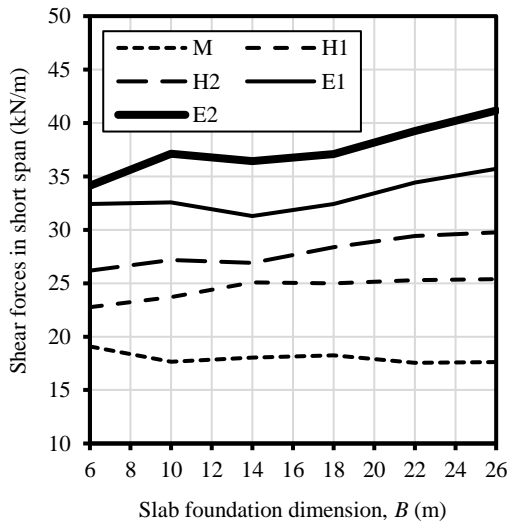
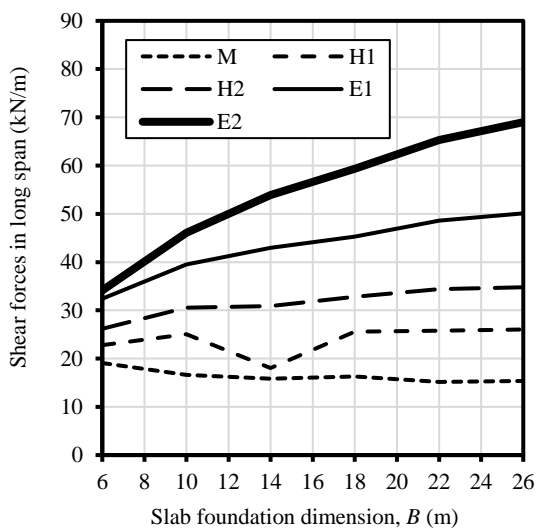
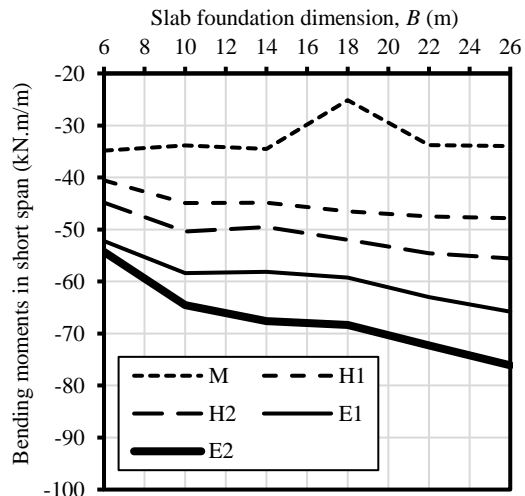
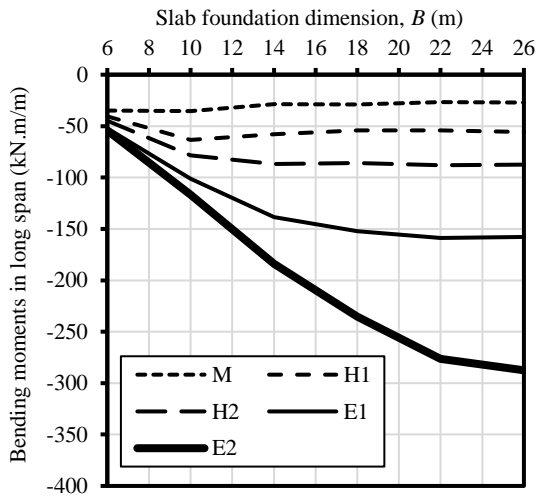
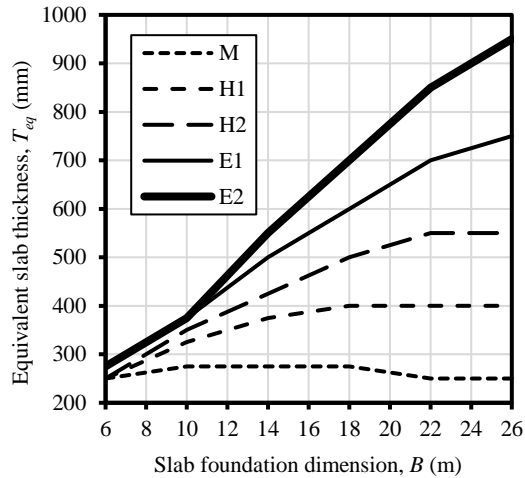


Figure B-4: $L = 6$ m, edge drop and $L_d/\Delta_{all} = 800$.

Slab foundation main span, L (m)	6.00
Edge lift scenario	EL
Span to deflection ratio (L_d/Δ_{all})	300
Service Loads:	
Internal wall loads (kPa)	2.6
Roof: 0.80 mm steel sheet (kPa)	0.1
10 mm Plasterboard (kPa)	0.083
12 mm hardwood lining	0.126
Insulation, wiring, fittings (kPa)	0.058
Flooring (13 mm clay tiling)	0.27
Permanent live load (kPa)	1.25
Total uniform load* (kPa)	4.50
Edge wall line load (kN/m)	6.00
*Without the self-weight of slab foundation	

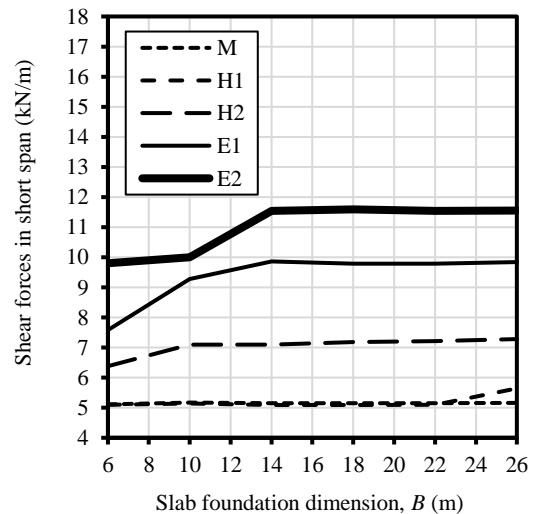
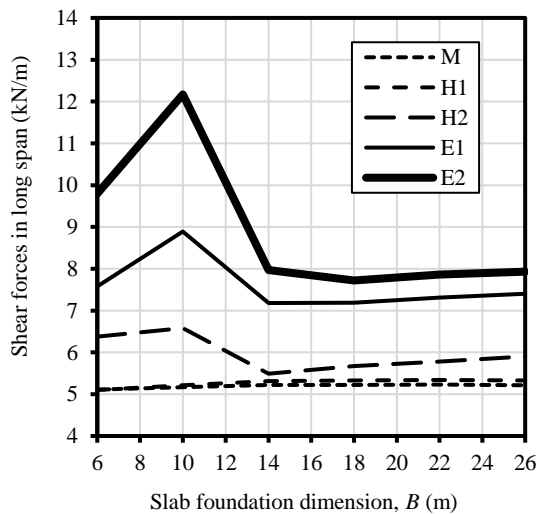
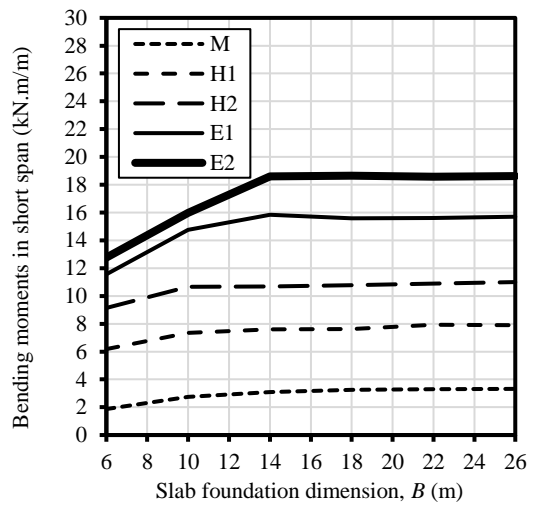
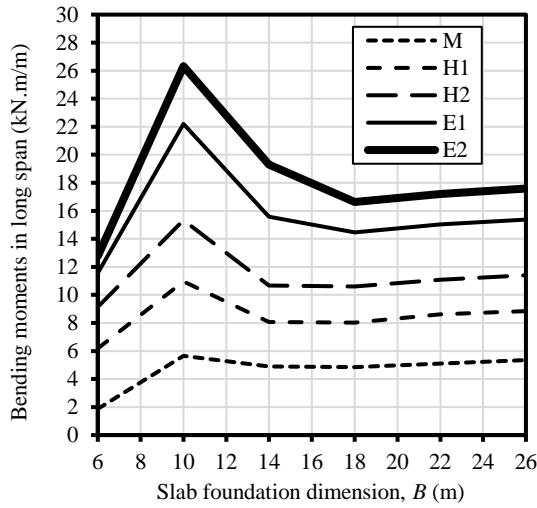
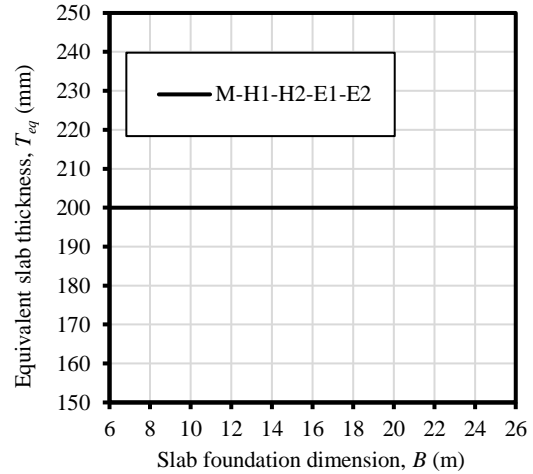


Figure B-5: $L = 6$ m, edge lift and $L_d/\Delta_{all} = 300$.

Slab foundation main span, L (m)	6.00
Edge lift scenario	EL
Span to deflection ratio (L_d/Δ_{all})	400
Service Loads:	
Internal wall loads (kPa)	2.6
Roof: 0.80 mm steel sheet (kPa)	0.1
10 mm Plasterboard (kPa)	0.083
12 mm hardwood lining	0.126
Insulation, wiring, fittings (kPa)	0.058
Flooring (13 mm clay tiling)	0.27
Permanent live load (kPa)	1.25
Total uniform load* (kPa)	4.50
Edge wall line load (kN/m)	6.00
*Without the self-weight of slab foundation	

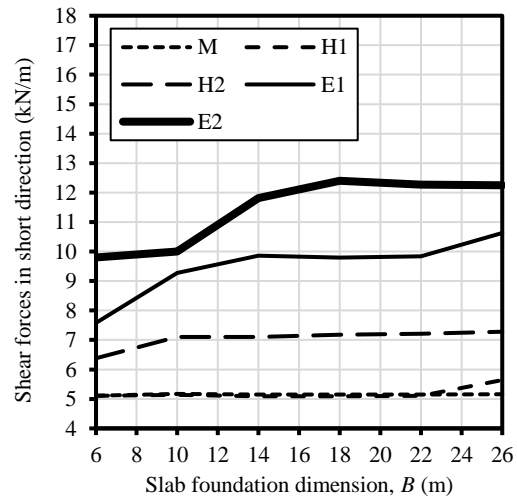
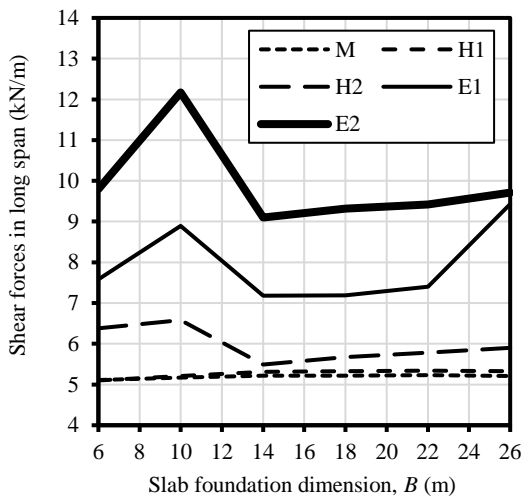
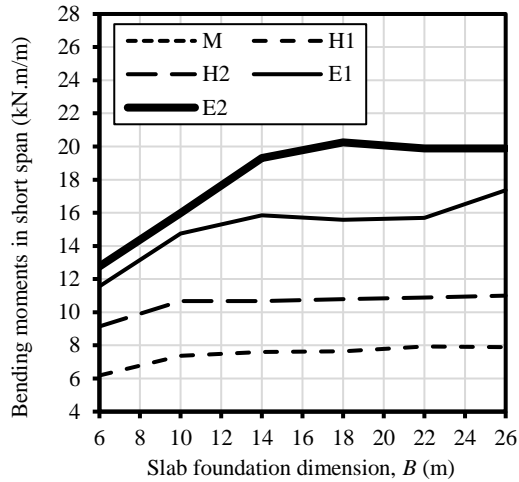
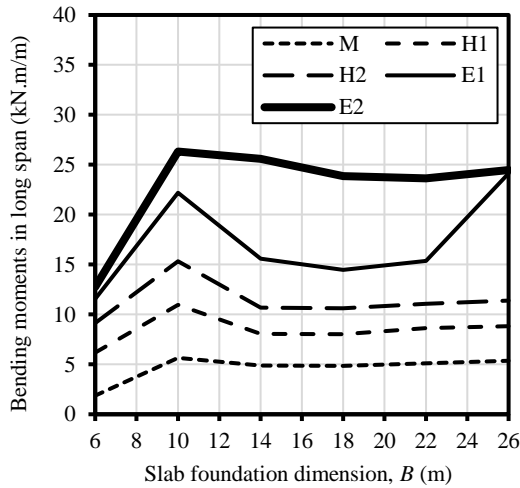
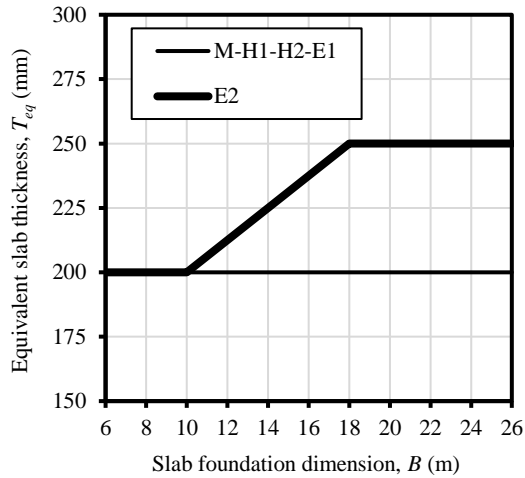


Figure B-6: $L = 6$ m, edge lift and $L_d/\Delta_{all} = 400$.

Slab foundation main span, L (m)	6.00
Edge lift scenario	EL
Span to deflection ratio (L_d/Δ_{all})	600
Service Loads:	
Internal wall loads (kPa)	2.6
Roof: 0.80 mm steel sheet (kPa)	0.1
10 mm Plasterboard (kPa)	0.083
12 mm hardwood lining	0.126
Insulation, wiring, fittings (kPa)	0.058
Flooring (13 mm clay tiling)	0.27
Permanent live load (kPa)	1.25
Total uniform load* (kPa)	4.50
Edge wall line load (kN/m)	6.00
*Without the self-weight of slab foundation	

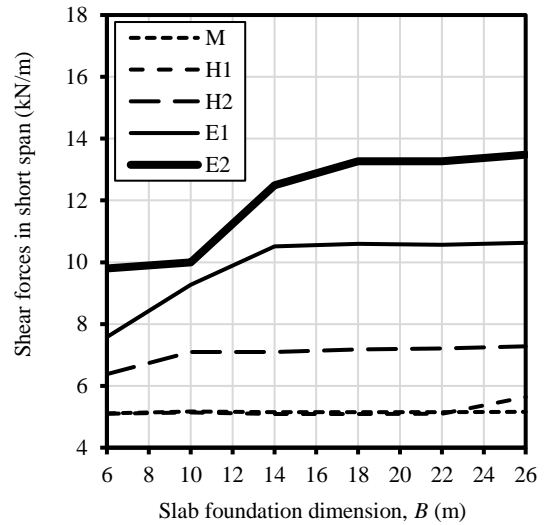
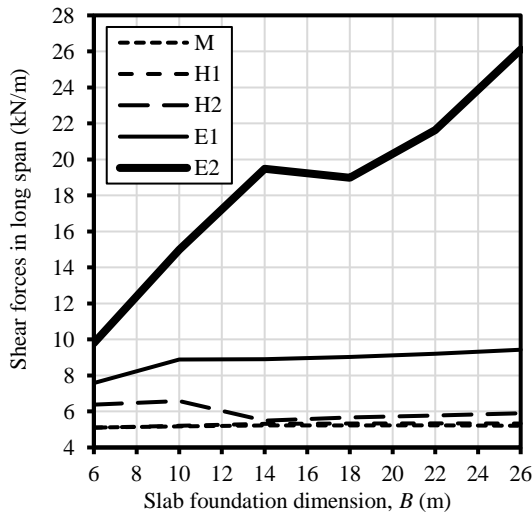
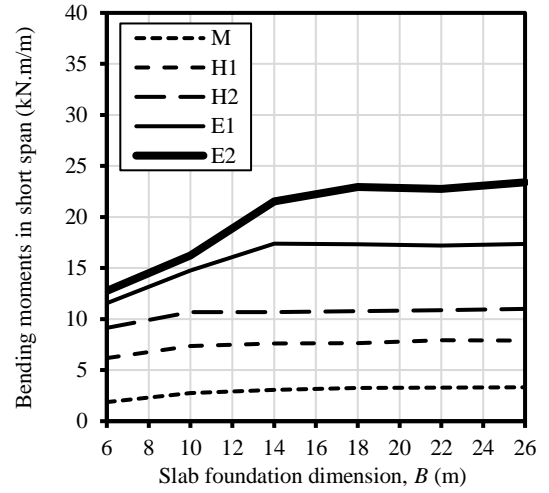
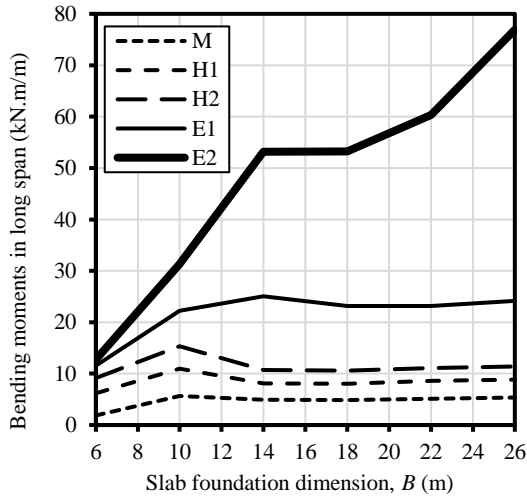
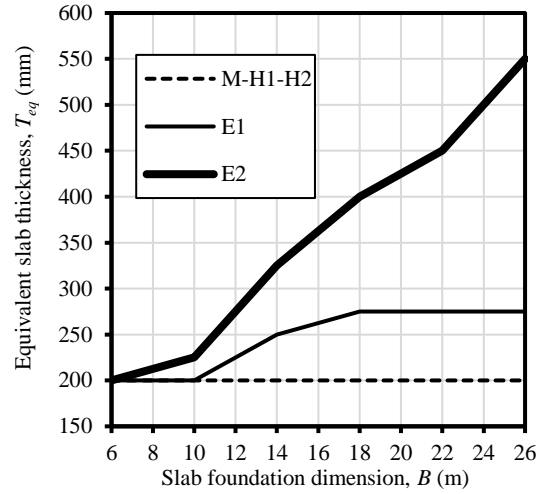


Figure B-7: $L = 6$ m, edge lift and $L_d/\Delta_{all} = 600$.

Slab foundation main span, L (m)	6.00
Edge lift scenario	EL
Span to deflection ratio (L_d/Δ_{all})	800
Service Loads:	
Internal wall loads (kPa)	2.6
Roof: 0.80 mm steel sheet (kPa)	0.1
10 mm Plasterboard (kPa)	0.083
12 mm hardwood lining	0.126
Insulation, wiring, fittings (kPa)	0.058
Flooring (13 mm clay tiling)	0.27
Permanent live load (kPa)	1.25
Total uniform load* (kPa)	4.50
Edge wall line load (kN/m)	6.00
*Without the self-weight of slab foundation	

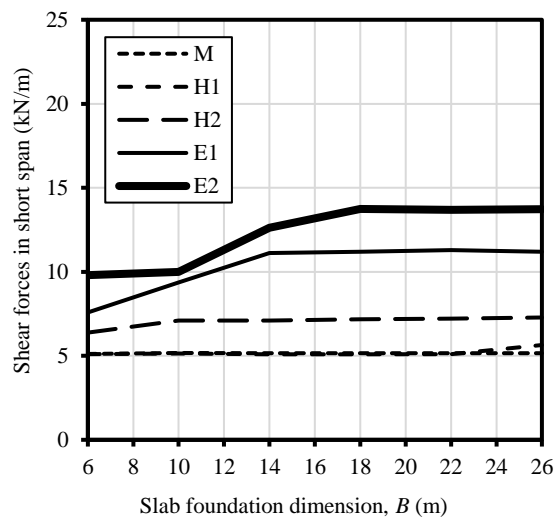
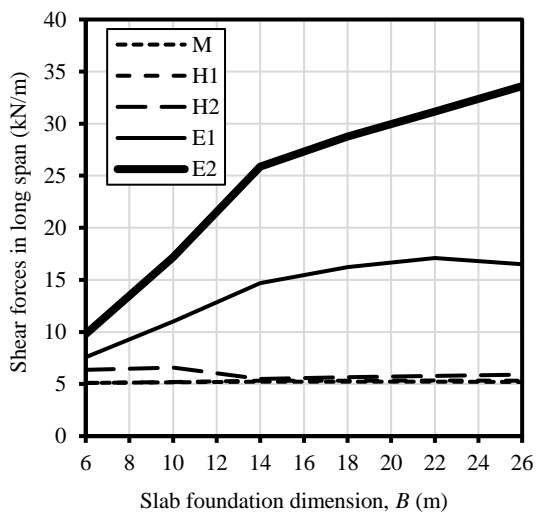
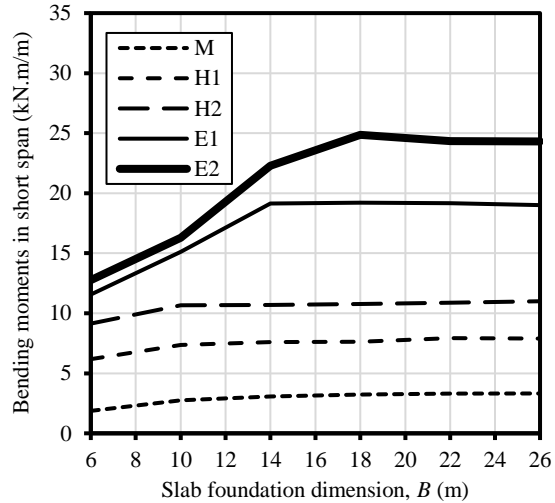
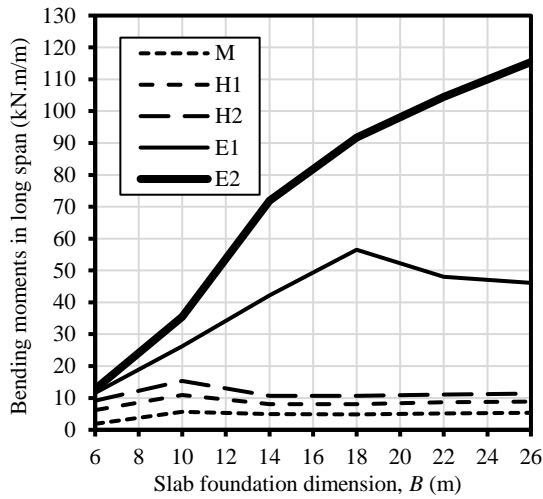
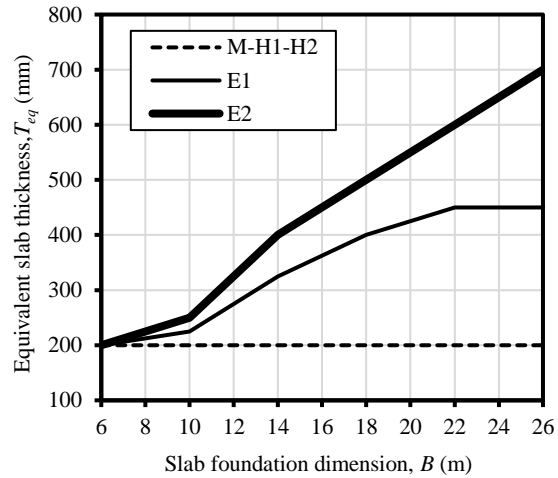


Figure B-8: $L = 6$ m, edge lift and $L_d/\Delta_{all} = 800$.

Slab foundation main span, L (m)	10.00
Edge drop scenario	ED
Span to deflection ratio (L_d/Δ_{all})	300
Service Loads:	
Internal wall loads (kPa)	2.6
Roof: 0.80 mm steel sheet (kPa)	0.1
10 mm Plasterboard (kPa)	0.083
12 mm hardwood lining	0.126
Insulation, wiring, fittings (kPa)	0.058
Flooring (13 mm clay tiling)	0.27
Permanent live load (kPa)	1.25
Total uniform load* (kPa)	4.50
Edge wall line load (kN/m)	6.00
*Without the self-weight of slab foundation	

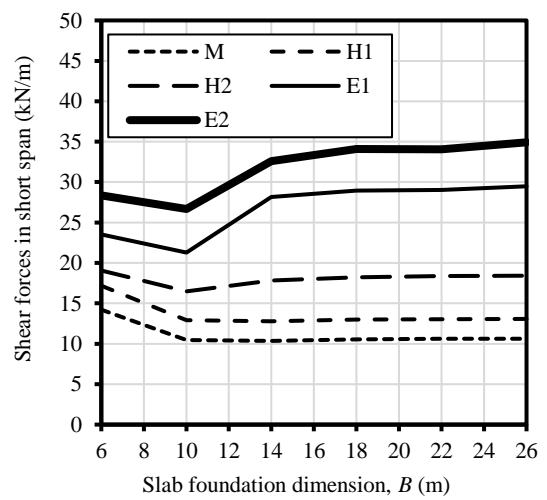
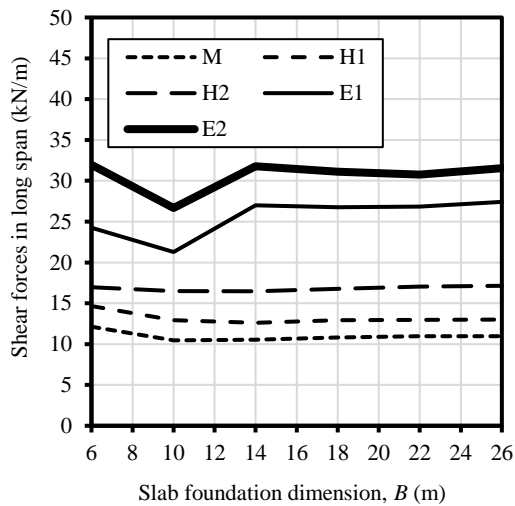
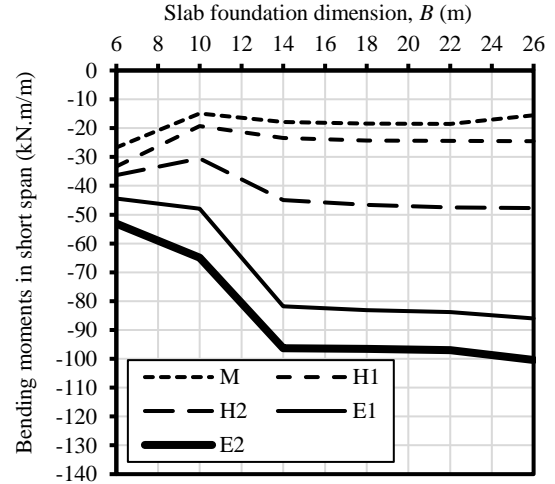
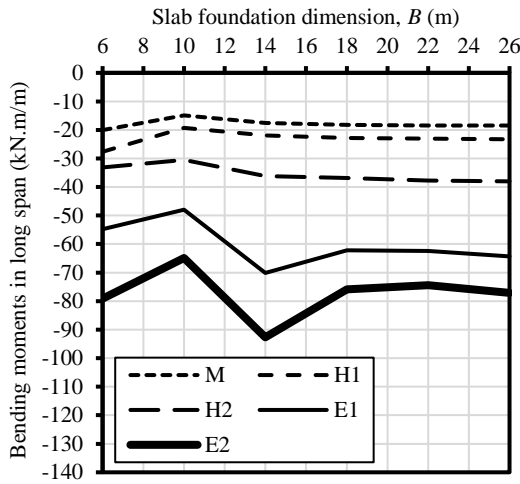
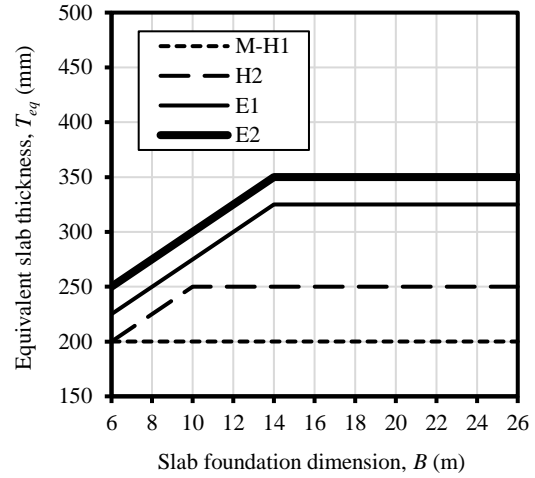


Figure B-9: $L = 10$ m, edge drop and $L_d/\Delta_{all} = 300$.

Slab foundation main span, L (m)	10.00
Edge drop scenario	ED
Span to deflection ratio (L_d/Δ_{all})	400
Service Loads:	
Internal wall loads, W_{int} (kPa)	2.6
Roof: 0.80 mm steel sheet (kPa)	0.1
10 mm Plasterboard (kPa)	0.083
12 mm hardwood lining	0.126
Insulation, wiring, fittings (kPa)	0.058
Flooring (13 mm clay tiling)	0.27
Permanent live load, q (kPa)	1.25
Total uniform load* (kPa)	4.50
Edge wall line load (kN/m)	6.00
*Without the self-weight of slab foundation	

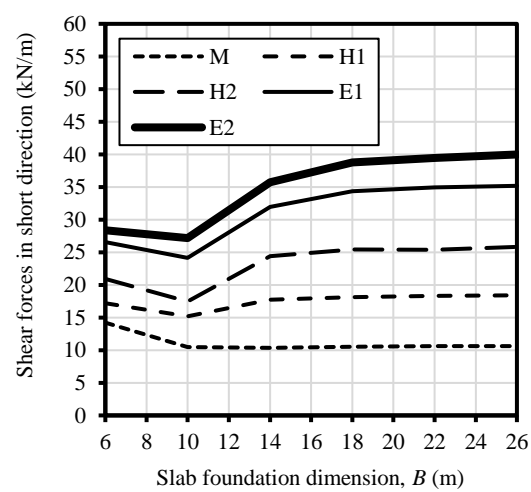
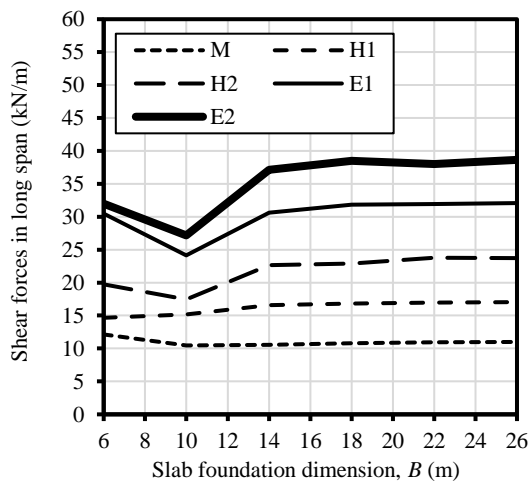
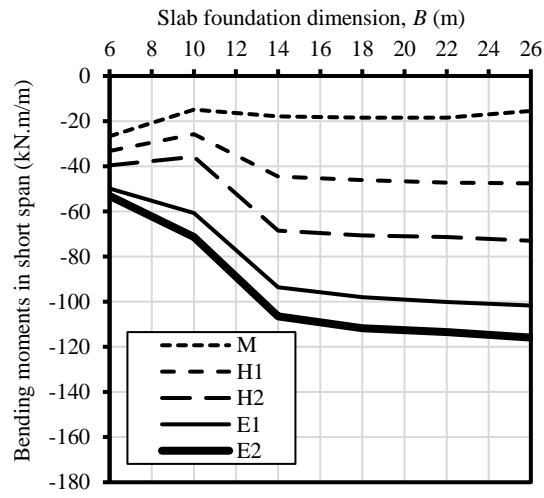
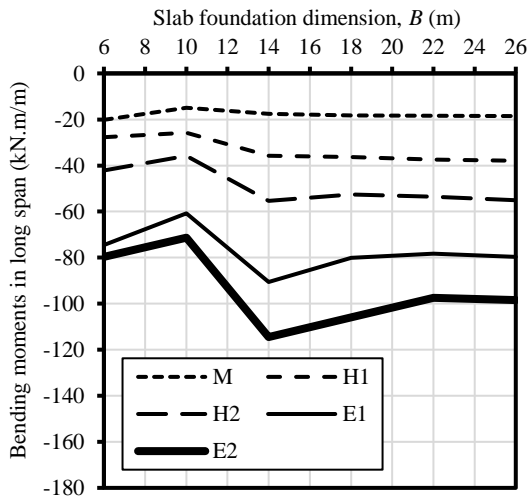
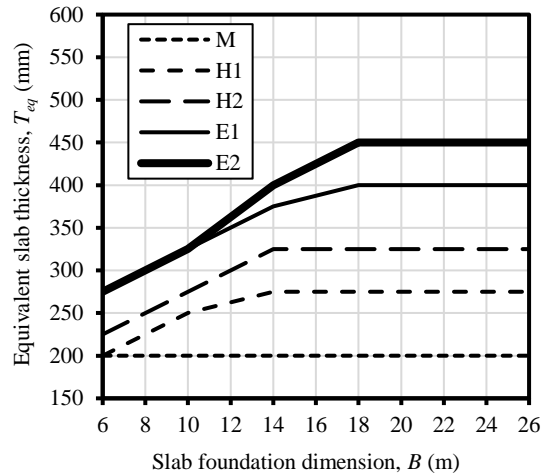


Figure B-10: $L = 10$ m, edge drop and $L_d/\Delta_{all} = 400$.

Slab foundation main span, L (m)	10.00
Edge drop scenario	ED
Span to deflection ratio (L_d/Δ_{all})	600
Service Loads:	
Internal wall loads (kPa)	2.6
Roof: 0.80 mm steel sheet (kPa)	0.1
10 mm Plasterboard (kPa)	0.083
12 mm hardwood lining	0.126
Insulation, wiring, fittings (kPa)	0.058
Flooring (13 mm clay tiling)	0.27
Permanent live load (kPa)	1.25
Total uniform load* (kPa)	4.50
Edge wall line load (kN/m)	6.00
*Without the self-weight of slab foundation	

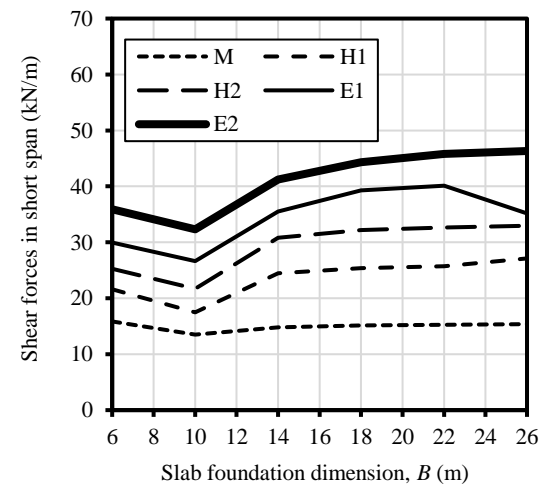
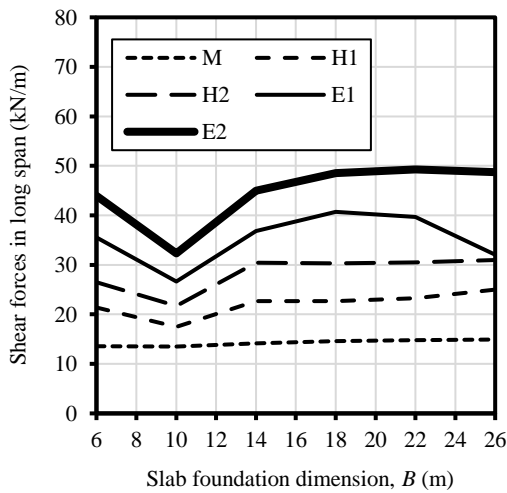
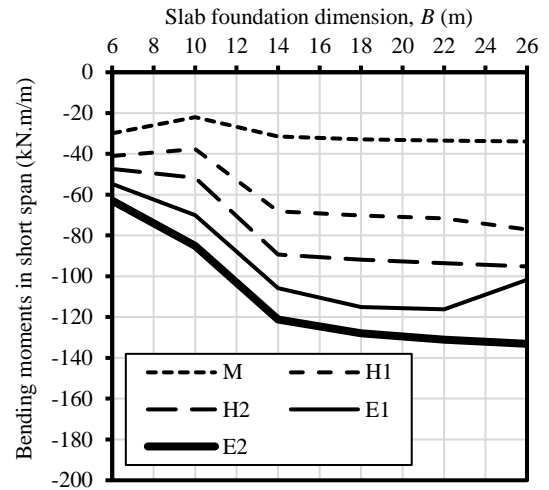
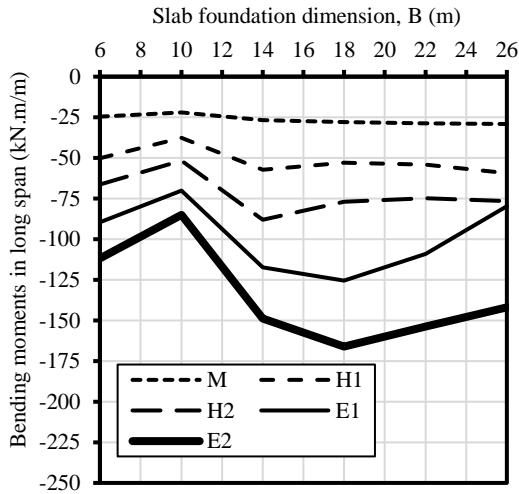
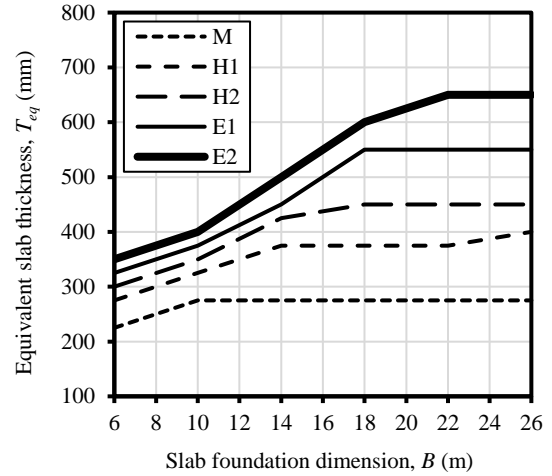


Figure B-11: $L = 10$ m, edge drop and $L_d/\Delta_{all} = 600$.

Slab foundation main span, L (m)	10.00
Edge drop scenario	ED
Span to deflection ratio (L_d/Δ_{all})	800
Service Loads:	
Internal wall loads (kPa)	2.6
Roof: 0.80 mm steel sheet (kPa)	0.1
10 mm Plasterboard (kPa)	0.083
12 mm hardwood lining	0.126
Insulation, wiring, fittings (kPa)	0.058
Flooring (13 mm clay tiling)	0.27
Permanent live load (kPa)	1.25
Total uniform load* (kPa)	4.50
Edge wall line load (kN/m)	6.00
*Without the self-weight of slab foundation	

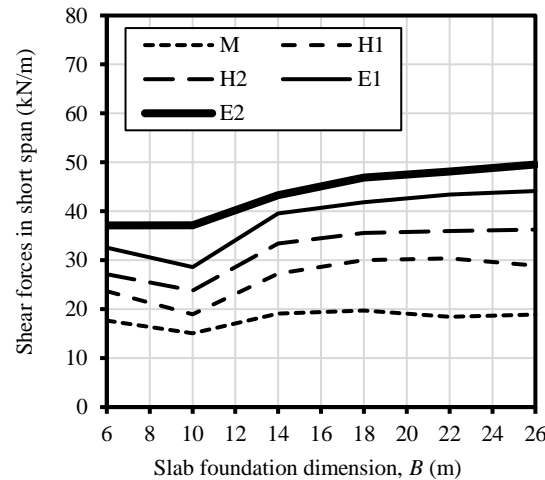
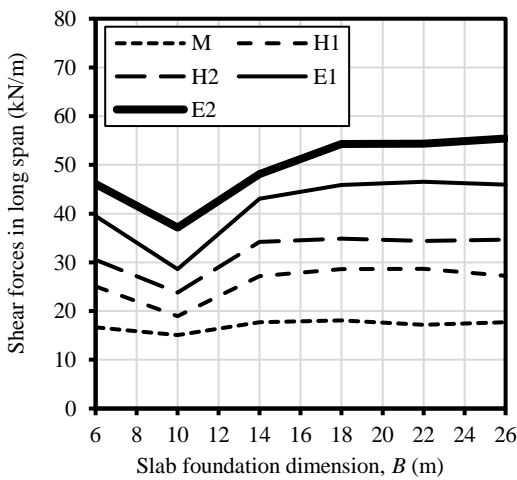
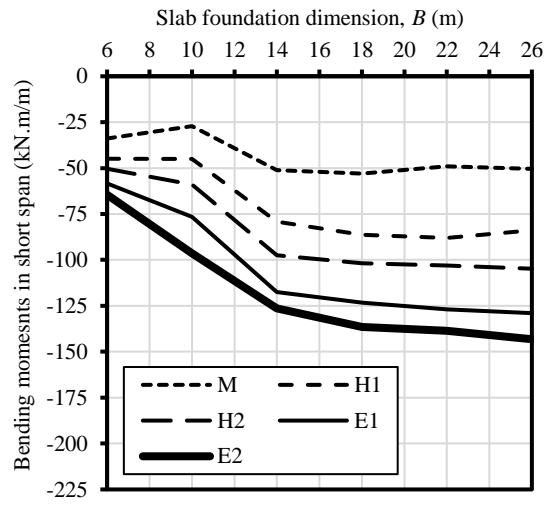
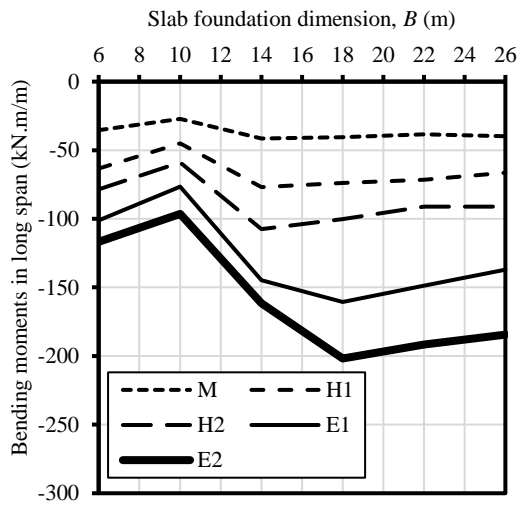
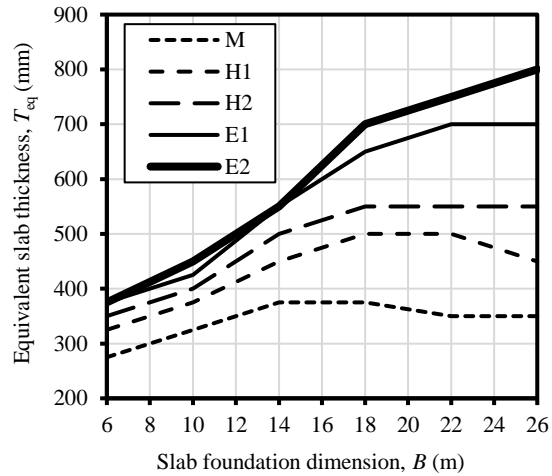


Figure B-12: $L = 10$ m, edge drop and $L_d/\Delta_{all} = 800$.

Slab foundation main span, L (m)	10.00
Edge lift scenario	EL
Span to deflection ratio (L_d/Δ_{all})	300
Service Loads:	
Internal wall loads (kPa)	2.6
Roof: 0.80 mm steel sheet (kPa)	0.1
10 mm Plasterboard (kPa)	0.083
12 mm hardwood lining	0.126
Insulation, wiring, fittings (kPa)	0.058
Flooring (13 mm clay tiling)	0.27
Permanent live load (kPa)	1.25
Total uniform load* (kPa)	4.50
Edge wall line load (kN/m)	6.00
*Without the self-weight of slab foundation	

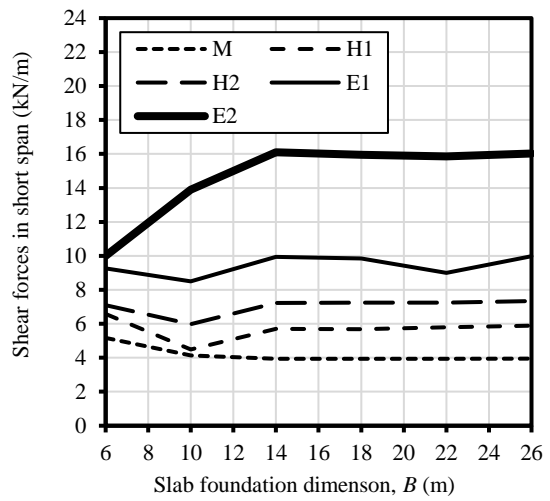
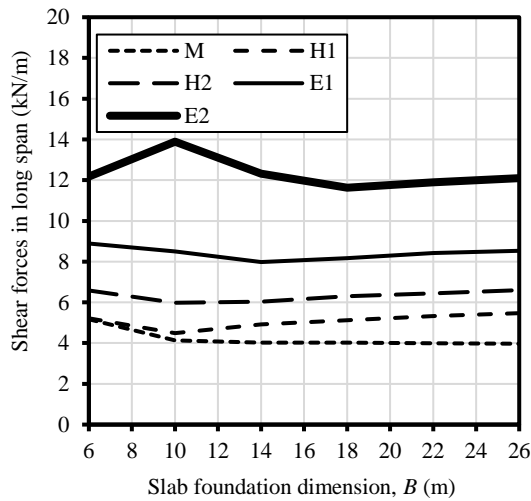
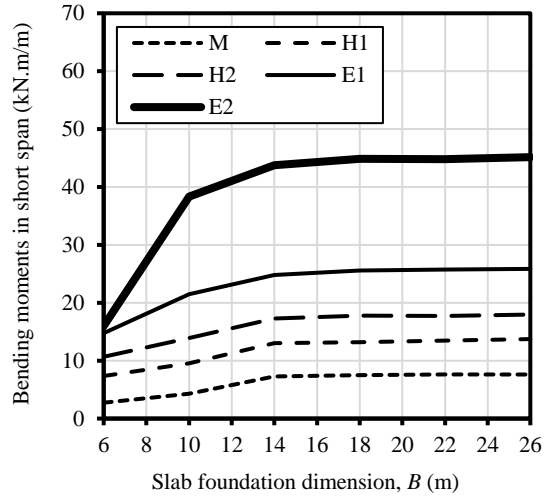
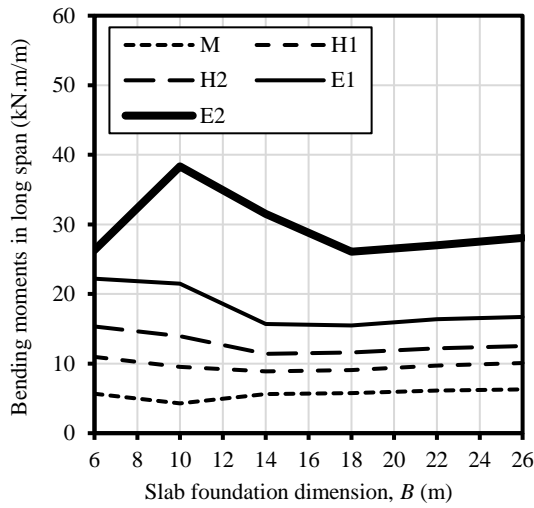
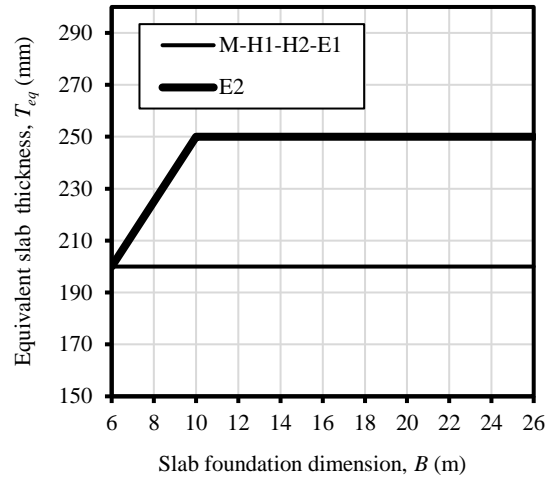


Figure B-13: $L = 10$ m, edge lift and $L_d/\Delta_{all} = 300$.

Slab foundation main span, L (m)	10.00
Edge lift scenario	EL
Span to deflection ratio (L_d/Δ_{all})	400
Service Loads:	
Internal wall loads (kPa)	2.6
Roof: 0.80 mm steel sheet (kPa)	0.1
10 mm Plasterboard (kPa)	0.083
12 mm hardwood lining	0.126
Insulation, wiring, fittings (kPa)	0.058
Flooring (13 mm clay tiling)	0.27
Permanent live load (kPa)	1.25
Total uniform load* (kPa)	4.50
Edge wall line load (kN/m)	6.00
*Without the self-weight of slab foundation	

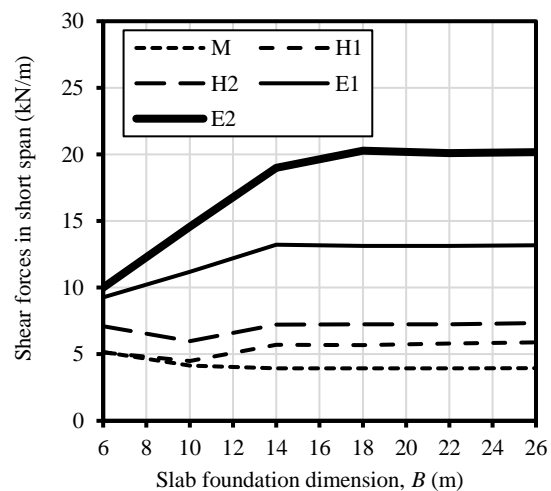
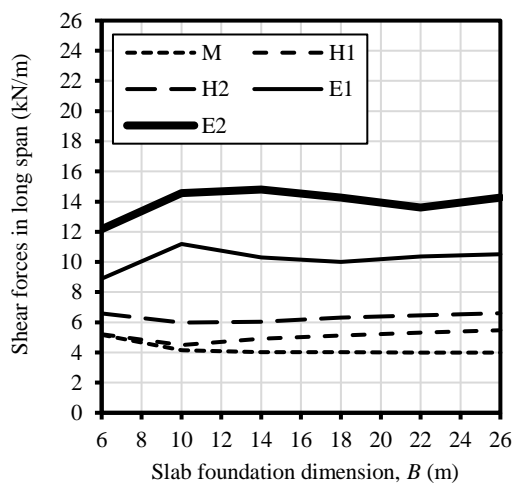
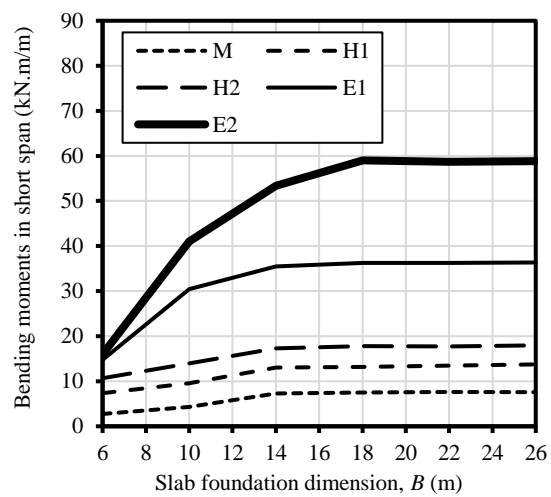
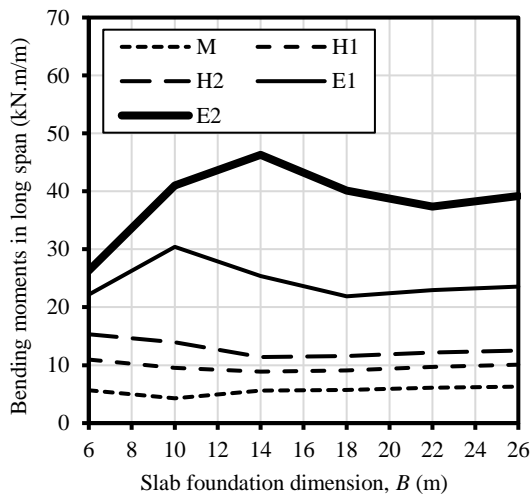
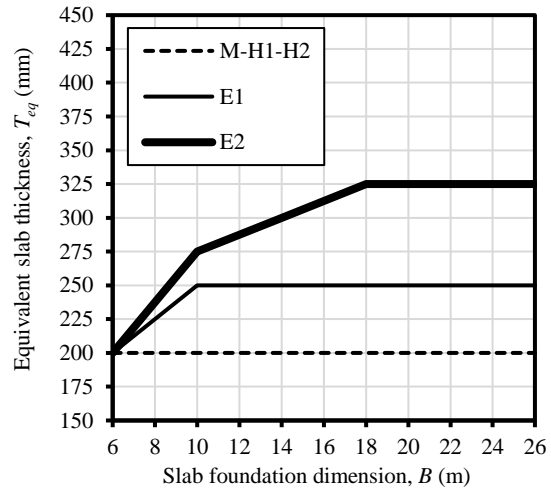


Figure B-14: $L = 10$ m, edge lift and $L_d/\Delta_{all} = 400$.

Slab foundation main span, L (m)	10.00
Edge lift scenario	EL
Span to deflection ratio (L_d/Δ_{all})	600
Service Loads:	
Internal wall loads (kPa)	2.6
Roof: 0.80 mm steel sheet (kPa)	0.1
10 mm Plasterboard (kPa)	0.083
12 mm hardwood lining	0.126
Insulation, wiring, fittings (kPa)	0.058
Flooring (13 mm clay tiling)	0.27
Permanent live load (kPa)	1.25
Total uniform load* (kPa)	4.50
Edge wall line load (kN/m)	6.00
*Without the self-weight of slab foundation	

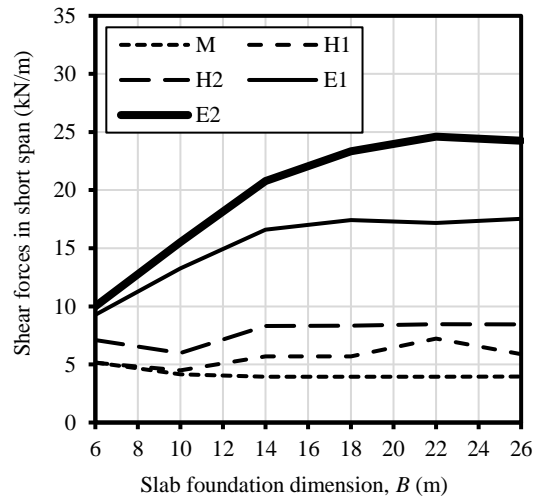
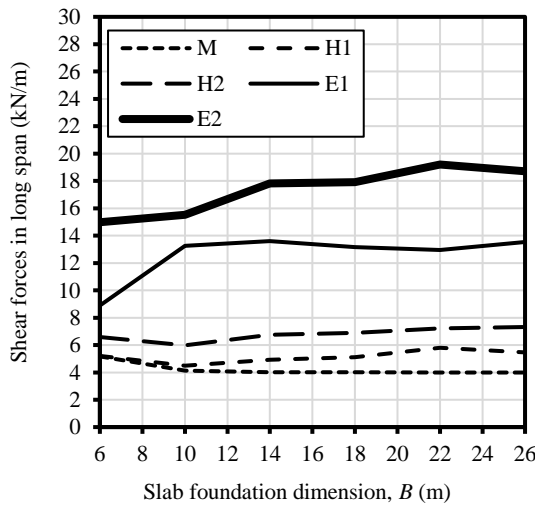
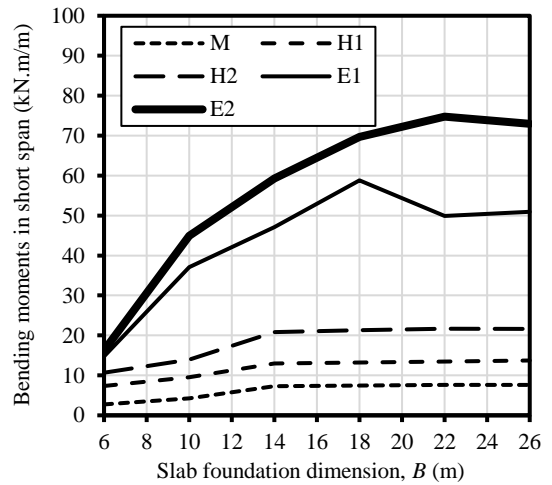
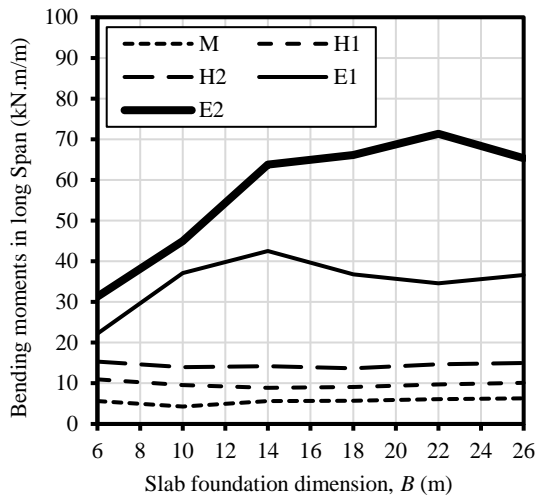
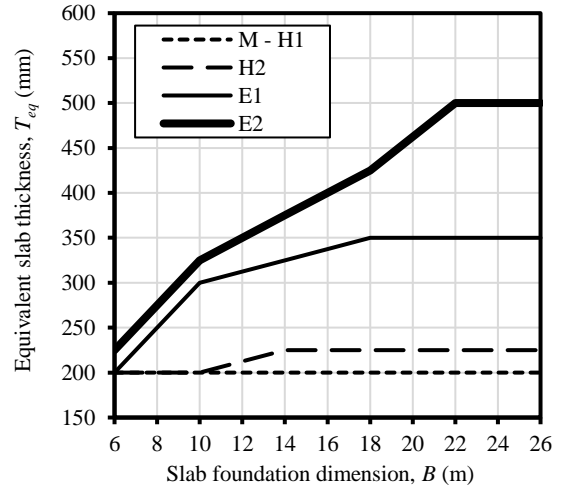


Figure B-15: $L = 10$ m, edge lift and $L_d/\Delta_{all} = 600$.

Slab foundation main span, L (m)	10.00
Edge lift scenario	EL
Span to deflection ratio (L_d/Δ_{all})	800
Service Loads:	
Internal wall loads (kPa)	2.6
Roof: 0.80 mm steel sheet (kPa)	0.1
10 mm Plasterboard (kPa)	0.083
12 mm hardwood lining	0.126
Insulation, wiring, fittings (kPa)	0.058
Flooring (13 mm clay tiling)	0.27
Permanent live load (kPa)	1.25
Total uniform load* (kPa)	4.50
Edge wall line load (kN/m)	6.00
*Without the self-weight of slab foundation	

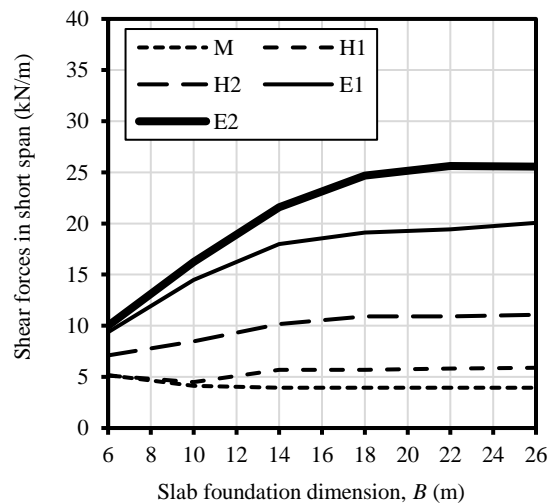
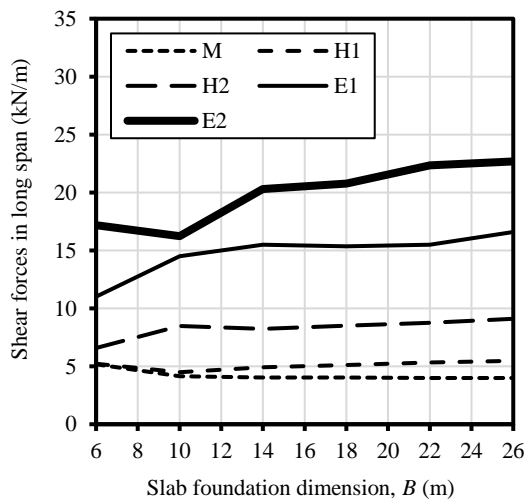
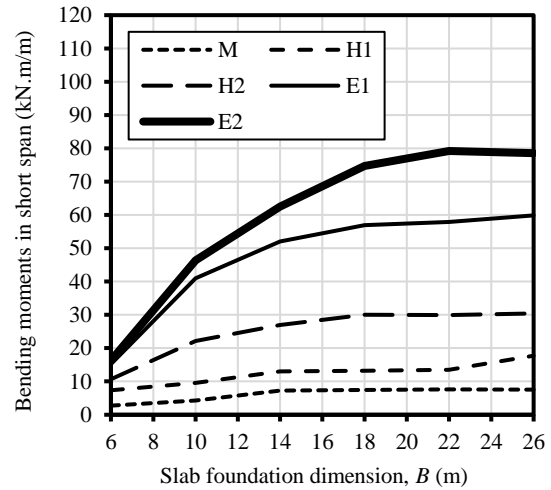
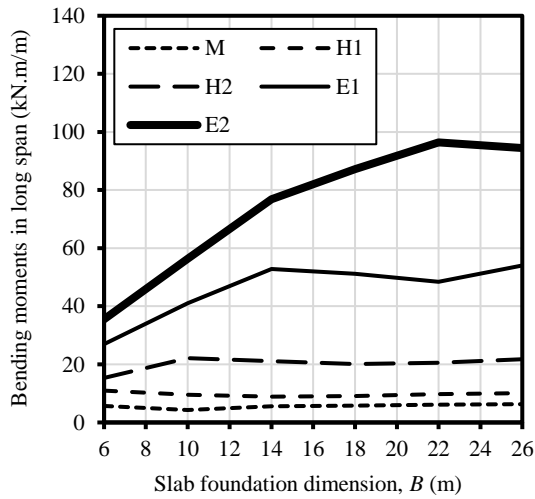
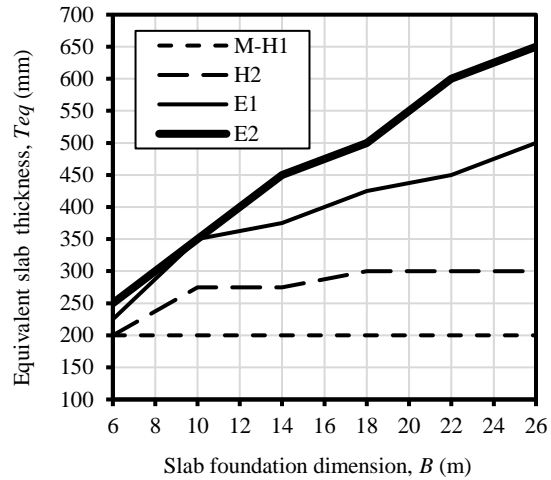


Figure B-16: $L = 10$ m, edge lift and $L_d/\Delta_{all} = 800$.

Slab foundation main span, L (m)	14.00
Edge drop scenario	ED
Span to deflection ratio (L_d/Δ_{all})	300
Service Loads:	
Internal wall loads (kPa)	2.6
Roof: 0.80 mm steel sheet (kPa)	0.1
10 mm Plasterboard (kPa)	0.083
12 mm hardwood lining	0.126
Insulation, wiring, fittings (kPa)	0.058
Flooring (13 mm clay tiling)	0.27
Permanent live load (kPa)	1.25
Total uniform load* (kPa)	4.50
Edge wall line load (kN/m)	6.00
*Without the self-weight of slab foundation	

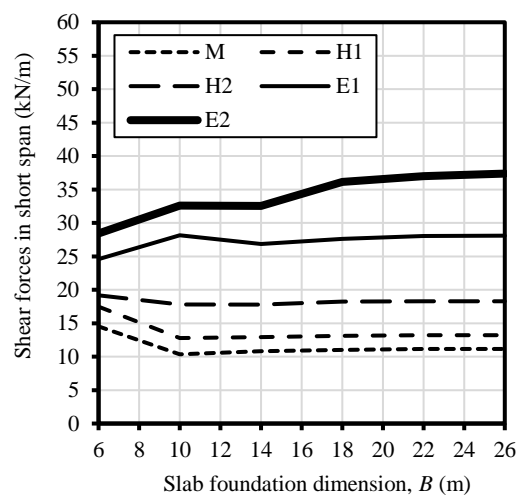
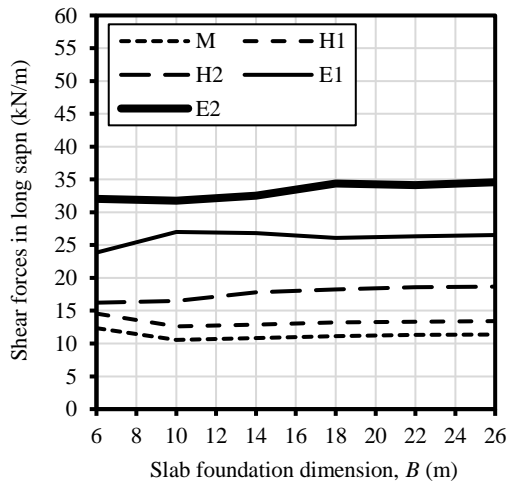
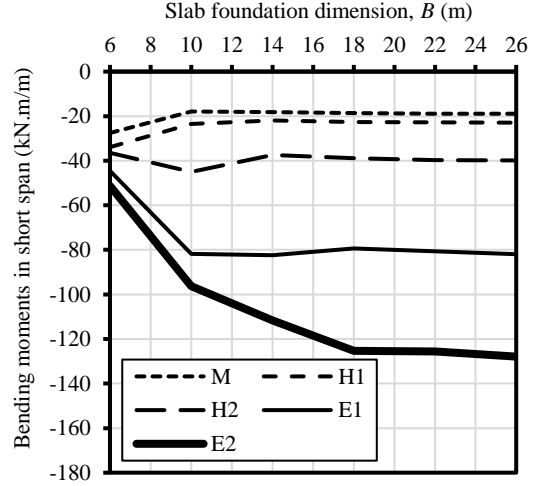
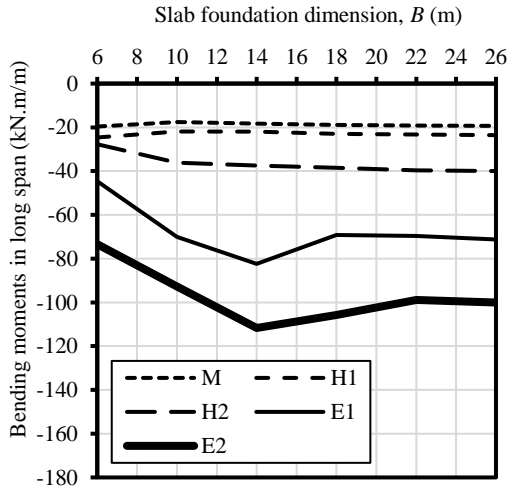
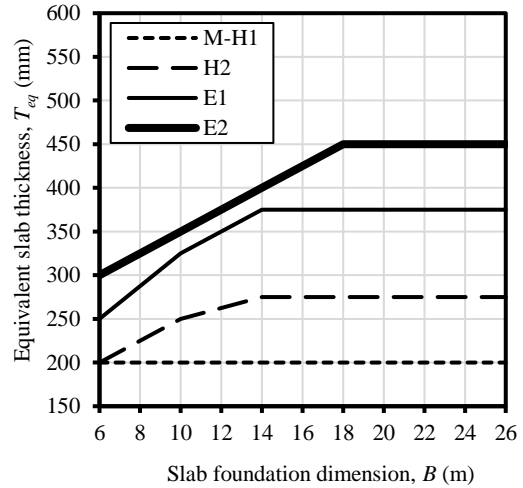


Figure B-17: $L = 14$ m, edge drop and $L_d/\Delta_{all} = 300$.

Slab foundation main span, L (m)	14.00
Edge drop scenario	ED
Span to deflection ratio (L_d/Δ_{all})	400
Service Loads:	
Internal wall loads (kPa)	2.6
Roof: 0.80 mm steel sheet (kPa)	0.1
10 mm Plasterboard (kPa)	0.083
12 mm hardwood lining	0.126
Insulation, wiring, fittings (kPa)	0.058
Flooring (13 mm clay tiling)	0.27
Permanent live load (kPa)	1.25
Total uniform load* (kPa)	4.50
Edge wall line load (kN/m)	6.00
*Without the self-weight of slab foundation	

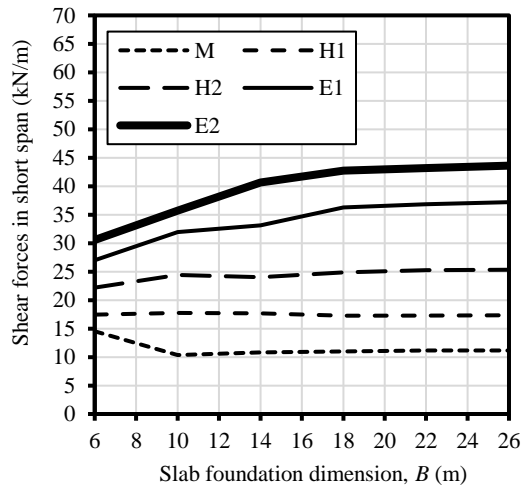
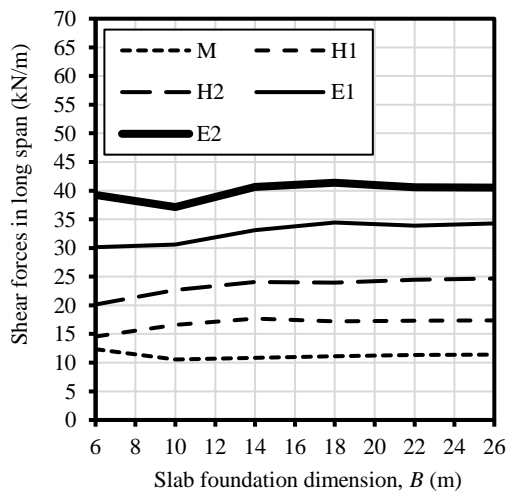
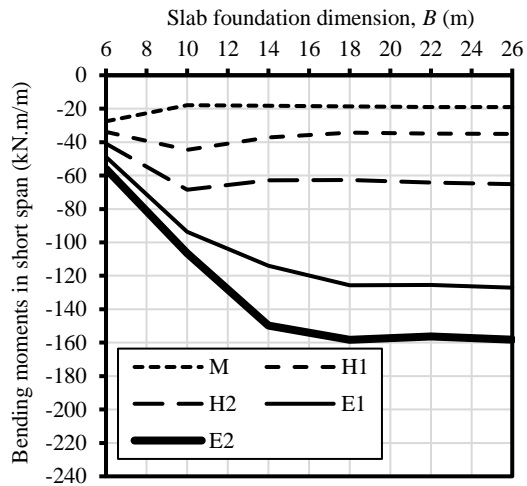
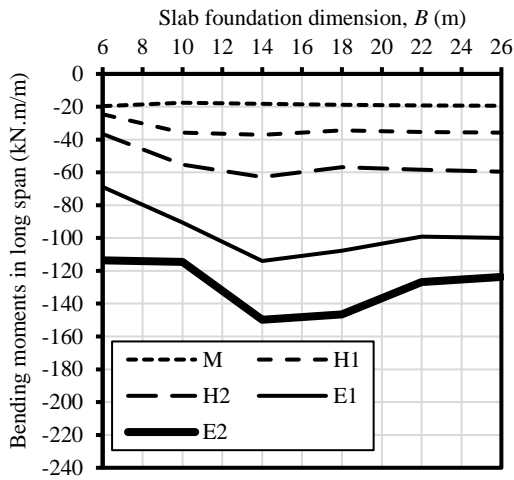
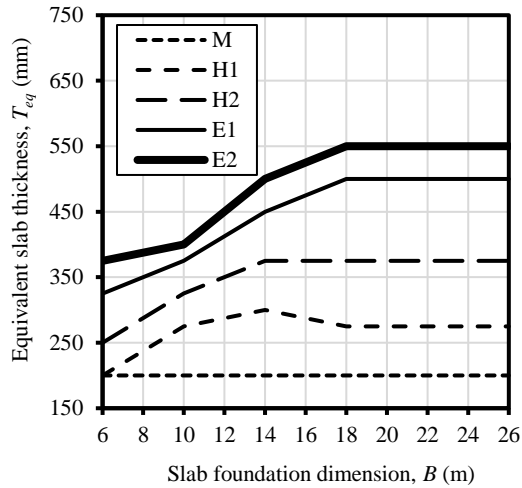


Figure B-18: $L = 14$ m, edge drop and $L_d/\Delta_{all} = 400$.

Slab foundation main span, L (m)	14.00
Edge drop scenario	ED
Span to deflection ratio (L_d/Δ_{all})	600
Service Loads:	
Internal wall loads (kPa)	2.6
Roof: 0.80 mm steel sheet (kPa)	0.1
10 mm Plasterboard (kPa)	0.083
12 mm hardwood lining	0.126
Insulation, wiring, fittings (kPa)	0.058
Flooring (13 mm clay tiling)	0.27
Permanent live load (kPa)	1.25
Total uniform load* (kPa)	4.50
Edge wall line load (kN/m)	6.00
*Without the self-weight of slab foundation	

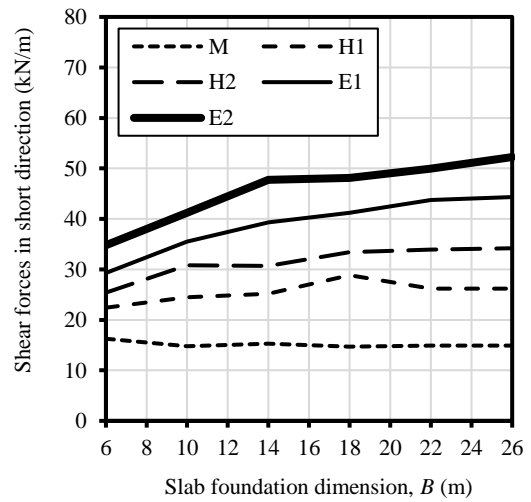
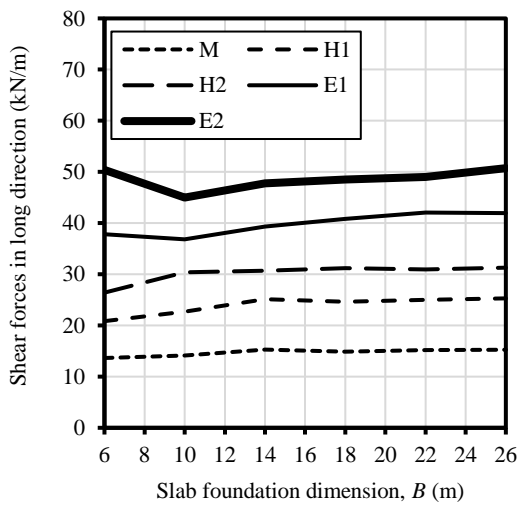
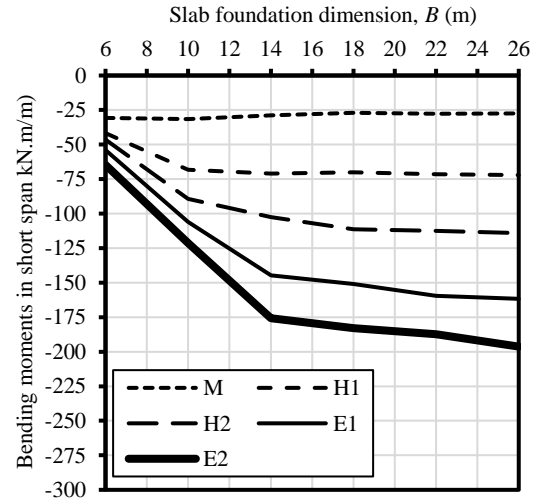
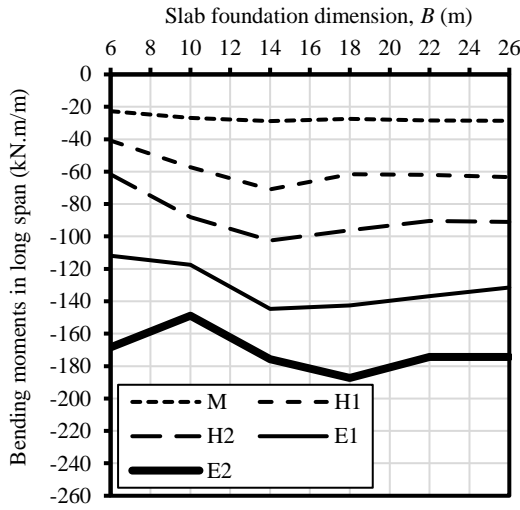
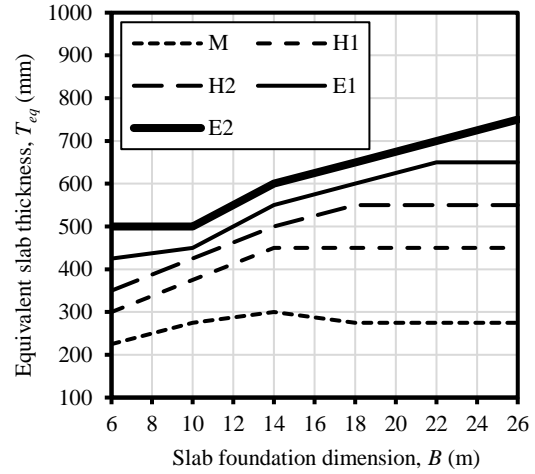


Figure B-19: $L = 14$ m, edge drop and $L_d/\Delta_{all} = 600$.

Slab foundation main span, L (m)	14.00
Edge drop scenario	ED
Span to deflection ratio (L_d/Δ_{all})	800
Service Loads:	
Internal wall loads (kPa)	2.6
Roof: 0.80 mm steel sheet (kPa)	0.1
10 mm Plasterboard (kPa)	0.083
12 mm hardwood lining	0.126
Insulation, wiring, fittings (kPa)	0.058
Flooring (13 mm clay tiling)	0.27
Permanent live load (kPa)	1.25
Total uniform load* (kPa)	4.50
Edge wall line load (kN/m)	6.00
*Without the self-weight of slab foundation	

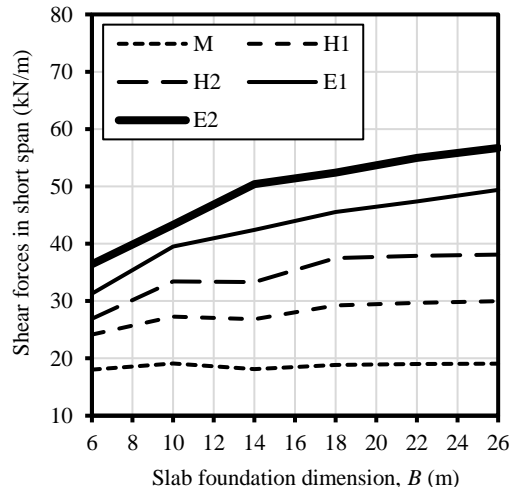
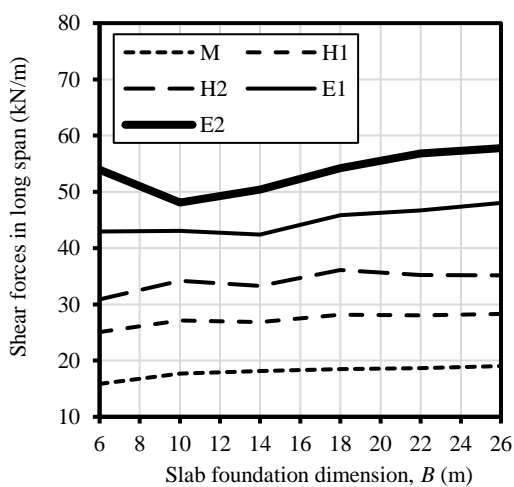
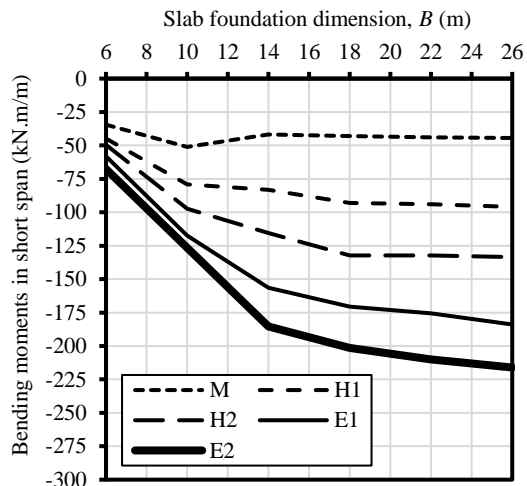
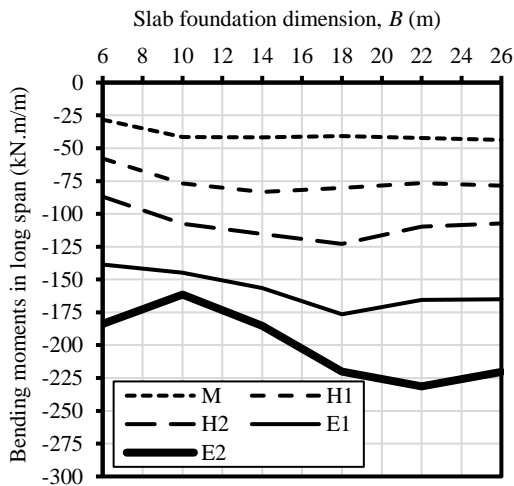
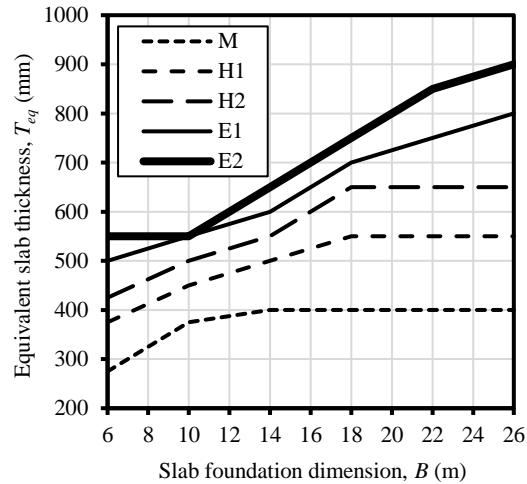


Figure B-20: $L = 14$ m, edge drop and $L_d/\Delta_{all} = 800$.

Slab foundation main span, L (m)	14.00
Edge lift scenario	EL
Span to deflection ratio (L_d/Δ_{all})	300
Service Loads:	
Internal wall loads (kPa)	2.6
Roof: 0.80 mm steel sheet (kPa)	0.1
10 mm Plasterboard (kPa)	0.083
12 mm hardwood lining	0.126
Insulation, wiring, fittings (kPa)	0.058
Flooring (13 mm clay tiling)	0.27
Permanent live load (kPa)	1.25
Total uniform load* (kPa)	4.50
Edge wall line load (kN/m)	6.00
*Without the self-weight of slab foundation	

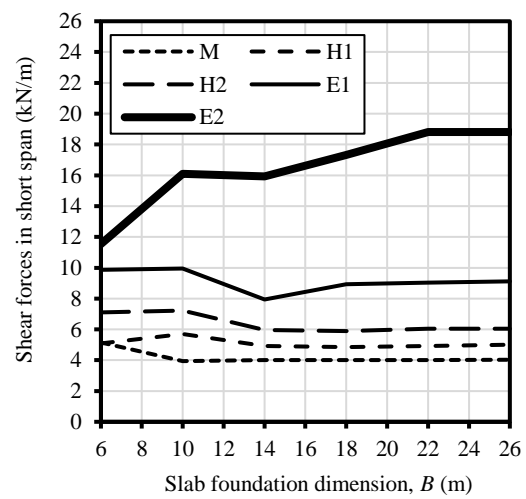
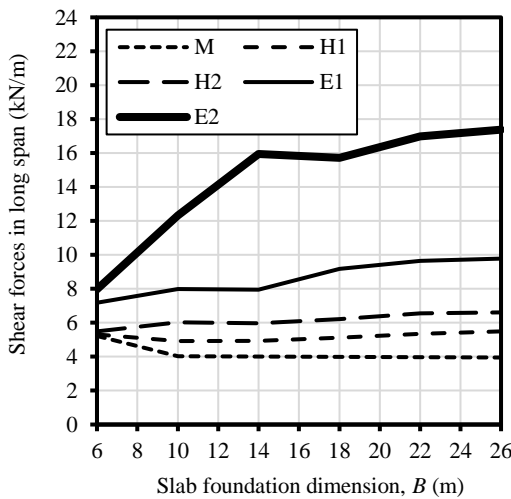
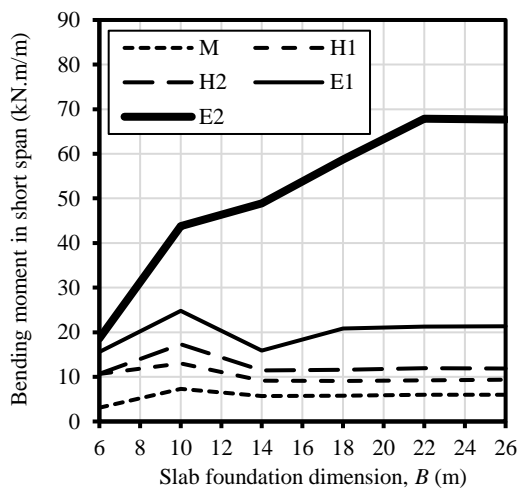
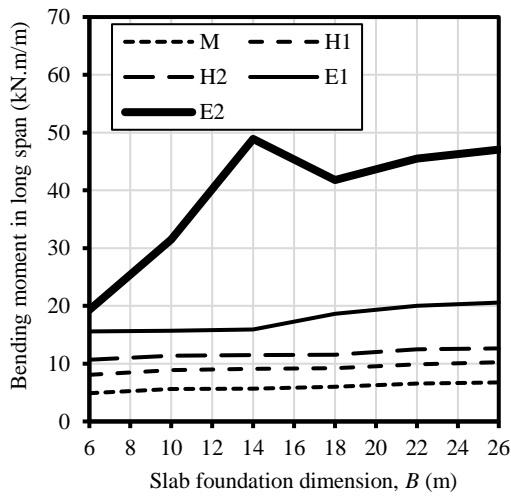
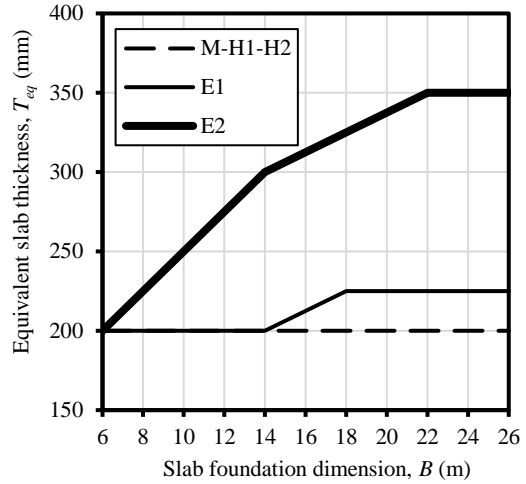


Figure B-21: $L = 14$ m, edge lift and $L_d/\Delta_{all} = 300$.

Slab foundation main span, L (m)	14.00
Edge lift scenario	EL
Span to deflection ratio (L_d/Δ_{all})	400
Service Loads:	
Internal wall loads (kPa)	2.6
Roof: 0.80 mm steel sheet (kPa)	0.1
10 mm Plasterboard (kPa)	0.083
12 mm hardwood lining	0.126
Insulation, wiring, fittings (kPa)	0.058
Flooring (13 mm clay tiling)	0.27
Permanent live load (kPa)	1.25
Total uniform load* (kPa)	4.50
Edge wall line load (kN/m)	6.00
*Without the self-weight of slab foundation	

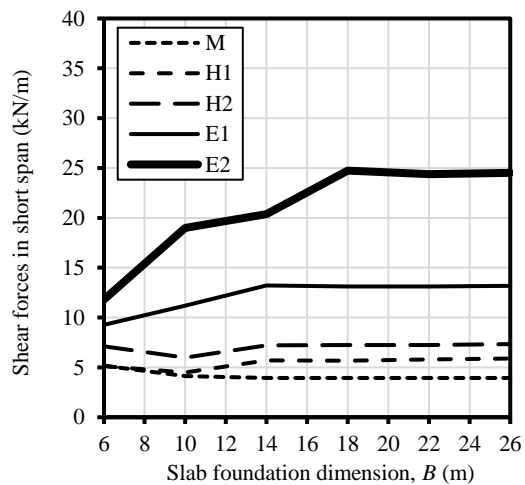
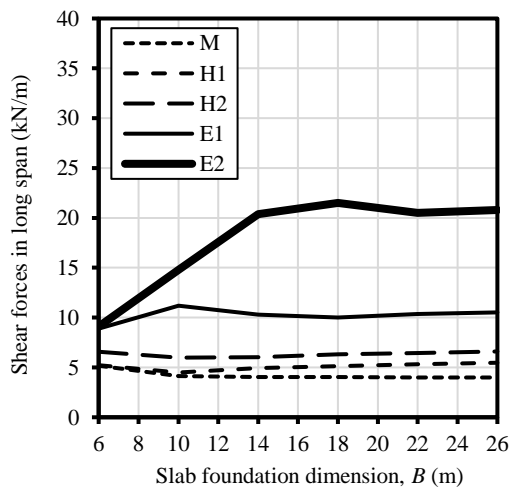
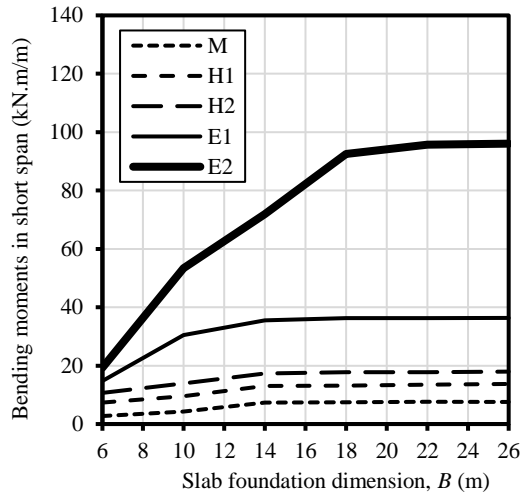
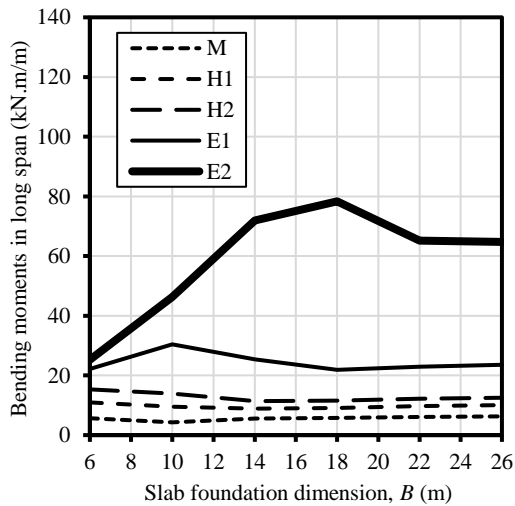
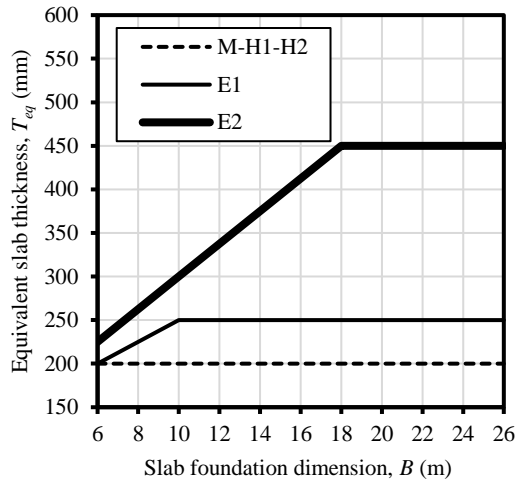


Figure B-22: $L = 14$ m, edge lift and $L_d/\Delta_{all} = 400$.

Slab foundation main span, L (m)	14.00
Edge lift scenario	EL
Span to deflection ratio (L_d/Δ_{all})	600
Service Loads:	
Internal wall loads (kPa)	2.6
Roof: 0.80 mm steel sheet (kPa)	0.1
10 mm Plasterboard (kPa)	0.083
12 mm hardwood lining	0.126
Insulation, wiring, fittings (kPa)	0.058
Flooring (13 mm clay tiling)	0.27
Permanent live load (kPa)	1.25
Total uniform load* (kPa)	4.50
Edge wall line load (kN/m)	6.00
*Without the self-weight of slab foundation	

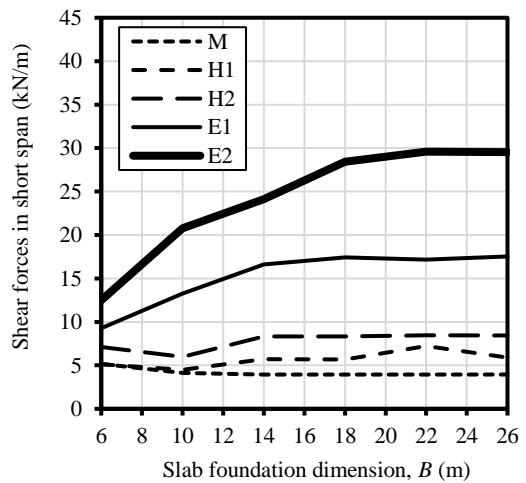
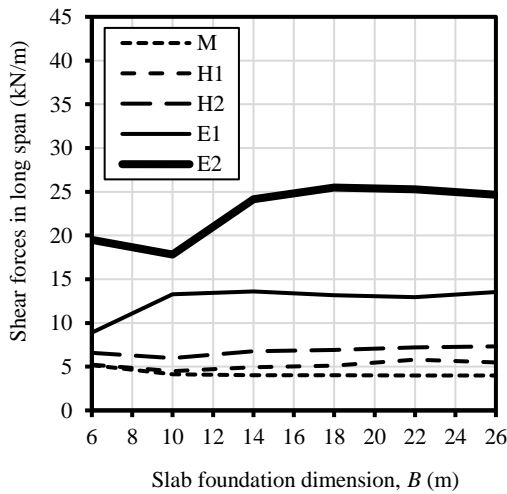
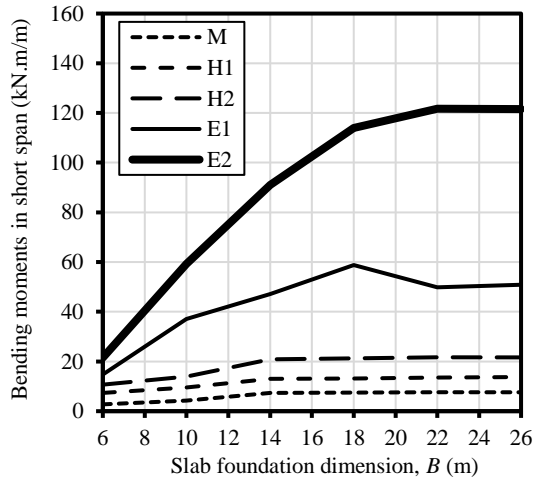
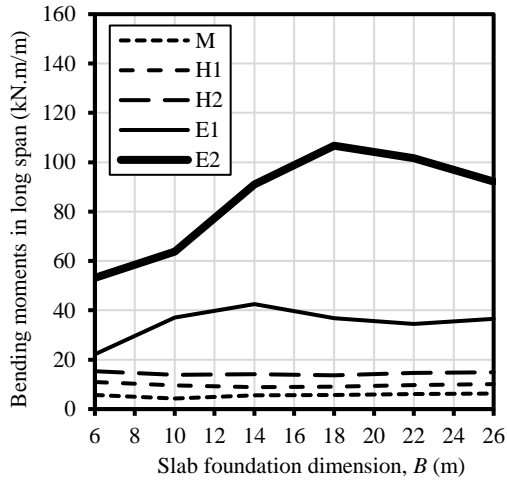
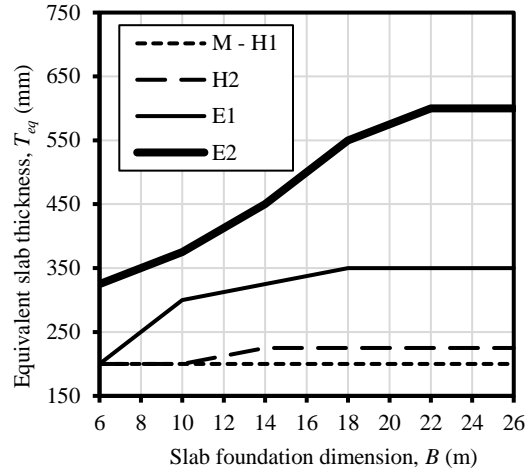


Figure B-23: $L = 14$ m, edge lift and $L_d/\Delta_{all} = 600$.

Slab foundation main span, L (m)	14.00
Edge lift scenario	EL
Span to deflection ratio (L_d/Δ_{all})	800
Service Loads:	
Internal wall loads (kPa)	2.6
Roof: 0.80 mm steel sheet (kPa)	0.1
10 mm Plasterboard (kPa)	0.083
12 mm hardwood lining	0.126
Insulation, wiring, fittings (kPa)	0.058
Flooring (13 mm clay tiling)	0.27
Permanent live load (kPa)	1.25
Total uniform load* (kPa)	4.50
Edge wall line load (kN/m)	6.00
*Without the self-weight of slab foundation	

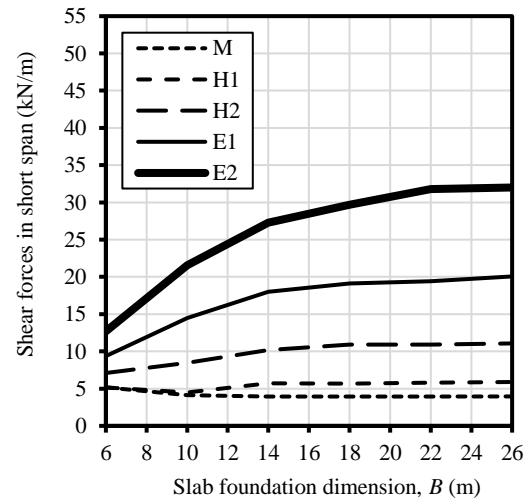
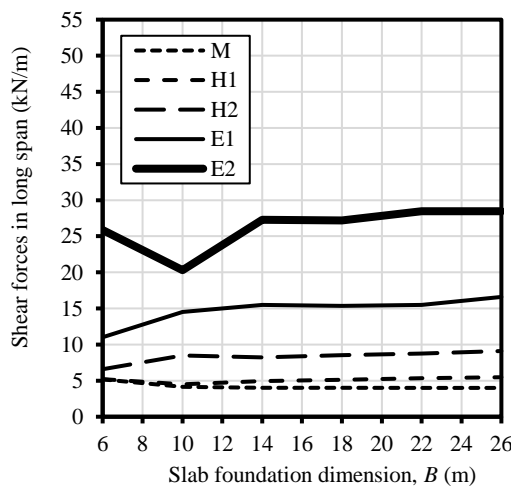
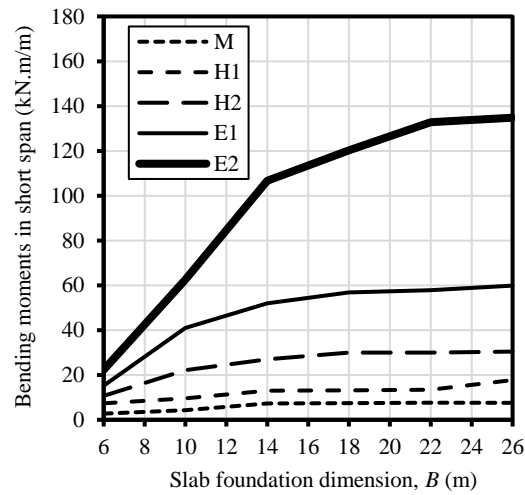
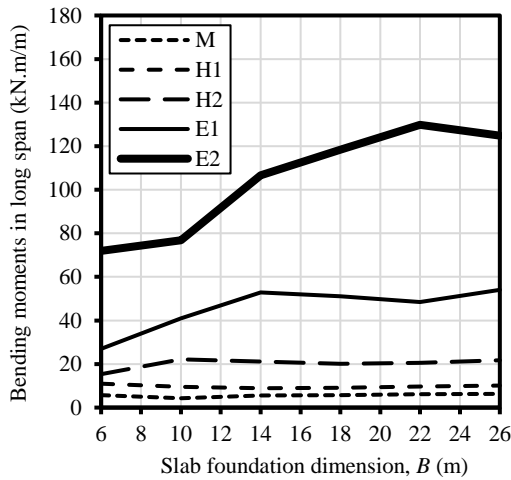
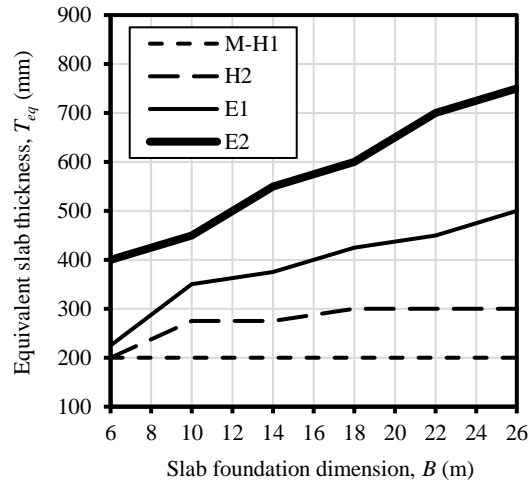


Figure B-24: $L = 14$ m, edge lift and $L_d/\Delta_{all} = 800$.

Slab foundation main span, L (m)	18.00
Edge drop scenario	ED
Span to deflection ratio (L_d/Δ_{all})	300
Service Loads:	
Internal wall loads (kPa)	2.6
Roof: 0.80 mm steel sheet (kPa)	0.1
10 mm Plasterboard (kPa)	0.083
12 mm hardwood lining	0.126
Insulation, wiring, fittings (kPa)	0.058
Flooring (13 mm clay tiling)	0.27
Permanent live load (kPa)	1.25
Total uniform load* (kPa)	4.50
Edge wall line load (kN/m)	6.00
*Without the self-weight of slab foundation	

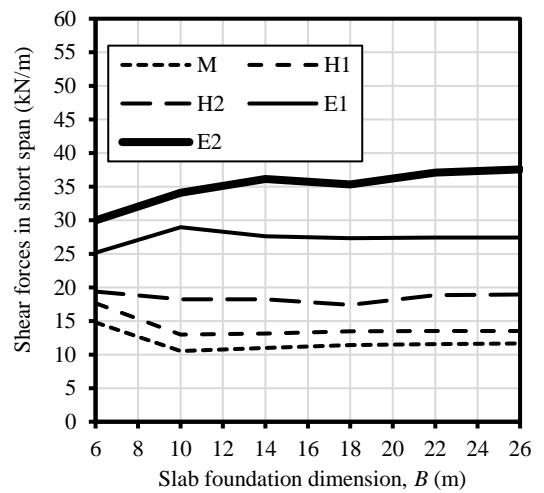
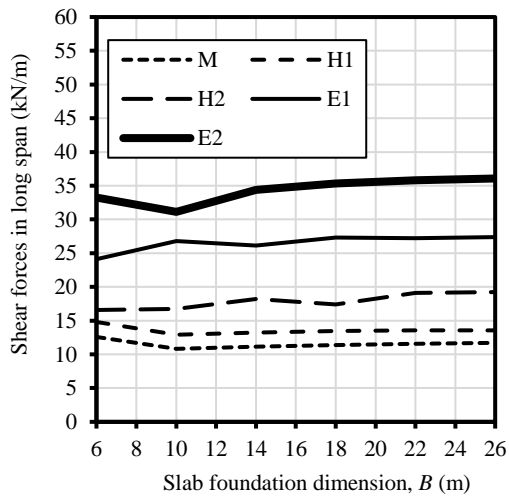
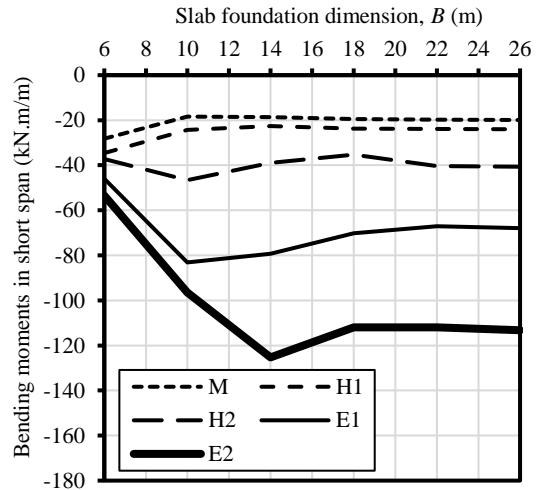
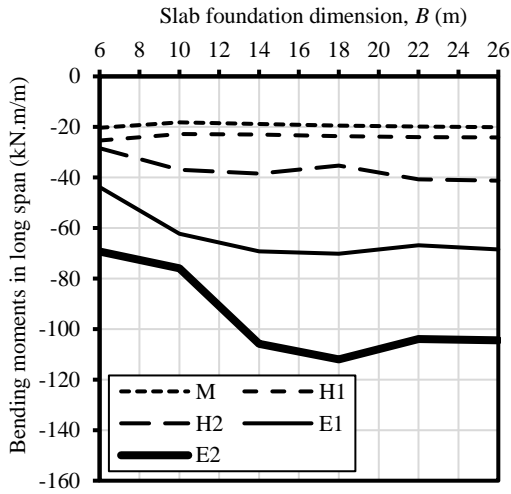
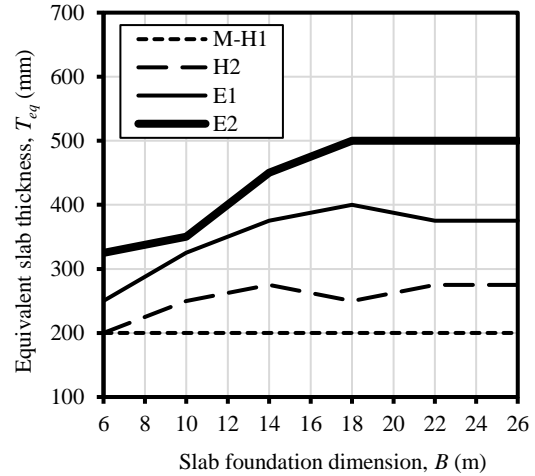


Figure B-25: $L = 18$ m, edge drop and $L_d/\Delta_{all} = 300$.

Slab foundation main span, L (m)	18.00
Edge drop scenario	ED
Span to deflection ratio (L_d/Δ_{all})	400
Service Loads:	
Internal wall loads (kPa)	2.6
Roof: 0.80 mm steel sheet (kPa)	0.1
10 mm Plasterboard (kPa)	0.083
12 mm hardwood lining	0.126
Insulation, wiring, fittings (kPa)	0.058
Flooring (13 mm clay tiling)	0.27
Permanent live load (kPa)	1.25
Total uniform load* (kPa)	4.50
Edge wall line load (kN/m)	6.00
*Without the self-weight of slab foundation	

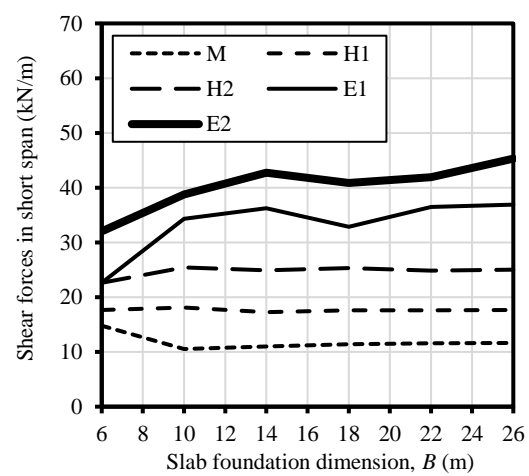
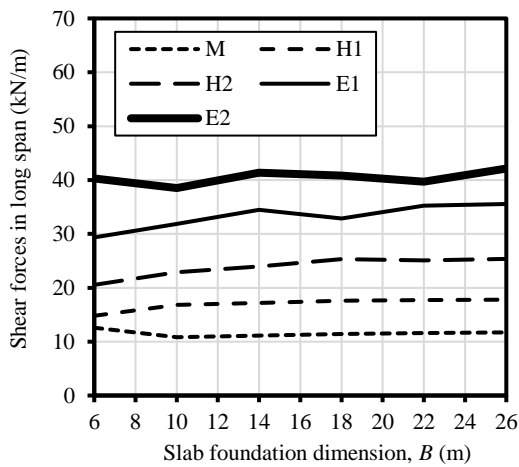
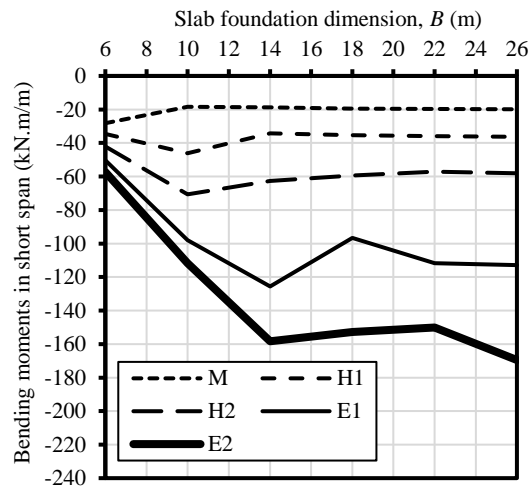
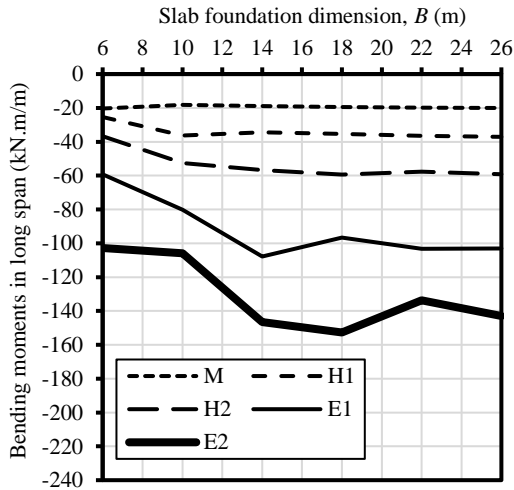
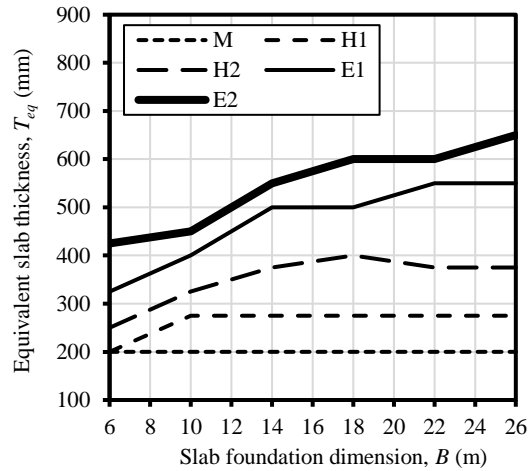


Figure B-26: $L = 18$ m, edge drop and $L_d/\Delta_{all} = 400$.

Slab foundation main span, L (m)	18.00
Edge drop scenario	ED
Span to deflection ratio (L_d/Δ_{all})	600
Service Loads:	
Internal wall loads (kPa)	2.6
Roof: 0.80 mm steel sheet (kPa)	0.1
10 mm Plasterboard (kPa)	0.083
12 mm hardwood lining	0.126
Insulation, wiring, fittings (kPa)	0.058
Flooring (13 mm clay tiling)	0.27
Permanent live load (kPa)	1.25
Total uniform load* (kPa)	4.50
Edge wall line load (kN/m)	6.00
*Without the self-weight of slab foundation	

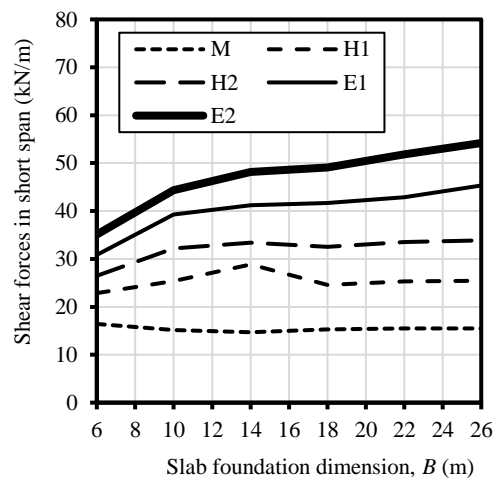
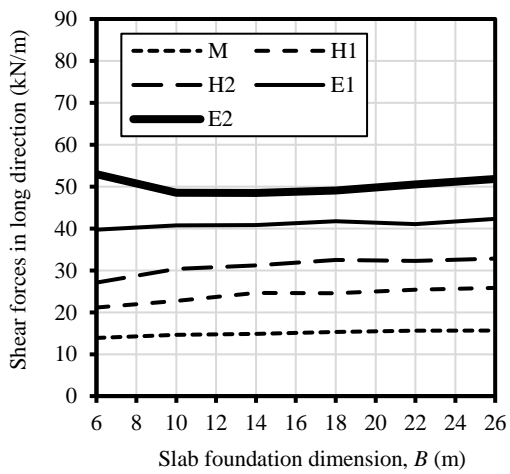
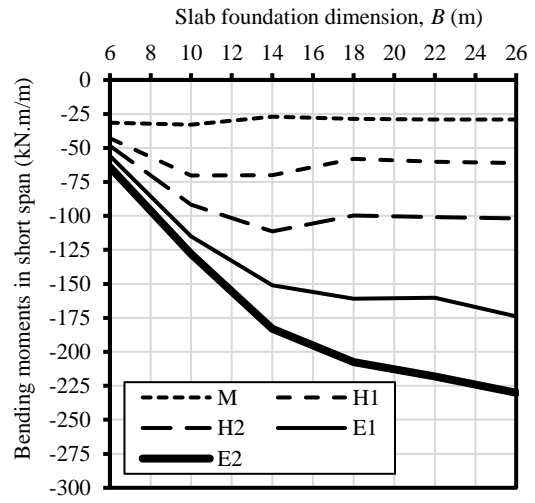
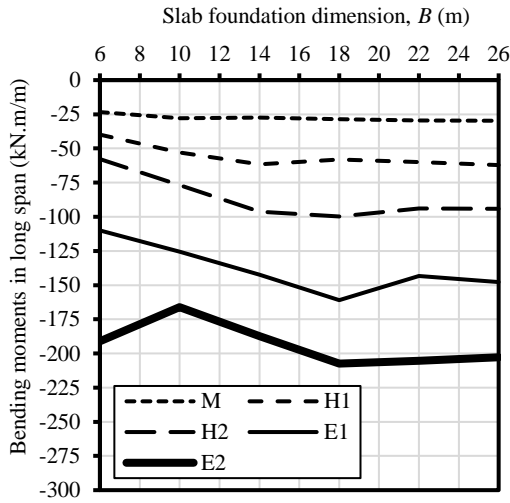
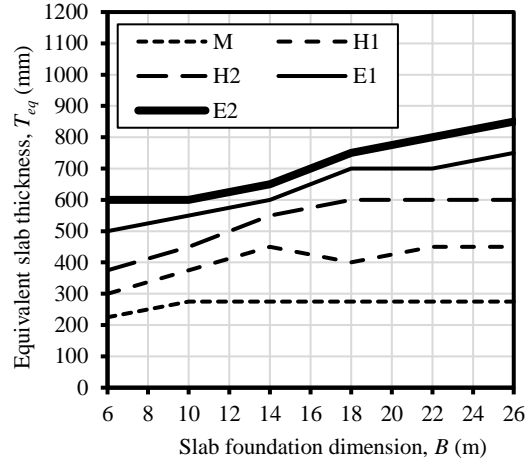


Figure B-27: $L = 18$ m, edge drop and $L_d/\Delta_{all} = 600$.

Slab foundation main span, L (m)	18.00
Edge drop scenario	ED
Span to deflection ratio (L_d/Δ_{all})	800
Service Loads:	
Internal wall loads (kPa)	2.6
Roof: 0.80 mm steel sheet (kPa)	0.1
10 mm Plasterboard (kPa)	0.083
12 mm hardwood lining	0.126
Insulation, wiring, fittings (kPa)	0.058
Flooring (13 mm clay tiling)	0.27
Permanent live load (kPa)	1.25
Total uniform load* (kPa)	4.50
Edge wall line load (kN/m)	6.00
*Without the self-weight of slab foundation	

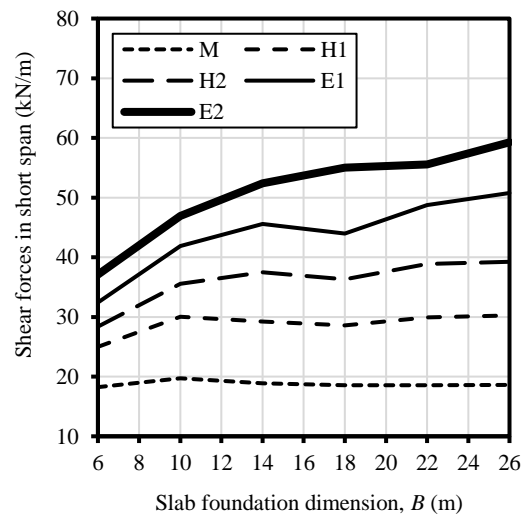
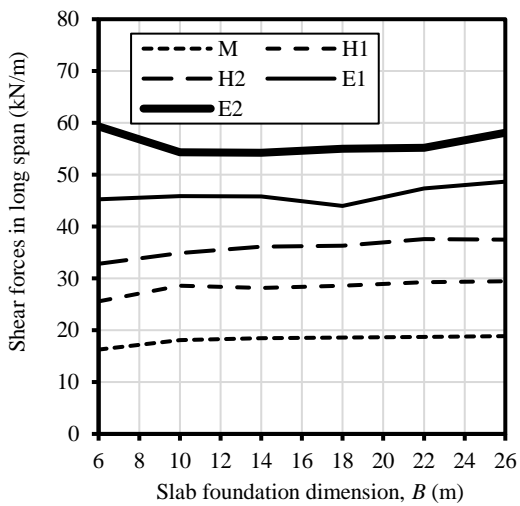
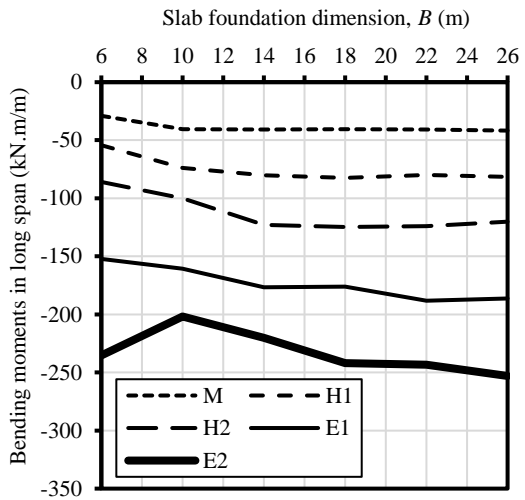
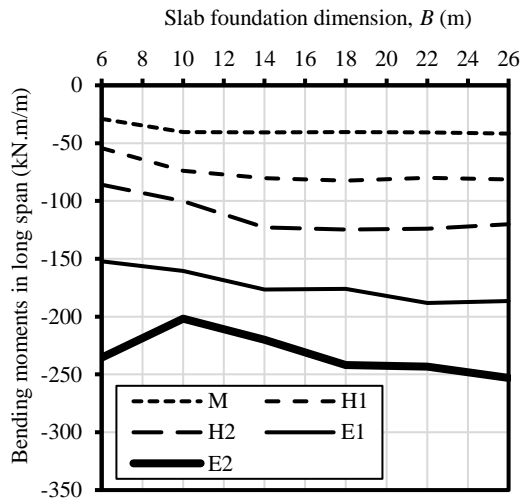
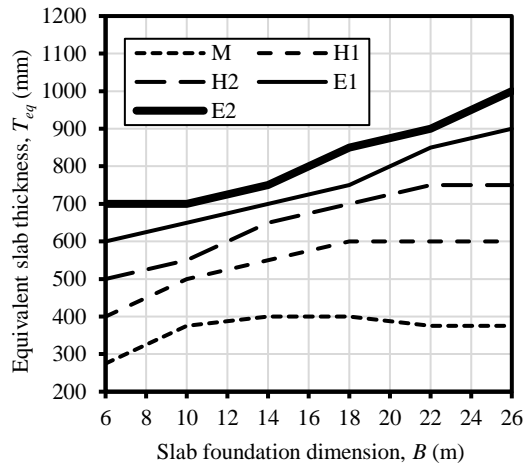


Figure B-28: $L = 18$ m, edge drop and $L_d/\Delta_{all} = 800$.

Slab foundation main span, L (m)	18.00
Edge lift scenario	EL
Span to deflection ratio (L_d/Δ_{all})	300
Service Loads:	
Internal wall loads (kPa)	2.6
Roof: 0.80 mm steel sheet (kPa)	0.1
10 mm Plasterboard (kPa)	0.083
12 mm hardwood lining	0.126
Insulation, wiring, fittings (kPa)	0.058
Flooring (13 mm clay tiling)	0.27
Permanent live load (kPa)	1.25
Total uniform load* (kPa)	4.50
Edge wall line load (kN/m)	6.00
*Without the self-weight of slab foundation	

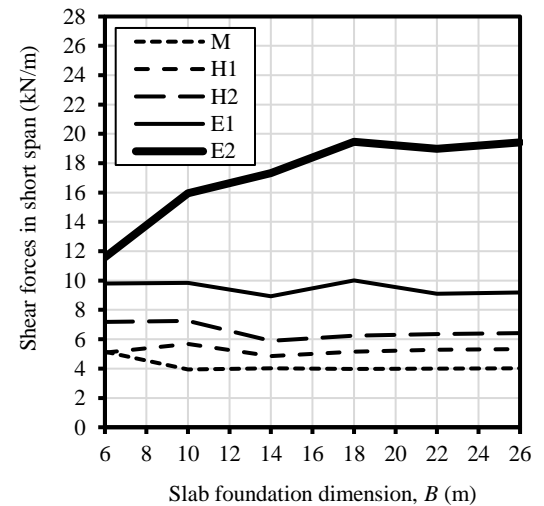
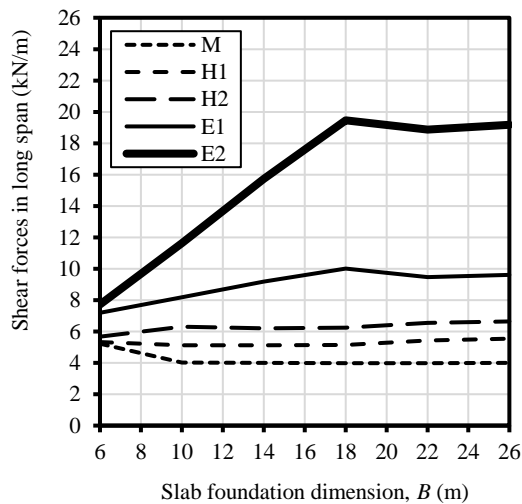
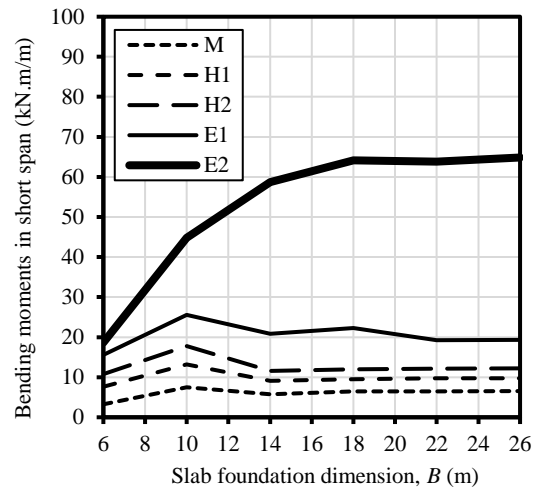
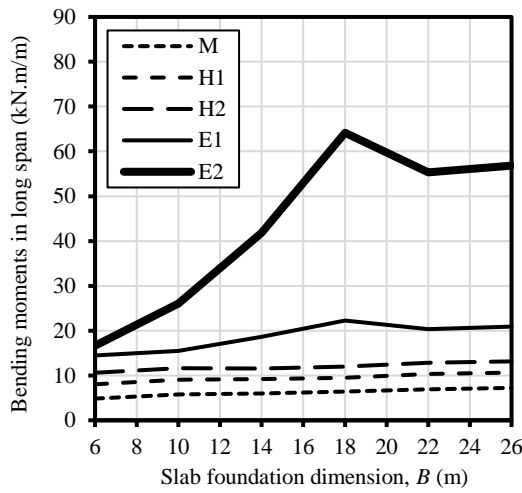
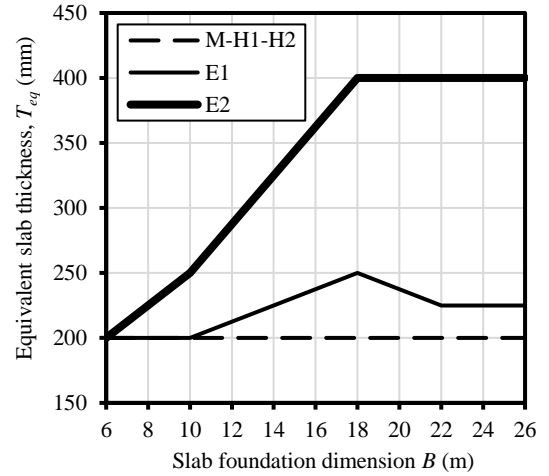


Figure B-29: $L = 18$ m, edge lift and $L_d/\Delta_{all} = 300$.

Slab foundation main span, L (m)	18.00
Edge lift scenario	EL
Span to deflection ratio (L_d/Δ_{all})	400
Service Loads:	
Internal wall loads (kPa)	2.6
Roof: 0.80 mm steel sheet (kPa)	0.1
10 mm Plasterboard (kPa)	0.083
12 mm hardwood lining	0.126
Insulation, wiring, fittings (kPa)	0.058
Flooring (13 mm clay tiling)	0.27
Permanent live load (kPa)	1.25
Total uniform load* (kPa)	4.50
Edge wall line load (kN/m)	6.00
*Without the self-weight of slab foundation	

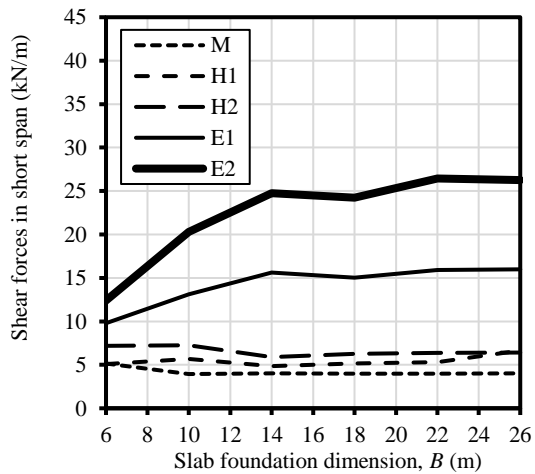
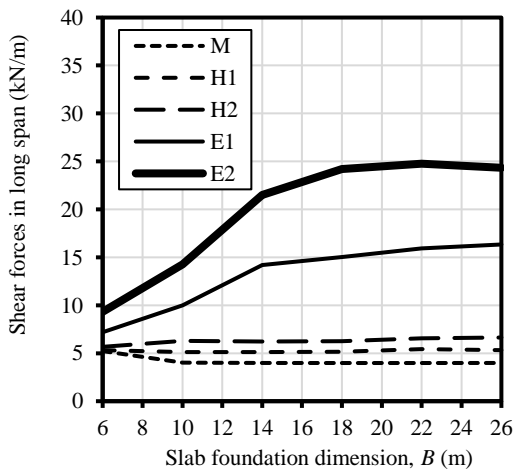
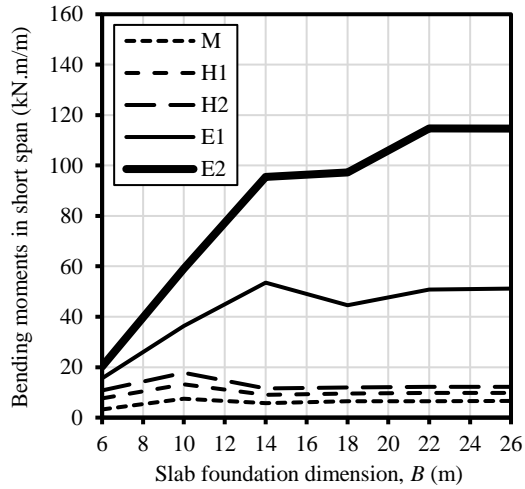
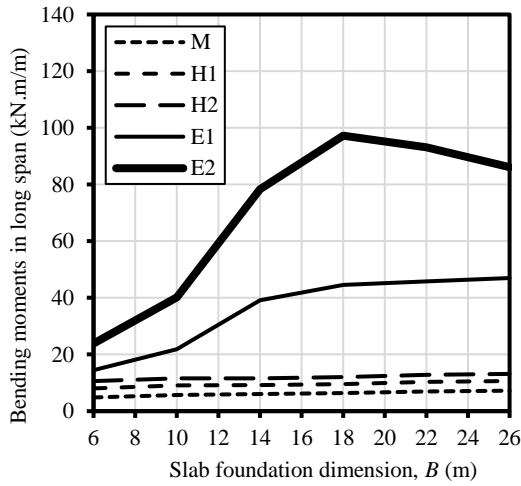
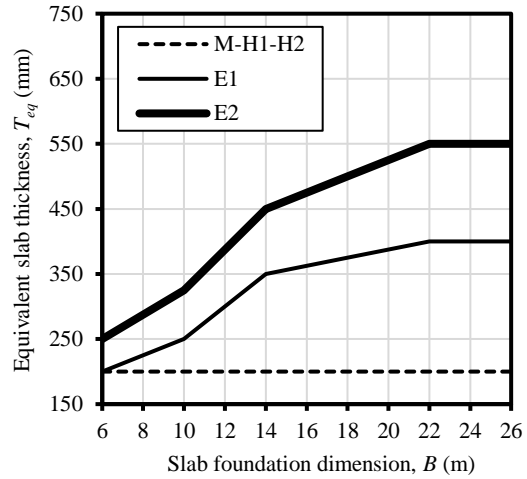


Figure B-30: $L = 18$ m, edge lift and $L_d/\Delta_{all} = 400$.

Slab foundation main span, L (m)	18.00
Edge lift scenario	EL
Span to deflection ratio (L_d/Δ_{all})	600
Service Loads:	
Internal wall loads (kPa)	2.6
Roof: 0.80 mm steel sheet (kPa)	0.1
10 mm Plasterboard (kPa)	0.083
12 mm hardwood lining	0.126
Insulation, wiring, fittings (kPa)	0.058
Flooring (13 mm clay tiling)	0.27
Permanent live load (kPa)	1.25
Total uniform load* (kPa)	4.50
Edge wall line load (kN/m)	6.00
*Without the self-weight of slab foundation	

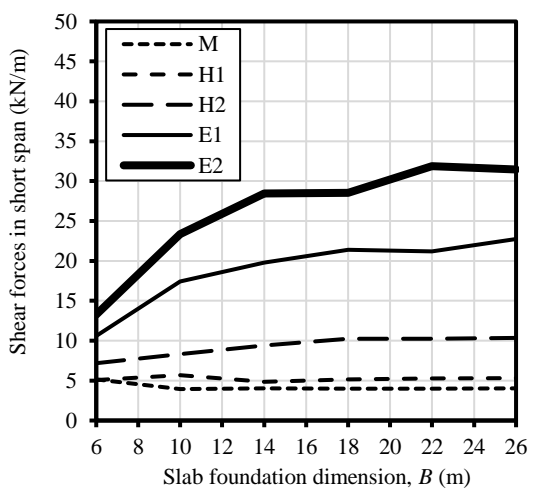
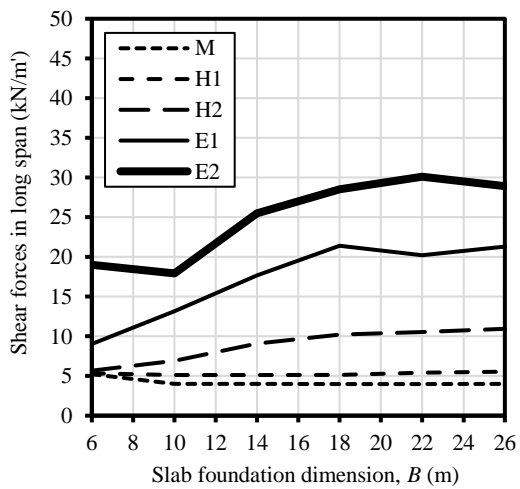
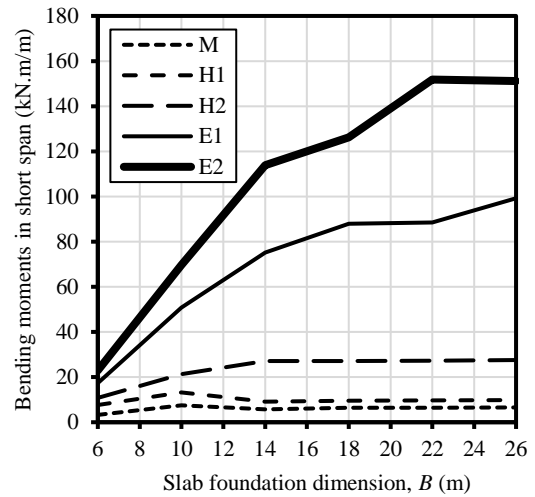
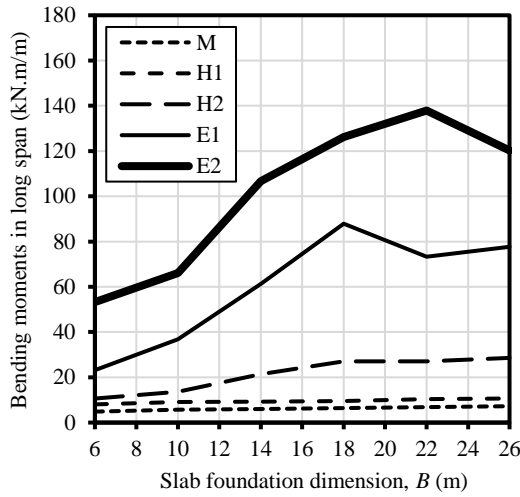
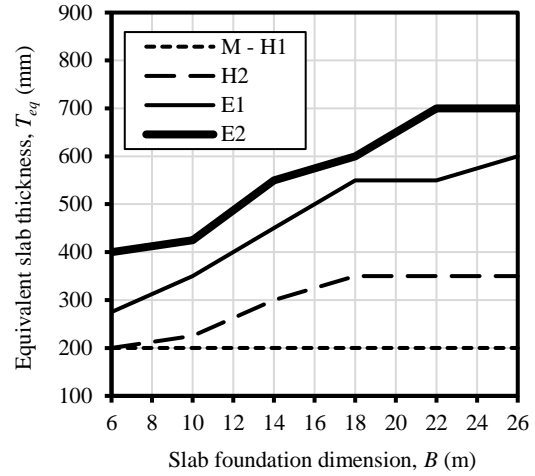


Figure B-31: $L = 18$ m, edge lift and $L_d/\Delta_{all} = 600$.

Slab foundation main span, L (m)	18.00
Edge lift scenario	EL
Span to deflection ratio (L_d/Δ_{all})	800
Service Loads:	
Internal wall loads (kPa)	2.6
Roof: 0.80 mm steel sheet (kPa)	0.1
10 mm Plasterboard (kPa)	0.083
12 mm hardwood lining	0.126
Insulation, wiring, fittings (kPa)	0.058
Flooring (13 mm clay tiling)	0.27
Permanent live load (kPa)	1.25
Total uniform load* (kPa)	4.50
Edge wall line load (kN/m)	6.00
*Without the self-weight of slab foundation	

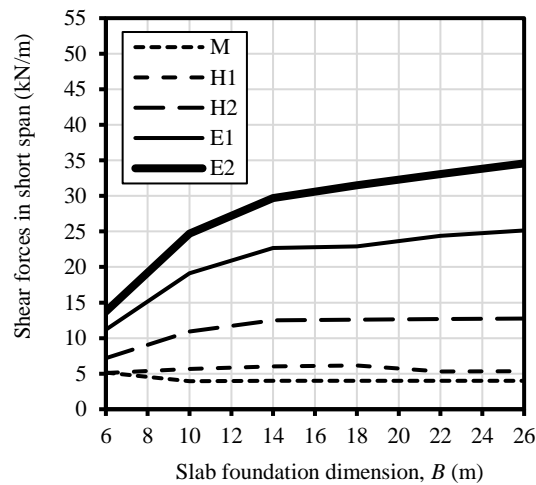
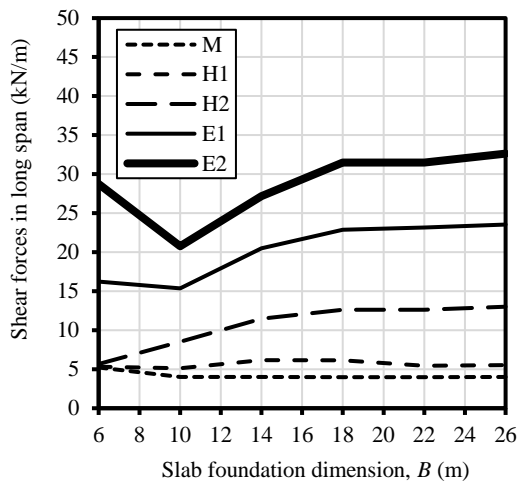
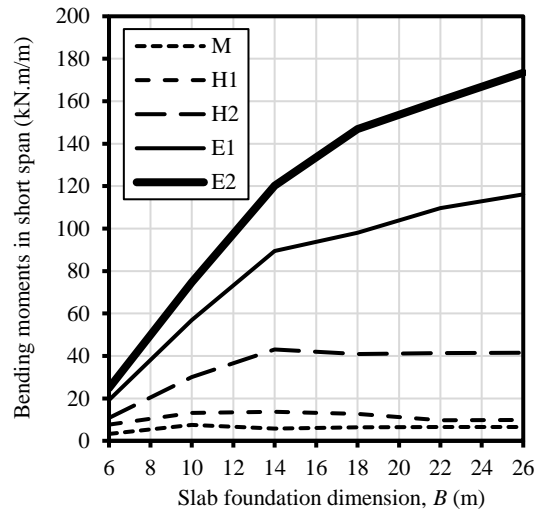
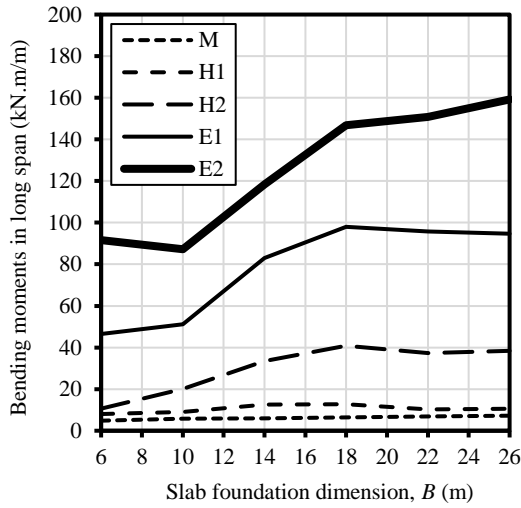
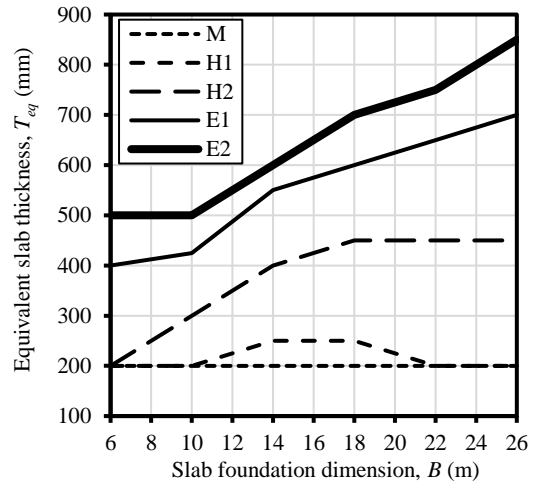


Figure B-32: $L = 18$ m, edge lift and $L_d/\Delta_{all} = 800$.

Slab foundation main span, L (m)	22.00
Edge drop scenario	ED
Span to deflection ratio (L_d/Δ_{all})	300
Service Loads:	
Internal wall loads (kPa)	2.6
Roof: 0.80 mm steel sheet (kPa)	0.1
10 mm Plasterboard (kPa)	0.083
12 mm hardwood lining	0.126
Insulation, wiring, fittings (kPa)	0.058
Flooring (13 mm clay tiling)	0.27
Permanent live load (kPa)	1.25
Total uniform load* (kPa)	4.50
Edge wall line load (kN/m)	6.00
*Without the self-weight of slab foundation	

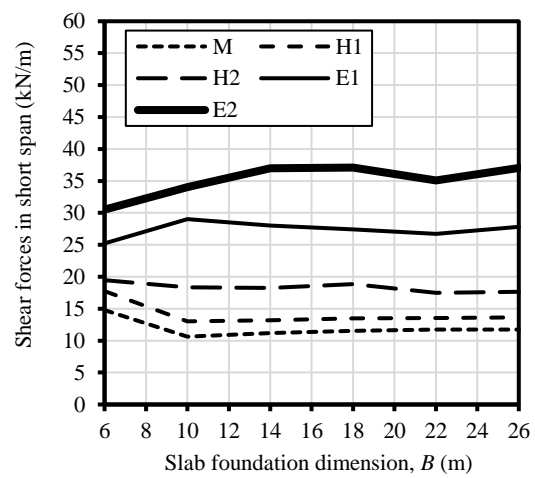
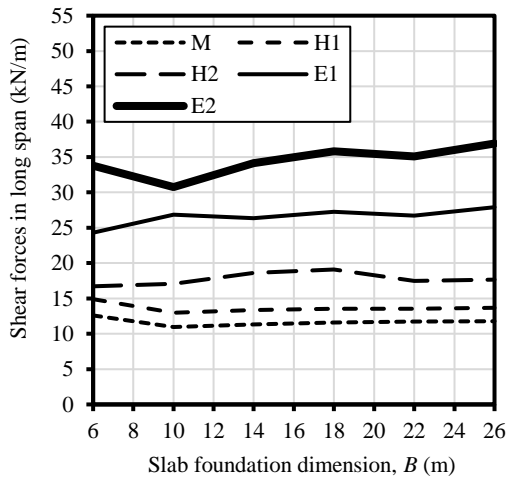
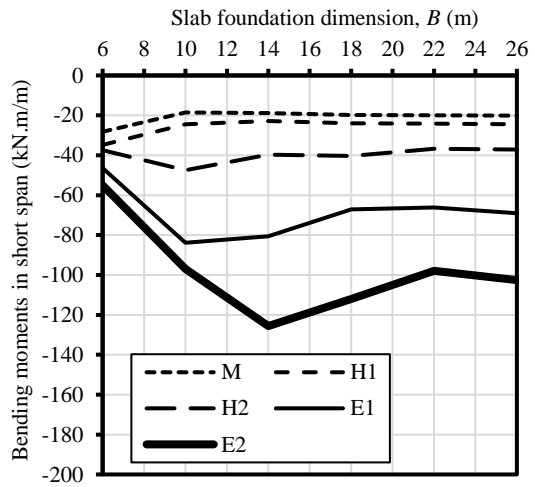
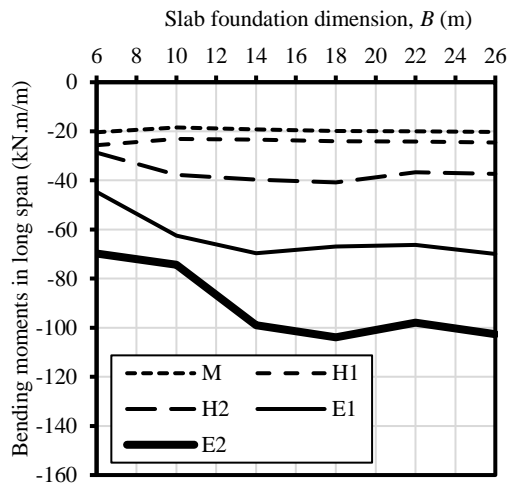
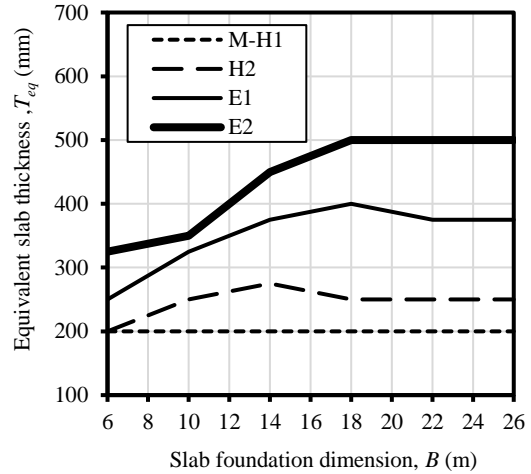


Figure B-33: $L = 22$ m, edge drop and $L_d/\Delta_{all} = 300$.

Slab foundation main span, L (m)	22.00
Edge drop scenario	ED
Span to deflection ratio (L_d/Δ_{all})	300
Service Loads:	
Internal wall loads (kPa)	2.6
Roof: 0.80 mm steel sheet (kPa)	0.1
10 mm Plasterboard (kPa)	0.083
12 mm hardwood lining	0.126
Insulation, wiring, fittings (kPa)	0.058
Flooring (13 mm clay tiling)	0.27
Permanent live load (kPa)	1.25
Total uniform load* (kPa)	4.50
Edge wall line load (kN/m)	6.00
*Without the self-weight of slab foundation	

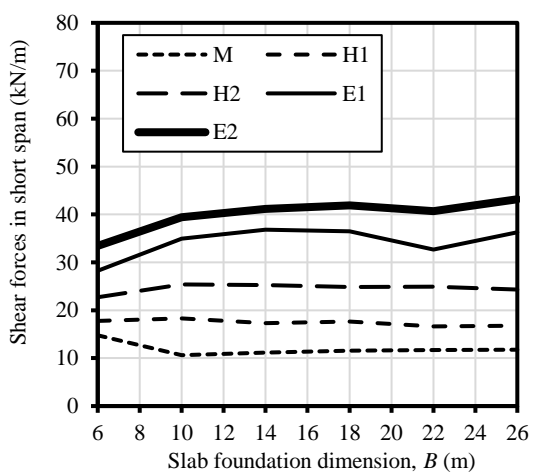
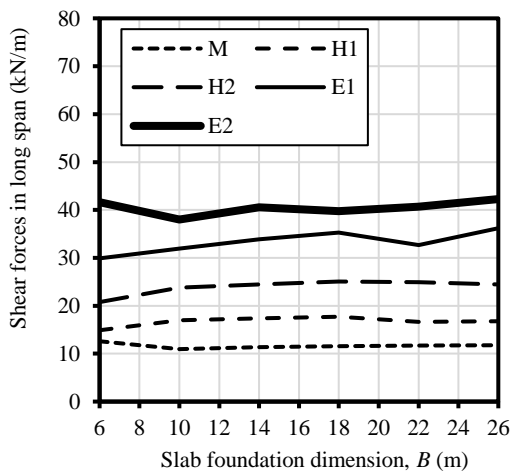
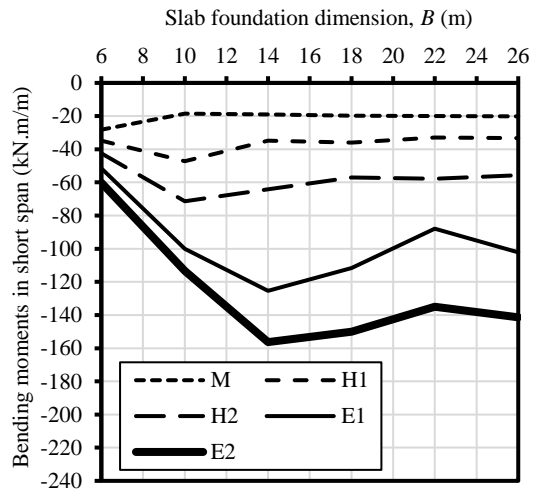
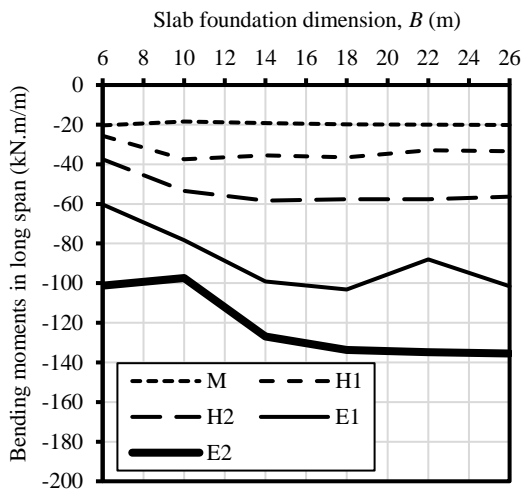
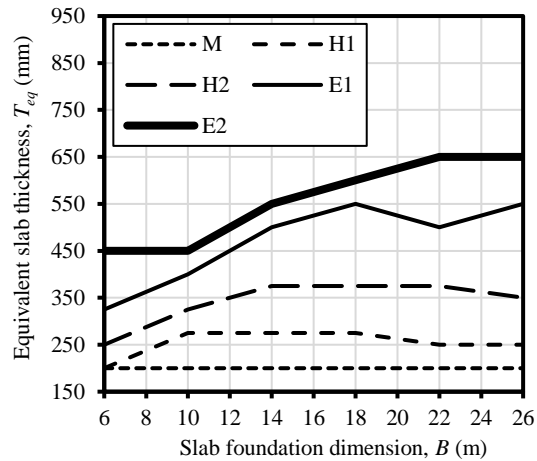


Figure B-34: $L = 22$ m, edge drop and $L_d/\Delta_{all} = 400$.

Slab foundation main span, L (m)	22.00
Edge drop scenario	ED
Span to deflection ratio (L_d/Δ_{all})	600
Service Loads:	
Internal wall loads (kPa)	2.6
Roof: 0.80 mm steel sheet (kPa)	0.1
10 mm Plasterboard (kPa)	0.083
12 mm hardwood lining	0.126
Insulation, wiring, fittings (kPa)	0.058
Flooring (13 mm clay tiling)	0.27
Permanent live load (kPa)	1.25
Total uniform load* (kPa)	4.50
Edge wall line load (kN/m)	6.00
*Without the self-weight of slab foundation	

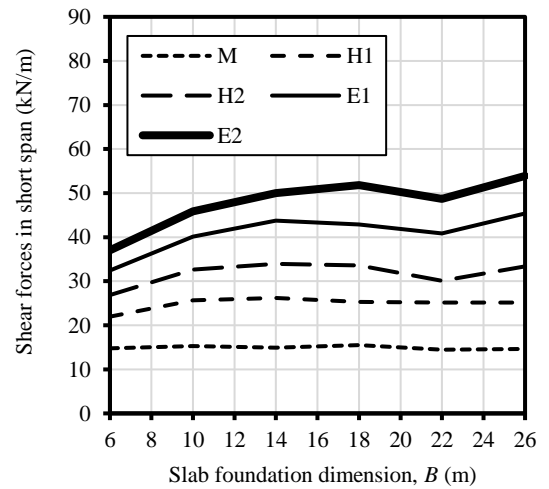
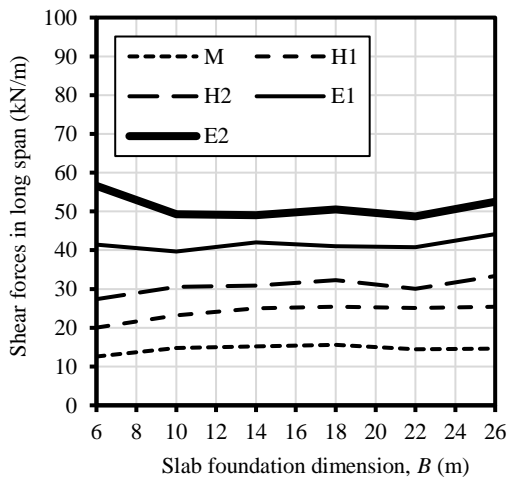
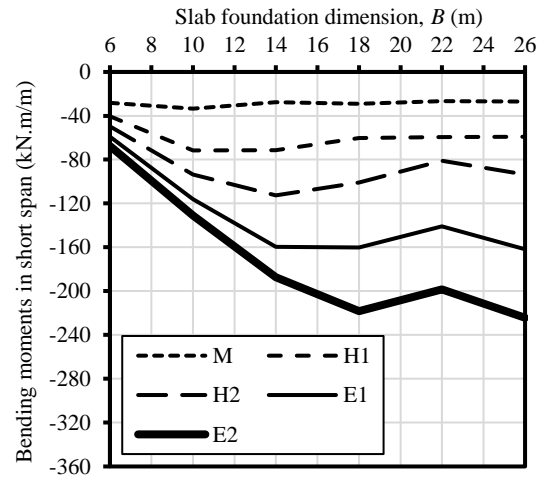
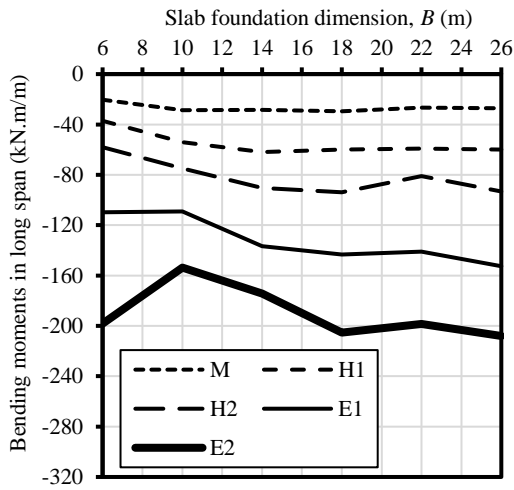
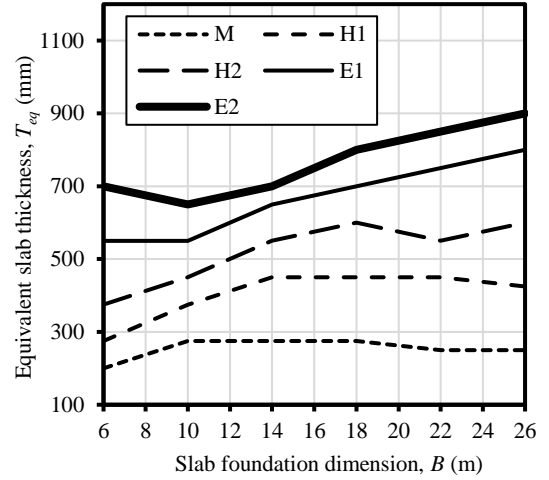


Figure B-35: $L = 22$ m, edge drop and $L_d/\Delta_{all} = 600$.

Slab foundation main span, L (m)	22.00
Edge drop scenario	ED
Span to deflection ratio (L_d/Δ_{all})	800
Service Loads:	
Internal wall loads (kPa)	2.6
Roof: 0.80 mm steel sheet (kPa)	0.1
10 mm Plasterboard (kPa)	0.083
12 mm hardwood lining	0.126
Insulation, wiring, fittings (kPa)	0.058
Flooring (13 mm clay tiling)	0.27
Permanent live load (kPa)	1.25
Total uniform load* (kPa)	4.50
Edge wall line load (kN/m)	6.00
*Without the self-weight of slab foundation	

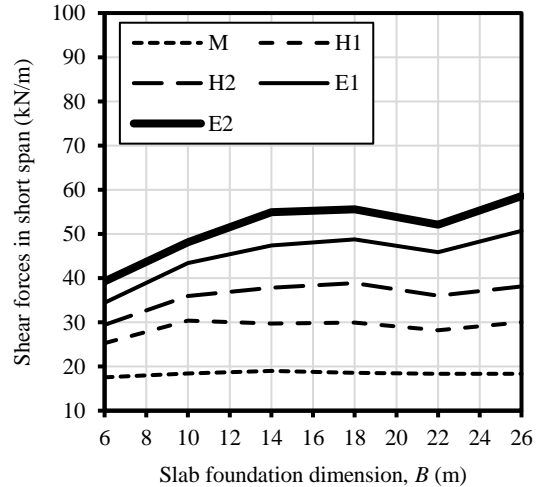
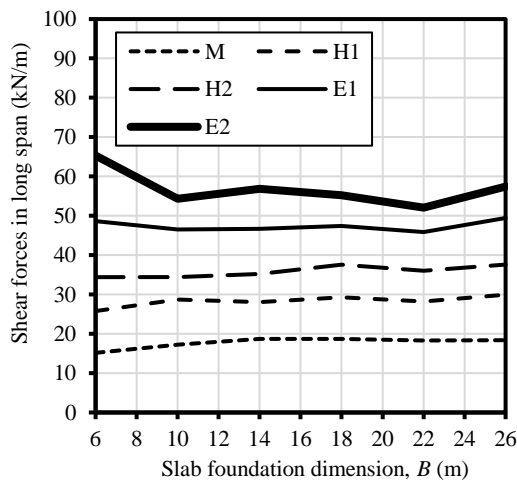
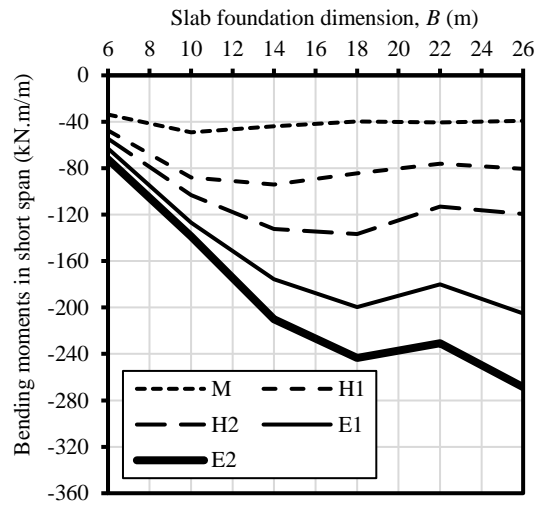
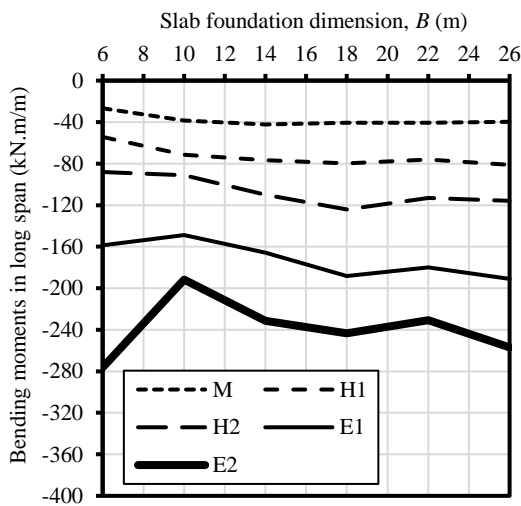
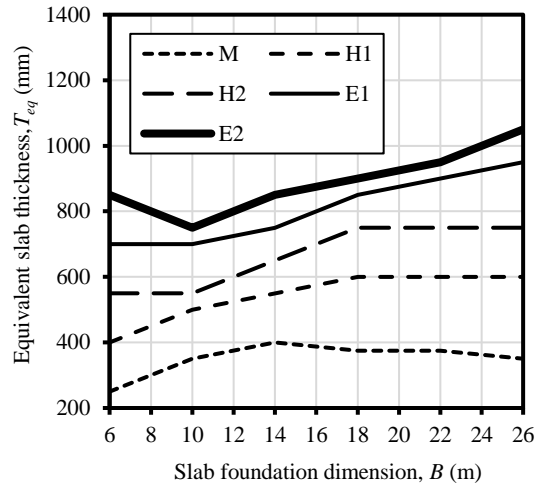


Figure B-36: $L = 22$ m, edge drop and $L_d/\Delta_{all} = 800$.

Slab foundation main span, L (m)	22.00
Edge lift scenario	EL
Span to deflection ratio (L_d/Δ_{all})	300
Service Loads:	
Internal wall loads (kPa)	2.6
Roof: 0.80 mm steel sheet (kPa)	0.1
10 mm Plasterboard (kPa)	0.083
12 mm hardwood lining	0.126
Insulation, wiring, fittings (kPa)	0.058
Flooring (13 mm clay tiling)	0.27
Permanent live load (kPa)	1.25
Total uniform load* (kPa)	4.50
Edge wall line load (kN/m)	6.00
*Without the self-weight of slab foundation	

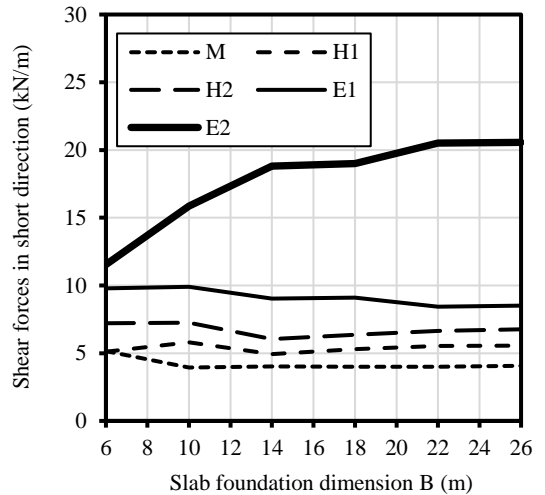
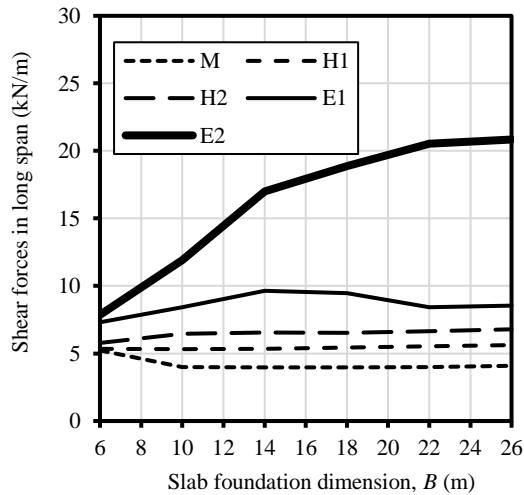
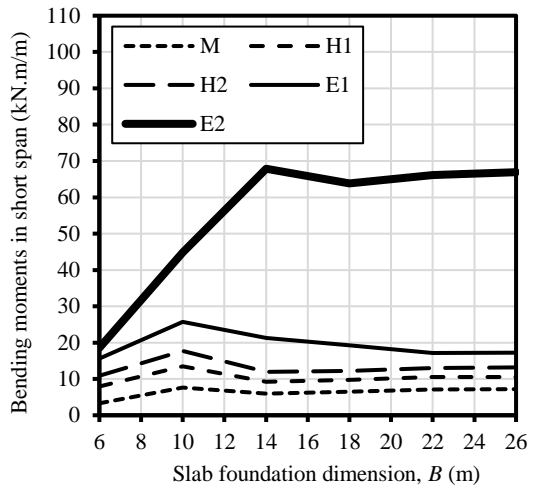
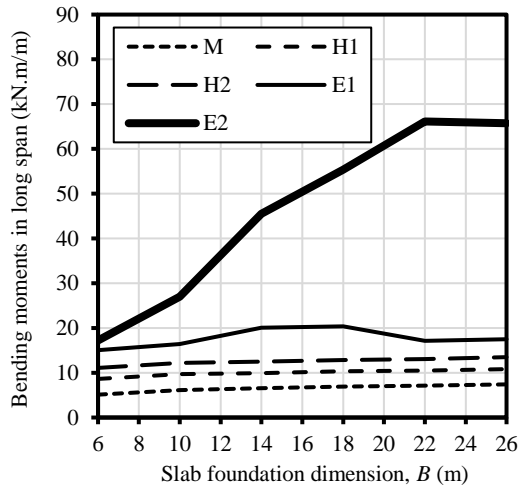
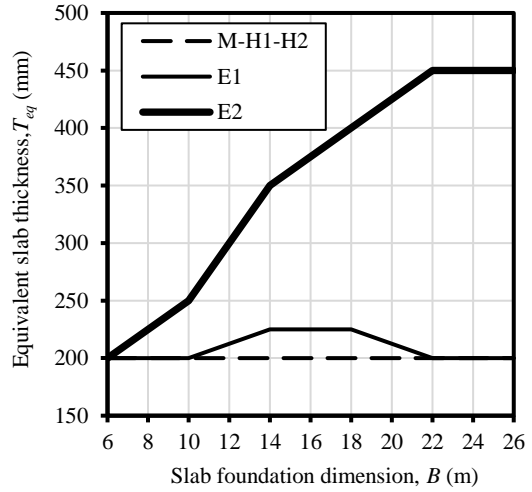


Figure B-37: $L = 22$ m, edge lift and $L_d/\Delta_{all} = 300$.

Slab foundation main span, L (m)	22.00
Edge lift scenario	EL
Span to deflection ratio (L_d/Δ_{all})	400
Service Loads:	
Internal wall loads (kPa)	2.6
Roof: 0.80 mm steel sheet (kPa)	0.1
10 mm Plasterboard (kPa)	0.083
12 mm hardwood lining	0.126
Insulation, wiring, fittings (kPa)	0.058
Flooring (13 mm clay tiling)	0.27
Permanent live load (kPa)	1.25
Total uniform load* (kPa)	4.50
Edge wall line load (kN/m')	6.00
*Without the self-weight of slab foundation	

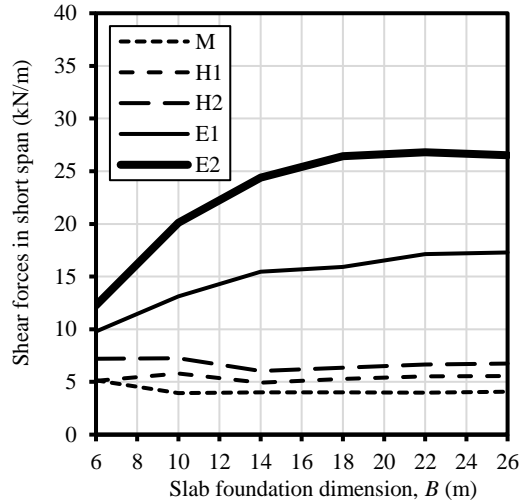
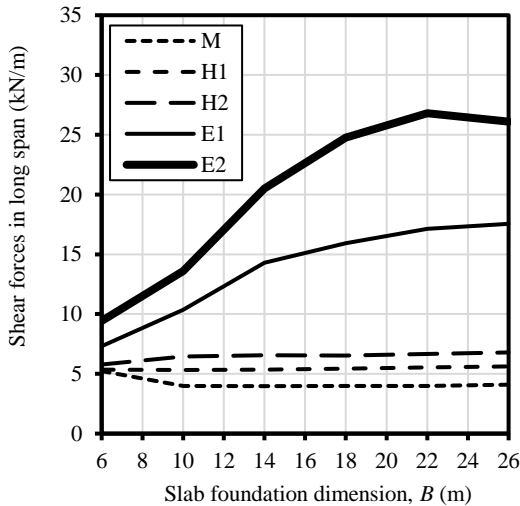
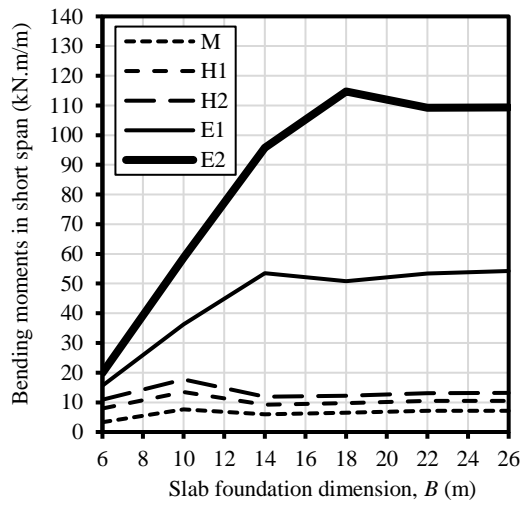
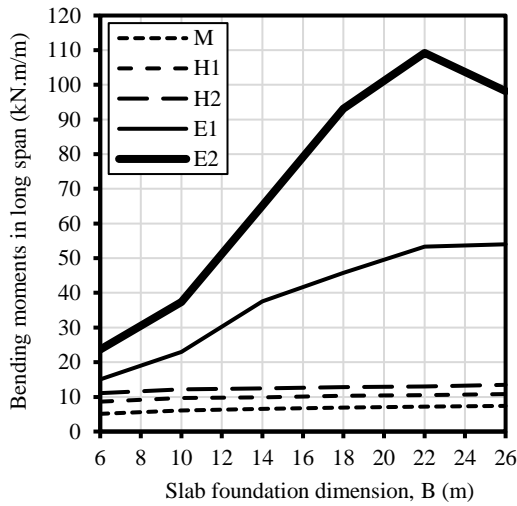
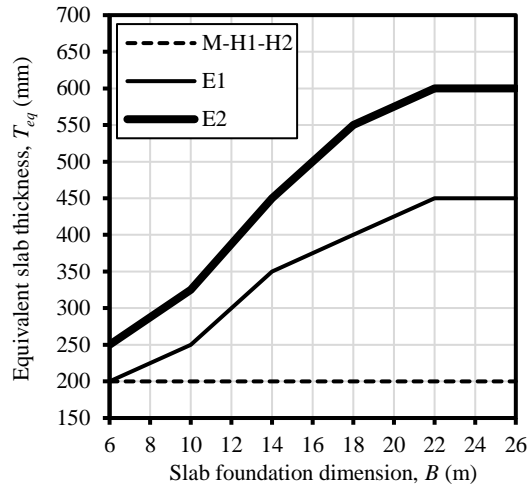


Figure B-38: $L = 22$ m, edge lift and $L_d/\Delta_{all} = 400$.

Slab foundation main span, L (m)	22.00
Edge lift scenario	EL
Span to deflection ratio (L_d/Δ_{all})	600
Service Loads:	
Internal wall loads (kPa)	2.6
Roof: 0.80 mm steel sheet (kPa)	0.1
10 mm Plasterboard (kPa)	0.083
12 mm hardwood lining	0.126
Insulation, wiring, fittings (kPa)	0.058
Flooring (13 mm clay tiling)	0.27
Permanent live load (kPa)	1.25
Total uniform load* (kPa)	4.50
Edge wall line load (kN/m)	6.00
*Without the self-weight of slab foundation	

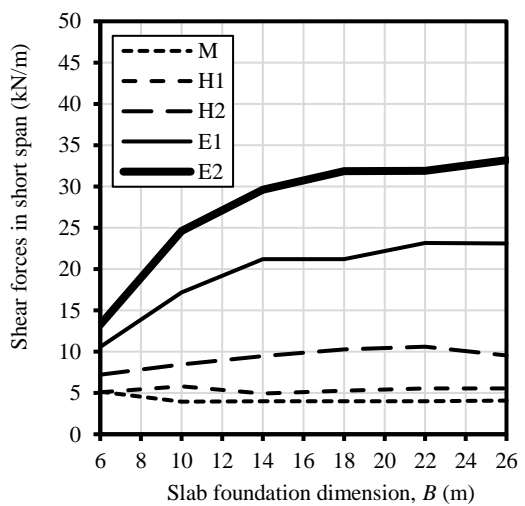
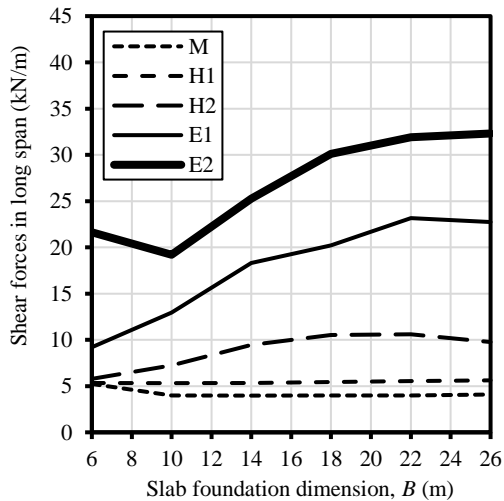
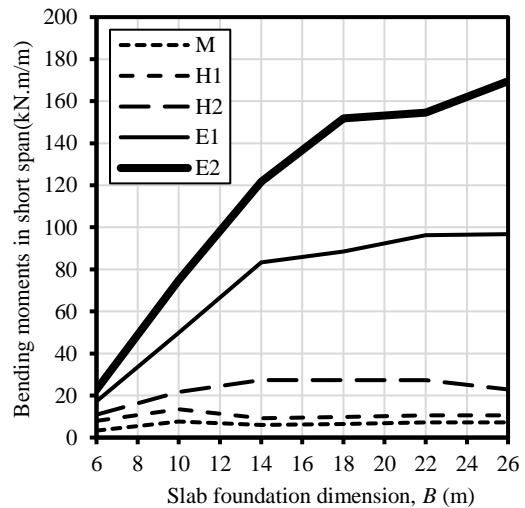
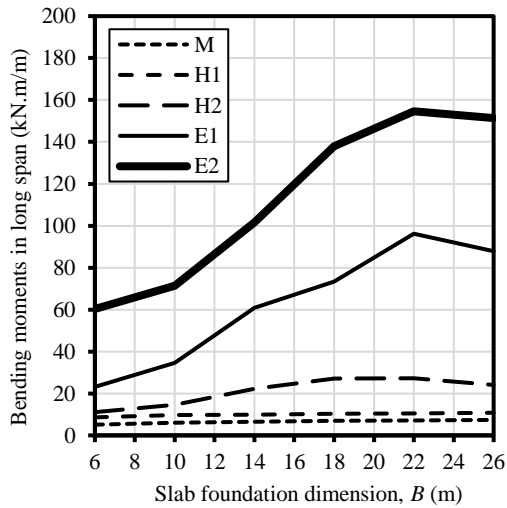
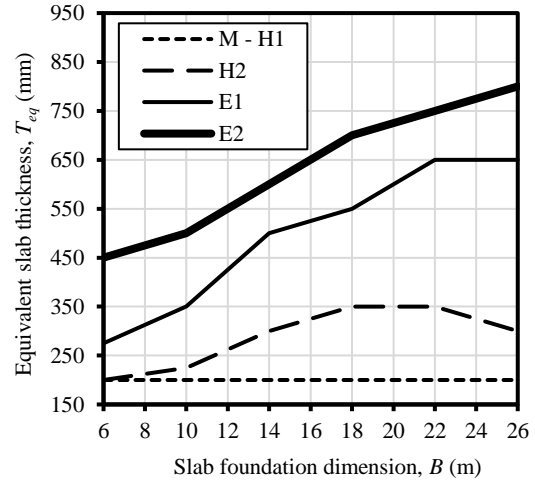


Figure B-39: $L = 22$ m, edge lift and $L_d/\Delta_{all} = 600$.

Slab foundation main span, L (m)	22.00
Edge lift scenario	EL
Span to deflection ratio (L_d/Δ_{all})	800
Service Loads:	
Internal wall loads (kPa)	2.6
Roof: 0.80 mm steel sheet (kPa)	0.1
10 mm Plasterboard (kPa)	0.083
12 mm hardwood lining	0.126
Insulation, wiring, fittings (kPa)	0.058
Flooring (13 mm clay tiling)	0.27
Permanent live load (kPa)	1.25
Total uniform load* (kPa)	4.50
Edge wall line load (kN/m)	6.00
*Without the self-weight of slab foundation	

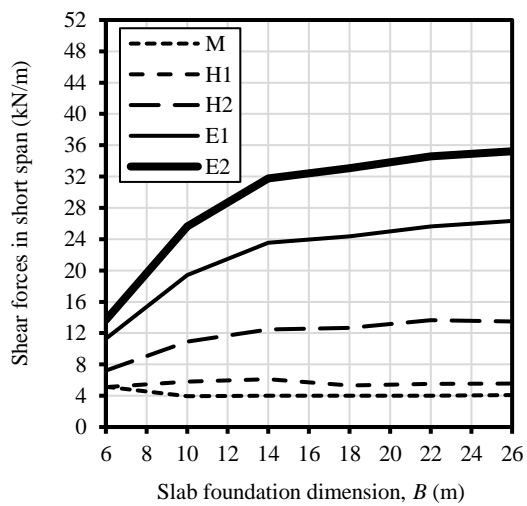
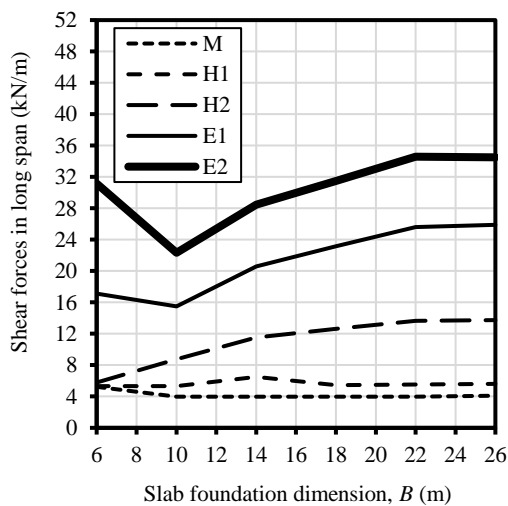
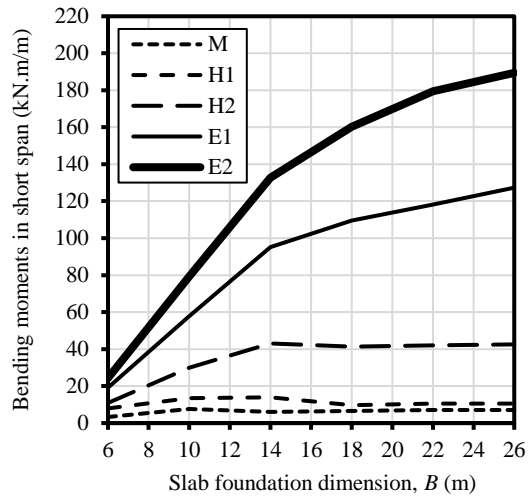
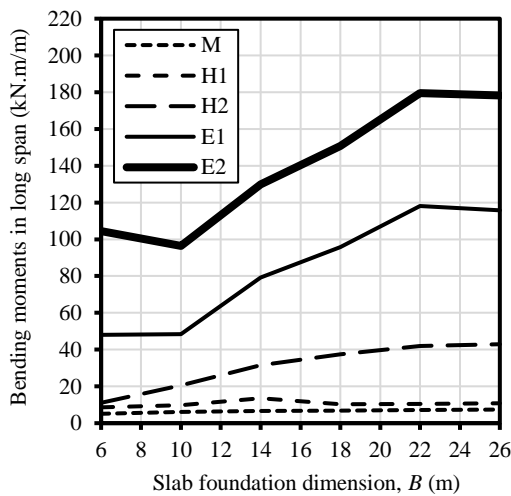
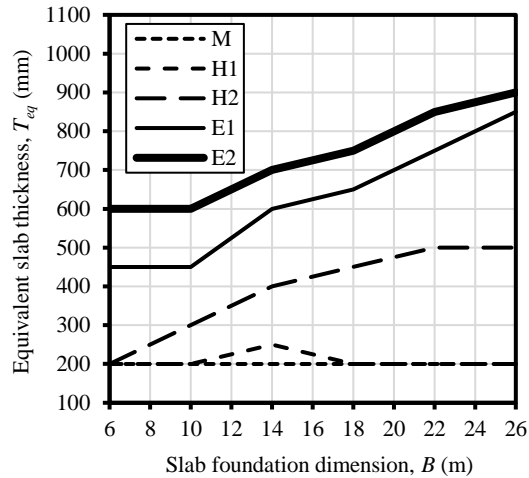


Figure B-40: $L = 22$ m, edge lift and $L_d/\Delta_{all} = 800$.

Slab foundation main span, L (m)	26.00
Edge lift scenario	ED
Span to deflection ratio (L_d/Δ_{all})	300
Service Loads:	
Internal wall loads (kPa)	2.6
Roof: 0.80 mm steel sheet (kPa)	0.1
10 mm Plasterboard (kPa)	0.083
12 mm hardwood lining	0.126
Insulation, wiring, fittings (kPa)	0.058
Flooring (13 mm clay tiling)	0.27
Permanent live load (kPa)	1.25
Total uniform load* (kPa)	4.50
Edge wall line load (kN/m)	6.00
*Without the self-weight of slab foundation	

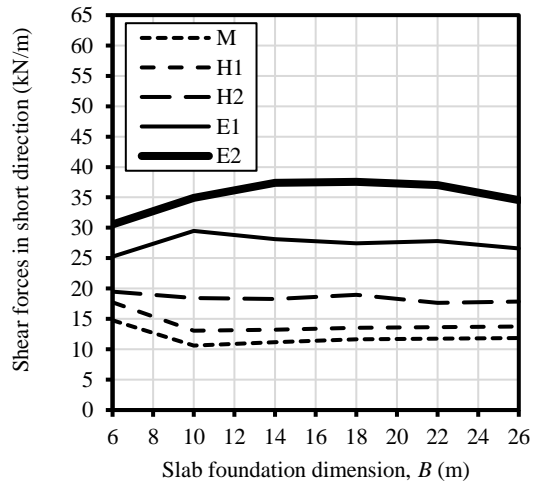
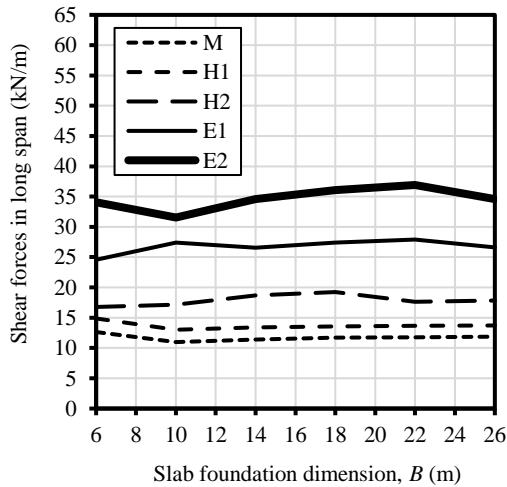
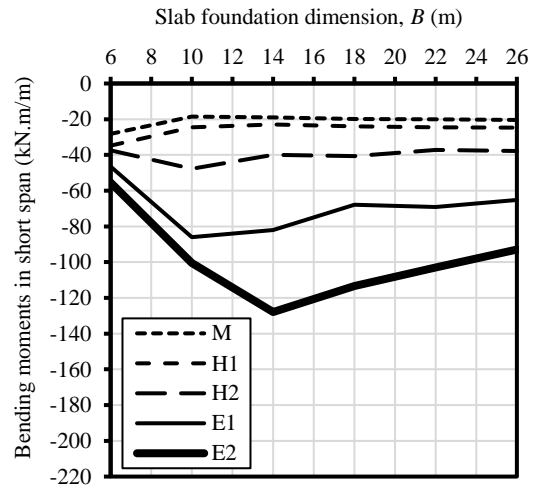
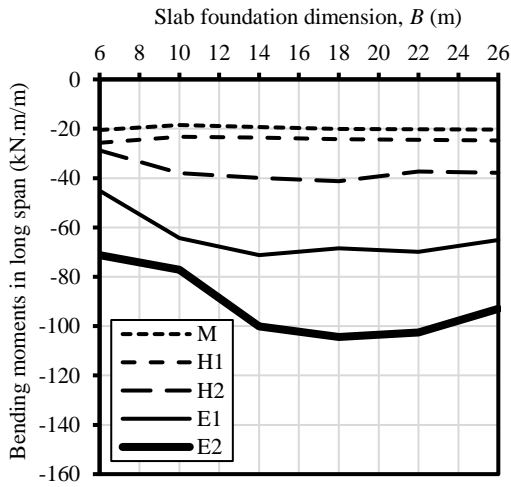
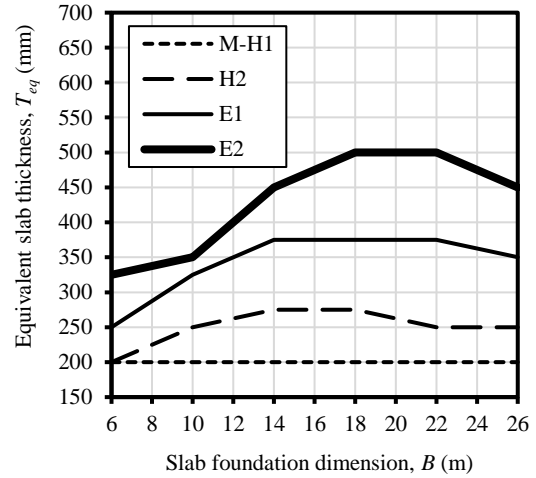


Figure B-41: $L = 26$ m, edge drop and $L_d/\Delta_{all} = 300$.

Slab foundation main span, L (m)	26.00
Edge lift scenario	ED
Span to deflection ratio (L_d/Δ_{all})	400
Service Loads:	
Internal wall loads (kPa)	2.6
Roof: 0.80 mm steel sheet (kPa)	0.1
10 mm Plasterboard (kPa)	0.083
12 mm hardwood lining	0.126
Insulation, wiring, fittings (kPa)	0.058
Flooring (13 mm clay tiling)	0.27
Permanent live load (kPa)	1.25
Total uniform load* (kPa)	4.50
Edge wall line load (kN/m)	6.00
*Without the self-weight of slab foundation	

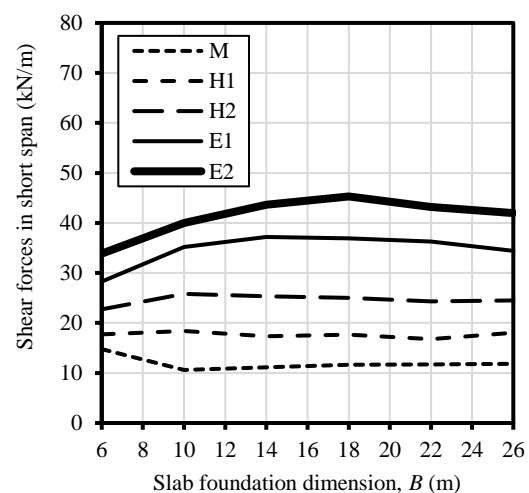
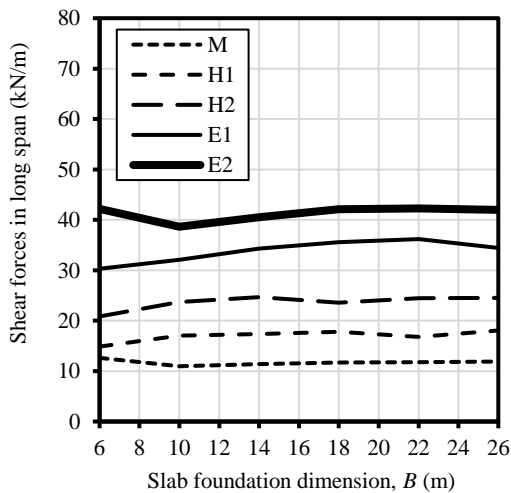
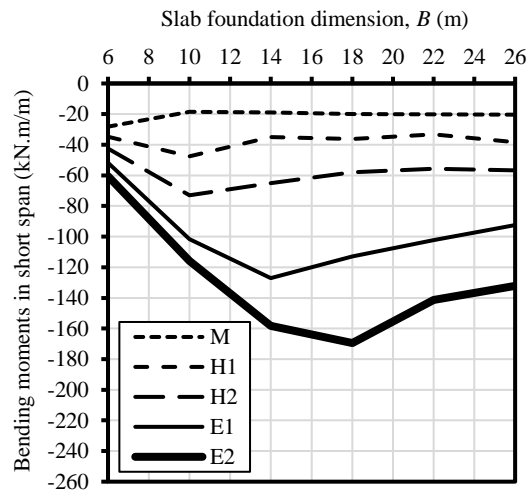
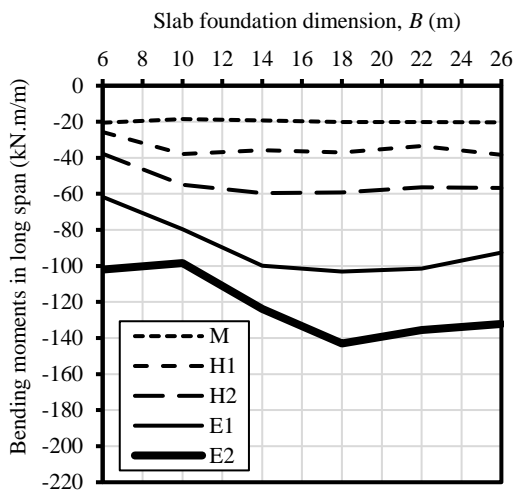
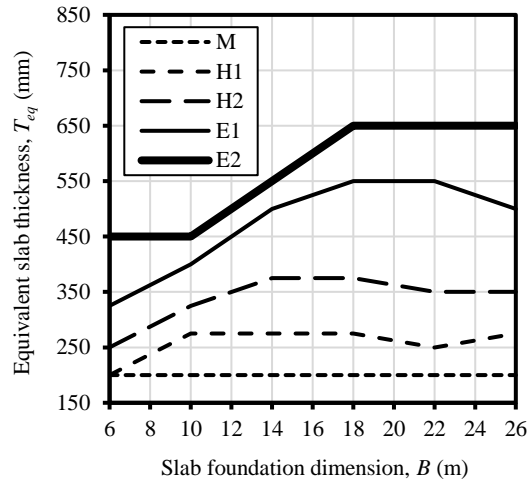


Figure B-42: $L = 26$ m, edge drop and $L_d/\Delta_{all} = 400$.

Slab foundation main span, L (m)	26.00
Edge lift scenario	ED
Span to deflection ratio (L_d/Δ_{all})	600
Service Loads:	
Internal wall loads (kPa)	2.6
Roof: 0.80 mm steel sheet (kPa)	0.1
10 mm Plasterboard (kPa)	0.083
12 mm hardwood lining	0.126
Insulation, wiring, fittings (kPa)	0.058
Flooring (13 mm clay tiling)	0.27
Permanent live load (kPa)	1.25
Total uniform load* (kPa)	4.50
Edge wall line load (kN/m)	6.00
*Without the self-weight of slab foundation	

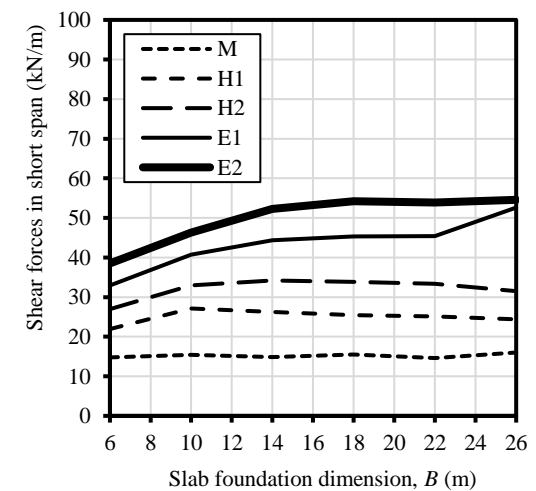
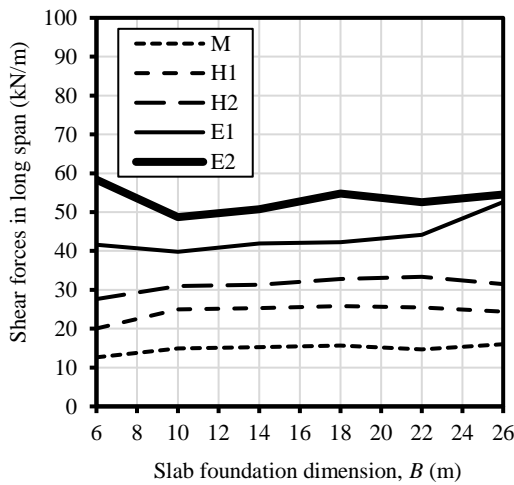
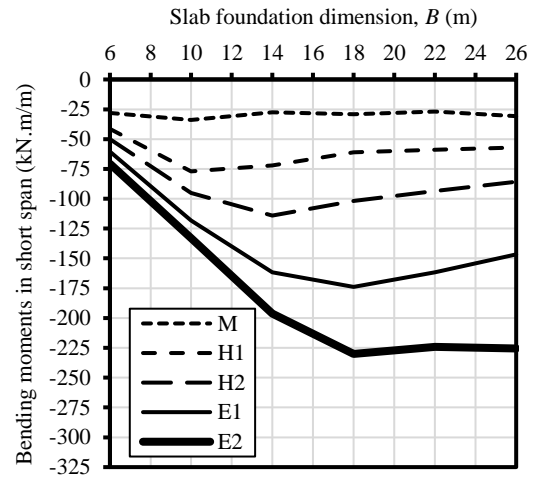
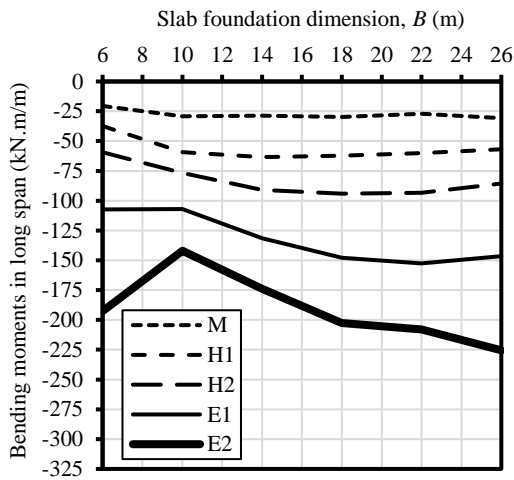
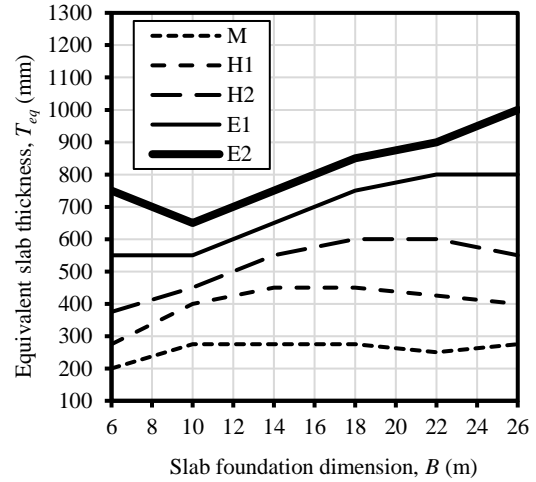


Figure B-43: $L = 26$ m, edge drop and $L_d/\Delta_{all} = 600$.

Slab foundation main span, L (m)	26.00
Edge lift scenario	ED
Span to deflection ratio (L_d/Δ_{all})	800
Service Loads:	
Internal wall loads (kPa)	2.6
Roof: 0.80 mm steel sheet (kPa)	0.1
10 mm Plasterboard (kPa)	0.083
12 mm hardwood lining	0.126
Insulation, wiring, fittings (kPa)	0.058
Flooring (13 mm clay tiling)	0.27
Permanent live load (kPa)	1.25
Total uniform load* (kPa)	4.50
Edge wall line load (kN/m)	6.00
*Without the self-weight of slab foundation	

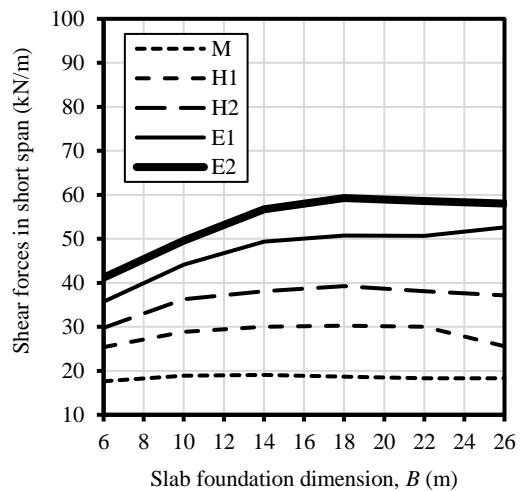
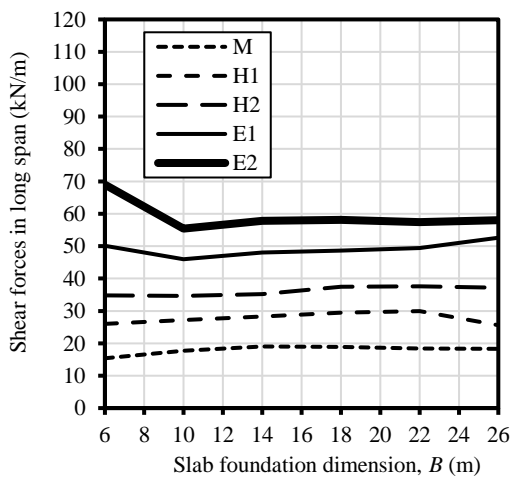
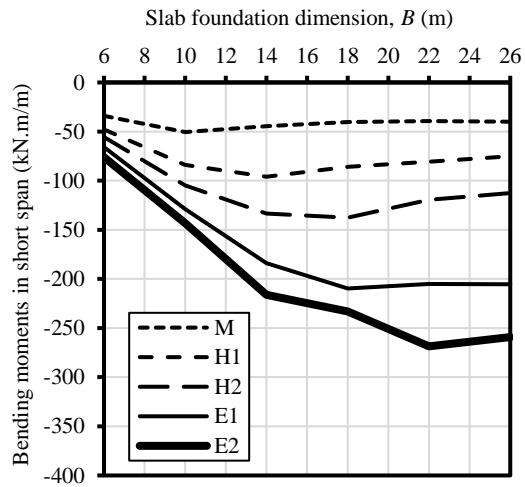
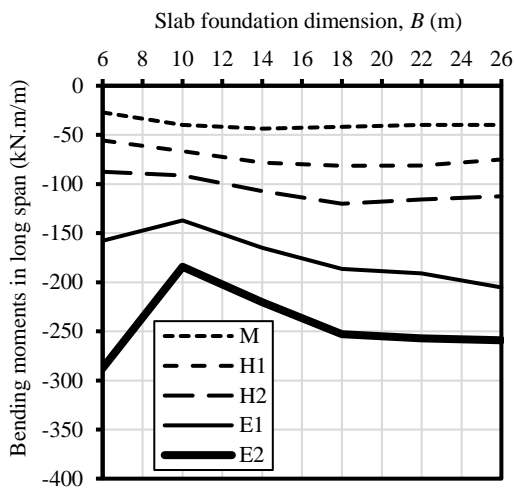
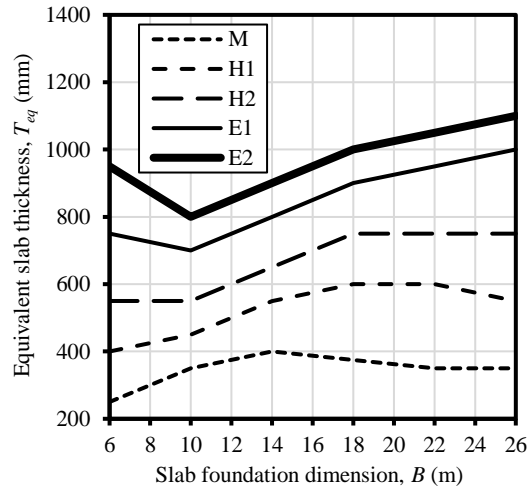


Figure B-44: $L = 26$ m, edge drop and $L_d/\Delta_{all} = 800$.

Slab foundation main span, L (m)	26.00
Edge lift scenario	EL
Span to deflection ratio (L_d/Δ_{all})	300
Service Loads:	
Internal wall loads (kPa)	2.6
Roof: 0.80 mm steel sheet (kPa)	0.1
10 mm Plasterboard (kPa)	0.083
12 mm hardwood lining	0.126
Insulation, wiring, fittings (kPa)	0.058
Flooring (13 mm clay tiling)	0.27
Permanent live load (kPa)	1.25
Total uniform load* (kPa)	4.50
Edge wall line load (kN/m)	6.00
*Without the self-weight of slab foundation	

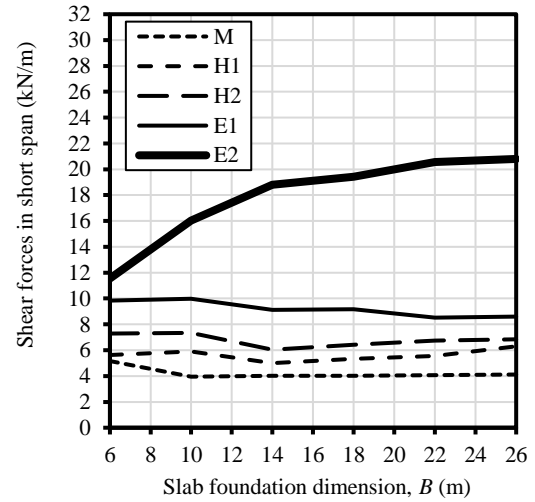
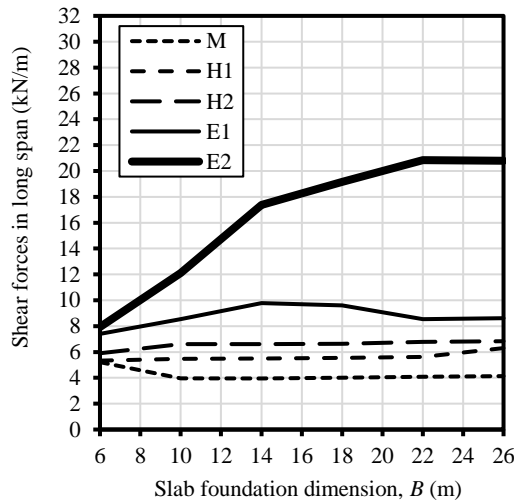
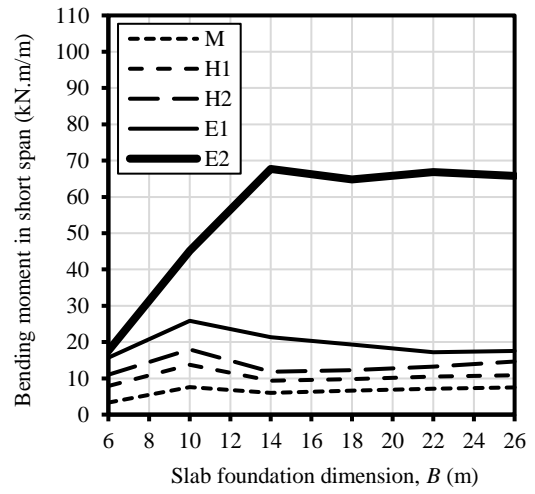
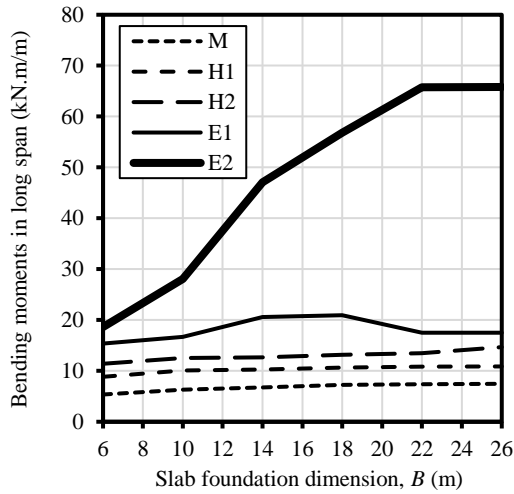
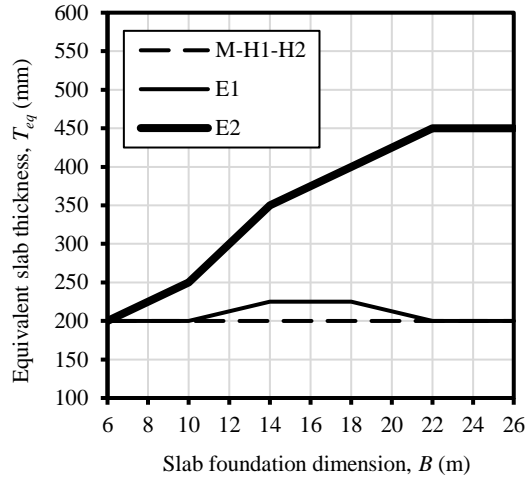


Figure B-45: $L = 26$ m, edge lift and $L_d/\Delta_{all} = 300$.

Slab foundation main span, L (m)	26.00
Edge lift scenario	EL
Span to deflection ratio (L_d/Δ_{all})	400
Service Loads:	
Internal wall loads (kPa)	2.6
Roof: 0.80 mm steel sheet (kPa)	0.1
10 mm Plasterboard (kPa)	0.083
12 mm hardwood lining	0.126
Insulation, wiring, fittings (kPa)	0.058
Flooring (13 mm clay tiling)	0.27
Permanent live load (kPa)	1.25
Total uniform load* (kPa)	4.50
Edge wall line load (kN/m)	6.00
*Without the self-weight of slab foundation	

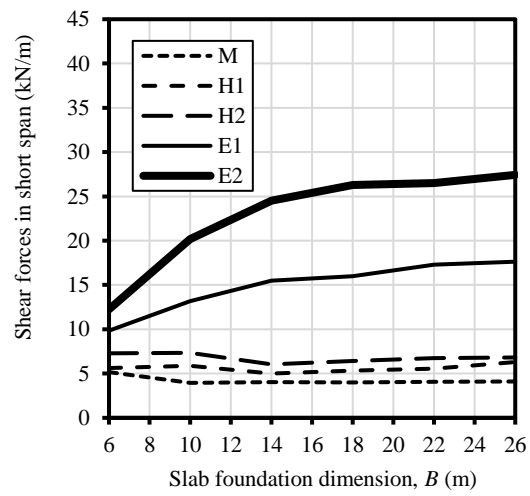
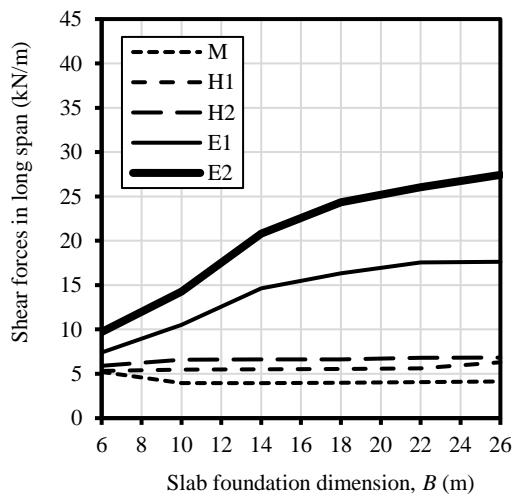
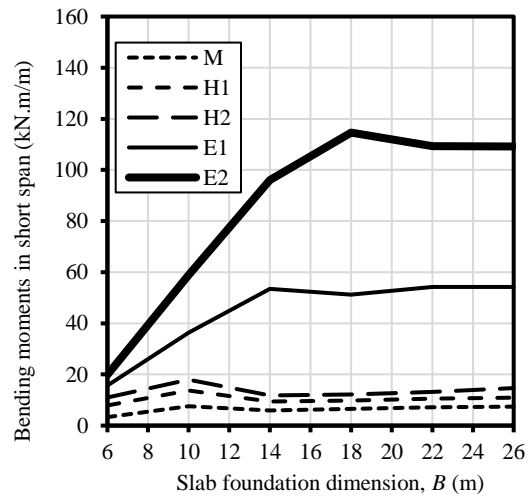
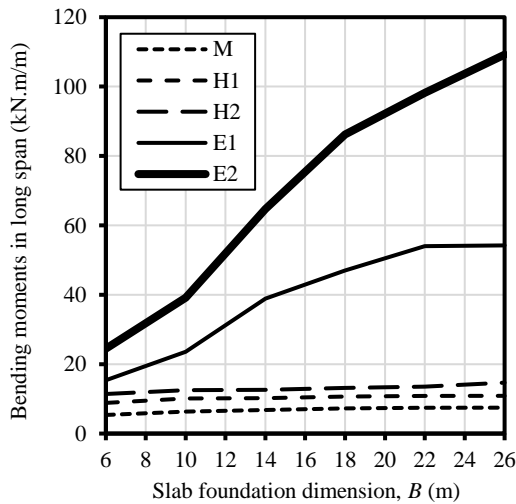
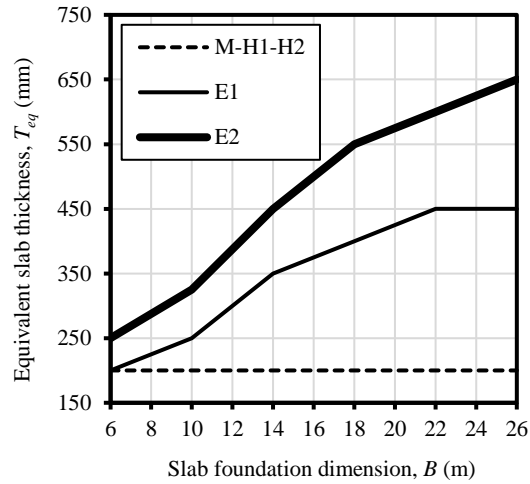


Figure B-46: $L = 26$ m, edge lift and $L_d/\Delta_{all} = 400$.

Slab foundation main span, L (m)	26.00
Edge lift scenario	EL
Span to deflection ratio (L_d/Δ_{all})	600
Service Loads:	
Internal wall loads (kPa)	2.6
Roof: 0.80 mm steel sheet (kPa)	0.1
10 mm Plasterboard (kPa)	0.083
12 mm hardwood lining	0.126
Insulation, wiring, fittings (kPa)	0.058
Flooring (13 mm clay tiling)	0.27
Permanent live load (kPa)	1.25
Total uniform load* (kPa)	4.50
Edge wall line load (kN/m)	6.00
*Without the self-weight of slab foundation	

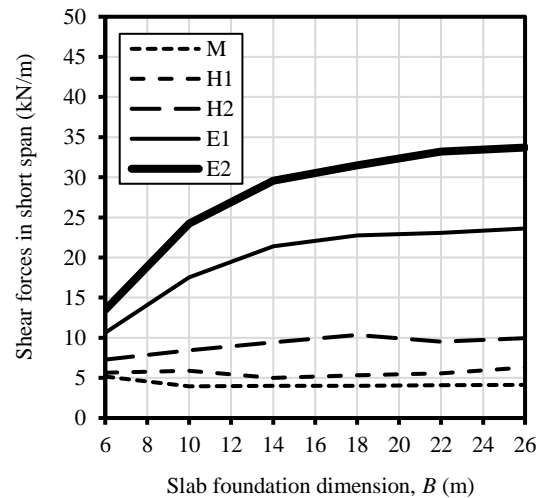
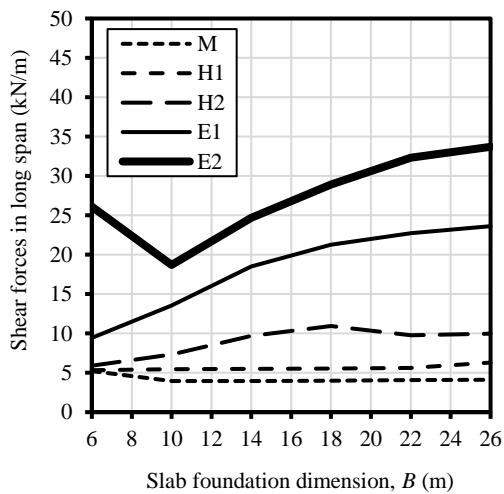
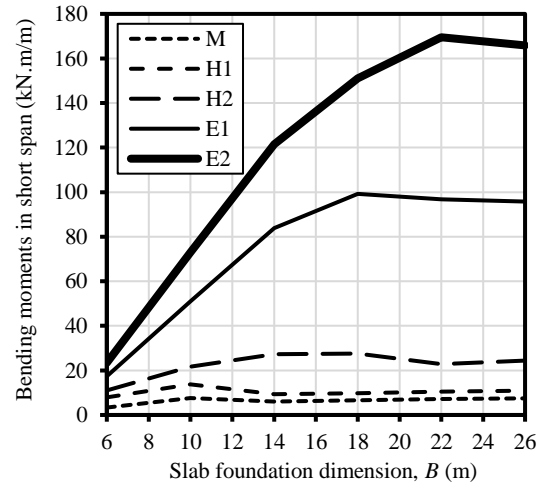
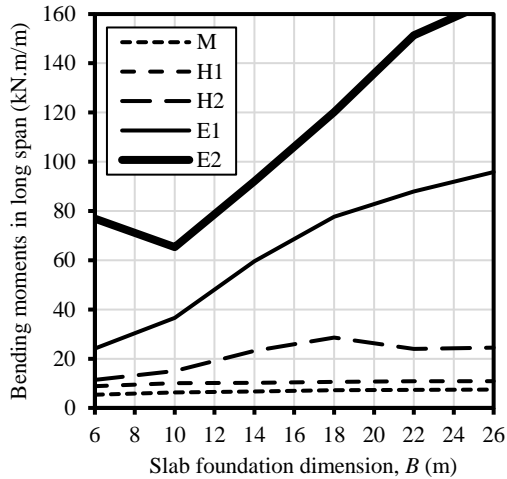
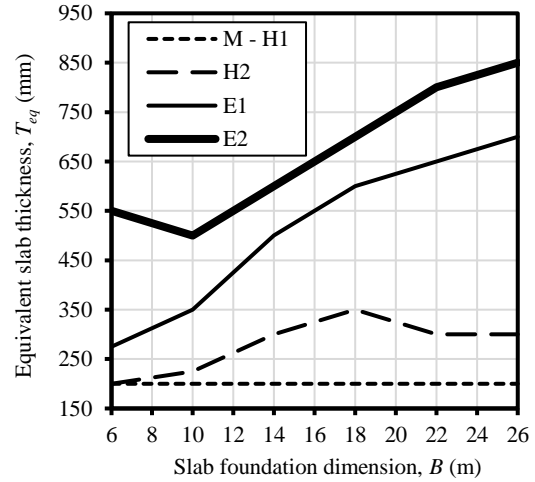


Figure B-47: $L = 26$ m, edge lift and $L_d/\Delta_{all} = 600$.

Slab foundation main span, L (m)	26.00
Edge lift scenario	EL
Span to deflection ratio (L_d/Δ_{all})	800
Service Loads:	
Internal wall loads (kPa)	2.6
Roof: 0.80 mm steel sheet (kPa)	0.1
10 mm Plasterboard (kPa)	0.083
12 mm hardwood lining	0.126
Insulation, wiring, fittings (kPa)	0.058
Flooring (13 mm clay tiling)	0.27
Permanent live load (kPa)	1.25
Total uniform load* (kPa)	4.50
Edge wall line load (kN/m)	6.00
*Without the self-weight of slab foundation	

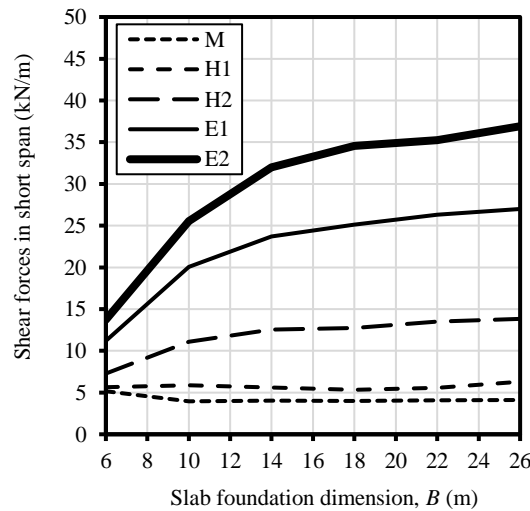
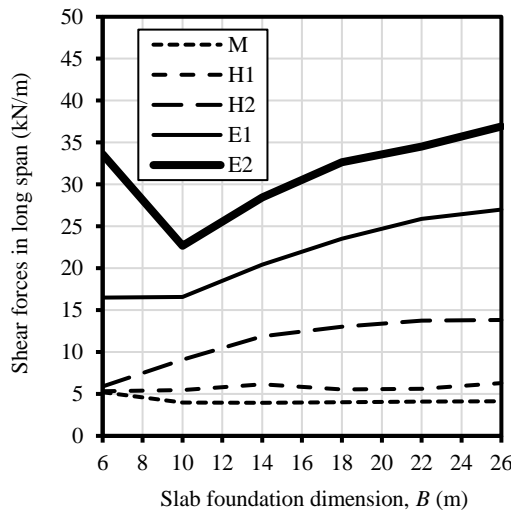
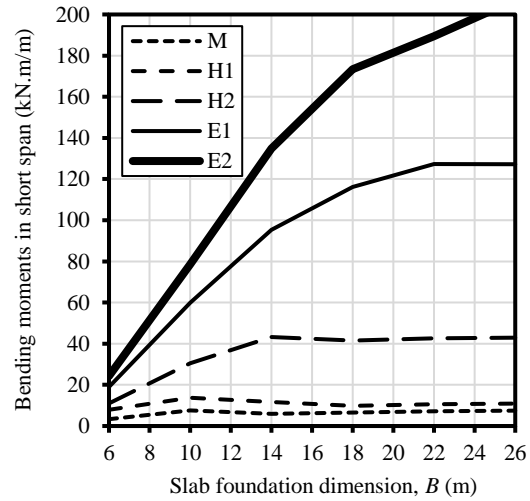
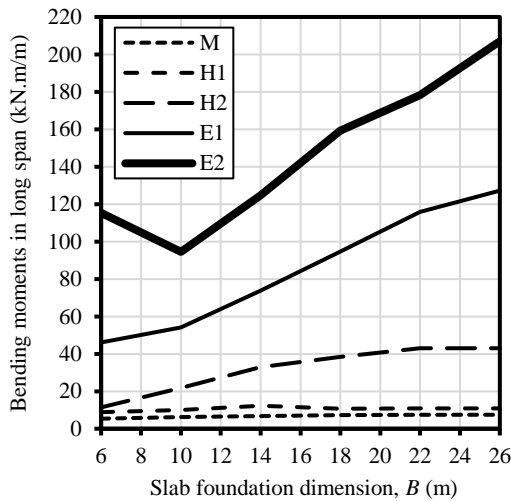
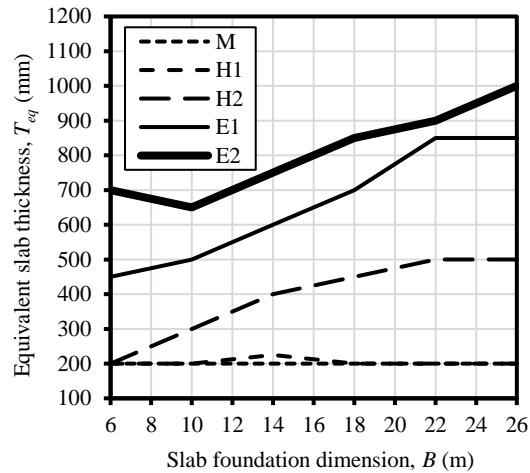





Figure B-48: $L = 26$ m, edge lift and $L_d/\Delta_{all} = 800$.

APPENDIX C: COPYRIGHT HOLDERS PERMISSION STATEMENTS

 Reply all |   Delete Junk |  ...

RE: Permission request

BL Barry Lehane <barry.lehane@uwa.edu.au>   Reply all | 
Yesterday, 8:50 AM
ANZ Geomechanics 2019 <anzgeomechanics2019@arinex.com.au>; Mohamed Shazwan <shazwan@arinex.com.au>

Inbox

You replied on 2/14/2019 5:56 AM.

Hi Steph/Mohamed

There are no copyright issues with these proceedings.

Mohamed, you would clearly need to refer to the source reference when re-printing these figures.

Regards

Barry

Prof. Barry Lehane

Winthrop Professor of Geotechnical Engineering

Department of Civil, Environmental and Mining Engineering, Rm. 2.76A

Faculty of Engineering and Mathematical Sciences • M021, Perth WA 6009 Australia

T +61 8 6488 2417 • M +614 26210262 • E Barry.Lehane@uwa.edu.au



From: ANZ Geomechanics 2019 [mailto:anzgeomechanics2019@arinex.com.au]

Sent: Tuesday, 12 February 2019 5:25 PM

To: Barry Lehane <barry.lehane@uwa.edu.au>

Subject: FW: Permission request

Hi Barry,

Kel & I are stuck on the below delegates request – Do you understand?

Thanks,
Steph

 Reply all |   Delete Junk |  

Sinha, J., and Poulos, H. G. (1996). "Behaviour of stiffened raft foundations.", *7th Australia New Zealand Conference on Geomechanics: Geomechanics in a Changing World*, Institution of Engineers, Australia, Barton, ACT, 704-709.

I have contacted Engineers Australia first for it looks like they are holding the copyrights of the paper but they asked me to contact you.

The figures will be cited in my thesis as shown above and the thesis will be made available online via Curtin's Institutional Repository, espace.

Please note that the use of these figures is for non-commercial and educational purposes.

Regards

Mohamed Shams

BSc, MSc, Civil Engineering

Mob | +61 4 06300653

Email | mohamed.shams@postgrad.curtin.edu.au

Disclaimer

The information contained in this communication from the sender is confidential. It is intended solely for use by the recipient and others authorized to receive it. If you are not the recipient, you are hereby notified that any disclosure, copying, distribution or taking action in relation of the contents of this information is strictly prohibited and may be unlawful.

This email has been scanned for viruses and malware, and may have been automatically archived by **Mimecast Ltd**, an innovator in Software as a Service (SaaS) for business. Providing a **safer** and **more useful** place for your human generated data. Specializing in; Security, archiving and compliance. To find out more [Click Here](#).

Reply all | Delete | Junk | ...

RE: Permission request

BJ Briaud, Jean-Louis <briaud@tamu.edu>
Yesterday, 10:59 AM
Mohamed Shams

Reply all |

Inbox

No problem with me Mohamed. Just please cite the source, and good luck to you. Jean-Louis

ASCE President Elect Nominee

Jean-Louis BRIAUD, PhD, PE, DGE, Distinguished Member ASCE
University Distinguished Professor and Buchanan Chair Holder
Zachry Dpt. of Civil Engineering, Texas A&M University
College Station, Texas, 77843-3136, USA
Tel: 979-845-3795, Cell: 979-777-1692
Email: briaud@tamu.edu
<https://ceprofs.civil.tamu.edu/briaud/>

From: Mohamed Shams <mohamed.shams@postgrad.curtin.edu.au>
Sent: Friday, February 8, 2019 9:00 PM
To: Briaud, Jean-Louis <briaud@tamu.edu>
Subject: Permission request

Dear Dr. Briaud,

I am a PhD student in Curtin university in Australia and I want your permission to reprint Figure 10 from your published paper:

Briaud, J. L., Abdelmalak, R., Xiong, Z., and Magbo, C. (2016). "Stiffened slab-on-grade on shrink-swell soil: New design method." *Journal of Geotechnical and Geoenvironmental Engineering*, 142 (7): 04016017, doi: 10.1061/(ASCE)GT.1943-5606.0001460.

The figure will be cited in my thesis as shown above.

The thesis will be made available online via Curtin's Institutional Repository, espace.

Please note that the use of these figures is for non-commercial and educational purposes.

Regards

Mohamed Shams
BSc, MSc, Civil Engineering

 Reply all |   Delete Junk |  ...

RE: Permission requested

RJ

Reins, John <JReins@wje.com>

Yesterday, 7:11 PM

Mohamed Shams 

  Reply all | 

Inbox

Mohamed:

You certainly have my permission to reprint those figures. Good luck with your thesis.

John D. Reins, PE

Principal

Wiss, Janney, Elstner Associates, Inc.*Engineers | Architects | Materials Scientists*[3609 South Wadsworth Blvd, Suite 400](#)[Lakewood, Colorado 80235](#)

tel 303.914.4300 | direct 303.914.4313 | fax 303.914.3000 | mobile 303.618.1832

From: Mohamed Shams [mailto:mohamed.shams@postgrad.curtin.edu.au]**Sent:** Friday, February 08, 2019 12:00 AM**To:** Reins, John <JReins@wje.com>**Subject:** Permission requested

Dear Sir,

I am a PhD student in Curtin university in Australia and I want your permission to reprint Figure 1 and 2 from your published paper:

"Monitoring and mitigation of movements affecting foundations on expansive soils in Colorado."

Journal of Performance of Constructed Facilities, 27 (6): 731-736.

The thesis will be made available online via Curtin's Institutional Repository, espace.

Please note that the use of these figures is for non-commercial and educational purposes.

Regards

Mohamed Shams

BSc, MSc, Civil Engineering

Mob | +61 4 06300653

Email | mohamed.shams@postgrad.curtin.edu.au


 Reply all |  Delete Junk | 

Re: Permission request

MD

Muawia Dafalla <mdafalla@gmail.com>

Today, 9:02 AM

Mohamed Shams 

  Reply all | 

Inbox

Dear Shams

I am pleased to grant the permission.

Muawia Dafalla

On Sun, 10 Feb 2019 at 06:16, Mohamed Shams <mohamed.shams@postgrad.curtin.edu.au> wrote:

Dear Dr. Muawia,

I am a PhD student in Curtin university in Australia and I need your kind permission to reprint Figure 3 from your published paper:

Dafalla, M. A., Al-Shamrani, M. A., Puppala, A. J., and Ali, H. E. (2011). "Design guide for rigid foundation systems on expansive soils." *International Journal of Geomechanics*, 12 (5): 528-536.

The figure will be cited in my thesis as shown above.

The thesis will be made available online via Curtin's Institutional Repository, espace.

Please note that the use of the figures is for non-commercial and educational purposes.

Regards

Mohamed Shams



[Home \(https://ww...](#) > [About \(https://...](#) > [Policies \(https:/...](#) > [Copyright \(http...](#) > [Permissions \(ht...](#)

Permissions

As a general rule, permission should be sought from the rights holder to reproduce any substantial part of a copyrighted work. This includes any text, illustrations, charts, tables, photographs, or other material from previously published sources. Obtaining permission to re-use content published by Elsevier is simple. Follow the guide below for a quick and easy route to permission.

Permission guidelines	ScienceDirect content	Non-ScienceDirect content	Tutorial videos	Help and support
---------------------------------------	---------------------------------------	---	---------------------------------	----------------------------------

Permission guidelines

For further guidelines about obtaining permission, please review our [Frequently Asked Questions](#) below:

[When is permission required?](#)

[When is permission not required?](#)

[From whom do I need permission?](#)

[How do I obtain permission to use photographs or illustrations?](#)

[Do I need to obtain permission to use material posted on a website?](#)

[What rights does Elsevier require when requesting permission?](#)

[How do I obtain permission from another publisher?](#)

[What is Rightslink?](#)

[What should I do if I am not able to locate the copyright owner?](#)

[What is Elsevier's policy on using patient photographs?](#)

[Can I obtain permission from a Reproduction Rights Organization \(RRO\)?](#)

This page is available in the following languages:



Creative Commons License Deed

Attribution-NonCommercial-NoDerivatives 4.0 International (CC BY-NC-ND 4.0)

This is a human-readable summary of (and not a substitute for) the [license](#).

You are free to:

Share — copy and redistribute the material in any medium or format

The licensor cannot revoke these freedoms as long as you follow the license terms.

Under the following terms:

Attribution — You must give appropriate credit, provide a link to the license, and indicate if changes were made. You may do so in any reasonable manner, but not in any way that suggests the licensor endorses you or your use.

NonCommercial — You may not use the material for commercial purposes.

NoDerivatives — If you remix, transform, or build upon the material, you may not distribute the modified material.

No additional restrictions — You may not apply legal terms or technological measures that legally restrict others from doing anything the license permits.

Notices:

You do not have to comply with the license for elements of the material in the public domain or where your use is permitted by an applicable exception or limitation.

No warranties are given. The license may not give you all of the permissions necessary for your intended use. For example, other rights such as publicity, privacy, or moral rights may limit how you use the material.